U.S. CENTERS FOR DISEASE CONTROL AND PREVENTION

EMERGING INFECTIOUS DISEASES®

Vectorborne Diseases

October 2024

Alfred Sisley (1839–1899), *Flood at Port-Marly*, 1872. Oil on canvas. 18 1/4 in × 24 in/46.4 cm × 61 cm. Collection of Mr. and Mrs. Paul Mellon. National Gallery of Art, Washington, DC, USA.

EMERGING INFECTIOUS DISEASES®

Emerging Infectious Diseases is published monthly by the Centers for Disease Control and Prevention, 1600 Clifton Rd NE, Mailstop H16-2, Atlanta, GA 30329-4018, USA. Telephone 404-639-1960; email, eideditor@cdc.gov

EMERGING INFECTIOUS DISEASES®

Vectorborne Diseases

October 2024

On the Cover

Alfred Sisley (1839–1899). *Flood at Port-Marly*, 1872. Oil on canvas. 18 1/4 in x 24 in/46.4 cm x 61 cm. Collection of Mr. and Mrs. Paul Mellon. National Gallery of Art, Washington, DC, USA. Open access image.

About the Cover p. 1500

Synopses

Medscape EDUCATION ACTIVITY

Research

Medscape EDUCATION ACTIVITY

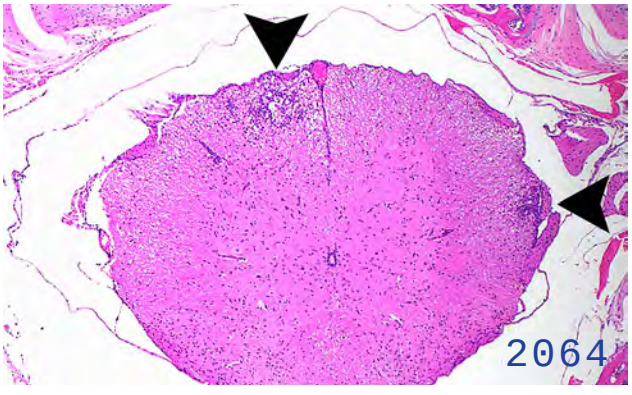

Dispatches

EMERGING INFECTIOUS DISEASES®
October 2024

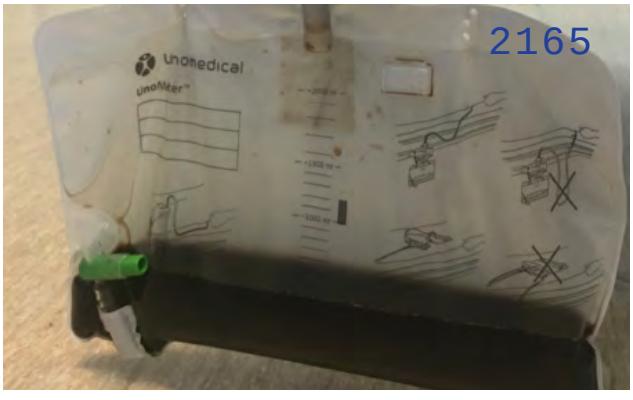

EMERGING INFECTIOUS DISEASES®
October 2024

Research Letters

Emerging Infections Network Letter

About the Cover

Etymologia

Corrections

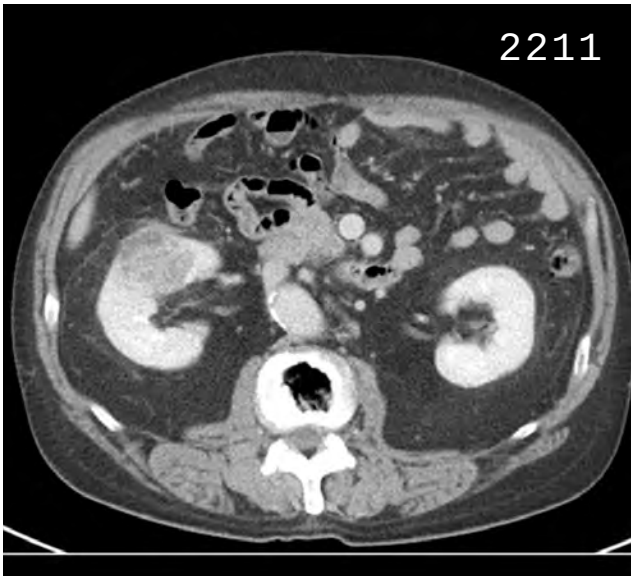

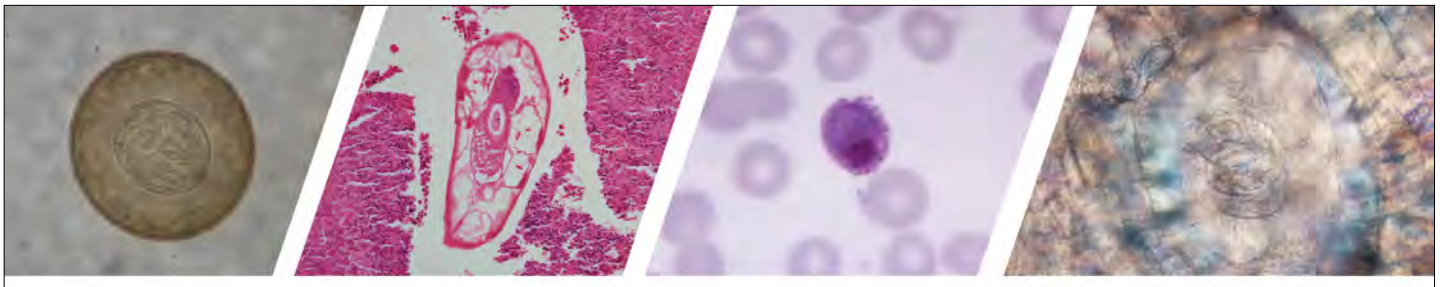

DPDx

Diagnostic Assistance and Training in Laboratory Identification of Parasites

A free service of CDC available to laboratorians, pathologists, and other health professionals in the United States and abroad

- Diagnosis from photographs of worms, histological sections, fecal, blood, and other specimen types
- Expert diagnostic review
- Formal diagnostic laboratory report
- Submission of samples via secure file share

Visit the DPDx website for information on laboratory diagnosis, geographic distribution, clinical features, parasite life cycles, and training via Monthly Case Studies of parasitic diseases.

www.cdc.gov/dpdx
dpdx@cdc.gov

U.S. Department of Health and Human Services
Centers for Disease Control and Prevention

CS272346-DE

Pasteurella Infections in South Korea and Systematic Review and Meta-analysis of *Pasteurella* Bacteremia

Seri Jeong, Eunjin Chang, Nuri Lee, Hyun Soo Kim, Han-Sung Kim, Jae-Seok Kim, Young Ah Kim, Chang Ki Kim, Kyungwon Lee, Hyukmin Lee, Seok Hoon Jeong, Wonkeun Song

Medscape CME Activity

In support of improving patient care, this activity has been planned and implemented by Medscape, LLC and Emerging Infectious Diseases. Medscape, LLC is jointly accredited with commendation by the Accreditation Council for Continuing Medical Education (ACCME), the Accreditation Council for Pharmacy Education (ACPE), and the American Nurses Credentialing Center (ANCC), to provide continuing education for the healthcare team.

Medscape, LLC designates this Journal-based CME activity for a maximum of 1.00 ***AMA PRA Category 1 Credit(s)™***. Physicians should claim only the credit commensurate with the extent of their participation in the activity.

Successful completion of this CME activity, which includes participation in the evaluation component, enables the participant to earn up to 1.0 MOC points in the American Board of Internal Medicine's (ABIM) Maintenance of Certification (MOC) program. Participants will earn MOC points equivalent to the amount of CME credits claimed for the activity. It is the CME activity provider's responsibility to submit participant completion information to ACCME for the purpose of granting ABIM MOC credit.

All other clinicians completing this activity will be issued a certificate of participation. To participate in this journal CME activity: (1) review the learning objectives and author disclosures; (2) study the education content; (3) take the post-test with a 75% minimum passing score and complete the evaluation at http://www.medscape.org/journal/eid; and (4) view/print certificate. For CME questions, see page 2224.

NOTE: It is Medscape's policy to avoid the use of Brand names in accredited activities. However, in an effort to be as clear as possible, trade names are used in this activity to distinguish between the mixtures and different tests. It is not meant to promote any particular product.

Release date: September 20, 2024; Expiration date: September 20, 2025

Learning Objectives

Upon completion of this activity, participants will be able to:

- Distinguish the most common species of *Pasteurella* implicated in infection in the current study
- Analyze characteristics of persons infected with *Pasteurella*
- Assess the management and outcomes of *Pasteurella* infection
- Estimate the global burden and outcomes of *Pasteurella* infection

CME Editor

Dana C. Dolan, BS, Technical Writer/Editor, Emerging Infectious Diseases. *Disclosure: Dana C. Dolan, BS, has no relevant financial relationships.*

CME Author

Charles P. Vega, MD, Health Sciences Clinical Professor of Family Medicine, University of California, Irvine School of Medicine, Irvine, California. *Disclosure: Charles P. Vega, MD, has the following relevant financial relationships: served as consultant or advisor for Boehringer Ingelheim; GlaxoSmithKline.*

Authors

Seri Jeong, MD, PhD; Eunjin Chang, MS; Nuri Lee, MD, PhD; Hyun Soo Kim, MD, PhD; Han-Sung Kim, MD, PhD; Jae-Seok Kim, MD, PhD; Young Ah Kim, MD, PhD; Chang Ki Kim, MD, PhD; Kyungwon Lee, MD, PhD; Hyukmin Lee, MD, PhD; Wonkeun Song MD, PhD.

Author affiliations: Hallym University College of Medicine, Seoul, South Korea (S. Jeong, E. Chang. N. Lee, J.-S. Kim, W. Song); Hallym University College of Medicine, Hwaseong, South Korea (H.S. Kim); Hallym University College of Medicine, Anyang, South Korea (H.-S. Kim); Ilsan Hospital, Goyang, South Korea (Y.A. Kim); Seoul Clinical Laboratories Academy, Yongin, South Korea (C.K. Kim, K. Lee); Yonsei University College of Medicine, Seoul (K. Lee, H. Lee, S.H. Jeong)

DOI: https://doi.org/10.3201/eid3010.240245

Pasteurella spp. can cause fatal zoonotic infections in humans. We performed a multicenter study to investigate the prevalence and clinical features of *Pasteurella* infections in South Korea during 2018–2022. We also conducted a collaborative systematic review and meta-analysis of the global burden of *Pasteurella* bacteremia. The study included 283 cases and found an increasing trend in *Pasteurella* infections. Blood cultures were positive in 8/35 (22.9%) cases sampled, for an overall bacteremia-associated rate of 2.8% (8/283). Aging was a significant risk factor for bacteremia (odds ratio 1.05 [95% CI 1.01–1.10]), according to multivariate analyses. For the meta-analysis, we included a total of 2,012 cases from 10 studies. The pooled prevalence of bacteremia was 12.4% (95% CI 7.3%–18.6%) and of mortality 8.4% (95% CI 2.7%–16.5%). Our findings reflect the need for greater understanding of the increase in *Pasteurella* infections and the global burden of *Pasteurella* bacteremia to determine appropriate case management.

Pasteurella spp. can cause fatal zoonotic infections in humans (*1*,*2*). *Pasteurella* spp., which are nonmotile, facultatively anaerobic bacteria, form the oral and gastrointestinal flora of many animals including companion and common livestock animals such as dogs, cats, and pigs (*3*–*5*). The health risk for humans and public health concerns regarding *Pasteurella* spp. should not be ignored when considering the increase in the numbers of those animals, caused by global economic and social development (*1*,*6*,*7*).

Strains of *P. multocida*, one of the most commonly isolated *Pasteurella* pathogens, have the capacity to invade human bronchial epithelial cells (*1*,*2*). The characteristics of human *Pasteurella* infections range from the commonly reported localized infection of a bite wound (*8*,*9*) to invasive infections such as bacteremia (*10*,*11*), meningitis (*12*), and infective endocarditis (*13*), especially in immunocompromised patients. Those invasive infections are associated with higher mortality rates in patients with pasteurellosis (*10*,*14*). However, only a few cohort studies on the epidemiology and clinical characteristics of *Pasteurella* infections have been published, mostly in Europe and the United States. Most studies regarding *Pasteurella* infections are reports of individual cases. Furthermore, the number of companion animals and the occurrence of humans having close contact with such animals have increased substantially (*15*).

We conducted a multicenter study of infections caused by *Pasteurella* spp. from various locations in South Korea during 2018–2022 to investigate their prevalence and clinical features. In addition, we conducted a comprehensive systematic review and meta-analysis to characterize the global burden of bacteremia as a representative disease of invasive infection caused by *Pasteurella* spp. We performed subgroup analyses stratified by publication periods and study locations. The Institutional Review Board of Kangnam Sacred Heart Hospital, Seoul (HKS 2023-01-008) approved the study and waived the need for informed consent because of participant anonymity.

Methods

Ethics

Study Design and Patients

We designed a retrospective multicenter study of the prevalence of infections caused by *Pasteurella* spp. combined with a meta-analysis to determine the burden of these infections, especially bacteremia. We obtained data for *Pasteurella* species infections during 2018–2022 from 7 university hospitals in metropolitan areas (4 in Seoul and 3 in Gyeonggi-do) and 1 reference laboratory, where samples from general and small- and medium-sized hospitals were tested, in South Korea to investigate the overall burden of these infections throughout the country. Patients were included if they had a microbiological examination that was positive for *Pasteurella* species. We identified isolated species by matrix-assisted laser desorption/ionization time-of-flight mass spectrometry on a Vitek-MS instrument (bioMérieux) or Bruker instrument (Bruker Daltonik), Vitek 2 system (bioMérieux), and the MicroScan Walkaway-96 system (Siemens). We obtained the following clinical variables from patient charts: basic demographics, hospital region of origin, sampling year, isolation site, the presence of polymicrobial infection, any animal contact such as bite or scratch history, and the antibiotics and therapies used. We also collected data for hospitalization and outcomes. From the 316 participants, we excluded 31 whose records lacked basic demographic information, such as age and sex (Figure 1). We included a total of 283 patients after excluding 2 patients whose *Pasteurella* species were isolated in 2017 and 2023. We obtained only basic data—age, sex, sampling year, isolation site, and region—for 213 participants from the reference laboratory.

Search Strategy and Selection Criteria for Meta-analysis

We performed a systematic review as described in the Cochrane handbook (*16*) to estimate the global prevalence of bacteremia caused by *Pasteurella* spp. We referred to the Preferred Reporting Items for Systematic Review and Meta-analysis (*17*,*18*)

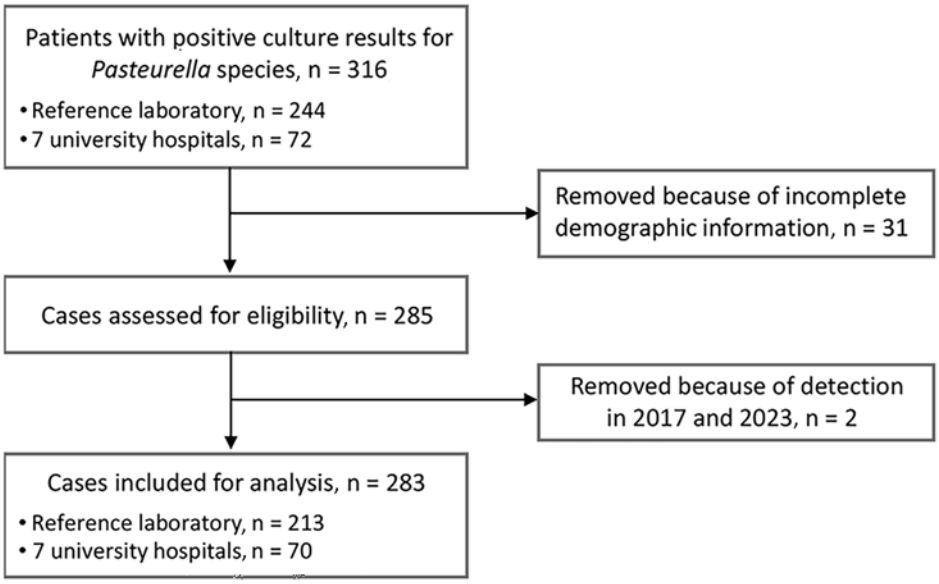

Figure 1. Flow diagram of study population selection for study of *Pasteurella* infection, South Korea, 2018–2022.

checklist (Appendix Table 1, https://wwwnc.cdc.gov/EID/article/30/10/24-0245-App1.pdf). We included studies that reported prevalence data for patients with *Pasteurella* species infection and bacteremia based on laboratory results. We included observational cohort studies, regardless of language or publication year. We excluded studies without the necessary data for the calculation of the prevalence of bacteremia (Appendix Table 2).

We performed a comprehensive search of PubMed, Ovid-EMBASE, and the Cochrane Library for articles published through November 1, 2023. The search strategy included use of the keywords "Pasteurella infections," "bacteremia," "prevalence," and "epidemiology." We included Medical Subject Heading and Emtree terms, text words, and equivalent subject heading and thesaurus terms to ensure inclusivity; we also performed manual searches of the references of relevant articles for completeness (Appendix Table 3). We registered the protocol in the international prospective register for systematic reviews (registration no. CRD42023484039).

Analysis of the Study Population Data and Meta-analysis

For statistical analysis of data from multiple centers in South Korea, we used the Mann-Whitney U test or Pearson's χ^2 test to compare groups. We applied multivariate binary logistic regression analyses to investigate variables that correlated independently with the occurrence of bacteremia in patients with *Pasteurella* spp. infections.

For the meta-analysis, we conducted title and abstract screening of studies selected through the search strategy on the basis of the eligibility criteria (Figure 2). Two reviewers (E.J. and N.L.) independently assessed the full texts of the studies. We settled disagreements by consensus after all reviewers reviewed the data. We extracted the following variables if they were available: demographic information about the study population, collection periods, the presence of animal exposure, the identified species, regions, and outcome measures. We documented the data for hospitalization and death, as well as the prevalence of bacteremia, our primary outcomes. We used the Joanna Briggs Institute checklist (*19*) to evaluate the quality of the included articles at the study level. We considered scores >70% as high quality. Two reviewers (E.J. and N.L.) assessed the quality of the included studies. S.J. resolved any disagreements.

We calculated the proportion of patients with positive blood cultures for the determining the rate of bacteremia among the total number of patients with bacterial infections. We based the calculation on all types of samples for which culture tests were requested (*3*,*4*,*10*,*20*). Although simultaneous blood culture is necessary for a more accurate determination of the rates of bacteremia, it was not routinely performed. Blood culture was performed only in 35/283 cases in which the clinician deemed it necessary. We transformed single raw prevalence using the Freeman-Tukey Double arcsine method (*21*) to stabilize variances. We used the random effects model to calculate the pooled prevalence with 95% CI across studies.

We assessed heterogeneity using Cochran's Q test and the degree of heterogeneity using the Higgins I^2 statistic. Indices with values of >75% represented high heterogeneity (*22*). We performed

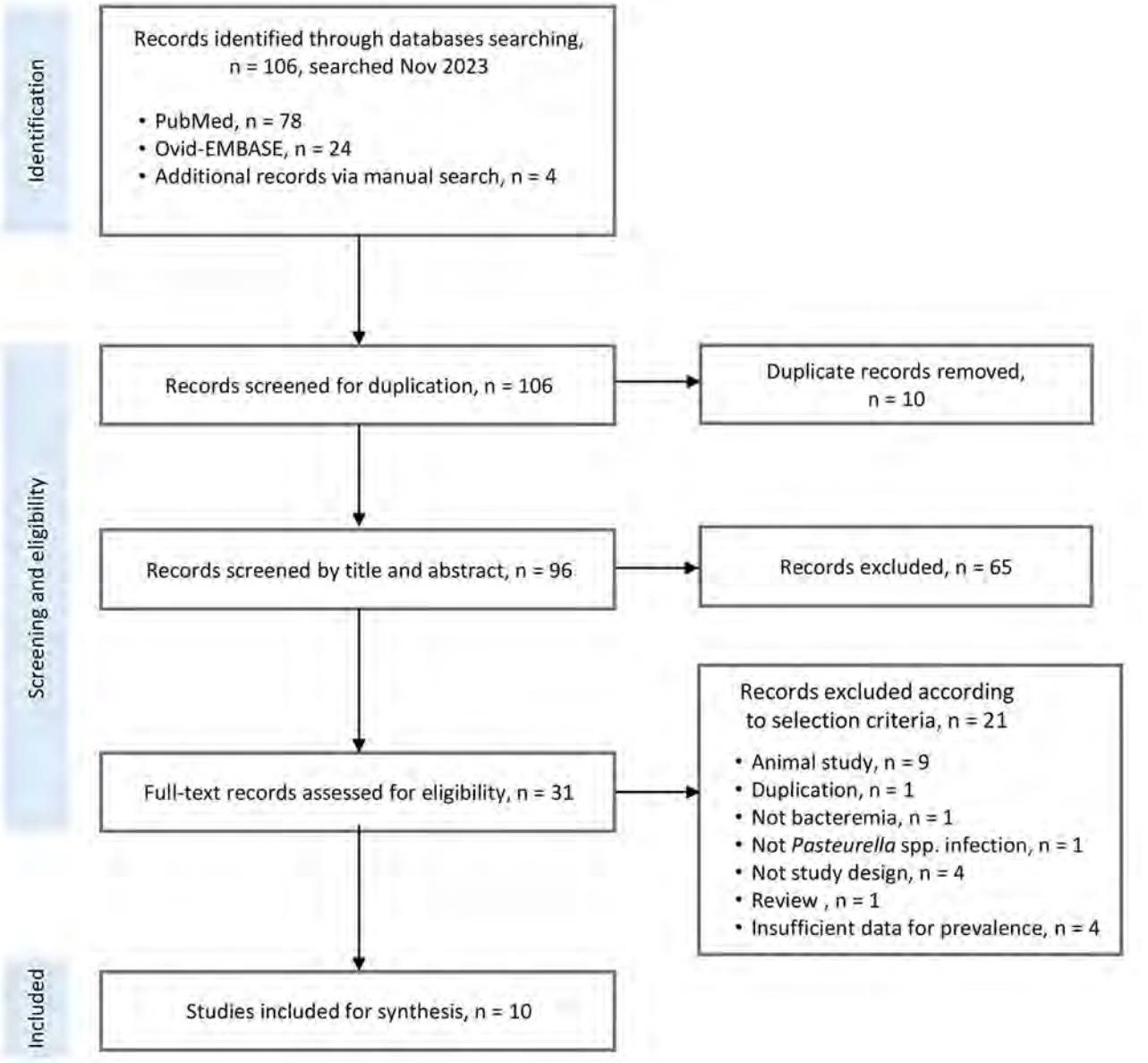

Figure 2. Flow diagram of study selection process in systematic review and meta-analysis of studies of human bacteremia caused by *Pasteurella* spp..

subgroup analyses to explore potential sources of heterogeneity by study location and period. In addition, we conducted sensitivity analysis to further assess the robustness of the estimates. The software we used for those analyses was the moonBook package in R (The R Project for Statistical Computing), MedCalc software, version 19.8 (MedCalc Software Ltd), Analyze-it Method Evaluation Edition software version 2.26 (Analyze-it Software Ltd), and Stata version 18 (StataCorp LLC). We have deposited the raw data used in this study (Appendix Tables 4, 5) in the Harvard Dataverse (https://doi.org/10.7910/DVN/1QQ9KK).

Results

Prevalence and Clinical Features of *Pasteurella* Infections

We included a total of 283 cases in the study, 70 from hospital patients with complete data and 213 cases from the main reference laboratory with basic information. We observed an increase in the number of infections caused by *Pasteurella* spp. from 2018 (n = 46) to 2022 (n = 72) (Figure 3); the increase was significant on the basis of the national population data extracted from the Korean Statistical Information Service (p = 0.012). The median number of cases per year

was 55. The predominant species were *P. multocida* (68.9%, 195/283) and *P. canis* (25.4%, 72/283), both of which contributed to the increase in infections. The median age of patients with positive culture results was 52.0 years. The number of *Pasteurella* isolation samples was higher in women (66.4%, 188/283) than in men (33.6%, 95/283). We observed the most cases in patients in the 50–59-year age group (Figure 3). The ratio of female to male patients was the highest (3.4:1) for patients 20–29 years of age. Most patients had a history of companion animal exposure (88.6%, 62/70) (Appendix Table 6); half had history of dog exposure and 38.7% (24/62) cat exposure. The rate of polymicrobial infection was 25.7% (18/70). The detected isolates were *Staphylococcus aureus* (n = 2), *Actinomyces* spp. (n = 2), *Streptococcus sanguinis* (n = 1), *Proteus mirabilis* (n = 1), and *Dermabacter hominis* (n = 1). The rate of hospitalization was 54.3% (38/70). We noted no significant differences in characteristics between inpatients and outpatients (Appendix Table 7). Among all the patients, most patients were mainly from Seoul (23.0%, 65/283), whereas those included in the reference laboratory study were predominantly from Gyeongsang-do (33.0%, 71/213) and Gyeonggi-do (17.4%, 37/213) (Appendix Figure 1). All patients, except for 3 outpatients, had received antimicrobial therapy. The most frequently prescribed antibiotics were penicillin/β-lactamase inhibitor combinations and first-generation cephalosporins (Appendix Table 4).

The rates of bacteremia were 2.8% (8/283) among all included infections and 7.1% (5/70) among the 7 university-hospital cases (Appendix Table 8). The median age was higher in bacteremia (68.5 years) than that in nonbacteremia (52.0 years). Patients with bacteremia had no animal exposure history. According to the multivariate regression analyses, including sex as the confounder, only increasing age was a significant risk factor for bacteremia (odds ratio 1.05, 95% CI 1.01–1.10; p = 0.024) (Figure 4). Among all bacteremia cases, 1 patient with septic shock caused by *P. multocida* died after 4 days of hospitalization; that patient had alcoholic liver cirrhosis and asthma as underlying diseases.

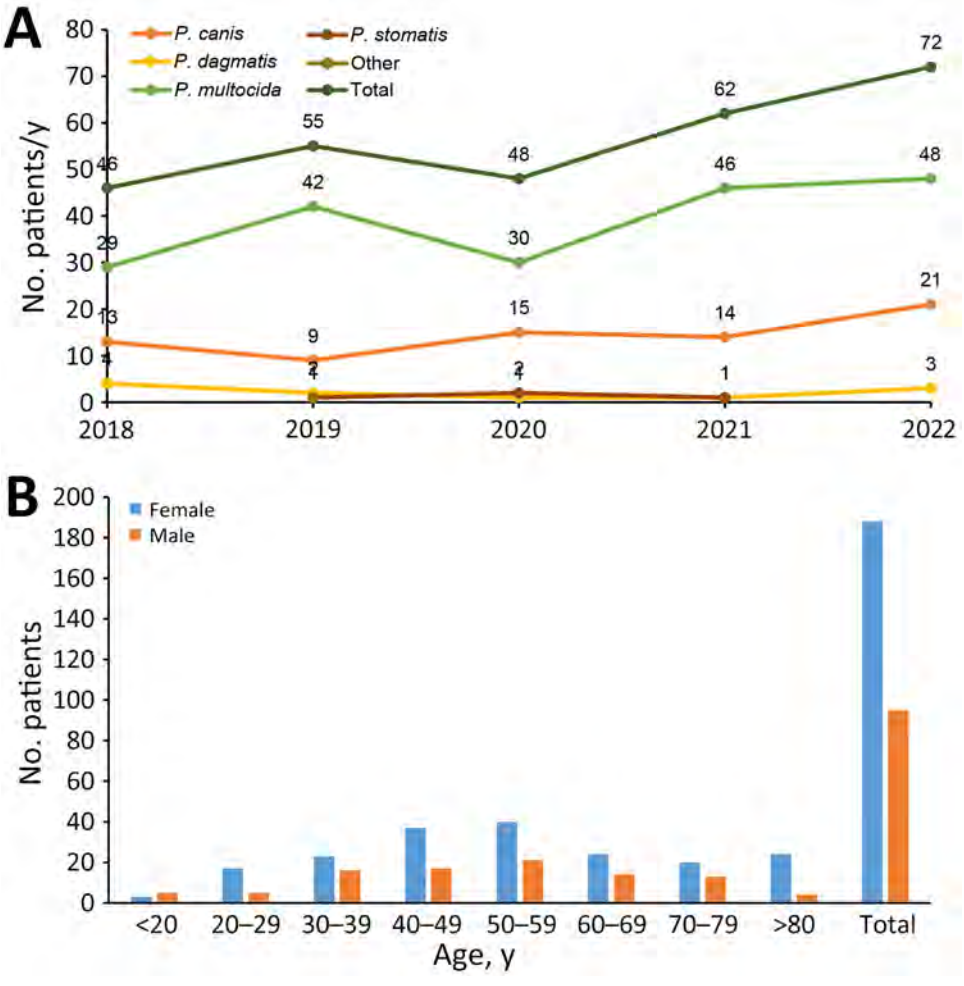

Figure 3. Prevalence of *Pasteurella* infections in South Korea, 2018–2022. A) Distribution of *Pasteurella* infections classified by year and species. B) Distribution of *Pasteurella* infections classified by age group and sex.

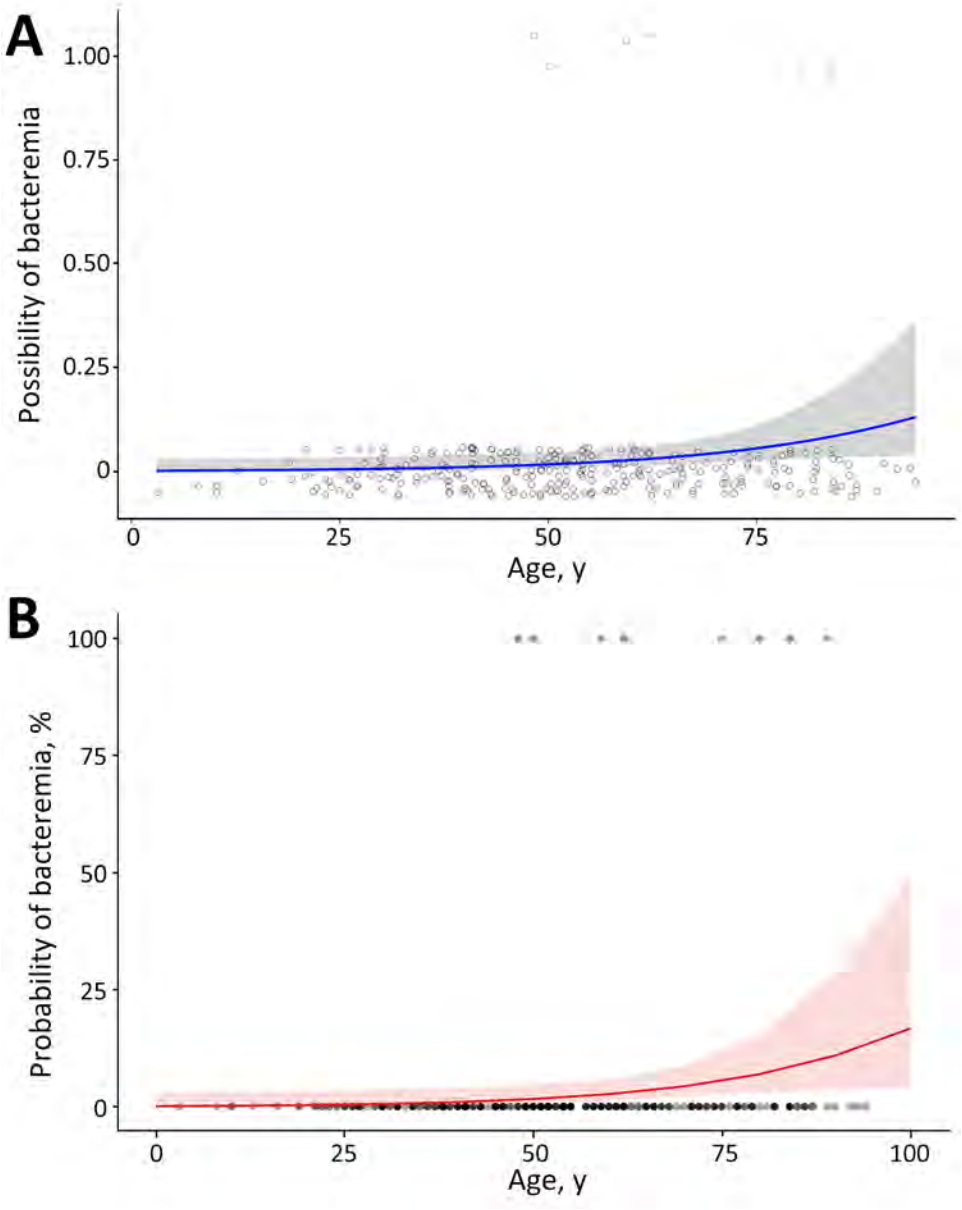

Figure 4. Regression model of bacteremia caused by *Pasteurella* spp., South Korea, 2018–2022. A) Univariate analysis of age and the probability of bacteremia caused by *Pasteurella* spp. The smoothing method was a generalized linear model. Blue line indicates the estimated values of the possibility of bacteremia; shading indicates 95% CI; black circles indicate cases with bacteremia; and gray circles indicate cases without bacteremia. B) Final model after multivariate analysis of age and sex for the predicted probability of bacteremia caused by *Pasteurella* spp. Red line indicates the estimated values of the probability of bacteremia; shading indicates 95% CI; black dots indicate cases with bacteremia; and gray dots indicate cases with nonbacteremia.

Meta-analyses for Global Burden of *Pasteurella* Bacteremia

The study screening method for the meta-analysis (Figure 2) identified 106 studies, of which 96 articles were relevant and were subsequently screened. A total of 31 reports were available for full-text screening. We excluded papers with insufficient study populations and design and insufficient data for the calculation of the prevalence of *Pasteurella* spp. bacteremia from the current review (Appendix Table 2). Finally, we included 10 studies in the systematic review (*3*,*4*,*6*,*7*,*10*,*20*,*23*–*26*).

We included a total of 2,012 participants from the 10 studies in the meta-analysis (Table). The studies were published during 1985–2021, half before 2010 (*4*,*10*,*20*,*25*,*26*) and half after 2010 (*3*,*6*,*7*,*23*,*24*). We observed more than 50% of study participants were female in all the included studies. The occurrence of animal exposure calculated from available study data was 34.3%–97.3%. The most commonly isolated species were *P. multocida* and *P. canis*. The rates of hospitalization were higher in cases of invasive infection (83.3% [*23*] and 97.0% [*24*]) than those in other cases (*3*,*6*,*7*,*20*). The death rates range was 0.6%–27.2%. Six studies were conducted in Europe and the United States (*3*,*7*,*10*,*20*,*23*–*26*). Based on the assessment using the Joanna Briggs Institute checklist, all studies showed scores >70%, indicating that they were of high quality.

Four studies that included only *P. multocida* infections had lower scores in the samples frame appropriate to address the target population (*3*,*4*,*20*,*25*).

The prevalence of bacteremia caused by *Pasteurella* spp. from 10 studies was 3.4%–32.5%. The random effects pooled prevalence from the 2,012 cases was 12.4% (95% CI 7.3%–18.6%). The Cochran Q test revealed significant heterogeneity (Q = 52.1, p<0.001). The I^2 index of the included studies indicated high heterogeneity (I^2 = 90.7) (Figure 5).

We calculated the pooled prevalence estimates of *Pasteurella* infection stratified by publication year. The pooled value of 5 studies published before 2010 (*4*,*10*,*20*,*25*,*26*) was 12.7% (95% CI 4.1%–24.6%) and of 5 studies published after 2010 (*3*,*6*,*7*,*23*,*24*) was 12.1% (95% CI 6.6%–18.9%). Although the I^2 index for studies published after 2010 (78.9%) was lower than that for studies before 2010 (94.4%), we noted no significant differences in pooled prevalence and heterogeneity. In a subgroup analysis of different regions, the estimated prevalence infection in 6 studies conducted in Europe (9.8%, 95% CI 4.5%–16.6%) was not different from that of 2 studies conducted in the United States (11.6%, 95% CI 3.3%–23.6%). We excluded 1 of the 10 studies from the sensitivity analyses. We compared estimated prevalence to the estimated total prevalence (Appendix Table 9). The pooled estimates from the sensitivity analyses were 9.9%–13.8%, consistent with the total pooled prevalence without statistical differences. The pooled death rate was 8.4% (95% CI 2.7%–16.5%) (Appendix Figure 2).

Discussion

In this analysis of data from 8 centers in South Korea and a meta-analysis of the global burden of *Pasteurella* infections, we included 283 cases of infection caused by *Pasteurella* spp. in South Korea and 2,012 cases from 10 previous studies. We observed an increasing

Table. Characteristics of study of *Pasteurella* infections in South Korea and 10 studies included in meta-analysis of bacteremia caused by *Pasteurella* spp.*

Study location	No. patients	Collection period	Age, y†	Sex ratio, M:F	No. (%) with animal exposure	Species (no.)	Hospitalizations, no. (%)	No. (%) deaths	Ref
South Korea	283‡	2018–2022	52.0	95:188	62/70‡ (88.6)	*P. multocida* (195), *P. canis* (72), *P. dagmatis* (11), *P. stomatis* (4)	38/70‡ (54.3)	1/70‡ (1.4)	This study
Greece	13	1993–2004	64.4	10:3	5 (38.5); 2 unknown	*P. multocida* (13)	NR	3 (23.1)	(*25*)
France	215: 45 invasive, 170 local	2005–2018	59.8 for invasive, 49.1 for local	29:16 for invasive, 64:106 for local	16 of invasive, 21 of complicated local	*P. multocida* (169/215 total), *P. canis* (32/170 local)	65/67 (97.0) invasive and complicated local	10/45 (22.2) invasive	(*23*)
United States	179	1987–2007	66	6:8	7 (50.0) of 14 hospitalized	*P. multicida* (179)	14 (7.8)	1 (0.6)	(*20*)
France	958	1985–1991	NR	NR	35/102§ (34.3)	*P. multocida* (460), *P. canis* (105), *P. dagmatis* (48), *P. stomatis* (38)	NR	12/87 (13.8) with septicemia	(*10*)
United States	44	2000–2014	64	14:30	25 (56.8)	*P. multocida* (44)	27 (61.4)	4 (9.1)	(*3*)
Denmark	146	1989–1992	NR	NR	142 (97.3)	*P. multocida* (95), *P. canis* (28), *P. septica* (21), *P. stomatis* (10), *P. dagmatis* (5)	NR	NR	(*26*)
Hungary	162	2002–2015	57	78:84	114 (70.4)	*P. multocida* (160), *P. canis* (36), *P. pneumotropica* (11)	71/114 (62.3) local, 40/48 (83.3) invasive	44 (27.2)	(*24*)
Australia	190	2000–2021	49.7	93:97	145 (76.3)	*P. multocida* (121), *P. canis* (45), *P. dagmatis* (2)	148 (77.9)	2 (1.1)	(*6*)
France	102: 74 local, 28 invasive	2000–2015	63 for invasive, 50 for local	38:64	NR	*P. multocida* (86), *P. canis* (10), *P. dagmatis* (1), *P. stomatis* (1)	75 (73.5)	4 (3.9)	(*7*)
Israel	77	2000–2005	49.2	38:39	46 (59.7)	*P. multocida* (77)	NR	2 (2.6)	(*4*)

*NR, not reported; ref, reference.
†Mean or median, as reported in article.
§15 cases of bacteremia and 87 cases of septicemia.
‡70 hospital patients with complete data and 213 cases from the main reference laboratory records.

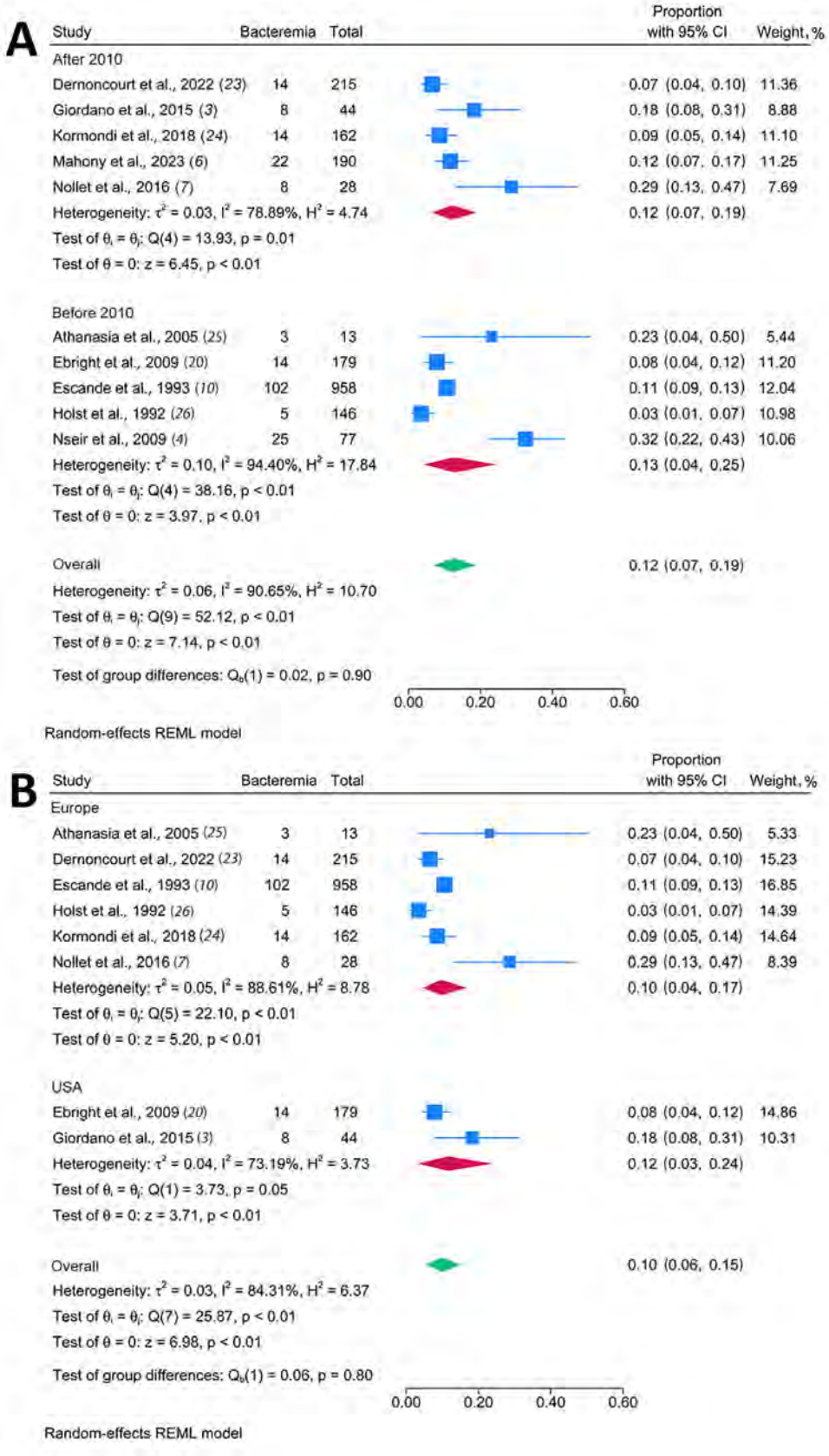

Figure 5. Forest plots for the pooled prevalence rates in systematic review and meta-analysis of studies of human bacteremia caused by *Pasteurella* spp. A) Subgroup analysis by year study was published. B) Subgroup analysis by study location. Blue squares indicate the rates of bacteremia of the included studies; error bars indicate 95% Cis. Red diamonds indicate the pooled rates of the included studies in the subgroup analysis, and green diamonds indicate the pooled rates of all studies presented in each subgroup analysis.

trend of *Pasteurella* infections during 2018–2022; South Korea had a median of 55 cases/year. The increasing trend of *Pasteurella* infections we observed in this study was consistent with the results of studies conducted in Australia (*6*) and Hungary (*24*). Those findings can be attributed to the increasing number of companion animals and their close contact with humans in South Korea. In Canada, ≈57% of households have ≥1 companion animal (*27*). The mean number of animal bites per year in Israel is 15,000, according to data from the Israeli Ministry of Health (*4*). In the United States, emergency departments observe ≈3 million dog bite injuries that lead to 10,000 hospitalizations and 20 deaths annually (*28*).

Among *Pasteurella* species, *P. multocida* is the most frequently isolated, followed by *P. canis* (*6*,*7*,*10*,*23*,*24*). Our results were consistent with those findings. The polymicrobial nature of *Pasteurella* infection was persistently reported. Mahony et al. (*6*) reported that 23.8% of cases exhibited polymicrobial infection, which was similar to the rate (25.7%) we observed in our study. *Staphylococcus aureus*, *Actinomyces* spp., *Streptococcus sanguinis*, and *Dermatobia hominis*, which were the co-isolated strains in this study, usually act as commensal bacteria in humans. *S. aureus* has been frequently isolated in several studies (*6*,*24*), concordant to our results.

For the demographic distribution, our study confirmed the predominance of infections in female patients, which has been consistently observed in previous studies, despite some variations (*3*,*7*,*24*). Dernoncourt et al. (*23*) observed this female predominance in localized infection cases rather than invasive infection cases, which might be associated with the higher proportions of localized infection we observed. Patients 50–59 years of age exhibited the most infections in this study. A survey in Canada found that the rate of pet ownership was highest among middle-aged persons (*27*), which supports our results, considering that pet-associated infections are frequently derived from injuries or animal bites (*24*). The high ratio of female to male patients 20–29 years of age could be because the primary responsibility for the care of companion animals is mostly that of female persons (72.8%) within households (*29*); another possible cause is that some nonmarried women spend substantial time with their cats (*29*).

Regarding bacteremia, older age groups are associated with bacteremia caused by *Pasteurella* spp. (*4*,*6*,*7*), consistent with the results of our study. Age-related dysfunction of the immune system and underlying diseases contribute to the increased risk for invasive infections (*24*). Underlying conditions such as diabetes mellitus and cirrhosis were commonly reported risk factors for bacteremia (*11*,*30*). Nollet et al. (*7*) determined by univariate analysis that chronic liver disease and alcohol consumption were risk factors for invasive *Pasteurella* infection; however, multivariate analysis showed that age was a significant risk factor (*7*). For animal contact, bacteremia was associated with the absence of animal bites or contacts (*7*,*24*), similar to our results. A previous study reported acute epiglottis without animal exposure (*31*), and a review described 79 cases including 34 of nonbite transmission (*14*). This type of transmission was related to comorbidities resulting in life-threatening infections. For example, contaminating a metatarsal ulcer by stepping on dog drool or wearing socks covered with cat hair could lead to bacteremia. The protection of open wounds is necessary for prevention because they were the most common entry method for non–bite-associated infections.

Several case reports or reviews have described severe systemic infections caused by *Pasteurella* spp., such as bacteremia and endocarditis. A review of *P. multocida* bacteremia presented the clinical features and outcome of 13 patients (*32*). A recent review focused on epidemiology, diagnosis, host–pathogen interactions, clinical manifestation, management, and prognosis of *P. multocida* infections (*2*). In addition, a systematic review of infective endocarditis caused by *Pasteurella* species described the clinical characteristics and outcomes of patients on the basis of data from 28 studies (*13*). However, meta-analyses with specified values have not been performed. Therefore, we conducted meta-analyses assessing the global burden of *Pasteurella* bacteremia as a representative invasive infection.

The pooled prevalence from 10 studies was 12.4%, which was higher than the rate of bacteremia observed in this study (2.8% from all episodes and 7.1% from 7 hospital cases). The study populations of the included studies included patients in tertiary and university hospitals (*3*,*6*,*23*–*26*) or with hospitalization (*4*), which may have influenced this high prevalence. In addition, high medical accessibility with a reimbursement system and health screenings for the elderly could be the cause of the significantly low prevalence of bacteremia we observed in our study. The high heterogeneity may be derived from the different periods of isolation and publication and by the variation across geographic regions of the country. We performed subgroup analyses stratified by publication year and study locations, which showed no significant differences, except for a slightly lower I^2 index (from 94.4% before 2010 to

78.9% after 2010). The overlap of data collection periods caused by long (median 13 years) study durations might have affected these results. In addition, the small number of studies on *Pasteurella* bacteremia used for this analysis might have affected the statistical results.

The number of deaths caused by *Pasteurella* infection is increasing in the United States (*33*). Meta-analyses revealed that the pooled estimate of deaths was 8.4%, which was much higher than the death rate measured in our study (0.4% for all and 1.4% for hospital cases). The low rate in our study is consistent with the low prevalence of bacteremia in our cohort; the mortality rate for patients with invasive infections was higher (*10*,*23*). Although the rate of infections is low, mortality rate may increase as the prevalence of *Pasteurella* infection increases.

One limitation of this study was its retrospective nature; some clinical information documented in the medical record was incomplete or missing. In particular, only basic demographic information was available for patients from the reference laboratory. Therefore, we included data from hospitals; data from multiple centers are a strength of this study. However, diverse identification methods and the inherent limitations of the applied methods may affect the results (*12*). The relatively small size of our cohort might influence the statistical analysis. Studies with larger study populations, including hospitals in rural and farming areas, are necessary. Detailed descriptions of the methods used for calculating the bacteremia rate would be useful to estimate the specified rate of bacteremia; in addition, further studies with concurrent blood culture data are needed to determine more accurate rates of bacteremia. For meta-analyses, additional studies from diverse countries are necessary for generalization. We could not sufficiently analyze publication bias because we included a limited number of studies. In addition, the heterogeneity of the included studies may have affected the results; we conducted subgroup analyses, a random effects model, and sensitivity analyses to overcome this limitation.

In conclusion, this study highlights the increasing trend and clinical features of *Pasteurella* infections, the rate of bacteremia, and older age as a risk factor for bacteremia based on data from 8 centers in South Korea. We estimated the global prevalence of bacteremia and related death rates through a collaborative approach with systematic meta-analysis. Our findings indicate that more attention needs to be paid to *Pasteurella* infection to enable appropriate management of these cases.

Acknowledgments

We thank all the personnel of the centers and participants, without whom this study could not be possible. We thank Editage for English language editing.

The protocol was registered in PROSPERO (registration no. CRD42023484039). The raw data used in this study (Appendix Table 4, 5) are available in the Harvard Dataverse (https://doi.org/10.7910/DVN/1QQ9KK).

This study was supported by the Seoul Clinical Laboratories Academy (grant no. 2023AR10) and the National Research Foundation of Korea (grant no. NRF-2022R1A2C1003503).

K.L. and W.S. conceptualized and designed the study. H.S.K., H.-SK., J.-SK., Y.A.K., C.K.K., H.L., and S.H.J. contributed to data collection and curation. E.C., N.L., and S.J. performed the formal analysis and visualization. S.J. prepared the first draft of the manuscript. K.L. and W.S. reviewed, edited, and verified all the data reported in the study.

About the Author

Dr. Jeong is a professor of Hallym University College of Medicine. Her research focuses on the microbiology and evidence-based medicine.

References

1. Peng Z, Lin L, Wang X, Chen H, Wu B. The public health concern of *Pasteurella multocida* should not be ignored. Lancet Microbe. 2022;3:e560. https://doi.org/10.1016/S2666-5247(22)00152-5
2. Piorunek M, Brajer-Luftmann B, Walkowiak J. *Pasteurella multocida* infection in humans. Pathogens. 2023;12:1210. https://doi.org/10.3390/pathogens12101210
3. Giordano A, Dincman T, Clyburn BE, Steed LL, Rockey DC. Clinical features and outcomes of *Pasteurella multocida* infection. Medicine (Baltimore). 2015;94:e1285. https://doi.org/10.1097/MD.0000000000001285
4. Nseir W, Giladi M, Moroz I, Moses AE, Benenson S, Finkelstein R, et al.; Israeli Group for Study of Pasteurella Infections. A retrospective six-year national survey of *P. multocida* infections in Israel. Scand J Infect Dis. 2009; 41:445–9. https://doi.org/10.1080/00365540902968035
5. Abreu F, Rodríguez-Lucas C, Rodicio MR, Vela AI, Fernández-Garayzábal JF, Leiva PS, et al. Human *Pasteurella multocida* infection with likely zoonotic transmission from a pet dog, Spain. Emerg Infect Dis. 2018;24:1145–6. https://doi.org/10.3201/eid2406.171998
6. Mahony M, Menouhos D, Hennessy J, Baird RW. Spectrum of human *Pasteurella* species infections in tropical Australia. PLoS One. 2023;18:e0281164. https://doi.org/10.1371/journal.pone.0281164
7. Nollet V, Souply L, Rosolen B, Mohseni-Zadeh M, Martinot M. Risk factors for invasive pasteurellosis: a retrospective case study. Eur J Clin Microbiol Infect Dis. 2016;35:1975–81. https://doi.org/10.1007/s10096-016-2749-y

8. Talan DA, Citron DM, Abrahamian FM, Moran GJ, Goldstein EJ; Emergency Medicine Animal Bite Infection Study Group. Bacteriologic analysis of infected dog and cat bites. N Engl J Med. 1999;340:85–92. https://doi.org/10.1056/NEJM199901143400202
9. Weber DJ, Wolfson JS, Swartz MN, Hooper DC. *Pasteurella multocida* infections. Report of 34 cases and review of the literature. Medicine (Baltimore). 1984;63:133–54. https://doi.org/10.1097/00005792-198405000-00001
10. Escande F, Lion C. Epidemiology of human infections by *Pasteurella* and related groups in France. Zentralbl Bakteriol. 1993;279:131–9. https://doi.org/10.1016/S0934-8840(11)80499-8
11. Laupland KB, Stewart AG, Edwards F, Harris P, Heney C, George N, et al. *Pasteurella* species bloodstream infections in Queensland, Australia, 2000-2019. Eur J Clin Microbiol Infect Dis. 2022;41:609–14. https://doi.org/10.1007/s10096-022-04411-w
12. Morsli M, Bechah Y, Coulibaly O, Toro A, Fournier PE, Houhamdi L, et al. Direct diagnosis of *Pasteurella multocida* meningitis using next-generation sequencing. Lancet Microbe. 2022;3:e6. https://doi.org/10.1016/S2666-5247(21)00277-9
13. Alifragki A, Kontogianni A, Protopapa I, Baliou S, Ioannou P. Infective endocarditis by *Pasteurella* species: a systematic review. J Clin Med. 2022;11:5037. https://doi.org/10.3390/jcm11175037
14. Kannangara DW, Pandya D, Patel P. *Pasteurella multocida* infections with unusual modes of transmission from animals to humans: a study of 79 cases with 34 nonbite transmissions. Vector Borne Zoonotic Dis. 2020;20:637–51. https://doi.org/10.1089/vbz.2019.2558
15. Kim SA, Kenyon CJ, Cheong S, Lee J, Hart LA. Attitudes and practices toward feral cats of male and female dog or cat owners and non-owners in Seoul, South Korea. Front Vet Sci. 2023;10:1230067. https://doi.org/10.3389/fvets.2023.1230067
16. Higgins JGS. Assessing risk of bias in included studies. In: J Higgins and S Green, editors. Cochrane handbook for systematic reviews of interventions, vol. 4. Chichester: John Wiley & Sons; 2011.
17. Moher D, Liberati A, Tetzlaff J, Altman DG; PRISMA Group. Preferred reporting items for systematic reviews and meta-analyses: the PRISMA statement. PLoS Med. 2009;6:e1000097. https://doi.org/10.1371/journal.pmed.1000097
18. Page MJ, McKenzie JE, Bossuyt PM, Boutron I, Hoffmann TC, Mulrow CD, et al. The PRISMA 2020 statement: an updated guideline for reporting systematic reviews. BMJ. 2021;372:n71. https://doi.org/10.1136/bmj.n71
19. Munn Z, Moola S, Lisy K, Riitano D, Tufanaru C. Methodological guidance for systematic reviews of observational epidemiological studies reporting prevalence and cumulative incidence data. Int J Evid-Based Healthc. 2015;13:147–53. https://doi.org/10.1097/XEB.0000000000000054
20. Ebright J, Frey AB, Fairfax MR. Pasteurella multocida infections and bacteremia: a twenty-year experience at an urban medical center. Infect Dis Clin Pract. 2009;17:102–4. https://doi.org/10.1097/IPC.0b013e318195e1ab
21. Freeman MF, Tukey JW. Transformations related to the angular and the square root. Ann Math Stat. 1950;21:607–11. https://doi.org/10.1214/aoms/1177729756
22. Higgins JP, Thompson SG, Deeks JJ, Altman DG. Measuring inconsistency in meta-analyses. BMJ. 2003;327:557–60. https://doi.org/10.1136/bmj.327.7414.557
23. Dernoncourt A, Lacroix M, Duhaut P, Salle V, Schmidt J, Batteux B, et al. Prognostic factors of *Pasteurella* infections: a single-center retrospective cohort study over a 14-year period (2005-2018). Int J Infect Dis. 2022;116:197–203. https://doi.org/10.1016/j.ijid.2022.01.028
24. Körmöndi S, Terhes G, Pál Z, Varga E, Harmati M, Buzás K, et al. Human pasteurellosis health risk for elderly persons living with companion animals. Emerg Infect Dis. 2019;25:229–35. https://doi.org/10.3201/eid2502.180641
25. Athanasia C, Maraki S, Gitti Z, Yiannis T. Review of *Pasteurella multocida* infections over a twelve-year period in a tertiary care hospital. Am J Infect Dis. 2005;02:107–10.
26. Holst E, Rollof J, Larsson L, Nielsen JP. Characterization and distribution of *Pasteurella* species recovered from infected humans. J Clin Microbiol. 1992;30:2984–7. https://doi.org/10.1128/jcm.30.11.2984-2987.1992
27. Alberta Ministry of Agriculture and Rural Development. Consumer corner: Canadian pet market outlook. 2014 [cited 2023 Nov 27]. http://www1.agric.gov.ab.ca/$department/deptdocs.nsf/all/sis14914/$file/sarah_pet_june20_2014.pdf
28. Weiss HB, Friedman DI, Coben JH. Incidence of dog bite injuries treated in emergency departments. JAMA. 1998;279:51–3. https://doi.org/10.1001/jama.279.1.51
29. Sarmicanic LL. Human and pet interaction: companion animals and the formation of identity. Las Vegas (NV): University of Nevada; 2007.
30. Chatelier E, Mahieu R, Hamel JF, Chenouard R, Lozac'h P, Sallé A, et al. *Pasteurella* bacteraemia: Impact of comorbidities on outcome, based on a case series and literature review. Int J Infect Dis. 2020;92:89–96. https://doi.org/10.1016/j.ijid.2020.01.003
31. Glickman M, Klein RS. Acute epiglottitis due to *Pasteurella multocida* in an adult without animal exposure. Emerg Infect Dis. 1997;3:408–9. https://doi.org/10.3201/eid0303.970328
32. Raffi F, Barrier J, Baron D, Drugeon HB, Nicolas F, Courtieu AL. *Pasteurella multocida* bacteremia: report of thirteen cases over twelve years and review of the literature. Scand J Infect Dis. 1987;19:385–93. https://doi.org/10.3109/00365548709021670
33. Wilson BA, Ho M. *Pasteurella multocida:* from zoonosis to cellular microbiology. Clin Microbiol Rev. 2013;26:631–55. https://doi.org/10.1128/CMR.00024-13

Address for correspondence: Wonkeun Song, Hallym University Kangnam Sacred Heart Hospital, Hallym University College of Medicine, 1, Shingil-ro, Youngdeungpo-gu, Seoul 07441, South Korea; email: swonkeun@hallym.or.kr

Campylobacteriosis Outbreak Linked to Municipal Water, Nebraska, USA, 2021[1]

Lauren Jansen, Rachael Birn,[2] Samir Koirala, Sadie Oppegard,[3] Brianna Loeck, Jeff Hamik, Elizabeth Wyckoff,[4] Dana Spindola, Sue Dempsey, Amanda Bartling, Alexis Roundtree, Amy Kahler, Charlotte Lane, Nancy Hogan, Nancy Strockbine, Haley McKeel, Jonathan Yoder, Mia Mattioli, Matthew Donahue,[5] Bryan Buss

In September 2021, eight campylobacteriosis cases were identified in a town in Nebraska, USA. We assessed potential exposures for a case–control analysis. We conducted whole-genome sequencing on *Campylobacter* isolates from patients' stool specimens. We collected large-volume dead-end ultrafiltration water samples for *Campylobacter* and microbial source tracking testing at the Centers for Disease Control and Prevention. We identified 64 cases in 2 waves of illnesses. Untreated municipal tap water consumption was strongly associated with illness (wave 1 odds ratio 15.36; wave 2 odds ratio 16.11). Whole-genome sequencing of 12 isolates identified 2 distinct *Campylobacter jejuni* subtypes (1 subtype/wave). The town began water chlorination, after which water testing detected coliforms. One dead-end ultrafiltration sample yielded nonculturable *Campylobacter* and avian-specific fecal rRNA genomic material. Our investigation implicated contaminated, untreated, municipal water as the source. Results of microbial source tracking supported mitigation with continued water chlorination. No further campylobacteriosis cases attributable to water were reported.

Campylobacter is a gram-negative, microaerophilic, flagellated, helical bacterium (*1*). *Campylobacter* infection, or campylobacteriosis, is the most common bacterial cause of diarrhea in the United States, producing ≈1.5 million illnesses each year (*2*). Serious sequelae of infection can occur, including prolonged bowel symptoms (5%–20% of reported cases), reactive arthritis (1%–5% of reported cases), and Guillain-Barré syndrome (0.001% of reported cases) (*2*). Common causes of *Campylobacter* infection include consuming contaminated foods (especially poultry, meat, and dairy) or contaminated water or having contact with animals (*3*). Campylobacteriosis outbreaks associated with water have been linked to contamination of groundwater sources after heavy rainfall and problematic water system cross-connections (*4*,*5*).

In Nebraska, USA, incidence of campylobacteriosis increased from 599 cases/year in 2016 to 811 cases/year in 2019 (*6*,*7*). This observed increase coincided with an increased use of culture-independent

Author affiliations: Nebraska Department of Health and Human Services, Lincoln, Nebraska, USA (L. Jansen, R. Birn, S. Koirala, S. Oppegard, B. Loeck, J. Hamik, E. Wyckoff, M. Donahue, B. Buss); Centers for Disease Control and Prevention, Atlanta, Georgia, USA (L. Jansen, E. Wyckoff, A. Kahler, C. Lane, N. Hogan, N. Strockbine, H. McKeel, J. Yoder, M. Mattioli, B. Buss); Council of State and Territorial Epidemiologists, Atlanta (R. Birn); University of Nebraska–Lincoln, Lincoln (S. Koirala, B. Loeck, J. Hamik); East Central District Health Department, Columbus, Nebraska, USA (D. Spindola); University of Nebraska Medical Center, Omaha, Nebraska, USA (S. Dempsey, A. Bartling); Chenega Enterprise System and Solutions, Chesapeake, Virginia, USA (A. Roundtree); US Public Health Service, Lincoln (B. Buss)

DOI: https://doi.org/10.3201/eid3010.231509

[1]Results from this investigation were presented at the following conferences: InFORM Conference; April 26–29, 2022 (virtual event); Epidemic Intelligence Service Conference; May 2–5, 2022, Atlanta, Georgia, USA; and Council of State and Territorial Epidemiologists Conference; June 19–23, 2022, Louisville, Kentucky, USA.

[2]Current affiliation: University of Nebraska Medical Center, Omaha, Nebraska, USA.

[3]Current affiliation: Lincoln–Lancaster County Health Department, Lincoln, Nebraska, USA.

[4]Current affiliation: University of Washington, Seattle, Washington, USA.

[5]Current affiliation: Iowa Department of Health and Human Services, Des Moines, Iowa, USA

diagnostic methods. As of 2015, Nebraska had the second-highest incidence of campylobacteriosis in the United States, at 26.6 cases/100,000 population, second only to South Dakota (*8*). Given competing priorities for public health, particularly during the COVID-19 pandemic, investigation of campylobacteriosis cases is sometimes limited to application of case definitions and assignment of case status, consistent with the National Notifiable Disease Surveillance System designation (*9*). Most cases are classified as sporadic infections. Selected cases are further investigated by local or state public health authorities, particularly if spatial or temporal clustering is observed.

Nondisinfected drinking water systems are common in the United States; >20 million US residents were served by nondisinfected water in 2006 (*10*). Nebraska is 1 of 6 states where ground water is used for >75% of public water supplies (*11*). In most Nebraska communities, ground water supplies are not treated with a disinfectant before being supplied to the public (*12*). Under the US Environmental Protection Agency (EPA) Ground Water Rule, ground water sourced systems can be untreated if certain monitoring procedures, which depend on the population size, are followed (*13*,*14*).

Contamination of drinking water systems can occur by many routes. One study reported contamination by animal feces and wastewater to be the most common source of contamination in ground water systems (*15*). Microbial source tracking (MST) is a molecular tool used to identify sources of fecal pollution in water. This technique is specialized and is not part of routine ground water monitoring procedures. MST uses quantitative PCR to detect molecular evidence of microbes unique to the guts of humans or specific animal species (*16*,*17*). MST assays have been developed to identify multiple species in the United States, including humans, cattle, and birds (*18*–*20*). Moreover, recently EPA and the National Institute for Standards validated standard material for MST biological markers, enabling use of these MST methods in outbreak response (*21*).

In September 2021, the East Central District Health Department and Nebraska Department of Health and Human Services were notified by electronic laboratory reporting of 8 campylobacteriosis cases clustering in 1 week's time in a small town in east central Nebraska that had a population of ≈330 persons. During 2011–2020, median annual campylobacteriosis case count in the affected town was 1 (range 0–8). The Nebraska Department of Health and Human Services collaborated with the East Central District Health Department to investigate, find the exposure and contamination sources, and prevent additional illness. In this report, we describe this outbreak of campylobacteriosis that was linked to municipal drinking water and animal contamination and identified by using MST.

Methods

Epidemiologic Investigation Methods

In response to the cluster of 8 campylobacteriosis cases, we sought to find additional cases. We used the case definitions from the 2015 National Notifiable Disease Surveillance System case definition for campylobacteriosis, in which a probable case is defined as "a case that meets the probable laboratory criteria for diagnosis or a clinically compatible case that is epidemiologically linked to a probable or confirmed case of campylobacteriosis" and a confirmed case is defined as "a case that meets the confirmed laboratory criteria for diagnosis" (*22*). We created a broad hypothesis-generating questionnaire in REDCap (a web-based interface for secure data collection; https://www.project-redcap.org) to address consumption of meats and other food items; consumption of different water sources, including methods of in-home water treatment (e.g., filtration, reverse osmosis); attendance at 2 known large community gatherings (i.e., a town bazaar and a wedding); and recent animal contact. We sought to reach as many town residents, workers, and visitors as possible with this questionnaire, including those sickened during the outbreak and those who remained healthy. To solicit participation among community members, the questionnaire link was distributed using Facebook (Meta Platforms, https://www.meta.com) posts by willing town residents and the local health jurisdiction's Facebook page. We deployed the questionnaire on September 16, 2021. On the basis of preliminary results of this initial questionnaire, which included multiple, free-text responses noting consumption of home-grown produce, we developed a second supplemental questionnaire through REDCap. By using respondent emails collected in the initial questionnaire, we deployed the website for this second questionnaire on September 28, 2021, to address produce consumption, with a particular focus on locally grown items and home gardens. If respondents to the first questionnaire did not respond to the second questionnaire but had previously provided a telephone number, we made attempts to complete the second questionnaire with the resident by telephone. Finally, both questionnaires were administered during door-to-door canvassing in the affected community, with 6 investigators working in pairs to conduct

in-person interviews with residents. We obtained verbal consent from each adult or legal guardian before administering interview questionnaires. We did not document refusal to participate.

This activity was reviewed by CDC and was conducted consistent with applicable federal law and CDC policy (e.g., 45 C.F.R. part 46, 21 C.F.R. part 56; 42 U.S.C. §241(d); 5 U.S.C. §552a; 44 U.S.C. §3501 et seq.). This activity was determined to be public health surveillance and therefore did not require CDC Human Research Protection Office review. We completed data collection through both questionnaires on October 21, 2021. We also obtained data from Nebraska's Electronic Disease Surveillance System (NEDSS), particularly in cases when a person could not be reached for an interview. Given the potential for nonresidents to have been exposed in the affected town, we also used NEDSS to search for other campylobacteriosis cases occurring within bordering counties during the outbreak, from mid-August 2021 to October 2021, to identify additional cases potentially associated with the outbreak.

Where possible, we combined results of the 2 questionnaires (or NEDSS data if questionnaire data were unavailable) to create 1 entry per person sick with campylobacteriosis. We used questionnaire results for a case-control analysis. We defined probable or suspect cases as self-reported diarrheal illness (≥3 stools/24 h for probable cases; 1–2 stools/24 h for suspect cases) among town residents, or among workers or visitors with exposure in the town, with onset during August 30–October 8, 2021; confirmed cases had *Campylobacter* spp. detected in stool (e.g., by antigen testing, PCR, or culture). Controls were persons who denied any diarrheal illness. We did not conduct any matching. If *Campylobacter* culture isolates were obtained from a specimen, whole-genome sequencing (WGS) was performed by the Nebraska Public Health Laboratory using the MagNA Pure Compact Nucleic Acid Isolation Kit version 19 (Roche, https://lifescience.roche.com) (*23*–*27*). We submitted sequences to GenBank.

We extracted data from REDCap by using Excel (Microsoft, https://www.microsoft.com) and performed descriptive analysis and calculated odds ratios (ORs) by using CDC's EpiInfo 7.2.4.0 (https://www.cdc.gov/epiinfo). We conducted analyses of questionnaire results and conducted separate subanalyses for each wave of illness. We calculated 95% CIs by using OpenEpi version 3.01 (https://www.openepi.com). We applied the modified Haldane–Anscombe correction in a case of a zero cell. We classified users of water-filtering pitchers or refrigerator water filters as being exposed to untreated water and those using reverse osmosis as being unexposed to untreated water.

Environmental Investigation Methods

Epidemiologic investigation findings guided the environmental investigation that followed outbreak detection. The town's ground water wells were routinely tested monthly for coliform. In Nebraska, water operators must be licensed and complete continuing education, and all public water testing results are documented in the Safe Drinking Water Information System database and are available to the public (*28*). A 100-mL sample was collected by the town water operator at a predetermined site in accordance with the water system's approved sample site plan. Testing was conducted by the state laboratory. When coliforms were detected, repeat samples were collected from the original site and locations upstream and downstream of the original site. Trigger samples (i.e., samples collected in response to coliform detection) were also collected from groundwater sources after a routine coliform detection. Routine maintenance chlorination of the system, typically done in spring and fall each year, was begun on October 1, 2021.

While the outbreak investigation was ongoing, the Nebraska Department of Environment and Energy (NDEE) began a comprehensive evaluation of the municipal water system. NDEE conducted an external inspection of the town's water tower by using an NDEE drone on October 18, 2021. NDEE drinking water field representatives performed a walkthrough backflow inspection in the town on October 20, 2021. When routine maintenance chlorination was stopped, postchlorination water testing was carried out on October 26 and October 29, 2021; positive results prompted NDEE to issue a boil water advisory on October 30, 2021, and to request specialized *Campylobacter* water testing from CDC.

On November 4, 2021, a total of 6 large-volume (>100-L), dead-end ultrafiltration (DEUF) water samples were collected by NDEE by using methods described previously (*29*). Sampled locations included the 2 active town wells and 4 additional sites from the distribution system in the town that we selected on the basis of previous coliform bacteria detections. We conducted sampling in areas within the distribution system with recently positive total coliform testing or in areas of concern, including areas with potential cross-connections, suspected backflow, dead ends, or high water age (i.e., the time water spends within the distribution system before use) (Appendix Table 1,

https://wwwnc.cdc.gov/EID/article/30/10/23-1509-App1.pdf). After sample collection, water chlorination resumed. We submitted all DEUF samples to CDC for *Campylobacter*-specific DNA testing and culture. In addition, CDC performed MST by using previously described PCR methods to identify bacteria molecular markers unique to human, ruminant, and bird feces (known environmental fecal shedders of *Campylobacter*) (*18*–*20*).

Results

Epidemiologic Investigation Results

A total of 138 questionnaires were completed. Of those, 129 were completed by persons connected to the affected community (121 town residents [37% of the town's population] and 8 with exposure in the community but not residing there). Of the 129 questionnaires, 26% (34/129) were completed during door-to-door canvassing efforts and the remainder by Facebook recruitment, email, or telephone (percentage completed by each method was not captured). According to US Census American Community Survey data, the median age of town residents was 36.8 years, and 55% identified as female in 2021 (*30*). By comparison, the median age of the 129 community-linked questionnaire respondents was 56 years, and 63% were female.

We identified 64 total campylobacteriosis cases (21 confirmed, 38 probable, and 5 suspect). Ill persons had a median age of 56 years (range 2–90 years); 33 (52%) were female and 31 (48%) male. Seven (11%) persons reported hospitalization (median length of stay 1 night [range 1–3 nights]), and no deaths occurred. Ill persons experienced diarrhea (64/64, as described in the case definition), abdominal cramping (48/64), nausea (34/64), fever (33/64), and vomiting (12/64).

We identified 2 distinct waves of illness; the first occurred during August 30–September 15 and the second during September 29–October 8 (Figure). Peak reported illness onset was during or shortly after the 2021 Labor Day holiday weekend (September 4–6, 2021). For wave 1, all but 1 (48/49 [98%]) of ill persons reported municipal water exposure, compared with 76% (25/33) of controls (OR 15.36 [95% CI 1.82–129.82]). For wave 2, all 14 (100%) ill persons reported municipal water exposure, compared with 65% (22/34) of controls (OR undefined). To account for no unexposed ill persons, we applied a modified Haldane–Anscombe correction, which yielded an OR of 16.11 (95% CI 0.88–293.6). Among all other exposures analyzed, including 50 separate food items, contact with animals or manure, and attendance at a community gathering, we found no other statistically significant associations with illness (Appendix Tables 2, 3).

Among 21 cases confirmed by laboratory testing, 8 were by antigen testing only, 1 by PCR, and 12 by stool culture. We speciated and identified all 12 clinical isolates as *C. jejuni*. WGS of 12 *Campylobacter* isolates from 12 patients' stool specimens identified 2 distinct *C. jejuni* subtypes, with 1 subtype/wave. In wave 1, a total of 7 isolates from 7 persons in 6 separate households were a 100% match (0 single-nucleotide polymorphisms [SNPs] difference). In wave 2, a total of 5 isolates from persons in 5 separate households matched each other (0–1 SNPs difference). The 2 distinct subtypes differed by 1,178 SNPs. Of the 12 with WGS, we uploaded 10 to GenBank (accession nos. PDT001144782.1, PDT001144787.1, PDT001144788.1, PDT001161287.1, PDT001161298.1, PDT001161283.1, PDT001161285.1, PDT001166739.1, PDT001166745.1, and PDT001175404.1).

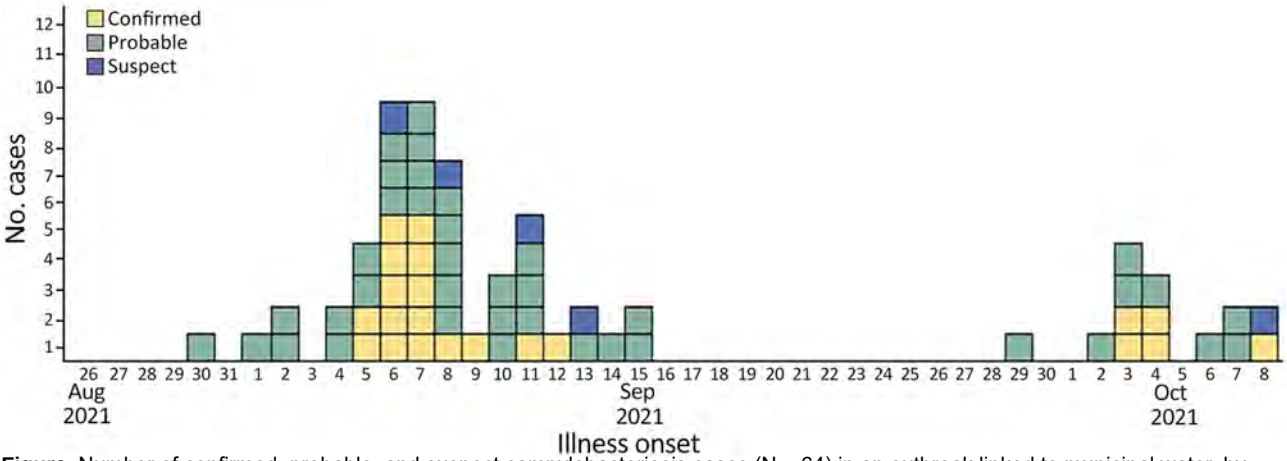

Figure. Number of confirmed, probable, and suspect campylobacteriosis cases (N = 64) in an outbreak linked to municipal water, by illness onset date, Nebraska, USA, August–October 2021.

Environmental Investigation Results

Municipal water in the town is supplied by 2 wells, each 170 feet deep. As permitted by the EPA Ground Water Rule, ground water from those wells was not treated before storage and distribution (*13*). In the 3 years preceding the outbreak, routine monthly coliform testing was positive on 5 occasions (range 1–3 instances/year). Regulatory coliform testing was negative on August 17, 2021, just before the outbreak, and on September 14, while wave 1 of the outbreak was occurring. Routine maintenance chlorination of the system, a common public water system practice typically conducted twice yearly in spring and fall, was begun by the town water operator on October 1. While the municipal water system was evaluated, chlorination of the system was continued. When chlorination was stopped on October 22, postchlorination testing detected coliform in the distribution system and in 1 source water well. Coliform detection and associated outbreak epidemiologic findings resulted in concern about possible *Campylobacter* contamination of the water supply. The town has 2 active wells located on either end of a recreation field area, a centrally located water tower, and a distribution system with 2 loops, 1 serving the bulk of the town and 1 serving newer buildings in the western part of the town. All 6 DEUF samples from the distribution system were culture-negative for *Campylobacter*. Of those, 1 sample was positive by PCR for presence of *Campylobacter* DNA. We did not detect human and bovine molecular fecal markers, but we did detect avian-specific fecal rRNA genomic material in 1 sample that also had low levels of culturable coliforms (0.72 most probable number/100 mL). This finding, together with the detected *Campylobacter* DNA, suggested the water contamination likely came from bird feces.

The most likely place for bird feces intrusion on the water system was the single, aged water tower (dating to the 1910s) pressurizing the municipal water system. Inspection of the tower by drone flyover during NDEE's initial inspection revealed no deficits. However, given increased concern after testing results, the affected town's leadership requested visual internal water tower inspection, which was completed on December 9 by a firm specializing in water tower maintenance. The internal tower inspection revealed damage to the tower's cap. Gaps present between the tower's cap and sidewall were large enough to permit direct intrusion by birds or allow bird feces from the tower's exterior to wash inside. The town's water was chlorinated until the tower was repaired January 28, 2022. No additional cases of campylobacteriosis were identified after chlorination of the water system was initiated while awaiting tower repair, and no campylobacteriosis clusters among community members were identified since tower repair was completed (at which time chlorination was stopped) through 1 year after tower repair completion (January 2023). In the affected community in the year after tower repair, only 1 person tested positive for *Campylobacter* by PCR. No isolate was obtained for typing because sequencing is not routinely completed in Nebraska for sporadic *Campylobacter* detections.

Discussion

We report a large campylobacteriosis outbreak in Nebraska in which ≈19% of the town's population reported as ill (64/≈330). In comparison, the next largest outbreak, in 2017, had 39 ill persons identified, which represented ≈6.5% of the city's population (*31*). Identifying the outbreak cause required the combination of epidemiologic, engineering, and environmental laboratory methods. MST is an emerging surface-water quality-monitoring technique that has recently been used to support outbreak response (*32*). This investigation demonstrates the value of this combination of methods, which was essential to identify the probable source and specific site of fecal intrusion in the water system, enabling corrective action to be taken. By implicating bird contamination (probably on 2 separate occasions as suggested by WGS), our findings provided clear motivation to conduct a timely internal water tower inspection, which is technically difficult and costly.

Nebraska has a plentiful ground water supply from the High Plains Aquifer, which underlies ≈90% of the state (*12*). In total, 88% of all Nebraska residents drink ground water, and although the larger municipal water systems in the state disinfect, ≈85% of Nebraska's 550 public ground water systems, predominantly in smaller communities, are not disinfected, (*12*,*33*). Although many states have abundant ground water from aquifers, contamination of water in the aquifer itself was never in question. Rather, aging water system infrastructure, as is often found in small or rural communities, can increase risk for enteric disease outbreaks, independent of the water's actual source. Distribution system aging or disruption of the system during repairs can enable microbial intrusion into untreated drinking water systems (*34*).

Water towers are a common method of water storage and pressurization in Nebraska (*35*). Rural areas, especially, are more likely to have aging water towers, sometimes more than a century old. Similar large outbreaks of enteric disease have been linked to water towers, such as a 1993 outbreak in Missouri that

involved ≥650 cases of salmonellosis, linked to a water tower with an uncovered hatch, enabling possible entry by birds (*36*). The compromised water tower that led to this campylobacteriosis outbreak was inspected and maintained (per Title 179 NAC 21-008 and 22-008, which states that water systems must "inspect, and clean if necessary, water storage facilities equipped for accessibility, no less often than once every 5 years") (*37*), but routine maintenance either did not identify the cap damage or the changes occurred between instances of maintenance. Our findings might indicate a need for managers of aged systems to increase scrutiny on system components and help ensure the safety of the water delivered to their residents. This need is nationwide, as demonstrated by a 2021 US infrastructure bill that has committed to "invest in water infrastructure" and particularly emphasizes this need in rural areas served by untreated ground water drinking systems (*38*).

One limitation of our study is that water testing was not undertaken until after the water system was chlorinated, 5–10 weeks after the 2 most likely periods of exposure. The inability to culture *Campylobacter* from the water samples might have been the result of previous chlorine treatment of the system or might simply reflect the common difficulty of growing *Campylobacter* in the laboratory. Had water testing been completed sooner, culturable organisms might have been found, which would have enabled genomic comparison of environmental contamination and clinical infections. In addition, selection bias probably occurred because of our use of convenience sampling. Median age of town residents was 36 years, but our questionnaire respondents' median age was 56 years, so our respondents skewed older. Questionnaire distribution through Facebook could have created bias toward users of that social network and persons motivated to complete the questionnaires because they had been sick. However, door-to-door canvassing efforts probably helped mitigate this potential bias, given that sick and healthy persons might have been encountered equally when canvassing the town as a whole. Furthermore, given such a high proportion of town residents who used municipal water, we would not expect our results to be substantially affected based on selection. Moreover, recall bias might have occurred because questionnaire forms relied on detailed recollection of exposures potentially as long as 6 weeks after the likely exposure period. However, because the outbreak source was not a food item, respondents' knowledge of their water source and recollection of water consumption presumably would be more reliable.

The marriage of shoe-leather epidemiology and advanced and emerging environmental microbiologic methods, with cooperation between community, local, state, and federal partners, helped establish the etiology of this large campylobacteriosis outbreak. After exposure at highly attended community gatherings was ruled out, municipal water was suspected as the cause, and then temporary disinfection and strategic investigation of the water distribution system further established the probable source of contamination. This investigation also highlights the usefulness of MST to support mitigation strategies directed at the source of fecal contamination of water systems and, in turn, to prevent future exposures. Untreated ground water systems with aging infrastructure are vulnerable to fecal intrusion, increasing the risk for large outbreaks of enteric disease. Public health authorities can encourage communities and managers of aged water systems to increase scrutiny of system components to help ensure drinking water safety.

Acknowledgments

We thank Tammy Dawdy, Halie Smith, the residents and municipal leaders of the affected community, the East Central District Health Department, and the Nebraska Department of Health and Human Services.

This work was supported by a grant through CDC's Epidemiology and Laboratory Capacity Program.

About the Author

Dr. Jansen served as a CDC Epidemic Intelligence Service Officer assigned to Nebraska Department of Health and Human Services in Lincoln and now serves as an assistant professor in the Department of Family Medicine and Community Health at the University of Massachusetts Chan Medical School in Worcester, Massachusetts. Her primary research interests include infectious disease epidemiology and emerging infectious disease.

References

1. Perez-Perez GI, Blaser MJ. *Campylobacter* and *Helicobacter*. In: Baron S, editor. Medical microbiology. 4th ed. Galveston (TX): University of Texas Medical Branch at Galveston; 1996 [cited 2022 Nov 7]. http://www.ncbi.nlm.nih.gov/books/NBK8417
2. Centers for Disease Control and Prevention. Questions and answers: *Campylobacter*. 2019 [cited 2022 Nov 7]. https://www.cdc.gov/campylobacter/faq.html
3. Centers for Disease Control and Prevention. *Campylobacter* (Campylobacteriosis). 2021 [cited 2022 Nov 7]. https://www.cdc.gov/campylobacter/index.html
4. Kuhn KG, Falkenhorst G, Emborg HD, Ceper T, Torpdahl M, Krogfelt KA, et al. Epidemiological and serological investigation of a waterborne *Campylobacter jejuni* outbreak in a Danish town. Epidemiol Infect. 2017;145:701–9. https://doi.org/10.1017/S0950268816002788

5. O'Reilly CE, Bowen AB, Perez NE, Sarisky JP, Shepherd CA, Miller MD, et al.; Outbreak Working Group. A waterborne outbreak of gastroenteritis with multiple etiologies among resort island visitors and residents: Ohio, 2004. Clin Infect Dis. 2007;44:506–12. https://doi.org/10.1086/511043
6. Centers for Disease Control and Prevention. Table 2d. Reported cases of notifiable diseases, by region and reporting area—United States and U.S. territories, 2016 [cited 2022 Nov 7]. https://wonder.cdc.gov/nndss/static/2016/annual/2016-table2d.html
7. Centers for Disease Control and Prevention. Table 2d. Annual reported cases of notifiable diseases, by region and reporting area, United States and U.S. territories, excluding non-U.S. residents, 2019 [cited 2022 Nov 7]. https://wonder.cdc.gov/nndss/static/2019/annual/2019-table2d.html
8. Adams DA, Thomas KR, Jajosky RA, Foster L, Baroi G, Sharp P, et al.; Nationally Notifiable Infectious Conditions Group. Summary of notifiable infectious diseases and conditions—United States, 2015. MMWR Morb Mortal Wkly Rep. 2017;64:1–143. https://doi.org/10.15585/mmwr.mm6453a1
9. Centers for Disease Control and Prevention. National notifiable diseases surveillance system [cited 2022 Dec 12]. https://www.cdc.gov/nndss/index.html
10. US Environmental Protection Agency. Economic analysis for the final ground water rule. EPA-815-R-06-014. 2019 Aug 19 [cited 2023 May 18]. https://www.regulations.gov/document/EPA-HQ-OW-2018-0780-0214
11. Dieter CA, Maupin MA, Caldwell RR, Harris MA, Ivahnenko TI, Lovelace JK, et al. Estimated use of water in the United States in 2015. Report no. 1441. Reston (VA): US Geological Survey; 2018 [cited 2022 Nov 7]. http://pubs.er.usgs.gov/publication/cir1441
12. Nebraska Department of Environment and Energy. 2020 Nebraska groundwater quality monitoring report. 2020 Dec 1 [cited 2022 Nov 2]. http://dee.ne.gov/Publica.nsf/PubsForm.xsp?documentId=C3C47F71DBDA83338625863100728C51&action=openDocument
13. US Government Printing Office. Federal Register, volume 71, issue 216. 2006 Nov 8 [cited 2022 Nov 7]. https://www.govinfo.gov/content/pkg/FR-2006-11-08/html/06-8763.htm
14. US Environmental Protection Agency. Ground water rule triggered and representative monitoring: a quick reference guide. 2008 [cited 2022 Nov 7]. https://nepis.epa.gov/Exe/ZyPDF.cgi?Dockey=P1001KJG.txt
15. Moreira NA, Bondelind M. Safe drinking water and waterborne outbreaks. J Water Health. 2017;15:83–96. https://doi.org/10.2166/wh.2016.103
16. Jamison MN, Hart JJ, Szlag DC. Improving the identification of fecal contamination in recreational water through the standardization and normalization of microbial source tracking. ACS ES T Water. 2022;2:2305–11. https://doi.org/10.1021/acsestwater.2c00185
17. Boehm AB, Van De Werfhorst LC, Griffith JF, Holden PA, Jay JA, Shanks OC, et al. Performance of forty-one microbial source tracking methods: a twenty-seven lab evaluation study. Water Res. 2013;47:6812–28. https://doi.org/10.1016/j.watres.2012.12.046
18. Green HC, Haugland RA, Varma M, Millen HT, Borchardt MA, Field KG, et al. Improved HF183 quantitative real-time PCR assay for characterization of human fecal pollution in ambient surface water samples. Appl Environ Microbiol. 2014;80:3086–94.
19. Mieszkin S, Yala J-F, Joubrel R, Gourmelon M. Phylogenetic analysis of Bacteroidales 16S rRNA gene sequences from human and animal effluents and assessment of ruminant faecal pollution by real-time PCR. J Appl Microbiol. 2010;108:974–84. https://doi.org/10.1111/j.1365-2672.2009.04499.x
20. Weller D, Belias A, Green H, Roof S, Wiedmann M. Landscape, water quality, and weather factors associated with an increased likelihood of foodborne pathogen contamination of New York streams used to source water for produce production. Front Sustain Food Syst. 2020;3:124. https://doi.org/10.3389/fsufs.2019.00124
21. Sivaganesan M, Willis JR, Karim M, Babatola A, Catoe D, Boehm AB, et al. Interlaboratory performance and quantitative PCR data acceptance metrics for NIST SRM® 2917. Water Res. 2022;225:119162. https://doi.org/10.1016/j.watres.2022.119162
22. Centers for Disease Control and Prevention. Campylobacteriosis (*Campylobacter* spp.) 2015 case definition. 2022 [cited 2024 Jul 11]. https://ndc.services.cdc.gov/case-definitions/campylobacteriosis-2015
23. Association of Public Health Laboratories. PulseNet standard operating procedure for DNA library preparation using the Illumina DNA Prep Kit. Document no. PNL35. Version no. 3. 2021 Apr 13.
24. Illumina. Illumina DNA Prep reference guide. 2021 August [cited 2021 Nov 15]. https://support.illumina.com/sequencing/sequencing_kits/illumina-dna-prep/documentation.html
25. Association of Public Health Laboratories. PulseNet standard operating procedure for the Reference Identification Database Workflow. Document no. PND20. Version no. 1. 2020 Dec 9 [cited 2021 Nov 15]. https://www.aphl.org/programs/food_safety/Documents/PND20_RefID_database_workflow.pdf
26. Association of Public Health Laboratories. PulseNet standard operating procedure for the organism-specific surveillance database workflow. Document no. PND05. Version no. 1. 2020 Jun 15 [2021 Nov 15]. https://www.aphl.org/programs/.../PND05_Surveillance_database_workflow.pdf
27. Association of Public Health Laboratories. PulseNet standard operating procedure for local cluster detection and matching against the national database. Document no. PND06. Version no. 1. 2020 Jun 23 [cited 2021 Nov 15]. https://www.aphl.org/programs/food_safety/Documents/PND06_Cluster_detection.pdf
28. US Environmental Protection Agency. Safe Drinking Water Information System (SDWIS) federal reports search [cited 2024 Jul 8]. https://sdwis.epa.gov/ords/sfdw_pub/r/sfdw/sdwis_fed_reports_public/200
29. Smith CM, Hill VR. Dead-end hollow-fiber ultrafiltration for recovery of diverse microbes from water. Appl Environ Microbiol. 2009;75:5284–9. https://doi.org/10.1128/AEM.00456-09
30. US Census Bureau. American Community Survey (ACS) demographic and housing estimates [cited 2023 Jun 29]. https://data.census.gov/table/ACSDP5Y2022.DP05?g=160XX00US3138995
31. Pedati C, Koirala S, Safranek T, Buss BF, Carlson AV. Campylobacteriosis outbreak associated with contaminated municipal water supply—Nebraska, 2017. MMWR Morb Mortal Wkly Rep. 2019;68:169–73. https://doi.org/10.15585/mmwr.mm6807a1
32. Mattioli MC, Benedict KM, Murphy J, Kahler A, Kline KE, Longenberger A, et al. Identifying septic pollution exposure routes during a waterborne norovirus outbreak—a new application for human-associated microbial source tracking qPCR. J Microbiol Methods. 2021;180:106091. https://doi.org/10.1016/j.mimet.2020.106091

33. Skipton S, Dvorak B, Woldt W. An introduction to drinking water. University of Nebraska–Lincoln. 2011 Jan [cited 2023 Jan 25]. https://extensionpublications.unl.edu/assets/html/g1539/build/g1539.htm
34. Nygård K, Wahl E, Krogh T, Tveit OA, Bøhleng E, Tverdal A, et al. Breaks and maintenance work in the water distribution systems and gastrointestinal illness: a cohort study. Int J Epidemiol. 2007;36:873–80. https://doi.org/10.1093/ije/dym029
35. University of Nebraska–Lincoln. Water towers. In: Encyclopedia of the Great Plains. Wishart DJ, editor. 2011 [cited 2022 Nov 3]. http://plainshumanities.unl.edu/encyclopedia/doc/egp.wat.037
36. Angulo FJ, Tippen S, Sharp DJ, Payne BJ, Collier C, Hill JE, et al. A community waterborne outbreak of salmonellosis and the effectiveness of a boil water order. Am J Public Health. 1997;87:580–4. https://doi.org/10.2105/AJPH.87.4.580
37. Nebraska Department of Health and Human Services. Title 179 public water systems [cited 2022 Nov 4]. https://dhhs.ne.gov/Pages/Title-179.aspx
38. The White House. Fact sheet: the bipartisan infrastructure deal. 2021 Nov 6 [cited 2024 Jul 8]. https://www.whitehouse.gov/briefing-room/statements-releases/2021/11/06/fact-sheet-the-bipartisan-infrastructure-deal

Address for correspondence: Bryan Buss, Nebraska Department of Health and Human Services, 301 Centennial Mall S, Fl 6, Epidemiology, Lincoln, NE 68509, USA; email: feu7@cdc.gov

Age- and Sex-Specific Differences in Lyme Disease Health-Related Behaviors, Ontario, Canada, 2015–2022

Janica A. Adams, Victoria Osasah, Katherine Paphitis, Affan Danish, Richard G. Mather, Curtis A. Russell, Jennifer Pritchard, Mark P. Nelder

Medscape CME Activity

In support of improving patient care, this activity has been planned and implemented by Medscape, LLC and Emerging Infectious Diseases. Medscape, LLC is jointly accredited with commendation by the Accreditation Council for Continuing Medical Education (ACCME), the Accreditation Council for Pharmacy Education (ACPE), and the American Nurses Credentialing Center (ANCC), to provide continuing education for the healthcare team.

Medscape, LLC designates this Journal-based CME activity for a maximum of 1.00 ***AMA PRA Category 1 Credit(s)™***. Physicians should claim only the credit commensurate with the extent of their participation in the activity.

Successful completion of this CME activity, which includes participation in the evaluation component, enables the participant to earn up to 1.0 MOC points in the American Board of Internal Medicine's (ABIM) Maintenance of Certification (MOC) program. Participants will earn MOC points equivalent to the amount of CME credits claimed for the activity. It is the CME activity provider's responsibility to submit participant completion information to ACCME for the purpose of granting ABIM MOC credit.

All other clinicians completing this activity will be issued a certificate of participation. To participate in this journal CME activity: (1) review the learning objectives and author disclosures; (2) study the education content; (3) take the post-test with a 75% minimum passing score and complete the evaluation at https://www.medscape.org/qna/processor/72617?showStandAlone=true&src=prt_jcme_eid_mscpedu; and (4) view/print certificate. For CME questions, see page 2225.

NOTE: It is Medscape's policy to avoid the use of Brand names in accredited activities. However, in an effort to be as clear as possible, trade names are used in this activity to distinguish between the mixtures and different tests. It is not meant to promote any particular product.

Release date: September 23, 2024; Expiration date: September 23, 2025

Learning Objectives

Upon completion of this activity, participants will be able to:

- Assess trends in the epidemiology of Lyme disease in Canada
- Distinguish which age groups were at highest risk for Lyme disease based on age
- Analyze trends in Lyme disease incidence based on gender
- Evaluate risk factors for Lyme disease among patients

CME Editor

Tony Pearson-Clarke, MS, Technical Writer/Editor, Emerging Infectious Diseases. *Disclosure: Tony Pearson-Clarke, MS, has no relevant financial relationships.*

CME Author

Charles P. Vega, MD, Health Sciences Clinical Professor of Family Medicine, University of California, Irvine School of Medicine, Irvine, California. *Disclosure: Charles P. Vega, MD, has the following relevant financial relationships: served as consultant or advisor for Boehringer Ingelheim; GlaxoSmithKline.*

Authors

Janica A. Adams, MSc; Victoria Osasah, MPH; Katherine Paphitis, PhD, MSc; Affan Danish, BS; Richard G. Mather, MD, MSc; Curtis A. Russell, PhD; Jennifer Pritchard, MPH; Mark P. Nelder, PhD.

Author affiliations: Public Health Ontario, Toronto, Ontario, Canada (J.A. Adams, V. Osasah, K. Paphitis, A. Danish, R.G. Mather, C.A. Russell, J. Pritchard, M.P. Nelder); Johns Hopkins Bloomberg School of Public Health, Baltimore, Maryland, USA (V. Osasah); Queen's University, Kingston, Ontario, Canada (R.G. Mather)

DOI: https://doi.org/10.3201/eid3010.240191

We investigated differences in risk factors and preventive behaviors by age and sex among persons with reported Lyme disease in Ontario, Canada, during 2015–2022. Incidence rates peaked among children 5–9 and adults 50–79 years of age. Median age was higher for female than male case-patients (54 vs. 51 years). Male case-patients reported more activity in wooded and tall grass areas than did female case-patients; fewer male case-patients reported sharing living space with outdoor-exposed companion animals. As age increased, more case-patients reported activity in blacklegged tick habitats, exposure to ticks, and wearing adequate clothing, but fewer reported sharing living space with outdoor-exposed companion animals. Adoption of preventive behaviors was relatively low and did not differ by sex. Male case-patients, children 5–9 years of age and their parents or caregivers, and adults >59 years of age represent populations that would benefit from tailored public health messaging on Lyme disease prevention.

Lyme disease is the most reported vectorborne disease affecting humans in Canada, and incidence continues to increase (*1*). In eastern North America, the blacklegged tick (*Ixodes scapularis*) is the primary vector of *Borrelia burgdorferi* sensu stricto, the causative agent of Lyme disease. About half of all cases of Lyme disease in Canada are reported from Ontario, a province in which blacklegged tick range has rapidly expanded northward by ≈50 km/year (*2*–*5*). *I. scapularis* ticks were first detected in Ontario along the northern shore of Lake Erie in the early 1970s (*6*). From the 1970s through the 2000s, blacklegged tick populations remained relatively isolated along the northern shores of the St. Lawrence River, Lake Ontario, and Lake Erie; however, in the 2010s, populations expanded or were established anew throughout the province (*7*). Climate and land-use changes will continue influencing the expansion of blacklegged tick range, increasing the risk for Lyme disease (*8*–*10*).

Blacklegged ticks transmit pathogens in addition to *B. burgdorferi* to humans, including *Anaplasma phagocytophilum*, *B. mayonii*, *B. miyamotoi*, *Babesia microti*, Powassan virus (lineage 2, or deer tick virus), and *Ehrlichia muris eauclairensis* (*11*). In 2023, postexposure prophylaxis was made available to residents of Ontario as part of a new Lyme disease prevention option, enabling pharmacists to treat patients after assessing their symptoms and tick exposure history (*12*). Optimizing public health guidance for preventing Lyme disease requires approaches focused on minimizing exposure to blacklegged ticks.

Our goal was to examine sex- and age-specific differences in exposures to Lyme disease risk factors and preventive behaviors adopted, which might increase or decrease risk of exposure to blacklegged ticks and local transmission of Lyme disease in Ontario compared with neighboring jurisdictions (e.g., the province of Quebec, as well as the continental United States, including New Jersey and New York) (*13*–*17*). Because climate and land-use changes affect the expansion of ranges among ticks, awareness of population subgroups experiencing increased rates of illness can help inform evidence-based public health messaging. We performed a retrospective cross-sectional study, using provincially reportable Lyme disease data to examine age- and sex-specific differences in self-reported risk factors and preventive behaviors associated with Lyme disease in Ontario during 2015–2022.

This project did not require research ethics committee approval because the activities were considered public health surveillance. Those activities were conducted in fulfillment of a Public Health Ontario legislative mandate "to provide scientific and technical advice and support to the health care system and the Government of Ontario in order to protect and promote the health of Ontarians." (Ontario Agency for Health Protection and Promotion Act, SO 2007, c 10, Schedule K).

Methods

Surveillance

In Ontario, 34 local public health units (PHUs) are responsible for the surveillance, investigation, and management of Lyme disease cases and also take part in active (dragging) and passive (identification of publicly submitted ticks) tick surveillance (*18*,*19*). PHUs classify confirmed and probable cases of Lyme disease on the basis of current provincial case definitions (Appendix Table, https://wwwnc.cdc.gov/EID/article/30/10/24-0191-App1.pdf). By telephone interview, investigators from the PHU area within which the case-patient lived at time of illness collected information using the provincial Lyme disease investigation tool, a standardized questionnaire for Lyme disease (*20*). Case information collected included likely location of tick bite (e.g., cottage, house, park), risk factors (e.g., exposure to ticks, activities in wooded areas), and preventive behaviors (e.g., checking self for ticks, wearing appropriate clothing, using tick repellents) associated with decreased risk for Lyme disease infection. Case-patients who reported health behaviors that potentially increased risk for developing Lyme disease during the telephone interview were asked about the most likely location of tick exposure (*7*) and might have voluntarily provided additional information on exposures, risk factors, and preventive behaviors.

Table 1. Demographics of Lyme disease case-patients in Ontario, Canada, 2015–2022*

Demographics	Value	Average annual incidence rate†
Age, y, n = 7,758‡		
Median (IQR)	53 (32–64)	NA
Range	<1–95	NA
Age group, y, n = 7,762		
<5	180 (2.3)	3.1
5–9	440 (5.7)	7.2
10–19	557 (7.2)	4.3
20–29	567 (7.3)	3.5
30–39	733 (9.5)	4.6
40–49	975 (12.6)	6.5
50–59	1,497 (19.3)	9.2
60–69	1,636 (21.1)	11.8
70–79	954 (12.3)	10.8
≥80	219 (2.8)	4.2
Unknown	4 (<0.5)	NA
Sex/gender, n = 7,762§		
M	4,371 (56.3)	7.6
F	3,364 (43.3)	5.7
Transgender/other/unknown	27 (<0.5)	NA

*Values are no. (%) patients except as indicated. IQR, interquartile range; NA, not available
†Rates per 100,000 persons were calculated for each age group using age-stratified annual population estimates in Ontario and for each sex using sex-stratified annual population estimates in Ontario.
‡Data for age were unavailable for 4 case-patients. Analysis was restricted to case-patients with complete data for age.
§Analysis was restricted to case-patients who self-identified as male or female because of low counts (n<5) observed in other reported categories.

Additional information collected from all case-patients included age, sex/gender (male, female, transgender, other, or unknown), and month and year of episode. Case-patient demographic and exposure data were reported to provincial public health authorities through the integrated Public Health Information System, an online surveillance platform.

Statistical Analyses

We conducted a descriptive analysis of Lyme disease risk factors and preventive behaviors to explore sex- and age-specific differences among case-patients. We recorded month and year of episode using, in order of preference, time of onset, specimen collection, laboratory testing, or case reported. We used patient's age at date of episode. We categorized case-patients ≥10 years of age into 10-year age groups (e.g., 10–19, 20–29). However, we determined 5-year age groups for patients <10 years of age because some previous literature suggested a relatively higher incidence of Lyme disease among children 5–9 years of age than children of other ages (*14*). To calculate average incidence rates per 100,000 persons, we used Government of Canada annual population estimates for Ontario (*21*).

For analyses involving sex as a variable, we included only case-patients who self-identified as male or female because of low counts (n<5) for other sex/gender categories. We compared demographic characteristics of male and female case-patients across age groups. For analyses involving geographic location, we included only cases with reported exposures within Ontario; we excluded from subsequent analyses all case data from persons reporting travel outside of Ontario during the exposure period. We used the Mann-Whitney U test to assess differences in medians, the Pearson χ^2 test to compare risk factors reported by male and female case-patients, and the Cochran-Mantel-Haenszel test to assess associations between age group and sex and between age group and self-reported risk factors. We performed all analyses, data cleaning and classification of exposures, risk factors, and preventive behaviors in Microsoft Excel (Microsoft, https://www.microsoft.com) and SAS Enterprise Guide 8.2 (SAS Institute Inc., https://www.sas.com). We considered differences among variables to be statistically significant at $p<0.05$.

Results

Epidemiology

During 2015–2022, there were 7,762 cases of Lyme disease reported in Ontario; 7,213 (92.9%) cases were confirmed and 549 (7.1%) probable (Table 1; Figure 1). Incidence increased 3-fold during the study period. Annually, the highest proportion of cases occurred during the summer, from June through August (Appendix Figure 1).

Twenty-seven case-patients entered sex as other than male or female (27/7,762, 0.3%), 3 as transgender or other and 24 as unknown; because of low numbers, we excluded those 27 case-patients from analyses involving sex. In addition, we excluded 4 case-patients with no data for age from analyses involving age. The median age of case-patients was 53.0 years; the most common age groups were 60–69 years (1,636/7,758 [21.1%]) and 50–59 years (1,497/7,758 [19.3%]) (Table 1). By sex, 56.3% of case-patients were male and 43.3% female; <5% were categorized as transgender, other, or unknown (Table 1). Annual Lyme disease incidence rates were higher among male than female case-patients (Table 2; Figure 2). Median age was lower for male than female case-patients (51.0 years vs. 54.0 years; $\chi^2 = 16.08$; $p<0.001$). Average annual incidence rates per 100,000 persons peaked among children 5–9 years of age (7.2%) and adults in age groups 50–59 (9.2%), 60–69 (11.8%), and 70–79 (10.8%) years of age (Appendix Figure 2). Although the number of cases generally increased each year, overall annual rates did not differ significantly by sex or age group ($p>0.05$).

Exposures, Risk Factors, and Preventive Behaviors

A total of 4,108 case-patients voluntarily reported ≥1 specific exposure activities (results not shown); interviewers using the Ontario Lyme disease questionnaire did not routinely ask case-patients about specific exposures. Among common exposure activities, 1,891/4,108 (46.0%) case-patients providing responses reported visiting a secondary residence, such as a cottage; 1,264 (30.8%) reported exposure to a tick habitat in the primary residence or when visiting a friend or relative's home, and 474 (11.5%) reported visiting a park. Less commonly reported activities included camping (170/4,108 [4.1%]), visiting a hiking or cycling trail (150 [3.7%]), and visiting a conservation area (127 [3.1%]).

Interviewers using the Ontario Lyme disease questionnaire asked all case-patient respondents about risk factors and preventive behaviors. Of case-patients providing (yes/no) responses, 81% (6,289/7,762) reported ≥1 risk factor or preventive behavior; ≈89% (4,430/4,937) of case-patients provided responses to ≥1 question about exposure to an at-risk area for Lyme disease, tick habitat, or reported activities in blacklegged tick habitats (wooded or tall grass areas); 4,020 (86.0%) recalled an exposure to ticks or having a tick bite; and 1,486 (41.9%) reported sharing a bed or indoor living space with a companion animal that had access to the outdoors (Table 3).

Male case-patients had higher odds than female of reporting activities in blacklegged tick habitats (crude odds ratio [OR] 1.77, 95% CI 1.47–2.13; p<0.001) and lower odds of sharing living space with an outdoor companion animal (OR 0.82, 95% CI 0.72–0.94; p = 0.004). There was also a significant association between age and reported activities, and in general, as age increased, respondents reported more activities in blacklegged tick habitats (n = 4,948, degrees of freedom [df] = 1, χ^2 = 15.69; p<0.001) and finding a tick on themselves (n = 4,680, df = 1, χ^2 = 14.22; p<0.001) (Table 4). As age increased, fewer case-patients reported sharing living space with an outdoor companion animal (n = 3,555, df = 1, χ^2 = 8.71; p = 0.003).

Relatively few case-patients who self-identified as male or female reported specific preventive behaviors while outdoors in wooded or tall grass areas (Table 3). Among respondents to specific preventive behavior questions, 1,265/3,915 (32.3%) of case-patients reported checking themselves for ticks, 1,046/3,750 (27.9%) reported wearing adequate clothing, and 958/3,763 (25.5%) reported using insect repellents in regions known to be habitats for ticks. Practicing preventive behaviors did not differ by sex (p>0.05). As age increased, more case-patients reported wearing adequate protective clothing while in tick habitats (n = 3,757, df = 1, χ^2 = 27.9; p<0.001) (Table 4).

Discussion

Lyme disease continues to spread in Ontario; incidence rates increased 3-fold during the 2015–2022 study period. Incidence rates increased in a biennial pattern, similar to nationwide trends in Canada

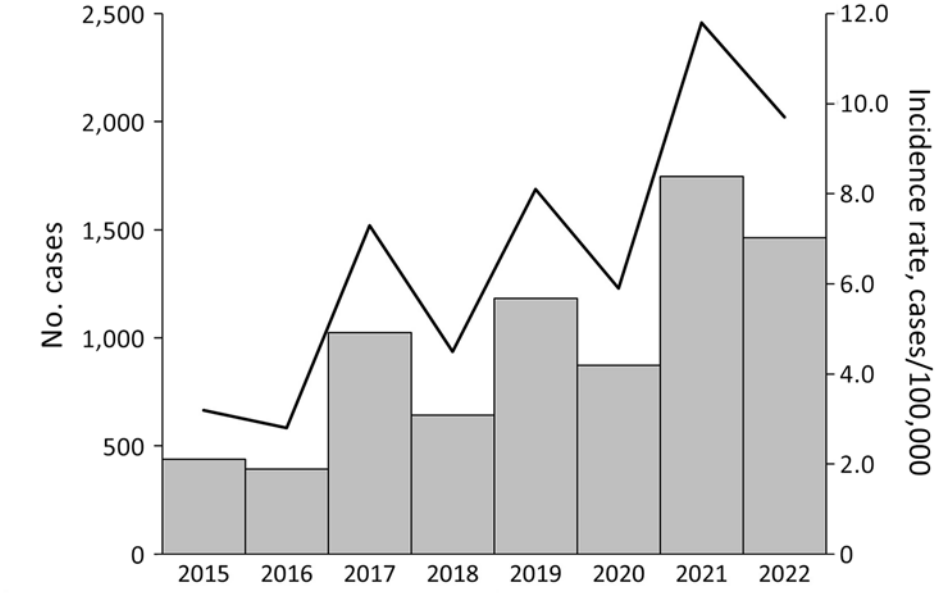

	2015	2016	2017	2018	2019	2020	2021	2022
No. cases	438	392	1,025	642	1,182	873	1,747	1,463
Rate	3.2	2.8	7.3	4.5	8.1	5.9	11.8	9.7

Figure 1. Annual case counts and incidence rates for Lyme disease in Ontario, Canada, 2015–2022. Denominators used in rate calculations based on annual provincial population estimates.

Table 2. Demographics of Lyme disease case-patients, by sex, Ontario, Canada, 2015–2022*

Demographics	Total, n = 7,731	Female, n = 3,362	Male, n = 4,369	Test of association	p value
Age, y					
Median (IQR)	53.0 (32.0–64.0)	54.0 (35.0–65.0)	51.0 (31.0–64.0)	16.08†	<0.001
Range	<1–95	<1–94	<1–95		
Age group, y					
<5	180 (2.3)	81 (45.0)	99 (55.0)	16.89‡	<0.001
5–9	438 (5.7)	191 (43.6)	247 (56.4)		
10–19	556 (7.2)	212 (38.1)	344 (61.9)		
20–29	565 (7.3)	212 (37.5)	353 (62.5)		
30–39	730 (9.4)	300 (41.1)	430 (58.9)		
40–49	972 (12.6)	382 (39.3)	590 (60.7)		
50–59	1,488 (19.2)	683 (45.9)	805 (54.1)		
60–69	1,633 (21.1)	791 (48.4)	842 (51.6)		
70–79	950 (12.3)	409 (43.1)	541 (57.0)		
≥80	219 (2.8)	101 (46.1)	118 (53.9)		

*Values are no. (%) patients except as indicated. IQR, interquartile range.
†Mann-Whitney U test; p<0.05 represents a statistically significant difference in the median age of female and male case-patients.
‡Cochran-Mantel-Haenszel test; p<0.05 represents a statistically significant relationship between increasing age groups and sex.

during 2016–2022 and the United States during 2004–2021 (*1*,*5*,*22*). The biennial trend likely reflects changes in the abundance of *B. burgdorferi*–infected nymph-stage blacklegged ticks; that stage is responsible for most summertime infections from ticks. Abundance of ticks is governed by ecologic variables such as temperature, precipitation, host abundance, tick distribution, and human exposure levels (*23*,*24*). Male case-patients, children <10 years of age, and adults >59 years of age were the groups with the highest Lyme disease illness rates in Ontario; however, exposures indicative of risk or protective behaviors depended on demographics. This information presents an opportunity to develop educational resources targeted to persons less likely to wear appropriate clothing or repellents while in tick habitats. Our research constitutes an initial step toward identifying behavioral, ecologic, and biomedical factors contributing to sex- and age-specific risks of Lyme disease.

Male case-patients, children 5–9 years of age, and adults 50–79 years of age experienced higher Lyme disease incidence than female case-patients and other age groups, similar to trends reported elsewhere (*4*,*13*,*25*–*27*). In the United States in 2021, of persons taking part in outdoor recreational activities (e.g., hiking, camping, fishing), 54% (95.5 million/176.7 million) were male, potentially disproportionately exposing males to blacklegged ticks (*28*). Data from Ontario during 2005–2014 indicated 50% of case-patients were male, compared with 56% in our study, with a relatively higher incidence among those 5–9 and 50–74 years of age (*25*). Similarly, in Canada during 2009–2019, a total of 57% of case-patients were male, and the highest incidence was among those 5–14 and 50–84 years of age (*5*). In

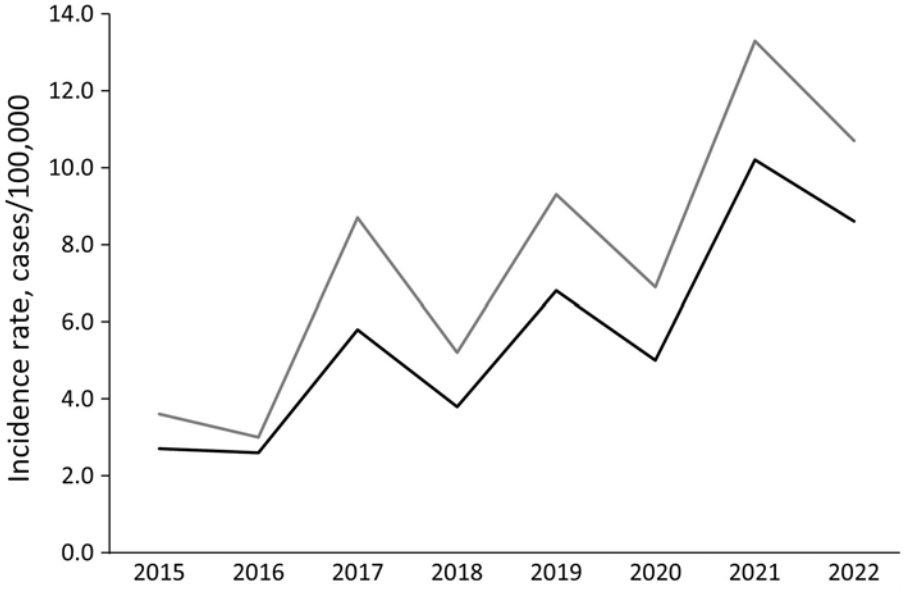

Figure 2. Annual incidence rates of Lyme disease case-patients, by sex, Ontario, Canada, 2015–2022. Denominators used in rate calculations include annual population estimates stratified by sex.

Table 3. Specific risk factors and preventive behaviors reported by Lyme disease case-patients, by sex, Ontario, Canada, 2015–2022*

Exposure activities	No. (%) cases			Crude OR (95% CI)†	p value‡
	Total	Female	Male		
Risk factors					
Participated in activities in wooded or tall grass areas§					
N	507	282 (55.6)	225 (44.4)	1.77 (1.47–2.13)	<0.001
Y	4,430	1,835 (41.4)	2,595 (58.6)		
Recalled finding tick or tick bite on self					
N	652	301 (46.2)	351 (53.8)	1.18 (1.00–1.39)	0.05
Y	4,020	1,691 (42.1)	2,329 (57.9)		
Contacted outdoor dog or cat that shared bed or living space					
N	2,062	864 (41.9)	1,198 (58.1)	0.82 (0.72–0.94)	0.004
Y	1,486	696 (46.8)	790 (53.2)		
Preventive behaviors					
Checked for ticks after being outdoors in wooded or tall grass areas					
N	2,650	1,107 (41.8)	1,543 (58.2)	0.88 (0.77–1.01)	0.07
Y	1,265	567 (44.8)	698 (55.2)		
Used insect repellant when outdoors in wooded or tall grass areas					
N	2,805	1,187 (42.3)	1,618 (57.7)	0.89 (0.77–1.03)	0.12
Y	958	433 (45.2)	525 (54.8)		
Used adequate clothing protection in wooded or tall grass areas¶					
N	2,704	1,128 (41.7)	1,576 (58.3)	0.87 (0.76–1.01)	0.07
Y	1,046	471 (45.0)	575 (55.0)		

*Case-patients were queried on risk factors and preventive behaviors in the 30 d before illness onset. A low percentage of case-patients provided responses to queries on risk factors (46%–64%) and preventive behaviors (48%–50%). OR, odds ratio.
†Reference group used in OR calculations is female case-patients.
‡χ^2 test; p<0.05 represents a statistically significant relationship between risk factor/preventive behavior and sex.
§For activities in wooded or tall grass areas, case-patients were asked about specific activities such as hiking, camping, or hunting.
¶Adequate clothing included long sleeves, long pants, and covered shoes.

the United States during 2012–2016, the proportion of cases peaked among those 5–9 and 45–70 years of age; the proportion of male case-patients with Lyme disease and the median case-patient age increased over the broader study period, 1992–2016 (*14*). Lyme disease incidence trends likely reflect sex- and age-specific behavioral differences; however, case trends follow in part from susceptibility of individual persons to clinical disease and subsequent likelihood of case detection and the population structure in areas of highest incidence (*14*). Furthermore, the higher incidence among young children might reflect increased healthcare-seeking behavior by parents and children who spend more time outdoors in potential tick habitats. Trends in found ticks submitted by healthcare providers and the public (i.e., passive tick surveillance) parallel the epidemiologic picture of Lyme disease (*29*–*31*). Those epidemiologic trends indicating possible associations between increased healthcare-seeking behaviors and tick submissions provide rationale for developing targeted public health messaging for specific groups, such as young children (including parents and caregivers), older adults, and persons who take part in outdoor activities. Additional research to assess the most effective public health messaging for preventing Lyme disease in these groups is warranted.

The evidence is inconsistent for increased risk for *B. burgdorferi* infection among owners of companion animals, despite companion animal owners having an increased risk for tick exposure (*32*,*33*). Because our analyses did not adjust for potential confounding or effect modification by other variables, factors related to ownership of companion animals with access to the outdoors or living in rural areas might have interacted with one another to influence reported Lyme disease incidence. For example, companion animals and their owners in rural areas might be more likely to share exposures to more blacklegged tick habitats than those in urban or suburban areas (*34*–*36*). Male case-patients and children <10 years of age engaged more often in outdoor activities with the potential for exposure to blacklegged ticks. The increased risk of Lyme disease for males is evident not only for other vectorborne diseases (e.g., West Nile virus infection) but is also associated with poor health-seeking behaviors, childhood obesity, and poor nutrition (*37*–*40*). Previous behavioral surveys and seroprevalence surveys in North America have found that female and older participants were more often knowledgeable than male participants and younger children about Lyme disease, risk factors for infection, and adopting preventive behaviors (e.g., use of repellents, wearing protective clothing) (*17*,*41*,*42*). Similar to our finding that female case-patients were more likely to report practicing preventive behaviors than male case-patients, in a study from the Estrie region of Québec, female participants were more aware of Lyme disease and more concerned about infection than male participants; Lyme disease awareness was also higher

among persons >35 years compared with those <25 years of age (*17*). Female participants used tick repellents and performed tick checks more often than male participants, although male participants showered after outdoor activities more often than female participants (*17*). In contrast to the literature, aside from some older case-patients reporting wearing adequate clothing in tick habitats, we identified no additional sex- or age-related differences in use of preventive measures. Although provincial questionnaires aimed to standardize case interviewing, not all case-patients were asked about all risks and preventive behaviors (i.e., questions about some variables were reported as not asked), potentially concealing differences associated with age and sex. Readers should interpret our results with caution, as a low percentage of case-patients provided responses to queries on risk factors (46%–64%) and preventive behaviors (48%–50%); the lack of responses was likely because of lack of prompting by the interviewer, rather than declining to answer. Investigators might benefit from training and reminders to ensure consistency and completeness in case interviewing.

The most common voluntarily reported locations for exposure among case-patients in Ontario occurred in the peridomestic environment, either at a secondary (46%) or primary residence (31%); however, only 53% of case-patients reported information on exposure location. Because peridomestic and areawide tick and rodent control are yet to show efficacy in reducing Lyme disease incidence, alternative and complementary methods should be explored (*43*,*44*). Focused public health messaging for those at higher risk of developing Lyme disease is vital, but the incidence of peridomestic Lyme disease warrants focused public health guidance on preventing tick exposures through activities around the home (e.g., gardening).

Among limitations to our study, aside from those already discussed, true incidence of Lyme disease is subject to underreporting, which can be caused by multiple factors, such as low disease awareness, poor

Table 4. Risk factors and preventive behaviors reported by Lyme disease case-patients, by age group, Ontario, Canada, 2015–2022*

Exposure activities	No. (%) case-patients by age group, y											χ^2†	p value
	Total	<5	5–9	10–19	20–29	30–39	40–49	50–59	60–69	70–79	≥80		
Risk factors													
Participated in activities in wooded or tall grass areas‡													
N	507 (10.2)	18 (15.1)	20 (6.5)	25 (6.7)	41 (10.9)	44 (8.8)	63 (9.8)	111 (11.4)	99 (9.8)	70 (13.3)	16 (14.6)	15.69	<0.001
Y	4,441 (89.8)	101 (84.9)	290 (93.6	346 (93.3)	336 (89.1)	458 (91.2)	581 (90.2)	863 (88.6)	915 (90.2)	457 (86.7)	94 (85.5)		
Recalled finding tick or tick bite on self													
N	653 (14.0)	18 (18.2)	47 (17.3)	60 (19.5)	47 (15.1)	53 (12.5)	106 (18.0)	127 (13.6)	118 (11.5)	63 (10.8)	14 (10.9)	14.22	<0.001
Y	4,027 (86.0)	81 (81.8)	224 (82.7)	248 (80.5)	265 (84.9)	371 (87.5)	483 (82.0)	806 (86.4)	912 (88.5)	522 (89.2)	115 (89.2)		
Contacted outdoor dog or cat that shared bed or living space													
N	2,066 (58.1)	53 (56.4)	121 (53.8)	154 (56.4)	168 (63.9)	173 (49.4)	273 (57.6)	376 (54.6)	442 (60.2)	243 (66.2)	63 (73.3)	8.71	0.003
Y	1,489 (41.9)	41 (43.6)	104 (46.2)	119 (43.6)	95 (36.1)	177 (50.6)	201 (42.4)	313 (45.4)	292 (39.8)	124 (33.8)	23 (26.7)		
Preventive behaviors													
Checked for ticks after being outdoors in wooded or tall grass areas													
N	2,657 (67.7)	62 (63.9)	170 (68.0)	209 (70.1)	211 (69.9)	266 (67.7)	354 (67.6)	506 (66.8)	528 (65.8)	278 (68.8)	73 (77.7)	0.46	0.50
Y	1,266 (32.3)	35 (36.1)	80 (32.0)	89 (29.9)	91 (30.1)	127 (32.3)	170 (32.4)	252 (33.3)	275 (34.3)	126 (31.2)	21 (22.3)		
Used insect repellant when outdoors in wooded or tall grass areas													
N	2,812 (74.6)	67 (72.8)	169 (70.1)	227 (79.7)	216 (74.2)	287 (75.5)	382 (76.1)	538 (74.0)	557 (72.0)	296 (76.1)	73 (81.1)	0.05	0.82
Y	959 (25.4)	25 (27.2)	72 (29.9)	58 (20.4)	75 (25.8)	93 (24.5)	120 (23.9)	189 (26.0)	217 (28.0)	93 (23.9)	17 (18.9)		
Used adequate clothing protection in wooded or tall grass areas§													
N	2,710 (78.4)	68 (72.3)	189 (77.5)	239 (82.7)	203 (69.8)	281 (76.0)	377 (75.6)	530 (73.3)	508 (65.9)	258 (66.5)	57 (64.8)	27.87	<0.001
Y	1,047 (30.3)	26 (27.7)	55 (22.5)	50 (17.3)	88 (30.2)	89 (24.1)	122 (24.5)	193 (26.7)	263 (34.1)	130 (33.5)	31 (35.2)		

*Case-patients were queried on risk factors and preventive behaviors in the 30 d before illness onset. A low percentage of case-patients provided responses to queries on risk factors (46%–64%) and preventive behaviors (48%–50%).
†Cochran-Mantel-Haenszel test; p<0.05 represents a statistically significant relationship between risk factor/preventive behavior and increasing age group.
‡For activities in wooded or tall grass areas, case-patients were asked about specific activities such as hiking, camping, or hunting.
§Adequate clothing included long sleeves, long pants, and covered shoes.

healthcare-seeking behaviors, preferential ascertainment of severe disease, limitations of serology during early infection, and reporting practices (*45*,*46*). Underreporting of Lyme disease in Ontario likely occurred during the study; however, we do not expect any difference in demographics and exposures of patients between reported and unreported cases. Second, the Ontario provincial electronic reportable disease system does not provide closed-ended questions on Lyme disease exposure locations (i.e., secondary residence), and completeness and entry of case exposure information relied on the data entry practices of PHUs and individual investigators. Consequently, some cases might not have a reported exposure location, and others might have multiple reported exposure locations. In future enhancements to the system, developers should consider adding specific questions regarding exposure locations. Third, there was potential for misclassification of exposure in our study because not all reported exposures contributed to *B. burgdorferi* transmission and additional contributing exposures might not have been reported; the exact location of tick acquisition was not identifiable and had to be inferred. Fourth, there is potential for recall bias among study case-patients, because those who found ticks on themselves might have spent more time thinking about whether they engaged in higher risk activities or took preventive measures. Fifth, case-patients were not asked specifically about use of other preventive measures (e.g., putting clothes in the dryer after being in tick habitats, limiting tick habitats around the home, use of tick prevention on pets); therefore, data are likely incomplete on the use of other preventive measures.

Despite limitations, the data we collected provided an opportunity to identify factors responsible for differences in observed sex- and age-specific exposures. Standardized epidemiologic studies (e.g., case-control) will improve the ability to identify the factors underlying the demographic patterns seen in Lyme disease surveillance. A proposal in Quebec aims to prioritize prevention efforts using a One Health approach that includes integrating behavioral (preventive) methods and ecologic (tick surveillance) risks into risk mapping (*47*). Protection motivation theory states that a person's use of protective measures increases along with the perceived seriousness of tick bites and Lyme disease (*48*). Protection motivation theory has the potential to predict the demographic and environmental factors that would increase the likelihood of the public using preventive measures; interventions to address those factors include messaging targeted to at-risk subpopulations that currently do not perceive tick bites and Lyme disease as serious threats to their health. A 2022 systematic review (*49*) found the effectiveness of various personal protection measures inconsistent and no single method effectively prevented Lyme disease. The success of prevention depends on effective public health actions that include passive and active surveillance, health messaging on personal preventive measures, and increasing Lyme disease awareness (e.g., risks posed by tick bites, seriousness of disease, risk mapping, epidemiology).

Using disease data in Ontario reported during 2015–2022, we found higher incidence of Lyme disease among male case-patients, children <10 years of age, and adults >59 years of age. In general, male case-patients were more likely than female to report finding a tick on themselves, and older age groups reported wearing adequate protective clothing while in blacklegged tick habitats more often than younger age groups. Until populationwide prevention methods (e.g., vaccines, areawide tick and rodent control) effective at reducing Lyme disease incidence become available, education and guidance should focus on behavioral change and personal protection targeted to specific subpopulations at high risk for disease.

Acknowledgments

We thank the public health units of Ontario for their commitment to surveillance and management of diseases of public health significance.

About the Author

Ms. Adams is an epidemiologist at Public Health Ontario, Toronto, Ontario, Canada. Her primary research interests are population health and the epidemiology of infectious diseases.

References

1. Public Health Agency of Canada. Lyme disease surveillance in Canada: annual edition 2022. Ottawa (ON): Public Health Agency of Canada; 2024.
2. Clow KM, Leighton PA, Ogden NH, Lindsay LR, Michel P, Pearl DL, et al. Northward range expansion of *Ixodes scapularis* evident over a short timescale in Ontario, Canada. PLoS One. 2017;12:e0189393. https://doi.org/10.1371/journal.pone.0189393
3. Tardy O, Acheson ES, Bouchard C, Chamberland É, Fortin A, Ogden NH, et al. Mechanistic movement models to predict geographic range expansions of ticks and tick-borne pathogens: case studies with *Ixodes scapularis* and *Amblyomma americanum* in eastern North America. Ticks Tick Borne Dis. 2023;14:102161. https://doi.org/10.1016/j.ttbdis.2023.102161
4. Nelder MP, Wijayasri S, Russell CB, Johnson KO, Marchand-Austin A, Cronin K, et al. The continued rise of Lyme disease in Ontario, Canada: 2017. Can Commun Dis Rep. 2018;44:231–6. https://doi.org/10.14745/ccdr.v44i10a01

5. Gasmi S, Koffi JK, Nelder MP, Russell C, Graham-Derham S, Lachance L, et al. Surveillance for Lyme disease in Canada, 2009–2019. Can Commun Dis Rep. 2022;48:219–27. https://doi.org/10.14745/ccdr.v48i05a05
6. Watson TG, Anderson RC. *Ixodes scapularis* Say on white-tailed deer (*Odocoileus virginianus*) from Long Point, Ontario. J Wildl Dis. 1976;12:66–71. https://doi.org/10.7589/0090-3558-12.1.66
7. Ontario Agency for Health Protection and Promotion. Ontario Lyme disease estimated risk areas map, 2019. Toronto (ON): Queen's Printer for Ontario; 2019.
8. McPherson M, García-García A, Cuesta-Valero FJ, Beltrami H, Hansen-Ketchum P, MacDougall D, et al. Expansion of the Lyme disease vector *Ixodes scapularis* in Canada inferred from CMIP5 climate projections. Environ Health Perspect. 2017;125:057008. https://doi.org/10.1289/EHP57
9. Ogden NH, Mechai S, Margos G. Changing geographic ranges of ticks and tick-borne pathogens: drivers, mechanisms and consequences for pathogen diversity. Front Cell Infect Microbiol. 2013;3:46. https://doi.org/10.3389/fcimb.2013.00046
10. Diuk-Wasser MA, VanAcker MC, Fernandez MP. Impact of land use changes and habitat fragmentation on the eco-epidemiology of tick-borne diseases. J Med Entomol. 2021;58:1546–64. https://doi.org/10.1093/jme/tjaa209
11. Nelder MP, Russell CB, Sheehan NJ, Sander B, Moore S, Li Y, et al. Human pathogens associated with the black-legged tick *Ixodes scapularis*: a systematic review. Parasit Vectors. 2016;9:265. https://doi.org/10.1186/s13071-016-1529-y
12. Ontario Ministry of Health. Management of tick bites and investigation of early localized Lyme disease. Toronto (ON): King's Printer for Ontario; 2023.
13. Schwartz AM, Kugeler KJ, Nelson CA, Marx GE, Hinckley AF. Use of commercial claims data for evaluating trends in Lyme disease diagnoses, United States, 2010–2018. Emerg Infect Dis. 2021;27:499–507. https://doi.org/10.3201/eid2702.202728
14. Kugeler KJ, Mead PS, Schwartz AM, Hinckley AF. Changing trends in age and sex distributions of Lyme disease—United States, 1992–2016. Public Health Rep. 2022;137:655–9. https://doi.org/10.1177/00333549211026777
15. Chow CC, Evans AS Jr, Noonan-Toly CM, White D, Johnson GS, Marks SJ, et al. Lyme disease trends—Dutchess County, New York, 1992–2000. Mt Sinai J Med. 2003;70:207–13.
16. New Jersey Department of Health. New Jersey State health assessment data: complete health indicator report of Lyme disease [cited 2024 May 15]. https://www-doh.nj.gov/doh-shad/indicator/view/LymeDisease.html
17. Aenishaenslin C, Charland K, Bowser N, Perez-Trejo E, Baron G, Milord F, et al. Behavioral risk factors associated with reported tick exposure in a Lyme disease high incidence region in Canada. BMC Public Health. 2022;22:807. https://doi.org/10.1186/s12889-022-13222-9
18. Nelder MP, Russell CB, Dibernardo A, Clow KM, Johnson S, Cronin K, et al. Monitoring the patterns of submission and presence of tick-borne pathogens in *Ixodes scapularis* collected from humans and companion animals in Ontario, Canada (2011–2017). Parasit Vectors. 2021;14:260. https://doi.org/10.1186/s13071-021-04750-1
19. Ontario Agency for Health Protection and Promotion. Blacklegged tick surveillance in Ontario: a systematic review. Toronto (ON): Queen's Printer for Ontario; 2016.
20. Ontario Agency for Health Protection and Promotion. Lyme disease investigation tool. Toronto (ON): King's Printer for Ontario; 2023.
21. Statistics Canada. Population estimates 2001–2022. Table 1. Annual population estimates by age and sex for July 1, 2001–2022, health regions, Ontario. Ottawa (ON): Government of Canada; 2023.
22. Centers for Disease Control and Prevention. Lyme disease: surveillance data [cited 2023 Nov 11]. https://www.cdc.gov/lyme/datasurveillance/surveillance-data.html
23. Schauber EM, Ostfeld RS, Evans J Jr, Andrew S. What is the best predictor of annual Lyme disease incidence: weather, mice, or acorns? Ecol Appl. 2005;15:575–86. https://doi.org/10.1890/03-5370
24. Stafford KC III, Cartter ML, Magnarelli LA, Ertel SH, Mshar PA. Temporal correlations between tick abundance and prevalence of ticks infected with *Borrelia burgdorferi* and increasing incidence of Lyme disease. J Clin Microbiol. 1998;36:1240–4. https://doi.org/10.1128/JCM.36.5.1240-1244.1998
25. Johnson KO, Nelder MP, Russell C, Li Y, Badiani T, Sander B, et al. Clinical manifestations of reported Lyme disease cases in Ontario, Canada: 2005–2014. PLoS One. 2018;13:e0198509. https://doi.org/10.1371/journal.pone.0198509
26. Hassenstein MJ, Janzen I, Krause G, Harries M, Melhorn V, Kerrinnes T, et al. Seroepidemiology of *Borrelia burgdorferi* s.l. among German National Cohort (NAKO) participants, Hanover. Microorganisms. 2022;10:2286. https://doi.org/10.3390/microorganisms10112286
27. Vrbova L, Middleton D. Descriptive epidemiology of Lyme disease in Ontario: 1999–2004. Can Commun Dis Rep. 2006;32:247–57.
28. Outdoor Foundation. 2022 outdoor participation trends report. Boulder (CO): Outdoor Foundation; 2022.
29. Nelder MP, Russell C, Lindsay LR, Dhar B, Patel SN, Johnson S, et al. Population-based passive tick surveillance and detection of expanding foci of blacklegged ticks *Ixodes scapularis* and the Lyme disease agent *Borrelia burgdorferi* in Ontario, Canada. PLoS One. 2014;9:e105358. https://doi.org/10.1371/journal.pone.0105358
30. Gasmi S, Ogden NH, Leighton PA, Lindsay LR, Thivierge K. Analysis of the human population bitten by *Ixodes scapularis* ticks in Quebec, Canada: increasing risk of Lyme disease. Ticks Tick Borne Dis. 2016;7:1075–81. https://doi.org/10.1016/j.ttbdis.2016.09.006
31. Marx GE, Spillane M, Beck A, Stein Z, Powell AK, Hinckley AF. Emergency department visits for tick bites—United States, January 2017–December 2019. MMWR Morb Mortal Wkly Rep. 2021;70:612–6. https://doi.org/10.15585/mmwr.mm7017a2
32. Jones EH, Hinckley AF, Hook SA, Meek JI, Backenson B, Kugeler KJ, et al. Pet ownership increases human risk of encountering ticks. Zoonoses Public Health. 2018;65:74–9. https://doi.org/10.1111/zph.12369
33. Ontario Agency for Health Protection and Promotion. Companion animals and tick-borne diseases: a systematic review. Toronto: Queen's Printer for Ontario; 2017.
34. Tan SML, Stellato AC, Niel L. Uncontrolled outdoor access for cats: an assessment of risks and benefits. Animals (Basel). 2020;10:258. https://doi.org/10.3390/ani10020258
35. Tan SML, Jajou S, Stellato AC, Niel L. Perspectives of Canadian and American cat owners on provision of uncontrolled outdoor access for owned domestic cats. Front Vet Sci. 2021;8:742245. https://doi.org/10.3389/fvets.2021.742245
36. Slatculescu AM, Pugliese M, Sander B, Zinszer K, Nelder MP, Russell CB, et al. Rurality, socioeconomic status, and residence in environmental risk areas associated with increased Lyme disease incidence in Ontario, Canada:

a case-control study. Vector Borne Zoonotic Dis. 2022;22:572–81. https://doi.org/10.1089/vbz.2022.0044
37. Galasso V, Pons V, Profeta P, Becher M, Brouard S, Foucault M. Gender differences in COVID-19 attitudes and behavior: panel evidence from eight countries. Proc Natl Acad Sci U S A. 2020;117:27285–91. https://doi.org/10.1073/pnas.2012520117
38. Shah B, Tombeau Cost K, Fuller A, Birken CS, Anderson LN. Sex and gender differences in childhood obesity: contributing to the research agenda. BMJ Nutr Prev Health. 2020;3:387–90. https://doi.org/10.1136/bmjnph-2020-000074
39. Thompson AE, Anisimowicz Y, Miedema B, Hogg W, Wodchis WP, Aubrey-Bassler K. The influence of gender and other patient characteristics on health care-seeking behaviour: a QUALICOPC study. BMC Fam Pract. 2016;17:38. https://doi.org/10.1186/s12875-016-0440-0
40. Varì R, Scazzocchio B, D'Amore A, Giovannini C, Gessani S, Masella R. Gender-related differences in lifestyle may affect health status. Ann Ist Super Sanita. 2016;52:158–66.
41. Niesobecki S, Hansen A, Rutz H, Mehta S, Feldman K, Meek J, et al. Knowledge, attitudes, and behaviors regarding tick-borne disease prevention in endemic areas. Ticks Tick Borne Dis. 2019;10:101264. https://doi.org/10.1016/j.ttbdis.2019.07.008
42. Finch C, Al-Damluji MS, Krause PJ, Niccolai L, Steeves T, O'Keefe CF, et al. Integrated assessment of behavioral and environmental risk factors for Lyme disease infection on Block Island, Rhode Island. PLoS One. 2014;9:e84758. https://doi.org/10.1371/journal.pone.0084758
43. Ostfeld RS, Keesing F. Does experimental reduction of blacklegged tick (*Ixodes scapularis*) abundance reduce Lyme disease incidence? Pathogens. 2023;12:714. https://doi.org/10.3390/pathogens12050714
44. Eisen L. Rodent-targeted approaches to reduce acarological risk of human exposure to pathogen-infected *Ixodes* ticks. Ticks Tick Borne Dis. 2023;14:102119. https://doi.org/10.1016/j.ttbdis.2023.102119
45. Nelson CA, Saha S, Kugeler KJ, Delorey MJ, Shankar MB, Hinckley AF, et al. Incidence of clinician-diagnosed Lyme disease, United States, 2005–2010. Emerg Infect Dis. 2015;21:1625–31. https://doi.org/10.3201/eid2109.150417
46. Hinckley AF, Connally NP, Meek JI, Johnson BJ, Kemperman MM, Feldman KA, et al. Lyme disease testing by large commercial laboratories in the United States. Clin Infect Dis. 2014;59:676–81. https://doi.org/10.1093/cid/ciu397
47. Bouchard C, Dumas A, Baron G, Bowser N, Leighton PA, Lindsay LR, et al. Integrated human behavior and tick risk maps to prioritize Lyme disease interventions using a 'One Health' approach. Ticks Tick Borne Dis. 2023;14:102083. https://doi.org/10.1016/j.ttbdis.2022.102083
48. Hansen MF, Sørensen PK, Sørensen AE, Krogfelt KA. Can protection motivation theory predict protective behavior against ticks? BMC Public Health. 2023;23:1214. https://doi.org/10.1186/s12889-023-16125-5
49. Schwartz AM, Mackeprang JM, Mead PS, Hinckley AF. Effectiveness of personal protection measures against Lyme disease: a review of epidemiologic studies from the United States. Zoonoses Public Health. 2022;69:777–91. https://doi.org/10.1111/zph.12984

Address for correspondence: Janica A. Adams, Enteric, Zoonotic and Vector-Borne Diseases, Health Protection, Operations and Response, Public Health Ontario, 661 University Ave, 17th Fl, Toronto, ON M5G 1M1, Canada; email: janica.adams@gmail.com

Associations between Minority Health Social Vulnerability Index Scores, Rurality, and Histoplasmosis Incidence, 8 US States

Dallas J. Smith, Malavika Rajeev, Kristina Boyd, Kaitlin Benedict, Ian Hennessee, Laura Rothfeldt, Connie Austin, Mary-Elizabeth Steppig, Dimple Patel, Rebecca Reik, Malia Ireland, Judi Sedivy, Suzanne Gibbons-Burgener, Renee M. Calanan, Samantha L. Williams, Sarah Rockhill, Mitsuru Toda

To explore associations between histoplasmosis and race and ethnicity, socioeconomic status, and rurality, we conducted an in-depth analysis of social determinants of health and histoplasmosis in 8 US states. Using the Minority Health Social Vulnerability Index (MH SVI), we analyzed county-level histoplasmosis incidence (cases/100,000 population) from the 8 states by applying generalized linear mixed hurdle models. We found that histoplasmosis incidence was higher in counties with limited healthcare infrastructure and access as measured by the MH SVI and in more rural counties. Other social determinants of health measured by the MH SVI tool either were not significantly or were inconsistently associated with histoplasmosis incidence. Increased awareness of histoplasmosis, more accessible diagnostic tests, and investment in rural health services could address histoplasmosis-related health disparities.

Histoplasmosis is an environmentally acquired fungal disease caused by *Histoplasma* species. In the United States, *Histoplasma* most commonly lives in central and eastern states, but infections also have been acquired outside of those areas (*1*,*2*). Globally, *Histoplasma* has been acquired in Latin America, Central Africa, and Southeast Asia but probably has worldwide distribution (*3*). Transmission involves inhalation of fungal spores from the environment; the incubation period is 3–17 days, and the primary clinical manifestation is pulmonary disease, although dissemination can occur (*4*,*5*). Commonly reported exposures include handling plant matter, disturbing material with bird or bat droppings, and cleaning, remodeling, or tearing down buildings (*6*,*7*). Persons who live in rural areas appear to be disproportionately affected by histoplasmosis, although outbreaks also can occur in urban settings (*6*–*8*).

Health disparities have been identified for fungal diseases in general, although additional analyses are needed to explore the underlying causes (*8*,*9*). Those disparities probably are related to environmental, behavioral, demographic, occupational, and socioeconomic factors. For histoplasmosis, previous reports have shown that men and boys and persons 41–80 years of age are more likely to have the disease diagnosed. Although incidence rates have been found to be similar across racial and ethnic categories (*1*,*6*), some studies of hospitalization data have found lower histoplasmosis-associated hospitalization rates among White patients (*10*). A previous study showed higher histoplasmosis hospitalization rates among non-Hispanic White patients and more histoplasmosis diagnoses among adult, low-income, and rural patients; however, analyses of associations between social, structural, and geographic factors that affect

Author affiliations: Centers for Disease Control and Prevention, Atlanta, Georgia, USA (D.J. Smith, M. Rajeev, K. Boyd, K. Benedict, I. Hennessee, R.M. Calanan, S.L. Williams, S. Rockhill, M. Toda); Arkansas Department of Health, Little Rock, Arkansas, USA (L. Rothfeldt); Illinois Department of Public Health, Springfield, Illinois, USA (C. Austin); Indiana Department of Health, Indianapolis, Indiana, USA (M.-E. Steppig); Kentucky Department of Public Health, Frankfort, Kentucky, USA (D. Patel); Michigan Department of Health and Human Services, Lansing, Michigan, USA (R. Reik); Minnesota Department of Health, St. Paul, Minnesota, USA (M. Ireland); Pennsylvania Department of Health, Harrisburg, Pennsylvania, USA (J. Sedivy); Wisconsin Department of Health Services, Madison, Wisconsin, USA (S. Gibbons-Burgener)

DOI: https://doi.org/10.3201/eid3010.231700

health and histoplasmosis incidence are lacking (*8*). Understanding such associations can inform educational outreach and other public health interventions to prevent illness and death from histoplasmosis in communities at higher risk.

To explore associations between histoplasmosis incidence, social determinants of health and rurality, we analyzed county-level histoplasmosis incidence from 8 US states reporting histoplasmosis to public health authorities. For this study, we used the Minority Health Social Vulnerability Index (MH SVI) and the National Center for Health Statistics (NCHS) urban–rural classification scheme.

Methods

Histoplasmosis Incidence

During 2011–2014 and 2019, a total of 8 US states (Arkansas, Illinois, Indiana, Kentucky, Michigan, Minnesota, Pennsylvania, Wisconsin) encompassing 698 counties reported county-level histoplasmosis case counts directly to the Centers for Disease Control and Prevention (CDC) Mycotic Diseases Branch (housed in the Division of Foodborne, Waterborne and Environmental Diseases, National Center for Emerging and Zoonotic Infectious Diseases). In 2020, those states reported histoplasmosis data to the National Notifiable Disease Surveillance System. Data from 2015–2018 were not reported to CDC. We calculated 6-year cumulative county-level incidence and 95% CIs by using county of residence and US Census population estimates across the years included in the study (*11*).

Minority Health Social Vulnerability Index

The MH SVI, launched in 2021, was developed by the US Department of Health and Human Services Office of Minority Health and CDC as an expanded version of CDC's Social Vulnerability Index. The MH SVI organizes 34 county-level social and structural factors that affect health into 6 distinct themes: socioeconomic status, household composition and disability, minority status and language, housing type and transportation, healthcare infrastructure and access, and medical vulnerability (*12*). This tool supports identification of racial and ethnicity minority communities that may be disproportionately affected by public health threats. MH SVI theme scores are interpreted as percentile rankings and expressed as decimals from 0 to 1; higher scores represent more vulnerable counties. We applied the methods for calculating and ranking the national MH SVI scores to obtain a regional score for each theme by including only data from the 8 states submitting histoplasmosis data (Appendix Figure 1, https://wwwnc.cdc.gov/EID/article/30/10/23-1700-App1.pdf). We also calculated MH SVI scores stratified by urban–rural classifications.

NCHS Urban–Rural Classification Scheme

The 2013 NCHS urban–rural classification scheme categorizes counties based on 6 levels of urbanization and is useful for assessing and monitoring health differences between counties (*13*). Level 1 (large central metropolitan) is the most urban, whereas level 6 (noncore) is the most rural. We condensed the NCHS classifications into 3 categories by combining large central metropolitan (level 1 [10 counties]) and large fringe metropolitan (level 2 [89 counties]), medium metropolitan (level 3 [71 counties]) and small metropolitan (level 4 [164 counties]), and micropolitan (level 5 [164 counties]) and noncore (level 6 [279 counties]). We collapsed the classifications on the basis of sparse data in the most urban category and a similar study of Social Vulnerability Index metrics and rurality (*14*).

Statistical Analyses

We used generalized linear mixed hurdle models to model 2 outcomes: the probability of observing ≥1 case (the zero-inflated component of the model [i.e., logistic regression]), and 6-year cumulative case counts at the county level (conditional component of the model [i.e., truncated Poisson regression]). We used a hurdle model to account for excess zeros in the data (i.e., counties that did not report any histoplasmosis cases) that might be attributable to sampling processes (e.g., limited surveillance or chance) (*15*). We summed case counts and population estimates across the 6 years (2011–2014 and 2019–2020) of available data. We ran models with counties categorized into low (referent), medium, and high-ranking tertiles for each MH SVI theme. As a sensitivity analysis, we also ran models with the MH SVI themes as continuous covariates. We included a state random intercept to account for state-specific differences in incidence and case detection and used the 3-category NCHS urban–rural classification to account for associations between rurality and histoplasmosis incidence. We included all covariates in both the zero-inflated and conditional components of the model. In addition, we included county population size as an offset in the conditional component and as a covariate (centered and scaled) in the zero-inflated component. To account for potential confounding between rurality and MH SVI metrics, we

ran an analysis stratified by urban–rural classification, running models for 443 micropolitan and noncore counties, 156 medium and small metropolitan counties, and 99 large metropolitan counties by using stratified MH SVI measures (recalculated for the subset of counties in each stratum).

We conducted analyses by using R version 4.2.2 (*16*). We implemented all models by using the R package glmmTMB (*15*) and used the R package DHARMa for model residual diagnostics, testing for uniformity of residuals, outlier predictions, and over- and underdispersion (*17*).

Results

During 2011–2014 and 2019–2020, a total of 4,854 histoplasmosis cases were reported in the 8 states included in this study. Of 698 total counties in the 8 states, 531 reported ≥1 case. For counties reporting ≥1 case, incidence ranged from 0.06 to 28.57 cases/100,000 persons. Both the proportion of counties with a case and the incidence varied by state (Figure 1); Minnesota had the highest average county-level incidence and Pennsylvania the lowest (Figures 2, 3). Median annual incidence was generally consistent across years, and of the counties reporting ≥1 case, most reported ≥1 across multiple years (73%) (Appendix Figure 2).

For counties reporting ≥1 case of histoplasmosis, all MH SVI themes were significantly associated with incidence in the count model (Appendix Table). MH SVI scores for the socioeconomic status and minority status and language themes were negatively associated with incidence; counties in the medium and high tertiles for those themes (more vulnerable counties) had significantly lower incidence compared with counties in the low tertile. In contrast, counties with higher vulnerability scores for the household composition and disability, healthcare infrastructure and access, and medical vulnerability themes had significantly higher incidence compared with low vulnerability counties. Counties classified as micropolitan and noncore and small and medium metropolitan had significantly higher incidence compared with the most urban counties (large metropolitan counties) (Figures 4, 5; Appendix Table).

Because rurality was significantly associated with incidence and the distribution of MH SVI scores, we ran models with counties stratified by rurality and recalculated MH SVI for the subset of counties in each urban–rural class to mitigate these associations (Appendix Figure 3). Many of the associations observed between MH SVI themes and incidence in the unstratified model were inconsistent in direction and statistical significance in the stratified models (Figure 3). Healthcare infrastructure and access was the only theme that had a consistent association and significance across urban–rural strata; counties with mid-vulnerability, high-vulnerability, or both had significantly higher incidence than low-vulnerability counties (Figure 6). The positive association between higher minority status and language vulnerability score and histoplasmosis incidence only remained

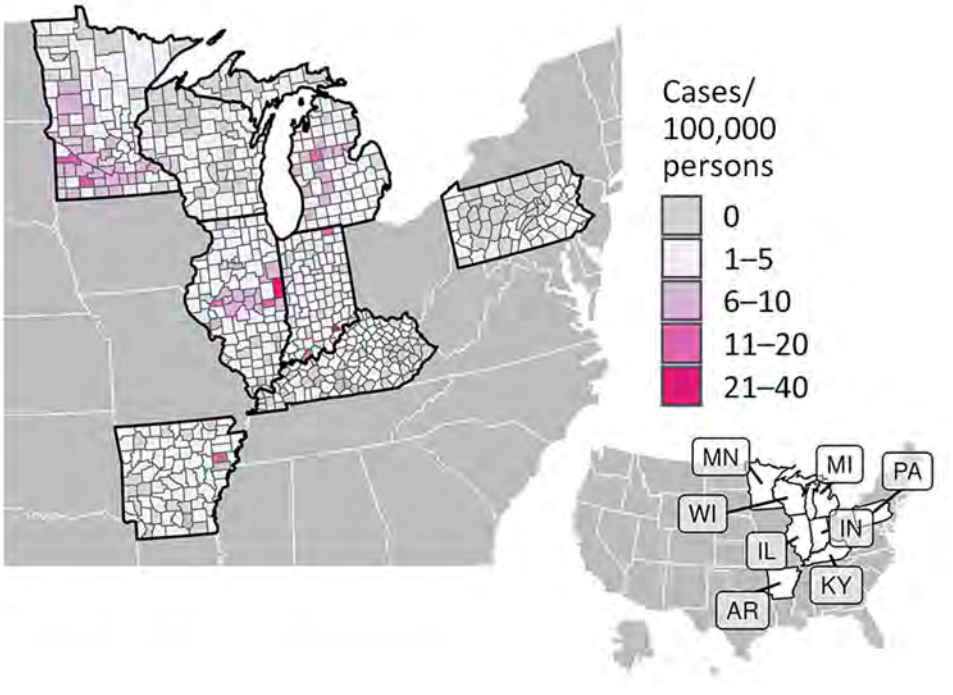

Figure 1. County-level histoplasmosis incidence (cases/100,000 persons) in 8 US states for which data were available, 2011–2014 and 2019–2020. Inset map indicates the 8 states.

statistically significant in the model with large metropolitan counties. In the unstratified model, more vulnerable counties for the socioeconomic status theme had lower incidence; however, the direction of that association flipped for micropolitan and noncore and large metropolitan counties and was not statistically significant for small and medium metropolitan counties (Figure 6). The association between the socioeconomic status theme and incidence was sensitive to our classification of counties into MH SVI tertiles; this association was not statistically significant in models with MH SVI themes as continuous covariates (Appendix Figure 4).

Minority status and language was the only MH SVI theme significantly associated with the probability of observing ≥1 case at the county level in the zero-inflated model (Appendix Table). County population size was associated with higher probability of observing a case, but rural classification did not have a statistically significant effect (Appendix Table, Figure 4). Rural classification, population size, and the minority status and language theme were correlated (Appendix Figure 5), and when we stratified by urban–rural classification, the association between minority status and language and observing a case was not significant (Figure 6). For the model with large metropolitan counties, socioeconomic status and medical vulnerability themes were significantly associated with case observation, but with only 99 counties in that category, the model also had the highest uncertainty (Figure 6; Appendix Figure 4).

Our key findings were not dependent on classification of counties into vulnerability tertiles; models with MH SVI themes as continuous covariates showed the same results for rurality and the healthcare access and infrastructure theme as the tertile models and overall were mostly congruent in the estimated associations and statistical significance for all other covariates (Appendix Figure 4). Estimates for state intercepts were also consistent across all models (Appendix Figure 6); however, much of the variation in incidence could not be explained by associations with MH SVI themes, rurality, or state-specific differences in incidence (Appendix Figure 7). Although models were robust when tested for outlier predictions, overdispersion, and underdispersion, the models with all counties and micropolitan and noncore counties did have significant nonuniformity of residuals (Appendix Figure 8), indicating potential issues with model fit.

Discussion

We found that histoplasmosis incidence was higher in counties with limited healthcare infrastructure and access as measured by the MH SVI theme and in more rural counties. In the full model, many of the other themes also were significantly associated with histoplasmosis incidence; however, these effect sizes

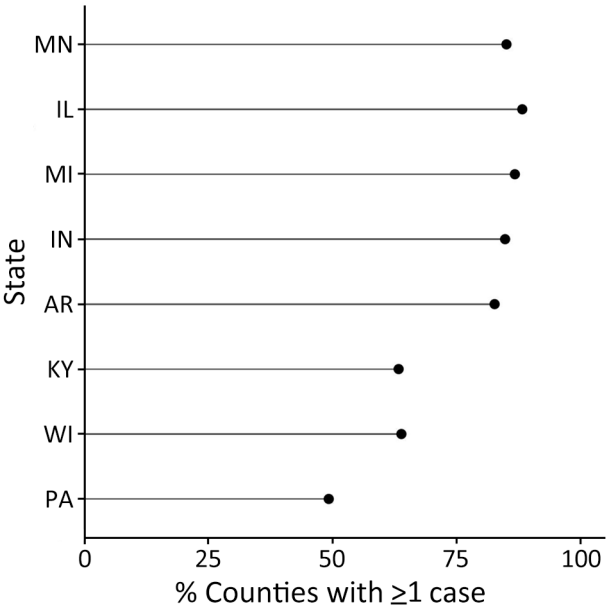

Figure 2. Percentage of counties in each state with ≥1 reported case of histoplasmosis in 8 US states for which data were available, 2011–2014 and 2019–2020.

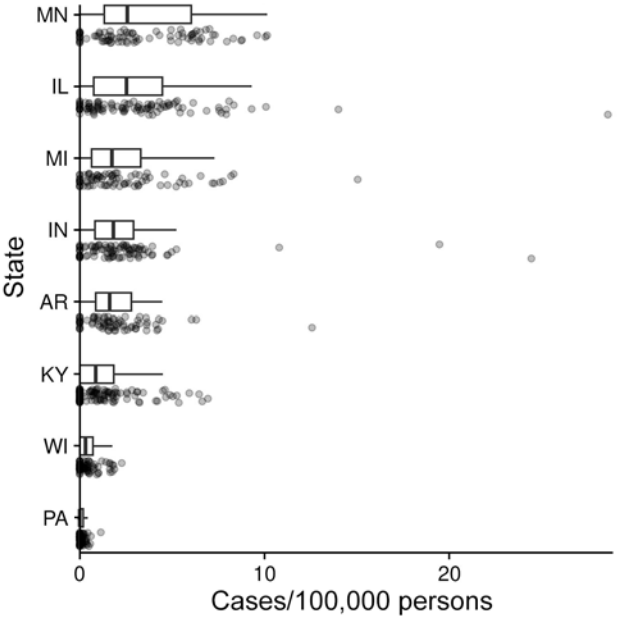

Figure 3. Distribution of county-level incidence (ordered from highest mean incidence to lowest mean incidence) in 8 US states for which data were available, 2011–2014 and 2019–2020. Boxplots show the medians (vertical black lines), interquartile ranges (box left and right ends), and range ±1.5 × interquartile range (error bars); the points show the raw data.

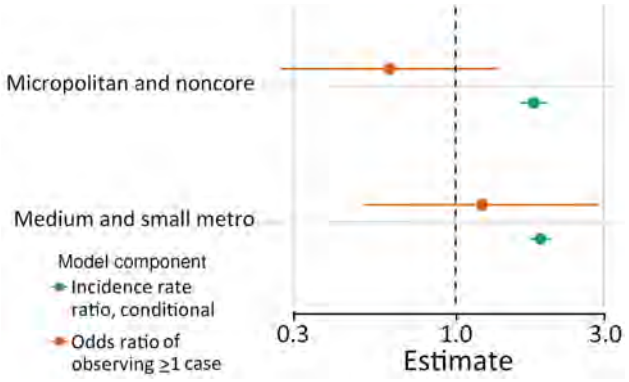

Figure 4. Associations between rurality and histoplasmosis incidence for counties reporting ≥1 case in 8 US states for which data were available, 2011–2014 and 2019–2020. Incidence rate ratios for conditional component (green) and odds ratios for the probability of observing ≥1 case in the zero-inflated component (orange) are shown 95% CIs (error bars) by county rural classification; reference group is large metropolitan counties.

were inconsistent in statistical significance and direction of the effect when stratified by urban–rural classification (i.e., household composition and disability and medical vulnerability). By using a hurdle model, we were able to model case observation separately from incidence and found that MH SVI themes were poor predictors of whether a county reported ≥1 histoplasmosis case during the study period.

Counties in the highest vulnerability tertile for the healthcare infrastructure and access theme had higher histoplasmosis incidence rates than did low-vulnerability counties. Counties in the highest vulnerability tertile probably have less access to hospitals, urgent care clinics, pharmacies, and primary-care physicians, perhaps making a diagnosis of histoplasmosis more difficult to obtain, which means histoplasmosis incidence probably is underestimated in these counties. Previous reports have shown that many patients with histoplasmosis experience >3 missed opportunities for diagnosis, leading to diagnostic delays of >3 weeks (*6*,*18*). Most histoplasmosis diagnoses are made by pulmonologists and infectious disease physicians (*6*). Access to such specialized providers is limited in the highly vulnerable communities. Considering there are more hospital closures than openings and few urgent care centers, especially in rural areas, it is critical for primary-care providers to consider histoplasmosis in patients who live in or have traveled to histoplasmosis-endemic areas who have compatible signs and symptoms (e.g., fever, cough, fatigue, chills, headache, chest pain, body aches) without improvement after empiric antibacterial medications (*19*,*20*). Extensive exposure to bird or bat droppings, a chest radiograph demonstrating new nodules or lymphadenopathy consistent with histoplasmosis, or an epidemiologic link to a histoplasmosis outbreak may be obtained from a patient's medical history when determining whether to test for histoplasmosis (*7*,*21*).

Equipping healthcare facilities with appropriate diagnostic tools might reduce histoplasmosis disparities related to healthcare infrastructure and access. Current diagnostic options are limited and can have long turnaround times, and test results can be difficult to interpret (*5*). For example, certain *Histoplasma* antigen assays are not commercially available; the assays that are available may be cost-prohibitive in rural healthcare facilities. Multiple and repeated diagnostic tests may be needed for an accurate diagnosis

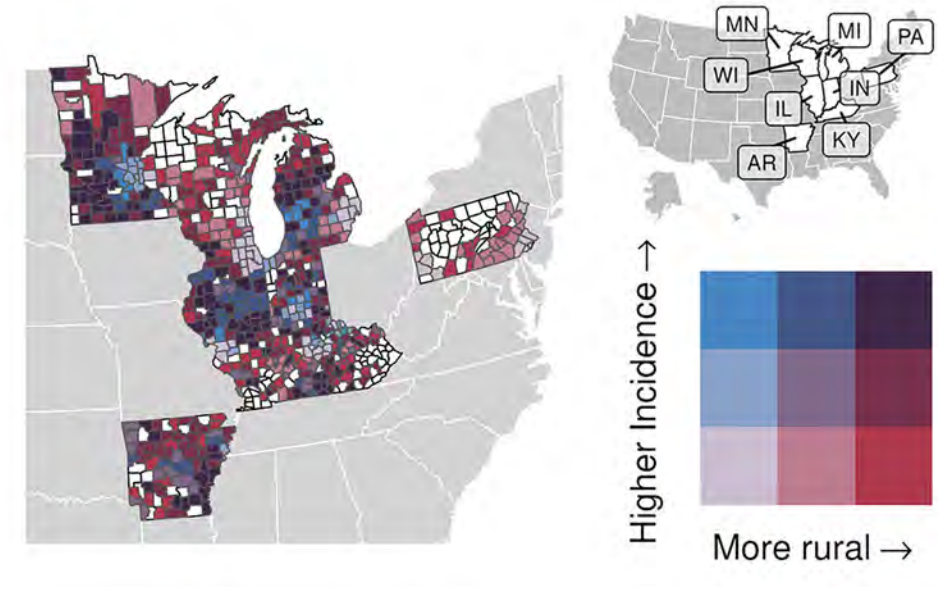

Figure 5. Associations between rurality and histoplasmosis incidence for counties reporting ≥1 case in 8 US states for which data were available, 2011–2014 and 2019–2020. For counties with ≥1 case of histoplasmosis, bivariate map shows county incidence (split into low-, mid-, and high-incidence tertiles) versus rurality (micropolitan and noncore, medium and small metropolitan, and large metropolitan counties); colors indicate the combination of incidence-rurality levels for each county. Counties without a case are shown in white. Inset map indicates names of the 8 states.

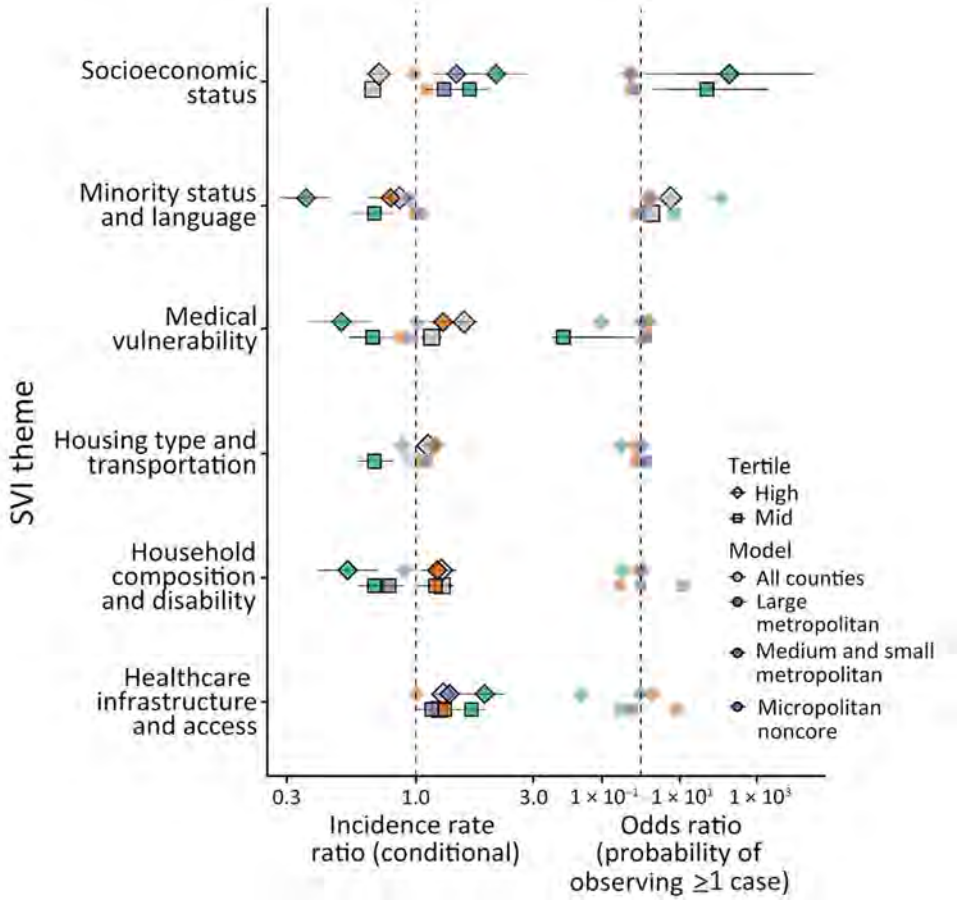

Figure 6. Model effect estimates for association of histoplasmosis incidence with MH SVI themes in 8 US states for which data were available, 2011–2014 and 2019–2020. MH SVI theme scores are interpreted as percentiles; higher scores represent more vulnerable counties. Left column shows incidence rate ratios for the conditional component; right column shows odds ratios for the probability of observing a case in the zero-inflated component. Error bars indicate 95% CIs. Shapes indicate the tertile (mid-tertile or high-tertile, with low-tertile as the reference level), and color indicates the model (model with all counties vs. those stratified by rural classification). Statistically significant effects are indicated by a black outline and increased opacity of points. MH SVI, Minority Health Social Vulnerability Index.

(*22*,*23*). Healthcare systems could use clinical diagnostic guidance for histoplasmosis to prioritize appropriate testing to manage resources and diagnostic access issues (*3*).

Promising diagnostic technologies may be able to revolutionize testing for histoplasmosis to prevent delayed diagnoses and misdiagnoses. *Histoplasma* antigen lateral flow assays (LFAs) show promise as point-of-care screening tests with high sensitivity (although further testing is needed in persons not living with HIV), are noninvasive, and have quick turnaround times (*24*–*28*). Encouragingly, multiple LFAs are undergoing diagnostic performance evaluation (*28*). LFAs could help mitigate vulnerabilities related to poor healthcare infrastructure and access by expediting diagnosis and subsequent treatment. Government-supported flexibilities for telemedicine and ordering diagnostic tests, like those implemented during the COVID-19 pandemic, especially in high-vulnerability counties, could improve access to care for patients with histoplasmosis (*29*).

Consistent with findings from previous studies, we found that the higher incidence rates in rural areas might be related to activities and occupations resulting in exposure to *Histoplasma* (*6*). Construction, excavation, agriculture, forestry, and hunting occupations have been linked to increased risks for acquiring histoplasmosis (*30*). Gardening, landscaping, or other handling of plant matter (48%); digging in soil (37%); and handling bird or bat droppings (24%) were identified as common exposures in patients with histoplasmosis in a recent surveillance report (*6*). Those occupations and activities might be more prevalent in rural areas. For workers at risk for histoplasmosis, appropriate prevention methods are critical (*30*). Interventions could include removing bats or birds from buildings, limiting dust exposure, communicating hazards, educating on histoplasmosis, and encouraging use of National Institute for Occupational Safety and Health–approved respirators for high-risk activities. We found that even among rural counties, those with higher vulnerability in the healthcare access and infrastructure theme had higher incidence of histoplasmosis, suggesting that interactions between exposure factors in rural areas and social and structural vulnerabilities may compound the risk for histoplasmosis.

Neither MH SVI themes nor rurality were strong predictors of which counties reported any histoplasmosis cases. County- and state-level differences in case detection and reporting and other factors that influence baseline risk (e.g., underlying conditions and environmental conditions) might be more predictive. Histoplasmosis surveillance in the United States is limited in terms of the number of states reporting, the data collected about cases, and the fact that histoplasmosis is not a nationally notifiable disease. A national case definition for histoplasmosis was established in 2017; state public health authorities used varying case definitions during 2011–2014 (*31*), making intrastate and interstate comparisons of histoplasmosis incidence difficult.

The medical vulnerability theme captures certain underlying conditions but does not capture severity of the condition (e.g., poorly controlled diabetes) and is not comprehensive; for example, autoimmune disease is not included, yet it was the most common underlying condition reported among patients with histoplasmosis in an enhanced surveillance study (*6*). *Histoplasma* is not distributed uniformly among counties, and our analysis was not able to account for hot spots or foci of *Histoplasma*, which are often associated with accumulated bird or bat droppings (*7*). Other environmental conditions that are incompletely understood also may influence *Histoplasma* hot spots. Modeling efforts have begun to explore areas where *Histoplasma* may be more prevalent (e.g., using suitability scores based on preferred soil environments) (*32*,*33*). More research is needed in that area, but such models could account for geographic variation at a more granular level than our study. Other social determinants of health (e.g., occupation and working conditions) not measured by the MH SVI tool have been linked to histoplasmosis outbreaks and probably are associated with higher histoplasmosis incidence (*30*). In future analyses, additional determinants could be included to further explore factors related to histoplasmosis incidence and guide public health response (*34*).

One limitation of our analysis is that MH SVI measures are composite ranks and therefore only can be interpreted in relative terms and within the context of the locations represented in the analysis. We found that it was critical to recalculate indices for the subset of states analyzed and stratify by rurality when examining associations between themes and incidence, both of which are associated with rurality. Extrapolation to the entire United States may not be appropriate because only 8 states were included in this study. MH SVI metrics are snapshots rather than temporal measures and thus do not capture changes in the individual factors that may occur over the time. In addition, the NCHS urban–rural classification scheme is largely based on proximity to a large metropolitan area and therefore may not capture aspects of rurality that might be more strongly associated with histoplasmosis incidence. It does not directly correlate with population density or other factors, such as land use or occupational composition, which may be more directly related to exposure risk. Our analyses also were limited to data aggregated to the county level. Rurality, population density, access to services, racial and ethnic diversity, and other social factors can vary widely within counties, and our estimates could not include individual-level risk factors for histoplasmosis. Future studies could address some of these limitations by incorporating more specific measures of rurality and social vulnerability (e.g., land use or individual data elements within the MH SVI themes), higher resolution spatial data (e.g., at the census tract), or individual-level sociodemographic and behavioral data (e.g., insurance status, care-seeking behavior, and occupational or environmental exposures). Moreover, county-level case counts were based on county of residence. Acquisition of histoplasmosis can be related to activities or an occupation that may not take place within a patient's county of residence; thus, county of residence may not always represent the location where the infection was acquired. Also, data on histoplasmosis outcome (e.g., illness, decreased quality of life, and death) and clinical manifestations (e.g., pulmonary or disseminated) were not available, but understanding the associations of those variables with social determinants of health could be critical to save lives and could be explored with enhanced histoplasmosis surveillance. Further, changes (e.g., in the economy and climate) may have occurred during 2011–2019 in the counties that were not captured in this analysis. We saw consistent incidence in states across years and counties reporting ≥1 case, but we cannot rule out the possibility of bias introduction by the gaps in data during 2015–2018.

In conclusion, our study found histoplasmosis incidence was higher in counties with limited healthcare infrastructure and access and in rural counties. Other social determinants of health measured by the MH SVI tool were not associated with histoplasmosis incidence. Increased awareness of histoplasmosis among healthcare providers and the public, implementation of prevention measures for occupational-related disease, point-of-care histoplasmosis diagnostic tools, and overall investment in rural health services are needed to help address histoplasmosis-related health disparities.

Acknowledgments

We thank Katelyn Lazenby, Stephen Hedges, and state and local health departments for collecting these data and Mohammed Khan for statistical support. We also recognize the CDC Health Equity Science Manuscript Development Program, in partnership with University of California–San Francisco, for the dedicated training and collaboration that have contributed to this article.

Code used in the study is available at https://github.com/CDCgov/histo_svi_smithetal_2024 and archived at https://zenodo.org/doi/10.5281/zenodo.13323658. Data are available on request and subject to state-specific approvals.

About the Author

Dr. Smith is an epidemiologist with the Mycotic Diseases Branch in the Division of Foodborne, Waterborne and Environmental Diseases, National Center for Zoonotic and Emerging Infectious Diseases, CDC. His primary research interests include dimorphic fungal diseases, fungal neglected tropical diseases, and antifungal stewardship.

References

1. Smith DJ, Williams SL, Benedict KM, Jackson BR, Toda M, Adame G, et al.; Endemic Mycoses State Partners Group. Surveillance for coccidioidomycosis, histoplasmosis, and blastomycosis—United States, 2019. MMWR Surveill Summ. 2022;71:1–14. https://doi.org/10.15585/mmwr.ss7107a1
2. Mazi PB, Sahrmann JM, Olsen MA, Coler-Reilly A, Rauseo AM, Pullen M, et al. The geographic distribution of dimorphic mycoses in the United States for the modern era. Clin Infect Dis. 2023;76:1295–301. https://doi.org/10.1093/cid/ciac882
3. Smith DJ, Free RJ, Thompson GR III, Baddley JW, Pappas PG, Benedict K, et al.; Endemic Mycoses Diagnostic Algorithm Subject Matter Expert Group. Clinical testing guidance for coccidioidomycosis, histoplasmosis, and blastomycosis in patients with community-acquired pneumonia for primary and urgent care providers. Clin Infect Dis. 2024;78:1559–63. https://doi.org/10.1093/cid/ciad619
4. Wheat J. Histoplasmosis. Experience during outbreaks in Indianapolis and review of the literature. Medicine (Baltimore). 1997;76:339–54. https://doi.org/10.1097/00005792-199709000-00002
5. Linder KA, Kauffman CA. Histoplasmosis: epidemiology, diagnosis, and clinical manifestations. Curr Fungal Infect Rep. 2019;13:120–8. https://doi.org/10.1007/s12281-019-00341-x
6. Benedict K, McCracken S, Signs K, Ireland M, Amburgey V, Serrano JA, et al. Enhanced surveillance for histoplasmosis—9 states, 2018–2019. Open Forum Infect Dis. 2020;7:ofaa343. https://doi.org/10.1093/ofid/ofaa343
7. Benedict K, Mody RK. Epidemiology of histoplasmosis outbreaks, United States, 1938–2013. Emerg Infect Dis. 2016;22:370–8. https://doi.org/10.3201/eid2203.151117
8. Rayens E, Rayens MK, Norris KA. Demographic and socioeconomic factors associated with fungal infection risk, United States, 2019. Emerg Infect Dis. 2022;28:1955–69. https://doi.org/10.3201/eid2810.220391
9. Gold JAW, Ahmad FB, Cisewski JA, Rossen LM, Montero AJ, Benedict K, et al. Increased deaths from fungal infections during the COVID-19 pandemic—National Vital Statistics System, United States, January 2020–December 2021. Clin Infect Dis. 2023;76:e255–62. https://doi.org/10.1093/cid/ciac489
10. Armstrong PA, Jackson BR, Haselow D, Fields V, Ireland M, Austin C, et al. Multistate epidemiology of histoplasmosis, United States, 2011–2014. Emerg Infect Dis. 2018;24:425–31. https://doi.org/10.3201/eid2403.171258
11. US Census Bureau. 2019 national and state population estimates. Annual population estimates, estimated components of resident population change, and rates of the components of resident population change for the United States, States, and Puerto Rico: April 1, 2010 to July 1, 2019 [cited 2023 Oct 5]. https://www.census.gov/newsroom/press-kits/2019/national-state-estimates.html
12. Centers for Disease Control and Prevention. CDC and OMH Minority Health Social Vulnerability Index [cited 2022 Nov 17]. https://www.minorityhealth.hhs.gov/minority-health-svi
13. Ingram DD, Franco SJ. NCHS urban-rural classification scheme for counties. Vital Health Stat 2. 2013;2014:1–73.
14. Fletcher KM, Espey J, Grossman MK, Sharpe JD, Curriero FC, Wilt GE, et al. Social vulnerability and county stay-at-home behavior during COVID-19 stay-at-home orders, United States, April 7-April 20, 2020. Ann Epidemiol. 2021;64:76–82. https://doi.org/10.1016/j.annepidem.2021.08.020
15. Brooks ME, Kristensen K, van Benthem KJ, Magnusson A, Berg CW, Nielsen A, et al. glmmTMB balances speed and flexibility among packages for zero-inflated generalized linear mixed modeling. R J. 2017;9:378–400. https://doi.org/10.32614/RJ-2017-066
16. R Core Team. R: a language and environment for statistical computing. 2022 [cited 2023 Oct 5]. https://www.R-project.org
17. Hartig F. DHARMa: residual diagnostics for hierarchical (multi-level / mixed) regression models. R package version 0.4.6 [cited 2023 Oct 5]. https://CRAN.R-project.org/package=DHARMa
18. Miller AC, Arakkal AT, Koeneman SH, Cavanaugh JE, Thompson GR, Baddley JW, et al. Frequency and duration of, and risk factors for, diagnostic delays associated with histoplasmosis. J Fungi (Basel). 2022;8:438. https://doi.org/10.3390/jof8050438
19. Health Affairs. Solving rural US health care challenges with frugal innovation. low-costs, high returns. 2022 [cited 2022 Nov 18]. http://www.healthaffairs.org/do/10.1377/forefront.20220222.972908/full
20. Ashraf N, Kubat RC, Poplin V, Adenis AA, Denning DW, Wright L, et al. Re-drawing the maps for endemic mycoses. Mycopathologia. 2020;185:843–65. https://doi.org/10.1007/s11046-020-00431-2
21. Kauffman CA. Histoplasmosis: a clinical and laboratory update. Clin Microbiol Rev. 2007;20:115–32. https://doi.org/10.1128/CMR.00027-06
22. Govindarajan A, Sous R, Venter F, Torrico T, Karapetians N, Heidari A, et al. A case of disseminated histoplasmosis from California, in the setting of secondary hemophagocytic lymphohistiocytosis: a diagnostic challenge. J Investig Med High Impact Case

Rep. 2023;11:23247096231156007. https://doi.org/10.1177/23247096231156007
23. Sabzanov S, Ganz M, Mishail B, Yusupov D, Fried P, Jacobs M, et al. A complex case of histoplasmosis in an immunocompromised patient: diagnostic challenges, multidisciplinary collaboration, and environmental factors. Cureus. 2023;15:e51276. https://doi.org/10.7759/cureus.51276
24. Cáceres DH, Gómez BL, Tobón AM, Chiller TM, Lindsley MD. Evaluation of a *Histoplasma* antigen lateral flow assay for the rapid diagnosis of progressive disseminated histoplasmosis in Colombian patients with AIDS. Mycoses. 2020;63:139–44. https://doi.org/10.1111/myc.13023
25. Abdallah W, Myint T, LaRue R, Minderman M, Gunn S, Wheat LJ, et al. Diagnosis of histoplasmosis using the MVista *Histoplasma* galactomannan antigen qualitative lateral flow-based immunoassay: a multicenter study. Open Forum Infect Dis. 2021;8:ofab454. https://doi.org/10.1093/ofid/ofab454
26. Cáceres DH, Gómez BL, Tobón ÁM, Minderman M, Bridges N, Chiller T, et al. Validation and concordance analysis of a new lateral flow assay for detection of *Histoplasma* antigen in urine. J Fungi (Basel). 2021;7:799. https://doi.org/10.3390/jof7100799
27. Andreani M, Frola CE, Caceres DH, Canteros CE, Rolón MJ, Chiller T, et al. Validation of a lateral flow assay for rapid diagnosis of histoplasmosis in advanced HIV disease, Buenos Aires, Argentina. Appl Microbiol. 2022;2:950–5. https://doi.org/10.3390/applmicrobiol2040072
28. Villareal K, Price A, Pasqualotto AC, Bahr NC. The current and future states of diagnostic tests for histoplasmosis with a focus on people with HIV and disseminated histoplasmosis. J Fungi (Basel). 2023;9:793. https://doi.org/10.3390/jof9080793
29. Centers for Medicare and Medicaid Services. Physicians and other clinicians: CMS flexibilities to fight COVID-19. 2023 Nov 6 [cited 2023 Dec 3]. https://www.cms.gov/files/document/physicians-and-other-clinicians-cms-flexibilities-fight-covid-19.pdf
30. de Perio MA, Benedict K, Williams SL, Niemeier-Walsh C, Green BJ, Coffey C, et al. Occupational histoplasmosis: epidemiology and prevention measures. J Fungi (Basel). 2021;7:510. https://doi.org/10.3390/jof7070510
31. Council of State and Territorial Epidemiologists. Standardized surveillance case definition for histoplasmosis. 2016 [cited 2023 Oct 5]. https://cdn.ymaws.com/www.cste.org/resource/resmgr/2016PS/16_ID_02.pdf
32. Maiga AW, Deppen S, Scaffidi BK, Baddley J, Aldrich MC, Dittus RS, et al. Mapping *Histoplasma capsulatum* exposure, United States. Emerg Infect Dis. 2018;24:1835–9. https://doi.org/10.3201/eid2410.180032
33. Hepler SA, Kaufeld KA, Benedict K, Toda M, Jackson BR, Liu X, et al. Integrating public health surveillance and environmental data to model presence of histoplasma in the United States. Epidemiology. 2022;33:654–9. https://doi.org/10.1097/EDE.0000000000001499
34. Jenks JD, Prattes J, Wurster S, Sprute R, Seidel D, Oliverio M, et al. Social determinants of health as drivers of fungal disease. EClinicalMedicine. 2023;66:102325. https://doi.org/10.1016/j.eclinm.2023.102325

Address for correspondence: Dallas Smith, Centers for Disease Control and Prevention, 1600 Clifton Rd NE, Mailstop H24-11, Atlanta, GA 30333-4027, USA; email: rhq8@cdc.gov

One Health Investigation into Mpox and Pets, United States

Clint N. Morgan, Natalie M. Wendling, Nicolle Baird, Chantal Kling, Leah Lopez, Terese Navarra, Gracie Fischer, Nhien Wynn, Leslie Ayuk-Takor, Brandy Darby, Julia Murphy, Rachel Wofford, Emma Roth, Stacy Holzbauer, Jayne Griffith, Ali Ruprecht, Charlalynn Harris, Nadia Gallardo-Romero, Jeffrey B. Doty

Monkeypox virus (MPXV) is zoonotic and capable of infecting many mammal species. However, whether common companion animals are susceptible to MPXV infection is unclear. During July 2022–March 2023, we collected animal and environmental swab samples within homes of confirmed human mpox case-patients and tested for MPXV and human DNA by PCR. We also used ELISA for orthopoxvirus antibody detection. Overall, 12% (22/191) of animal and 25% (14/56) of environmental swab samples from 4 households, including samples from 4 dogs and 1 cat, were positive for MPXV DNA, but we did not detect viable MPXV or orthopoxvirus antibodies. Among MPXV PCR-positive swab samples, 82% from animals and 93% from the environment amplified human DNA with a statistically significant correlation in observed cycle threshold values. Our findings demonstrate likely DNA contamination from the human mpox cases. Despite the high likelihood for exposure, we found no indications that companion animals were infected with MPXV.

Before 2022, the primary mode for monkeypox virus (MPXV) transmission was known to be zoonotic, and only limited human-to-human transmission was documented (*1*,*2*). Human MPXV infections resulting in mpox disease were hypothesized to be the result of direct or potentially indirect contact with infected wild mammals in Central and Western Africa (*3*,*4*). Our understanding of the potential for human-to-human spread of MPXV considerably broadened in the spring of 2022 (*5*,*6*). During that time, variant of clade II MPXV (clade IIb) was found in to be transmitted via direct contact among human populations and spreading primarily through sexual networks outside of mpox endemic regions (*5*,*6*).

Given the zoonotic origin and reported broad host-range of MPXV, efforts to understand and limit potential human-to-animal transmission are ongoing (*4*,*7*). The Centers for Disease Control and Prevention (CDC) provides guidance that persons with mpox stop or avoid contact with animals and that animals should be kept away from potentially infectious lesion material, objects, or surfaces (*8*). Mpox patients are generally urged by public health agencies to isolate at home unless hospitalization is clinically necessary (*9*,*10*). A person with mpox is considered infectious throughout their illness and until lesions have fully healed with new skin underneath; therefore, public health officials recommend that mpox patients isolating at home take proper infection control measures to prevent spread of infectious particles throughout the home (*11*–*13*). Unless infected persons take measures to completely isolate or reduce transmission potential, companion animals in close contact with mpox patients and their environments could be at higher risk for MPXV exposure than other mammal species, warranting special concern and investigation.

As of July 2024, no cases of MPXV infection or mpox disease had been confirmed in common domestic animals, such as dogs and cats, during the current global outbreak or any past outbreaks. One study in July 2022 described a 4-year-old dog in France that had been living and co-sleeping with 2 mpox case-patients

Author affiliations: Centers for Disease Control and Prevention, Atlanta, Georgia, USA (C.N. Morgan, N.M. Wendling, N. Baird, C. Kling, L. Lopez, T. Navarra, G. Fischer, N. Wynn, S. Holzbauer, C. Harris, N. Gallardo-Romero, J.B. Doty); Oak Ridge Institute for Science and Education, Oak Ridge, Tennessee, USA (L. Lopez, T. Navarra, G. Fischer); DC Department of Health, Washington, DC, USA (L. Ayuk-Takor); Virginia Department of Health, Richmond, Virginia, USA (B. Darby, J. Murphy); Council of State and Territorial Epidemiologists, Applied Epidemiology Fellowship Program, Atlanta (R. Wofford); Tennessee Department of Health, Nashville, Tennessee, USA (R. Wofford, E. Roth); Minnesota Department of Health, Saint Paul, Minnesota, USA (S. Holzbauer, J. Griffith, A. Ruprecht); Chenega Enterprise Systems and Solutions, Chesapeake, Virginia, USA (C. Harris)

DOI: https://doi.org/10.3201/eid3010.240632

(*14*). In that study, MPXV DNA was identified in swab samples from the dog's skin and surface of mucosal lesions and in anal and oral swab samples (*14*). However, follow-up investigations suggested that the animal was not infected with MPXV (*15*). A similar case was documented in Brazil in August 2022, when a 5-month-old dog had lesions that were MPXV-positive by quantitative PCR (*16*). Whether viral DNA detection was a result of MPXV infection in those animals or the result of environmental contamination due to close contact with infected humans is unclear. We conducted a One Health investigation in the United States to assess the susceptibility of companion animals to mpox and the risk for reverse-zoonotic transmission within households.

Methods and Materials

Study Population

The CDC Multi-National Mpox Response's One Health Team worked in collaboration with state and local jurisdictions to investigate the susceptibility of companion animals to MPXV infection. As part of that effort, CDC and state public health investigators collected blood samples from companion animals and swab specimens from companion animals and animal-associated objects. CDC tested swab and serum specimens via real-time PCR, orthopoxvirus (OPXV) serology, and viral culture. All animals tested were companion animals in a residence of a person with probable or confirmed mpox while the person was infectious. Animal sampling occurred within 21 days of any direct contact with the ill person before the person recovered (Table 1).

During July 2022–March 2023, we conducted sample collection in the District of Columbia, Virginia, Minnesota, and Tennessee, USA. After the initial sampling timepoint, we attempted follow-up sampling from all households 3–4 months later to collect animal serum samples and assess postexposure or postinfection immune responses.

Questionnaire and Consent

State and local public health personnel from the District of Columbia, Virginia, Minnesota, and Tennessee assisted with the study by interviewing mpox cases in their jurisdictions and requesting their voluntary participation in the study. After a person gave verbal consent to participate, they were provided with a survey questionnaire and consent forms. The questionnaire ascertained details and a timeline of the human case, the animal's health condition, general household information, types of contact between the person with mpox and the animal or animals in the household, and information about wild or domestic animals in and around the household. This project was reviewed by CDC clearance, cleared for human subjects, and determined to be nonresearch public health surveillance that did not require submission to the CDC institutional review board (project no. 0900f3eb81f79d72).

Swab Sample Collection

We performed all animal handling and sampling procedures in accordance with the approved CDC Institutional Animal Care Use Committee protocol (no. DOTMULX3183), in collaboration with state public health agencies, and with written consent of the animal's owner. We collected a standardized set of polyester swab (Puritan, https://www.puritanmedproducts.com) samples from the animal's dorsum fur, ventral abdomen, oral cavity, and anorectal area under supervision of the owner. We sampled animal lesions, if present. We also collected animal-associated environmental (AAE) specimens from objects and surfaces often used by the animal.

Sample Processing and PCR

We processed swab samples by using the swab extraction tube system (SETS; Roche, https://www.roche.com) with 400 µL of phosphate-buffered saline; after DNA extraction, we tested all samples for MPXV DNA by real-time PCR using an MPXV clade II–specific assay (*17*). In addition, we tested samples for human DNA by using the RNase-P PCR assay, which is used as an endogenous control when testing human specimens (*18*). We calculated Pearson correlation coefficients to assess the relationship between cycle threshold (Ct) values of MPXV clade II PCR–positive (Ct values $\leq$37) and RNase-P–reactive (Ct values <40) samples.

Viral Culture

We tested all PCR-positive swab samples for viable virus via cell culture by adding an aliquot of swab eluate to BSC-40 cell monolayers in T-25 flasks. We used an inoculation volume of 50 µL $\pm$25 µL, depending on available eluate volume. We incubated flasks at 35.5°C in an atmosphere of 6% CO_2 in Roswell Park Memorial Institute medium (*19*). We incubated and observed flasks $\leq$14 days or until $\approx$100% of monolayer showed cytopathic effect, following methods and media supplements described previously (*11*). To control the overgrowth of bacteria or fungi in T-25 flasks, we added penicillin/streptomycin, amphotericin B, and gentamicin to the cell culture medium. If we

detected any bacterial or fungal contamination, we performed 4 cycles of medium replacement to wash the monolayers and repeated this process as needed to prevent overgrowth.

Blood Collection and Serologic Testing

We attempted blood collection from all cooperative animals for which the owner provided consent. We collected ≤3 mL of blood from 20/34 animals during initial sampling and 21/25 animals during follow-up sampling. We cleaned the external venipuncture site with 90% ethanol and used a syringe or vacutainer needle for blood collection. For dogs and 1 rabbit, we collected blood via the cephalic or lateral saphenous veins. For cats, we collected blood via the jugular or medial saphenous veins. We stored and transported blood tubes at 4°C–20°C before centrifugation, after which we transferred serum into 2-mL cryotubes and stored at temperatures of at least –20°C until laboratory testing. We conducted a modified ELISA on all serum samples to determine presence of OPXV IgG antibodies, as previously described (*20*,*21*). We tested serum samples at a dilution of 1:100 by using microtiter plates coated with purified vaccinia virus (Dryvax strain) and using the A/G protein as the secondary antibody at a 1:10,000 concentration and developed plates for 25 minutes.

Data Analysis

When referring to animal swab samples, we defined prevalence as the proportion of total swabs collected from each animal from which we detected

Table 1. Summary of variables coded from household and questionnaire data used in a One Health investigation into mpox and pets, United States*

HH no.	Animal ID	DIS	CSI	AOA†	Household area, ft²‡	CCR	Rodents in household	Wildlife around household	SXDS	No. days exposure§	
										Before sampling	After recovery
1	DC-001	2	N	None	500–825	N	Y	Y	N	22	1
	DC-002	2	N	None					N	22	1
2	DC-003	6	N	None	500–825	N	N	N	N	22	13
3	DC-004	0	N	None	1,500–2,000	Y	N	N	Y	11	0
4	DC-005	5	Y	Walks	900–1,350	N	N	Y	Y	9	0
5	DC-006	6	N	Walks	500–825	Y	N	Y	N	16	6
6	DC-007	0	N	Walks	500–825	Y	N	Y	Y	28	0
7	DC-008	6	Y	Yard	1,500–2,000	Y	N	Y	Y	17	0
	DC-009	6	Y	Yard					Y	17	0
8	VA-001	2	N	Yard	1,500–2,000	Y	Y	Y	N	14	10
	VA-002	3	N	Yard					N	14	10
9	VA-003	2	N	Walks	500–825	Y	N	N	N	20	2
10	VA-004	7	Y	None	500–825	N	N	N	Y	18	0
11	VA-005	2	N	None	500–825	Y	N	N	N	12	12
	VA-006	2	N	None					N	10	12
12	MN-001	4	Y	None	500–825	Y	N	Y	Y	7	0
13	MN-002	3	Y	None	1,500–2,000	Y	Y	Y	Y	13	0
14	MN-003	5	Y	Walks	500–825	Y	N	Y	Y	46	0
15	MN-004	3	Y	Yard	1,500–2,000	Y	N	Y	Y	12	0
16	MN-005	6	N	None	1,500–2,000	N	Y	Y	N	26	17
	MN-006	6	N	None					N	26	17
	MN-007	6	N	None					N	26	17
	MN-008	6	N	None					N	26	17
	MN-009	6	N	Yard					N	26	17
	MN-010	6	N	Yard					N	26	17
17	TN-001	2	N	None	900–1,350	Y	N	Y	N	36	12
	TN-002	2	N	None					N	36	12
18	TN-003	2	N	None	1,500–2,000	Y	N	Y	N	25	14
	TN-004	2	N	None					N	25	14
19	TN-005	6	N	Yard	2,000–3,500	N	Y	Y	N	36	7
	TN-006	6	N	Yard					N	36	7
	TN-007	3	N	Yard					N	36	7
20	TN-008	5	N	Walks	1,500–2,000	Y	N	Y	N	UNK	27
21	TN-009	3	Y	None	900–1,350	N	N	Y	Y	17	0

*Variables relate to companion animals and peridomestic wildlife and include duration of potential monkeypox virus exposure to the animal within the household of the mpox case in relation to the date of sampling. AOA, animal outdoor activity; CCR, contact change with animals reported after mpox diagnosis in household member; CSI, co-sleeping with animal while owner infectious; DIS, direct interaction score comprised of the sum of all reported interaction types involving direct contact; HH, household; ID, identification; SXDS, mpox case-patient with symptoms during sampling; UNK, unknown.
†Considered as none (pet not allowed outside), walks (periodic or frequent supervised walks outside), or yard (periodic or prolonged unsupervised outdoor activity).
‡Based on data reported or estimated, the approximate area range is displayed for increased anonymity.
§Cumulative days potentially exposed to mpox.

either MPXV DNA or RNase-P (RNP) by PCR. When referring to AAE samples, we defined prevalence as the proportion of total swabs collected from the AAE samples within that animal's household that were MPXV-positive or RNP-positive. We also referred to detection of RNase-P via PCR as presence of human DNA.

For each animal, we calculated the duration of exposure, defined as cumulative number of days before sampling that an infectious owner had direct contact with the animal, including durations where direct contact was not reported but the animal was still sharing a common space with a person with mpox. Duration of exposure represented the total period that infectious lesion material (crusts or exudates) or other infectious particles were potentially shed or transferred within the home, to which the animal potentially had contact, either directly or via fomites.

We investigated factors reported in questionnaires that could affect animal MPXV exposure (Table 1). Those factors included whether the owner was symptomatic during time of sampling (coded SXDS); the degree of animal outdoor activity (coded AOA), which we stratified by none (no outdoor activity), walks (periodic or frequent supervised walks outside), and yard (allowed in yard or outside unsupervised frequently or for prolonged periods); co-sleeping with the animal while the owner was infectious (coded CSI); and a score comprised of the sum of all reported interaction types between animals and humans that involved direct contact (coded DIS), which included cuddling, hugging, petting, kissing, co-sleeping, sharing food, and grooming (Table 1).

We compared bivariate correlation coefficients among variables compiled from questionnaire data or diagnostic testing. We used SPSS Statistics 27 (IBM, https://www.ibm.com) to compute Pearson correlation coefficients. We performed 2-tailed tests of significance and considered p values of $\leq$0.05 or $\leq$0.01 statistically significant, as applicable.

Results

Overall, we sampled 34 individual companion animals from 21 households: 24 domestic dogs, 9 domestic cats, and 1 domestic rabbit (Table 2). The age of the animals ranged from 4 months to 16 years; 22 were male and 12 were female. All but 1 household had a single human mpox case; the other household had 2 cases. We collected a total of 191 swab specimens from animals and 56 AAE specimens. If excess blood was available, we opportunistically tested select blood specimens via PCR, including 10 whole blood specimens preserved in EDTA and 1 blood clot. At examination, we observed skin lesions in 6 dogs and 1 cat, and lesion features and locations varied.

PCR for Animal Samples

Samples collected from 5 individual animals (4 dogs, 1 cat) from 4 households were MPXV-positive; 2 of the dogs shared a household. Total animal swab MPXV positivity was 12% (22/191); 21 MPXV-positive swabs were from dogs, and 1 was from a cat (Table 3). All MPXV-positive animals also had $\geq$1 sample with an RNP-positive test result. Ct values of MPXV-positive samples were 25.2–36.7 (mean 34.5). Results of specific sample types collected were 29% (4/14) for skin lesions, 16% (6/37) for ventral skin or fur, 12% (4/33) for dorsal fur, 11% (4/35) for periocular area, 8% (3/36) for anorectal area, and 3% (1/36) for oral.

Among animal MPXV-positive specimens, 82% were RNP-positive, whereas 25% of the MPXV DNA–negative specimens were RNP-positive (Table 3). Ct values of MPXV-positive specimens that were RNP-positive positively correlated ($p<0.01$). In animal specimens, 18% (4/22) were MPXV-positive and RNP-negative, and positive Ct values (range 35.3–36.1) were near the upper limit of detection (Ct 37) for the assay. We did not detect MPXV DNA in any of the blood specimens tested via MPXV PCR. In addition, MPXV DNA prevalence in animal samples alone and when combined with AAE specimens significantly correlated with RNP prevalence in those same samples ($p<0.05$).

AAE PCR

We collected AAE specimens from 20/21 households, predominately from animal beds or bedding, toys, and food and water dishes. Among households, 29% (6/21) were positive for MPXV DNA, as were 25% (14/56) of collected specimens, 93% (13/14) of which were positive for MPXV and RNP (Table 3). In those same samples, AAE MPXV DNA prevalence positively correlated with human DNA prevalence ($p<0.05$). Of the 4 households with MPXV-positive animal swab specimens, all had MPXV-positive AAE swabs with Ct values of 29.9–35.9 (mean 32.8). For AAE specimens that were MPXV- and RNP-positive, the MPXV and RNase-P Ct values were significantly correlated ($p<0.01$). Of all AAE specimens, 66% (37/56) were RNP-positive, of which 82% (9/11) of specimens with Ct values <37 were in the 4 households with MPXV-positive AAE and animal swab samples.

Viral Culture and Serology

We attempted viral culture from all specimens with Ct values $\leq$36 (n = 31), and all were negative with

no signs of cytopathic effect. Three specimens from 2 dogs had bacterial contamination causing destruction of monolayer by day 6 or 7 postinfection, despite mitigating steps or retesting, and the harvested culture media tested negative by MPXV-specific PCR. In addition, all initial (n = 20) and follow-up (n = 22) serum specimens collected were ELISA-negative, and we detected no OPXV IgG. For 1 dog that had samples with the lowest MPXV Ct values, we collected 2 follow-up samples 2 months apart. Of the 5 animals that had MPXV-positive swab specimens, 3 did not have blood sampled at the initial timepoint due to noncompliance or aggression, and 3 were not available at the postexposure sampling timepoint.

Questionnaire Analysis

In total, 32% (11/34) of animals had preexisting health issues and 5 animals had preexisting skin lesions. In addition to the 5 animals with skin lesions that developed before owner symptom onset (all sampled), 2 additional animals had lesions that developed after owner symptom onset. We observed and sampled those lesions during the initial sampling visit, and 1 animal had skin and fur, periocular, and anorectal specimens that were PCR-positive for MPXV DNA, but we did not detect MPXV DNA from the lesion specimen, and serology results also were negative.

In total, 33% (7/21) of households reported no contact change with their animals. Reported types of changes in animal interactions included reducing frequency of interactions (9/21), stopping interactions (8/21), use of PPE during interactions (6/21), and relocating or isolating the animal (4/21); 1 household reported relegating animal care to uninfected persons outside the household. However, all but 1 household reported ≥1 type of direct contact activity with each animal after the MPXV-positive human in the household had symptoms develop (Table 1).

Households comprised apartments (n = 11) or single-family homes (n = 10), and approximate size

Table 2. Animal and environment sampling and diagnostic testing data from a One Health investigation into mpox and pets, United States*

Household no.	Animal ID	Species	Sex	Lesions sampled	Prevalence of animal sample PCR positivity†			Prevalence of environment sample PCR positivity		Serum timepoints
					MPXV	RNP	Ct	MPXV	RNP	
1	DC-001	Dog	M	N	0.0	0.8	ND	0.0	0.8	NC
	DC-002	Dog	M	N	0.0	0.6	ND	0.0	0.8	NC
2	DC-003	Cat	M	N	0.0	0.2	ND	0.0	0.3	1
3	DC-004	Dog	F	N	0.0	0.0	ND	0.0	0.5	NC
4	DC-005	Dog	M	Y	0.0	0.4	ND	0.0	0.7	1
5	DC-006	Dog	F	Y	0.0	0.3	ND	0.0	0.5	1
6	DC-007	Dog	M	N	0.0	0.4	ND	0.0	1.0	1
7	DC-008	Dog	F	N	0.0	0.6	ND	0.0	0.0	2
	DC-009	Dog	M	N	0.0	0.2	ND	0.0	0.0	2
8	VA-001	Dog	M	N	0.0	0.0	ND	0.0	0.0	1
	VA-002	Dog	M	Y	0.0	0.0	ND	0.0	0.0	2
9	VA-003	Dog	M	Y	0.7	0.6	35.4	1.0	0.7	1
10	VA-004	Cat	F	Y	0.2	0.3	36.4	1.0	1.0	NC
11	VA-005	Dog	M	Y	0.5	0.5	33	1.0	1.0	1
	VA-006	Dog	M	N	0.7	0.5	34.5	1.0	1.0	3
12	MN-001	Dog	F	N	0.5	0.6	34.4	1.0	1.0	NC
13	MN-002	Rabbit	M	N	0.0	0.2	ND	0.3	0.7	2
14	MN-003	Dog	M	Y	0.0	0.3	ND	0.0	0.3	2
15	MN-004	Dog	F	N	0.0	0.3	ND	0.0	1.0	2
16	MN-005	Cat	M	N	0.0	0.2	ND	NC	NC	2
	MN-006	Cat	M	N	0.0	0.4	ND	NC	NC	NC
	MN-007	Cat	M	N	0.0	0.0	ND	NC	NC	NC
	MN-008	Cat	M	N	0.0	0.0	ND	NC	NC	1
	MN-009	Dog	F	N	0.0	0.2	ND	NC	NC	2
	MN-010	Dog	M	N	0.0	0.5	ND	NC	NC	2
17	TN-001	Cat	M	N	0.0	0.2	ND	0.0	1.0	1
	TN-002	Cat	F	N	0.0	0.2	ND	0.0	1.0	2
18	TN-003	Dog	M	N	0.0	0.4	ND	0.0	0.7	1
	TN-004	Cat	F	N	0.0	0.4	ND	0.0	1.0	NC
19	TN-005	Dog	F	N	0.0	0.0	ND	0.0	0.0	2
	TN-006	Dog	F	N	0.0	0.3	ND	0.0	0.0	2
	TN-007	Dog	M	N	0.0	0.0	ND	0.0	0.0	2
20	TN-008	Dog	M	N	0.0	0.2	ND	0.3	0.7	1
21	TN-009	Dog	F	N	0.0	0.0	ND	0.0	0.0	2

*Ct, cycle threshold value; MPXV, monkeypox virus DNA; NC, no specimens collected; ND, not done; RNP, RNase-P DNA.
†Proportion of total swab specimens that were MPXV or RNP positive.

Table 3. PCR results for monkeypox virus clade II and RNase-P DNA assays from swab samples of companion animals and animal-associated objects and surfaces during a One Health investigation into mpox and pets, United States

	Monkeypox virus, no. (%)									RNase-P, no. (%)	
	Dogs		Cats		Rabbit		All				
Swab samples	Total	Positive	Total	Positive	Total	Positive	Total	Positive	Negative	Positive	Negative
Animal	140	21 (15)	47	1 (2)	4	0	191	22 (12)	169 (88)	18 (82)	42 (25)
Objects and surfaces	42	10 (24)	11	3(27)	3	1 (33)	56	14 (25)	42 (75)	13 (93)	24 (57)
Totals	182	31 (17)	58	4 (7)	7	1 (14)	247	36 (15)	211 (85)	31 (86)	66 (31)

range was 500–3,500 ft^2 (Table 1). We observed a significant negative correlation between household size and prevalence of either MPXV ($p<0.05$) or human DNA ($p<0.01$) in animal samples and human DNA prevalence in environmental samples ($p<0.01$). Apart from human DNA prevalence, household size, and environmental MPXV prevalence, we observed no other statistically significant relationships for other variables potentially influencing prevalence of MPXV DNA in animal samples.

Discussion

CDC advises that persons with mpox should avoid contact with animals, including pets, until lesions have fully healed to prevent potential virus spillback. That recommendation is because of uncertainty regarding susceptibility of companion animals to MPXV (*9*). If MPXV-infected persons cannot avoid contact with pets within the household, practicing appropriate infection control will prevent further exposure potential. In most households we visited, recommended quarantine and infection control procedures were not consistently followed.

Despite MPXV-positive swab specimens detected on the skin or fur of dogs and cats and in associated environmental samples, no dogs or cats with live virus or antibodies detected have been reported globally. In 2 cases outside of the United States in which MPXV DNA was detected in dogs (*14*,*16*), apart from apparent skin lesions, no other signs of infection were reported in the animals, including virus cultured from samples or OPXV antibodies detected by serology after additional investigation (*15*).

In our household study, skin lesions in 7 animals were the only observable clinical features that were potentially consistent with mpox disease. However, 5 animals exhibited lesions before owner symptom onset, and the 2 animals with skin lesions that were observed after owner symptom onset were negative for MPXV by PCR. Only 1 animal had MPXV-positive lesions sampled, a dog with lesion swab samples collected from a grouping of 3 large lesions on its rear leg, and the average Ct value of samples was 25.2. After further testing to consider potential DNA contamination from the owner, that sample also had the lowest average RNase-P Ct value (29.3) of all samples tested. In addition, that dog's lesions were reported to have formed before symptom onset in the owner, culture attempts from that and all other samples were negative, and OPXV antibodies were not detected during any timepoint tested. Therefore, after reviewing all the data, we did not consider this animal a confirmed mpox case.

All animals with MPXV-positive samples in this study also had RNP-positive specimens collected, indicating the presence of human DNA. The statistically significant correlation of MPXV- and RNP-positive samples, MPXV PCR results showing high Ct values indicating low viral DNA loads, and the lack of viable virus or antibodies in the collected samples strongly suggest that observed lesions or scabs in these animals were not the result of MPXV infection. In addition, from our knowledge of MPXV pathology, an MPXV lesion would most likely produce high viral loads and at levels higher than for other sample types (*22*).

As reported in other household environmental sampling studies, MPXV DNA can be widely detected in indoor or household settings (*11*,*12*,*23*–*25*). In this study, we found that households with smaller shared spaces were significantly correlated with both MPXV and human DNA prevalence, suggesting that the risk for MPXV exposure could be higher in smaller living quarters. Given the capability of MPXV DNA to disseminate within the household of a person with mpox, and after consideration of the PCR results detailed here, persons with mpox, not the companion animals, likely were the source of the MPXV DNA we detected in the household.

The potential for contamination from either direct contact with a person with mpox or indirect exposure to materials containing MPXV DNA should be considered when interpreting results of PCR testing from companion animals. In addition, case definitions should consider potential extraneous contamination and require more than a PCR-positive result from an animal to be considered a confirmed animal mpox case (*26*). Contamination should also be considered as a reason for a positive PCR result and false-positive results in humans with nonspecific lesions who have potentially had contact with an mpox case-patient.

MPXV infection in companion animals, if they are suitable hosts, is uncharacterized; clinical signs, viral shedding, and duration of infectious period are unknown. Thus, although unlikely, given the limits of our sampling design, it is possible that an infected animal escaped detection in our study. However, the overall PCR and serologic evidence best fits the hypothesis that the MPXV DNA detected in animal samples submitted for PCR testing is a result of DNA contamination from the infected human within the household.

More work is needed to determine the susceptibility of companion animals to clade IIb MPXV. Thus, CDC still recommends that companion animal owners with mpox limit their interactions with their pets while infectious, particularly if they are sharing smaller living spaces. That precautionary measure is recommended until more information is available about the susceptibility of common mammalian companion animal species to mpox.

In conclusion, no strong evidence yet exists to suggest that common companion animals, such as dogs or cats, are susceptible to infection with clade IIb MPXV. Given high likelihood for exposure among most of these animals, the paucity of evidence indicating infection might indicate resistance to infection. Nonetheless, to prevent further viral spread and potential evolution and establishment of new endemic areas, during public health emergencies caused by emerging zoonotic diseases, responders should apply a One Health approach to investigate potential spillback of human infections to animals, including pets.

Acknowledgments

The authors thank the Epidemiology, Laboratory and Testing, and STLT (State, Tribal, Local, or Territorial) Task Forces of the CDC 2022 Multinational Mpox Response and the CDC Poxvirus and Rabies Branch, Division of High Consequence Pathogens and Pathology, National Center for Emerging and Zoonotic Infectious Diseases. We also acknowledge additional persons and entities who assisted with this study, including the Minnesota Department of Health, including Patrice Vandelinde, Victoria Lappi, and Anna Strain; the Virginia Department of Health, including Kenneth Gordon, Christina Chommanard, Luisa Angel Cortes, Clarissa Bonnefond, Lisa Engle, and Cynthia Rieken; the Tennessee Department of Health and Agriculture, including Jane Yackley, Dilani Goonewardene, and Whitnie Smartt; and DC Department of Health, including Sarah Gillani, Will Still, and Karla Miletti. In addition, we acknowledge Casey Barton-Behravesh, Yoshinori Nakazawa, Modupe Osinubi, Ashutosh Wadhwa, and Ariel Caudle for their assistance.

All funding for this study was provided by the Centers for Disease Control and Prevention's 2022 Multinational Mpox Response (CDC Mpox Response). The CDC Mpox Response provided technical review and oversight of this manuscript before publication. This study and report were also supported in part by an appointment to the Applied Epidemiology Fellowship Program, administered by the Council of State and Territorial Epidemiologists and funded by the Centers for Disease Control and Prevention (cooperative agreement no. 1NU38OT000297-03-00).

About the Author

Mr. Morgan is a biologist in the Poxvirus and Rabies Branch, Division of High Consequence Pathogens and Pathology, National Center for Emerging and Zoonotic Infectious Diseases, Centers for Disease Control and Prevention. His research interests include the virus-host interactions of orthopoxviruses and lyssaviruses in the environment.

References

1. Nolen LD, Osadebe L, Katomba J, Likofata J, Mukadi D, Monroe B, et al. Extended human-to-human transmission during a monkeypox outbreak in the Democratic Republic of the Congo. Emerg Infect Dis. 2016;22:1014–21. https://doi.org/10.3201/eid2206.150579
2. Durski KN, McCollum AM, Nakazawa Y, Petersen BW, Reynolds MG, Briand S, et al. Emergence of monkeypox—West and Central Africa, 1970–2017. MMWR Morb Mortal Wkly Rep. 2018;67:306–10. https://doi.org/10.15585/mmwr.mm6710a5
3. Reynolds MG, Doty JB, McCollum AM, Olson VA, Nakazawa Y. Monkeypox re-emergence in Africa: a call to expand the concept and practice of One Health. Expert Rev Anti Infect Ther. 2019;17:129–39. https://doi.org/10.1080/14787210.2019.1567330
4. Reynolds MG, Guagliardo SAJ, Nakazawa YJ, Doty JB, Mauldin MR. Understanding orthopoxvirus host range and evolution: from the enigmatic to the usual suspects. Curr Opin Virol. 2018;28:108–15. https://doi.org/10.1016/j.coviro.2017.11.012
5. Sah R, Abdelaal A, Reda A, Katamesh BE, Manirambona E, Abdelmonem H, et al. Monkeypox and its possible sexual transmission: where are we now with its evidence? Pathogens. 2022;11:924. https://doi.org/10.3390/pathogens11080924
6. Low N, Bachmann LH, Ogoina D, McDonald R, Ipekci AM, Quilter LAS, et al. Mpox virus and transmission through sexual contact: defining the research agenda. PLoS Med. 2023;20:e1004163. https://doi.org/10.1371/journal.pmed.1004163
7. McQuiston JH, Braden CR, Bowen MD, McCollum AM, McDonald R, Carnes N, et al. The CDC domestic mpox response—United States, 2022–2023. MMWR Morb Mortal Wkly Rep. 2023;72:547–52. https://doi.org/10.15585/mmwr.mm7220a2
8. Centers for Disease Control and Prevention. Mpox in the home [cited 2023 Dec 8]. https://www.cdc.gov/poxvirus/mpox/veterinarian/mpox-in-animals.html

9. Adler H, Gould S, Hine P, Snell LB, Wong W, Houlihan CF, et al. Clinical features and management of human monkeypox: a retrospective observational study in the UK. Lancet Infect Dis. 2022;22:1153–62. https://doi.org/10.1016/S1473-3099(22)00228-6
10. Minhaj FS, Ogale YP, Whitehill F, Schultz J, Foote M, Davidson W, et al.; Monkeypox Response Team 2022. Monkeypox outbreak—nine states, May 2022. MMWR Morb Mortal Wkly Rep. 2022;71:764–9. https://doi.org/10.15585/mmwr.mm7123e1
11. Morgan CN, Whitehill F, Doty JB, Schulte J, Matheny A, Stringer J, et al. Environmental persistence of monkeypox virus on surfaces in household of person with travel-associated infection, Dallas, Texas, USA, 2021. Emerg Infect Dis. 2022;28:1982–9. https://doi.org/10.3201/eid2810.221047
12. Pfeiffer JA, Collingwood A, Rider LE, Minhaj FS, Matheny AM, Kling C, et al. High-contact object and surface contamination in a household of persons with monkeypox virus infection—Utah, June 2022. MMWR Morb Mortal Wkly Rep. 2022;71:1092–4. https://doi.org/10.15585/mmwr.mm7134e1
13. Centers for Disease Control and Prevention. Mpox: isolation and infection control at home [cited 2023 Jan 21]. https://www.cdc.gov/poxvirus/monkeypox/clinicians/infection-control-home.html
14. Seang S, Burrel S, Todesco E, Leducq V, Monsel G, Le Pluart D, et al. Evidence of human-to-dog transmission of monkeypox virus. Lancet. 2022;400:658–9. https://doi.org/10.1016/S0140-6736(22)01487-8
15. The French Agency for Food. Monkeypox: what is the risk of spreading to pets? [in French] [cited 2022 Dec 16]. https://www.anses.fr/fr/content/variole-du-singe-quel-risque-de-diffusion-aux-animaux-de-compagnie
16. Brazilian Ministry of Health. Ministry of Health is notified of the first case of monkeypox in a domestic animal [in Portuguese] [cited 2022 Dec 3]. https://www.gov.br/saude/pt-br/assuntos/noticias/2022/agosto/ministerio-da-saude-e-notificado-do-primeiro-caso-de-variola-dos-macacos-em-animal
17. Li Y, Zhao H, Wilkins K, Hughes C, Damon IK. Real-time PCR assays for the specific detection of monkeypox virus West African and Congo Basin strain DNA. J Virol Methods. 2010;169:223–7. https://doi.org/10.1016/j.jviromet.2010.07.012
18. Centers for Disease Control and Prevention. Test procedure: monkeypox virus generic real-time PCR test [cited 2023 Oct 7]. https://www.cdc.gov/poxvirus/mpox/pdf/PCR-Diagnostic-Protocol-508.pdf
19. Hughes CM, Liu L, Davidson WB, Radford KW, Wilkins K, Monroe B, et al. A tale of two viruses: coinfections of monkeypox and varicella zoster virus in the Democratic Republic of Congo. Am J Trop Med Hyg. 2021;104:604–11. https://doi.org/10.4269/ajtmh.20-0589
20. Karem KL, Reynolds M, Braden Z, Lou G, Bernard N, Patton J, et al. Characterization of acute-phase humoral immunity to monkeypox: use of immunoglobulin M enzyme-linked immunosorbent assay for detection of monkeypox infection during the 2003 North American outbreak. Clin Diagn Lab Immunol. 2005;12:867–72.
21. Hutson CL, Olson VA, Carroll DS, Abel JA, Hughes CM, Braden ZH, et al. A prairie dog animal model of systemic orthopoxvirus disease using West African and Congo Basin strains of monkeypox virus. J Gen Virol. 2009;90:323–33. https://doi.org/10.1099/vir.0.005108-0
22. Kim H, Kwon R, Lee H, Lee SW, Rahmati M, Koyanagi A, et al. Viral load dynamics and shedding kinetics of mpox infection: a systematic review and meta-analysis. J Travel Med. 2023;30: taad111. https://doi.org/10.1093/jtm/taad111
23. Gould S, Atkinson B, Onianwa O, Spencer A, Furneaux J, Grieves J, et al. Air and surface sampling for monkeypox virus in a UK hospital: an observational study. Lancet Microbe. 2022;3:e904–11. https://doi.org/10.1016/S2666-5247(22)00257-9
24. Nörz D, Pfefferle S, Brehm TT, Franke G, Grewe I, Knobling B, et al. Evidence of surface contamination in hospital rooms occupied by patients infected with monkeypox, Germany, June 2022. Euro Surveill. 2022;27:2200477. https://doi.org/10.2807/1560-7917.ES.2022.27.26.2200477
25. Atkinson B, Burton C, Pottage T, Thompson K-A, Ngabo D, Crook A, et al. Infection-competent monkeypox virus contamination identified in domestic settings following an imported case of monkeypox into the UK. Environ Microbiol. 2022;24:4561–9. https://doi.org/10.1111/1462-2920.16129
26. Centers for Disease Control and Prevention. Interim CDC case definition for animal cases of monkeypox [cited 2023 Mar 14]. https://www.cdc.gov/poxvirus/mpox/veterinarian/animal-officials.html#case-def

Address for correspondence: Jeffrey B. Doty, Centers for Disease Control and Prevention, 4055 Tudor Center Dr, Anchorage, AK 99508, USA; email: uwb7@cdc.gov

Pathogenicity of Highly Pathogenic Avian Influenza A(H5N1) Viruses Isolated from Cats in Mice and Ferrets, South Korea, 2023

Il-Hwan Kim,[1] Jeong-Hyun Nam,[1] Chi-Kyeong Kim, Yong Jun Choi, Hyeokjin Lee, Bo Min An, Nam-Joo Lee, Hyoseon Jeong, Su-Yeon Lee, Sang-Gu Yeo, Eun-Kyoung Lee, Youn-Jeong Lee, Jee Eun Rhee, Sang Won Lee, Youngmee Jee, Eun-Jin Kim

The prevalence of highly pathogenic avian influenza (HPAI) A(H5N1) viruses has increased in wild birds and poultry worldwide, and concomitant outbreaks in mammals have occurred. During 2023, outbreaks of HPAI H5N1 virus infections were reported in cats in South Korea. The H5N1 clade 2.3.4.4b viruses isolated from 2 cats harbored mutations in the polymerase basic protein 2 gene encoding single amino acid substitutions E627K or D701N, which are associated with virus adaptation in mammals. Hence, we analyzed the pathogenicity and transmission of the cat-derived H5N1 viruses in other mammals. Both isolates caused fatal infections in mice and ferrets. We observed contact infections between ferrets, confirming the viruses had high pathogenicity and transmission in mammals. Most HPAI H5N1 virus infections in humans have occurred through direct contact with poultry or a contaminated environment. Therefore, One Health surveillance of mammals, wild birds, and poultry is needed to prevent potential zoonotic threats.

Since the emergence of the highly pathogenic avian influenza (HPAI) A(H5N1) virus (A/chicken/Scotland/59) in Scotland, UK, several outbreaks of H5Nx viruses have been reported in poultry worldwide (*1*). In 1996, an HPAI H5N1 virus, A/goose/Guangdong/1/1996 (Gs/GD), was identified, and the Gs/GD lineage H5 viruses have been circulating in poultry and wild aquatic bird reservoirs for >25 years (*1*,*2*). HPAI H5N1 viruses pose a global threat to the poultry industry and public health because of frequent outbreaks in chicken, ducks, and other poultry (*3*). According to the World Health Organization, 882 cases of avian influenza A(H5N1) infections in humans have been reported globally from January 1, 2003, to December 21, 2023, resulting in 461 deaths (52% mortality rate) (*4*).

Since 2005, HPAI H5N1 viruses have diversified genetically, forming numerous genotypes through reassortment with other avian influenza A viruses (*5*). HPAI H5N1 clade 2.3.4.4b viruses of the Gs/GD lineage emerged in Europe in 2020, causing outbreaks in wild birds and poultry in many countries (*5*). The spread of clade 2.3.4.4b viruses was reported in 26 countries worldwide; the virus infected >48 mammal species (*2*,*5*–*7*). In 2022, mass deaths of >20,000 sea lions from HPAI H5N1 infections were confirmed along the coast of South America, including coastal Peru, Chile, Argentina, Uruguay, and Brazil. In addition, in 2023, unusual deaths of cats were reported in Poland (*8*–*10*). Therefore, concerns about the risk for interspecies transmission and human-to-human spread of H5N1 viruses have been growing because of the acquisition of interhost transmission capability and the increase in HPAI H5N1 viruses found in mammals (*11*).

In South Korea, HPAI H5N1 clade 2.3.4.4.b viruses were identified in wild birds in 2021, which was followed by infection outbreaks in poultry farms (*12*). During autumn 2022, introductions of ≥2 types of HPAI H5N1 clade 2.3.4.4b viruses that originated from Eurasian breeding grounds and North America occurred simultaneously, and various genotypes were subsequently detected in wild birds and domestic poultry (*13*,*14*). During July 2023, unusual deaths

Author affiliations: Korea Disease Control and Prevention Agency, Cheongju, South Korea (I.-H. Kim, J.-H. Nam, C.-K. Kim, Y.J. Choi, H. Lee, B.M. An, N.-J. Lee, H. Jeong, S.-Y. Lee, S.-G. Yeo, J.E. Rhee, S.W. Lee, Y. Jee, E.-J. Kim); Animal and Plant Quarantine Agency, Gimcheon, South Korea (E.-K. Lee, Y.-J. Lee)

DOI: https://doi.org/10.3201/eid3010.240583

[1]These authors contributed equally to this article.

of cats at animal shelters occurred in the Yongsan and Gwanak Districts of Seoul, South Korea, caused by HPAI H5N1 viruses (*15*,*16*); viruses isolated from cats were obtained from each animal shelter. We analyzed the pathogenicity and transmission characteristics of 2 cat-derived virus isolates by using molecular methods and by conducting experiments in mouse and ferret infection models. We performed all animal experiments in strict accordance with general animal care guidelines mandated under the Guidelines for Animal Use and Care of the Korea Disease Control and Prevention Agency (KDCA).

Materials and Methods

Cells

We grew and maintained MDCK cells (American Type Culture Collection, https://www.atcc.org) in Eagle's Minimum Essential Medium (WELGENE, https://www.welgene.com) containing 5% fetal bovine serum, 1 mmol/L l-glutamine, and penicillin/streptomycin (Thermo Fisher Scientific, https://www.thermofisher.com). We incubated the cells at 37°C in 5% CO_2 until use.

Virus Distribution

The Animal and Plant Quarantine Agency (APQA), South Korea, provided 3 HPAI H5N1 virus isolates and deposited their whole-genome sequences in the GISAID EpiFlu database (http://www.gisaid.org). We propagated the isolates in specific pathogen-free embryonated chicken eggs (second passage) and confirmed that their sequences were identical to those provided by the APQA (Table 1). A/duck/Korea/H493/2022(H5N1) (GISAID accession no. EPI_ISL_15647834) originated from a duck farm in the Yecheon area in October 2022. A/feline/Korea/M302–6/2023(H5N1) (accession no. EPI_ISL_18819809) was from the Yongsan District, and A/feline/Korea/M305–7/2023(H5N1) (accession no. EPI_ISL_18819807) was from the Gwanak District; both of those viruses from cats were obtained from animal shelters during July 2023.

Genetic and Phylogenetic Analysis

We extracted virus RNA by using the RNeasy Mini Kit (QIAGEN, https://www.qiagen.com) and performed gene amplification and library preparation by using the Illumina Microbial Amplicon Prep-Influenza A/B kit (Illumina, https://www.illumina.com). Subsequently, we sequenced whole genomes of the viruses on a MiSeq instrument by using MiSeq Reagent Kit v2 (Illumina) to obtain 2 × 150-bp read lengths. For phylogenetic analysis, we searched for sequences, other than those analyzed in this study, in the GISAID database. We inferred phylogenetic relationships of sequences obtained in this study by using the maximum-likelihood method, 1,000 bootstrap values, and MEGA 7 software (*17*).

Virus Titrations

We determined virus titers of oropharyngeal and cloacal swab samples, nasal washes, and homogenized tissue samples by performing endpoint titrations in MDCK cell monolayers. We inoculated MDCK cells with 10-fold serial dilutions of each sample prepared in fetal bovine serum–free medium containing L-1-tosylamido-2-phenylethyl chloromethyl ketone–treated trypsin and penicillin/streptomycin. After a 72-hour incubation at 37°C, we detected viruses in a standard hemagglutination assay by using 0.5% turkey erythrocytes. We expressed mean virus titers as $\log_{10}$ 50% tissue culture infectious dose ($TCID_{50}$). The detection limit was 0.5 $\log_{10}$ $TCID_{50}$/mL. We estimated virus titers by using *t*-tests and 2-way analysis of variance in GraphPad Prism 9 (GraphPad Software Inc., https://www.graphpad.com).

Neuraminidase Inhibitor Resistance

We used the neuraminidase (NA) inhibitors oseltamivir and peramivir (Cayman Chemical, https://www.caymanchem.com) and zanamivir (Sigma-Aldrich, https://www.sigmaaldrich.com) to assess drug susceptibility of the 3 virus isolates. We used a fluorescence assay containing the 2′-(4-methylumbelliferyl)-α-D-*N*-acetylneuraminic acid substrate (Sigma-Aldrich) (*18*,*19*). We normalized influenza viruses to equivalent NA activities and incubated virus samples with 10-fold serial dilutions (0–30,000 nmol/L) of oseltamivir, zanamivir, or peramivir. We measured the fluorescence signal by using a Mithras LB 940 reader (Berthold Technologies, https://www.berthold.com) at excitation/emission wavelengths of 355/460 nm. We estimated the 50% inhibitory concentration (IC_{50}) for each sample from dose-response curves by using the sigmoidal, 4-parameter, logistic nonlinear regression equation in GraphPad Prism 9. To assess neuraminidase inhibitor (NAI) resistance, we divided the IC_{50} value of the virus being analyzed by the IC_{50} value of the NAI-sensitive influenza A(H1N1)pdm09 virus strain, which has the amino acid H274 in neuraminidase, making it NAI susceptible.

Experimental Infections of Mice and Ferrets

We anesthetized groups of 6-week-old BALB/c mice (SAMTAKO, http://www.samtako.com) (n = 5/

Table 1. Characteristics of highly pathogenic avian influenza A(H5N1) viruses isolated from cats, South Korea, 2023*

Virus	Origin	Passage no.†	Clade	MLD_{50}‡	Abbreviation
A/duck/Korea/H493/2022	Trachea from duck carcass	2	2.3.4.4b	$10^{4.8}$	YC/2022
A/feline/Korea/M302-6/2023	Trachea from cat carcass	2	2.3.4.4b	$10^{1.5}$	YS/2023
A/feline/Korea/M305-7/2023	Nasal swab sample from cat	2	2.3.4.4b	$10^{0.5}$	GA/2023

*MLD_{50}, 50% median lethal dose.
†Passage number of virus in embryonated eggs.
‡MLD_{50} was determined by measuring 50% tissue culture infectious dose/mL.

group) with ketamine and intranasally inoculated them with 50 μL of 10^0–10^6 $TCID_{50}$/mL of virus. After virus inoculation, we weighed the mice and monitored them for clinical signs and death for 14 days. For virus replication studies, we intranasally inoculated 15 mice per group with 50 μL of 10^3 50% median lethal dose (MLD_{50})/mL. We euthanized 5 mice per group on days 3, 5, and 7 postinoculation and assessed virus titers in brain, trachea, nasal turbinate, lung, heart, liver, kidney, spleen, and intestinal samples.

We anesthetized 20–22-week-old ferrets (IDBio, http://www.idbio.co.kr) (n = 12/group) with ketamine and intranasally inoculated them with 1 mL of 10^3 MLD_{50}/mL of virus. After virus inoculation, we weighed and monitored 3 ferrets per virus group for clinical signs and death for 14 days. We used the remaining 9 ferrets per group for virus replication studies. We euthanized 3 ferrets per virus group on days 3, 5, and 7 postinoculation and assessed virus titers in brain, trachea, nasal turbinate, lung, heart, liver, kidney, spleen, and intestinal samples. To assess virus transmission via contact infection, we intranasally inoculated 1 ferret (per virus) with 1 mL of 10^3 MLD_{50}/mL virus and then housed serologically-naive ferrets (n = 2) in the same cage the next day (1 cage/virus). We collected nasal wash samples from each ferret on days 3, 5, and 7 postinoculation and measured virus titers. We euthanized mice and ferrets showing >20% body weight loss, which we considered a humane endpoint.

Serologic Tests

We collected blood samples from ferrets in the infection groups 14 days postinfection and in the transmission groups 14 days after contact with a virus-infected ferret. We determined seroconversion by using a microneutralization assay.

Results

Genetic Characterization of H5N1 Viruses Isolated from Cats

The Korea Disease Control and Prevention Agency (KDCA) received 2 different HPAI H5N1 viruses from cats in animal shelters that were collected by APQA, which we used to characterize infections in other mammals. We used the 2 H5N1 viruses, A/feline/Korea/M302–6/2023(H5N1) from Yongsan (abbreviated as YS/2023) and A/feline/Korea/M305–7/2023(H5N1) from Gwanak (abbreviated as GA/2023), to determine how the pathogenicity and transmission of those H5N1 viruses differed from previously prevalent H5N1 viruses. We also analyzed the virus isolated from a duck, A/duck/Korea/H493/2022(H5N1) (abbreviated as YC/2022), representing the first poultry outbreak in autumn 2022.

We conducted whole-genome sequence analysis to confirm genetic characteristics of the YC/2022, YS/2023, and GA/2023 viruses and observed polybasic residues (REKRRKR/GLF) within the cleavage sites of hemagglutinin (HA), classifying all 3 viruses as HPAI. Phylogenetic analysis confirmed the viruses belonged to clade 2.3.4.4b (Table 1; Appendix Figure, https://wwwnc.cdc.gov/EID/article/30/10/24-0583-App1.pdf). YS/2023 and GA/2023 viruses shared 99.9%–100% genetic similarity (Appendix Table). They also showed close genetic relatedness to H5N1 viruses that have been circulating in wild birds and poultry in Asia since 2022, including in South Korea, China, and Japan (*15*).

We identified amino acid substitutions related to mammal adaptation in both YS/2023 and GA/2023 viruses. In both viruses, we found mutations S123P, S133A, and T156A (H5 numbering), which enhance binding affinity of the HA protein to α2,6-sialic acid on the host cell surface and contribute to increased mammal receptor tropism (*20*; J. Yang et al., unpub. data, https://doi.org/10.1101/2024.07.09.602706). In addition, in the polymerase basic 2 (PB2) gene segment, we identified mutations encoding D701N in YS/2023 and E627K in GA/2023; both substitutions are mammal-adapting mutations known to increase polymerase activity and virulence in mammals (Table 2) (*21*–*23*). However, mutations associated with antiviral drug resistance, such as H274Y in NA and S31N in the matrix protein, were not detected (*21*,*24*).

Virus Pathogenesis in a Mouse Model

We intranasally inoculated 10-fold serial dilutions of infectious dose for each virus into 6-week-old BALB/c mice. After a 2-week observation period, the MLD_{50} values were $10^{1.5}$ $TCID_{50}$/mL for YS/2023 and $10^{0.5}$ $TCID_{50}$/mL for GA/2023, whereas the MLD_{50} was

Table 2. Comparisons of major amino acid substitutions in protein segments from highly pathogenic avian influenza A(H5N1) viruses isolated from cats, South Korea, 2023*

	HA†					PB2‡				NA§	M¶
Virus	123	133	156	222	224	526	591	627	701	274	31
A/duck/Korea/H493/2022	**P**	**A**	**A**	Q	G	K	Q	E	D	H	S
A/feline/Korea/M302-6/2023	**P**	**A**	**A**	Q	G	K	Q	E	**N**	H	S
A/feline/Korea/M305-7/2023	**P**	**A**	**A**	Q	G	K	Q	**K**	D	H	S

*Bold letters indicate substitutions in each virus protein. HA, hemagglutinin; M, matrix protein; NA, neuraminidase; PB2, polymerase basic protein 2.
†H5 numbering was used. S123P, S133A, T156A, Q222L, and G224S affect α2,6-sialic acid receptor binding affinity.
‡K526R, Q591K, E627K, and D701N enhance virus replication in mammals.
§H274Y affects inhibition of NA.
¶S31N affects matrix protein inhibition.

$10^{4.8}$ $TCID_{50}$/mL for YC/2022. The 2 viruses isolated from cats had ≈10-fold difference in MLD_{50} values between them, but their MLD_{50} values were >1,000-fold lower than that of the duck isolate (Table 1; Figure 1).

To assess detailed clinical symptoms and virus replication in internal organs, we intranasally inoculated 50 μL of 10^3 MLD_{50}/mL (YS/2023, $10^{4.5}$ $TCID_{50}$/mL; GA/2023, $10^{3.5}$ $TCID_{50}$/mL; YC/2022, $10^{7.8}$ $TCID_{50}$/mL) of each virus into 6-week-old BALB/c mice (n = 15 in each group). All infected mice exhibited clinical symptoms, such as weight loss, ruffled fur, lethargy, and ataxia, within 5 days postinfection. Virus infection was confirmed in the respiratory tract of all mice on day 3 postinfection, and only viruses isolated from cats were detected in all organs (including the brain) by day 5 postinfection (Figure 2). Furthermore, all virus-infected mice had virus titers in lung, trachea, and nasal turbinate samples beginning on day 3 during the early stage of infection (Figure 2). By day 5, only mice infected with both cat isolates (YS/2023 and GA/2023) had virus titers in 9 organs; we observed high virus titers in brain, nasal turbinate, trachea, lung, and heart samples. In particular, mice infected with GA/2023 exhibited high titers in lung ($10^{5.4}$ $TCID_{50}$/mL) and trachea ($10^{5.1}$ $TCID_{50}$/mL) tissue on day 3 and in lung ($10^{4.9}$ $TCID_{50}$/mL) and brain ($10^{4.7}$ $TCID_{50}$/mL) tissue on day 5, but all mice died before day 7. Mice infected with YS/2023 had high titers ($10^{3.9}$–$10^{4.9}$ $TCID_{50}$/mL) in lung, trachea, and brain tissues on day 5 and in brain ($10^{4.8}$ $TCID_{50}$/mL) and nasal turbinate ($10^{4.25}$ $TCID_{50}$/mL) tissue on day 7. Both cat-derived virus isolates used to infect mice showed a systemic infection pattern and high lethality; high virus titers occurred in most organs, including the brain. The duck isolate, YC/2022, was detected only in the brain and respiratory organs (nasal turbinate, trachea, and lungs) by day 7; virus titers were lower than those for the cat isolates (Figure 2).

Virus Pathogenesis and Transmission in a Ferret Model

Ferrets intranasally infected with the 2 cat-derived H5N1 virus isolates showed severe clinical symptoms, including sneezing, nasal discharge, diarrhea, and neurologic complications. They also exhibited a mean peak reduction in bodyweight of 5.5%–25.7% and fever of 0.7°C–2.6°C above baseline temperature. All ferrets died by day 8 in the GA/2023 infection group and by day 9 in the YS/2023 group (100% mortality rate) (Figure 3). The ferrets infected with the GA/2023 and YS/2023 viruses showed a systemic infection pattern. In ferrets infected with GA/2023, the virus was detected in all organs except the kidneys by day 5, and virus titers of $10^{0.8}$–$10^{2.9}$ $TCID_{50}$/mL were detected in the brain and respiratory organs. Those titers were lower than titers observed in ferrets infected with YS/2023 ($10^{2.3}$–$10^{3.4}$ $TCID_{50}$/mL) that survived longer (Figure 4).

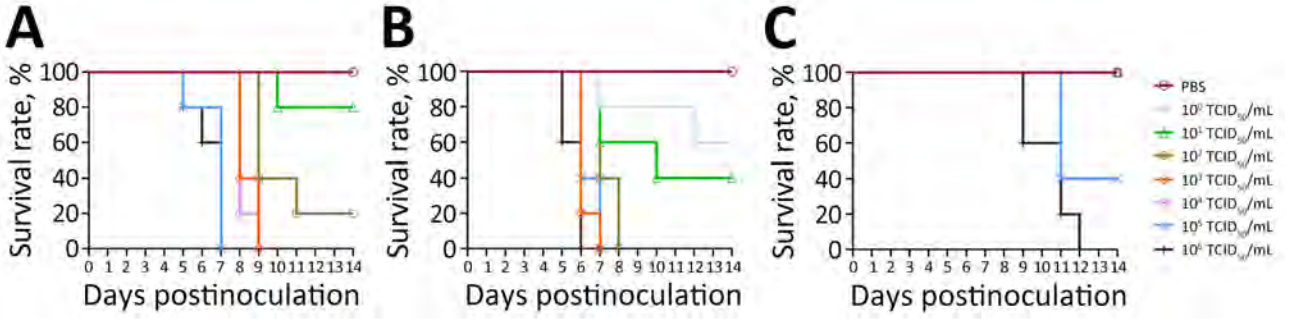

Figure 1. Survival of mice infected with highly pathogenic avian influenza A(H5N1) viruses isolated from cats in South Korea, 2023. Viruses were isolated from 2 cats and 1 duck. A) A/feline/Korea/M302-6/2023; B) A/feline/Korea/M305-7/2023; C) A/duck/Korea/H493/2022. BALB/c mice (n = 5/group) were intranasally inoculated with 10-fold serial dilutions (50 μL of 10° to 10^6 $TCID_{50}$/mL) of each H5N1 virus. PBS was used as a negative control inoculant. Mice were monitored for 14 days, and survival rates were compared. PBS, phosphate-buffered saline; $TCID_{50}$, 50% tissue culture infectious dose.

The ferrets infected with YC/2022 showed the highest virus titers in the respiratory tract ($10^{2.3}$–$10^{5.4}$ $TCID_{50}$/mL) until day 5, and infection was observed in all organs. However, 1 ferret died in the YC/2022 group on day 11, resulting in a survival rate of 66.6% (Figure 3).

To assess virus transmission via contact with YS/2023, GA/2023, and YC/2022, each virus was intranasally inoculated into 1 ferret and 2 serologically naive ferrets were moved into the same cage as the infected animal. The ferrets inoculated with either cat-derived virus died on day 8 postinoculation. In contrast, only 1 of 2 ferrets in contact with the YS/2023-infected ferret died on day 13; no seroconversion was observed in the surviving ferret. The 2 ferrets in contact with the GA/2023-infected ferret died by day 9 (100% mortality rate) (Figure 5). Virus concentrations increased ($10^{2.3}$–$10^{5.5}$ $TCID_{50}$/mL) in nasal wash samples collected from ferrets exposed to the cat-derived viruses on days 3, 5, and 7, confirming transmission and infection in naive ferrets through contact with infected animals (Figure 6). In contrast, the ferret infected intranasally with YC/2022 did not die, although the virus was detected in nasal washes. Both ferrets in that contact group survived; no virus was detected in nasal washes and no seroconversion was observed, inferring that contact transmission of YC/2022 did not occur.

Antiviral Drug Susceptibility of Influenza A(H5N1) Viruses Isolated from Cats

We experimentally analyzed NAI susceptibility to evaluate the effectiveness of existing influenza antiviral drugs against YS/2023, GA/2023, and YC/2022 viruses. We compared the IC_{50} values of the 3 viruses with that of an antiviral drug–susceptible human influenza A(H1N1)pdm09 reference virus. The high sensitivity of YS/2023, GA/2023, and YC/2022 viruses to NAIs confirmed the effectiveness of specific antiviral drugs (Table 3).

Discussion

HPAI H5N1 outbreaks continue worldwide, posing considerable threats to humans and animals. HPAI H5N1

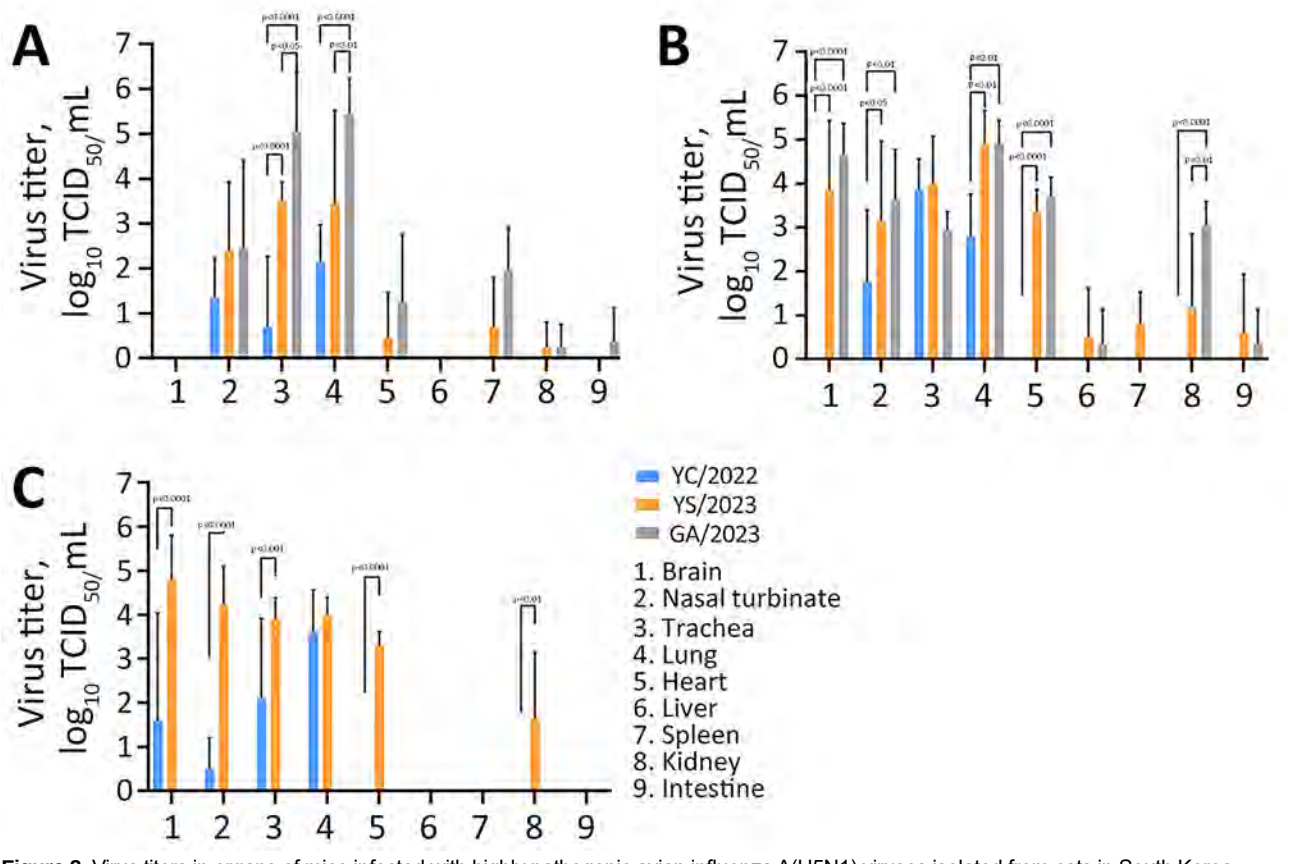

Figure 2. Virus titers in organs of mice infected with highly pathogenic avian influenza A(H5N1) viruses isolated from cats in South Korea, 2023. Viruses were isolated from 2 cats (YS/2023 and GA/2023) and 1 duck (YC/2022). BALB/c mice (n = 15/virus) were inoculated with 50 µL of 10^3 50% median lethal dose/mL of each virus; 5 mice/day from each virus group were euthanized on days 3 (A), 5 (B), and 7 (C) postinfection to measure and compare virus titers in organ tissues. GA/2023 virus titers were not measured on day 7 because all of those mice died by day 6 postinfection. p values were calculated by using 2-way analysis of variance. dpi, days postinoculation; GA/2023, A/feline/Korea/M305-7/2023; $TCID_{50}$, 50% tissue culture infectious dose; YC/2022, A/duck/Korea/H493/2022; YS/2023, A/feline/Korea/M302-6/2023.

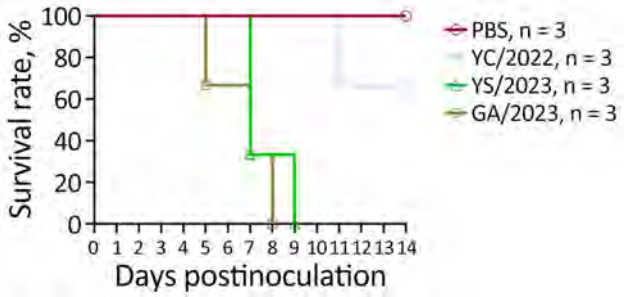

Figure 3. Survival of ferrets infected with highly pathogenic avian influenza A(H5N1) viruses isolated from cats in South Korea, 2023. Viruses were isolated from 1 duck (YC/2022) and 2 cats (YS/2023 and GA/2023). Ferrets (n = 3/group) were intranasally inoculated with 1 mL of 10^3 50% median lethal dose of each H5N1 virus; PBS was used as a negative control inoculant. Ferrets were monitored for 14 days, and survival rates were compared. GA/2023, A/feline/Korea/M305-7/2023; PBS, phosphate-buffered saline; YC/2022, A/duck/Korea/H493/2022; YS/2023, A/feline/Korea/M302-6/2023.

clade 2.3.4.4b viruses have been detected in wild birds and domestic poultry in South Korea (*14*). In addition, infection outbreaks in cats caused by HPAI H5N1 clade 2.3.4.4b viruses occurred in 2 animal shelters in South Korea during July 2023. Both H5N1 viruses isolated from cats had genetic constellations similar to that of the predominant influenza virus circulating in wild birds and poultry in South Korea during 2022–2023. An investigation of the source of infection found that the cats were infected by ingesting raw duck feed contaminated with the prevalent circulating virus. The raw feed–derived viruses were genetically identical to the poultry virus; however, the APGA found 2 mutations related to mammal adaptation (E627K and D701N) in PB2 of the isolates from cats (Y.M. Kang et al., onpub.data). Therefore, it is critical to prevent HPAI virus infections in mammals because avian-derived influenza viruses have been found to mutate after infecting mammals. We performed genetic analysis and animal model experiments to assess the potential mammal-to-mammal transmission and pathogenicity of HPAI H5N1 clade 2.3.4.4b viruses isolated from cat outbreaks in other mammals.

We analyzed 5 amino acids encoded by the HA gene segment (S123P, S133A, T156A, Q222L, and G224S). S123P, S133A, and T156A have been reported to increase mammal receptor affinity by enhancing binding to α2,6-sialic acid (*21*); however, S123P increased the affinity for α2,6-sialic acid only in the

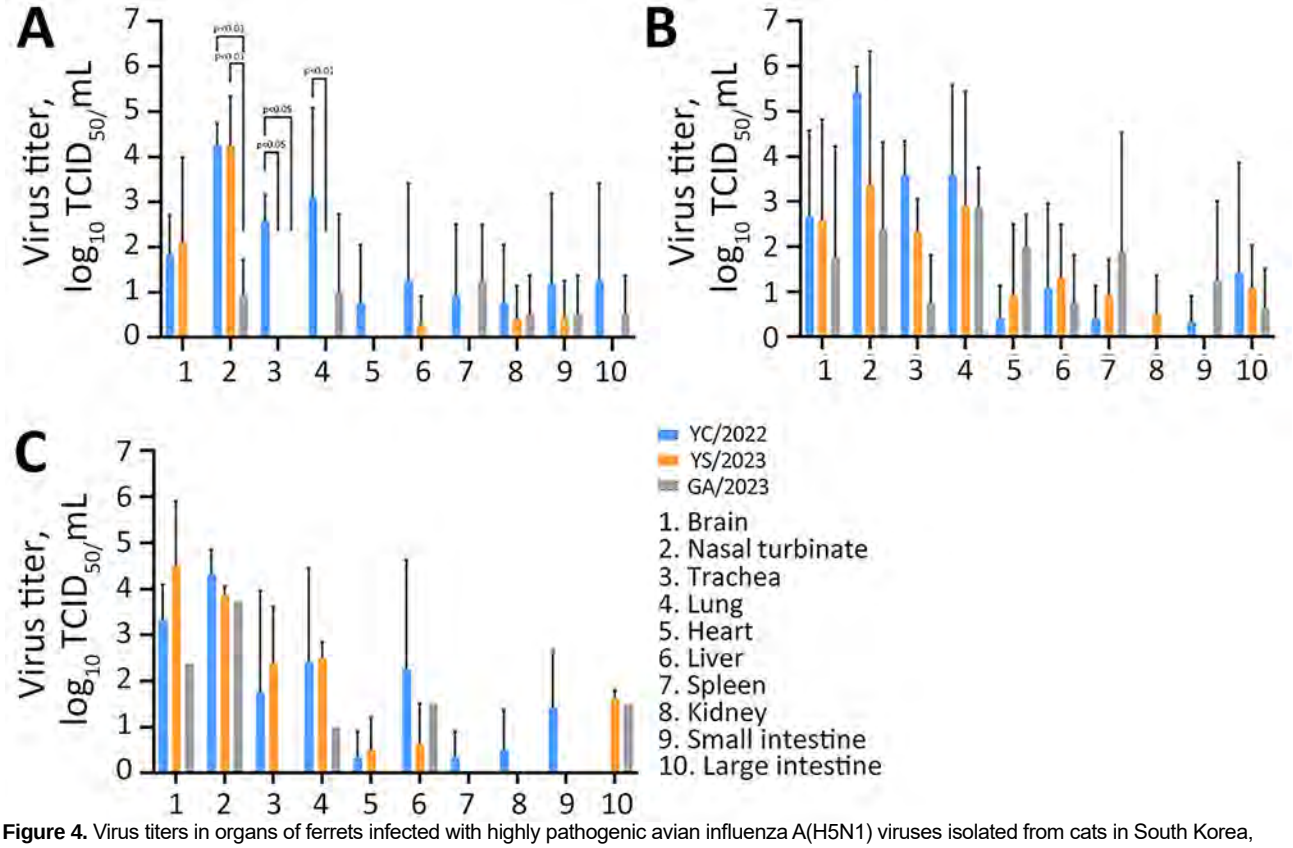

Figure 4. Virus titers in organs of ferrets infected with highly pathogenic avian influenza A(H5N1) viruses isolated from cats in South Korea, 2023. Viruses were isolated from 1 duck (YC/2022) and 2 cats (YS/2023 and GA/2023). Ferrets (n = 9/virus) were inoculated with 1 mL of 10^3 50% median lethal dose of each virus, and 3 ferrets/day from each virus group were euthanized on days 3 (A), 5 (B), and 7 (C) postinfection to measure and compare virus titers in organ tissues. p values were calculated by using 2-way analysis of variance. GA/2023, A/feline/Korea/M305-7/2023; $TCID_{50}$, 50% tissue culture infectious dose; YC/2022, A/duck/Korea/H493/2022; YS/2023, A/feline/Korea/M302-6/2023.

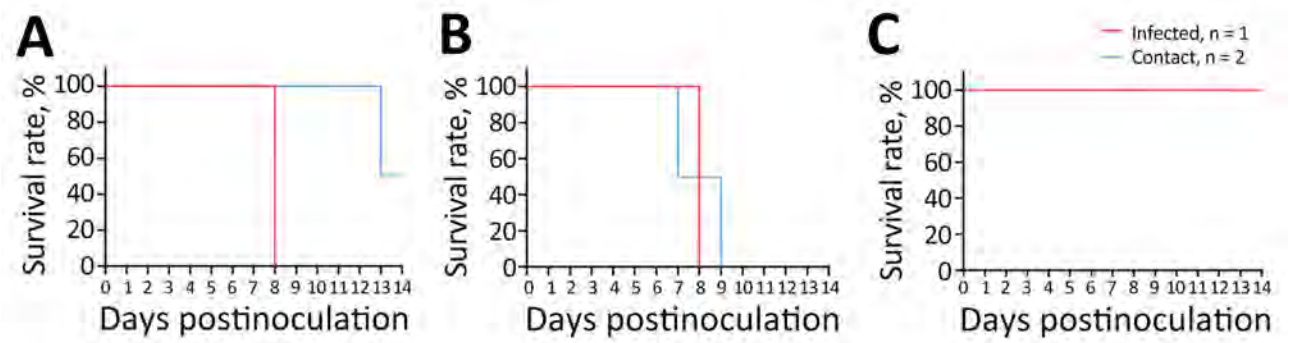

Figure 5. Survival rates after ferret-to-ferret contact transmission in study of pathogenicity of highly pathogenic avian influenza A(H5N1) viruses isolated from cats, South Korea, 2023. Viruses were isolated from 2 cats and 1 duck. A) A/feline/Korea/M302-6/2023; B) A/feline/Korea/M305-7/2023; C) A/duck/Korea/H493/2022. We intranasally inoculated 1 ferret with 1 mL of 10^3 50% median lethal dose of each virus (1 ferret/virus) and then housed serologically naive ferrets (n = 2) in the same cage the next day (1 cage/virus). Survival rates for the inoculated and naive ferrets were measured.

presence of E75K, N193K, or R437K substitutions (*20*). YC/2022, YS/2023, and GA/2023 viruses did not have E75K, N193K, or R437K substitutions. Clade 2.3.4.4b viruses have not shown increased affinity for α2,6-sialic acid, even with S133A and T156A substitutions in HA (J. Yang et al., unpub. data). We did not find the Q222L and G224S substitutions, which are associated with strong affinity for α2,6-sialic acid, in YC/2022, YS/2023, and GA/2023 viruses (*20*,*25*). Consequently, we do not consider the effects of HA mutations to be substantial for those viruses.

The H5N1 PB2 substitution E627K was observed in cats in Poland, and the PB2 D701N substitution was observed in sea lions in Argentina (*10*,*26*). According to sequence data registered in GISAID, >50% of human HPAI virus isolates exhibit E627K or D701N substitutions in PB2. Those mammal-adaptive mutations are critical factors that increase replication and virulence of H5N1 viruses in cell culture and animal experiments (*27*–*30*).

Ferrets are useful animal models to study influenza virus transmission and are frequently used for influenza pathogenicity evaluation because they exhibit influenza-like symptoms after infection, including fever, malaise, anorexia, sneezing, and nasal discharge (*31*–*33*). The H5N1 viruses isolated from cats exhibited high virus replication levels and systemic infection along with severe symptoms and high mortality rates in mice and ferrets; in addition, contact transmission among ferrets was confirmed. Therefore, it was inferred that YS/2023 and GA/2023 are highly pathogenic in mammals and are capable of mammal-to-mammal transmission. It was also presumed that the amino acid substitutions E627K and D701N in PB2, previously associated with increased replication and virulence in mammals (*29*), might be responsible for the pathogenicity and transmission of H5N1 viruses in mammals. YS/2023 and the GA/2023 are genetically similar, except for the PB2 substitutions D701N in YS/2023 and E627K in GA/2023. The GA/2023 virus with the E627K substitution showed stronger contact transmission in ferrets than the YS/2023 virus with the D701N substitution. It has been reported that the E627K substitution in PB2 of H5N1 viruses affects

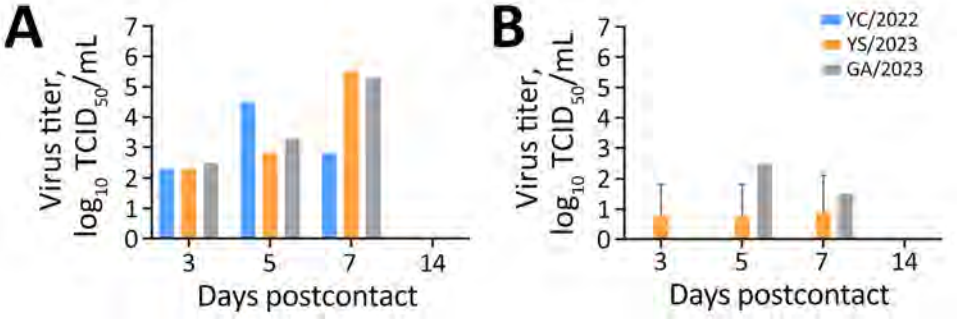

Figure 6. Virus titers after ferret-to-ferret contact transmission in study of pathogenicity of highly pathogenic avian influenza A(H5N1) viruses isolated from cats, South Korea, 2023. Virus titers were measured in nasal washes from ferrets initially inoculated with virus (A) and naive ferrets exposed to the infected ferret (B). Viruses were isolated from 2 cats (YS/2023 and GA/2023) and 1 duck (YC/2022). We intranasally inoculated 1 ferret with 1 mL of 10^3 50% median lethal dose of each virus (1 ferret/virus) and then housed serologically naive ferrets (n = 2) in the same cage the next day (1 cage/virus). To evaluate transmission of virus to naive animals, nasal wash samples were collected over time, and virus titers were measured. GA/2023, A/feline/Korea/M305-7/2023; $TCID_{50}$, 50% tissue culture infectious dose; YC/2022, A/duck/Korea/H493/2022; YS/2023, A/feline/Korea/M302-6/2023.

Table 3. Susceptibility of highly pathogenic avian influenza A(H5N1) viruses isolated from cats in South Korea, 2023, to antiviral drugs*

		Neuraminidase inhibitors					
		Oseltamivir		Zanamivir		Peramivir	
Virus	Subtype	IC_{50}, nM	Fold change	IC_{50}, nM	Fold change	IC_{50}, nM	Fold change
A/duck/Korea/H493/2022	H5N1	0.16	0.11	0.19	0.18	0.44	0.775
A/feline/Korea/M302-6/2023	H5N1	0.35	0.24	0.18	0.17	0.2	0.3
A/feline/Korea/M305/2023	H5N1	0.23	0.15	0.16	0.15	0.2	0.36
Influenza A(H1N1)pdm09	H1N1	1.47	1	1.09	1	0.57	1

*H5N1 virus from 1 duck was compared with 2 viruses isolated from cats. Fold change in drug susceptibility was measured relative to that of influenza A(H1N1)pdm09 containing the wild-type H274 amino acid in neuraminidase. IC_{50}, 50% inhibitory concentration.

airborne transmission in ferrets (*34*). Therefore, the E627K mutation might have a greater effect on transmission of the cat-derived viruses than D701N, although this possibility requires further investigation.

We compared the 2 cat-derived viruses with a duck-derived virus that occupied the same clade as the H5N1 virus circulating in poultry during 2022. However, the first limitation of our study is that direct comparisons of pathogenicity between isolates could not be completely assessed because of virus gene segmental differences. Nevertheless, it was clear that the H5N1 viruses isolated from cats were more pathogenic and transmissible among mammals than the duck-derived virus. Second, we analyzed mouse infections and contact transmission in ferrets, but we did not include an aerosol droplet transmission experiment to analyze the potential for human-to-human transmission. Consequently, assessing the public health risk to humans was also limited.

Increasing transmission of H5N1 viruses among mammals has been observed in countries in South America and in the United States. Most cases of spillover into humans have involved direct contact with infected poultry or a contaminated environment. The risk for human infection from recent outbreaks of HPAI influenza viruses in mammals, including tigers, leopards, domestic cats, domestic dogs, sea lions, and seals, has been assessed as low by the World Health Organization and other experts because of the lack of evidence for human-specific adaptive changes (*6*,*8*,*11*).

In conclusion, the increased pathogenicity and transmission among mammals observed in ferrets exposed to cat-derived HPAI H5N1 viruses indicate a need to conduct surveillance for H5N1 viruses in wild birds and mammals to prepare for potential zoonotic threats. A One Health surveillance approach is crucial, and sharing and integrating information, such as sequencing data, reference viruses, and experimental data, during outbreaks in birds and mammals are essential to prevent human HPAI H5N1 virus infections.

This work was supported by the Korea Disease Control and Prevention Agency (KDCA) (grant no. 6300-6331-301).

About the Author

Dr. Kim is a scientific deputy director of the Division of Emerging Infectious Diseases at the Korea Disease Control and Prevention Agency (KDCA). His main research interests are infectious disease and microbiology.

References

1. Lee DH, Criado MF, Swayne DE. Pathobiological origins and evolutionary history of highly pathogenic avian influenza viruses. Cold Spring Harb Perspect Med. 2021;11:a038679. https://doi.org/10.1101/cshperspect.a038679
2. Caliendo V, Lewis NS, Pohlmann A, Baillie SR, Banyard AC, Beer M, et al. Transatlantic spread of highly pathogenic avian influenza H5N1 by wild birds from Europe to North America in 2021. Sci Rep. 2022;12:11729. https://doi.org/10.1038/s41598-022-13447-z
3. Lewis NS, Banyard AC, Whittard E, Karibayev T, Al Kafagi T, Chvala I, et al. Emergence and spread of novel H5N8, H5N5 and H5N1 clade 2.3.4.4 highly pathogenic avian influenza in 2020. Emerg Microbes Infect. 2021;10:148–51. https://doi.org/10.1080/22221751.2021.1872355
4. World Health Organization. Avian influenza weekly update 2024. Human infection with avian influenza A(H5) viruses [cited 2024 Mar 8]. https://iris.who.int/handle/10665/375483
5. Centers for Disease Control and Prevention. Technical report: June 2023 highly pathogenic avian influenza A(H5N1) viruses [cited 2023 Jul 7]. https://www.cdc.gov/bird-flu/php/technical-report/h5n1-070723.html
6. Plaza PI, Gamarra-Toledo V, Euguí JR, Lambertucci SA. Recent changes in patterns of mammal infection with highly pathogenic avian influenza A(H5N1) virus worldwide. Emerg Infect Dis. 2024;30:444–52. https://doi.org/10.3201/eid3003.231098
7. Alkie TN, Lopes S, Hisanaga T, Xu W, Suderman M, Koziuk J, et al. A threat from both sides: multiple introductions of genetically distinct H5 HPAI viruses into Canada via both East Asia-Australasia/Pacific and Atlantic flyways. Virus Evol. 2022;8:veac077. https://doi.org/10.1093/ve/veac077
8. Plaza PI, Gamarra-Toledo V, Rodríguez Euguí J, Rosciano N, Lambertucci SA. Pacific and Atlantic sea lion mortality caused by highly pathogenic avian influenza A(H5N1) in South America. Travel Med Infect Dis. 2024;59:102712. https://doi.org/10.1016/j.tmaid.2024.102712
9. Gamarra-Toledo V, Plaza PI, Gutiérrez R, Inga-Diaz G, Saravia-Guevara P, Pereyra-Meza O, et al. Mass mortality of sea lions caused by highly pathogenic avian influenza A(H5N1) virus. Emerg Infect Dis. 2023;29:2553–6. https://doi.org/10.3201/eid2912.230192
10. Domańska-Blicharz K, Świętoń E, Świątalska A, Monne I, Fusaro A, Tarasiuk K, et al. Outbreak of highly pathogenic avian influenza A(H5N1) clade 2.3.4.4b virus in cats, Poland, June to July 2023. Euro Surveill. 2023;28:2300366. https://doi.org/10.2807/1560-7917.ES.2023.28.31.2300366

11. Pan American Health Organization. World Health Organization. Risk assessment for public health related to outbreaks caused by highly pathogenic avian influenza (HPAI) A(H5N1), clade 2.3.4.4b, in animal species in the region of the Americas—20 September 2023 [cited 2023 Sep 20]. https://www.paho.org/en/documents/risk-assessment-public-health-related-outbreaks-caused-highly-pathogenic-avian-influenza
12. Cha RM, Lee YN, Park MJ, Baek YG, Shin JI, Jung CH, et al. Genetic characterization and pathogenesis of H5N1 high pathogenicity avian influenza virus isolated in South Korea during 2021–2022. Viruses. 2023;15:1403. https://doi.org/10.3390/v15061403
13. Lee SH, Cho AY, Kim TH, Ahn SJ, Song JH, Lee H, et al. Novel highly pathogenic avian influenza A(H5N1) clade 2.3.4.4b virus in wild birds, South Korea. Emerg Infect Dis. 2023;29:1475–8. https://doi.org/10.3201/eid2907.221893
14. Kang YM, Heo GB, An SH, Lee YN, Cha RM, Cho HK, et al. Introduction of multiple novel high pathogenicity avian influenza (H5N1) virus of lade 2.3.4.4b into South Korea in 2022. Transbound Emerg Dis. 2023:8339427. https://doi.org/10.1155/2023/8339427
15. Lee K, Yeom M, Vu TTH, Do HQ, Na W, Lee M, et al. Characterization of highly pathogenic avian influenza A (H5N1) viruses isolated from cats in South Korea, 2023. Emerg Microbes Infect. 2024;13:2290835. https://doi.org/10.1080/22221751.2023.2290835
16. Ministry of Agriculture, Food and Rural Affairs. Feline highly pathogenic avian influenza epidemic prevention area lifted on August 21. Aug 22, 2023 [cited 2024 Jul 25]. https://www.mafra.go.kr/home/5109/subview.do?enc=Zm5jdDF8QEB8JTJGYmJzJTJGaG9tZSUyRjc5MiUyRjU2NzI1OCUyRmFydGNsVmlldy5kbyUzRnJnc0VuZGRlU3RyJTNEJTI2YmJzT3BlbldyZFNlcSUzRCUyNnBhc3N3b3JkJTNEJTI2cGFnZSUzRDEzMSUyNnJnc0JnbmRlU3RyJTNEJTI2cm93JTNEMTAlMjZiYnNDbFNlcSUzRCUyNnNyY2hDb2x1bW4lM0QlMjZpc1ZpZXdNaW5lJTNEZmFsc2UlMjZzcmNoV3JkJTNEJTI2
17. Kumar S, Stecher G, Li M, Knyaz C, Tamura K. MEGA X: molecular evolutionary genetics analysis across computing platforms. Mol Biol Evol. 2018;35:1547–9. https://doi.org/10.1093/molbev/msy096
18. Couzens L, Gao J, Westgeest K, Sandbulte M, Lugovtsev V, Fouchier R, et al. An optimized enzyme-linked lectin assay to measure influenza A virus neuraminidase inhibition antibody titers in human sera. J Virol Methods. 2014;210:7–14. https://doi.org/10.1016/j.jviromet.2014.09.003
19. Govorkova EA, Takashita E, Daniels RS, Fujisaki S, Presser LD, Patel MC, et al. Global update on the susceptibilities of human influenza viruses to neuraminidase inhibitors and the cap-dependent endonuclease inhibitor baloxavir, 2018–2020. Antiviral Res. 2022;200:105281. https://doi.org/10.1016/j.antiviral.2022.105281
20. Yamada S, Suzuki Y, Suzuki T, Le MQ, Nidom CA, Sakai-Tagawa Y, et al. Haemagglutinin mutations responsible for the binding of H5N1 influenza A viruses to human-type receptors. Nature. 2006;444:378–82. https://doi.org/10.1038/nature05264
21. Suttie A, Deng YM, Greenhill AR, Dussart P, Horwood PF, Karlsson EA. Inventory of molecular markers affecting biological characteristics of avian influenza A viruses. Virus Genes. 2019;55:739–68. https://doi.org/10.1007/s11262-019-01700-z
22. Gabriel G, Czudai-Matwich V, Klenk HD. Adaptive mutations in the H5N1 polymerase complex. Virus Res. 2013;178:53–62. https://doi.org/10.1016/j.virusres.2013.05.010
23. Medina RA, García-Sastre A. Influenza A viruses: new research developments. Nat Rev Microbiol. 2011;9:590–603. https://doi.org/10.1038/nrmicro2613
24. Holsinger LJ, Nichani D, Pinto LH, Lamb RA. Influenza A virus M2 ion channel protein: a structure-function analysis. J Virol. 1994;68:1551–63. https://doi.org/10.1128/jvi.68.3.1551-1563.1994
25. Alkie TN, Cox S, Embury-Hyatt C, Stevens B, Pople N, Pybus MJ, et al. Characterization of neurotropic HPAI H5N1 viruses with novel genome constellations and mammalian adaptive mutations in free-living mesocarnivores in Canada. Emerg Microbes Infect. 2023;12:2186608. https://doi.org/10.1080/22221751.2023.2186608
26. Rimondi A, Vanstreels RET, Olivera V, Donini A, Lauriente MM, Uhart MM. Highly pathogenic avian influenza A(H5N1) viruses from multispecies outbreak, Argentina, August 2023. Emerg Infect Dis. 2024;30:812–4. https://doi.org/10.3201/eid3004.231725
27. Subbarao EK, London W, Murphy BR. A single amino acid in the *PB2* gene of influenza A virus is a determinant of host range. J Virol. 1993;67:1761–4. https://doi.org/10.1128/jvi.67.4.1761-1764.1993
28. Van Hoeven N, Pappas C, Belser JA, Maines TR, Zeng H, García-Sastre A, et al. Human HA and polymerase subunit PB2 proteins confer transmission of an avian influenza virus through the air. Proc Natl Acad Sci USA. 2009;106:3366–71. https://doi.org/10.1073/pnas.0813172106
29. Steel J, Lowen AC, Mubareka S, Palese P. Transmission of influenza virus in a mammalian host is increased by PB2 amino acids 627K or 627E/701N. PLoS Pathog. 2009;5:e1000252. https://doi.org/10.1371/journal.ppat.1000252
30. Pulit-Penaloza JA, Brock N, Pappas C, Sun X, Belser JA, Zeng H, et al. Characterization of highly pathogenic avian influenza H5Nx viruses in the ferret model. Sci Rep. 2020;10:12700. https://doi.org/10.1038/s41598-020-69535-5
31. Bodewes R, Kreijtz JHCM, van Amerongen G, Fouchier RAM, Osterhaus ADME, Rimmelzwaan GF, et al. Pathogenesis of influenza A/H5N1 virus infection in ferrets differs between intranasal and intratracheal routes of inoculation. Am J Pathol. 2011;179:30–6. https://doi.org/10.1016/j.ajpath.2011.03.026
32. Bodewes R, Rimmelzwaan GF, Osterhaus ADME. Animal models for the preclinical evaluation of candidate influenza vaccines. Expert Rev Vaccines. 2010;9:59–72. https://doi.org/10.1586/erv.09.148
33. Thangavel RR, Bouvier NM. Animal models for influenza virus pathogenesis, transmission, and immunology. J Immunol Methods. 2014;410:60–79. https://doi.org/10.1016/j.jim.2014.03.023
34. Herfst S, Schrauwen EJA, Linster M, Chutinimitkul S, de Wit E, Munster VJ, et al. Airborne transmission of influenza A/H5N1 virus between ferrets. Science. 2012;336:1534–41. https://doi.org/10.1126/science.1213362

Address for correspondence: Eun-Jin Kim, Division of Emerging Infectious Diseases, Bureau of Infectious Disease Diagnosis Control, Korea Disease Control and Prevention Agency, 187, Osongsaengmyeong 2-ro, Osong-eup, Heungdeok-gu, Cheongju-si, Chungcheongbuk-do 28159, South Korea; email: ekim@korea.kr

Epidemiologic Quantities for Monkeypox Virus Clade I from Historical Data with Implications for Current Outbreaks, Democratic Republic of the Congo

Valentina Marziano, Giorgio Guzzetta, Ira Longini,[1] Stefano Merler[1]

We used published data from outbreak investigations of monkeypox virus clade I in the Democratic Republic of the Congo to estimate the distributions of critical epidemiological parameters. We estimated a mean incubation period of 9.9 days (95% credible interval [CrI] 8.5–11.5 days) and a mean generation time of 17.2 days (95% CrI 14.1–20.9 days) or 11.3 days (95% CrI 9.4–14.0 days), depending on the considered dataset. Presymptomatic transmission was limited. Those estimates suggest generally slower transmission dynamics in clade I than in clade IIb. The time-varying reproduction number for clade I in the Democratic Republic of the Congo was estimated to be below the epidemic threshold in the first half of 2024. However, in the South Kivu Province, where the newly identified subclade Ib has been associated with sustained human-to-human transmission, we estimated an effective reproduction number above the epidemic threshold (95% CrI 0.96–1.27).

A large outbreak of monkeypox virus (MPXV) clade I (previously known as the Congo-Basin clade) infections has been ongoing in the Democratic Republic of the Congo (DRC) since the autumn of 2023 and had caused >20,000 cases and 1,000 deaths (mostly among children <15 years of age) across the country as of May 26, 2024 (*1*). Infections with MPXV clade I have a case-fatality ratio of up to 10% (*1*; L.K. Whittles et al., unpub. data, https://www.medrxiv.org/content/10.1101/2024.04.23.24306209v1), substantially more deadly than for infections with clade IIb (formerly West African clade), which has spread internationally since 2022, mainly through sexual contact among men who have sex with men (MSM) (*2*).

Author affiliations: Center for Health Emergencies, Fondazione Bruno Kessler, Trento, Italy (V. Marziano, G. Guzzetta, S. Merler); University of Florida, Gainesville, Florida, USA (I. Longini)

DOI: https://doi.org/10.3201/eid3010.240665

The epidemiology of MPXV clade I seems to be evolving; until recently, it was mainly of zoonotic origin, and only sporadic human-to-human transmission occurred within households. Sexual transmission of MPXV clade I was observed during an outbreak investigation in Kwango Province, DRC, in March 2023 (*3*). A new subclade has been recently identified in Kamituga in the South Kivu Province, where extensive sexual transmission has been documented (*4*–*6*). Sustained human-to-human transmission, new routes of infections, and genetic evolution raise concerns about the potential risk for international spread, making estimating critical epidemiologic parameters specific to MPXV clade I urgent. In this study, we used previously published outbreak investigation data to provide novel estimates of probability distribution functions for epidemiologic parameters that are critical for monitoring and modeling the spread of MPXV clade I (K. Charniga et al., unpub. data, https://arxiv.org/abs/2405.08841).

Methods

To estimate the incubation period, we fitted 3 families of distributions (i.e., Weibull, gamma, and log-normal, with a possible offset parameter) to data from 15 cases with known incubation period (i.e., the time elapsed between the infection episode and rash onset) reported in a published study (*7*). We estimated the distribution of the serial interval (i.e., the time elapsed between the symptom onset in an index case and in their secondary cases) on the basis of 2 different datasets and considering the same 3 families of distributions. We obtained the first dataset (dataset 1) by pooling together symptom onset dates for 32 infector–infectee transmission links from 2 household

[1]These senior authors contributed equally to this article.

outbreaks in Sudan in 2005 (n = 13) (*8*) and in Central African Republic in 2021–2022 (n = 19) (*9*). The second dataset (dataset 2) consisted of 11 infector–infectee transmission links from a hospital-associated outbreak in the DRC in 2003 (*10*). In all 3 outbreaks, the chains of transmission were reconstructed through detailed epidemiologic investigations identifying the most likely infector.

We estimated the generation time (i.e., the time elapsed between the date of exposure of a confirmed case and those of their secondary cases) by considering the same data on infector–infectee pairs used for the estimate of the serial interval, following a Bayesian approach previously applied to MPXV clade IIb (*11*,*12*). The generation time was assumed to be distributed either as a gamma, a Weibull, or a log-normal function with offset; parameters of the distributions and dates of exposure for all cases were estimated within a Markov chain Monte Carlo procedure. If the sampled date of exposure for the infectee was earlier than the date of symptom onset for the infector, we considered that an episode of presymptomatic transmission.

In sensitivity analyses, we accounted for potential double interval censoring caused by the discretization of data at a 1-day resolution for the incubation period and the serial interval, and we reestimated the generation time by not allowing for presymptomatic transmission (i.e., setting a null prior for exposure dates of the infectee occurring before the symptom onset date of the infector).

We used estimates of the generation time to estimate reproduction numbers for MPXV clade I, using the time series of laboratory-confirmed mpox cases in the DRC during January 1–May 12, 2024 (*13*), and the time series of weekly hospitalized mpox case-patients (confirmed, probable, or suspected) in the Kamituga Health Zone, South Kivu Province, during late October 2023–April 21, 2024 (L.M. Masirika et al., unpub. data, https://www.medrxiv.org/content/10.1101/2024.05.10.24307057v1). The reproduction number, R_0, is defined as the average number of secondary cases per infectious person and represents a critical parameter to assess the transmissibility of an infection; when $R_0<1$, transmission is expected to fade out, whereas if $R_0>1$, the epidemic has the potential for further spread. We computed the time-varying reproduction number, R_t, representing transmissibility over time, and the effective reproduction number, R_{eff}, representing an average value of transmissibility over the study period. We used the renewal equation and the computation of the exponential growth rate of the number of cases to provide estimates (*14*–*16*) (Appendix, https://wwwnc.cdc.gov/EID/article/30/10/24-0665-App1.pdf).

Results

The best estimate for the incubation period was a Weibull distribution with an offset term of 4 days and mean of 9.9 days (95% credible interval [CrI] 8.5–11.5 days) (Figure, panel A). For the serial interval, we obtained as an optimal estimate a Weibull with an offset term of 1 day and mean of 17.5 days (95% CrI 14.1–21.5 days) for dataset 1 and a Weibull with offset 6 days and mean of 11.4 days (95% CrI 9.9–13.5 days) for dataset 2 (Figure, panel B).

The mean estimated generation time for the gamma distribution was 17.2 days (95% CrI 14.1–20.9 days) for dataset 1 and 11.3 days (95% CrI 9.4–14.0 days) for dataset 2 (Figure, panel C). For both considered datasets, presymptomatic transmission played a minor role (i.e., ≈20% of cases for dataset 1 and ≈17% of cases for dataset 2). For all parameters, variations were minimal when using the other 2 distribution families (Appendix). The distributions obtained from the sensitivity analyses accounting for potential double interval censoring and not allowing for presymptomatic transmission were practically overlapping with those from the baseline analysis (Appendix).

The mean R_t in the DRC was estimated to be under the epidemic threshold for most of 2024 (Appendix). However, the R_t estimated in Kamituga lay consistently above the epidemic threshold throughout the study period (Figure, panel D). Mean estimates for R_{eff} in Kamituga ranged from 1.08 to 1.18 (range of the 95% CrI 0.96–1.27), depending on the method and generation time considered. Additional results and full methods for the analysis are provided (Appendix).

Discussion

The estimated mean incubation period of MPXV clade I (9.9 days, 95% CrI 8.5–11.5 days) was longer than most estimates reported for MPXV clade IIb in a review by the World Health Organization (*17*) (although some of the studies reported in the review might use a different definition of incubation period [e.g., from exposure to first symptoms rather than from exposure to rash as in our data]). Available data, although limited in sample size, point to a variability in serial intervals/generation times depending on the observation settings, with cases from household outbreaks having mean values ranging from 14 to 21 days (mean 17 days) and cases from an outbreak associated to hospital cases ranging from 9 to 14 days (mean 11 days). The transmission dynamics of MPXV clade I

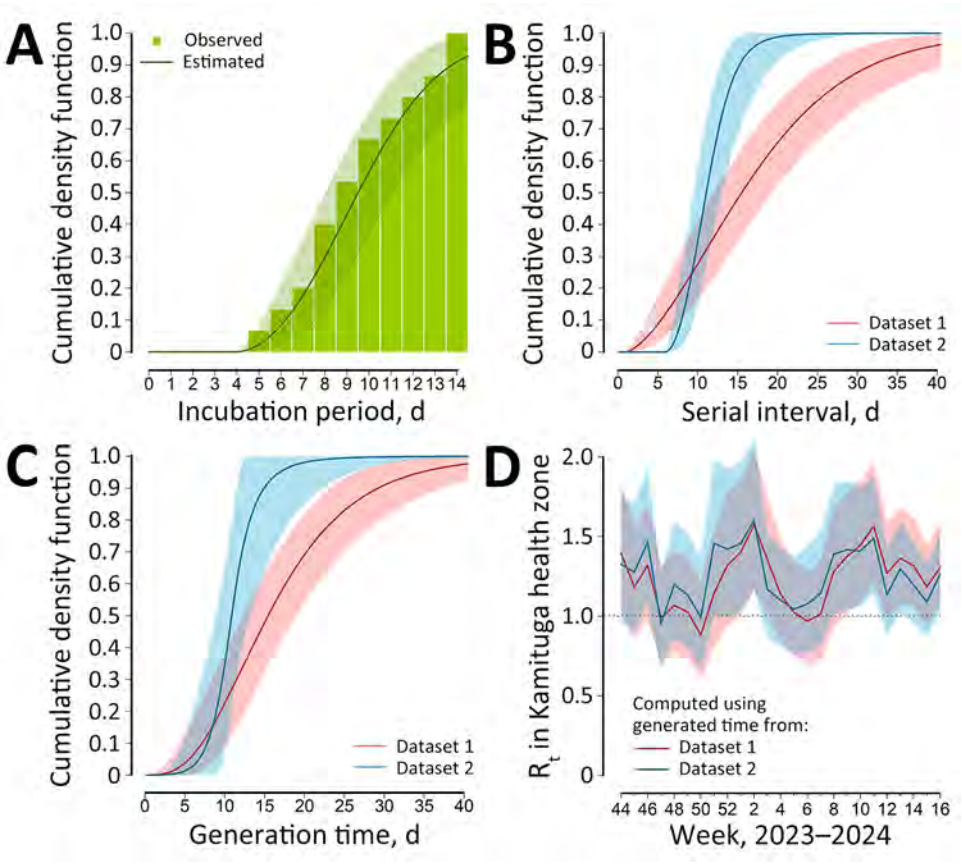

Figure. Estimates of key epidemiologic parameters for monkeypox virus clade I from historical data with implications for current outbreaks, Democratic Republic of the Congo. A) Cumulative density function of the incubation period, estimated from data on 15 cases reported in a previous study (*7*). B) Cumulative density function of the serial interval, estimated from data on 32 transmission links associated with household outbreaks (*8*,*9*), and on data on 11 transmission links associated with a hospital outbreak (*10*). C) Cumulative density function of the estimated generation time, based on the same data reported for the serial interval and on estimates of the incubation period. D) Estimates of R_t in the Kamituga Health Zone, obtained from the time-series of hospitalized cases (suspected, probable, and confirmed) (L.M. Masirika et al., unpub. data, https://www.medrxiv.org/content/10.1101/2024.05.10.24307057v1) and using the 2 estimates of the generation times. Lines indicate mean estimates; shaded areas indicate 95% credible intervals. R_t, time-varying reproduction number.

seem slower than clade IIb, for which mean estimates range from 5.6 to 9.4 days for serial intervals (*17*) and ≈12.5 days for generation times (*12*). We suggest a limited occurrence of presymptomatic transmission, on the basis of the estimated distribution of the infectious period and available data on serial intervals. This finding is again in contrast with MPXV clade IIb, for which substantial presymptomatic viral shedding and transmission has been demonstrated (*18*,*19*).

The estimated R_t for MPXV clade I in the DRC in 2024 has been hovering around values that are compatible with historical estimates of 0.75–0.86 (*20*–*22*), below the epidemic threshold of 1. However, the R_t estimated for the Kamituga Health Zone, South Kivu province, where a recently identified subclade has emerged (*5*), was above threshold; the mean value of R_{eff} was from 1.08 to 1.18 (95% CrI 0.96–1.27). This substantially higher value, compared with historical estimates, might be caused by possible viral adaptation to human transmission, as well as by higher local contact rates because of sexual transmission given the concentration of sex workers associated with the mining industry in the region (L.M. Masirika et al., unpub. data).

We acknowledge that parameter estimations could be affected by small sample sizes and by the limitations of primary studies, which makes extrapolating results to other transmission settings difficult (*7*–*10*). Further quantitative epidemiologic studies are warranted to improve the knowledge on this emerging pathogen. The precise estimation of R_t may be distorted by time-varying diagnostic delays, which shifts forward the epidemic curve and adds stochastic noise to the time series of cases. Estimation of R_t might also be affected by potential improvements in surveillance over time at the national level because of the outbreak declaration, by assumptions on the frequency of cases associated with zoonotic spillover, and by heterogeneous case definitions (laboratory-confirmed cases for the national-level curve vs. any hospitalized case for the Kamituga curve). Nonetheless, we do not expect the general conclusions to be affected by these potential biases. Estimates of the reproduction numbers might further be affected by the uncertainty of the distribution of the generation time; we note that, in principle, this distribution may be different for sexual transmission, which is currently

the main route in South Kivu. However, estimates of reproduction numbers were relatively stable when using the 2 alternative generation time distributions estimated from heterogeneous datasets.

Those results show a distinct timing of MPXV clade I epidemiology compared with MPXV clade IIb, which suggests the need for investigations into the contribution of sexual transmission and associated serial intervals and generation times, and also provides useful parameters for monitoring and modeling the transmission dynamics of MPXV clade I. Finally, if not controlled with contact tracing and vaccination, this continued relatively low-level but persistent transmission of MPXV clade I in the DRC could lead to further evolution of the virus toward higher person-to-person transmissibility and further spread beyond the current geographic focus of transmission (*23*).

This article was published as a preprint at https://www.medrxiv.org/content/10.1101/2024.05.10.24307157v1.

This research was supported by EU funding within the NextGeneration EU-MUR PNRR Extended Partnership Initiative on Emerging Infectious Diseases (project no. PE00000007, INF-ACT) received by S.M. and by funding from EU grant 101045989 VERDI received by S.M. I.L. received funding from the Epistorm: Center for Advanced Epidemic Analytics and Predictive Modeling Technology (CDC, NU38FT000013). I.L. was partially supported by cooperative agreement CDC-RFA-FT-23-0069 from the CDC's Center for Forecasting and Outbreak Analytics.

About the Author

Dr. Marziano is a researcher at the Bruno Kessler Foundation in Trento, Italy. Her primary research interests are mathematical models to investigate the epidemiology of infectious diseases, support public health decisions, and assess the effectiveness of interventions.

References

1. World Health Organization. Mpox—Democratic Republic of the Congo [cited 2024 Jun 25]. https://www.who.int/emergencies/disease-outbreak-news/item/2024-DON522
2. World Health Organization. Mpox (monkeypox) outbreak 2022 [cited 2024 Jun 25]. https://www.who.int/emergencies/situations/monkeypox-oubreak-2022
3. Kibungu EM, Vakaniaki EH, Kinganda-Lusamaki E, Kalonji-Mukendi T, Pukuta E, Hoff NA, et al.; International Mpox Research Consortium. Clade I–associated mpox cases associated with sexual contact, the Democratic Republic of the Congo. Emerg Infect Dis. 2024;30:172–6. https://doi.org/10.3201/eid3001.231164
4. Katoto PD, Muttamba W, Bahizire E, Malembaka EB, Bosa HK, Kazadi DM, et al. Shifting transmission patterns of human mpox in South Kivu, DR Congo. Lancet Infect Dis. 2024;24:e354–5. https://doi.org/10.1016/S1473-3099(24)00287-1
5. Vakaniaki EH, Kacita C, Kinganda-Lusamaki E, O'Toole Á, Wawina-Bokalanga T, Mukadi-Bamuleka D, et al. Sustained human outbreak of a new MPXV clade I lineage in eastern Democratic Republic of the Congo. Nat Med. 2024 Jun 13 [Epub ahead of print]. https://doi.org/10.1038/s41591-024-03130-3
6. Masirika LM, Udahemuka JC, Schuele L, Ndishimye P, Otani S, Mbiribindi JB, et al. Ongoing mpox outbreak in Kamituga, South Kivu province, associated with monkeypox virus of a novel clade I sub-lineage, Democratic Republic of the Congo, 2024. Euro Surveill. 2024;29:2400106. https://doi.org/10.2807/1560-7917.ES.2024.29.11.2400106
7. Nolen LD, Osadebe L, Katomba J, Likofata J, Mukadi D, Monroe B, et al. Extended human-to-human transmission during a monkeypox outbreak in the Democratic Republic of the Congo. Emerg Infect Dis. 2016;22:1014–21. https://doi.org/10.3201/eid2206.150579
8. Formenty P, Muntasir MO, Damon I, Chowdhary V, Opoka ML, Monimart C, et al. Human monkeypox outbreak caused by novel virus belonging to Congo Basin clade, Sudan, 2005. Emerg Infect Dis. 2010;16:1539–45. https://doi.org/10.3201/eid1610.100713
9. Besombes C, Mbrenga F, Malaka C, Gonofio E, Schaeffer L, Konamna X, et al. Investigation of a mpox outbreak in Central African Republic, 2021–2022. One Health. 2023;16:100523. https://doi.org/10.1016/j.onehlt.2023.100523
10. Learned LA, Reynolds MG, Wassa DW, Li Y, Olson VA, Karem K, et al. Extended interhuman transmission of monkeypox in a hospital community in the Republic of the Congo, 2003. Am J Trop Med Hyg. 2005;73:428–34. https://doi.org/10.4269/ajtmh.2005.73.428
11. Miura F, van Ewijk CE, Backer JA, Xiridou M, Franz E, Op de Coul E, et al. Estimated incubation period for monkeypox cases confirmed in the Netherlands, May 2022. Euro Surveill. 2022;27:2200448. https://doi.org/10.2807/1560-7917.ES.2022.27.24.2200448
12. Guzzetta G, Mammone A, Ferraro F, Caraglia A, Rapiti A, Marziano V, et al. Early estimates of monkeypox incubation period, generation time, and reproduction number, Italy, May–June 2022. Emerg Infect Dis. 2022;28:2078–81. https://doi.org/10.3201/eid2810.221126
13. Monkeypox in the Democratic Republic of the Congo: epidemiological situation report sitrep no. 014 (06–12 May 2024) [in French] [cited 2024 Jun 25]. https://reliefweb.int/report/democratic-republic-congo/la-variole-simienne-monkeypox-en-republique-democratique-du-congo-rapport-de-la-situation-epidemiologique-sitrep-no014-06-12-mai-2024
14. Cori A, Ferguson NM, Fraser C, Cauchemez S. A new framework and software to estimate time-varying reproduction numbers during epidemics. Am J Epidemiol. 2013;178:1505–12. https://doi.org/10.1093/aje/kwt133
15. Thompson RN, Stockwin JE, van Gaalen RD, Polonsky JA, Kamvar ZN, Demarsh PA, et al. Improved inference of time-varying reproduction numbers during infectious disease outbreaks. Epidemics. 2019;29:100356. https://doi.org/10.1016/j.epidem.2019.100356
16. Wallinga J, Lipsitch M. How generation intervals shape the relationship between growth rates and reproductive numbers. Proc Biol Sci. 2007;274:599–604.
17. World Health Organization. 2022–24 mpox (monkeypox) outbreak: global trends. Literature summary & epidemic

parameters [cited 2024 Jun 25]. https://worldhealthorg.shinyapps.io/mpx_global/#6_Literature_summary__epidemic_parameters
18. Brosius I, Van Dijck C, Coppens J, Vandenhove L, Bangwen E, Vanroye F, et al.; ITM MPOX Study Group. Presymptomatic viral shedding in high-risk mpox contacts: a prospective cohort study. J Med Virol. 2023;95:e28769. https://doi.org/10.1002/jmv.28769
19. Miura F, Backer JA, van Rijckevorsel G, Bavalia R, Raven S, Petrignani M, et al.; Dutch Mpox Response Team. Time scales of human mpox transmission in the Netherlands. J Infect Dis. 2024;229:800–4. https://doi.org/10.1093/infdis/jiad091
20. Fine PEM, Jezek Z, Grab B, Dixon H. The transmission potential of monkeypox virus in human populations. Int J Epidemiol. 1988;17:643–50. https://doi.org/10.1093/ije/17.3.643
21. Sun YQ, Chen JJ, Liu MC, Zhang YY, Wang T, Che TL, et al. Mapping global zoonotic niche and interregional transmission risk of monkeypox: a retrospective observational study. Global Health. 2023;19:58. https://doi.org/10.1186/s12992-023-00959-0
22. Charniga K, McCollum AM, Hughes CM, Monroe B, Kabamba J, Lushima RS, et al. Updating reproduction number estimates for mpox in the Democratic Republic of Congo using surveillance data. Am J Trop Med Hyg. 2024;110:561–8. https://doi.org/10.4269/ajtmh.23-0215
23. Johnson PLF, Bergstrom CT, Regoes RR, Longini IM, Halloran ME, Antia R. Evolutionary consequences of delaying intervention for monkeypox. Lancet. 2022;400:1191–3. https://doi.org/10.1016/S0140-6736(22)01789-5

Address for correspondence: Stefano Merler, Center for Health Emergencies, Bruno Kessler Foundation, Via Sommarive 18, 38123, Trento, Italy; email: merler@fbk.eu

Rapid Increase in Seroprevalence of *Borrelia burgdorferi* Antibodies among Dogs, Northwestern North Carolina, USA, 2017–2021[1]

Peyton K. Pretsch, Katherine Tyrlik-Olk, Hilary Sandborn, Dana A. Giandomenico, Alexis M. Barbarin, Carl Williams, Paul L. Delamater, Barbara Qurollo, Stephanie van der Westhuizen, Ross M. Boyce

We evaluated spatial-temporal risk for Lyme disease in northwestern North Carolina, USA, by using individual-level canine *Borrelia burgdorferi* seroprevalence data collected during 2017–2021 at routine veterinary screenings for tickborne diseases. Seroprevalence in dogs increased from 2.2% (47/2,130) in 2017 to 11.2% (339/3,033) in 2021. The percentage of incident seropositivity increased from 2.1% (45/2,130) in 2017 to 7.6% (231/3,033) in 2021. Exploratory geographic analyses found canine seroprevalence shifted from clustered (2017, Moran's *I* = 0.30) to dispersed (2021, Moran's *I* = −0.20). Elevation, slope, aspect, and forest land cover density were associated with canine seroprevalence within various household buffer regions in 2017. Slope was associated with seroprevalence at the household level in 2021. Results support the use of individual-level canine seroprevalence data for monitoring human risk for Lyme disease. Establishing sentinel veterinary clinics within Lyme disease–emergent communities might promote prevention and control efforts and provide opportunities for educational and behavioral interventions.

Lyme disease, caused primarily by infection with *Borrelia burgdorferi*, is the most frequently reported vectorborne disease in the United States, accounting for >75% of reported tickborne diseases (*1*). *B. burgdorferi* is transmitted to both humans and animals through the bite of infected *Ixodes* spp. ticks; *I. scapularis* is the primary tick vector in the eastern United States (*2*,*3*). Early during the disease course, humans typically experience rash (i.e., erythema migrans), fever, and malaise. Untreated, the disease can progress to more severe manifestations, including carditis and arthritis (*4*). Although most infections resolve after antimicrobial drug treatment, even with early and appropriate treatment, ≈15% of persons will experience posttreatment Lyme disease syndrome, characterized by chronic pain, fatigue, and cognitive impairment often described as brain fog (*5*–*7*).

The Centers for Disease Control and Prevention records ≈30,000 Lyme disease cases per year in the United States (*8*). Those data are collected through routine surveillance systems and might greatly underestimate true infection incidence (*9*–*12*). Underreporting can be caused by empirically treated but untested or frequently unreported cases, relatively complex case definitions that vary according to transmission setting, and variations in state resources dedicated to surveillance and case investigations (*10*,*11*). In the United States, Lyme disease has historically been associated with New England and upper Midwest and mid-Atlantic regions (*3*). However, studies have suggested that northern populations of *I. scapularis* ticks are expanding their geographic range southward along the Appalachian Mountains, affecting areas such as southwestern Virginia and northwestern North

Author affiliations: University of North Carolina, Chapel Hill, North Carolina, USA (P.K. Pretsch, K. Tylrik-Olk, H. Sandborn, D.A. Giandomenico, P.L. Delamater, R.M. Boyce); North Carolina Department of Health and Human Services, Raleigh, North Carolina, USA (K. Tylrik-Olk, A.M. Barbarin, C. Williams); North Carolina State University, Raleigh (B. Qurollo); Animal Hospital of Boone, Boone, North Carolina, USA (S. van der Westhuizen)

DOI: https://doi.org/10.3201/eid3010.240526

[1]Preliminary results from this study were presented at the Virginia Mosquito Control Association Annual Conference; February 14–15, 2023; Virginia Beach, Virginia, USA; and the North Carolina Mosquito and Vector Control Association Annual Meeting; November 15–17, 2023; Carolina Beach, North Carolina, USA.

Carolina (*13*–*16*). Medical providers might be less familiar with the diagnosis and management of Lyme disease in those areas, which might also contribute to underdiagnosis (*17*). Novel and more effective methods of surveillance that enable timely risk monitoring might help to overcome the prevention and awareness challenges caused by Lyme disease spread into new areas and populations. Seroprevalence among companion animals, specifically domestic dogs, has been shown to be a proxy measure for human disease risk (*18*–*21*). Although direct transmission of *B. burgdorferi* spirochetes between dogs and humans has not been reported, a pet dog would likely encounter many of the same environmental conditions that would expose humans to tick vectors (*3*,*22*). Multiple studies have shown a spatial overlap between *B. burgdorferi* seroprevalence in dogs and the incidence of human Lyme disease cases (*18*–*21*); a seroprevalence of ≥5% in dogs was reported to be a sensitive indicator for human infection risk (*20*).

In veterinary clinics, domestic dogs are tested for *B. burgdorferi* antibodies as part of their annual heartworm and tickborne disease screening, most commonly performed by using the SNAP 4DX Plus assay (IDEXX Laboratories, Inc., https://www.idexx.com) (*23*–*25*). SNAP assay data can provide a comprehensive and accessible mechanism for monitoring spatial-temporal changes in Lyme disease risk (*19*). However, research evaluating the trends of *B. burgdorferi* seroprevalence in individual dogs is limited because most studies have used aggregated, cross-sectional data to evaluate yearly state and county level trends (*19*,*20*). In contrast, a more detailed approach might provide crucial information that promotes timely identification of emerging risk areas, which could guide targeted educational campaigns and vector-control interventions.

The objective of this study was to evaluate the spatiotemporal risk for Lyme disease in northwestern North Carolina by using individual-level canine *B. burgdorferi* seroprevalence data. Specifically, we focused on Watauga County (Appendix Figure 1, https://wwwnc.cdc.gov/EID/article/29/1/22-0154-App1.pdf), which reported no Lyme disease cases in the 2020 North Carolina surveillance summary (*15*), despite being located in an area of emerging risk, according to entomologic and human surveillance reports (*13*,*15*,*16*,*26*). The contradictory nature of the data suggests that human cases might not have been reported or not identified and treated, potentially resulting in long-term adverse health consequences.

Methods

We conducted a retrospective cohort study of *B. burgdorferi* seroprevalence data collected from dogs primarily through routine screening for heartworm and tickborne disease exposure. We partnered with a large veterinary clinic that had ≈7,000 canine patients in 2021. The clinic is located in Boone, North Carolina, USA, the largest town (population ≈19,000 residents) in Watauga County (*27*). We collected data from tests completed during January 1, 2017–December 31, 2021. The University of North Carolina at Chapel Hill Institutional Review Board provided ethics approval for this study (approval no. 22–0152).

The veterinary clinic measured antibodies against *B. burgdorferi* by using the SNAP 4DX Plus assay. This point-of-care veterinary diagnostic test is an ELISA that uses the C6-peptide for detection of antibodies specifically produced during *B. burgdorferi* infections; the peptide does not cross-react with antibodies produced by canine Lyme disease vaccines (*28*,*29*). In addition, the SNAP 4DX Plus test enables simultaneous detection of *Dirofilaria immitis* antigen and antibodies against *Anaplasma phagocytophilum*, *A. platys*, *Ehrlichia canis*, and *E. ewingii* (*19*,*28*). We obtained SNAP 4DX Plus results from clinic records along with concurrent doxycycline prescriptions and client household addresses used for epidemiologic and geographic analyses.

The primary outcome measures for epidemiologic analysis were annual seroprevalence of canine *B. burgdorferi* and incident seropositivity. We defined canine *B. burgdorferi* seroprevalence as the proportion of test results positive for *B. burgdorferi* antibodies among all SNAP 4DX Plus tests completed for each year of the study period. We used incident seropositivity to measure the proportion of new *B. burgdorferi*–seropositive results that occurred among all annually completed tests and defined it as the dog's first positive result for *B. burgdorferi* antibodies detected by the SNAP 4DX Plus test over the course of the study. Unlike measures of seroprevalence, a dog could only be incident seropositive once. We evaluated annual seroprevalence and incident seropositivity for *Anaplasma* spp. as secondary epidemiologic outcomes. We considered a dog to be *Anaplasma* spp. positive if they had a positive result for *A. phagocytophilum* or *A. platys* antibodies; the SNAP 4DX Plus test does not differentiate between the 2 species. Additional secondary outcomes were *B. burgdorferi* and *Anaplasma* spp. co-positive seroprevalence and the number of doxycycline prescriptions, which we used as an estimate for symptomatic cases among dogs with a positive test result.

To explore the spatiotemporal risk for Lyme disease, we assessed geographic clustering of canine *B. burgdorferi* seroprevalence at the household level for each year. We geocoded client household addresses through Google's geocoding application programming interface. Then, environmental covariates were used in regression analyses to identify risk factors for annual canine *B. burgdorferi* seroprevalence during the first (2017) and last (2021) years of the study. Environmental risk factors of interest were elevation, slope, aspect, normalized difference vegetation index (NDVI), distance to green space, and forest, urban, and agricultural land cover densities. We derived elevation, slope, and aspect from the Shuttle Radar Topography Mission 30m digital elevation model using ArcGIS Pro version 3.1.2 (*30*). We derived NDVI from US Geological Survey Landsat 8 30m imagery from May 24, 2023 (*31*). NDVI is the difference between near-infrared (which vegetation reflects) and red light (which vegetation absorbs) and ranges from −1 (bare ground or water) to +1 (green vegetation). We collected land cover data from the National Land Cover Database through the Multi-Resolution Land Characteristics Consortium (*32*). For this study, forest land cover comprised deciduous, evergreen, and mixed forest classes; urban land cover comprised developed open space, low intensity, medium intensity, and high intensity classes; and agricultural land cover consisted of hay/pasture and cultivated crops classes.

We used prevalence differences (PDs) to quantify the change in annual canine *B. burgdorferi* seroprevalence and risk differences (RDs) to quantify the change in incident seropositivity for each year of the study, using 2017 as our referent year. To account for correlations that arise from repeated measures, we estimated absolute measures of effect (e.g., PD and RD) and corresponding 95% CIs by using binomial generalized estimating equations along with an identity link and robust variance estimators, assuming an exchangeable correlation structure (*33*–*37*). We iteratively estimated working correlation matrices by using all available pairs of nonmissing values in the moment estimators (*38*). We also used identical generalized estimating equations procedures and assumptions to calculate PDs to compare annual canine *Anaplasma* spp. seroprevalence and RDs to compare *Anaplasma* spp. incident seropositivity for each year, using 2017 as the referent group. We cross-sectionally evaluated the prevalence of *B. burgdorferi* and *Anaplasma* spp. co-positivity among all completed tests and the proportion of doxycycline prescriptions among positive test results for each year of the study. We used SAS version 9.4 (SAS Institute Inc., https://www.sas.com) to perform data analyses. We considered a p value <0.05 to be statistically significant.

We used Moran's *I* statistic, aggregated to the US census block group, to evaluate whether households with similar seroprevalence of canine *B. burgdorferi* were geographically clustered in Watauga County during 2017–2021. The metric returns a value ranging from −1 to 1; the −1 indicates perfect geographic dispersion, 0 indicates perfect geographic randomness, and 1 indicates perfect geographic clustering. Furthermore, we used bivariate ordinary least squares regression to analyze the associations between environmental characteristics and *B. burgdorferi* seroprevalence for years 2017 and 2021. To account for human and dog movement, we averaged environmental variables (except distance to the nearest national, state, or local park or forest edge) across buffer regions that had radii of 0, 0.5, 1, and 3 miles around each household. We calculated the percentages of each buffer region that had forest, urban, or agricultural cover and used them as explanatory variables. In addition, we calculated the Euclidean distances in meters from each household point location to the nearest national, state, or local park or forest edge; we collected those data by using Esri (*39*). We standardized regression coefficients, enabling comparisons of coefficient magnitudes across models by using the household buffer region of 0 miles as the referent.

Results

We identified 6,683 unique canine patients associated with 4,070 owners that had ≥1 completed SNAP 4DX Plus test during January 1, 2017–December 31, 2021. A total of 12,990 SNAP 4DX Plus test results were reported in clinic records. We excluded 649 SNAP 4DX Plus tests because either results were missing (n = 52) or testing was performed at a location outside of our partner clinic and those results were not accessible to study staff (n = 597), leaving 12,341 test results for inclusion in our analyses.

Over the entire study period, 914 (7.4%) tests were positive for *B. burgdorferi* antibodies, of which 690 (75.5%, 690/914) were defined as incident seropositive. Seroprevalence increased from 2.2% (47/2,130) in 2017 to 11.2% (339/3,033) in 2021 (PD = 9.39% [95% CI 8.12%–10.66%]) (Table 1). Incident *B. burgdorferi* seropositivity also increased; newly positive results increased from 2.1% (45/2,130) in 2017 to 7.6% (231/3,033) in 2021 (RD = 5.49% [95% CI 4.36%–6.62%]). However, when compared with 2017, the greatest increase in newly positive test results was observed in 2020 (RD = 5.82% [95% CI 4.61%–7.03%]).

Table 1. *Borrelia burgdorferi* seroprevalence and incident seropositivity among dogs screened for heartworm and tickborne diseases in Watauga County, North Carolina, USA, 2017–2021*

Year	No. tests	Seroprevalence, no. (%)	Seroprevalence difference, % (95% CI)†	Incident seropositivity, no. (%)	Risk difference, % (95% CI)†
2017	2,130	47 (2.2)	Referent	45 (2.1)	Referent
2018	2,114	77 (3.6)	1.54 (0.65–2.44)	60 (2.8)	0.71 (−0.23 to 1.65)
2019	2,447	163 (6.7)	4.83 (3.73–5.93)	145 (5.9)	3.74 (2.62–4.87)
2020	2,617	288 (11.0)	9.04 (7.76–10.31)	209 (8.0)	5.82 (4.61–7.03)
2021	3,033	339 (11.2)	9.39 (8.12–10.66)	231 (7.6)	5.49 (4.36–6.62)

*Dogs were screened by using the IDEXX SNAP 4DX Plus assay (IDEXX Laboratories, Inc., https://www.idexx.com). Seroprevalence was defined as the proportion of results positive for *Borrelia burgdorferi* antibodies among all IDEXX SNAP 4DX Plus tests completed for each year of the study. Incident seropositivity was defined as the dog's first *Borrelia burgdorferi*–positive result during the study period.
†Absolute measures of effect were analyzed by using generalized estimating equations with robust variance estimators to account to correlations that arise from repeated measures. Models assume an exchangeable correlation structure.

Among the 12,341 tests, 37 (0.3%) had a positive result for *Anaplasma* spp. antibodies, of which 35 (94.6%, 35/37) were newly positive. All *Anaplasma* s pp.–positive SNAP 4DX Plus test results in 2017, 2019, and 2020 were newly positive, yielding similar seroprevalence and incident seropositivity results within each year (Table 2). Canine *Anaplasma* spp. seroprevalence increased from 0.1% (2/2,130) in 2017 to 0.4% (12/3,033) in 2021 (PD = 0.30% [95% CI 0.04%–0.55%]). The percentage of newly positive test results increased from 0.1% (2/2,130) in 2017 to 0.3% (10/3,033) in 2021 (RD = 0.24% [95% CI −0.01%–0.48%]). The largest increase occurred in 2019; newly positive results were 0.5% (RD = 0.40% [95% CI 0.09%–0.70%]). Approximately 50% of the *Anaplasma* spp.–positive results were concurrently positive for *B. burgdorferi* (51.4% [19/37]). Of the 932 dogs that had a positive SNAP 4DX Plus result for *B. burgdorferi*, *Anaplasma* spp., or both, 391 (42.0%) were provided a concurrent doxycycline prescription.

Exploratory geographic analysis included 2,739 client households within Watauga County. Canine *B. burgdorferi* seroprevalence in 2017 appeared higher in more population-dense areas, such as Boone and the primarily residential areas south of Boone (Figure; Appendix Figure 2). In contrast, in 2021, when canine *B. burgdorferi* seroprevalence was significantly higher, we did not observe an apparent geographic correlation. The Moran's *I* values for canine *B. burgdorferi* seroprevalence were positive and significant for 2017 (p = 0.002), 2018 (p<0.001), and 2019 (p<0.001), indicating geographic clustering (Table 3). In the 2017 bivariate regression analysis (Table 4), elevation was positively associated with canine *B. burgdorferi* seroprevalence, and slope was negatively associated with seroprevalence in the 0.5-mile, 1-mile, and 3-mile buffer regions surrounding households. Aspect was positively associated with canine *B. burgdorferi* seroprevalence, and density of forest land cover was negatively associated with seroprevalence at the 3-mile level. In the 2021 bivariate regression analysis, only the slope was positively associated with canine *B. burgdorferi* seroprevalence at the household level.

Discussion

Seroprevalence and incident seropositivity of *B. burgdorferi* antibodies among domestic dogs in Watauga County, North Carolina, increased substantially from 2017 to 2021; the largest relative difference in proportions of newly positive test results occurred in 2020. Although less frequent, *Anaplasma* spp. seroprevalence and incident seropositivity also increased during 2017–2021, possibly indicating emergence of *Anaplasma spp*. in southern states. However, that result might indicate exposure to *A. platys*, which is not spread by *Ixodes* sp. ticks, unlike *A. phagocytophilum*.

Table 2. *Anaplasma* spp. seroprevalence and incident seropositivity among dogs screened for heartworm and tickborne diseases in Watauga County, North Carolina, USA, 2017–2021*

Year	No. tests	Seroprevalence, no. (%)	Seroprevalence difference, % (95% CI)†	Incident seropositivity, no. (%)	Risk difference, % (95% CI)†
2017	2,130	2 (0.1)	Referent	2 (0.1)	Referent
2018	2,114	0	NA	0	NA
2019	2,447	12 (0.5)	0.40 (0.09–0.71)	12 (0.5)	0.40 (0.09–0.70)
2020	2,617	11 (0.4)	0.32 (0.05–0.60)	11 (0.4)	0.33 (0.05–0.61)
2021	3,033	12 (0.4)	0.30 (0.04–0.55)	10 (0.3)	0.24 (−0.01 to 0.48)

*Dogs were screened by using the IDEXX SNAP 4DX Plus assay (IDEXX Laboratories, Inc., https://www.idexx.com). Seroprevalence was defined as the proportion of results positive for *Anaplasma* spp. antibodies among all IDEXX SNAP 4DX Plus tests completed for each year of the study. Incident seropositivity was defined as the dog's first *Anaplasma* spp.–positive result during the study period. A dog was considered *Anaplasma* spp. positive if it had a positive result for *Anaplasma phagocytophilum* or *Anaplasma platys* antibodies; the IDEXX SNAP 4DX Plus test does not differentiate between the 2 species. NA, not applicable.
†Absolute measures of effect were analyzed by using generalized estimating equations with robust variance estimators to account for correlations that arise from repeated measures. Models assume an exchangeable correlation structure.

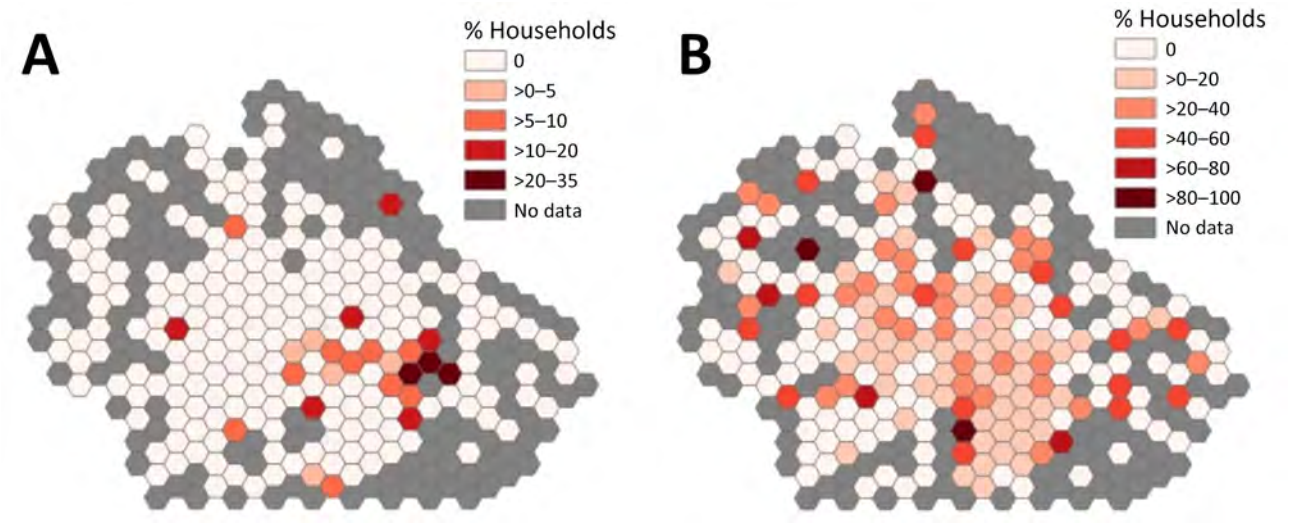

Figure. Canine *Borrelia burgdorferi* seroprevalence among surveyed households in Watauga County, North Carolina, USA, 2017–2021. Colored hexagons indicate the percentage of households with dogs positive for *B. burgdorferi* antibodies during 2017 (A) and 2021 (B). A total of 2,739 client households were included in the analysis. Seroprevalence was defined as the percentage of IDEXX SNAP 4DX Plus assay (IDEXX Laboratories, Inc., https://www.idexx.com) results that were positive for *B. burgdorferi* antibodies in dogs living within surveyed households. Lighter colors indicate areas with no or low canine *B. burgdorferi* seroprevalence; darker colors indicate areas with higher canine *B. burgdorferi* seroprevalence. Gray hexagons indicate areas with no household data.

Doxycycline was prescribed for ≈50% of dogs that had a positive test result. We used concurrent doxycycline prescriptions to measure symptomatic illness; however, this might have led to an overestimate because doxycycline could have also been prescribed for asymptomatic cases. Over the study period, canine *B. burgdorferi* seroprevalence shifted from clustering in distinct geographic areas to having no distinct clusters within the county. Moreover, the observed *B. burgdorferi* seroprevalence in 2021 (11.2%) falls within the sensitivity indicator (≥5%) for human infection risk (*20*) and is comparable to rates found in traditionally high-incidence states. For example, the Companion Animal Parasite Council reported an annual canine *B. burgdorferi* seroprevalence of 8.8% in Rhode Island, 11.9% in Connecticut, and 12.4% in Maine in 2021 (*40*). Therefore, our overall findings provide compelling evidence of change in canine *B. burgdorferi* seropositivity, supporting the conclusion that Lyme disease is rapidly emerging and is likely established in northwestern North Carolina (*14*).

Geographic analysis results were generally consistent with trends observed in the epidemiologic analysis. For example, in 2017, specific environmental factors were associated with canine *B. burgdorferi* seroprevalence, including elevation, slope, aspect, and density of forest land cover. This finding is consistent with previous research in southwestern Virginia that found associations between Lyme disease incidence and higher geographic elevation (*41*). In addition, others have found slope to be negatively associated with tick densities, and higher tick densities were associated with northerly aspects (*42*), consistent with our findings. Forest land cover density was negatively associated with *B. burgdorferi* seroprevalence in our study, consistent with a report that found Lyme disease risk was inversely related to forest patch area; small patches had higher risk because of a higher density of infected vectors (e.g., white-footed mouse) that thrive in fragmented forest areas (*43*). The absence of clustering or geographic associations seen in 2021 data suggests that Lyme disease risk is becoming widespread within the county without regard to specific environmental or ecologic factors.

Surveillance reports using human data have shown a similar Lyme disease trend in Watauga County; the number of reported human cases increased from 7 in 2017 to 31 in 2021 (*44*). However, well-documented limitations of traditional surveillance systems, such as

Table 3. Spatial autocorrelation of canine *Borrelia burgdorferi* seroprevalence among surveyed households in Watauga County, North Carolina, USA, 2017–2021*

Year	Moran's *I*	p value
2017	0.30	0.002
2018	0.38	<0.001
2019	0.38	<0.001
2020	0.10	0.207
2021	−0.20	0.128

*Number of surveyed households was 2,739. Moran's *I* values were aggregated to the US census block groups (n = 35).

Table 4. Associations between environmental characteristics and canine *Borrelia burgdorferi* seroprevalence across various household buffer regions in Watauga County, North Carolina, USA, 2017–2021*

	Buffer regions, 2017				Buffer regions, 2021			
Characteristics	Household†	0.5-mile radius	1-mile radius	3-mile radius	Household†	0.5-mile radius	1-mile radius	3-mile radius
Elevation	−0.03 (0.03)	0.07 (0.03)‡	0.06 (0.03)‡	0.06 (0.03)‡	0.00 (0.03)	0.01 (0.03)	0.02 (0.03)	0.00 (0.03)
Slope	0.00 (0.00)	−0.06 (0.03)‡	−0.06 (0.03)‡	−0.08 (0.03)§	0.01 (0.00)‡	−0.00 (0.03)	0.02 (0.03)	−0.02 (0.03)
Aspect	−0.01 (0.06)	−0.03 (0.03)	0.04 (0.03)	0.10 (0.03)¶	−0.02 (0.05)	−0.03 (0.03)	−0.01 (0.03)	−0.01 (0.03)
NDVI	0.04 (0.03)	−0.02 (0.03)	−0.03 (0.03)	−0.04 (0.03)	0.03 (0.03)	0.01 (0.03)	0.01 (0.03)	−0.00 (0.03)
Distance to green space	−0.04 (0.03)	−0.04 (0.03)	−0.04 (0.03)	−0.04 (0.03)	0.01 (0.03)	0.01 (0.03)	0.01 (0.03)	0.01 (0.03)
Forest land cover density	−0.03 (0.03)	−0.03 (0.03)	−0.07 (0.03)‡	−0.08 (0.03)§	0.01 (0.03)	0.03 (0.03)	0.01 (0.03)	−0.05 (0.03)
Urban land cover density	0.01 (0.03)	0.01 (0.03)	0.05 (0.03)	0.05 (0.03)	−0.02 (0.03)	−0.04 (0.03)	−0.02 (0.03)	0.02 (0.03)
Agriculture land cover density	0.04 (0.03)	0.03 (0.03)	0.01 (0.03)	0.05 (0.03)	0.01 (0.03)	0.05 (0.03)‡	0.04 (0.03)	0.05 (0.03)

*Values are regression coefficients (±SE). Bivariate ordinary least squares regression was performed to determine associations; coefficients were standardized, enabling magnitude comparisons of coefficients across models by using the household level as the referent. NDVI, normalized difference vegetation index.
†Household represents a buffer region radius of 0 miles.
‡p<0.05.
§p<0.01.
¶p<0.001.

underreporting, often underestimate the true risk for human infection and can, therefore, limit public health responses (*10*–*12*). Evidence of underreporting can clearly be seen during the COVID-19 pandemic, when surveillance reports from 2020 identified no human Lyme disease cases in Watauga County, despite being listed as a high-incidence North Carolina county several consecutive years before that time (*15*). This distinction is further exemplified in our findings for the year 2021, which identified 231 newly positive tests among dogs at 1 veterinary clinic in Watauga County alone compared with 31 human cases reported through traditional surveillance systems (*44*). Although data for both humans and dogs showed similar Lyme disease trends in Watauga County, monitoring changes in canine *B. burgdorferi* seroprevalence might help to overcome limitations of traditional surveillance systems by providing a more consistent, robust, and accessible data source. Furthermore, sentinel-based surveillance at veterinary clinics could be used to monitor Lyme disease risk in emergent areas at the leading edge of *Ixodes* sp. tick and *B. burgdorferi* endemicity through regular reporting of canine *B. burgdorferi* seroprevalence to local or state health departments. Observed changes in seroprevalence estimates could subsequently trigger public health interventions, such as targeted entomologic surveillance, educational efforts for clinical providers, and public awareness campaigns. Surveillance is likely to be most effective in areas where the ecology is suitable for vectors and where variations in land cover and ecologic features occur (*45*).

Most research evaluating trends in canine *B. burgdorferi* seroprevalence have used cross-sectional analysis and ecologic data (*19*,*20*). A previous observational study using data from the IDEXX Reference Laboratories network and from veterinarians who used the IDEXX VetLab Stations and software found that canine *B. burgdorferi* seroprevalence increased in North Carolina from 1.9% in 2010 to 2.3% in 2017; Watauga County was listed as 1 of the 12 counties contributing to the observed increase (*19*). Our results support and build upon those findings. However, our analysis differs because we evaluated our data on an individual level, further demonstrating the ability of canine seroprevalence to identify Lyme disease emergence into nonendemic areas, where populations might be at increased risk (*18*–*20*). By working directly with a local veterinary clinic, we obtained client addresses to further evaluate geographic risk factors associated with canine *B. burgdorferi* seroprevalence. Individual-level canine *B. burgdorferi* seroprevalence data has additional applications for human health that should be evaluated in future research. For example, knowledge of the dog's serostatus could be used to target educational and behavioral interventions for owners of *B. burgdorferi*–positive dogs, prioritizing prevention, control, and even vaccine efforts for high-risk persons. If a human Lyme disease vaccine becomes available, veterinary clinic visits could be used as an opportunity to inform the owner about the human vaccine and discuss their risk according to their dog's *B. burgdorferi* serostatus. This type of intervention might improve acceptance of human Lyme disease vaccines and could help counter vaccine hesitancy with nontraditional sources, such as veterinarians, providing education and individualized risk assessments to human clients (*46*,*47*).

Our study has notable strengths, including the use of a large individual-level dataset. However, the first limitation of our study is that we only collected data from 1 veterinary clinic within the county, which might limit the generalizability of our overall findings and interpretations. In addition, our results might also be less generalizable than previous studies that used publicly available data, which enabled larger scale analysis. However, we believe that the study population was representative of domestic dogs in Watauga County because our partner clinic is a large and established veterinary hospital in the community, completing >2,000 SNAP 4DX Plus tests annually. Second, the definition used to measure incident seropositivity might have included some dogs that were not tested before receiving their first positive result and, therefore, might not represent a true incident infection. However, we believe this number is low because of the relatively small proportion of dogs that tested positive during the first year of the study. Third, associated behavioral data was absent. Understanding the extent to which certain confounders influence *B. burgdorferi* seropositivity among dogs is crucial, especially among previously unexposed populations, where less is known about behavioral risk factors (*14*). For example, we did not collect information regarding the use of tick prevention or control products among dogs, which might influence a dog's susceptibility for infection and eventually human risk for tick exposure (*48*), although we have no reason to believe that marketing or use of those products during the study period would have changed. Future research should evaluate the extent to which covariates influence exposure and outcome relationships between humans and their pet dogs to help develop and implement community awareness and prevention campaigns in areas where Lyme disease is emerging. Furthermore, some tested dogs might have had antibodies against *B. burgdorferi* that reflect exposure from other higher transmission areas for various reasons, such as relocation of owners, recreational activities outside northwestern North Carolina (e.g., hiking, hunting), and movement of animals from breeders or shelters before residing with their current owner. Not adjusting for travel history might overestimate the human Lyme disease risk in Watauga County, especially in study years before 2020, because we believe travel might have been limited because of the COVID-19 pandemic. Future research should control for this potential bias by documenting residence and travel histories of both owners and animals.

In conclusion, our findings provide support for leveraging canine *B. burgdorferi* seroprevalence in sentinel surveillance to monitor human Lyme disease risk in Lyme disease–emergent areas. Sentinel veterinary clinics might also serve as critical partners, providing opportunities for education and individualized risk assessment delivered by trusted veterinarians. Our findings in Watauga County indicate the use of canine *B. burgdorferi* seroprevalence might help overcome limitations of traditional human surveillance systems by providing more accessible and cost-effective estimates of human Lyme disease risk.

Acknowledgments

We thank all veterinarians and staff at the Animal Hospital of Boone for their support and partnership.

Deidentified individual data that support the results will be shared beginning 9–36 months after publication of this manuscript provided the investigator who proposes to use the data has approval from an institutional review board, independent ethics committee, or research ethics board and executes a data use/sharing agreement with the University of North Carolina.

Funding was provided to R.M.B. by a Creativity Hub award from the University of North Carolina Office of the Vice Chancellor for Research. P.K.P. was supported by the Southeastern Center of Excellence in Vector Borne Diseases (cooperative agreement no. U01CK000662 from the US Centers for Disease Control and Prevention). B.Q. receives partial salary support from IDEXX Laboratories and has been a paid consultant during the development and validation of rapid assays developed by IDEXX Laboratories for veterinary medical applications.

About the Author

Ms. Pretsch is a PhD candidate at the University of North Carolina, Chapel Hill, NC, USA. Her primary research interests focus on vectorborne diseases and One Health strategies.

References

1. Rosenberg R, Lindsey NP, Fischer M, Gregory CJ, Hinckley AF, Mead PS, et al. Vital signs: trends in reported vectorborne disease cases—United States and Territories, 2004–2016. MMWR Morb Mortal Wkly Rep. 2018;67:496–501. https://doi.org/10.15585/mmwr.mm6717e1
2. Centers for Disease Control and Prevention. Lyme disease [cited 2023 Sep 24]. https://www.cdc.gov/lyme/index.html
3. Centers for Disease Control and Prevention. How Lyme disease spreads [cited 2023 Feb 13]. https://www.cdc.gov/lyme/causes
4. Centers for Disease Control and Prevention. Signs and symptoms of untreated Lyme disease [cited 2023 Sep 17]. https://www.cdc.gov/lyme/signs-symptoms
5. Centers for Disease Control and Prevention. Chronic symptoms and Lyme disease [cited 2023 Sep 17]. https://www.cdc.gov/lyme/signs-symptoms/chronic-symptoms-and-lyme-disease.html

6. Chung MK, Caboni M, Strandwitz P, D'Onofrio A, Lewis K, Patel CJ. Systematic comparisons between Lyme disease and post-treatment Lyme disease syndrome in the U.S. with administrative claims data. EBioMedicine. 2023;90:104524. https://doi.org/10.1016/j.ebiom.2023.104524
7. Aucott JN, Yang T, Yoon I, Powell D, Geller SA, Rebman AW. Risk of post-treatment Lyme disease in patients with ideally-treated early Lyme disease: a prospective cohort study. Int J Infect Dis. 2022;116:230–7. https://doi.org/10.1016/j.ijid.2022.01.033
8. Centers for Disease Control and Prevention. Lyme disease surveillance data [cited 2023 Feb 13]. https://www.cdc.gov/lyme/data-research/facts-stats/surveillance-data-1.html
9. Centers for Disease Control and Prevention. Lyme disease surveillance and data [cited 2023 Feb 13]. https://www.cdc.gov/lyme/data-research/facts-stats
10. Kugeler KJ, Schwartz AM, Delorey MJ, Mead PS, Hinckley AF. Estimating the frequency of Lyme disease diagnoses, United States, 2010–2018. Emerg Infect Dis. 2021;27:616–9. https://doi.org/10.3201/eid2702.202731
11. Schwartz AM, Kugeler KJ, Nelson CA, Marx GE, Hinckley AF. Use of commercial claims data for evaluating trends in Lyme disease diagnoses, United States, 2010–2018. Emerg Infect Dis. 2021;27:499–507. https://doi.org/10.3201/eid2702.202728
12. Nelson CA, Saha S, Kugeler KJ, Delorey MJ, Shankar MB, Hinckley AF, et al. Incidence of clinician-diagnosed Lyme disease, United States, 2005–2010. Emerg Infect Dis. 2015;21:1625–31. https://doi.org/10.3201/eid2109.150417
13. Barbarin AM, Seagle SW, Creede S. Notes from the field: four cases of Lyme disease at an outdoor wilderness camp—North Carolina, 2017 and 2019. MMWR Morb Mortal Wkly Rep. 2020;69:114–5. https://doi.org/10.15585/mmwr.mm6904a5
14. Lantos PM, Nigrovic LE, Auwaerter PG, Fowler VG Jr, Ruffin F, Brinkerhoff RJ, et al. Geographic expansion of Lyme disease in the southeastern United States, 2000–2014. Open Forum Infect Dis. 2015;2:ofv143. https://doi.org/10.1093/ofid/ofv143
15. North Carolina Department of Health and Human Services. Lyme disease surveillance summary from 2015–2020 [cited 2023 Feb 13]. https://epi.dph.ncdhhs.gov/cd/lyme/Lyme-SurveillanceSummary2020.pdf
16. North Carolina Department of Health and Human Services. Lyme disease surveillance summary from 2016–2021 [cited 2023 Feb 13]. https://epi.dph.ncdhhs.gov/cd/lyme/LymeSurveillanceSummary2021.pdf
17. Beck AR, Marx GE, Hinckley AF. Diagnosis, treatment, and prevention practices for Lyme disease by clinicians, United States, 2013–2015. Public Health Rep. 2021;136:609–17. https://doi.org/10.1177/0033354920973235
18. Little SE, Heise SR, Blagburn BL, Callister SM, Mead PS. Lyme borreliosis in dogs and humans in the USA. Trends Parasitol. 2010;26:213–8. https://doi.org/10.1016/j.pt.2010.01.006
19. Dewage BG, Little S, Payton M, Beall M, Braff J, Szlosek D, et al. Trends in canine seroprevalence to *Borrelia burgdorferi* and *Anaplasma* spp. in the eastern USA, 2010–2017. Parasit Vectors. 2019;12:476. https://doi.org/10.1186/s13071-019-3735-x
20. Mead P, Goel R, Kugeler K. Canine serology as adjunct to human Lyme disease surveillance. Emerg Infect Dis. 2011;17:1710–2. https://doi.org/10.3201/1709.110210
21. Liu Y, Nordone SK, Yabsley MJ, Lund RB, McMahan CS, Gettings JR. Quantifying the relationship between human Lyme disease and *Borrelia burgdorferi* exposure in domestic dogs. Geospat Health. 2019;14. https://doi.org/10.4081/gh.2019.750
22. Day MJ. One Health: the importance of companion animal vector-borne diseases. Parasit Vectors. 2011;4:49. https://doi.org/10.1186/1756-3305-4-49
23. Little S, Braff J, Place J, Buch J, Dewage BG, Knupp A, et al. Canine infection with *Dirofilaria immitis*, *Borrelia burgdorferi*, *Anaplasma* spp., and *Ehrlichia* spp. in the United States, 2013–2019. Parasit Vectors. 2021;14:10. https://doi.org/10.1186/s13071-020-04514-3
24. Littman MP, Gerber B, Goldstein RE, Labato MA, Lappin MR, Moore GE. ACVIM consensus update on Lyme borreliosis in dogs and cats. J Vet Intern Med. 2018;32:887–903. https://doi.org/10.1111/jvim.15085
25. American Heartworm Society. Heartworm guidelines [cited 2024 Mar 21]. https://www.heartwormsociety.org/veterinary-resources/american-heartworm-society- guidelines
26. North Carolina Digital Collections. Discovering the distribution of ticks and tickborne illness in North Carolina [cited 2024 Jul 21]. https://digital.ncdcr.gov/Documents/Detail/discovering-the-distribution-of-ticks-and-tickborne-illness-in-north-carolina/3689998
27. Data Commons. Boone [cited 2024 Feb 5]. https://datacommons.org/place/geoId/3707080
28. O'Connor TP. SNAP assay technology. Top Companion Anim Med. 2015;30:132–8. https://doi.org/10.1053/j.tcam.2015.12.002
29. Goldstein RE, Eberts MD, Beall MJ, Thatcher B, Chandrashekar R, Alleman AR. Performance comparison of SNAP 4Dx Plus and AccuPlex 4 for the detection of antibodies to *Borrelia burgdorferi* and *Anaplasma phagocytophilum*. Intern J Appl Res Vet Med. 2014;12:141–7.
30. Watkins D. 30-Meter SRTM elevation data downloader [cited 2023 Dec 13]. https://dwtkns.com/srtm30m
31. US Geological Survey. USGS EROS archive—Landsat archives—Landsat 8–9 OLI/TIRS collection 2 level-2 science products [cited 2023 Dec 13]. https://www.usgs.gov/centers/eros/science/usgs-eros-archive-landsat-archives-landsat-8-9-olitirs-collection-2-level-2
32. North Carolina State University Libraries. National land cover database (NLCD) [cited 2023 Dec 13]. https://www.lib.ncsu.edu/gis/nlcd
33. Penn State Department of Statistics. STAT 504: analysis of discrete data. 12.2—modeling binary clustered responses [cited 2023 Dec 13]. https://online.stat.psu.edu/stat504/lesson/12/12.2
34. SAS Institute Inc. Usage note 24200: when to use a nested effect in the SUBJECT= option of GENMOD's REPEATED statement [cited 2023 Dec 13]. https://support.sas.com/kb/24/200.html
35. Penn State Department of Statistics. STAT 504: analysis of discrete data. 12.1—introduction to generalized estimating equations [cited 2023 Dec 13]. https://online.stat.psu.edu/stat504/lesson/12/12.1
36. SAS Institute Inc. Usage note 24200: assessing choice of GEE working correlation structure [cited 2023 Dec 13]. https://support.sas.com/kb/23/109.html
37. Pedroza C, Truong VT. Performance of models for estimating absolute risk difference in multicenter trials with binary outcome. BMC Med Res Methodol. 2016;16:113. https://doi.org/10.1186/s12874-016-0217-0
38. SAS Institute Inc. SAS/STAT User's Guide. The GENMOD procedure: generalized estimating equations [cited 2024 Aug 30]. https://documentation.sas.com/doc/en/statcdc/14.2/statug/statug_genmod_details29.htm#statug.genmod.genmodmissinggee

39. Ersi; TomTom North America, Inc. USA parks [cited 2023 Dec 13]. https://www.arcgis.com/home/item.html?id=578968f975774d3fab79fe56c8c90941
40. Companion Animal Parasite Council. Tick borne disease agents—Lyme disease—dog [cited 2024 Feb 5]. https://capcvet.org/maps#/2021/all-year/lyme-disease/dog/united-states
41. Lantos PM, Tsao J, Janko M, Arab A, von Fricken ME, Auwaerter PG, et al. Environmental correlates of Lyme disease emergence in Southwest Virginia, 2005–2014. J Med Entomol. 2021;58:1680–5. https://doi.org/10.1093/jme/tjab038
42. Hahn MB, Jarnevich CS, Monaghan AJ, Eisen RJ. Modeling the geographic distribution of *Ixodes scapularis* and *Ixodes pacificus* (Acari: Ixodidae) in the contiguous United States. J Med Entomol. 2016;53:1176–91. https://doi.org/10.1093/jme/tjw076
43. Allan BF, Keesing F, Ostfeld RS. Effect of forest fragmentation on Lyme disease risk. Conserv Biol. 2003; 17:267–72. https://doi.org/10.1046/j.1523-1739.2003.01260.x
44. Centers for Disease and Prevention. Lyme disease case map [cited 2024 Mar 21]. https://www.cdc.gov/lyme/data-research/facts-stats/lyme-disease-case-map.html
45. Guillot C, Bouchard C, Aenishaenslin C, Berthiaume P, Milord F, Leighton PA. Criteria for selecting sentinel unit locations in a surveillance system for vector-borne disease: a decision tool. Front Public Health. 2022;10:1003949. https://doi.org/10.3389/fpubh.2022.1003949
46. Sajid A, Matias J, Arora G, Kurokawa C, DePonte K, Tang X, et al. mRNA vaccination induces tick resistance and prevents transmission of the Lyme disease agent. Sci Transl Med. 2021;13:eabj9827. https://doi.org/10.1126/scitranslmed.abj9827
47. Bézay N, Hochreiter R, Kadlecek V, Wressnigg N, Larcher-Senn J, Klingler A, et al. Safety and immunogenicity of a novel multivalent OspA-based vaccine candidate against Lyme borreliosis: a randomised, phase 1 study in healthy adults. Lancet Infect Dis. 2023;23:1186–96. https://doi.org/10.1016/S1473-3099(23)00210-4
48. Dantas-Torres F, Otranto D. Best practices for preventing vector-borne diseases in dogs and humans. Trends Parasitol. 2016;32:43–55. https://doi.org/10.1016/j.pt.2015.09.004

Address for correspondence: Peyton K. Pretsch, University of North Carolina at Chapel Hill, 130 Mason Farm Rd, CB 7030, Chapel Hill, NC 27516, USA; email: ppretsch@live.unc.edu

etymologia revisited

Dermatophilus congolensis
[dur"mə-tof'-s con-gō-len'sis]

From the Greek *derma* (skin) + *philos* (loving), *Dermatophilus congolensis* is a gram-positive, aerobic actinomycete, and facultatively anaerobic bacteria. *D. congolensis* infects the epidermis and produces exudative dermatitis termed dermatophilosis that was previously known as rain rot, rain scald, streptotrichosis, and mycotic dermatitis.

In 1915, René Van Saceghem, a Belgian military veterinarian stationed at a veterinary laboratory in the former Belgian Congo (thus, the species name *congolensis*), reported *D. congolensis* from exudative dermatitis in cattle. Local breeders and veterinarians had observed the disease since 1910, but the causal agent was not identified.

Dermatophilosis affects animals, mainly cattle, and more rarely humans. Outbreaks of *D. congolensis* infection have severe economic implications in the livestock and leather industries.

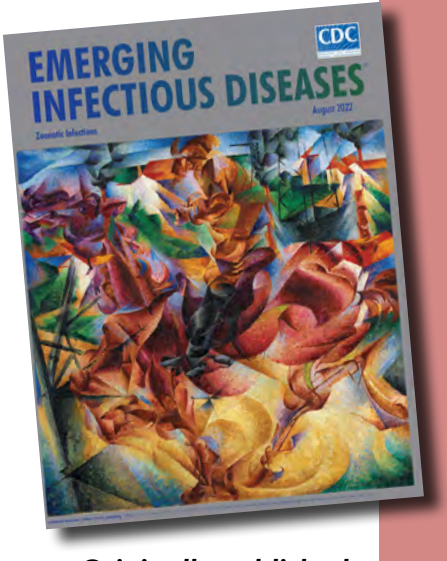

Originally published in August 2022

Sources

1. Amor A, Enríquez A, Corcuera MT, Toro C, Herrero D, Baquero M. Is infection by *Dermatophilus congolensis* underdiagnosed? J Clin Microbiol. 2011;49:449–51. https://doi.org/10.1128/JCM.01117-10
2. Branford I, Johnson S, Chapwanya A, Zayas S, Boyen F, Mielcarska MB, et al. Comprehensive molecular dissection of *Dermatophilus congolensis* genome and first observation of *tet*(z) tetracycline resistance. Int J Mol Sci. 2021;22:7128. https://doi.org/10.3390/ijms22137128
3. Dorland's illustrated medical dictionary. 32nd ed. Philadelphia: Elsevier Saunders; 2012.
4. Van Saceghem R. Contagious skin disease (contagious impetigo) [in French]. Bull Soc Pathol Exot. 1915;8:354–9.

https//wwwnc.cdc.gov/eid/article/28/8/et-2808_article

Virulence of *Burkholderia pseudomallei* ATS2021 Unintentionally Imported to United States in Aromatherapy Spray

Christopher K. Cote, Kevin D. Mlynek, Christopher P. Klimko, Sergei S. Biryukov, Sherry Mou, Melissa Hunter, Nathaniel O. Rill, Jennifer L. Dankmeyer, Jeremy A. Miller, Yuli Talyansky, Michael L. Davies, J. Matthew Meinig, Stephanie A. Halasohoris, Annette M. Gray, Jade L. Spencer, Ashley L. Babyak, M. Kelly Hourihan, Bobby J. Curry, Ronald G. Toothman, Sara I. Ruiz, Xiankun Zeng, Keersten M. Ricks, Tamara L. Clements, Christina E. Douglas, Suma Ravulapalli, Christopher P. Stefan, Charles J. Shoemaker, Mindy G. Elrod, Jay E. Gee, Zachary P. Weiner, Ju Qiu, Joel A. Bozue, Nancy A. Twenhafel, David DeShazer

In the United States in 2021, an outbreak of 4 cases of *Burkholderia pseudomallei*, the etiologic agent of melioidosis and a Tier One Select Agent (potential for deliberate misuse and subsequent harm), resulted in 2 deaths. The causative strain, *B. pseudomallei* ATS2021, was unintentionally imported into the United States in an aromatherapy spray manufactured in India. We established that ATS2021 represents a virulent strain of *B. pseudomallei* capable of robust formation of biofilm at physiologic temperatures that may contribute to virulence. By using mouse melioidosis models, we determined median lethal dose estimates and analyzed the bacteriologic and histopathologic characteristics of the organism, particularly the potential neurologic pathogenesis that is probably associated with the $bimA_{Bm}$ allele identified in *B. pseudomallei* strain ATS2021. Our data, combined with previous case reports and the identification of endemic *B. pseudomallei* strains in Mississippi, support the concept that melioidosis is emerging in the United States.

In the United States, melioidosis is an emerging infectious disease caused by *Burkholderia pseudomallei* (*1*,*2*). In melioidosis-endemic areas, the bacterium causes pneumonia and fatal bacteremia with diverse mortality rates that depend on the standard of care provided, patient risk factors (e.g., diabetes), and extent and location of the infection (*3*,*4*). Melioidosis clinical manifestation ranges from asymptomatic to acute pulmonary severe illness or chronic infection (*1*). In a subset of patients (1.5%–5%), *B. pseudomallei* infection leads to serious neurologic melioidosis (*5*,*6*). Clinical signs/symptoms are fever, headache, seizures, unilateral weakness, paralysis, encephalomyelitis, and brain abscesses. Treatment duration is typically ≥6 months and includes an intravenous intensive phase and an oral eradication phase (*7*). Most cases of neurologic melioidosis are reported in the melioidosis-endemic areas of Australia and India (*8*–*10*).

In 2021, melioidosis was confirmed in 4 patients in the United States who had not traveled internationally (*11*). Whole-genome sequencing and epidemiologic investigations linked the clonal isolates of *B. pseudomallei* ATS2021 from all 4 patients to an aromatherapy spray imported from India. Neurologic melioidosis affected 2 of the patients; 1 died and 1 experienced long-term sequelae (*11*). Of the 2 cases of melioidosis that were not shown to have substantial neurologic

Author affiliations: United States Army Medical Research Institute of Infectious Diseases, Fort Detrick, Frederick, Maryland, USA (C.K. Cote, K.D. Mlynek, C.P. Klimko, S.S. Biryukov, S. Mou, M. Hunter, N.O. Rill, J.L. Dankmeyer, J.A. Miller, Y. Talyansky, M.L. Davies, J.M. Meinig, S.A. Halasohoris, A.M. Gray, J.L. Spencer, A.L. Babyak, M.K. Hourihan, B.J. Curry, R.G. Toothman, S.I. Ruiz, X. Zeng, K.M. Ricks, T.L. Clements, C.E. Douglas, S. Ravulapalli, C.P. Stefan, C.J. Shoemaker, J. Qiu, J.A. Bozue, N.A. Twenhafel, D. DeShazer); Centers for Disease Control and Prevention, Atlanta, Georgia, USA (M.G. Elrod, J.E. Gee, Z.P. Weiner)

DOI: https://doi.org/10.3201/eid3010.240084

involvement, 1 was fatal and the other patient recovered. In addition, a pet raccoon that had direct contact with the contaminated spray exhibited neurologic signs approximately 2 weeks after contact with the contaminated spray and 3 days before death. Although viable bacteria were not recovered from the carcass, tissue samples were positive by PCR for *B. pseudomallei* DNA and provide support that the likely cause of death was neurologic melioidosis (*12*).

Inhaled *B. pseudomallei* can enter the central nervous system (CNS) through several portals (*13*–*15*). Previous studies in mice demonstrated colonization at the nasal mucosa-associated lymphoid tissue and the olfactory epithelium (*16*). Tracking *B. pseudomallei* after intranasal exposure demonstrates that the bacterium crosses the respiratory epithelium, but invasion likely requires that the olfactory epithelium be previously damaged (*16*). Neurologic disease is associated with the *Burkholderia* intracellular motility factor A (BimA) (*17*,*18*), a protein that is essential for actin-based motility, enabling intracellular movement and evasion of the immune system (*18*). Although all *B. pseudomallei* strains possess *bimA*, a subset encodes a variant gene ($bimA_{Bm}$) that is 95% homologous to the gene in the closely related *Burkholderia mallei*, which correlates with neurologic involvement (*8*,*18*). In our study, we characterized *B. pseudomallei* ATS2021 and laid the groundwork for using that strain to test medical countermeasures against melioidosis.

Materials and Methods

Growth Curve Determinations

B. pseudomallei strains were grown in either Luria broth with 4% glycerol (LBG), 4% glycerol, 1% tryptone, 5% NaCl broth (GTB), M9 (minimal medium) + 2 % glucose, (M9G), or M9G + 0.5% casamino acids (M9GC). We resuspended strains from an overnight broth culture to a 600 nm optical density (OD_{600}) of 0.5 in brain–heart infusion broth. We diluted suspensions 1:10 into a 96-well microtiter plate, grew them in a Spark (Tecan Group, https://www.tecan.com) microplate reader shaken at 37°C for ≈36 hours, and measured OD_{600} hourly. We obtained data by subtracting the value of the respective medium-only control from the measured OD_{600}.

Biofilm Assay

We used crystal violet staining to measure biofilm. We resuspended *B. pseudomallei* overnight broth cultures to an OD_{600} of ≈0.2 in phosphate-buffered saline (PBS) and diluted the bacterial suspensions 1:10 into LBG, GTB, M9G, or M9GC in CoStar polystyrene 96-well plates, incubated at room temperature or 37°C for 24 or 48 hours. Before staining, we measured the OD_{600}, after which we aspirated plates, washed 3 times with PBS to remove planktonic cells, and fixed with 100% ethanol for 30 minutes at room temperature. After fixing the samples in ethanol, we added 0.1% (wt/vol) crystal violet to each well for 15 minutes, and washed 3 times with PBS, after which we solubilized the remaining stain in 33% acetic acid. To quantify staining as an indicator of biofilm formation, we measured the OD_{600}. When necessary, we diluted samples in 33% acetic acid to ensure that readings were within linear range. We averaged ≥3 technical replicates in each experiment. Data reported are the result of ≥4 individual experiments.

Mouse Exposure to Aerosolized Bacteria

We started cultures by inoculating GTB with frozen bacterial stocks and growing them at 37°C while shaken at 200 rpm. We estimated bacterial concentrations by 620 nm OD (OD_{620}) and then determined CFU by growing *B. pseudomallei* on sheep blood agar plates (Remel; Thermo Fisher Scientific, https://www.thermofisher.com). We exposed mice to aerosolized *B. pseudomallei* ATS2021 at increasing concentrations in a whole-body aerosol exposure chamber equipped with the automated Biaera particle generator (*19*). The small-particle aerosol size diameter is ≈1–3 μm. To estimate inhaled doses, we serially diluted samples collected by using an all-glass impinger onto sheep blood agar plates (*20*).

Mouse 50% Lethal Dose Determinations and Bacterial Burden

At the time of exposure to aerosolized *B. pseudomallei*, female C57BL/6 and BALB/c mice (Charles River Laboratory) were 7–9 weeks of age. We exposed 48 C57BL/6 mice to 5 aerosolized doses of *B. pseudomallei* (Table). To calculate the 50% lethal dose (LD_{50}), we observed a subset of those mice for clinical signs for 60 days after exposure. We serially euthanized other mice for histopathologic and bacteriologic analyses. We also determined LD_{50} for BALB/c mice.

Capsule Detection

We detected *B. pseudomallei* capsular polysaccharide (CPS) in brain homogenates by using an antigen capture immunoassay developed on the Magpix platform (Thermo Fisher Scientific). We coupled *Burkholderia* CPS antibody, 4C4 (*21*), to magnetic beads by using a Luminex xMap kit and biotinylated by using an EZ-link Sulfo-NHS-LC-Biotin kit (Thermo Fisher Scientific). We added 4C4-coupled beads (2,500 beads/well), and 50 μL of study samples diluted 1:20 in 5%

skim milk in PBS with 0.5% Tween-20 (mixture called SM) to white, round-bottom 96-well plates and incubated for 1 hour with shaking. We washed the wells 3 times with 100 µL of PBS-T (PBS with Tween 20) before adding 50 µL of 4 µg/mL of biotinylated 4C4 in SM. After incubating the wells for 1 hour, we washed them before adding 50 µL of 10 µg/mL streptavidin phycoerythrin in SM. After the wells were incubated for 30 minutes, we washed the beads, resuspended then in 100 µL of PBS-T, and read them by using the Magpix instrument. We considered samples with a median fluorescent intensity 2-fold over naive brain homogenate to be positive.

Histopathologic Analyses

We examined a subset of mice histopathologically (Appendix 1 Table 1, https://wwwnc.cdc.gov/EID/article/30/10/24-0084-App1.pdf). We performed necropsies and processed the tissues after they had been in 10% buffered formalin for 21 days. We produced tissue blocks and slides and stained them with hematoxylin and eosin. We performed immunohistochemistry (IHC) on select animals by using the BOND RX Automated Stainer (Leica Biosystems, https://www.leicabiosystems.com). We used a rabbit polyclonal *Burkholderia* antibody (antibody no. 351; US Army Medical Research Institute of Infectious Diseases) at a dilution of 1:5,000. We counterstained the sections with hematoxylin and applied coverslips.

RNA Extraction and Nanostring Data Collection

We inactivated all brain homogenates with a 3:1 ratio of TRIzol LS (Thermo Fisher Scientific) and extracted total RNA as previously reported (*22*). We collected host gene expression data by using the nCounter mouse Neuroinflammation Panel on the SPRINT Profiler platform (NanoString Inc, https://nanostring.com). The panel consists of 770 genes spanning 23 neuroinflammation pathways and processes. In brief, we added 70 µL of hybridization buffer to the reporter code set to make a master mixture. We added 8 µL of the master mixture to 50 ng of extracted host RNA and 2 µL of the capture code set, incubated it at 65°C for 17 hours, and then incubated at 4°C until the samples were placed on a NanoString SPRINT Profiler and total fluorescent counts corresponding to target binding were collected. We extracted gene expression analysis and cell profiling data from Nanostring RCC files and analyzed by using the ROSALIND Bioinformatics suite (https://rosalind.bio). We generated normalized counts by using criteria provided by NanoString. ROSALIND follows the nCounter Advanced Analysis protocol (NanoString) of dividing counts within a lane by the geometric mean of the normalizer probes from the same lane. Housekeeping probes to be used for normalization are selected based on the geNorm algorithm as implemented in the NormqPCR R library1 (*23*). Unless otherwise noted, we based significance of differentially expressed genes on them passing a filter greater than ±1.5-fold linear threshold and an adjusted $p \leq 0.05$ relative to brain homogenates from an unchallenged mouse group. We based cell profiling data for oligodendrocytes on abundance scores provided by the ROSALIND NanoString Cell Type Profiling Module. We performed statistical analyses

Table. Median lethal dose of aerosolized *Burkholderia pseudomallei* ATS2021 in C57BL/6 and BALB/c mice*

Mice†	Day	Inhaled dose	LD_{50} (95% CI)	TTD median (95% CI)	TTD mean (SE)
C57BL/6	21	9.9×10^{-1}	56.4 CFU (21.3–150.2)	>21	>21
		1.32×10^{1}		>21	16.5 (0.7)
		1.07×10^{2}		18.0 (11.0–NC)	15.9 (0.9)
		1.15×10^{3}		4.0 (3.0–5.0)	4.4 (0.3)
		4.49×10^{3}		3.0 (NC)	3.1 (0.1)
	60	9.9×10^{-1}	5.8 CFU (2.0–15.1)	>60	51.0 (NC)
		1.32×10^{1}		41.5 (12.0– NC)	39.3 (5.6)
		1.07×10^{2}		18.0 (11.0–26.0)	20.9 (3.2)
		1.15×10^{3}		4.0 (3.0–5.0)	4.4 (0.3)
		4.49×10^{3}		3.0 (NC)	3.1 (0.1)
BALB/c	21	4.00×10^{-1}	4.1 CFU (1.8–11.3)	>21	4.0 (NC)
		2		>21	4.9 (0.1)
		2.05×10^{1}		4.0 (3.0 –4.0)	4.3 (0.3)
		1.86×10^{2}		3.0 (NC)	3.1 (0.1)
		9.60×10^{2}		3.0 (2.0–3.0)	2.9 (0.1)
	60	4.00×10^{-1}	4.1 CFU (1.8–11.3)	>60	4.0 (NC)
		2		>60	4.9 (0.1)
		2.05×10^{1}		4.0 (3.0–4.0)	4.3 (0.3)
		$1.86E \times 10^{2}$		3.0 (NC)	3.1 (0.1)
		9.60×10^{2}		3.0 (2.0–3.0)	2.9 (0.1)

*LD_{50}, 50% lethal dose; NC, noncalculable; TTD, time to death or euthanasia in accordance with early intervention criteria.
†Female; 7–9 weeks of age at time of exposure to aerosolized bacteria.

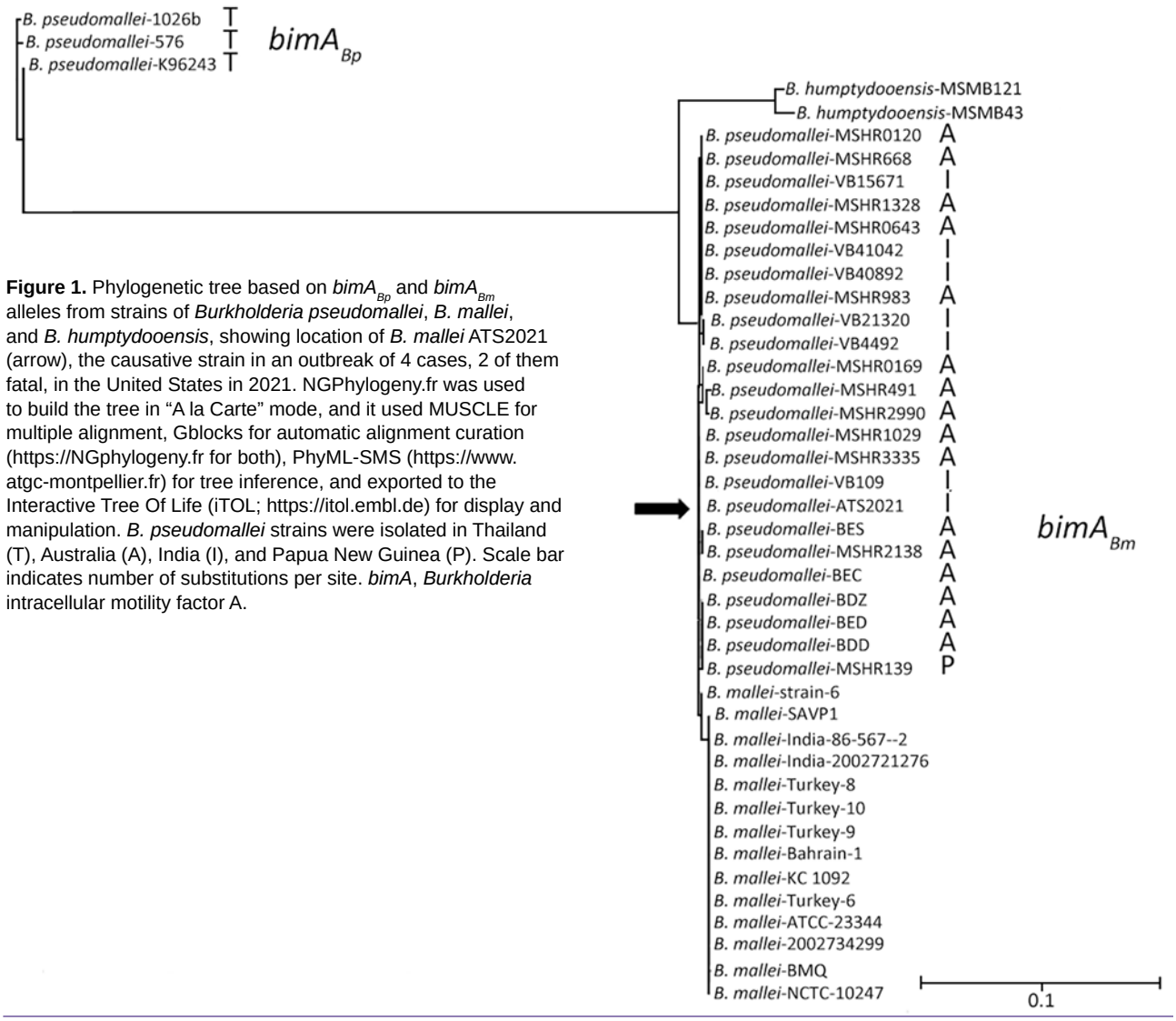

Figure 1. Phylogenetic tree based on *bimA*$_{Bp}$ and *bimA*$_{Bm}$ alleles from strains of *Burkholderia pseudomallei*, *B. mallei*, and *B. humptydooensis*, showing location of *B. mallei* ATS2021 (arrow), the causative strain in an outbreak of 4 cases, 2 of them fatal, in the United States in 2021. NGPhylogeny.fr was used to build the tree in "A la Carte" mode, and it used MUSCLE for multiple alignment, Gblocks for automatic alignment curation (https://NGphylogeny.fr for both), PhyML-SMS (https://www.atgc-montpellier.fr) for tree inference, and exported to the Interactive Tree Of Life (iTOL; https://itol.embl.de) for display and manipulation. *B. pseudomallei* strains were isolated in Thailand (T), Australia (A), India (I), and Papua New Guinea (P). Scale bar indicates number of substitutions per site. *bimA*, *Burkholderia* intracellular motility factor A.

and graphing for host gene expression on Graphpad Prism 9.4.0 (https://www.graphpad.com).

Statistical Analyses

We analyzed biofilm data analyzed by using a linear mixed effects model implemented in the GLIMMIX procedure of SAS version 9.4 (SAS Institute Inc., https://www.sas.com). We did not apply multiplicity adjustment. We estimated LD_{50} under a probit model with log_{10} transformation of the dose variable and obtained LD_{50} pairwise comparisons by using nonlinear mixed model on the log_{10} dose scale. We estimated median time to death or euthanasia in accordance with early endpoint euthanasia criteria and accompanying confidence limits, mean time to death, and SE by using Kaplan-Meier survival methods. We determined correlation between in vitro biofilm production and in vivo virulence by using Spearman rank order analyses. We performed analysis in SAS version 9.4.

Results

Genetic Analyses and Molecular Virulence Determinants of ATS2021

The ATS2021 whole-genome shotgun sequencing project was available in GenBank (accession no. JASCQT000000000.1). We examined the genetic sequence of known *B. pseudomallei* surface-associated virulence determinants, including the 6-deoxyheptan CPS (*24*), the lipopolysaccharide O-antigen (*25*), and the cluster 1 type 6 secretion system (*26*). Those gene clusters exhibited ≈99% identity with the corresponding gene clusters in the prototypic strain

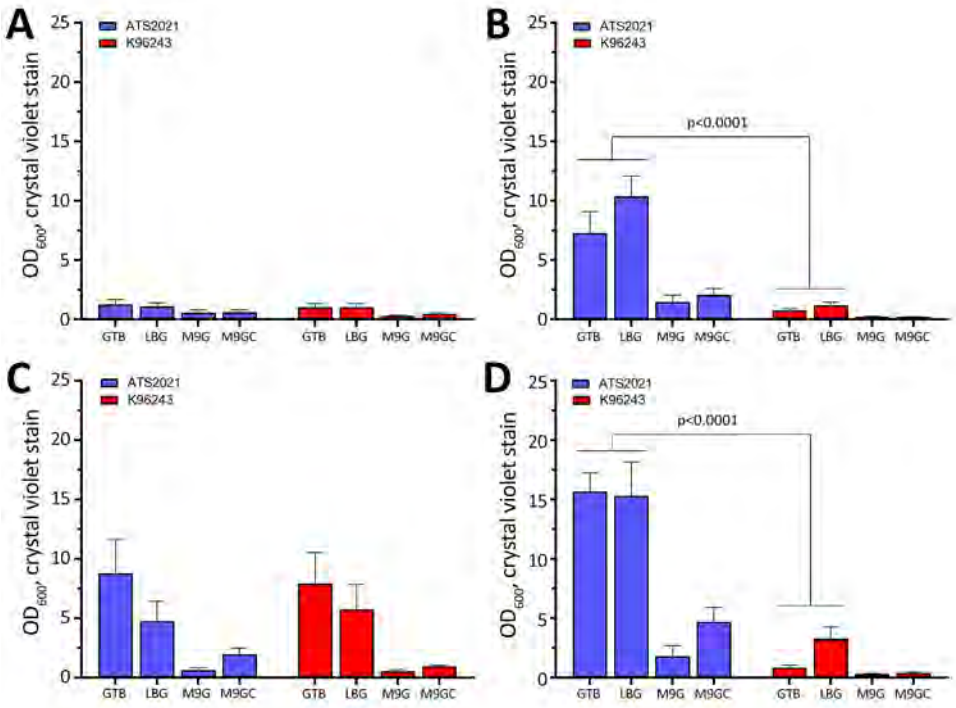

Figure 2. Biofilm formation of *Burkholderia pseudomallei* strains ATS2021, the causative strain in an outbreak of 4 cases, 2 of them fatal, in the United States in 2021, and K96243 under multiple test conditions. Biofilm formation of both strains was assessed by crystal violet staining as measured by OD_{600}. A) One day at room temperature; B) 1 day at 37°C; C) 2 days at room temperature; D) 2 days at 37°C. Error bars represent the SEs from mean values determined from 3 separate assays. p values determined by linear mixed effects model. M9G, M9 + glucose; M9GC, 0.2% glucose to M9 and casamino acids; OD_{600}, optical density at 600 nm.

B. pseudomallei K96243 (*27*). In addition, immunoblot analysis with specific antibodies demonstrated the production of CPS and type A lipopolysaccharide O-antigen when ATS2021 was grown in vitro (data not shown). Petras et al. recently revealed that ATS2021 harbors a *bimA* gene that closely resembles the *bimA* gene found in *B. mallei*, the etiologic agent of glanders (*12*). The *bimA* gene encodes a trimeric autotransported protein that mediates actin-based motility in infected host cells (*28*). Most *B. pseudomallei* strains from environmental or clinical sources contain the $bimA_{Bp}$ allele, but a relatively small number of strains possess the $bimA_{Bm}$ allele and are often isolated from patients with neurologic melioidosis

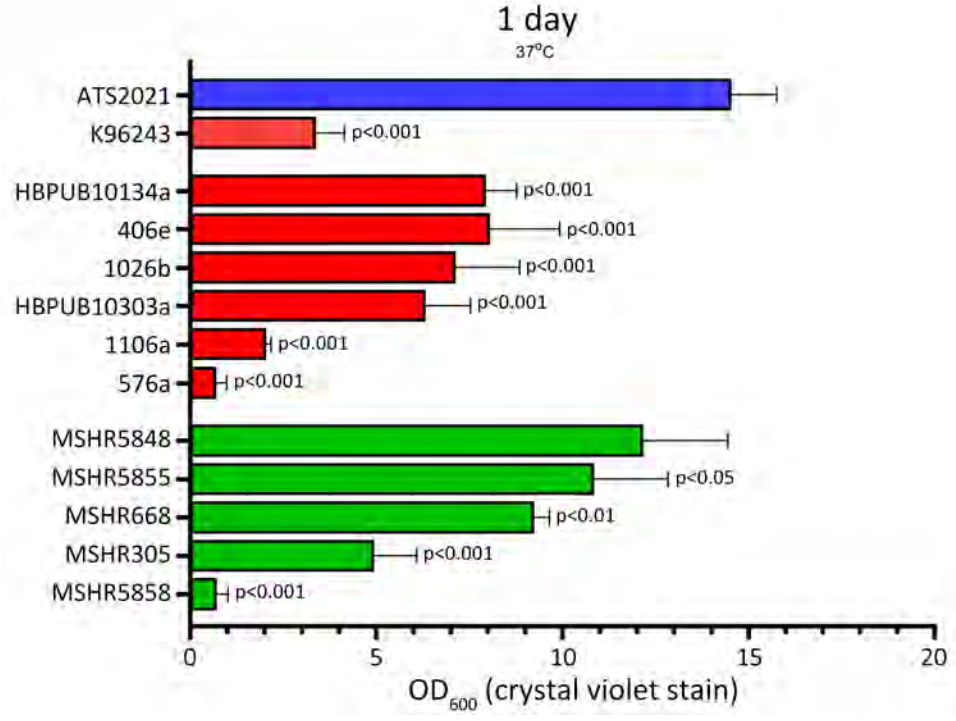

Figure 3. Biofilm production for *Burkholderia pseudomallei* strain ATS2021, the causative strain in an outbreak of 4 cases, 2 of them fatal, in the United States in 2021, in relation to other previously characterized *B. pseudomallei* clinical isolates. Biofilm formation of bacterial strains was assessed by crystal violet staining as measured by OD_{600}. Biofilm was allowed to form after static growth in LB+4% glycerol for 1 day at 37°C. Clinical isolates used in this assay originated from Thailand (red bars) or Australia (green bars). Error bars represent the SEs from mean values determined from 4 independent assays. ATS2021 formed significantly more biofilm under these conditions compared to all isolates except MSHR5848 as determined by a linear mixed effects model. OD_{600}, optical density at 600 nm.

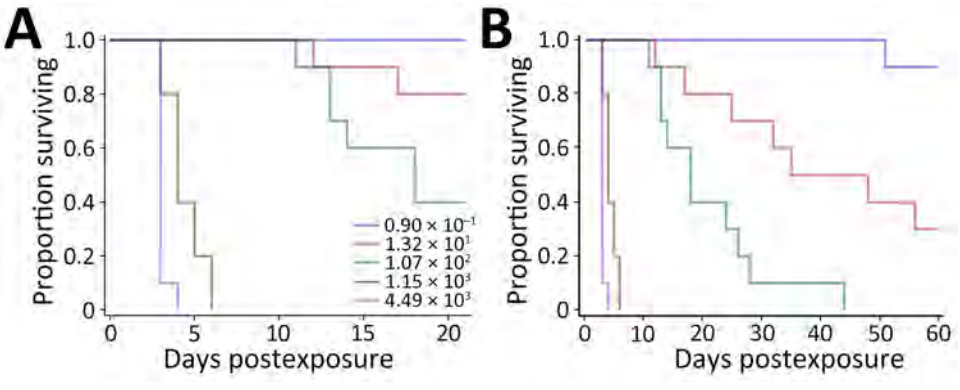

Figure 4. Kaplan-Meier survival plots calculated for C57BL/6 mice exposed to aerosolized *Burkholderia pseudomallei* ATS2021, the causative strain in an outbreak of 4 cases, 2 of them fatal, in the United States in 2021. A) Survival after 21 days; B) survival after 60 days. N = 10 per aerosolized dose of *B. pseudomallei.* The day 21 survival rates from highest to lowest calculated inhaled dose of *B. pseudomallei* ATS2021 (4,490 CFU, 1,150 CFU, 107 CFU, 13 CFU, 1 CFU) as depicted in panel A are 0/10, 0/10, 4/10, 8/10, and 10/10. The day 60 survival rates from highest to lowest calculated inhaled dose of *B. pseudomallei* ATS2021 as depicted in panel B are 0/10, 0/10, 0/10, 3/10, and 9/10.

(*17*,*18*,*29*,*30*). The presence of the $bimA_{Bm}$ allele is thought to exacerbate neurologic melioidosis by increasing rapidity of bacterial dissemination to various tissues and persistence in phagocytic cells (*29*). The phylogenetic tree is based on the unique $bimA_{Bm}$ alleles deposited in publicly available draft and complete genome sequence databases (Figure 1). The *B. pseudomallei* $bimA_{Bm}$ sequences are all derived from strains originating in Australia, Papua New Guinea, and India, differing from each primarily in the region encoding the proline-rich domain (*28*,*30*). The ATS2021 *bimA* (Figure 1, arrow) groups within the $bimA_{Bm}$ branch of the tree. *B. pseudomallei* strains with the $bimA_{Bm}$ allele have also been described in Sri Lanka (*31*), but the sequences of those isolates have not been made publicly available. Of note, 2 environmental isolates of *Burkholderia humptydooensis*, MSMB 43 and MSMB121, harbor genes that are closely related to the $bimA_{Bm}$ alleles in *B. mallei* and *B. pseudomallei* (*32*) (Figure 1). To demonstrate the sequence differences between the $bimA_{Bp}$ and $bimA_{Bm}$ alleles, we included 3 representative $bimA_{Bp}$ alleles from K96243, 1026b, and 576 (Figure 1).

ATS2021 Robust Biofilm

We compared growth of K96243 and ATS2021 in several types of rich or defined media to assess differences with nutritional requirements and observed no differences in growth between the 2 strains (Appendix 2 Figure, https://wwwnc.cdc.gov/EID/article/30/10/24-0084-App2.pdf). We measured the ability of K96243 and ATS2021 to produce biofilm by using different growth media, incubation times, and temperatures. Low-level biofilm was detected for both strains after 1 day at room temperature (Figure 2). However, after 2 days at room temperature, levels of biofilm were higher for K96243 and ATS2021, especially in the rich media (LBG and GTB). The difference in biofilm formation was greater after incubation at 37°C; ATS2021 produced more biofilm than K96243. To determine if the increased formation at 37°C was specific to ATS2021, we tested biofilm formation in *B. pseudomallei* strains that accounted for the previously described strain panel (*33*). The clinical isolates formed variable biofilms, but ATS2021 produced substantially more biofilm at 37°C than the

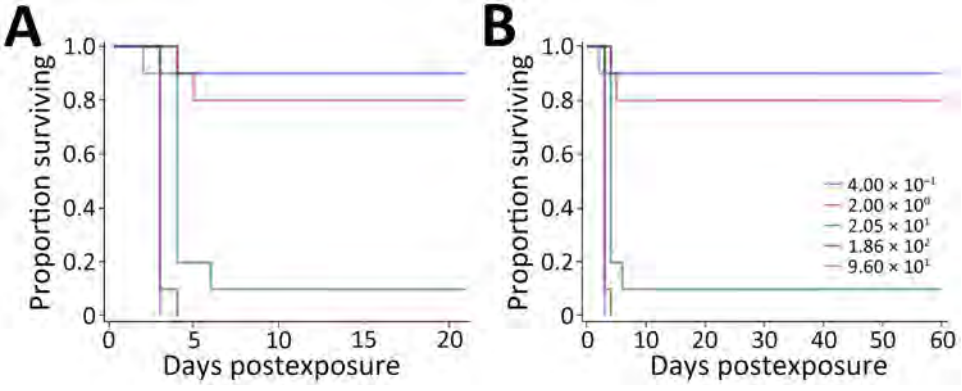

Figure 5. Kaplan-Meier survival plots calculated for BALB/c mice exposed to aerosolized *Burkholderia pseudomallei* ATS2021, the causative strain in an outbreak of 4 cases, 2 of them fatal, in the United States in 2021. A) Survival after 21 days; B) survival after 60 days. N = 10 per aerosolized dose of *B. pseudomallei.* The day 21 survival rates from highest to lowest calculated inhaled dose of *B. pseudomallei* ATS2021 (960 CFU, 186 CFU, 21 CFU, 2 CFU, 0.4 CFU) as depicted in panel A are 0/10, 0/10, 1/10, 8/10, and 9/10. The day 60 survival rates as depicted in panel B are 0/10, 0/10, 1/10, 8/10, and 9/10.

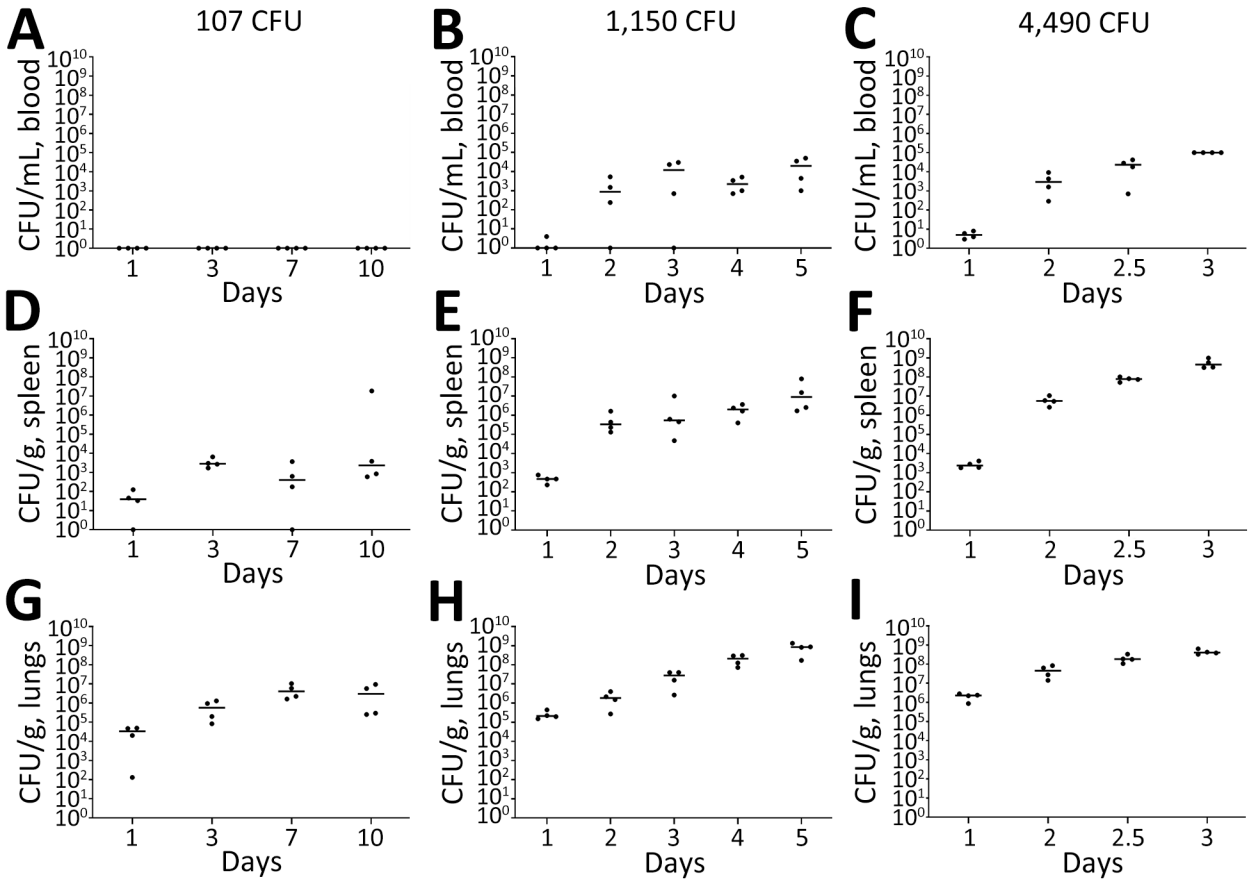

Figure 6. Serial sampling experiment to investigate bacterial dissemination in blood, spleens, and lungs of C57BL/6 mice at different challenge doses of aerosolized *Burkholderia pseudomallei* strain ATS2021, the causative strain in an outbreak of 4 cases, 2 of them fatal, in the United States in 2021. C57BL/6 mice were estimated to have inhaled various doses on day 0. A subset of mice was then deeply anesthetized for a terminal blood collection, euthanized, and then the spleens and lungs were removed to determine the bacteriologic burden in each organ at each time point indicated. Bacterial counts are shown for whole blood (A–C), spleen homogenate (D–F), and lung homogenate (G–I). N = 4 for each time point. The CFU burden is shown for each mouse; the geometric mean is depicted with the horizontal bar. Limit of detection is ≈100 CFU/mL of blood and 5 CFU/organ.

other strains, except MSHR5848 (Figure 3). Those differences were not observed when the bacteria were grown at room temperature (Figure 2; data not shown for all bacteria). Retrospective analyses demonstrated a negative correlation between in vitro biofilm formation and in vivo virulence in mice after exposure to aerosolized *B. pseudomallei* (Spearman correlation −0.70 and p = 0.017 for BALB/c mice; Spearman correlation −0.63 and p = 0.038 for C57BL/6 mice). Those analyses did not reveal statistically significant correlations between in vitro biofilm formation and in vivo virulence in mice after intraperitoneal injection of *B. pseudomallei*.

LD_{50} Determinations in Mice

We used C57BL/6 mice because they are an accepted model for vaccine development (*34*,*35*). The LD_{50} estimate after exposure to aerosolized ATS2021 was ≈56 CFU after 21 days and 6 CFU after 60 days (Table; Figure 4). We also determined the LD_{50} in BALB/c mice because they are used for pathogenesis and therapeutic studies (*19*,*33*,*36*). The LD_{50} estimate for 21 and 60 days after exposure to aerosolized ATS2021 was ≈4 CFU for both time frames (Table; Figure 5). Those LD_{50} values categorize the isolate to be among the most virulent we have characterized. Retrospective statistical analyses supported this observation and demonstrated similar (p>0.1) virulence to *B. pseudomallei* strains 1026b, MSHR5855, HBPUB10303a, and HBPBUB10134a in C57BL/6 mice exposed to aerosolized bacteria (*19*). Clinical signs assumed to be associated with neurologic melioidosis were observed in some mice (e.g., uncoordinated and impaired movement, tremors, and hypersensitivity to touch).

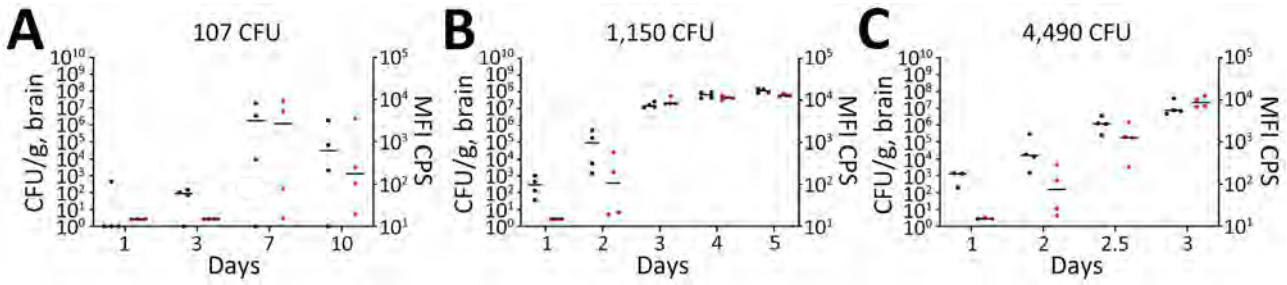

Figure 7. Serial sampling experiment to investigate bacterial dissemination in brains of C57BL/6 mice at different challenge doses of aerosolized *Burkholderia pseudomallei* strain ATS2021, the causative strain in an outbreak of 4 cases, 2 of them fatal, in the United States in 2021. C57BL/6 mice were estimated to have inhaled various doses of aerosolized *Burkholderia pseudomallei* ATS2021 on day 0: A) 107 CFU, B) 1,150 CFU, and C) 4,490 CFU. A subset of mice was then deeply anesthetized for a terminal blood collection, euthanized, and then brains were removed to determine the bacteriologic burden in each brain at each time point indicated. N = 4 for each time point. The CFU burden is shown for each mouse, depicted as a black circle; geometric mean is depicted with the horizontal bar. The brain homogenates were exposed to ≈21 kGy of gamma radiation, proven sterile, and then subjected to the *B. pseudomallei* capsule-specific immunodiagnostic assay. The MFI of each mouse is depicted by a red circle, and the geometric mean is depicted with the horizontal bar. Limit of detection is ≈5 CFU/organ. The detection of capsule in the irradiated brain homogenate is depicted in red and is displayed as MFI. MFI, mean fluorescent intensity.

Bacterial Burden in C57BL/6 Mice after Exposure to Aerosolized ATS2021

We performed a serial sampling experiment to investigate bacterial dissemination in C57BL/6 mice at different challenge doses (107 CFU, 1,150 CFU, and 4,490 CFU). Bacterial dissemination patterns depend on the dose of inhaled bacteria after aerosolization (Figure 6). The 2 highest inhaled doses resulted in early bacteremia (Figure 6, panels B, C). *B. pseudomallei* was detected in the spleens (Figure 6, panels D–F) of nearly all animals within 24 hours. Regardless of the exposure dose, all mice had substantial bacterial replication in the lungs within 24 hours, as expected, given that the lungs were the main portal of entry for the bacteria (Figure 6, panels G–I). We examined the brains and identified substantial bacterial burden within 24 hours after inhalation in the 3 doses (Figure 7, black data points). We also performed a capsule-specific immune-diagnostic assay on gamma-irradiated brain homogenates. Detection of capsule in those samples (Figure 7, red data points)

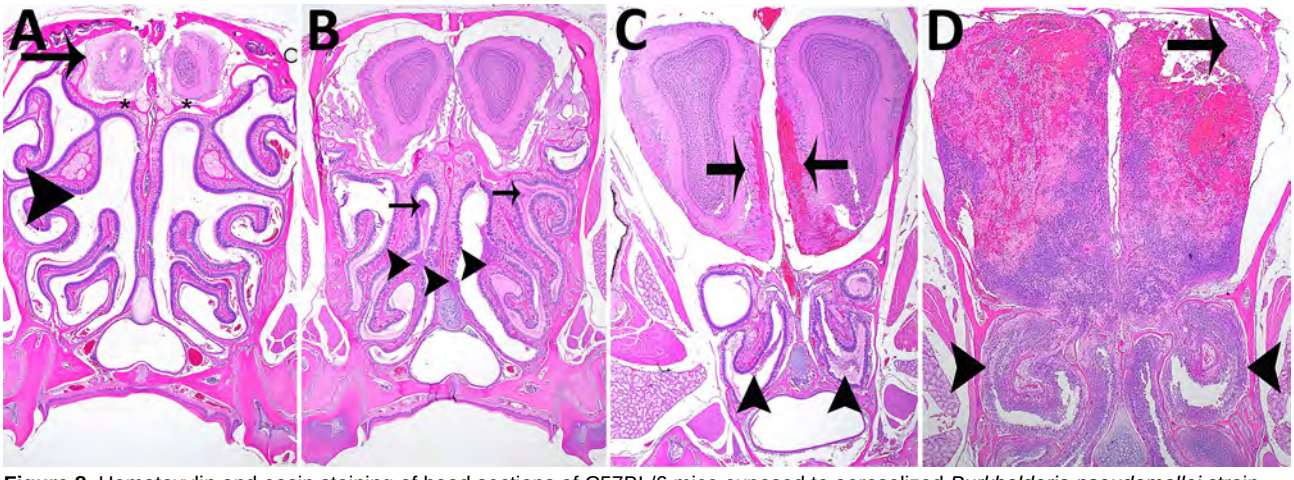

Figure 8. Hematoxylin and eosin staining of head sections of C57BL/6 mice exposed to aerosolized *Burkholderia pseudomallei* strain ATS2021, the causative strain in an outbreak of 4 cases, 2 of them fatal, in the United States in 2021. Shown are the nasal cavity (including nasal turbinates, nasal septum, respiratory and olfactory epithelium, lamina propria with supporting tissues and glands, nerve bundles, and nasal air passages); cribriform plate (bone and olfactory/trigeminal nerves); and cranial vault with olfactory bulb. A) Day 1 after exposure, dose 107 CFU, showing nasal turbinates (arrowhead), cribriform plate (asterisks), and olfactory bulb (arrow) that are essentially normal. Original magnification ×2. B) Day 2 after exposure, dose 4,490 CFU, showing mild necrosuppurative rhinitis (arrowheads) with edema, cellular debris and suppurative inflammation in few nasal air passages (arrows). Original magnification ×2. C) Day 3 after exposure, dose 4,490 CFU, showing multifocal moderate necrosuppurative rhinitis (arrowheads) and necrotizing and hemorrhagic meningoencephalitis of the olfactory bulb (arrows). Original magnification × e times 2. D) Day 4 after exposure, dose 1,150 CFU. There is diffuse necrosuppurative rhinitis of the nasal turbinates (arrowheads), showing extensive necrosis and hemorrhage of the olfactory bulb with a small portion of recognizable neural tissue evident (arrow). Original magnification ×2.

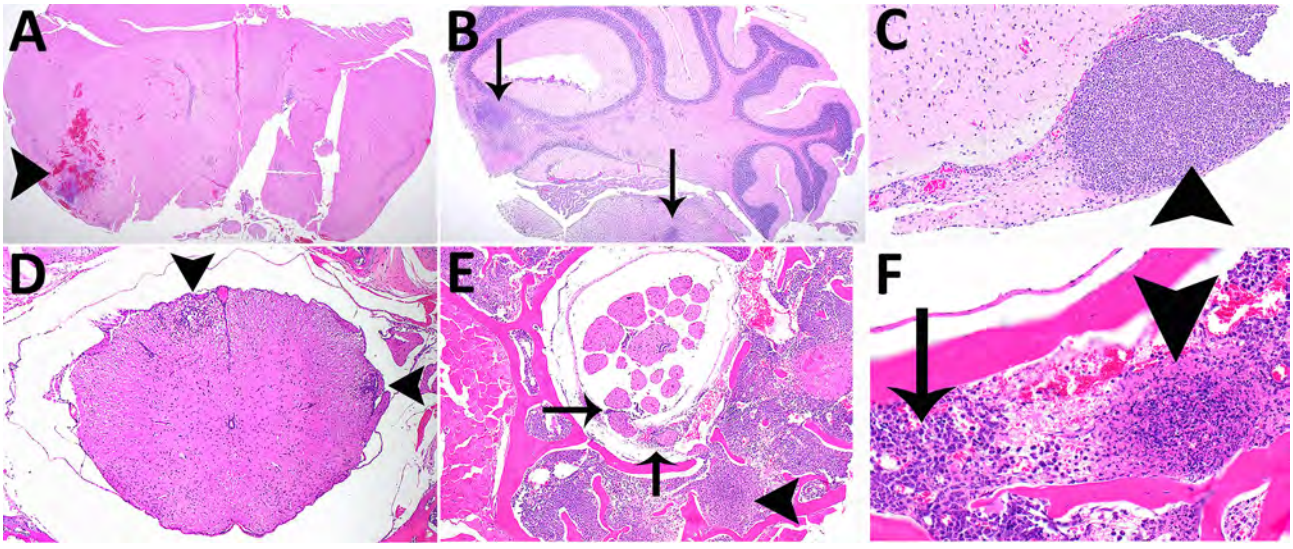

Figure 9. Histopathologic analyses of the neurologic system of C57BL/6 mice after inhalation of *Burkholderia pseudomallei* strain ATS2021, the causative strain in an outbreak of 4 cases, 2 of them fatal, in the United States in 2021. A) Day 5 after exposure, dose 1,150 CFU. Cerebrum showing focally extensive necrotizing and hemorrhagic meningoencephalitis (arrowhead). Hematoxylin and eosin (HE) stain; original magnification ×2. B) Day 9 after exposure, dose 107 CFU. Pons and cerebellum. There is multifocal necrotizing meningoencephalitis (arrows). HE stain; original magnification ×2. C) Day 10 after exposure, dose 1,150 CFU. Cerebrum with olfactory peduncle filled with viable and degenerate neutrophils with no recognizable peduncular tissue (arrowhead). HE stain; original magnification ×20. D) Day 9 after exposure, 107 CFU. Spinal cord, thoracic, shows multifocal meningomyelitis (arrowheads). HE stain; original magnification ×4. E) Day 5 after exposure, 1,150 CFU. Spinal cord and vertebrae, lumbar at cauda equina, show is multifocal suppurative perineuritis of spinal nerves (arrows). Note the necrotizing lesion within the vertebral bone marrow (arrowhead) HE stain; original magnification ×10. F) Day 4 after exposure, dose 1,150 CFU. Spinal cord and vertebra, thoracic, show necrotizing osteomyelitis (arrowhead). Note the loss of distinction of bone marrow cells compared to normal cells of the bone marrow (arrow). HE stain; original magnification ×40.

was reflective of the bacterial burden, but quantification of viable bacteria via culture was more sensitive.

Representative Histopathology in C57BL/6 Mice after Inhalation of ATS2021

We performed histopathologic analyses on a subset of animals. Animals that died 1–3 days after aerosol exposure probably did not have time for substantial tissue lesions to develop (despite high exposure doses) and may have received lower severity scores because of rapid time to death or euthanasia, which accounts for the lowest animal scores at days 1, 2, and 3 in all 3 groups (Appendix 1 Table 1). Pathologic lesions in mice were consistent with lesions produced by other strains of *B. pseudomallei* (*19*,*37*). In general, the focal-to-coalescing necrotizing lesions were accompanied by many degenerate neutrophils and accumulating necrotic debris to form variably sized necrosuppurative lesions, which expand to form more organized abscesses with time.

We prioritized the central nervous system to characterize the ATS2021 isolate after inhalation of small-particle aerosols (Figures 8, 9). Lesions consistent with *B. pseudomallei* were seen by day 1 in the lung and nasal turbinates, the sites of initial colonization. Subsequently, lesions were noted by day 2 in the brain, specifically the olfactory bulb, and in the olfactory nerves of many mice from 1,150 and 4,490 CFU doses. In addition, by day 2, lesions were present in the spleen and liver, as noted by increased pathology scores (Appendix 1 Table 1). Lesions of the vertebral bone marrow were noted after 1,150 and 4,490 CFU doses within 3 days. Bone marrow lesions were primarily noted in the groups that received higher doses. Lesions of the cerebrum, cerebellum, and brainstem were noted by day 4 and spinal cord lesions by day 5 (Figure 9). Lesions were noted in the olfactory bulb in mice that received doses of 1,150 CFU and in the olfactory nerves of mice that received 1,150 CFU and 4,490 CFU within 48 hours after exposure and an increased number of mice with lesions in the olfactory bulb by 36 hours.

We performed IHC to support histopathologic findings and provide additional evidence that the lesions resulted from infection with *B. pseudomallei* (Appendix 1 Table 2). IHC clearly identified bone marrow lesions that are difficult to appreciate with hematoxylin and eosin staining. Nasal turbinates showed *Burkholderia* positivity by IHC within 24 hours after exposure, and IHC positivity was found within 48 hours in the mice receiving the highest inhaled dose in the

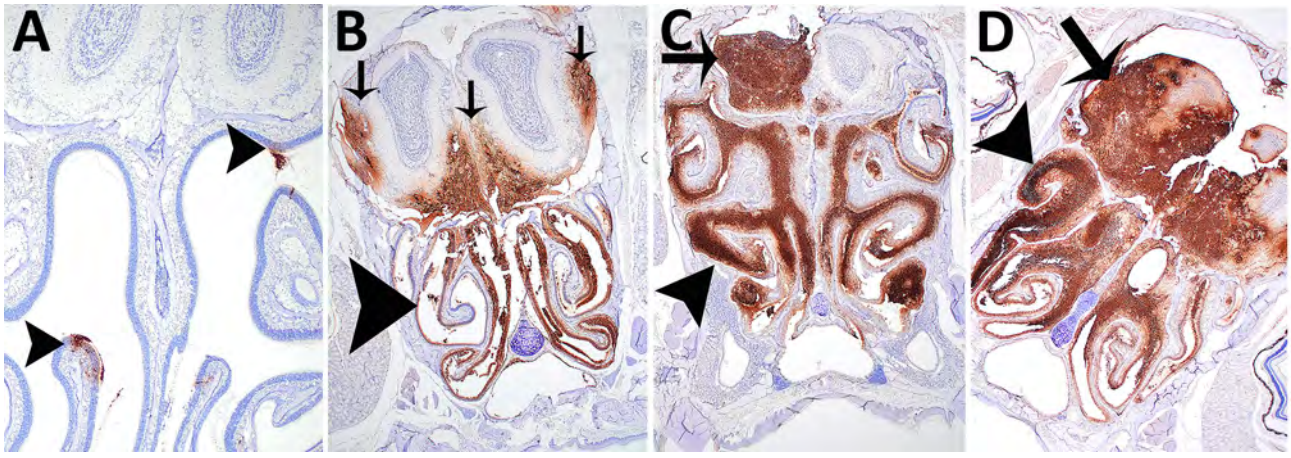

Figure 10. Immunohistochemical analyses of head sections of C57BL/6 mice exposed to aerosolized *Burkholderia pseudomallei* strain ATS2021, the causative strain in an outbreak of 4 cases, 2 of them fatal, in the United States in 2021. Shown are the nasal cavity (including nasal turbinates, nasal septum, respiratory and olfactory epithelium, lamina propria with supporting tissues and glands, nerve bundles, and nasal air passages); cribriform plate (bone and olfactory/trigeminal nerves); and cranial vault with olfactory bulb. A) Day 1 after exposure, dose 1,150 CFU, shows multifocal minimal positivity of the nasal cavity epithelium (arrowheads), which is most likely olfactory epithelium of the ethmoid turbinate. Original magnification ×2. B) Day 3 after exposure, dose 4,490 CFU, showing diffuse marked positivity of the nasal cavity epithelium (arrowhead) and multifocal moderate positivity of the olfactory bulb (arrows). Original magnification ×2. C) Day 6 after exposure, dose 107 CFU, showing diffuse severe positivity of the nasal cavity epithelium (arrowhead) and multifocal marked positivity of the olfactory bulb (arrow). Original magnification ×2. D) Day 4 after exposure, 1,150 CFU, showing diffuse severe positivity of the nasal cavity (arrowhead) and olfactory bulb (arrow). Original magnification ×2.

brain olfactory bulb, olfactory nerves, and nasal turbinates (Figures 10, 11).

Effects on Oligodendrocytes

We applied a transcriptomic approach targeted against a range of neuroinflammatory genes in brain homogenates from mice. According to targeted expression levels, we used a cell profiling module to identify changes in neuronal cell types based on relative abundance of marker genes associated with oligodendrocytes. In the 2 highest dose groups, we observed statistically significant drops in oligodendrocyte signatures, particularly on days 3 and 5 (Figure 12, panel A). A total of 27 genes constitute the oligodendrocyte cell profile, of which 23 had significant expression differences for ≥1 time point (Figure 12, panel B). Total numbers of significant genes were dependent on infectious dose with no differential gene expression observed in the 107 CFU group. We observed early and pronounced down-regulation of many of these genes, as early as day 1 in the 4,490 CFU group. Of the 27 genes, 6 are known to predominately constitute the oligodendrocyte cell profile and all encode proteins involved in myelination or lipid metabolism (Appendix 2 Table). All 6 of the signatures were significantly down-regulated, further suggesting dysregulation in oligodendrocytes in infected hosts (Figure 12, panel C).

Discussion

Knowledge of the diversity of virulence associated with distinct geographic isolates of *B. pseudomallei* is crucial to the further development, testing, and

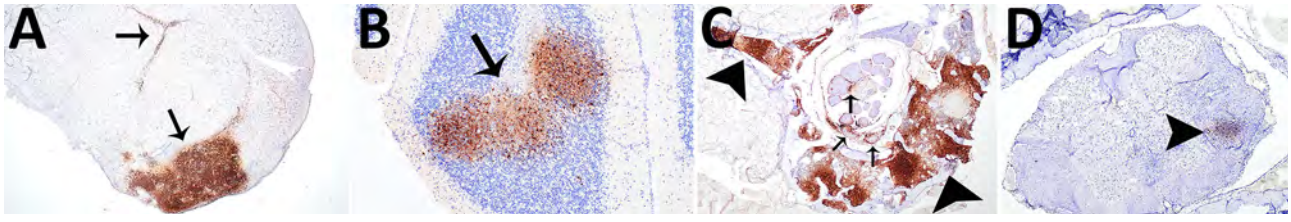

Figure 11. Immunohistochemical analyses of the neurologic system of C57BL/6 mice exposed to aerosolized *Burkholderia pseudomallei* strain ATS2021, the causative strain in an outbreak of 4 cases, 2 of them fatal, in the United States in 2021. A) Day 6 after exposure, dose 107 CFU. Cerebrum shows multifocal moderate positivity (arrows). Original magnification ×2. B) Day 6 after exposure, dose 107 CFU. Cerebellum shows multifocal moderate positivity (arrow). Original magnification ×10. C) Day 5 after exposure, dose 1,150 CFU. Lumbar spinal cord at cauda equina and vertebra shows multifocal mild perineural positivity (arrows) of spinal nerves at cauda equina and marked vertebral bone marrow positivity (arrowheads). Original magnification ×10. D) Day 9 after exposure, dose 107 CFU. Spinal cord, cervical, shows focal moderate positivity (arrowheads). Original magnification ×20.

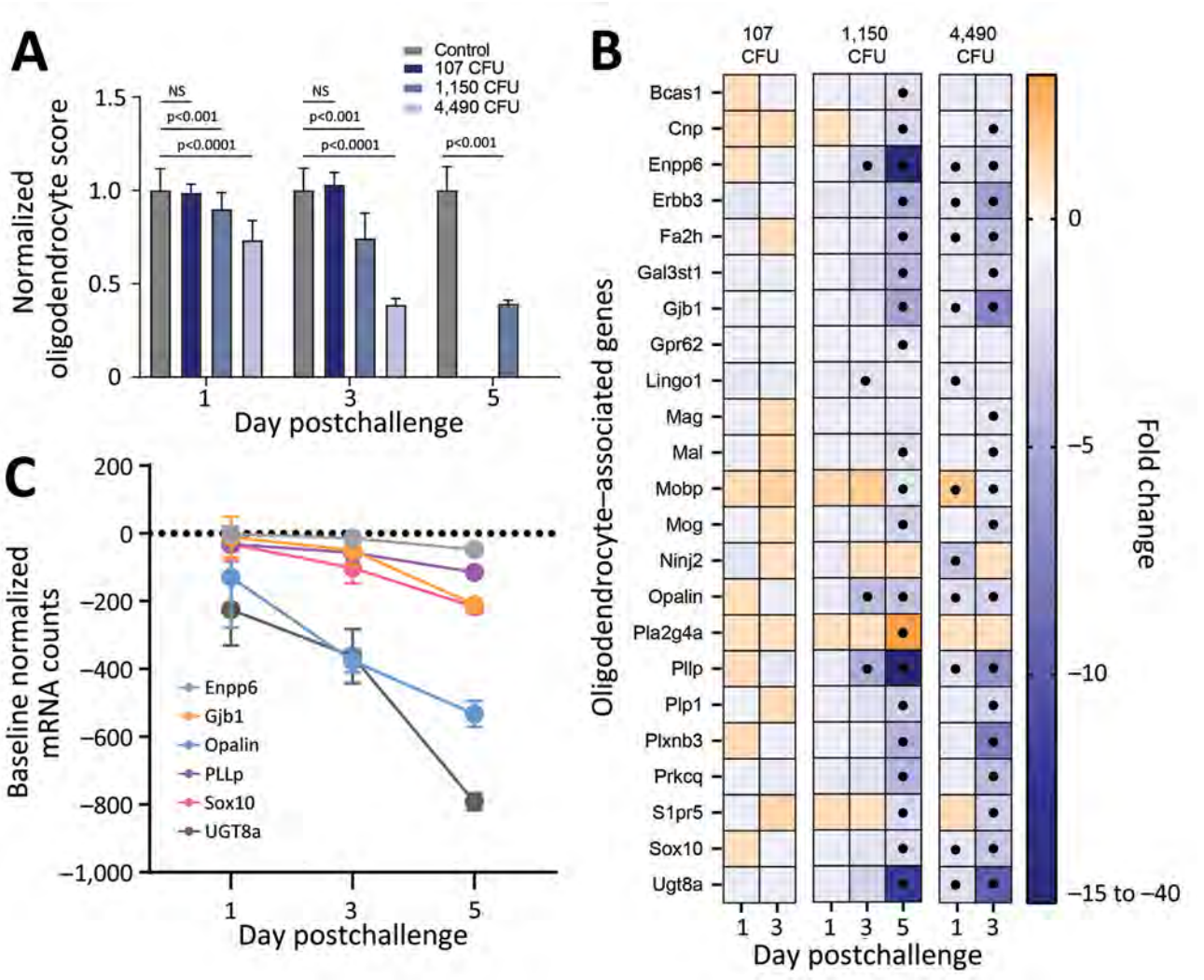

Figure 12. Profiling of differentially expressed genes revealing downregulation of markers associated with oligodendrocytes after exposure to aerosolized *Burkholderia pseudomallei* strain ATS2021, the causative strain in an outbreak of 4 cases, 2 of them fatal, in the United States in 2021. A) Significant downregulation or decreased expression of genes involved in oligodendrocyte function was observed in select challenge groups of mice on days 1,3, and 5 after challenge. Values are normalized to unchallenged control mice and represent 4 mice per group. Significance based on a 2-way analysis of variance. Error bars indicate 95% CIs. B) Heat map of differentially expressed genes associated with NanoString oligodendrocyte cell profiler panel (https://nanostring.com). Fold change is linear, and dots indicate gene changes that were above the significance threshold. C) Expression changes over time in select genes associated with oligodendrocyte function for the 1,150 CFU challenge group. In panels A and C, error bars represent standard deviation.

evaluation of medical countermeasures. We characterized several factors that may contribute to the virulence associated with ATS2021. We examined several key genetic virulence attributes of that strain and demonstrated considerable virulence in 2 mouse models of inhalational melioidosis. Because ATS2021 was shown to carry the $bimA_{Bm}$ allele and neurologic involvement of this strain played a role in human infections, we focused on analyzing the histopathology associated with the rapid neurologic invasion. The nasal turbinates were heavily colonized within the first day after exposure to aerosolized bacteria, leading to infection of the olfactory bulb by day 2; the cerebrum, cerebellum, and brain stem by day 4; and the spinal column by day 5 (with evidence of infection in vertebral bone marrow within 3 days for mice inhaling the highest dose of aerosolized bacteria).

RNA analyses indicated that the oligodendrocyte populations in the infected mouse brains were significantly affected by the infection in a dose- and time-dependent manner. The robust decreases in oligodendrocyte abundance, function, or both that we observed in the highest bacterial challenge groups (Figure 12, panels A, B) suggest pronounced impairment of a glial cell population that is critical for brain homeostasis and function. Oligodendrocytes are responsible for

myelination of the CNS, encapsulating neuronal axons in lipid-rich membranes that serve as insulators enabling rapid neuronal conduction (*38*,*39*). Given the role of oligodendrocytes in brain function, a variety of neurodegenerative disorders affecting the brain and spinal cord are associated with demyelination (e.g., multiple sclerosis) (*40*,*41*). There are known microbial-associated causes of oligodendrocyte dysfunction and associated demyelination; progressive multifocal leukoencephalopathy is caused by infection of oligodendrocytes by the JC virus (*42*), and *Borrelia burgdorferi* can induce oligodendrocyte apoptosis (*43*). Although more study is needed, the down-regulation of genes associated with myelination could account for some of the clinical signs observed in mice and nonhuman primates when infected with neurotropic strains of *B. pseudomallei*, including muscle weakness, tremors, and extreme sensitivity to touch (*37*,*44*).

Last, we are intrigued by the robust biofilm production at 37°C compared with other strains of *B. pseudomallei*. Although virulence (assayed by an intraperitoneal BALB/c infection model) did not correlate with biofilm production of *B. pseudomallei* isolates from Thailand (*45*), biofilm formation is associated with virulence of other bacteria (*46*,*47*). That this biofilm phenotype is exaggerated at 37°C suggests a potential role in pathogenesis that may be relevant to inhaled *B. pseudomallei* in the context of colonization of upper respiratory areas (e.g., nasal turbinates as the result of inhaling the bacteria) and may contribute to the intrinsic difficulty in successfully treating melioidosis with antimicrobial drugs (*48*). Our retrospective analyses support the data published by Taweechaisupapong et al., which demonstrate no correlation between biofilm formation and virulence associated with intraperitoneal injection (*45*), but we did identify a statistically significant negative correlation between in vitro biofilm formation and virulence as measured by mouse models of inhalational melioidosis. Future work focused on identifying correlations between biofilm formation and neurologic melioidosis should help clarify the effect of host–bacterial interactions on CNS demyelination.

Combined, our data, previous case-reports (*11*,*12*), and the identification of endemic strains in Mississippi (*49*) support the idea that melioidosis is an emerging infectious disease in the United States. Thus, it is imperative that we understand the new isolates in the context of inhalational and neurologic melioidosis to accurately predict the hazards associated with this emerging pathogen for the biodefense and public health communities. Clinical laboratories must continue to be on the alert for melioidosis within the United States, and new isolates should be used to develop and test novel medical countermeasures and diagnostic strategies.

Opinions, interpretations, conclusions, and recommendations are those of the authors and are not necessarily endorsed by the US Army, the US Defense Health Agency, or the Centers for Disease Control and Prevention. Research was conducted under an animal care and use protocol approved by the US Army Medical Research Institute of Infectious Diseases Institutional Animal Care and Use Committee in compliance with the Animal Welfare Act and other federal statutes and regulations relating to animals and experiments involving animals and adheres to principles stated in the Guide for the Care and Use of Laboratory Animals, National Research Council, 2011. The facility where this research was conducted is fully accredited by the Association for Assessment and Accreditation of Laboratory Animal Care International.

About the Author

Dr. Cote is the deputy chief of the Bacteriology Division at the US Army Medical Research Institute of Infectious Diseases. His interests are high-containment bacteriologic research to include medical countermeasure development, bacterial pathogenesis, and animal models of bacterial diseases.

References

1. Currie BJ. Melioidosis: evolving concepts in epidemiology, pathogenesis, and treatment. Semin Respir Crit Care Med. 2015;36:111–25. https://doi.org/10.1055/s-0034-1398389
2. Currie BJ, Meumann EM, Kaestli M. The expanding global footprint of *Burkholderia pseudomallei* and melioidosis. Am J Trop Med Hyg. 2023;108:1081–3.
3. Chantratita N, Phunpang R, wYarasai A, Dulsuk A, Yimthin T, Onofrey LA, et al. Characteristics and one year outcomes of melioidosis patients in northeastern Thailand: a prospective, multicenter cohort study. Lancet Reg Health Southeast Asia. 2023;9:9. https://doi.org/10.1016/j.lansea.2022.100118
4. Currie BJ, Mayo M, Ward LM, Kaestli M, Meumann EM, Webb JR, et al. The Darwin Prospective Melioidosis Study: a 30-year prospective, observational investigation. Lancet Infect Dis. 2021;21:1737–46. https://doi.org/10.1016/S1473-3099(21)00022-0
5. Currie BJ, Fisher DA, Howard DM, Burrow JN. Neurological melioidosis. Acta Trop. 2000;74:145–51. https://doi.org/10.1016/S0001-706X(99)00064-9
6. Wongwandee M, Linasmita P. Central nervous system melioidosis: a systematic review of individual participant data of case reports and case series. PLoS Negl Trop Dis. 2019;13:e0007320. https://doi.org/10.1371/journal.pntd.0007320
7. Sullivan RP, Marshall CS, Anstey NM, Ward L, Currie BJ. 2020 review and revision of the 2015 Darwin melioidosis treatment guideline; paradigm drift not shift. PLoS Negl Trop Dis. 2020;14:e0008659. https://doi.org/10.1371/journal.pntd.0008659

8. Gora H, Hasan T, Smith S, Wilson I, Mayo M, Woerle C, et al. Melioidosis of the central nervous system; impact of the *bimABm* allele on patient presentation and outcome. Clin Infect Dis. 2022:ciac111. https://doi.org/10.1093/cid/ciac111
9. Mukhopadhyay C, Kaestli M, Vandana KE, Sushma K, Mayo M, Richardson L, et al. Molecular characterization of clinical *Burkholderia pseudomallei* isolates from India. Am J Trop Med Hyg. 2011;85:121–3. https://doi.org/10.4269/ajtmh.2011.11-0166
10. Limmathurotsakul D, Dance DA, Wuthiekanun V, Kaestli M, Mayo M, Warner J, et al. Systematic review and consensus guidelines for environmental sampling of *Burkholderia pseudomallei*. PLoS Negl Trop Dis. 2013;7:e2105. https://doi.org/10.1371/journal.pntd.0002105
11. Gee JE, Bower WA, Kunkel A, Petras J, Gettings J, Bye M, et al. Multistate outbreak of melioidosis associated with imported aromatherapy spray. N Engl J Med. 2022;386:861–8. https://doi.org/10.1056/NEJMoa2116130
12. Petras JK, Elrod MG, Ty M, Adams P, Zahner D, Adams A, et al. Notes from the field: *Burkholderia pseudomallei* detected in a raccoon carcass linked to a multistate aromatherapy-associated melioidosis outbreak—Texas, 2022. MMWR Morb Mortal Wkly Rep. 2022;71:1597–8. https://doi.org/10.15585/mmwr.mm7150a5
13. Matthews RJ, Smith S, Wilson I, Tjahjono R, Young S, Hanson J. Case report: vagal nerve neuritis associated with pulmonary melioidosis provides potential insights into the pathophysiology of neuromelioidosis. Am J Trop Med Hyg. 2023;108:1212–4. https://doi.org/10.4269/ajtmh.22-0694
14. St John JA, Walkden H, Nazareth L, Beagley KW, Ulett GC, Batzloff MR, et al. *Burkholderia pseudomallei* rapidly infects the brain stem and spinal cord via the trigeminal nerve after intranasal inoculation. Infect Immun. 2016;84:2681–8. https://doi.org/10.1128/IAI.00361-16
15. Walkden H, Delbaz A, Nazareth L, Batzloff M, Shelper T, Beacham IR, et al. *Burkholderia pseudomallei* invades the olfactory nerve and bulb after epithelial injury in mice and causes the formation of multinucleated giant glial cells in vitro. PLoS Negl Trop Dis. 2020;14:e0008017. https://doi.org/10.1371/journal.pntd.0008017
16. St John JA, Ekberg JA, Dando SJ, Meedeniya AC, Horton RE, Batzloff M, et al. *Burkholderia pseudomallei* penetrates the brain via destruction of the olfactory and trigeminal nerves: implications for the pathogenesis of neurological melioidosis. MBio. 2014;5:e00025. https://doi.org/10.1128/mBio.00025-14
17. Burnard D, Bauer MJ, Falconer C, Gassiep I, Norton RE, Paterson DL, et al. Clinical *Burkholderia pseudomallei* isolates from north Queensland carry diverse *bimABm* genes that are associated with central nervous system disease and are phylogenomically distinct from other Australian strains. PLoS Negl Trop Dis. 2022;16:e0009482. https://doi.org/10.1371/journal.pntd.0009482
18. Sarovich DS, Price EP, Webb JR, Ward LM, Voutsinos MY, Tuanyok A, et al. Variable virulence factors in *Burkholderia pseudomallei* (melioidosis) associated with human disease. PLoS One. 2014;9:e91682. https://doi.org/10.1371/journal.pone.0091682
19. Trevino SR, Klimko CP, Reed MC, Aponte-Cuadrado MJ, Hunter M, Shoe JL, et al. Disease progression in mice exposed to low-doses of aerosolized clinical isolates of *Burkholderia pseudomallei*. PLoS One. 2018;13:e0208277. https://doi.org/10.1371/journal.pone.0208277
20. Guyton AC. Measurement of the respiratory volumes of laboratory animals. Am J Physiol. 1947;150:70–7. https://doi.org/10.1152/ajplegacy.1947.150.1.70
21. Marchetti R, Dillon MJ, Burtnick MN, Hubbard MA, Kenfack MT, Blériot Y, et al. *Burkholderia pseudomallei* capsular polysaccharide recognition by a monoclonal antibody reveals key details toward a biodefense vaccine and diagnostics against melioidosis. ACS Chem Biol. 2015;10:2295–302. https://doi.org/10.1021/acschembio.5b00502
22. Stefan CP, Arnold CE, Shoemaker CJ, Zumbrun EE, Altamura LA, Douglas CE, et al. Transcriptomic analysis reveals host miRNAs correlated with immune gene dysregulation during fatal disease progression in the Ebola virus cynomolgus macaque disease model. Microorganisms. 2021;9:665. https://doi.org/10.3390/microorganisms9030665
23. Perkins JR, Dawes JM, McMahon SB, Bennett DL, Orengo C, Kohl M. ReadqPCR and NormqPCR: R packages for the reading, quality checking and normalisation of RT-qPCR quantification cycle (Cq) data. BMC Genomics. 2012;13:296. https://doi.org/10.1186/1471-2164-13-296
24. Reckseidler SL, DeShazer D, Sokol PA, Woods DE. Detection of bacterial virulence genes by subtractive hybridization: identification of capsular polysaccharide of *Burkholderia pseudomallei* as a major virulence determinant. Infect Immun. 2001;69:34–44. https://doi.org/10.1128/IAI.69.1.34-44.2001
25. DeShazer D, Brett PJ, Woods DE. The type II O-antigenic polysaccharide moiety of *Burkholderia pseudomallei* lipopolysaccharide is required for serum resistance and virulence. Mol Microbiol. 1998;30:1081–100. https://doi.org/10.1046/j.1365-2958.1998.01139.x
26. Burtnick MN, Brett PJ, Harding SV, Ngugi SA, Ribot WJ, Chantratita N, et al. The cluster 1 type VI secretion system is a major virulence determinant in *Burkholderia pseudomallei*. Infect Immun. 2011;79:1512–25. https://doi.org/10.1128/IAI.01218-10
27. Holden MT, Titball RW, Peacock SJ, Cerdeño-Tárraga AM, Atkins T, Crossman LC, et al. Genomic plasticity of the causative agent of melioidosis, *Burkholderia pseudomallei*. Proc Natl Acad Sci U S A. 2004;101:14240–5. https://doi.org/10.1073/pnas.0403302101
28. Benanti EL, Nguyen CM, Welch MD. Virulent *Burkholderia* species mimic host actin polymerases to drive actin-based motility. Cell. 2015;161:348–60. https://doi.org/10.1016/j.cell.2015.02.044
29. Morris JL, Fane A, Sarovich DS, Price EP, Rush CM, Govan BL, et al. Increased neurotropic threat from *Burkholderia pseudomallei* strains with a *B. mallei*–like variation in the *bimA* motility gene, Australia. Emerg Infect Dis. 2017;23:740–9. https://doi.org/10.3201/eid2305.151417
30. Sitthidet C, Stevens JM, Chantratita N, Currie BJ, Peacock SJ, Korbsrisate S, et al. Prevalence and sequence diversity of a factor required for actin-based motility in natural populations of *Burkholderia* species. J Clin Microbiol. 2008;46:2418–22. https://doi.org/10.1128/JCM.00368-08
31. Jayasinghearachchi HS, Corea EM, Jayaratne KI, Fonseka RA, Muthugama TA, Masakorala J, et al. Biogeography and genetic diversity of clinical isolates of *Burkholderia pseudomallei* in Sri Lanka. PLoS Negl Trop Dis. 2021;15:e0009917. https://doi.org/10.1371/journal.pntd.0009917
32. Janesomboon S, Muangsombut V, Srinon V, Meethai C, Tharinjaroen CS, Amornchai P, et al. Detection and differentiation of *Burkholderia* species with pathogenic potential in environmental soil samples. PLoS One. 2021;16:e0245175. https://doi.org/10.1371/journal.pone.0245175
33. Welkos SL, Klimko CP, Kern SJ, Bearss JJ, Bozue JA, Bernhards RC, et al. Characterization of *Burkholderia pseudomallei* strains using a murine intraperitoneal infection model and in vitro macrophage assays. PLoS One. 2015;10:e0124667. https://doi.org/10.1371/journal.pone.0124667

34. Limmathurotsakul D, Funnell SG, Torres AG, Morici LA, Brett PJ, Dunachie S, et al.; Steering Group on Melioidosis Vaccine Development. Consensus on the development of vaccines against naturally acquired melioidosis. Emerg Infect Dis. 2015;21:e141480. https://doi.org/10.3201/eid2106.141480
35. Conejero L, Patel N, de Reynal M, Oberdorf S, Prior J, Felgner PL, et al. Low-dose exposure of C57BL/6 mice to *Burkholderia pseudomallei* mimics chronic human melioidosis. Am J Pathol. 2011;179:270–80. https://doi.org/10.1016/j.ajpath.2011.03.031
36. Nelson M, Barnes KB, Davies CH, Cote CK, Meinig JM, Biryukov SS, et al. The BALB/c mouse model for the evaluation of therapies to treat infections with aerosolized *Burkholderia pseudomallei.* Antibiotics (Basel). 2023;12:506. https://doi.org/10.3390/antibiotics12030506
37. Bearss JJ, Hunter M, Dankmeyer JL, Fritts KA, Klimko CP, Weaver CH, et al. Characterization of pathogenesis of and immune response to *Burkholderia pseudomallei* K96243 using both inhalational and intraperitoneal infection models in BALB/c and C57BL/6 mice. PLoS One. 2017;12:e0172627. https://doi.org/10.1371/journal.pone.0172627
38. Stassart RM, Möbius W, Nave KA, Edgar JM. The axon-myelin unit in development and degenerative disease. Front Neurosci. 2018;12:467. https://doi.org/10.3389/fnins.2018.00467
39. Molina-Gonzalez I, Miron VE, Antel JP. Chronic oligodendrocyte injury in central nervous system pathologies. Commun Biol. 2022;5:1274. https://doi.org/10.1038/s42003-022-04248-1
40. Kenigsbuch M, Bost P, Halevi S, Chang Y, Chen S, Ma Q, et al. A shared disease-associated oligodendrocyte signature among multiple CNS pathologies. Nat Neurosci. 2022;25:876–86. https://doi.org/10.1038/s41593-022-01104-7
41. Graf LM, Rosenkranz SC, Hölzemer A, Hagel C, Goebell E, Jordan S, et al. Clinical presentation and disease course of 37 consecutive cases of progressive multifocal leukoencephalopathy (PML) at a German tertiary-care hospital: a retrospective observational study. Front Neurol. 2021;12:632535. https://doi.org/10.3389/fneur.2021.632535
42. Cortese I, Reich DS, Nath A. Progressive multifocal leukoencephalopathy and the spectrum of JC virus-related disease. Nat Rev Neurol. 2021;17:37–51. https://doi.org/10.1038/s41582-020-00427-y
43. Ramesh G, Borda JT, Dufour J, Kaushal D, Ramamoorthy R, Lackner AA, et al. Interaction of the Lyme disease spirochete *Borrelia burgdorferi* with brain parenchyma elicits inflammatory mediators from glial cells as well as glial and neuronal apoptosis. Am J Pathol. 2008;173:1415–27. https://doi.org/10.2353/ajpath.2008.080483
44. Trevino SR, Dankmeyer JL, Fetterer DP, Klimko CP, Raymond JLW, Moreau AM, et al. Comparative virulence of three different strains of *Burkholderia pseudomallei* in an aerosol non-human primate model. PLoS Negl Trop Dis. 2021;15:e0009125. https://doi.org/10.1371/journal.pntd.0009125
45. Taweechaisupapong S, Kaewpa C, Arunyanart C, Kanla P, Homchampa P, Sirisinha S, et al. Virulence of *Burkholderia pseudomallei* does not correlate with biofilm formation. Microb Pathog. 2005;39:77–85. https://doi.org/10.1016/j.micpath.2005.06.001
46. Boisvert AA, Cheng MP, Sheppard DC, Nguyen D. Microbial biofilms in pulmonary and critical care diseases. Ann Am Thorac Soc. 2016;13:1615–23. https://doi.org/10.1513/AnnalsATS.201603-194FR
47. Chakraborty P, Bajeli S, Kaushal D, Radotra BD, Kumar A. Biofilm formation in the lung contributes to virulence and drug tolerance of *Mycobacterium tuberculosis.* Nat Commun. 2021;12:1606. https://doi.org/10.1038/s41467-021-21748-6
48. Nyanasegran PK, Nathan S, Firdaus-Raih M, Muhammad NAN, Ng CL. Biofilm signaling, composition and regulation in *Burkholderia pseudomallei.* J Microbiol Biotechnol. 2023;33:15–27. https://doi.org/10.4014/jmb.2207.07032
49. Petras JK, Elrod MG, Ty MC, Dawson P, O'Laughlin K, Gee JE, et al. Locally acquired melioidosis linked to environment—Mississippi, 2020–2023. N Engl J Med. 2023;389:2355–62. https://doi.org/10.1056/NEJMoa2306448

Address for correspondence: Christopher K. Cote and David DeShazer, US Army Medical Research Institute of Infectious Diseases, Bacteriology Division, 1425 Porter St, Fort Detrick, Frederick, MD 21702, USA; email: christopher.k.cote.civ@health.mil; david.deshazer.civ@health.mil

Economic Analysis of National Program for Hepatitis C Elimination, Israel, 2023[1]

Yuval Dadon, Francis B. Mimouni, Ariella Toren, Tal Morgenstern, Lior Barak, Joseph Mendlovic

In 2021, the Israel Ministry of Health began a national hepatitis C elimination program. Implementing a World Health Organization goal, Israel's program involved targeted screening, barrier minimization, workup simplification, awareness campaigns, and a patient registry. We evaluated program costs for testing and treatment. By May 15, 2023, the program had identified 865,382 at-risk persons, of whom 555,083 (64.3%) were serologically screened for hepatitis C virus (HCV), which was detected in 24,361 (4.4%). Among 20,928 serologically positive patients, viremia was detected in 13,379 (63.9%), of whom 10,711 (80%) were treated, and 4,618 (96.5%) of 4,786 persons receiving posttreatment HCV RNA testing had sustained virologic response. We estimated costs of ₪14,426 (new Israel shekel; ≈$3,606 USD) per person whose HCV infection was diagnosed and successfully treated. The program yielded screening and treatment in almost two thirds of the identified at-risk population. Although not eliminated, HCV prevalence will likely decrease substantially by the 2030 target.

Active hepatitis C virus (HCV) prevalence (i.e., HCV PCR positivity) in Israel is estimated to range from 0.1% to >5.5%, depending on risk group affiliation; seroprevalence (i.e., HCV antibody positivity) among the general population is ≈1.96% (*1*–*3*). In Israel, risk groups include immigrants from the former Soviet Union; persons who received blood transfusion before 1992, when HCV testing for blood donations was initiated; persons who inject drugs (PWID); persons with other bloodborne diseases, such as HIV or hepatitis B; and persons who have undergone invasive procedures in places lacking universal precautions to bloodborne infections (*1*,*4*). Untreated HCV infection spontaneously resolves within 6 months postinfection in ≈25% of patients (*5*), but HCV can continue latently for years until complications such as liver cirrhosis or carcinoma emerge (*6*). In addition, chronic HCV carriers remain contagious.

The availability of highly effective direct-acting antiviral (DAA) medications enabled a sustained virologic response (SVR) in >95% of cases, prompting the World Health Organization (WHO) to declare in 2016 that the goal of eliminating HCV by 2030 was achievable (*7*). Subsequently, Israel's Ministry of Health (MoH) launched an HCV elimination program in 2021 (*8*).

We hypothesized that a targeted approach to HCV elimination enabled detection of active disease in >5% of high-risk persons. In addition, we believed that a systematic program could lead to more carrier detection and substantially increase the number of patients treated over time. Finally, we hypothesized that the SVR rate exceeded 95% in compliant patients. Thus, we aimed to evaluate the costs of the HCV elimination program, assess program efficacy in terms of SVR in treated patients, and develop policies for improving program compliance and maximizing SVR.

Methods

Program Elements

The Israel MoH used 5 principles to guide development of the HCV elimination program. Those 5 principles were targeted screening guidelines; identification of barriers and development of strategies to minimize those barriers; clinical workup simplification; awareness campaigns; and a national patient registry.

Author affiliations: Ministry of Health, Jerusalem, Israel (Y. Dadon, A. Toren, T. Morgenstern, L. Barak, J. Mendlovic); Leumit Health Care, Tel Aviv, Israel (F.B. Mimouni); Sackler School of Medicine, Tel Aviv (F.B. Mimouni); Shaare Zedek Medical Center, Hadassah-Hebrew University School of Medicine, Jerusalem (J. Mendlovic)

DOI: https://doi.org/10.3201/eid3010.240210

[1]Preliminary results from this study were presented at the Israel National Institute for Health Policy Research conference; May 31, 2023; Tel Aviv, Israel.

Targeted Screening Guidelines

In 2021, MoH implemented new directives mandating that every citizen who emigrated from an endemic country or identified in any of the risk groups be referred for HCV antibody screening testing. Screening was conducted by each of the 4 health maintenance organizations (HMO), the Health System of the Israeli Defense Forces (IDF) for drafted soldiers, and the Israeli Prison Services (IPS) for long-term prisoners and incomers. MoH also deployed dedicated microelimination taskforces for subpopulations that did not regularly visit a primary care physician (PCP) and that required proactive outreach, such as PWID. Subsequently, all serologically positive persons with a positive reflex PCR test indicative of viremia were started on DAA treatments, as dictated by the Healthcare Basket, the funding system for healthcare in Israel.

Identification and Minimization of Barriers

The MOH developed a taskforce networking policy to assure ongoing collaboration between all relevant parties. Networking involved extensive discussions with all HMOs, IPS, IDF, physician and patient union representatives, the National Councils, and the public. All taskforce delegates were asked to identify potential challenges in program materialization and to offer tailored solutions. Recognized challenges included at-risk population identification, treatment costs, workup and testing costs, and clinic availability.

To address challenges in identifying at-risk populations, when an HMO identified persons with possible inaccurate birth country data, MoH assisted in data retrieval from the national citizen registry. Those data were later transcribed into the well-established HMO electronic medical record (EMR) system. The EMR could automatically alert healthcare workers of persons at high risk for HCV, advise on HCV risks, and refer those patients for testing.

HCV treatment cost gradually extended over time to include a wide range of indications for all disease severity and genotyping (Appendix, https://wwwnc.cdc.gov/EID/article/30/10/24-0210-App1.pdf). Thus, every HCV patient in Israel eventually was eligible for free treatment.

Workup and testing costs were minimized by cancelling the requirement of genotyping assessment because pan-genotypic DAA medications were available (*9*). In addition, costly measures for fibrosis assessment, such as imaging-based diagnostic testing, were replaced by serum laboratory parameter–based assessments.

To address clinic availability, MOH used geographic information systems to map areas of high-risk populations. Using those maps, HMO clinic distribution was adjusted to address targeted populations (Figure 1).

Clinical Workup Simplification

Subsequent workup for patients with HCV viremia was minimized to include only FIB-4 classification assessment, a blood-based diagnostic test for liver fibrosis that relies on 4 parameters: alanine aminotransferase, aspartate aminotransferase, platelet count, and patient age (*10*). FIB-4 eliminated the need for fibrosis and genotyping assessment via time-consuming measures. Use of FIB-4 was based on current clinical guidelines and availability of DAA drugs that do not require genotyping (*11*). FIB-4 reduced the burden on persons with a diagnosed HCV infection and enabled rapid treatment initiation.

FIB-4 index of 1.4 was the defined cutoff for patients with mild disease; those patients could be treated by their PCP and then have HCV RNA PCR testing 12 weeks after treatment. Severe cases (i.e., FIB-4 $\geq$1.4) were referred for gastroenterology evaluation, which previously was used for all HCV-positive cases, regardless of severity (*12*).

Awareness Campaigns

MoH provided healthcare workers with online e-tutorials on the HCV elimination program and their role in it. MOH and HMOs distributed leaflets on HCV to the public in all relevant languages. Leaflets described the HCV asymptomatic phase and the need for early diagnosis and treatment. In addition, MoH opened an HCV web portal (https://govextra.gov.il/ministry-of-health/hepatitis/c-en) and uploaded a questions and answers video to the MOH YouTube channel https://www.youtube.com/watch?v=9Z8vivI0kqA). The strategic network distributed links to the public. MoH representatives also executed media interviews, advertisements, and awareness campaigns. Finally, MoH collaborated with municipalities, unions, and other ministries (e.g., immigration and social affairs) as a major component for increasing awareness and compliance to encourage citizens to undergo HCV screening.

National Patient Registry

The status of each identified patient was monitored via a national registry reported to the MoH in an individualized, yet anonymized, format. Registry data

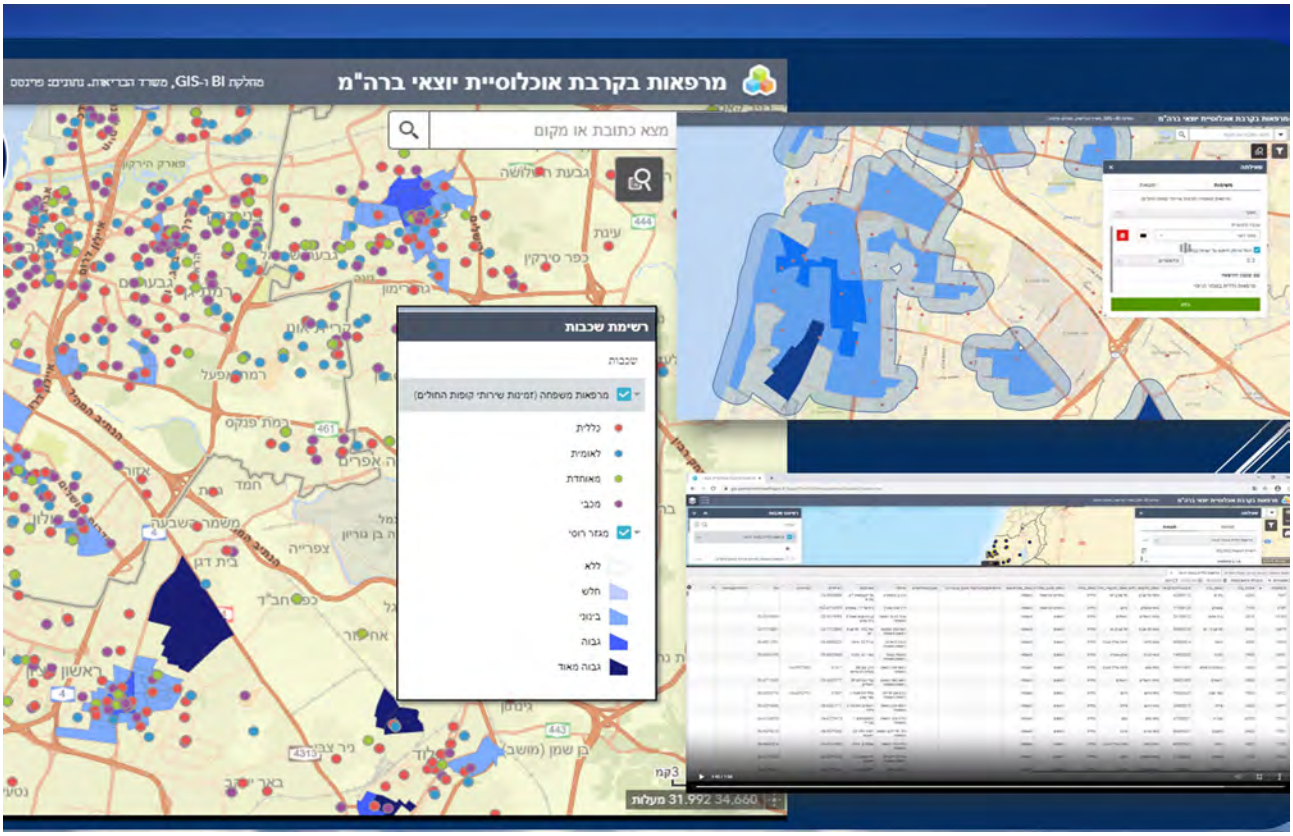

Figure 1. Geographic mapping in an economic analysis of a national program for hepatitis C elimination, Israel, 2023. Screenshot shows Hebrew-language mapping by Points Location Intelligence company (https://points.co.il) in ArcGIS (www.arcgis.com). Upper right inset shows clinic locations (orange dots) at the beginning of the program. Blue shading indicates areas with higher populations of immigrants from the former Soviet Union, who are at higher risk for hepatitis C virus infection; intensity of shading increases as population numbers rise. Detail on left shows increased clinical sites added as part of the hepatitis C elimination program. Each colored dot (orange, blue, green, purple) represents a clinic and its affiliation to 1 of the 4 health maintenance organizations, shaded areas that represent the prevalence of population at risk in a given geographic area. Darker blue indicates higher concentrations of at-risk populations. Combining the 2 parameters (clinics distribution and density of population at risk density) enabled a systematic strategy for a targeted approach to identify and list clinics for higher yield in program accomplishment.

included patient's status from the initial serology testing through subsequent PCR testing, treatment, and eventually SVR, where indicated.

Program Cost Estimation

Annual healthcare costs in Israel are mostly financed by MoH via Healthcare Basket. All citizens have mandatory coverage through 1 of the 4 available HMOs. Coverage comprises all medications, tests, and services that HMOs are obligated to provide to insured patients.

Each year, a joint government–HMO committee examines the scope and costs of the Healthcare Basket. The committee recommends an annual cost expansion by adding new medical treatments to the existing budget of the previous year on the basis of an estimation of the number of eligible patients and the cost of the new treatment. Each HMO is granted funds proportional to the number of enrolled patients. The entire HCV elimination program, including healthcare workforce, testing, and treatment, is provided at no cost to all HMO members. Although we do not provide details of the exact calculations, the costs estimated in this study likely reflect those agreed upon by finance specialists from both the government and the HMOs.

To assess the cost per resolved HCV case, we considered costs for laboratory testing, government budget to cover treatment costs, and costs for liver fibrosis testing. We considered laboratory testing costs throughout a patient's workup process, including serologic screening, subsequent PCR testing, and PCR testing for SVR confirmation. We used MoH's tariff to determine the cost of each laboratory test (*13*). We calculated cost for a subpopulation that had already been tested for HCV and for the subpopulation for

which testing was pending. To calculate the number of required subsequent HCV PCR tests for serologically HCV-positive patients, we assumed the proportion of positive persons among the not-yet-tested subpopulation on the basis of the findings from the tested population. We then estimated overall costs using those assumptions.

We assessed the governmental budget to cover HCV treatment costs, including the gradual expansion of indications over the study period (*13*) (Appendix). Medication pricing represents the final price after MoH negotiated with pharmaceutical companies.

We also included testing for liver fibrosis via imaging or biomarker testing and genotyping for patients with viremia in the assessment. Those tests were later found to be redundant when DAA medications became available. DAA medications are effective against all HCV subtypes and require no prior testing; thus, the overall cost for liver fibrosis assessment was virtually exchanged to cover the cost of other supportive HMO promotional activities, also budgeted by MoH, as part of the Healthcare Basket.

We used available 2021 pricing to calculate all the costs and assumed that pricing changes were essentially unchanged throughout the observation period. We divided the sum of those elements by the number of all resolved HCV infections over the study period, as reported annually to MoH by the different HMOs.

Statistical Analysis

We characterized and summarized at-risk persons by their workup and treatment stage at the country and HMO levels. At the HMO level, we calculated the number of persons in the target risk-group population who participated in the screening process; the prevalence of HCV positivity among persons serologically screened for HCV antibodies; and the prevalence of viremia among seropositive persons tested by PCR. We used χ^2 tests to statistically assess differences between the rates of positivity among HMOs and considered $p<0.001$ statistically significant. We also reported HCV treatment over the study years and number of HCV patients treated on the state and HMO levels.

Results

Findings of Program Progress

Risk Group Identification

By June 13, 2022, the national registry identified a total of 865,382 persons at risk for HCV infection and their birth countries. Among at-risk persons, 98% (863,909) were actively insured by 1 of the 4 HMOs, and the other 2% were either at IPS or IDF or had emigrated out of Israel. At-risk persons included 26,004 persons who immigrated to Israel from Russia and Ukraine during the immigration wave of 2022 due to the escalation of the Russo-Ukrainian War.

We classified immigration data by HMO affiliation. The 2 largest HMOs in Israel had the largest percentage of immigrants, 40.6% and 37.6% (Table 1). We noted no major differences in origin country or age-group distribution when comparing those distributions among HMOs.

HCV Screening Performance

By May 15, 2023, a total of 555,083 (64.3%) persons in the target risk group population had already been screened for HCV (Figure 2). Screening occurred either through the national program or previously as part of the standard workup assessment per clinical requirement, such as liver enzyme elevation assessment.

HCV Seroprevalence

Overall, HCV seroprevalence was 4.4% among the 555,083 persons tested (i.e., 24,361 persons positive for previous infection) (Table 1; Figure 2). Seroprevalence ranged from 3.1% to 6.0% in the different HMOs (Table 1), and those differences were statistically significant ($p<0.001$).

Table 1. Distribution of identified risk groups by HMOs in an economic analysis of a national program for hepatitis C elimination, Israel, 2023*

HMO no.	At-risk persons†	Immigrants‡	Total at-risk persons	Screened for HCV	Serology			
					Testing pending	Positive	Seropositive + PCR-positive	% Viremia
1	73,023 (8.4)	859 (3.2)	73,882 (8.6)	51,891 (70.2)	21,991	2,396 (4.6)	748 (31)	1.4
2	113,982 (13.2)	1,680 (6.5)	114,426 (13.2)	50,387 (44.0)	64,039	1,545 (3.1)	235 (15)	0.5
3	318,380 (36.8)	6,621 (25.5)	325,001 (37.6)	163,386 (50.3)	161,615	9,795 (6.0)	5,614 (57)	3.4
4	359,997 (41.6)	16,844 (64.8)	350,600 (40.6)	289,419 (82.5)	61,181	10,625 (3.7)	6,782 (64)	2.3
Total	865,382	26,004	863,909	555,083 (64.3)	308,826 (35.7)	24,361 (4.4)	13,379 (54.9)	2.4

*Values were assessed by phase of screening status, prevalence of HCV serology and viremia in 4 HMOs. Values are no. (%) except as indicated. HCV, hepatitis C virus; HMO, health maintenance organization.
†Data on at-risk persons included country of birth.
‡Persons who immigrated to Israel from Russia and Ukraine during the immigration wave of 2022 due to the Russia–Ukraine war.

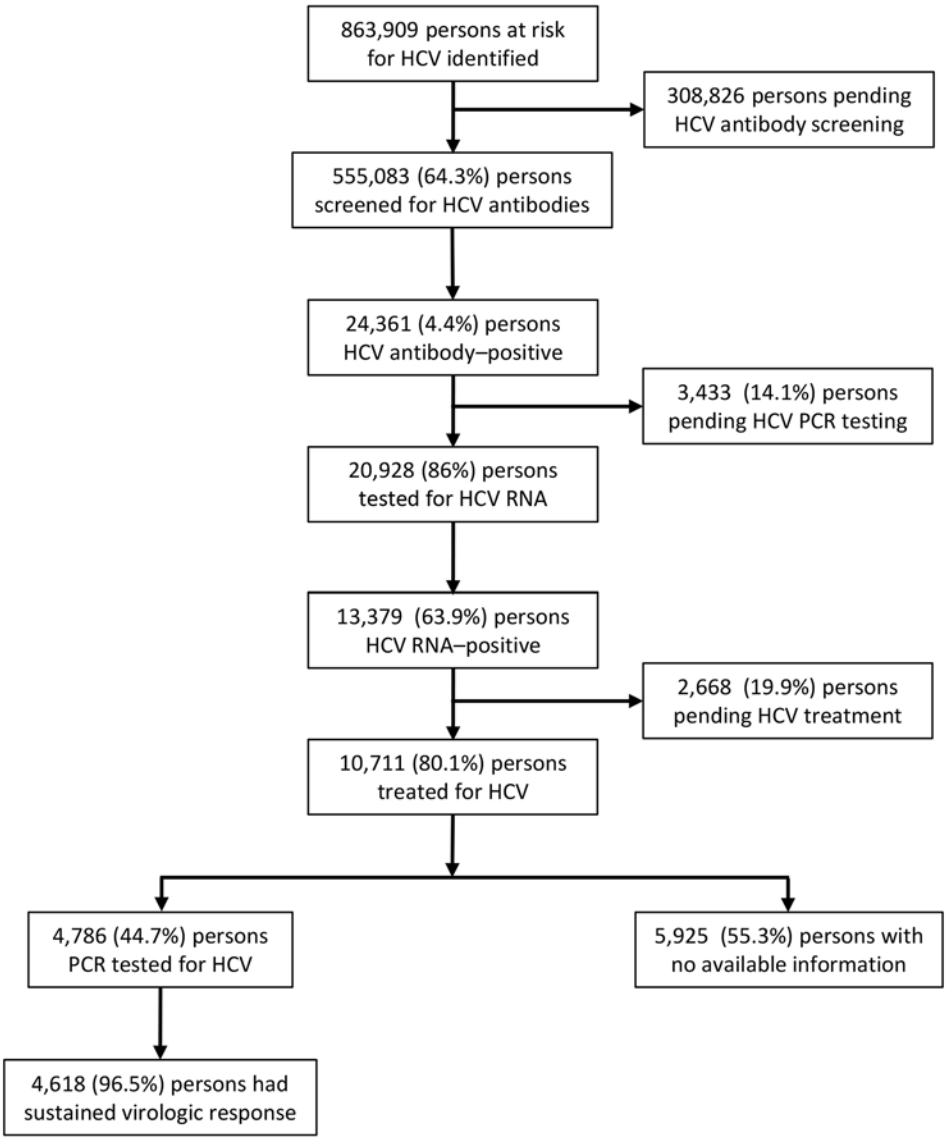

Figure 2. Flowchart of participant enrollment, virologic screening, and HCV treatment in an economic analysis of a national program for hepatitis C elimination, Israel, 2023. HCV, hepatitis C virus.

Subsequent HCV PCR testing for 20,928 (86%) HCV antibody–positive patients identified 13,379 (63.9%) persons with an active HCV infection (Figure 1). The other 3,433 seropositive persons had not yet received further PCR testing, mostly because of noncompliance, despite HMO PCP reminders to get tested. DAA treatment was started and documented in 10,711 (80%) persons (Figure 3), according to MoH's registry for drug prescriptions during 2018–2022.

SVR

Among 10,711 persons treated for HCV, 44.7% (4,786) had available data on HCV RNA testing 12 weeks after treatment completion, among whom 4,618 (96.5%) showed SVR. Patients who did not reach SVR as measured by posttreatment HCV RNA testing continued the standard care follow-up under their HMO, including repeated testing and follow-up. No data are available for that ongoing follow-up.

Pending Workup and Treatment

At the cutoff date for retrieved data, a total of 2,668 (19.9%) HCV patients had not yet started treatment. In addition, 14.1% (3,433) of serologically positive patients had not yet been tested for viremia.

Estimation of Program Cost Per Resolved HCV Case

The overall cost per documented resolved HCV case was ₪14,426 (Israeli new shekel; ≈$3,606 USD). That estimation considers initial serology testing for the identified at-risk population, subsequent PCR testing

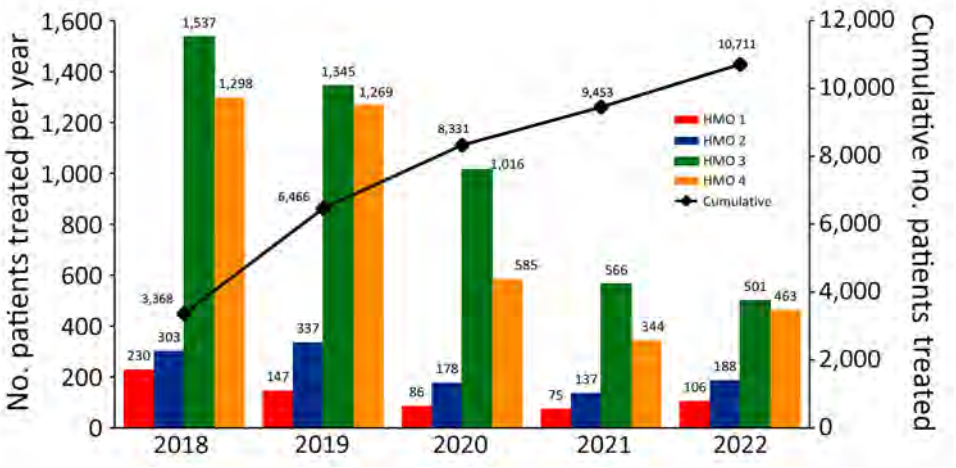

Figure 3. Assessment of patients treated in 4 HMOs in an economic analysis of a national program for hepatitis C elimination, Israel, 2023. Scales for the y-axes differ substantially to underscore patterns but do not permit direct comparisons. HMO, health maintenance organization.

for the seropositive patients, and PCR testing to confirm SVR (Table 2). The cost of the initial serology screening testing for the entire at-risk population of 863,909 identified persons was ₪20.3 million. PCR testing for all 24,361 seropositive patients was ₪10.61 million, and PCR testing for the 13,588 potentially seropositive patients was ₪5.92 million (assuming 4.4% positivity for HCV serology testing), which totaled ₪16.53 million for the entire at-risk population. However, in a worst-case scenario in which Israel could not test or treat additional persons, our assumptions show the country would spend ≈₪290.349 million to treat HCV, or ≈₪28,000 per resolved case. During the study period, the overall HCV treatment cost from the Healthcare Basket was ₪260.86 million (Appendix).

In the program, posttreatment PCR for SVR was performed for tested and potentially PCR-positive patients. Costs for that testing were ₪5.83 million for 13,379 HCV-confirmed and ₪3.79 million for 8,697 potentially PCR-positive patients, which assumes a 64% positivity for HCV PCR testing. Total costs for SVR testing were ₪9.61 million.

Our cost analysis assumptions might provide overly optimistic calculations. Indeed, by the analysis date, only 10,711 persons had started DAA treatment, and only 44.7% of those patients had data on posttreatment SVR. However, the cost analysis assumed that 21,303 persons would achieve SVR, which resulted in an estimated cost of ₪14,426 per resolved HCV case. For example, if 96.5% of persons treated with DAA medications achieved SVR, costs would be ≈₪30,000 per person with SVR.

Discussion

Our data analysis shows that, within a 27-month period, Israel tested 555,083 (64.3%) of 863,909 persons at risk for HCV infection. The program aimed to identify all patients needing treatment by 2030, and our results indicate the program could be construed as a remarkable success. However, the program still has a long way to go to get as close to 100% as possible.

Table 2. Cost estimation per a resolved HCV case in an economic analysis of a national program for hepatitis C elimination, Israel, 2023*

Category	HCV antibody tested			Pending testing			Program total cost
	No. patients	Cost per patient	Total cost	No. patients	Cost per patient	Total cost	
Initial serology	555,083	23.5	13,044,451	308,826	23.5	7,257,411	20,301,862
PCR for positive serology	24,361	435.5	10,609,216	13,588†	435.5	5,917,724	16,526,939
Treatment							260,869,000‡
Posttreatment PCR for SVR	13,379	435.5	5,826,555	8,697§	435.5	3,787,544	9,614,099
No. SVR patients	12,911	NA	NA	8,392¶	NA	21,303	
Total program cost							307,311,900
Cost per resolved HCV case							14,426 ($3,606)#

*A total of 863,909 persons were evaluated via serologic testing for HCV antibodies. Costs are in Israeli new shekel, except where indicated. HCV, hepatitis C virus; NA, not applicable; SVR, sustained viral response.
†Given 4.4% positivity for HCV serology tested.
‡Overall treatment cost at Health Basket.
§Given 64% positivity for HCV PCR testing.
¶Given 96.5% HCV resolution.
#Conversion to US dollars based on 2012 data from ExchangeRates.org (https://www.exchangerates.org). Data should be inflation adjusted for accumulated inflation during 1999–2021.

In addition, of the 555,083 persons tested, HCV seroprevalence was 4.4%, meaning 24,361 persons had positive results of previous infection. Subsequent PCR testing for 20,928 HCV seropositive persons yielded 13,379 (63.9%) with an active infection. Thus, 14.1% (3,433/24,361) seropositive persons had not yet received further PCR testing, despite PCP reminders to get tested. That 14.1% noncompliance rate is concerning because the PCR positivity rate among those persons may be much higher than the 64% positivity rate documented among compliant persons. Moreover, 80.1% (10,711/13,379) of persons received DAA treatment for HCV, indicating a treatment noncompliance rate of 19.9%. Furthermore, SVR was not evaluated in all treated patients, probably because eradication rates from DAA treatment are known to be extremely high. However, among 4,786 (44.7%) persons who received PCR tests, 3.5% still tested HCV RNA–positive.

Nevertheless, compared with other countries facing WHO's initiative for 2030 HCV elimination, Israel shows great progress. A 2022 review of status of the HCV initiative in Europe showed that most countries are not on track to reach the WHO target (*14*). Some countries have not established policies or guidelines for treatment, prevention, or harm reduction. Moreover, because many existing national plans do not include wide-scale screening, HCV treatment rates have even been declining over the past few years. In contrast, in Egypt, a total of 49,630,319 (79.4%) persons out of a target population of 62.5 million spontaneously participated in screening during October 1, 2018–April 30, 2019 (*15*). In just over 7 months, 2.2 million HCV-seropositive persons in Egypt were referred for evaluation and treatment (*15*).

From our data, in view of the lack of absolute compliance in serologic screening, HCV PCR testing, treatment completion, and post treatment testing, HCV likely will not be eradicated in Israel by 2030. Nonetheless, HCV prevalence likely will be substantially reduced, leading to a decrease in the number of new cases.

The program received heavy political support, which likely explains its sustainability. Estimated cost for HCV treatment in Israel gradually expanded by ≈2.63-fold over the years after initial inclusion of DAA medications in 2012. At that time, the overall aggregated Healthcare Basket allocation to treat HCV was ₪99.1 million a year. Allocations rose to ₪261 million in 2018, when all available HCV DAA medications were included and the indications for DAA use expanded to all disease severity and HCV subtypes (Appendix). Of note, policy makers were convinced of the value of investments in resolving HCV cases by 2016, when they included not only therapeutic agents but also ancillary diagnostic testing (i.e., laboratory and imaging for fibrosis assessment) that covered the additional ₪5.58 million per year in workup costs.

By enabling a risk-sharing model between the HMOs and pharmaceutical companies, MoH was able to provide no-cost testing and treatment to patients and later DAA medications free of charge. No-cost testing and treatment is a major factor driving adherence to the program. Also of note, the observed active HCV prevalence of 2.4% in the at-risk population in Israel seems to be lower than the expected prevalence of ≤5.5% for this subgroup based upon previous research (*1*–*3*). We suggest that HCV spontaneous recovery might be higher than 25% and might have increased over the years to >45.5% (*5*).

In 2020, the US Preventive Services Task Force issued a new recommendation for HCV screening, advising that all adults aged 18–79 in the United States without liver disease undergo screening for HCV (*15*). That updated screening recommendation expands the previous guideline, indicating screening only for persons born during 1945–1965 (*16*). Although Israel's MoH did not adopt this recommendation, the results of our study could provide additional support for nonuniversal screening of adults in view of the higher degree of spontaneous recovery among infected persons. Nevertheless, additional investigation, such as a random sample of the general population, may be required to support a change in policy.

Our findings address the overall cost of Israel's HCV elimination program, which is assumed to prevent long-term consequences among persons with resolved infection. Our findings require validation through epidemiologic investigations to verify the effects of the program on the incidence of HCV-related liver disease, residual chronic infection, and associated complications. Furthermore, additional research to accurately assess future cost savings and the impact on disability-adjusted life-years saved is warranted.

The first limitation of our study is that we based it on at-risk population testing and not on universal testing; thus, we cannot estimate the rate of seropositivity in the general population in Israel. Second, we did not have information on persons who emigrated from Israel; thus, our seropositivity rate could be underestimated. Third, completed data on treatment outcome and SVR status were lacking, partly because PCPs assume the high rate of resolution for DAA treatment might not warrant further PCR assessment;

thus, SVR rates might be underestimated. Fourth, PWID are difficult for HMOs to follow, which might have contributed to noncompliance rates. Fifth, ≈36% of the at-risk population had not completed the initial screening despite HMO outreach attempts, and a fraction of those patients persistently refused to undergo any evaluation, although their motives for noncompliance are not completely clear. Thus, those patients, might be the most noncompliant, and might not have achieved HCV resolution even if treated. Sixth, the costs we report reflect costs for medications, tests, and scans going back to 1999 (Appendix). Those costs probably do not accurately reflect the cost to treat the active hepatitis C cohort identified through the elimination program, which formally initiated in 2021. In addition, the cost calculations provided here are estimates based on published information, such as pricing of medications or laboratory tests, and might differ from the real costs incurred by HMOs; thus, our treatment and testing costs could be underestimated. Finally, risk factors for HCV seropositivity, including age, sex, socioeconomic status, and area of residence, were not recorded in a comprehensive registry, as planned, because of operational limitations and the desire to initiate the program as soon as possible. Consequently, valuable analyses, such as differences between patients with and without viremia, could not be assessed and deserve further evaluation.

In conclusion, this study demonstrated that a targeted approach provided HCV screening to a large percentage (64.3%) of identified at-risk persons in Israel and a substantial steady increase in the number of patients treated over time. The SVR results confirm previous research showing HCV resolution in >95% of treated patients. Israel initiated and executed a comprehensive HCV screening and treatment program on a national scale in just 2 years, aligning with WHO's global initiative for HCV elimination. By implementing clear criteria for identifying targeted at-risk persons, mandating their screening, and financially supporting and adequately using existing HMOs' EMR infrastructure, almost two thirds of the at-risk population was screened and treated in less than 2 years. Nonetheless, in view of the above-mentioned limitations, HCV likely will not be eliminated in Israel by 2030, but HCV prevalence will substantially decrease.

Acknowledgments

We thank all our collaborators from the health maintenance organizations, the Israeli National Council of Gastroenterology, and World Health Organization management, and the following for their collaboration: Avital Weiss, Daniella Cohen-Rahamim, Isana Kaplan-Lavi, Shlomit Yaron, Eran Matz, Ziv Ben-Ari, Oren Shibolet, Eli Zukerman, Michelle Thiornine, Julio Burman, Liav Goldstein, and Itamar Grotto.

About the Author

Dr. Dadon is the head of the National Program for Hepatitis C Elimination in Israel at the Israeli Ministry of Health, Jerusalem, Israel. His research interests include policy making for preventable long-term harmful consequences resulting from infectious diseases.

References

1. Cornberg M, Razavi HA, Alberti A, Bernasconi E, Buti M, Cooper C, et al. A systematic review of hepatitis C virus epidemiology in Europe, Canada and Israel. Liver Int. 2011;31:30–60. https://doi.org/10.1111/j.1478-3231.2011.02539.x
2. Weil C, Nwankwo C, Friedman M, Kenet G, Chodick G, Shalev V. Epidemiology of hepatitis C virus infection in a large Israeli health maintenance organization. J Med Virol. 2016;88:1044–50. https://doi.org/10.1002/jmv.24426
3. Blach S, Terrault NA, Tacke F, Gamkrelidze I, Craxi A, Tanaka J, et al.; Polaris Observatory HCV Collaborators. Global change in hepatitis C virus prevalence and cascade of care between 2015 and 2020: a modelling study. Lancet Gastroenterol Hepatol. 2022;7:396–415. https://doi.org/10.1016/S2468-1253(21)00472-6
4. Mukomolov S, Trifonova G, Levakova I, Bolsun D, Krivanogova E. Hepatitis C in the Russian Federation: challenges and future directions. Hepat Med. 2016;8:51–60.
5. Micallef JM, Kaldor JM, Dore GJ. Spontaneous viral clearance following acute hepatitis C infection: a systematic review of longitudinal studies. J Viral Hepat. 2006;13:34–41. https://doi.org/10.1111/j.1365-2893.2005.00651.x
6. Forman MS, Valsamakis A. Hepatitis C virus. In: Versalovic J, Carrol KC, Funke G, Jorgensen JH, Landry ML, Warrock DW, editors. Murray's manual of clinical microbiology, 10th ed. Washington: American Society of Microbiology Press; 2011. p. 1437–55.
7. World Health Organization. Global health sector strategy on viral hepatitis [cited 2023 Dec 30]. http://apps.who.int/gb/ebwha/pdf_files/WHA69/A69_32-en.pdf
8. Israeli Ministry of Health. Press release: the National Program for Hepatitis C Elimination [in Hebrew] [cited 2023 Dec 12]. https://www.gov.il/he/departments/policies/mmk01-2021
9. Sterling RK, Lissen E, Clumeck N, Sola R, Correa MC, Montaner J, et al.; APRICOT Clinical Investigators. Development of a simple noninvasive index to predict significant fibrosis in patients with HIV/HCV coinfection. Hepatology. 2006;43:1317–25. https://doi.org/10.1002/hep.21178
10. Pawlotsky J-M, Negro F, Aghemo A, Berenguer M, Dalgard O, Dusheiko G, et al.; European Association for the Study of the Liver. EASL recommendations on treatment of hepatitis C 2018. J Hepatol. 2018;69:461–511. https://doi.org/10.1016/j.jhep.2018.03.026
11. Blanco-Grau A, Gabriel-Medina P, Rodriguez-Algarra F, Villena Y, Lopez-Martínez R, Augustín S, et al. Assessing liver fibrosis using the FIB4 index in the community setting. Diagnostics (Basel). 2021;11:2236. https://doi.org/10.3390/diagnostics11122236

12. Israeli Ministry of Health. Healthcare basket [in Hebrew] [cited 2023 Dec 30]. https://www.gov.il/en/departments/topics/health-services-subject/govil-landing-page
13. Israeli Ministry of Health. Tariff index [in Hebrew] [cited 2023 Dec 9]. https://www.gov.il/he/departments/dynamiccollectors/moh-price-list
14. Wedemeyer H, Tergast TL, Lazarus JV, Razavi H, Bakoyannis K, Baptista-Leite R, et al. Securing wider EU commitment to the elimination of hepatitis C virus. Liver Int. 2023;43:276–91. https://doi.org/10.1111/liv.15446
15. US Preventive Services Task Force; Owens DK, Davidson KW, Krist AH, Barry MJ, Cabana M, Caughey AB, et al. Screening for hepatitis C virus infection in adolescents and adults: US Preventive Services Task Force recommendation statement. JAMA. 2020;323:970–5. https://doi.org/10.1001/jama.2020.1123
16. Razavi H, Elkhoury AC, Elbasha E, Estes C, Pasini K, Poynard T, et al. Chronic hepatitis C virus (HCV) disease burden and cost in the United States. Hepatology. 2013;57:2164–70. https://doi.org/10.1002/hep.26218

Address for correspondence: Yuval Dadon, Deputy Director Office, Ministry of Health, 116 Menachem Begin St, Tel Aviv 6473912, Israel; email: Yuval.dadon@moh.gov.il

etymologia revisited

Treponema
[trep″o-ne′mə]

From the Greek *trepo* (rotate, turn) and *ne¯ma* (thread), *Treponema* is a genus of gram-negative, anaerobic or microaerophilic bacteria. They are spiral-shaped and have flagella, which extend from motors at the pole, producing undulating movement through fluids, enabling tissue invasion and dissemination. In 1905, microbiologist Fritz Richard Schaudinn and dermatologist Paul Erich Hoffmann described *Treponema pallidum* subsp. *pallidum* as *Spirochaeta pallida* from a fresh human vulvar lesion.

Treponema spp. can invade the epidermis and oral, intestinal, and genital mucosa of humans and animals. They cause human diseases, such as syphilis, yaws, pinta, and bejel, and animal diseases, such as digital dermatitis. *T. phagedenis*, *T. pedis*, and *T. medium* infect mainly cattle. *T. paraluiscuniculi* can cause syphilis in rabbits.

Most *Treponema* spp. are not cultivable, except for *T. palllidum* subsp. *pallidum* and *T. phagedenis*. *T. pallidum* subsp. *pallidum* causative syphilis is a reemerging disease in industrialized countries. Digital dermatitis, a polytreponemaldisease, is considered to be the major infectious claw disease in cattle worldwide.

Sources

1. Dorland's illustrated medical dictionary. 32nd ed. Philadelphia: Elsevier Saunders; 2012.
2. Edmondson DG, Hu B, Norris SJ. Long-term in vitro culture of the syphilis spirochete *Treponema pallidum* subsp. *pallidum*. MBio. 2018;9:e01153. https://doi.org/10.1128/mBio.01153-18
3. Nally JE, Hornsby RL, Alt DP, Whitelegge JP. Phenotypic and proteomic characterization of treponemes associated with bovine digital dermatitis. Vet Microbiol. 2019;235:35–42. https://doi.org/10.1016/j.vetmic.2019.05.023
4. Oriel JD. The scars of Venus: a history of venereology. London: Springer-Verlag; 1994.
5. Šmajs D, Zobaníková M, Strouhal M, Čejková D, Dugan-Rocha S, Pospíšilová P, et al. Complete genome sequence of *Treponema paraluiscuniculi*, strain Cuniculi A: the loss of infectivity to humans is associated with genome decay. PLoS One. 2011;6:e20415. https://doi.org/10.1371/journal.pone.0020415

Originally published in April 2021

https//wwwnc.cdc.gov/eid/article/27/4/et-2704_article

Population Structure and Antimicrobial Resistance in *Campylobacter jejuni* and *C. coli* Isolated from Humans with Diarrhea and from Poultry, East Africa

Nigel P. French, Kate M. Thomas, Nelson B. Amani, Jackie Benschop, Godfrey M. Bigogo, Sarah Cleaveland, Ahmed Fayaz, Ephrasia A. Hugho, Esron D. Karimuribo, Elizabeth Kasagama, Ruth Maganga, Matayo L. Melubo, Anne C. Midwinter, Blandina T. Mmbaga, Victor V. Mosha, Fadhili I. Mshana, Peninah Munyua, John B. Ochieng, Lynn Rogers, Emmanuel Sindiyo, Emanuel S. Swai, Jennifer R. Verani, Marc-Alain Widdowson, David A. Wilkinson, Rudovick R. Kazwala, John A. Crump,[1] Ruth N. Zadoks[1]

Campylobacteriosis and antimicrobial resistance (AMR) are global public health concerns. Africa is estimated to have the world's highest incidence of campylobacteriosis and a relatively high prevalence of AMR in *Campylobacter* spp. from humans and animals. Few studies have compared *Campylobacter* spp. isolated from humans and poultry in Africa using whole-genome sequencing and antimicrobial susceptibility testing. We explored the population structure and AMR of 178 *Campylobacter* isolates from East Africa, 81 from patients with diarrhea in Kenya and 97 from 56 poultry samples in Tanzania, collected during 2006–2017. Sequence type diversity was high in both poultry and human isolates, with some sequence types in common. The estimated prevalence of multidrug resistance, defined as resistance to ≥3 antimicrobial classes, was higher in poultry isolates (40.9%, 95% credible interval 23.6%–59.4%) than in human isolates (2.5%, 95% credible interval 0.3%–6.8%), underlining the importance of antimicrobial stewardship in livestock systems.

Campylobacter jejuni and *C. coli* are causes of foodborne enteric infection worldwide (*1*). *Campylobacter* spp. are among the most frequent pathogens identified in diarrheal samples from persons in Africa, particularly in children (*2*), and among World Health Organization regions, the highest burden of campylobacteriosis is observed in the Africa Region (*1*). Lack of surveillance data hinders attempts to assess the actual burden in this setting (*2*), however, and determining whether *Campylobacter* is the causal agent of diarrhea can be difficult (*3*). *Campylobacter* spp. are increasingly recognized as associated with other conditions, including stunting (*4*).

Animals and foods of animal origin make an increasing contribution to human nutrition in low- and middle-income countries as sources of high-quality

Author affiliations: Massey University, Palmerston North, New Zealand (N.P. French, J. Benschop, A. Fayaz, A.C. Midwinter, L. Rogers, D.A. Wilkinson); Ministry for Primary Industries, Wellington, New Zealand (K.M. Thomas); Kilimanjaro Clinical Research Institute, Kilimanjaro Christian Medical Centre, Moshi, Tanzania (N.B. Amani, E.A. Hugho, E. Kasagama, M.L. Melubo, B.T. Mmbaga, V.V. Mosha, F.I. Mshana); Centre for Global Health Research, Kenya Medical Research Institute, Kisumu, Kenya (G.M. Bigogo, J.B. Ochieng); University of Glasgow, Glasgow, Scotland, UK (S. Cleaveland, R. Maganga, R.N. Zadoks); Sokoine University of Agriculture, Morogoro, Tanzania (E.D. Karimuribo, R.R. Kazwala); Kilimanjaro Christian Medical University College, Moshi (B.T. Mmbaga), US Centers for Disease Control and Prevention, Nairobi, Kenya (P. Munyua, J.R. Verani, M.-A. Widdowson); Nelson Mandela African Institution of Science and Technology, Arusha, Tanzania (E. Sindiyo), Ministry of Livestock and Fisheries, Dodoma, Tanzania (E.S. Swai); University of Otago, Dunedin, New Zealand (J.A. Crump); University of Sydney, Sydney, New South Wales, Australia (R.N. Zadoks)

DOI: https://doi.org/10.3201/eid3010.231399

[1]These senior authors contributed equally to this article.

protein and micronutrients (*5*). Food of animal origin is also a source of zoonotic pathogens, including *Campylobacter* spp.; 3 systematic reviews identified poultry (*6*–*8*) as a source of *Campylobacter* spp. in Africa. In Tanzania, consumption of chicken meat was the only animal-related risk factor for human campylobacteriosis (*9*), and genetic studies demonstrate the possibility of transmission between poultry and children (*10*).

Molecular epidemiologic approaches have improved our understanding of sources of human *Campylobacter* infection and contributed to campylobacteriosis control programs in high-income countries (*11*,*12*). Earlier molecular studies used low-resolution techniques such as 7-gene multilocus sequence typing (MLST) (*11*,*12*), whereas in recent years, whole-genome sequencing (WGS) has played an increasing role in informing control strategies (*13*). To date, few studies of *Campylobacter* spp. in Africa using WGS exist (*14*,*15*), and even fewer have been conducted comparing human and poultry isolates (*16*).

The prevalence of antimicrobial resistance (AMR) is high among *C. jejuni* and *C. coli* isolated from humans (*9*,*16*), poultry (*16*–*18*), and other animals (*7*) in sub-Saharan Africa. Examining the genomic epidemiology of *Campylobacter* spp. and evidence for AMR in isolates from poultry and humans in this region is necessary. To this end, we integrated food safety research in northern Tanzania (*19*) with an established diarrheal disease etiology surveillance system in neighboring Kenya to provide detailed WGS and AMR data on *Campylobacter* spp. isolated from persons with diarrhea and from poultry in East Africa and to explore similarities and differences between isolates from humans and from chickens reared in different farming systems.

Materials and Methods

Study Setting and Sampling

Chicken Isolates from Tanzania

We conducted sampling during October 10, 2016–July 24, 2017, at 66 poultry farms in Arusha City and Moshi Municipal Districts, Tanzania (Figure 1). We collected cloacal swab specimens from ≤10 visually healthy chickens per farm in 8 randomly selected wards in Arusha City District and 10 randomly selected wards in Moshi Municipal District. Per ward, we included up to 1 farm per production system; production systems were classified as extensive (not housed, indigenous breeds), semi-intensive (partly housed, indigenous breeds), intensive (fully housed, indigenous breeds), and broiler (fully housed, exotic breeds) (*20*). We collected cloacal swab specimens from live animals using Amies charcoal transport swabs (Sterilin Ltd, http://www.sterilin.co.uk) and transported samples in a cooler box with freezer packs to Kilimanjaro Clinical Research Institute Biotechnology Laboratory in Moshi for processing on the day of sampling. We isolated and identified *Campylobacter* as described by Sindiyo et al. (*20*) (Appendix, https://wwwnc.cdc.gov/EID/article/30/10/23-1399-App1.pdf).

Human Isolates from Kenya

We requested *Campylobacter* isolates collected from human stool (n = 81) from Tabitha Clinic, Kibera, Nairobi (urban informal settlement), and St. Elizabeth Lwak Mission Hospital, Asembo, western Kenya (rural site), during December 14, 2006–March 22, 2016, from the Population-Based Infectious Disease Surveillance platform, implemented by the Kenya

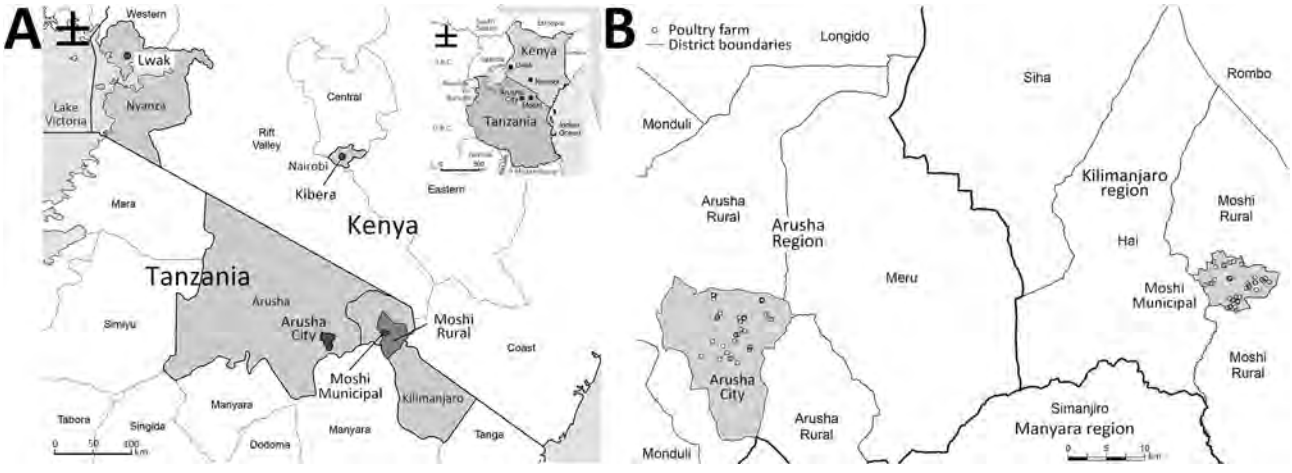

Figure 1. Location of sampling sites in study of population structure and antimicrobial resistance in *Campylobacter jejuni* and *C. coli* isolated from humans with diarrhea and from poultry, East Africa, 2006–2017. A) Data collection sites in Lwak and Kibera in Kenya and Arusha and Kilimanjao in northern Tanzania. Inset shows location of Kenya and Tanzania in East Africa. B) Poultry farm locations sampled in Arusha and Kilimanjaro regions, northern Tanzania.

Medical Research Institute in collaboration with the US Centers for Disease Control and Prevention (CDC) as described in Crump et al. (*19*). Isolates were shipped to Kilimanjaro Clinical Research Institute in Trypticase Soya Broth with 20% glycerol (BD Diagnostics, https://www.bd.com) and stored at −80°C (Appendix).

Molecular Confirmation and WGS Analysis of *Campylobacter* Isolates

We sent *Campylobacter* isolates in brain–heart infusion plus glycerol on dry ice to mEpiLab, Hopkirk Research Institute, Massey University (Palmerston North, New Zealand), for WGS and analysis. Isolates were subcultured on Columbia horse blood agar (Fort Richard Laboratories, https://www.fortrichard.com) at 42°C in a microaerobic atmosphere (5% O_2, 10% CO_2, 85% N_2) provided by a MACS VA500 incubator (Don Whitley Scientific, https://www.dwscientific.com). We extracted DNA using the QiaAmp DNA minikit (QIAGEN, https://www.qiagen.com) and confirmed *Campylobacter* isolates by PCR using *hipO* (*21*) and *ceuE* primers (*22*). We performed library preparation using an Illumina NexteraXT library preparation kit (Illumina, https://www.illumina.com) according to the manufacturer's instructions. We submitted prepared libraries to New Zealand Genomics Limited (University of Otago, Dunedin, New Zealand), which performed sequencing using Illumina HiSeq 2 × 125-bp PE v4 instrument. We submitted raw sequence data to the National Center for Biotechnology Information (NCBI) (https://www.ncbi.nlm.nih.gov/bioproject) under BioProject no. PRJNA1026168, and we use accession numbers to refer to the sequences.

Antimicrobial Susceptibility Testing and Analysis

We performed antimicrobial susceptibility testing (AST) against gentamicin, ampicillin, ciprofloxacin, nalidixic acid, erythromycin, trimethoprim/sulfamethoxazole, and tetracycline on all human and poultry isolates as described by the EUCAST disk diffusion method (*23*,*24*). We used horse blood Mueller-Hinton agar supplemented with β-nicotinamide adenine dinucleotide (Fort Richard Laboratories) with microaerobic atmosphere (MACS VA500) at 41°C for 24 ±2 hours. We interpreted data according to EUCAST guidelines for *Campylobacter* for ciprofloxacin, erythromycin, and tetracycline; EUCAST guidelines for Enterobacterales for ampicillin, gentamicin, and trimethoprim/sulfamethoxazole; and Clinical and Laboratory Standards Institute guidelines for Enterobacterales for nalidixic acid (*25*). We displayed the frequencies of AMR phenotypes using UpSet plots in R (The R Project for Statistical Computing, https://www.r-project.com) using the packages ComplexUpset and ComplexHeatmap (https://github.com/krassowski/complex-upset).

We evaluated estimates of the prevalence of AMR in human and poultry isolates, where the outcome of interest was defined as resistance to ≥1 (AMR) or ≥3 (multidrug resistance [MDR]) classes, using intercept-only Bayesian regression models with AMR and MDR as Bernoulli distributed response variables. We assumed isolates from humans were statistically independent. To account for nonindependence between multiple isolates from the same flock or bird, we randomly selected 1 isolate from each farm. We repeated this random selection to create 500 random datasets, then used those datasets to create a combined posterior distribution using the outputation method (*26*). We fitted models using the R package brms (*27*) using 4 chains with 2,000 iterations per chain for each of the 500 poultry datasets and 1×10^6 iterations for the human dataset and a 50% burn in. To improve convergence and avoid overfitting, we specified mildly informative, conservative priors on the fixed effects (Normal [0, 5]). We describe results as mean prevalence estimates and mean differences in prevalence between poultry and human isolates with 95% credible intervals (CrIs).

Genetic and Phylogenetic Analyses

We characterized all isolates according to their 7-gene sequence type (ST) and clonal complex (CC) by uploading contig fasta files to the PubMLST *Campylobacter* website (*28*). In addition, we identified genes and alleles associated with resistance using the Comprehensive Antibiotic Resistance Database (*29*) and customized scripts for extracting and aligning individual genes and detecting mutations associated with resistance.

We established cgMLST allele profiles by using the 1343 gene cgMLST scheme (*30*) and plotted them as a minimum spanning tree using the MSTree V2 algorithm in GrapeTree (*31*). We created a circular dendrogram based on single linkage clustering of isolates and their cgMLST profiles with metadata on the host, farm type, *Campylobacter* species, resistome, and AST using the Interactive Tree of Life online tool (*32*).

Ethics Statement

This study was approved by the Tanzania National Institutes for Medical Research National Research Ethics Coordinating Committee, Kilimanjaro Christian Medical University College Research Ethics Committee, the Kenya Medical Research Institute

Scientific and Ethics Review Unit, the University of Otago Human Ethics Committee, and the University of Glasgow School of Veterinary Medicine Research Ethics Committee. The protocol for the source of the human isolates was approved by the Kenya Medical Research Institute Scientific and Ethics Review Committee (SSC protocol nos. 1899 and 2761). This activity was reviewed by CDC and was conducted consistent with applicable federal law and CDC policy as provided for in the Code of Federal Regulations (45 C.F.R part 46 and 21 C.F.R. part 56). Written informed consent was obtained from participants (or parent or guardian) before stool specimen collection.

Results

Campylobacter spp. Prevalence and Population Structure

We isolated *Campylobacter* spp. from 56 (8.6%) of 649 chicken cloacal swab specimens (Table). Differences in prevalence between farm types were not significant (χ^2 test at farm level p>0.05).

All isolates (n = 178) were confirmed as *C. jejuni* or *C. coli* and used for WGS and AST, including 81 from patients with diarrhea (44 from Lwak and 37 from Kibera) and 97 from 56 poultry samples (15 singletons and 82 pairs of isolates from 41 birds from 33 farms). *C. coli* made up 6 (7.4%) of 81 human isolates and 18 (18.6%) of 97 poultry isolates. The remaining isolates were *C. jejuni*.

We identified 11 *C. coli* STs and 67 *C. jejuni* STs, including 57 STs from patients with diarrhea and 29 STs in poultry samples. The most common STs were *C. jejuni* ST353 (4 human and 10 poultry isolates from 6 farms), ST2122 (10 poultry isolates from 4 farms), and ST1932 (9 poultry isolates from 5 farms), and *C. coli* ST8043 (11 poultry isolates from 5 farms), each of which comprised <6.2% of the isolate collection. The most common CCs were CC353 (7 human and 20 poultry isolates), CC354 (7 human and 4 poultry isolates), and CC828 (6 human and 5 poultry isolates). Human and poultry isolates were distributed around the minimum spanning tree showing the population structure according to cgMLST (Figure 2); some clusters represented 7-gene CC or ST derived from mixed host populations and others associated with a single host (e.g., CC257, CC460/ST1932, ST2122, and ST8043 in poultry; CC45 and CC403 in humans).

By cgMLST, isolates were largely clustered according to their STs and CCs, with some exceptions. For example, *C. jejuni* CC49 isolates clustered in 2 distinct clades; 1 included ST479 and ST10922 and 1 included ST3720 and ST4624. Further, most isolates belonging to *C. jejuni* CC353 clustered together, with the exception of 1 isolate belonging to ST1036. The most closely related human and poultry isolates differed by 53 alleles on the basis of cgMLST; all were identified as ST362 based on 7-gene MLST.

At the time of writing, 22 (12.4%) isolates belonged to STs that were unique to this study (ST numbers 10893 and above). Three (1.7%) were *C. coli* isolates from CC828 and the remainder were *C. jejuni* (Appendix Tables 1, 2).

Of the 29 STs from poultry samples, 9 (31%) were identified on multiple farms (e.g., ST353 on 6 [9.1%] farms, ST1932 and ST8043 on 5 [7.6%] farms each, and ST2122 on 4 [4.5%] farms) (Figure 3). ST353, ST1932, and ST2122 were identified in Arusha and Moshi, whereas ST8043 was only identified in Moshi. For isolates belonging to the same ST, the median pairwise allele difference between isolates from the same farm on the basis of cgMLST was 46 (interquartile range [IQR] 38–59.75, range 15–230), whereas the median pairwise allele difference between isolates from different farms was 167 (IQR 102.5–245, range 24–497).

Table. Prevalence of *Campylobacter* spp. in poultry by region and production type, Tanzania, 2016–2017*

Characteristic	Farm-level prevalence		
	Prevalence, %	No. positive	No. sampled
Region			
Arusha City	42.3	11	26
Moshi Municipal	55.0	22	40
Production type			
Extensive	37.5	6	16
Semi-intensive	43.8	7	16
Intensive indigenous	72.2	13	18
Intensive broiler	43.8	7	16

*There were no significant differences in prevalence between regions and production types (χ^2 test p >0.6 for both contingency tables).

Antimicrobial Resistance

AMR was detected in 75.3% (95% CrI 65.4–83.9%) and MDR was detected in 2.5% (95% CrI 0.3–6.8%) of 81 human isolates, and the point estimates of prevalence were similar in both regions (75.7% in Kibera and 75.0% in Lwak for AMR and 2.7% in Kibera and 2.3% in Lwak for MDR). No evidence of a trend in resistance in human isolates over the period of collection was seen. In poultry, the crude estimate of AMR prevalence was 85.7% of 97 poultry isolates from 87.5% of 56 poultry samples. The crude estimate of MDR prevalence was 40.2% of 97 poultry isolates from 44.6% of 56 poultry samples. After allowing for clustering of isolates within farms, the estimated prevalence in poultry was 85.4% (95% CrI 70.6–95.8%) for AMR and 43.1% (95% CrI 25.6%–61.4%) for MDR. The estimated difference between poultry and humans was

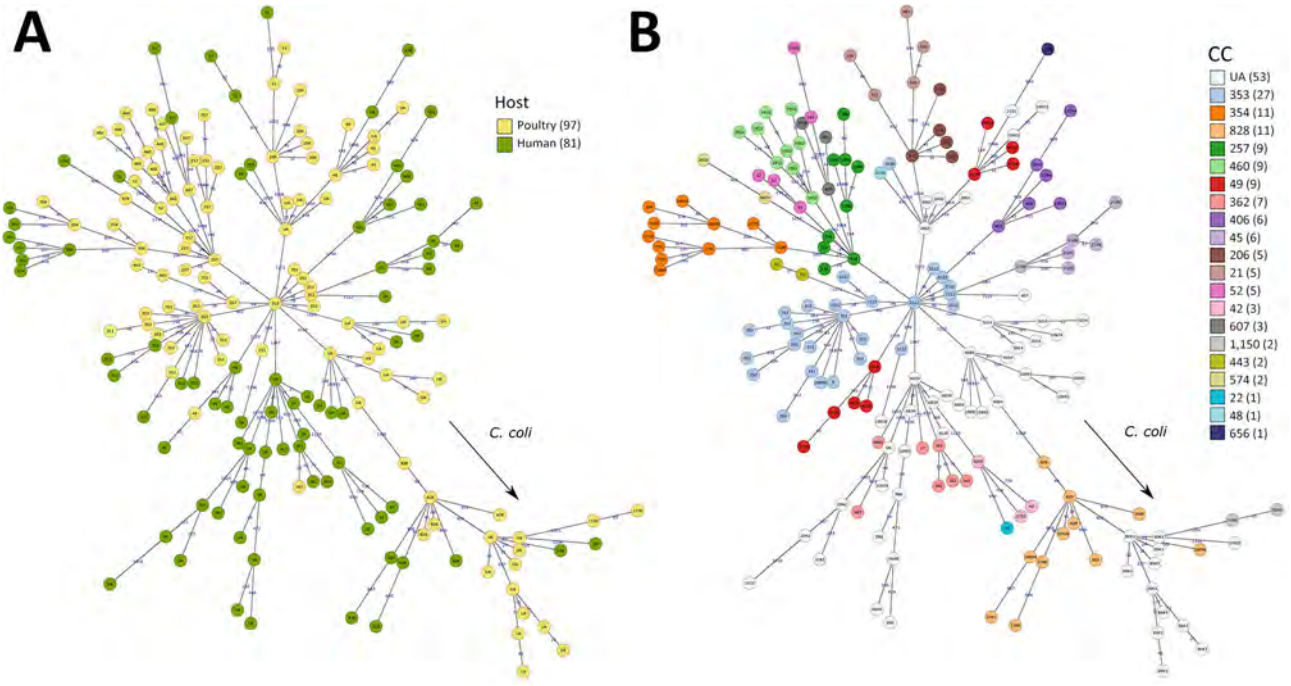

Figure 2. Minimum spanning tree population structure of *Campylobacter jejuni* and *C. coli* isolated from humans with diarrhea and from poultry from Kenya and Tanzania, 2006–2017 (human) or 2016–2017 (poultry), based on core genome multilocus sequence types profiles. A) Plot colored by host (human or poultry) with CC indicated in each node; B) plot colored by CC with sequence type indicated in each node. Core-genome multilocus sequence type allele differences are indicated on each branch. CC, clonal complex; UA, unassigned.

nonsignificant for AMR (10.1% [95% CrI −7.0% to 24.8%, including 0]), but significant for MDR (40.6% [95% CrI 22.7%–59.1%, excluding 0]).

The most resistant isolates were resistant to 5 of the 6 classes of antimicrobial drugs tested. That phenotype was observed in 5 isolates from 3 birds from 2 farms, an intensive indigenous farm and a broiler farm, and all were *C. coli* belonging to ST8043.

The distribution of AST profiles differed between human and poultry isolates; 6 of the 9 MDR profiles were only found in poultry, and of the 5 most common resistance profiles among poultry isolates, only 1 was also detected in human isolates (Figure 4). The most common AMR profile in human isolates was resistance to trimethoprim/sulfamethoxazole, whereas the most common profile in poultry isolates was resistance to ciprofloxacin, nalidixic acid, trimethoprim/sulfamethoxazole, and tetracycline. Of the 41 birds with 2 isolates, 36 (87.8%) had pairs of isolates with identical AST profiles (Figure 5). All isolates were susceptible to gentamicin.

Relationship among AST, Genotype, and Host

The relationship among the population structure, as determined by single linkage clustering of cgMLST profiles, and other epidemiologic, genotypic, and phenotypic variables was displayed as a circular dendrogram (Figure 5). We observed near-complete concordance between the genomically derived resistome and AST phenotypes associated with fluoroquinolone, macrolide, and tetracycline resistance. All isolates that were resistant to ciprofloxacin and nalidixic acid carried the C257T mutation, associated with fluoroquinolone resistance in the *gyr*A gene. Similarly, we observed complete concordance between the presence of the A2075G mutation in the 23S rRNA gene, associated with macrolide resistance and resistance to erythromycin. Tetracycline resistance was found in all isolates with the *tet*O gene, with the exception of isolate ZLB391b. In contrast, agreement was relatively poor between the presence of the β-lactamase–encoding gene bla_{OXA} and ampicillin resistance, and no isolates with genes associated with aminoglycoside resistance were resistant to gentamicin.

Discussion

This study provides a detailed description of the population structure of *Campylobacter* spp. isolated from clinically healthy poultry and persons with diarrhea in East Africa and associations with AMR phenotypes, genes, and alleles. Key findings include evidence of a relatively high prevalence of AMR (>75%) in both human and poultry isolates and a higher prevalence of MDR in isolates from poultry

than in those from humans. Further, considerable genetic heterogeneity within and between human and poultry *Campylobacter* isolates and many previously unreported STs were observed. The absence of dominant STs is in contrast to findings for nontyphoidal *Salmonella* collected from the same region over the same time period where 2 STs include almost two thirds of human diarrhea–derived isolates and 4 STs account for more than three quarters of poultry-derived isolates (*19*).

Earlier studies conducted in Tanzania estimated a similarly high farm-level prevalence of *Campylobacter* in poultry and also provided evidence of a higher prevalence of *C. jejuni* than *C. coli* and a higher prevalence in free-range chicken than in broilers (*10*,*33*). Those Tanzania studies did not examine AMR or sequence data. In contrast, a study conducted in Botswana showed evidence of a relatively higher prevalence of *C. coli* than *C. jejuni* in broilers compared with free-range poultry (*16*), and a higher

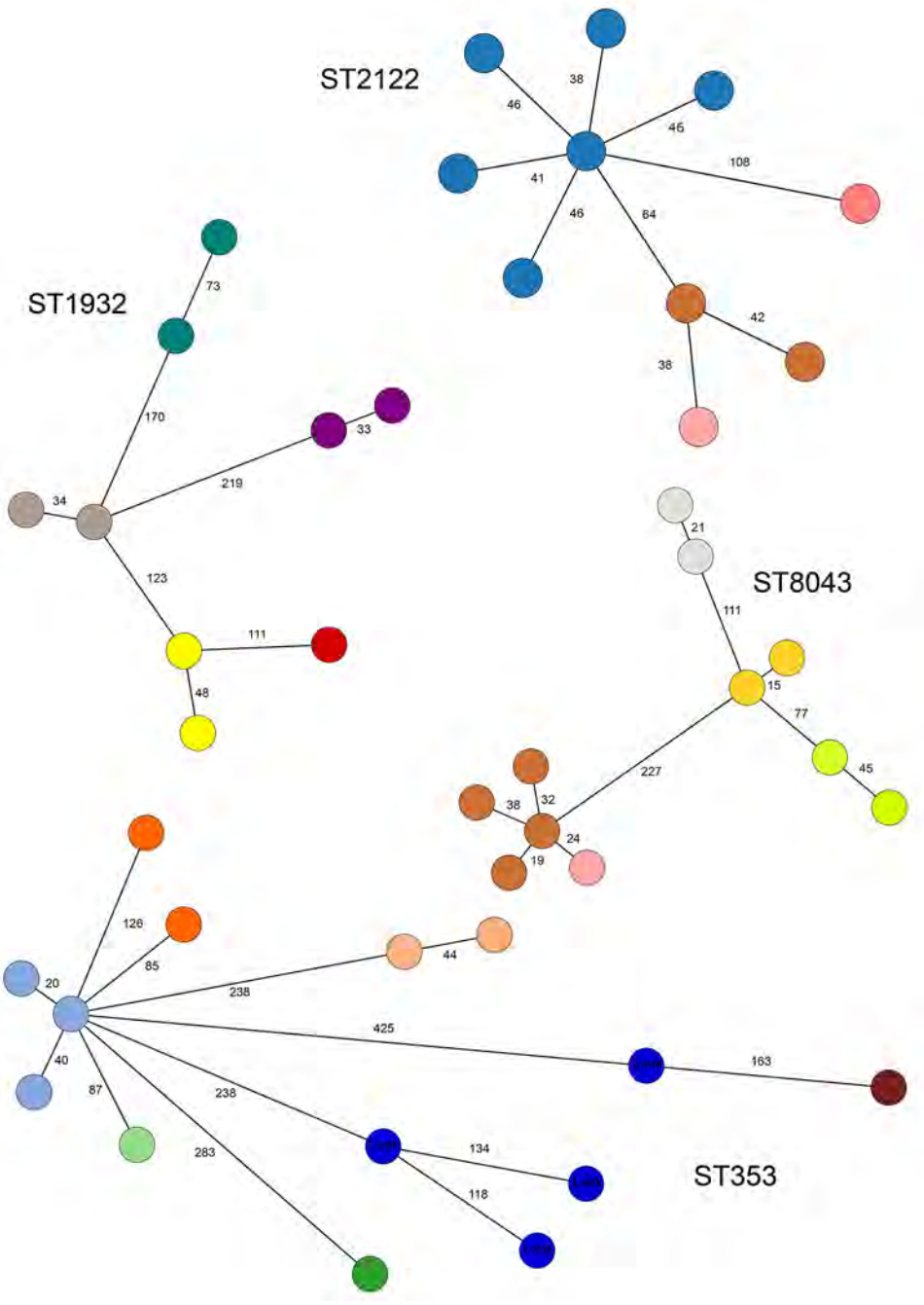

Figure 3. Minimum spanning tree of core-genome multilocus sequence types profiles from the 4 most prevalent 7-gene multilocus sequence type–based ST isolated from poultry in Tanzania, 2016–2017, in a study of *Campylobacter jejuni* and *C. coli,* East Africa. Each color represents a different farm, with the exception of 4 ST353 isolates from human cases (dark blue). Core genome multilocus sequence type allele differences are indicated on each branch. The 2 pairs of isolates from different farms with the lowest number of allele differences, belonging to ST8043 (24 allele differences) and ST2122 (38 allele differences) (shown in brown and light pink) were from 2 farms in the same location in Luongo, Moshi. One was an intensive indigenous farm (light pink isolates), and the other was an intensive broiler farm (brown isolates). ST, sequence type.

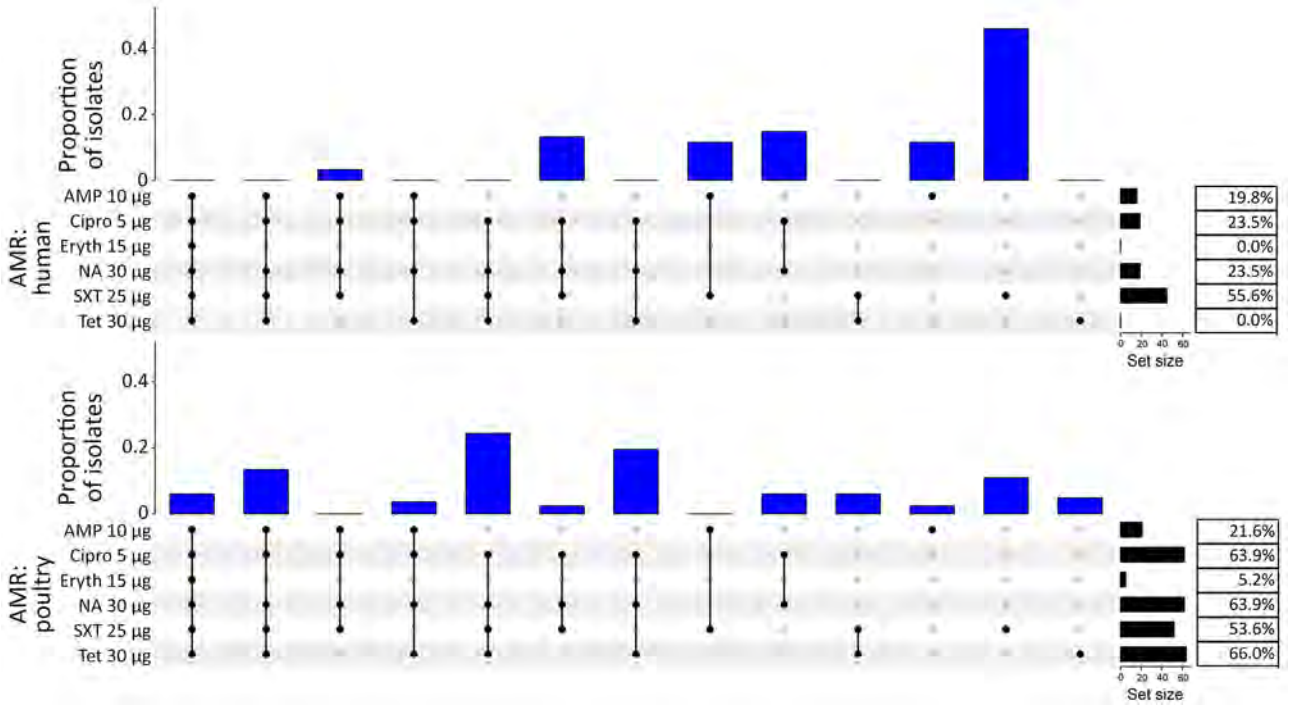

Figure 4. Distribution of different combinations of AMR in *Campylobacter jejuni* and *C. coli* human isolates from Kenya (top, n = 81) and poultry isolates from Tanzania (bottom, n = 97) in study of population structure and AMR in *C. jejuni* and *C. coli* isolated from humans with diarrhea and from poultry, East Africa, 2006–2017. The percentage of isolates resistant to each antimicrobial is given in the table to the right of each plot. All isolates were susceptible to gentamicin. The histogram represents proportion of isolates by antimicrobial resistance pattern. Black dots represent AMR and gray dots represent absence of AMR to the specific antimicrobial agent listed. Black lines join black dots to visualize patterns of AMR. AMP, ampicillin; AMR, antimicrobial resistance; Cipro, ciprofloxacin; Eryth, erythromycin; NA, nalidixic acid; SXT, trimethoprim/sulfamethoxazole; Tet, tetracycline.

prevalence of AMR was observed in *C. coli* than in *C. jejuni*. In common with our Tanzania study, the Botswana study used WGS and included 3 isolates belonging to *C. coli* ST8043, all of which carried *tetO* and bla_{OXA} genes; 1 had the *gyrA* C257T mutation encoding for quinolone resistance. Both in our study and in the study from Botswana, some STs were shared between humans and poultry, suggesting the possibility of interspecies transmission as also observed for certain types of nontyphoidal *Salmonella* (*19*). However, both studies were population-level studies, and analysis of epidemiologically linked isolates (e.g., from humans and animals within the same household or farm, or from poultry meat and its handlers and consumers) would be needed to generate direct evidence of interspecies transmission.

Comparison of the cgMLST allele differences within and between poultry farms showed greater similarity of isolates within farms compared with between farms, consistent with lower between-farm transmission than within-farm transmission. However, the 2 pairs of isolates from different farms with the lowest number of allele differences, belonging to ST8043 (24 allele differences) and ST2122 (38 allele differences) (Figure 3), were from 2 farms in the same location in Luongo, Moshi. Of those farms, 1 was an intensive indigenous farm and the other an intensive broiler farm. This finding is consistent with local spread or spread from a common source, such as shared equipment, inputs, or the environment (*34*), underlining the importance of biosecurity for preventing the spread of foodborne pathogens and AMR within the poultry sector.

Other studies of potential sources of human campylobacteriosis in Tanzania include *C. jejuni* and *C. coli* in duck intestinal contents (*35*), pig fecal samples (*36*), and beef carcasses and raw milk (*37*). In the study of beef carcasses and raw milk, prevalence of AMR was similar to that observed in poultry in our study.

Few studies have reported MDR prevalence estimates in human isolates in Kenya. However, 1 review (*6*) indicates a low prevalence of AMR in human isolates across multiple antimicrobials, similar to other countries in Africa and this study. By inference from individual AMR prevalence estimates, MDR in *C. jejuni* in Kenya was at most ≈10% (*6*).

Of the 78 STs identified in this study, 27 have been isolated from other countries in Africa and

recorded on PubMLST. Those isolates include the most prevalent STs: ST353, which has also been isolated from Malawi, and ST1932 and ST8043, which have been isolated from Botswana (Appendix Table 2).

With the exception of β-lactams and aminoglycosides, the resistome was strongly correlated with the AST results; the *tetO* gene was associated with tetracycline resistance (*38*), the C257T mutation in *gyrA* was associated with fluoroquinolone resistance (*39*), and the A2075G mutation in the 23S rRNA was associated with macrolide resistance (*40*). The A2075G mutation in the 23S rRNA (*E. coli* equivalent base 2058) was observed only in *C. coli* isolates in this study, which is consistent with other international studies (*40*). The relatively high prevalence of tetracycline and fluoroquinolone resistance in human or poultry isolates might be the result of selection pressure resulting from the widespread use of these antimicrobials in humans, food production, or both. A recent study in Dar es Salaam, Tanzania, indicated widespread use

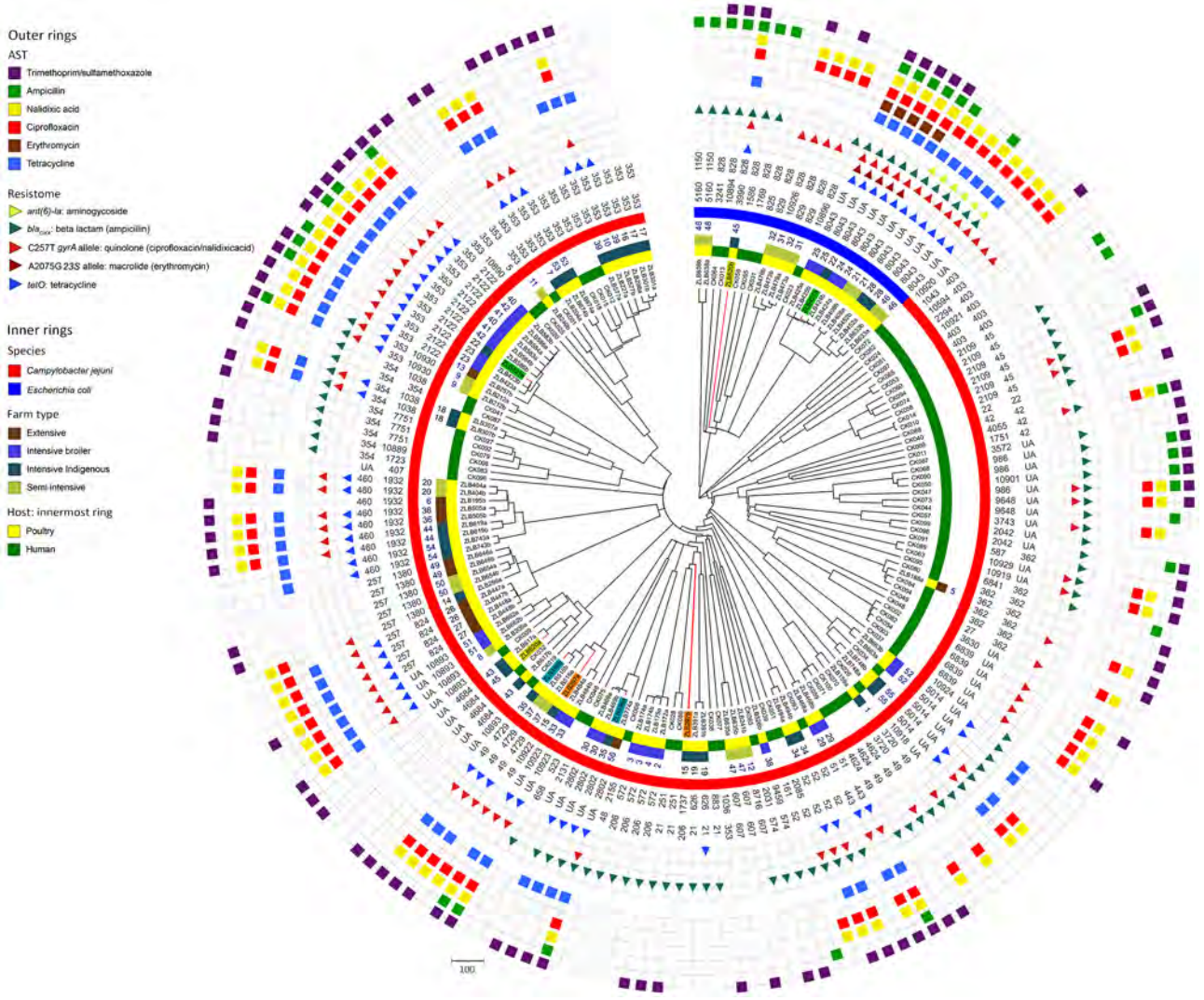

Figure 5. Circular dendrogram showing, from outer to inner rings, AST in study of population structure and antimicrobial resistance in *Campylobacter jejuni* and *C. coli* isolated from humans with diarrhea and from poultry, East Africa, 2006–2017. Colored blocks indicate resistance (all isolates were susceptible to gentamicin so this ring is not included), resistome, clonal complex (CC), sequence type (ST), *Campylobacter* species, poultry sample number, farm type, host and isolate ID for isolates from Kenya and Tanzania, 2006–2017 (human) or 2016–2017 (poultry). Isolates from the same poultry sample that belonged to a different ST are highlighted (samples 15, 22, 35, and 45) using colored isolate identification labels. The resistome indicates detection of resistance genes (encoding for resistance to some aminoglycosides, β-lactam antimicrobials and tetracyclines) and alleles (encoding for resistance for fluoroquinolones in the gyrase A gene, and macrolides in the 23S rRNA gene). Clustering of antimicrobial resistance phenotypes and the resistome with some CCs and STs is evident. For example, multidrug resistance is observed in *C. jejuni* ST2122 and *C. coli* ST8043 isolates. Scale bar indicates number of core-genome multilocus-sequence typing allele differences. AST, antimicrobial sensitivity.

of both tetracyclines and fluoroquinolones in poultry and cattle production; >40% of farmers surveyed were not compliant with drug withdrawal periods (*41*). Evidence of noncompliance with withdrawal periods was also reported in a study of commercial smallholder egg producers in Morogoro, Tanzania (*42*). In human medicine, evidence exists of wide availability and sale of fluoroquinolones in authorized and unauthorized drug outlets. More than 70% of pharmacists surveyed reported dispensing antimicrobial drugs without a prescription, including penicillins, macrolides, and fluoroquinolones (*43*).

Our study had relatively low power to detect associations between epidemiologic variables and AMR and did not assess all transmission pathways. In addition, human diarrheal isolates were sourced from a wider temporal range (2006–2016) than poultry isolates (2016–2017), and isolates were co-located at regional rather than village or household level. However, although the human isolates were from a different country to the poultry isolates, it is worth noting that Nairobi is 272 km by road from Arusha and 326 km from Moshi, closer than other locations in Tanzania with human *Campylobacter* isolates potentially available for sequencing. Chicken production systems are largely similar across East Africa, including flock sizes and extensive, semi-intensive and intensive management systems between Kenya and Tanzania (*44*).

In conclusion, this study provides a detailed examination of the population structure of isolates of *C. jejuni* and *C. coli* in a region of East Africa. Although this study was smaller than similar studies conducted in high-income countries (*13*), it is one of the largest studies using WGS to characterize *Campylobacter* spp. isolates in Africa and has generated several valuable insights. The study showed a striking diversity of *Campylobacter* in both humans and poultry, with some STs common to multiple farms or to humans and poultry. AMR was highly prevalent, particularly to tetracyclines, fluoroquinolones, or sulphonamides, and MDR was prevalent in a high proportion of poultry compared with human isolates. The high prevalence of MDR and the identification of previously undescribed STs highlights the need for ongoing investigation of enteric pathogens, such as *Campylobacter* spp., in low-resource settings. That effort would require genomic tools to be embedded within formal and transparent surveillance systems, in addition to a greater understanding of the role of antimicrobial use and biosecurity measures as drivers of the emergence of resistance in human health and food production and improved governance of antimicrobial use in both sectors.

Acknowledgments

We would like to acknowledge the invaluable contributions made to this study, and to the SEEDZ, HAZEL and Brucella Projects supported by the BBSRC- ZELS initiative by our coauthor, Professor Rudovick Kazwala, who passed away on April 3, 2023, in Dar es salaam, Tanzania. He was one of Tanzania's most prominent researchers and a mentor, colleague, and friend to many of us. We would also like to thank Jane Juma and Newton Wamola for their contribution to the initial isolation of the bacteria from human cases.

This work was supported by the UK Biotechnology and Biological Sciences Research Council, the UK Department for International Development, the UK Economic and Social Research Council, the UK Medical Research Council, the UK Natural Environment Research Council, and the UK Defense Science and Technology Laboratory through the Zoonoses and Emerging Livestock Systems programme (grant nos. BB/L017679/1 and BB/N503563/1).

About the Author

Dr. French is distinguished professor of infectious disease epidemiology and public health at Massey University, New Zealand, chief science advisor for Te Niwha, the Infectious Diseases Research Platform, and emeritus director of the New Zealand Food Safety Science and Research Centre. His main research interests are molecular and genomic epidemiology, pathogen evolution, ecosystem health, and food and environmental pathogens.

References

1. Kirk MD, Pires SM, Black RE, Caipo M, Crump JA, Devleesschauwer B, et al. World Health Organization estimates of the global and regional disease burden of 22 foodborne bacterial, protozoal, and viral diseases, 2010: a data synthesis. PLoS Med. 2015;12:e1001921. https://doi.org/10.1371/journal.pmed.1001921
2. Asuming-Bediako N, Parry-Hanson Kunadu A, Abraham S, Habib I. *Campylobacter* at the human-food interface: the African perspective. Pathogens. 2019;8:87. https://doi.org/10.3390/pathogens8020087
3. Liu J, Platts-Mills JA, Juma J, Kabir F, Nkeze J, Okoi C, et al. Use of quantitative molecular diagnostic methods to identify causes of diarrhoea in children: a reanalysis of the GEMS case-control study. Lancet. 2016;388:1291–301. https://doi.org/10.1016/S0140-6736(16)31529-X
4. Amour C, Gratz J, Mduma E, Svensen E, Rogawski ET, McGrath M, et al.; Etiology, Risk Factors, and Interactions of Enteric Infections and Malnutrition and the Consequences for Child Health and Development Project (MAL-ED) Network Investigators. Epidemiology and impact of *Campylobacter* infection in children in 8 low-resource settings: results from the MAL-ED study. Clin Infect Dis. 2016;63:1171–9.
5. Rukambile E, Sintchenko V, Muscatello G, Kock R, Alders R. Infection, colonization and shedding of *Campylobacter* and

Salmonella in animals and their contribution to human disease: a review. Zoonoses Public Health. 2019;66:562–78. https://doi.org/10.1111/zph.12611
6. Gahamanyi N, Mboera LEG, Matee MI, Mutangana D, Komba EVG. Prevalence, risk factors, and antimicrobial resistance profiles of thermophilic *Campylobacter* species in humans and animals in sub-Saharan Africa: a systematic review. Int J Microbiol. 2020;2020:2092478. https://doi.org/10.1155/2020/2092478
7. Hlashwayo DF, Sigaúque B, Bila CG. Epidemiology and antimicrobial resistance of *Campylobacter* spp. in animals in sub-Saharan Africa: a systematic review. Heliyon. 2020;6:e03537. https://doi.org/10.1016/j.heliyon.2020.e03537
8. Thomas KM, de Glanville WA, Barker GC, Benschop J, Buza JJ, Cleaveland S, et al. Prevalence of *Campylobacter* and *Salmonella* in African food animals and meat: a systematic review and meta-analysis. Int J Food Microbiol. 2020; 315:108382. https://doi.org/10.1016/j.ijfoodmicro.2019.108382
9. Komba EV, Mdegela RH, Msoffe PL, Nielsen LN, Ingmer H. Prevalence, antimicrobial resistance and risk factors for thermophilic *Campylobacter* infections in symptomatic and asymptomatic humans in Tanzania. Zoonoses Public Health. 2015;62:557–68. https://doi.org/10.1111/zph.12185
10. Chuma IS, Nonga HE, Mdegela RH, Kazwala RR. Epidemiology and RAPD-PCR typing of thermophilic campylobacters from children under five years and chickens in Morogoro Municipality, Tanzania. BMC Infect Dis. 2016;16:692. https://doi.org/10.1186/s12879-016-2031-z
11. Mughini Gras L, Smid JH, Wagenaar JA, de Boer AG, Havelaar AH, Friesema IH, et al. Risk factors for campylobacteriosis of chicken, ruminant, and environmental origin: a combined case-control and source attribution analysis. PLoS One. 2012;7:e42599. https://doi.org/10.1371/journal.pone.0042599
12. Sears A, Baker MG, Wilson N, Marshall J, Muellner P, Campbell DM, et al. Marked campylobacteriosis decline after interventions aimed at poultry, New Zealand. Emerg Infect Dis. 2011;17:1007–15. https://doi.org/10.3201/eid/1706.101272
13. Mughini-Gras L, Pijnacker R, Coipan C, Mulder AC, Fernandes Veludo A, de Rijk S, et al. Sources and transmission routes of campylobacteriosis: a combined analysis of genome and exposure data. J Infect. 2021;82:216–26. https://doi.org/10.1016/j.jinf.2020.09.039
14. Chen D, McKune SL, Singh N, Yousuf Hassen J, Gebreyes W, Manary MJ, et al. *Campylobacter* colonization, environmental enteric dysfunction, stunting, and associated risk factors among young children in rural Ethiopia: a cross-sectional study from the *Campylobacter* Genomics and Environmental Enteric Dysfunction (CAGED) Project. Front Public Health. 2021;8:615793. https://doi.org/10.3389/fpubh.2020.615793
15. Osei Sekyere J, Reta MA. Genomic and resistance epidemiology of Gram-negative bacteria in Africa: a systematic review and phylogenomic analyses from a One Health perspective. mSystems. 2020;5:e00897-20. https://doi.org/10.1128/mSystems.00897-20
16. de Vries SPW, Vurayai M, Holmes M, Gupta S, Bateman M, Goldfarb D, et al. Phylogenetic analyses and antimicrobial resistance profiles of *Campylobacter* spp. from diarrhoeal patients and chickens in Botswana. PLoS One. 2018; 13:e0194481. https://doi.org/10.1371/journal.pone.0194481
17. Abubakar MK, Muigai AW, Ndung'u P, Kariuki S. Investigating carriage, contamination, antimicrobial resistance and assessment of colonization risk factors of *Campylobacter* spp. in broilers from selected farms in Thika, Kenya. Microbiol Res J Int. 2019;27:1–16. https://doi.org/10.9734/mrji/2019/v27i630119
18. Kinana AD, Cardinale E, Tall F, Bahsoun I, Sire JM, Garin B, et al. Genetic diversity and quinolone resistance in *Campylobacter jejuni* isolates from poultry in Senegal. Appl Environ Microbiol. 2006;72:3309–13. https://doi.org/10.1128/AEM.72.5.3309-3313.2006
19. Crump JA, Thomas KM, Benschop J, Knox MA, Wilkinson DA, Midwinter AC, et al. Investigating the meat pathway as a source of human nontyphoidal *Salmonella* bloodstream infections and diarrhea in East Africa. Clin Infect Dis. 2021;73:e1570–8. https://doi.org/10.1093/cid/ciaa1153
20. Sindiyo E, Maganga R, Thomas KM, Benschop J, Swai E, Shirima G, et al. Food safety, health management, and biosecurity characteristics of poultry farms in Arusha City, Northern Tanzania, along a gradient of intensification. East Afr Health Res J. 2018;2:168–80. https://doi.org/10.24248/eahrj.v2i2.580
21. Wang G, Clark CG, Taylor TM, Pucknell C, Barton C, Price L, et al. Colony multiplex PCR assay for identification and differentiation of *Campylobacter jejuni*, *C. coli*, *C. lari*, *C. upsaliensis*, and *C. fetus* subsp. fetus. J Clin Microbiol. 2002;40:4744–7. https://doi.org/10.1128/JCM.40.12.4744-4747.2002
22. Denis M, Refrégier-Petton J, Laisney MJ, Ermel G, Salvat G. *Campylobacter* contamination in French chicken production from farm to consumers. Use of a PCR assay for detection and identification of *Campylobacter jejuni* and *Camp. coli*. J Appl Microbiol. 2001;91:255–67. https://doi.org/10.1046/j.1365-2672.2001.01380.x
23. European Committee on Antimicrobial Susceptibility Testing. Antimicrobial susceptibility testing EUCAST disk diffusion method. Version 9.0 (January 2021) [cited 2024 Sep 9]. https://www.eucast.org/fileadmin/src/media/PDFs/EUCAST_files/Disk_test_documents/2021_manuals/Manual_v_9.0_EUCAST_Disk_Test_2021.pdf
24. European Committee on Antimicrobial Susceptibility Testing. Breakpoint tables for interpretation of MICs and zone diameters. Version 10.0. 2020 [cited 2024 Sep 9]. https://www.eucast.org/fileadmin/src/media/PDFs/EUCAST_files/Breakpoint_tables/v_10.0_Breakpoint_Tables.pdf
25. Clinical and Laboratory Standards Institute. Performance standards for antimicrobial susceptibility testing. Supplement M100-29 (29th ed.). Wayne (PA): The Institute; 2019.
26. Follmann D, Proschan M, Leifer E. Multiple outputation: inference for complex clustered data by averaging analyses from independent data. Biometrics. 2003;59:420–9. https://doi.org/10.1111/1541-0420.00049
27. Bürkner P-C. brms: an R package for Bayesian multilevel models using Stan. J Stat Softw. 2017;80:1–28. https://doi.org/10.18637/jss.v080.i01
28. Jolley KA, Bray JE, Maiden MCJ. Open-access bacterial population genomics: BIGSdb software, the PubMLST.org website and their applications. Wellcome Open Res. 2018;3:124. https://doi.org/10.12688/wellcomeopenres.14826.1
29. Alcock BP, Raphenya AR, Lau TTY, Tsang KK, Bouchard M, Edalatmand A, et al. CARD 2020: antibiotic resistome surveillance with the comprehensive antibiotic resistance database. Nucleic Acids Res. 2020;48(D1):D517–25.
30. Cody AJ, Bray JE, Jolley KA, McCarthy ND, Maiden MCJ. Core genome multilocus sequence typing scheme for stable, comparative analyses of *Campylobacter jejuni* and *C. coli* human disease isolates. J Clin Microbiol. 2017;55:2086–97. https://doi.org/10.1128/JCM.00080-17
31. Zhou Z, Alikhan NF, Sergeant MJ, Luhmann N, Vaz C, Francisco AP, et al. GrapeTree: visualization of core

genomic relationships among 100,000 bacterial pathogens. Genome Res. 2018;28:1395–404. https://doi.org/10.1101/gr.232397.117
32. Letunic I, Bork P. Interactive Tree Of Life (iTOL) v4: recent updates and new developments. Nucleic Acids Res. 2019;47(W1):W256–9. https://doi.org/10.1093/nar/gkz239
33. Kazwala RR, Jiwa SF, Nkya AE. The role of management systems in the epidemiology of thermophilic campylobacters among poultry in eastern zone of Tanzania. Epidemiol Infect. 1993;110:273–8. https://doi.org/10.1017/S0950268800068205
34. Kazwala RR, Collins JD, Hannan J, Crinion RA, O'Mahony H. Factors responsible for the introduction and spread of *Campylobacter jejuni* infection in commercial poultry production. Vet Rec. 1990;126:305–6.
35. Nonga HE, Muhairwa AP. Prevalence and antibiotic susceptibility of thermophilic *Campylobacter* isolates from free range domestic duck (*Cairina moschata*) in Morogoro municipality, Tanzania. Trop Anim Health Prod. 2010;42:165–72. https://doi.org/10.1007/s11250-009-9401-0
36. Mdegela RH, Laurence K, Jacob P, Nonga HE. Occurrences of thermophilic *Campylobacter* in pigs slaughtered at Morogoro slaughter slabs, Tanzania. Trop Anim Health Prod. 2011;43:83–7. https://doi.org/10.1007/s11250-010-9657-4
37. Kashoma IP, Kassem II, John J, Kessy BM, Gebreyes W, Kazwala RR, et al. Prevalence and antimicrobial resistance of *Campylobacter* isolated from dressed beef carcasses and raw milk in Tanzania. Microb Drug Resist. 2016;22:40–52. https://doi.org/10.1089/mdr.2015.0079
38. Manavathu EK, Fernandez CL, Cooperman BS, Taylor DE. Molecular studies on the mechanism of tetracycline resistance mediated by Tet(O). Antimicrob Agents Chemother. 1990;34:71–7. https://doi.org/10.1128/AAC.34.1.71
39. Wang Y, Huang WM, Taylor DE. Cloning and nucleotide sequence of the *Campylobacter jejuni gyrA* gene and characterization of quinolone resistance mutations. Antimicrob Agents Chemother. 1993;37:457–63. https://doi.org/10.1128/AAC.37.3.457
40. Gibreel A, Kos VN, Keelan M, Trieber CA, Levesque S, Michaud S, et al. Macrolide resistance in *Campylobacter jejuni* and *Campylobacter coli*: molecular mechanism and stability of the resistance phenotype. Antimicrob Agents Chemother. 2005;49:2753–9. https://doi.org/10.1128/AAC.49.7.2753-2759.2005
41. Azabo R, Mshana S, Matee M, Kimera SI. Antimicrobial usage in cattle and poultry production in Dar es Salaam, Tanzania: pattern and quantity. BMC Vet Res. 2022;18:7. https://doi.org/10.1186/s12917-021-03056-9
42. Nonga HE, Simon C, Karimuribo ED, Mdegela RH. Assessment of antimicrobial usage and residues in commercial chicken eggs from smallholder poultry keepers in Morogoro municipality, Tanzania. Zoonoses Public Health. 2010;57:339–44.
43. Poyongo BP, Sangeda RZ. Pharmacists' knowledge, attitude and practice regarding the dispensing of antibiotics without prescription in Tanzania: an explorative cross-sectional study. Pharmacy (Basel). 2020;8:238. https://doi.org/10.3390/pharmacy8040238
44. Mujyambere V, Adomako K, Olympio SO, Ntawubizi M, Nyinawamwiza L, Mahoro J, et al. Local chickens in East African region: their production and potential. Poult Sci. 2022;101:101547. https://doi.org/10.1016/j.psj.2021.101547

Address for correspondence: Nigel P. French, Tāwharau Ora, School of Veterinary Science, Massey University, Tennent Dr, Palmerston North 4410, New Zealand; email: rn.p.french@massey.ac.nz

Evidence of Lineage 1 and 3 West Nile Virus in Person with Neuroinvasive Disease, Nebraska, USA, 2023

Emily Davis,[1] Jason Velez,[1] Jeff Hamik, Kelly Fitzpatrick, Jacki Haley, Jeremy Eschliman, Amanda Panella, J. Erin Staples, Amy Lambert, Matthew Donahue, Aaron C. Brault, Holly R. Hughes

West Nile virus (WNV) is the most common cause of human arboviral disease in the contiguous United States, where only lineage 1 (L1) WNV had been found. In 2023, an immunocompetent patient was hospitalized in Nebraska with West Nile neuroinvasive disease and multisystem organ failure. Testing at the Centers for Disease Control and Prevention indicated an unusually high viral load and acute antibody response. Upon sequencing of serum and cerebrospinal fluid, we detected lineage 3 (L3) and L1 WNV genomes. L3 WNV had previously only been found in Central Europe in mosquitoes. The identification of L3 WNV in the United States and the observed clinical and laboratory features raise questions about the potential effect of L3 WNV on the transmission dynamics and pathogenicity of WNV infections. Determining the distribution and prevalence of L3 WNV in the United States and any public health and clinical implications is critical.

West Nile virus (WNV) is a flavivirus within the family Flaviviridae. Since WNV was identified in New York, USA, in 1999, it has become the leading cause of arboviral disease in the contiguous United States (*1*–*3*). WNV is maintained in a transmission cycle between mosquitoes and birds, in which infection can range from asymptomatic to lethal depending on the avian species (*4*). Similarly, in dead-end hosts, such as humans, disease severity varies. Most human WNV infections are asymptomatic; however, <1% of infections result in severe neurologic disease (*3*). WNV disease risk generally increases with age and underlying conditions (*5*).

The diagnosis of WNV disease is typically made on the basis of clinical symptoms and serologic testing because viremia is typically transient and low titer. WNV IgM is detected by using immunosorbent assays, and diagnosis is confirmed with a plaque reduction neutralization test. In persons who are immunosuppressed, or when serologic findings are not conclusive, molecular detection of WNV RNA in serum or cerebrospinal fluid (CSF) can be used to make the diagnosis (*6*)

Up to 9 distinct lineages of WNV have been proposed on the basis of genotypic analyses of the envelope and nonstructural protein 5 genes (*1*,*7*–*11*). Sublineage 1a is broadly distributed in Africa, Europe, and the Americas. Lineage 2 (L2) WNV was primarily found in sub-Saharan Africa until the early 2000s, when it rapidly emerged in Europe. Many WNV lineages are referred to by other names, including Kunjin (L1b) (*12*), Koutango (L7) (*13*), and Rabensburg (L3) viruses (*14*,*15*).

Murine virulence studies and clinical testing of humans has shown that L1 and L2 can cause neuroinvasive disease (*16*,*17*). In contrast, L3 WNV has not been found to cause disease or pathology in birds or mammals, being detected only in mosquito pools in the Czech Republic (*7*,*15*,*18*,*19*). The restricted host range of L3 WNV was confirmed in experiments in which viremia and antibodies were not detected after avian infection (*14*). Furthermore, the virus did not replicate in mammalian cell culture at physiologic temperatures and was highly attenuated in adult mouse models (*14*,*18*–*20*).

In 2023, an immunocompetent patient was hospitalized in Nebraska, USA, with West Nile neuroinvasive disease and multisystem organ failure. Testing

Author affiliations: Centers for Disease Control and Prevention, Fort Collins, Colorado, USA (E. Davis, J. Velez, K. Fitzpatrick, A. Panella, J.E. Staples, A. Lambert, A.C. Brault, H.R. Hughes); Nebraska Department of Health and Human Services, Lincoln, Nebraska, USA (J. Hamik, M. Donahue); Two Rivers Public Health Department, Kearney, Nebraska, USA (J. Haley, J. Eschliman)

DOI: https://doi.org/10.3201/eid3010.240595

[1]These first authors contributed equally to this article.

at the Centers for Disease Control and Prevention (CDC) indicated an unusually high viral load. The high viremia prompted genomic surveillance testing to investigate whether mutations in L1 WNV could potentially explain the high viremia findings. High-throughput sequencing (HTS) indicated the presence of L1 and L3 WNV RNA in the patient's serum and CSF. In this article, we describe the clinical features and course of disease in the patient and the initial virologic findings that might affect the transmission dynamics and pathogenicity of WNV infections.

Materials and Methods

Case Information

We collected case information as part of surveillance and follow-up of a nationally notifiable disease. We conducted interviews to determine potential travel and exposure history and obtained clinical information from the patient and healthcare providers.

Case-Patient Clinical Description

A man 70–79 years of age who had coronary artery disease, hyperlipemia, controlled type 2 diabetes mellitus, obesity, and mild chronic kidney disease was in his usual state of health until mid-August 2023, when he had onset of fever, myalgias, diarrhea, headache, dyspnea on exertion, and decreased appetite. Four days after symptom onset, the patient visited a local hospital, where he was noted to have increased inflammatory markers (C-reactive protein 17 mg/dL [reference range <0.3 mg/dL], erythrocyte sedimentation rate 43 mm/h [reference range 0–15 mm/h], and procalcitonin 1.48 ng/mL [reference range <0.1 ng/mL]), as well as leukopenia (leukocytes 2,700 cells/μL [reference range 4,000–11,000 cells/μL]) and thrombocytopenia (platelets 115,000/μL [reference range 150,000–450,000/μL]). He was hospitalized and given ceftriaxone.

Two days after admission, he continued to have fevers with increasing headaches and neurologic signs and symptoms, including bilateral fine tremors in his hands, decreased strength, slower gait, stiff neck, and difficulty in responding to questions. A lumber puncture revealed an decreased leukocyte count (1,939 cells/mm^3 [reference range 4,000–11,000 cells/mm^3]) with a neutrophilic predominance (72%), elevated protein (242 mg/dL [reference range 60–83 mg/dL], and <3,000 erythrocytes cells/mm^3 (reference range 3.93–5.96 million erythrocytes /mm^3); glucose was within reference range (54 mg/dL [reference range 50–75 mg/dL]). The patient was transferred to the intensive care unit, and his antimicrobial drug treatment regimen was broadened to include vancomycin, meropenem, acyclovir, and doxycycline.

The patient became more confused and then unresponsive and had onset of ascending paralysis to his thoracic region; seizure-like activity was noted on day 3 of hospitalization. A contrast magnetic resonance imaging of his spine and brain had no acute findings, and an electroencephalogram revealed non-localized cerebral dysfunction without seizures. He was transferred to a tertiary-care center the following day (day 8 after illness onset), where he was intubated and found to have acute kidney injury. The patient remained critically ill on a ventilator until his mental status began to improve on hospital day 9. He eventually had a percutaneous endoscopic gastrostomy tube placed, and a tracheostomy was performed before the patient was transferred to a long-term care hospital and then a skilled nursing facility, where he remained for >3 months.

Two weeks before illness onset, the patient had traveled to northeast Colorado for 2 nights, but otherwise he did not have other domestic or international travel. He reported no known mosquito or tick bites when recreating outdoors, which he did often. He did not have pets or exposure to other animals.

Serologic Testing

We had ELISA testing performed at a commercial reference laboratory. The laboratory then sent positive serum and CSF samples to the CDC Arboviral Diseases Branch (Division of Vector-Borne Diseases, National Center for Emerging and Zoonotic Infectious Diseases; Fort Collins, CO, USA) for confirmation, where we performed plaque-reduction neutralization tests as previously described (*21*). In brief, we diluted an aliquot of the patient's serum sample 1:5 before 2-fold serial dilutions, whereas the CSF starting dilution was 1:2. We incubated these dilutions with 100 PFUs of L1 WNV (strain NY99) and used them to infect Vero cells followed by an agarose overlay. After 3 days, we placed an overlay including neutral red on top of the monolayer and counted plaques the next day. The diagnostic cutoff for positivity was a 90% reduction in PFUs.

Molecular Testing

We extracted viral RNA from clinical samples by using the QIAmp Viral RNA Mini Kit (QIAGEN, https://www.qiagen.com). We followed the manufacturer's protocol unless otherwise stated. We determined input and elution volume on the basis of sample availability (for serum, input 500 μL and elution 60 μL; for CSF, input 80 μL and elution 50 μL). We

completed an additional low-volume extraction on the remaining volume of serum (20 μL input and 30 μL elution volume). To confirm a laboratory contamination event had not occurred, we performed the CSF and second serum extraction in a separate laboratory that only handled bacteria and where WNV had never been present. We performed real-time reverse transcription PCR (rRT-PCR) by using the QuantiTect Probe RT-PCR Kit (QIAGEN) and L1-specific (*1*) and L3-specific (*22*) primers according to the manufacturers' protocols.

Virus Isolation

We grew and maintained Vero cells at 37°C as previously described (*23*). We inoculated cell monolayers with 200 μL of the patient's serum and monitored them daily for cytopathic effects (CPE). At 3 days after inoculation, 50% of the cells demonstrated CPE and we harvested an isolate (Vero passage 1 [Vp1]). We centrifuged cell supernatant to clear cell debris, then aliquoted and stored it at −80°C. We extracted RNA by using an input of 100 μL and used an elution of 100 μL for rRT-PCR testing, as described.

We inoculated Vp1 onto Vero cells at 32°C and 28°C, allowed it to incubate for 1 hour, and then overlaid it. After 3 days, we added to a second overlay to the wells, including neutral red. We monitored plates for plaque formation for 11 days. We picked plaques and suspended them in BA-1 diluent before using this inoculum to inoculate Vero cells, and we monitored CPE as described previously. We also isolated RNA as described.

Next-Generation Sequencing and Analysis

We generated complementary DNA (cDNA) by using the Ovation RNA-Seq System V2 (Tecan Life Sciences, https://lifesciences.tecan.com). We prepared sequencing libraries by using the Nextera XT DNA Library Prep Kit (Illumina, https://www.illumina.com) and IDT DNA/RNA UD indexes (IDT, https://www.idtdna.com). We completed sequencing on RNA extracted from the clinical samples and Vp1 by using the NextSeq1000 and a P1, 300-cycle kit or a MiSeq and a V2 300-cycle kit (Illumina).

We completed de novo assembly by using SPAdes version 3.15.3 (https://github.com/ablab/spades) and its RNA viral presets. We searched the resulting contigs for viral origin by using the viral_nt database and CLI of BLASTn version 2.12.0 (https://ftp.ncbi.nlm.nih.gov/blast/executables/LATEST) and confirmed them by using the nucleotide BLAST database (https://blast.ncbi.nlm.nih.gov). To resolve areas of overlap between WNVs lineages, we also completed reference alignment and used it to generate consensus sequences as previously described (*24*). We used Bowtie2 version 2.2.5 (https://github.com/BenLangmead/bowtie2) to align samples to references by using very-sensitive-local presets. We used Samtools version 1.15.1 (https://github.com/samtools/samtools/releases) to sort reads by coordinate, from which we then removed duplicates by using Picard version 2.23.0 https://github.com/broadinstitute/picard/releases). We calculated coverage by using Bamtools version 2.5.2 (https://github.com/pezmaster31/bamtools).

Results

Case-Patient Testing

For the case-patient, testing for various bacterial and viral pathogens was negative on the serum and CSF samples (Appendix Table 1, https://wwwnc.cdc.gov/EID/article/30/10/24-0595-App1.pdf 1). Samples of serum collected 4 days and CSF collected 6 days after illness onset were tested by using WNV IgM ELISA at a commercial reference laboratory. Both serum and CSF samples were identified to be IgM-positive.

Diagnostic Evaluation of Presumptive WNV Infection

To confirm the WNV IgM results, serum and CSF samples were sent to CDC's Arboviral Diseases Branch, where we conducted plaque reduction neutralization testing. We observed reduced plaque sizes compared with control WNV L1 plaques, and the degree of neutralization did not meet the cutoff for positivity for either serum or CSF. However, we confirmed WNV infection by using the L1-specific WNV rRT-PCR assay with an average cycle threshold (Ct) of 21.3 on serum. By using an on-plate standard curve of L1 WNV RNA (R^2 = 0.9802), we calculated that this Ct approximated 5.5 $\log_{10}$ PFU equivalents of L1 WNV (Appendix Figure). We detected L1 WNV RNA again in Vp1 by using rRT-PCR (Ct 11, estimated titer 8.9 $\log_{10}$ PFU equivalents). Volume did not allow for L3-specific molecular detection to be performed on the serum sample. Results of a retrospective rRT-PCR test using L3 primers on the Vp1 sample was negative.

Metagenomic Sequencing Confirmation of L1 and Detection of L3 WNV RNA

We used RNA from serum and Vp1 to perform metagenomic sequencing on the NextSeq1000 platform. In serum, we detected full-length L1 WNV

(4,299,218 total reads, 4,505 average reads/base; GenBank accession no. PP445211) and full-length L3 WNV (542,849 reads, 1,012 average reads/base; GenBank accession no. PP445212) by de novo assembly (Figure 1, panel A). We completed a second, low-volume extraction to confirm the presence of L3 WNV RNA in the serum that had undergone freeze-thaw and sequenced it on the MiSeq platform. We detected L1 and L3 WNV RNA by using de novo assembly (2,038-nt–long contig of L1 WNV and 510-nt contig of L3) and subsequent reference guided assembly (1,376 reads for L1 and 334 reads for L3). We detected full-length L1 WNV RNA by using de novo assembly in Vp1 (27,347,544 total reads and 39,600 average reads/base) (Figure 1, panel B). We compared both serum and Vp1 sequences of L1 with NY99 (GenBank accession no. MZ605381); the serum sequence had 98.7% nucleotide identity and the Vp1 sequence had 98.6% nucleotide identity. We detected L3 WNV in Vp1 (97.3% genome coverage) through reference guided assembly (380,953 reads and 3,326 average reads/base) (Figure 1, panel B; Appendix Table 4). We sequenced RNA from the CSF on the MiSeq platform. We detected only 2 reads of L1 WNV RNA (Figure 1, panel C), mapping to 10,679–10,909 nt. We detected 20 reads of L3 WNV (18.8% genome coverage) (Figure 1, panel C).

Comparison of the serum and Vp1 L1 WNV revealed 134 synonymous nucleotide changes, 12 nonsynonymous nucleotide changes, and 7 changes within the 3′ untranslated region (UTR), which corresponds to 98.6% nucleotide identity (Figure 2, panel A; Appendix Table 2). Comparison of the serum L3 WNV RNA and the L3 WNV detected in Vp1 revealed 1 change in the 5′ UTR, 68 synonymous nucleotide changes, 21 nonsynonymous nucleotide changes, and three 3′ UTR changes, which equates to 97.2% nucleotide identity between L3 detected in serum and Vp1 (Figure 2, panel B; Appendix Table 3).

We compared the consensus sequence of the serum L3 sequence with historical strains of L3 WNV: 97-103 (GenBank accession no. AY765264, isolated in 1997), 99-222 (GenBank accession no. GQ421359, isolated in 1999), and 06-222 (GenBank accession no. GQ421358, isolated in 2006). Compared with 97–103, the only available full-length sequence of L3 in GenBank, the serum L3 WNV strain was 99.1% identical at the nucleotide level (8 synonymous changes, 5 nonsynonymous changes, 1 change in the 5′ UTR, and 2 changes in the 3′ UTR). The serum L3 WNV strain was 99.6% identical at the nucleotide level with the partial sequences of 99–222 and 99.9% identical at the nucleotide level with the partial sequences of 06-222 (Figure 2, panel C; Appendix Table 5).

When the partial consensus sequence of L3 detected in CSF was compared with L3 WNV detected in the serum, we detected 9 nucleotide changes, all resulting in amino acid substitutions (Figure 1, panel

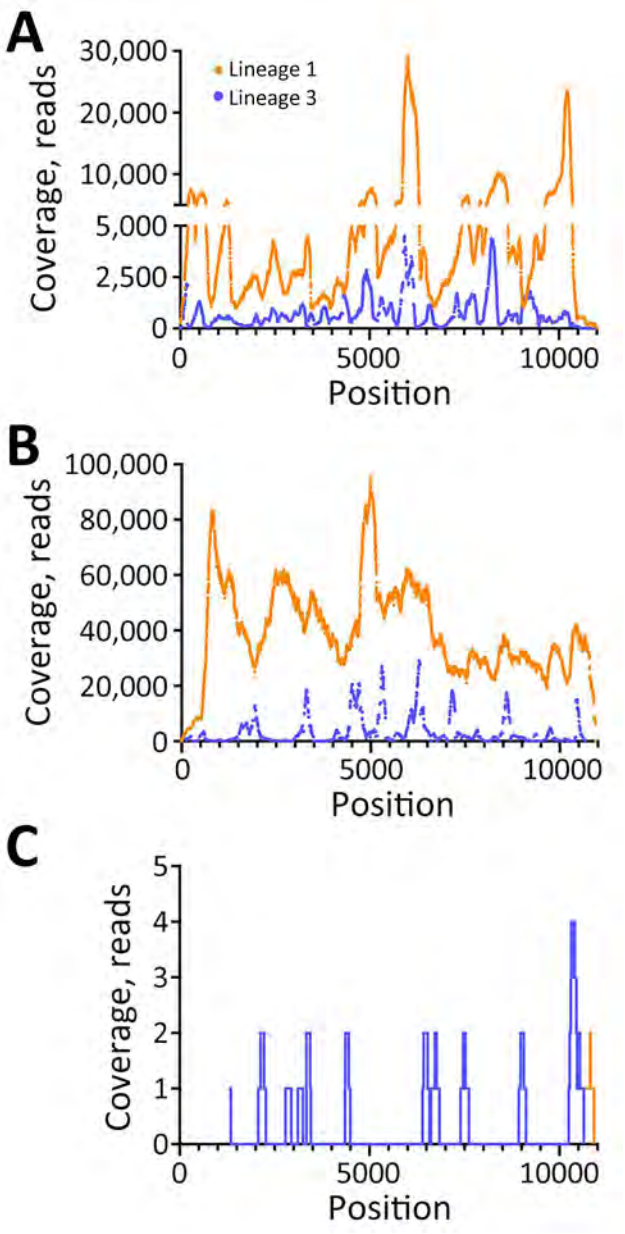

Figure 1. Coverage of lineage 1 and lineage 3 WNV as determined by reference guided assembly in samples from a patient with neuroinvasive disease and evidence of lineage 1 and 3 WNV infection, Nebraska, USA, 2023. Using de novo assembled consensus sequences, a reference guided assembly was completed. Reads mapped to lineage 1 (orange) and lineage 3 (purple) WNV are shown in serum (A), after Vero passage 1 (B), and in cerebrospinal fluid (C). WNV, West Nile virus.

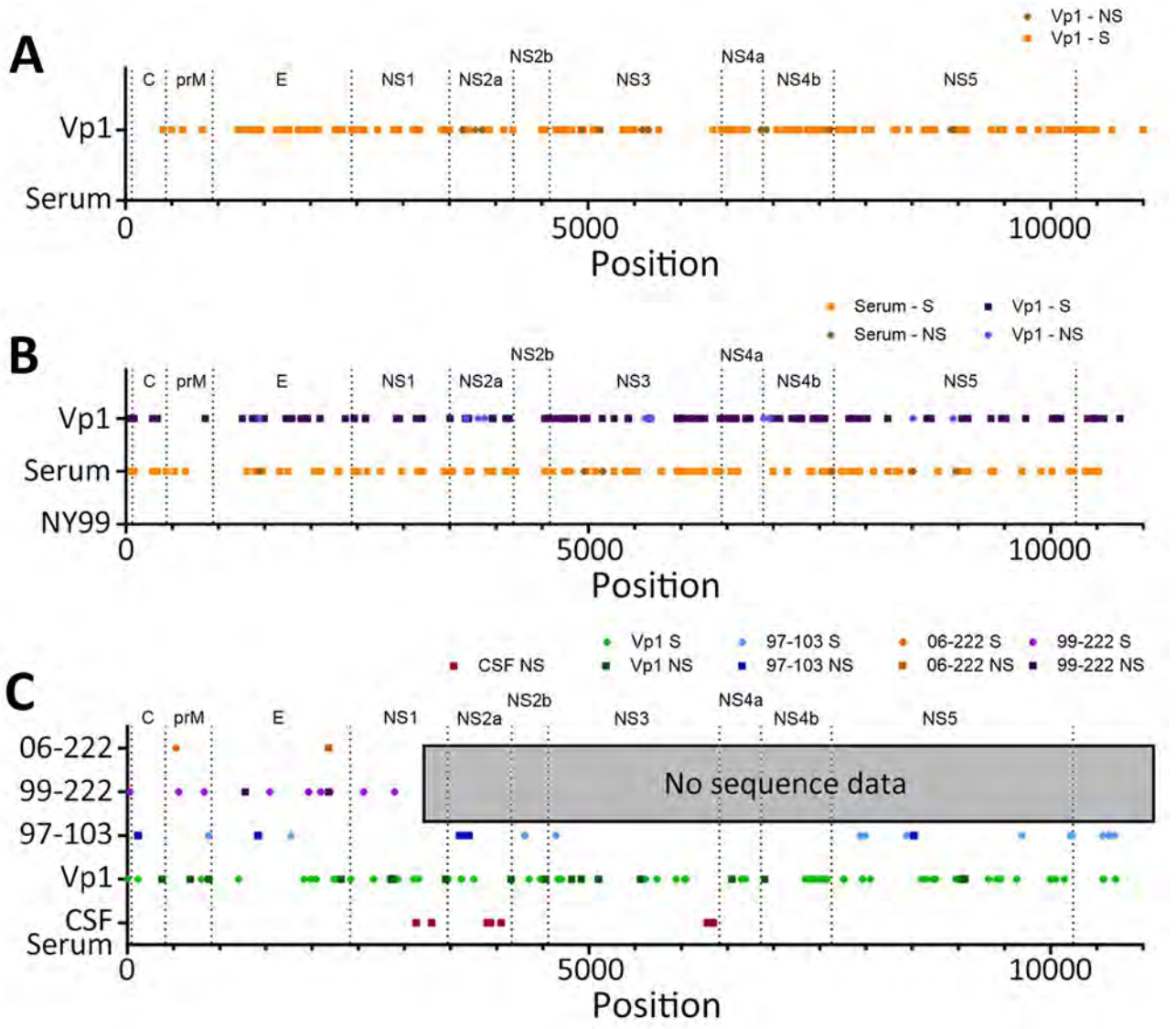

Figure 2. Consensus sequences for lineage 1 and lineage 3 WNV in serum and after Vp1 in samples from a patient with neuroinvasive disease and evidence of lineage 1 and 3 WNV infection, Nebraska, USA, 2023. Lineage 1 and lineage 3 WNV are distinct at the consensus level compared with Vp1 and historical strains. A, B) The consensus sequence of lineage 1 WNV in serum was compared with that of Vp1 (A), and those 2 sequences were then compared with the prototypical North American lineage 1 WNV strain, NY99 (B). C) Serum lineage 3 WNV consensus sequence was compared with the partial lineage 3 WNV sequences determined from Vp1 and CSF and historical lineage 3 WNV strains. C, capsid; CSF, cerebrospinal fluid; E, envelope; NS, nonstructural; prM, premembrane; Vp1, Vero passage 1; WNV, West Nile virus.

C; Appendix Table 6). The contig mapping to L1 had 100% identity to that of the serum L1 WNV.

Plaque Pick Isolation of L1 and L3 WNV at Low Temperature

We selected 3 plaques for HTS on the basis of the time needed for visualization after neutral red overlay. All plaque picks (Pp) were positive for L1 by rRT-PCR. None were positive by L3 specific rRT-PCR. Pp1 was similar to the expected WNV plaque phenotype but appeared at 3 days after overlay (1 day later than normal) and was picked from plates incubated at 32°C. Pp2 also was derived from a plate incubated at 32°C but appeared 9 days after overlay. Pp3 was picked from cells held at 28°C and appeared 7 days after overlay. Upon reference guided assembly, we detected L3 WNV in all plaques at a much lower rate than L1 WNV (Appendix Table 7).

Discussion

We describe evidence of L3 WNV in the United States and L3 WNV detection in an immunocompetent

patient's samples with atypical diagnostic test findings. The patient had detectable WNV IgM antibodies without sufficient neutralizing antibodies to be considered WNV positive on a day 4 serum and day 6 CSF samples. We did not collect convalescent samples to test for a delayed neutralizing or a cross-reactive neutralizing response; however, L1 rRT-PCR results demonstrated an uncharacteristically low Ct value, indicating a high level of virus in the patient's serum. HTS conducted to investigate whether mutations in L1 WNV could potentially explain the diagnostic findings indicated the presence of L1 and L3 WNV in the patient's serum and CSF.

Viremia is transient in patients with WNV disease, and the period of viremia typically ends with development of IgM, often before symptom onset (*25*). The estimated 5.5 $\log_{10}$ PFU/mL of virus in the serum of a patient who was not taking immunosuppressive medications or known to have a medical condition that caused substantial immunosuppression is abnormal. Data from asymptomatic blood donors who screen positive for WNV RNA typically demonstrate a level of viremia <80 PFU/mL, although blood donors often can have extended RNA positivity in whole blood (*26*,*27*). It is unclear whether the ability of L1 WNV to replicate to high titer without eliciting a neutralizing antibody response is caused by an interaction with L3 virus, alterations in the immune response (given the 2 viral infections), an unknown host factor, or the timing of sample collection. However, the amount of virus present in the patient exceeds a level where mosquitoes are known to become infected in laboratory setting (*28*,*29*). Additional work will be necessary to determine if this level of virus in human blood can lead to humans playing a role in the WNV transmission cycle.

Across multiple lineages, WNV has been demonstrated to infect 75 mosquito species and 300 bird, reptile, and mammal species (*30*–*32*). This broad host range is attributed to the ability of WNV to replicate efficiently because of rapid evolution in the new host (*33*). However, L3 WNV was previously thought to exist only in the mosquito vector (*Culex pipiens* and *Aedes rossicus*), with maintenance being completely reliant on vertical transmission (*14*,*20*,*22*). Although L3 WNV was demonstrated to grow in avian cell culture (*22*), no viremia or antibodies have been detected in vivo in experiments using chickens and house sparrows (*14*). L3 WNV is unable to grow in mammalian cell culture (e.g., Vero, Vero E6, human embryonic kidney 293, and baby hamster kidney cells) at 37°C unless RNA is electroporated into cells (*22*). Furthermore, L3 WNV has been demonstrated to display restricted virulence compared with other lineages of WNV(*18*,*19*). L3 WNV causes no disease in adult outbred mice, regardless of the route of infection (including intracranial), and caused reduced disease in the highly susceptible suckling mouse model (*18*,*19*). The identification of L3 RNA in a human might have occurred through replication complex interactions between L1 and L3 WNV in co-infected cells; however, we did not test this hypothesis in our study.

Flavivirus co-infection of mosquitoes, birds, and humans has been observed in many flavivirus-endemic regions (*34*–*40*). Alterations in pathogenesis caused by dual infections is complex because groups have demonstrated both increased (*41*,*42*) and decreased (*36*,*43*) disease in cases in which 2 flaviviruses infect a host simultaneously. A study in which mosquitoes were coinfected with dengue and Zika viruses demonstrated that flaviviruses can interact through their replication complexes, substantially enhancing viral replication in the vector and vector competence (*44*). The potential for viral interaction in the patient described here is supported by identification of both L1 and L3 WNV RNA in plaque picks of Vp1 grown at low temperatures, suggesting that the co-infection of L1 and L3 result in hybrid replication complexes and the viruses are co-packaged to some degree. Supporting this theory, the partial L3 genomes detected in plaque picks corresponded to regions of high coverage observed in Vp1 L3, indicating that degraded L3 RNA was replicated and packaged with L1. The large disparity between the number of reads associated with both lineages upon sequencing does suggest that far less L3 than L1 WNV RNA was present in the clinical sample, which probably led to a failure to isolate L3 virus or detect L3 RNA by rRT-PCR in Vp1.

The L3 WNV we detected is similar to the only other complete isolate (97–103), differing at only 15-nt; of those differences, 5 were nonsynonymous. Because of nucleotide similarities between the L3 and historical strains, because the 97–103 isolate exists at CDC, and because L3 was only detected by using a very sensitive HTS (*44*), RNA was re-extracted from the clinical samples in a laboratory only conducting bacterial assays to exclude contamination issues. Although contamination of the samples before arriving at CDC cannot be excluded, the 1 other laboratory in the United States that handles L3 is in New York, a different location from where the patient samples were handled and tested. Another factor potentially supporting the finding of L3 in the clinical samples was that the L3 WNV genome detected in serum was most similar to the partial sequence from L3 WNV strain 06–222, which is not present at CDC.

The 06-222 isolate of L3 WNV was collected in 2006 and was demonstrated to be more virulent than the prototype strain of L3 WNV, 97-103, in suckling mice (*14*). Overall, it is unclear why the virus has changed so little over 26 years; however, viral evolution is necessitated by rapid replication at elevated temperatures and host-specific pressures (*22*,*45*–*49*). Because L3 WNV grows slower at lower temperatures and purportedly in fewer hosts, virus evolution might be slower. The L3 WNV we observed is more distinct from historical strains than historical strains are from themselves, which indicates some evolution has occurred, just at a slower rate than the more rapidly replicating L1 WNV. The similarity could also indicate a more recent introduction of L3 into the United States, but more work is necessary, including field work to identify where L3 virus might be circulating, to determine how the virus might have evolved and adapted to a specific ecologic niche.

The effect of dual infection with L1 and L3 WNV on the patient's clinical course and outcome is unclear because the patient's age and underlying conditions are risk factors for more severe WNV disease. The patient had encephalitis, required intensive care, and had multiple organ system failure. He survived but did have several sequelae requiring long-term assisted care. Of note, none of the amino acid changes in the L3 WNV RNA we have described have been associated with alterations in virulence in L1 WNV; however, molecular determinants of virulence probably differ between the 2 lineages.

Current methods of surveillance do not include assays that will detect L3 WNV by molecular testing (*14*) or differentiate L3 from L1 through serologic testing (*15*), so the distribution and prevalence of disease related to L3 infection in the United States is not known. More work is needed to be determine the effect that L3 has, either with or without concurrent infection with L1, on WNV transmission dynamics and pathogenicity. Retrospective and prospective vector surveillance efforts are planned to determine how pervasive L3 WNV is among native mosquito species. In addition, CDC is working with the Nebraska Department of Health and Human Services to determine if additional L1 and L3 infections or only L3 infections have occurred in patients with similar clinical or diagnostic findings.

Acknowledgments

We thank the CDC Bacterial Diseases Branch Diagnostic and Reference Team (Division of Vector-Borne Diseases, National Center for Emerging and Zoonotic Infectious Diseases) for allowing confirmatory testing to take place in their laboratory space, Carolyn Gould for her review of the manuscript, and the patient for sharing clinical and exposure history.

About the Author

Dr. Davis is a postdoctoral fellow at the Arboviral Diseases Branch, Division of Vector-Borne Diseases, National Center for Emerging and Zoonotic Infectious Diseases, CDC. Her primary research interests include viral pathogenicity and genomics. Mr. Velez oversees the Arboviral Diseases Branch cell culture laboratory. His primary research interests include clinical virus isolation and diagnostic molecular testing.

References

1. Lanciotti RS, Roehrig JT, Deubel V, Smith J, Parker M, Steele K, et al. Origin of the West Nile virus responsible for an outbreak of encephalitis in the northeastern United States. Science. 1999;286:2333–7. https://doi.org/10.1126/science.286.5448.2333
2. Soto RA, Hughes ML, Staples JE, Lindsey NP. West Nile virus and other domestic nationally notifiable arboviral diseases—United States, 2020. MMWR Morb Mortal Wkly Rep. 2022;71:628–32. https://doi.org/10.15585/mmwr.mm7118a3
3. Fagre AC, Lyons S, Staples JE, Lindsey N. West Nile virus and other nationally notifiable arboviral diseases—United States, 2021. MMWR Morb Mortal Wkly Rep. 2023;72:901–6. https://doi.org/10.15585/mmwr.mm7234a1
4. Komar N, Langevin S, Hinten S, Nemeth N, Edwards E, Hettler D, et al. Experimental infection of North American birds with the New York 1999 strain of West Nile virus. Emerg Infect Dis. 2003;9:311–22. https://doi.org/10.3201/eid0903.020628
5. McDonald E, Mathis S, Martin SW, Staples JE, Fischer M, Lindsey NP. Surveillance for West Nile virus disease—United States, 2009–2018. MMWR Surveill Summ. 2021;70:1–15. https://doi.org/10.15585/mmwr.ss7001a1
6. Kapadia RK, Staples JE, Gill CM, Fischer M, Khan E, Laven JJ, et al. Severe arboviral neuroinvasive disease in patients on rituximab therapy: a review. Clin Infect Dis. 2023;76:1142–8. https://doi.org/10.1093/cid/ciac766
7. Bakonyi T, Hubálek Z, Rudolf I, Nowotny N. Novel flavivirus or new lineage of West Nile virus, central Europe. Emerg Infect Dis. 2005;11:225–31. https://doi.org/10.3201/eid1102.041028
8. Bondre VP, Jadi RS, Mishra AC, Yergolkar PN, Arankalle VA. West Nile virus isolates from India: evidence for a distinct genetic lineage. J Gen Virol. 2007;88:875–84. https://doi.org/10.1099/vir.0.82403-0
9. Berthet FX, Zeller HG, Drouet MT, Rauzier J, Digoutte JP, Deubel V. Extensive nucleotide changes and deletions within the envelope glycoprotein gene of Euro-African West Nile viruses. J Gen Virol. 1997;78:2293–7. https://doi.org/10.1099/0022-1317-78-9-2293
10. Savage HM, Ceianu C, Nicolescu G, Karabatsos N, Lanciotti R, Vladimirescu A, et al. Entomologic and avian investigations of an epidemic of West Nile fever in Romania in 1996, with serologic and molecular characterization of a virus isolate from mosquitoes. Am J Trop Med Hyg. 1999;61:600–11. https://doi.org/10.4269/ajtmh.1999.61.600

11. Pachler K, Lebl K, Berer D, Rudolf I, Hubalek Z, Nowotny N. Putative new West Nile virus lineage in *Uranotaenia unguiculata* mosquitoes, Austria, 2013. Emerg Infect Dis. 2014;20:2119–22. https://doi.org/10.3201/eid2012.140921
12. Scherret JH, Poidinger M, Mackenzie JS, Broom AK, Deubel V, Lipkin WI, et al. The relationships between West Nile and Kunjin viruses. Emerg Infect Dis. 2001;7:697–705. https://doi.org/10.3201/eid0704.017418
13. Mackenzie JS, Williams DT. The zoonotic flaviviruses of southern, south-eastern and eastern Asia, and Australasia: the potential for emergent viruses. Zoonoses Public Health. 2009;56:338–56. https://doi.org/10.1111/j.1863-2378.2008.01208.x
14. Aliota MT, Jones SA, Dupuis AP II, Ciota AT, Hubalek Z, Kramer LD. Characterization of Rabensburg virus, a flavivirus closely related to West Nile virus of the Japanese encephalitis antigenic group. PLoS One. 2012;7:e39387. https://doi.org/10.1371/journal.pone.0039387
15. Hubálek Z, Halouzka J, Juricová Z, Sebesta O. First isolation of mosquito-borne West Nile virus in the Czech Republic. Acta Virol. 1998;42:119–20.
16. Beasley DW, Li L, Suderman MT, Barrett AD. Mouse neuroinvasive phenotype of West Nile virus strains varies depending upon virus genotype. Virology. 2002;296:17–23. https://doi.org/10.1006/viro.2002.1372
17. Bakonyi T, Ivanics E, Erdélyi K, Ursu K, Ferenczi E, Weissenböck H, et al. Lineage 1 and 2 strains of encephalitic West Nile virus, central Europe. Emerg Infect Dis. 2006;12:618–23. https://doi.org/10.3201/eid1204.051379
18. Hubálek Z, Rudolf I, Bakonyi T, Kazdová K, Halouzka J, Sebesta O, et al. Mosquito (Diptera: Culicidae) surveillance for arboviruses in an area endemic for West Nile (lineage Rabensburg) and Tahyna viruses in Central Europe. J Med Entomol. 2010;47:466–72. https://doi.org/10.1603/ME09219
19. Hubálek Z, Savage HM, Halouzka J, Juricová Z, Sanogo YO, Lusk S. West Nile virus investigations in South Moravia, Czechland. Viral Immunol. 2000;13:427–33. https://doi.org/10.1089/vim.2000.13.427
20. Aliota MT, Kramer LD. Replication of West Nile virus, Rabensburg lineage in mammalian cells is restricted by temperature. Parasit Vectors. 2012;5:293. https://doi.org/10.1186/1756-3305-5-293
21. Hughes HR, Velez JO, Fitzpatrick K, Davis EH, Russell BJ, Lambert AJ, et al. Genomic evaluation of the genus *Coltivirus* indicates genetic diversity among Colorado tick fever virus strains and demarcation of a new species. Diseases. 2021;9:9. https://doi.org/10.3390/diseases9040092
22. Ngo KA, Rose JT, Kramer LD, Ciota AT. Adaptation of Rabensburg virus (RBGV) to vertebrate hosts by experimental evolution. Virology. 2019;528:30–6. https://doi.org/10.1016/j.virol.2018.11.015
23. Lambert AJ, Velez JO, Brault AC, Calvert AE, Bell-Sakyi L, Bosco-Lauth AM, et al. Molecular, serological and in vitro culture-based characterization of Bourbon virus, a newly described human pathogen of the genus *Thogotovirus*. J Clin Virol. 2015;73:127–32. https://doi.org/10.1016/j.jcv.2015.10.021
24. Hughes HR, Velez JO, Davis EH, Laven J, Gould CV, Panella AJ, et al. Fatal human infection with evidence of intrahost variation of eastern equine encephalitis virus, Alabama, USA, 2019. Emerg Infect Dis. 2021;27:1886–92. https://doi.org/10.3201/eid2707.210315
25. Ratterree MS, Gutierrez RA, Travassos da Rosa AP, Dille BJ, Beasley DW, Bohm RP, et al. Experimental infection of rhesus macaques with West Nile virus: level and duration of viremia and kinetics of the antibody response after infection. J Infect Dis. 2004;189:669–76. https://doi.org/10.1086/381461
26. Cervantes DT, Chen S, Sutor LJ, Stonecipher S, Janoski N, Wright DJ, et al. West Nile virus infection incidence based on donated blood samples and neuroinvasive disease reports, northern Texas, USA, 2012. Emerg Infect Dis. 2015;21:681–3. https://doi.org/10.3201/eid2104.141178
27. Pealer LN, Marfin AA, Petersen LR, Lanciotti RS, Page PL, Stramer SL, et al.; West Nile Virus Transmission Investigation Team. Transmission of West Nile virus through blood transfusion in the United States in 2002. N Engl J Med. 2003;349:1236–45. https://doi.org/10.1056/NEJMoa030969
28. Platt KB, Tucker BJ, Halbur PG, Blitvich BJ, Fabiosa FG, Mullin K, et al. Fox squirrels (*Sciurus niger*) develop West Nile virus viremias sufficient for infecting select mosquito species. Vector Borne Zoonotic Dis. 2008;8:225–33. https://doi.org/10.1089/vbz.2007.0182
29. Goddard LB, Roth AE, Reisen WK, Scott TW. Vector competence of California mosquitoes for West Nile virus. Emerg Infect Dis. 2002;8:1385–91. https://doi.org/10.3201/eid0812.020536
30. Higgs S, Snow K, Gould EA. The potential for West Nile virus to establish outside of its natural range: a consideration of potential mosquito vectors in the United Kingdom. Trans R Soc Trop Med Hyg. 2004;98:82–7. https://doi.org/10.1016/S0035-9203(03)00004-X
31. Marra PP, Griffing SM, McLean RG. West Nile virus and wildlife health. Emerg Infect Dis. 2003;9:898–9. https://doi.org/10.3201/eid0907.030277
32. Klenk K, Snow J, Morgan K, Bowen R, Stephens M, Foster F, et al. Alligators as West Nile virus amplifiers. Emerg Infect Dis. 2004;10:2150–5. https://doi.org/10.3201/eid1012.040264
33. Añez G, Grinev A, Chancey C, Ball C, Akolkar N, Land KJ, et al. Evolutionary dynamics of West Nile virus in the United States, 1999–2011: phylogeny, selection pressure and evolutionary time-scale analysis. PLoS Negl Trop Dis. 2013;7:e2245. https://doi.org/10.1371/journal.pntd.0002245
34. Tamba M, Bonilauri P, Bellini R, Calzolari M, Albieri A, Sambri V, et al. Detection of Usutu virus within a West Nile virus surveillance program in northern Italy. Vector Borne Zoonotic Dis. 2011;11:551–7. https://doi.org/10.1089/vbz.2010.0055
35. Santos PD, Michel F, Wylezich C, Höper D, Keller M, Holicki CM, et al. Co-infections: simultaneous detections of West Nile virus and Usutu virus in birds from Germany. Transbound Emerg Dis. 2022;69:776–92. https://doi.org/10.1111/tbed.14050
36. Aberle SW, Kolodziejek J, Jungbauer C, Stiasny K, Aberle JH, Zoufaly A, et al. Increase in human West Nile and Usutu virus infections, Austria, 2018. Euro Surveill. 2018;23:23. https://doi.org/10.2807/1560-7917.ES.2018.23.43.1800545
37. Carrillo-Hernández MY, Ruiz-Saenz J, Villamizar LJ, Gómez-Rangel SY, Martínez-Gutierrez M. Co-circulation and simultaneous co-infection of dengue, chikungunya, and Zika viruses in patients with febrile syndrome at the Colombian–Venezuelan border. BMC Infect Dis. 2018;18:61. https://doi.org/10.1186/s12879-018-2976-1
38. Perera-Lecoin M, Luplertlop N, Surasombatpattana P, Liégeois F, Hamel R, Thongrungkiat S, et al. Dengue and chikungunya coinfection—the emergence of an underestimated threat. In: Rodriguez-Morales AJ, editor. Current topics in chikungunya. Rijeka (Croatia): InTech; 2016. p. 67.
39. Nimmannitya S, Halstead SB, Cohen SN, Margiotta MR. Dengue and chikungunya virus infection in man in Thailand, 1962–1964. I. Observations on hospitalized patients with

hemorrhagic fever. Am J Trop Med Hyg. 1969;18:954–71. https://doi.org/10.4269/ajtmh.1969.18.954
40. Chahar HS, Bharaj P, Dar L, Guleria R, Kabra SK, Broor S. Co-infections with chikungunya virus and dengue virus in Delhi, India. Emerg Infect Dis. 2009;15:1077–80. https://doi.org/10.3201/eid1507.080638
41. Mercado M, Acosta-Reyes J, Parra E, Pardo L, Rico A, Campo A, et al. Clinical and histopathological features of fatal cases with dengue and chikungunya virus co-infection in Colombia, 2014 to 2015. Euro Surveill. 2016;21:21. https://doi.org/10.2807/1560-7917.ES.2016.21.22.30244
42. Worobey M, Rambaut A, Holmes EC. Widespread intra-serotype recombination in natural populations of dengue virus. Proc Natl Acad Sci U S A. 1999;96:7352–7. https://doi.org/10.1073/pnas.96.13.7352
43. Tazeen A, Afreen N, Abdullah M, Deeba F, Haider SH, Kazim SN, et al. Occurrence of co-infection with dengue viruses during 2014 in New Delhi, India. Epidemiol Infect. 2017;145:67–77. https://doi.org/10.1017/S0950268816001990
44. Lin DC, Weng SC, Tsao PN, Chu JJH, Shiao SH. Co-infection of dengue and Zika viruses mutually enhances viral replication in the mosquito *Aedes aegypti*. Parasit Vectors. 2023;16:160. https://doi.org/10.1186/s13071-023-05778-1
45. Vogels CB, Fros JJ, Göertz GP, Pijlman GP, Koenraadt CJ. Vector competence of northern European *Culex pipiens* biotypes and hybrids for West Nile virus is differentially affected by temperature. Parasit Vectors. 2016;9:393. https://doi.org/10.1186/s13071-016-1677-0
46. Fay RL, Ngo KA, Kuo L, Willsey GG, Kramer LD, Ciota AT. Experimental evolution of West Nile virus at higher temperatures facilitates broad adaptation and increased genetic diversity. Viruses. 2021;13:13. https://doi.org/10.3390/v13101889
47. Caldwell HS, Ngo K, Pata JD, Kramer LD, Ciota AT. West Nile Virus fidelity modulates the capacity for host cycling and adaptation. J Gen Virol. 2020;101:410–9. https://doi.org/10.1099/jgv.0.001393
48. Ciota AT, Lovelace AO, Jones SA, Payne A, Kramer LD. Adaptation of two flaviviruses results in differences in genetic heterogeneity and virus adaptability. J Gen Virol. 2007;88:2398–406. https://doi.org/10.1099/vir.0.83061-0
49. Ciota AT, Ngo KA, Lovelace AO, Payne AF, Zhou Y, Shi PY, et al. Role of the mutant spectrum in adaptation and replication of West Nile virus. J Gen Virol. 2007;88:865–74. https://doi.org/10.1099/vir.0.82606-0

Address for corresponding author: Holly R. Hughes, Centers for Disease Control and Prevention, 3156 Rampart Rd, Mailstop PO2, Fort Collins, CO 80521, USA, email: ltr8@cdc.gov

etymologia revisited

Tularemia [t-lə-rē-mē-ə]

An infectious, plaguelike, zoonotic disease caused by the bacillus *Francisella tularensis*. The agent was named after Tulare County, California, where the agent was first isolated in 1910, and Edward Francis, an Officer of the US Public Health Service, who investigated the disease. Dr. Francis first contracted deer fly fever from a patient he visited in Utah in the early 1900s. He kept a careful record of his 3-month illness and later discovered that a single attack confers permanent immunity. He was exposed to the bacterium for 16 years and even deliberately reinfected himself 4 times.

Tularemia occurs throughout North America, many parts of Europe, the former Soviet Union, the People's Republic of China, and Japan, primarily in rabbits, rodents, and humans. The disease is transmitted by the bites of deerflies, fleas, and ticks; by contact with contaminated animals; and by ingestion of contaminated food or water.

Clinical manifestations vary depending on the route of introduction and the virulence of the agent. Most often, an ulcer is exhibited at the site of introduction, together with swelling of the regional lymph nodes and abrupt onset of fever, chills, weakness, headache, backache, and malaise.

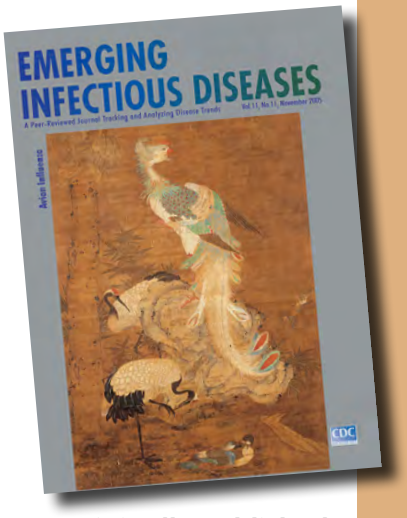

Originally published in November 2007

Reference

Dorland's illustrated medical dictionary, 31st edition. Philadelphia: Saunders; 2007; Benenson AS, editor. Control of communicable diseases manual. Washington: American Public Health Association; 1995; https://www.whonamedit.com

https://wwwnc.cdc.gov/eid/article/13/11/e1-1311_article

Bartonella spp. in Phlebotominae Sand Flies, Brazil

Daniel Antônio Braga Lee, Paloma Helena Fernandes Shimabukuro, Andréia Fernandes Brilhante, Paulo Vitor Cadina Arantes, Gustavo Seron Sanches, Eliz Oliveira Franco, Rosangela Zacarias Machado, Ricardo G. Maggi, Edward B. Breitschwerdt, Marcos Rogério André

Bartonella spp. are opportunistic, vectorborne bacteria that can cause disease in both animals and humans. We investigated the molecular occurrence of *Bartonella* spp. in 634 phlebotomine sand fly specimens, belonging to 44 different sand fly species, sampled during 2017–2021 in north and northeastern Brazil. We detected *Bartonella* sp. DNA in 8.7% (55/634) of the specimens by using a quantitative real-time PCR targeting the 16S-23S internal transcribed spacer intergenic region. Phylogenetic analysis positioned the *Lutzomyia longipalpis* sand fly–associated *Bartonella gltA* gene sequence in the same subclade as *Bartonella ancashensis* sequences and revealed a *Bartonella* sp. sequence in a *Dampfomyia beltrani* sand fly from Mexico. We amplified a bat-associated *Bartonella nuoG* sequence from a specimen of *Nyssomyia antunesi* sand fly. Our findings document the presence of *Bartonella* DNA in sand flies from Brazil, suggesting possible involvement of these insects in the epidemiologic cycle of *Bartonella* species.

The genus *Bartonella* (Alphaproteobacteria: Bartonellaceae) comprises emergent and re-emergent opportunistic bacteria classified in 39 validated species (https://lpsn.dsmz.de/genus/bartonella), some of them capable of causing disease in both animals and humans (*1*). Mammals (e.g., rodents, bats, cats, dogs, ruminants), including humans, are the main reservoirs for bartonellae. The *Bartonella* species most often associated with disease in humans are *B. henselae* (the causative agent of cat scratch disease), *B. quintana* (the causative agent of trench fever), and *B. bacilliformis* and *B. ancashensis* (the causative agents of Carrion's disease and verruga peruana) (*2*–*4*). Other species, including *B. clarridgeiae*, *B. koehlerae*, *B. vinsonii* subspecies *berkhoffii*, *B. elizabethae*, and Candidatus *Bartonella mayotimonensis*, also have been associated with disease in humans, especially in fever of unknown origin and culture-negative endocarditis cases (*5*,*6*). *Bartonella* spp. infect a variety of cells, including erythrocytes, pericytes, endothelial, dendritic, and macrophage cells and are associated with persistent intraerythrocytic bacteremia, suggesting a possible coevolution between these bacteria and their hosts, which may explain their remarkable adaptability to ≥1 mammal species (*2*,*7*,*8*). The ability of those bacterial species to maintain a persistent bacteremia over time dovetails with their main route of transmission, via bloodsucking arthropods (*9*). On the basis of molecular epidemiologic surveys and clinical observations, researchers have implicated many hematophagous arthropods in the transmission cycles of *Bartonella* spp.—mosquitoes (*9*), biting midges (*10*), triatomine bugs (*11*), mites (*12*,*13*), and flies (*14*)—adding to the list of those already identified as competent vectors (fleas, lice, phlebotomine sand flies, ticks) (*15*,*16*).

Phlebotomine sand flies (Diptera: Psychodidae: Phlebotominae) comprise >1,060 species, distributed worldwide, especially in tropical and subtropical regions (*17*). Given their hematophagous feeding habit, female sand flies are insects of considerable public health concern, because they act as vectors in the transmission of different pathogenic agents (bacteria, protozoa, virus), such as *Bartonella* sp., *Leishmania* sp., and Phleboviruses (*18*). Within the Bartonellaceae family, *B. bacilliformis* is notably the most important agent transmitted by phlebotomine sand flies. This *Bartonella* species is the causative agent of Carrion's disease, which can manifest as 2 different syndromes (that can occur sequentially or independently): Oroya fever, characterized by an acute

Author affiliations: São Paulo State University, Jaboticabal, Brazil (D.A.B. Lee, P.V.C. Arantes, G.S. Sanches, E.O. Franco, R.Z. Machado, M.R. André); Oswaldo Cruz Foundation, Belo Horizonte, Brazil (P.H.F. Shimabukuro); Federal University of Acre, Rio Branco, Acre, Brazil (A.F. Brilhante); North Carolina State University College of Veterinary Medicine, Raleigh, North Carolina, USA (R.G. Maggi, E.B. Breitschwerdt)

DOI: https://doi.org/10.3201/eid3010.240397

hemolytic anemia with an untreated fatality rate of up to 90%, and verruga peruana (also called Peruvian warts), characterized by a widespread formation of hemangiomas (verrugas) on the skin, along with a persistent bacteremia (*3*,*7*). The primary vectors of *B. bacilliformis* are *Pintomyia verrucarum* and *Lutzomyia peruensis* sand flies, which can be found in the Inter-Andean valleys of Peru, at altitudes ranging from 500 to 3,200 meters (*7*).

Carrion's disease is a neglected disease because of its focal occurrence (Andean valleys of Peru and, to a lesser extent, in Colombia and Ecuador) and challenges in establishing diagnosis (lack of resources and difficult access to endemic areas). The occurrence of the disease in nonendemic areas and the detection of *B. bacilliformis* DNA in a growing range of sand fly species suggests that the epidemiologic cycle of Carrion's disease might involve more sand fly species than first suspected (*19*). Researchers have detected *B. bacilliformis* DNA in wild-captured *Pintomyia robusta* sand flies in the border region between Ecuador and Peru (A.R. Carrazco-Montalvo unpub. data, https://doi.org/10.13140/RG.2.2.17645.00481) and in *Pintomyia maranonensis* sand flies in northern Peru (*20*), but data have yet to confirm their role as vectors. Other possible vectors of Carrion's disease were noted in Colombia, including *Lutzomyia gomezi*, *Psychodopygus panamensis*, *Pintomyia serrana*, and most notably *Pintomyia columbiana* sand flies, because of their presence in areas of disease outbreaks (*21*,*22*); however, those observations lacked molecular confirmation of the presence of *Bartonella* DNA in those sand fly specimens. Other suggested vectors for transmission of *B. bacilliformis* include *Lutzomyia pescei*, *L. noguchii*, and *L. ayacuchensis* sand flies (*19*,*22*,*23*).

Reports have identified *Bartonella ancashensis*, a species closely related to *B. bacilliformis*, from blood samples of patients undergoing treatment for verruga peruana in the rural region of Ancash, Peru (*24*,*25*). Although that species has not been isolated from blood samples of patients with Oroya fever and seems to be less pathogenic than *B. bacilliformis*, co-infections can occur, given that the geographic distribution of *B. ancashensis* overlaps with *B. bacilliformis* (*4*,*25*). Still, no reports have elucidated the involvement of sand flies in the transmission cycle of *B. ancashensis*.

Brazil has a rich diversity of 304 phlebotomine sand fly species (89 endemic), classified within 19 genera, distributed across all 5 federative regions of Brazil: 218 species in the north, 155 in the midwest, 132 in the southeast, 129 in the northeast, and 49 in the south (*26*). Despite the diverse phlebotomine sand fly fauna present in Brazil and the proximity to regions endemic for or reporting cases of Carrion's disease, previous studies have not investigated the occurrence of *Bartonella* spp. in those dipterans. However, studies from other countries have detected the presence of *Bartonella* sp. DNA in sand fly species that inhabit Brazil. In Peru, individual female *Pintomyia nevesi* and *Lutzomyia sherlocki* sand flies and pooled female *Nyssomyia whitmani* and *Psychodopygus hirsutus* sand fly tested positive for *Bartonella* sp. DNA, phylogenetically associated with *B. bacilliformis* and *Candidatus* Bartonella rondoniensis (*27*). Researchers in Mexico detected *Bartonella gltA* genotypes, which have been associated with a putative new lineage of *Bartonella* in sand flies, in females *Lutzomyia cruciata* and *Psathyromyia shannoni* sand fly (*28*). In this study, we investigated the occurrence and molecular identity of *Bartonella* spp. in sand flies collected in 7 states across the north and northeast regions of Brazil.

Material and Methods

Sand Fly Specimens and Studied Areas

We analyzed sand fly specimens collected during November 2017–December 2021, captured by using Shannon traps or traps designed by the Centers for Disease Control and Prevention set up in ecologic reserves and parks throughout Brazil. Locations included preserved forest areas in the cities of Xapuri and Rio Branco (Acre); Murici Ecologic Station (Alagoas); Pau Brasil National Park (Bahia); Ubajara National Park (Ceará); Tapajós National Forest (Pará); Dois Irmãos State Park (Pernambuco); and Viruá National Park (Roraima). We extracted DNA from dissected sand flies by using Invitrogen TRIzol Reagent (Thermo Fisher Scientific, https://www.thermofisher.com); specimens were without heads and 3 last abdominal segments, which were used for morphologic identification according to previously described taxonomic keys (*29*). We evaluated DNA concentration and quality (260/280 ratio) with the use of a spectrophotometer (Nanodrop; Thermo Fisher Scientific). We assessed the presence of potential PCR inhibitors by using a conventional PCR based on cytochrome c oxidase subunit 1 (*cox1*), an endogenous gene among invertebrates. We investigated the occurrence of *Bartonella* sp. DNA in a total of 634 individual sand fly DNA samples, which we classified into 44 species belonging to 14 genera, obtained from 7 different states across north and northeast Brazil (Table 1).

Table. Species and number of sand flies, including regions they were collected, after PCR screening for amplification of the endogenous gene *cox*1 for investigation of *Bartonella spp.* in phlebotomine sand flies, Brazil*

Genera, no.	Species, no.	State of sampling
Bichromomyia, 4	*flaviscutellata*, 4	Acre
Brumptomyia, 12	sp., 12	Acre
Evandromyia, 60	*begonae*, 1	Acre
	infraspinosa, 1	Acre
	saulensis, 14	Acre
	termitophila, 1	Acre
	walkeri, 43	Acre
Lutzomyia, 46	*longipalpis*, 27	Ceará
	sherlocki, 19	Acre
Micropygomyia, 2	*trinidanensis*, 1	Acre
	sp., 1	Pará
Nyssomyia, 132	*antunesi*, 76	Acre
	shawi, 15	Acre
	umbratilis, 28	Pará, n = 14; Pernambuco, n = 14
	whitmani, 12	Acre
	sp., 1	Acre
Pintomyia, 13	*nevesi*, 5	Acre
	serrana, 6	Acre
	sp., 2	Bahia
Pressatia, 28	*choti*, 15	Bahia
	sp., 13	Acre, n = 5; Bahia, n = 8
Psathyromia, 3	*elizabethdorvalae*, 2	Acre
	sp., 1	Acre
Psychodopygus, 163	*amazonensis*, 3	Acre
	ayrozai, 40	Alagoas, n = 2; Bahia, n = 8; Roraima, n = 30
	carreirai, 25	Acre, n = 22; Roraima, n = 3
	chagasi, 26	Alagoas, n = 2; Pará, n = 6; Roraima, n = 18
	complexus, 3	Alagoas, n = 2; Pará, n = 1
	davisi, 30	Acre, n = 24; Pará, n = 6
	guyanensis, 1	Pará
	hirsutus, 2	Alagoas, n = 1; Bahia, n = 1
	lainsoni, 2	Acre
	llanosmartinsi, 11	Acre
	paraensis, 17	Pará, n = 5; Roraima, n = 12
	squamiventris, 1	Roraima
	sp., 2	Acre, n = 1; Roraima, n = 1
Sciopemyia, 2	*sordelli*, 2	Acre
Trichophoromyia, 106	*ubiquitalis*, 1	Pará
	viannamartins, 65	Alagoas
	sp., 40	Acre, n = 24; Pará, n = 16
Trichopygomyia, 61	*dasypodogeton*, 2	Acre
	longispina, 55	Bahia
	sp., 4	Bahia, n = 2; Roraima, n = 2
Viannamyia, 2	*furcata*, 2	Acre

*All sand fly samples were used for PCR amplification and phylogenetic characterization of *Bartonella* spp.

Molecular Assays

We conducted molecular screening for *Bartonella* spp. by using a quantitative real-time PCR (qPCR) based on a 243-bp fragment of the 16S-23S ribosomal DNA internal transcribed spacer (ITS). We performed all reactions in a final volume of 10 μL containing 2× qPCRBIO Probe Master Mix Buffer (PCR Biosystems, https://pcrbio.com), 1.2 μM of each primer and probe, 1 μL of DNA sample, and ultrapurified, sterilized water qsp (Appendix Table 1, https://wwwnc.cdc.gov/EID/article/30/10/24-0397-App1.pdf). For the construction of the standard curve of each reaction, we performed serial dilutions at different concentrations (10^7–10^1 copies) of a gBlock gene fragment encoding a 243-bp fragment of the ITS genic region of *Bartonella henselae* (GenBank accession no. L35101) (Integrated DNA Technologies, https://www.idtdna.com). We also used the gBlocksas positive controls.

We determined the number of gene copies by the formula (XG/μL DNA/[gene block length, bp × 660]) × 6.22 × 10^{23} × gene copies/μL. We calculated the amplification efficiency (E) according to the slope of the standard curve by using the formula $E = 10^{-1/\text{slope}}$. We evalutated each DNA sample in duplicate and retested in triplicate those samples that presented differences in Cq values >0.5. We considered a Cq value cutoff of 42 for negative results. We carried out reactions in a C1000-CFX96 thermocycler (Bio-Rad Laboratories, https://www.bio-rad.com), using ultrapurified, sterilized water as a negative control.

We noted samples revealed to be positive in the screening qPCR and characterized them by using conventional PCRs based on 8 different molecular markers: *gltA* (380–400 bp), (767 bp), *ftsZ* (515 bp), *groEL* (752 bp), *nuoG* (346 bp), *pap31* (564 bp), *rpoB* (825 bp), *ribC* (585–588 bp), and 16S-23S ITS (453–717 bp) (Appendix Table 1).

Purification and Phylogenetic Analyzes

We purified the amplicons obtained in the PCRs by using Wizard SV Gel and PCR Clean-Up System (Promega Corporation, https://www.promega.com). We submitted purified amplicons for Sanger sequencing in both directions (forward and reverse) at the Centro de Estudos do Genoma Humano e Células Tronco (University of São Paulo, São Paulo, Brazil) by using the BigDye Terminator v3.1 Cycle Sequencing Kit (Thermo Fisher Scientific). We assembled a consensus sequence for each sample by using Geneious Prime 2023.2 (Geneious, https://www.geneious.com) and BioEdit 7.2 (*30*) software programs.

We conducted BLASTn analyzes (https://blast.ncbi.nlm.nih.gov) to produce an alignment for each genetic region, by using the obtained sequences, closely related sequences, and reference sequences previously deposited in GenBank. We created alignments by using the MAFFT version 7 software (https://mafft.cbrc.jp/alignment/server/index.html) and trimmed by using BioEdit 7.2 software (*30*). For phylogenetic inferences, we performed a maximum-likelihood analysis, with 10^3 ultraFast bootstrap replicates for each alignment, by using IQTREE2 1.6.12 software (http://www.iqtree.org). We chose the best-fitting evolutionary model for each alignment by using MrModeltest2 2.4 (MrModeltest 2.4; https://github.com/nylander/MrModeltest2) through the PAUP4* Version 4c software (https://paup.phylosolutions.com). We rooted (via outgroups) and edited the resulting phylogenetic trees by using FigTree 1.4.4 (https://tree.bio.ed.ac.uk/software/figtree) and iTOL version 5 (https://itol.embl.de) software programs.

Results

The DNA extraction of individual specimens of sand flies by using TRIzol was satisfactory, yielding DNA concentrations ranging from 1 to 15 ng/μL. We were able to obtain positive samples in the *cox1* conventional PCR for all 634 (100%) specimens.

Using the qPCR assay targeting the 16S-23S ITS region, we found that 55 (8.67%) of 634 sand flies tested positive for *Bartonella* spp. in the molecular screening: 48 from Acre (*Nyssomyia antunesi* [n = 18], *Evandromyia walkeri* [n = 7], *Trichophoromyia* sp. [n = 5], *L. sherlocki* [n = 4], *Nyssomyia shawi* [n = 3]; *Psychodopygus llanosmartinsi* [n = 2]; *Psychodopygus davisi* [n = 2]; *Bichromomyia flaviscutellata* [n = 1]; *Evandromyia saulensis* [n = 1]; *Nyssomyia* sp. [n = 1]; *N. whitmani* [n = 1]; *P. nevesi* [n = 1]; *Pintomyia serrana* [n = 1]; *Viannamyia furcata* [n = 1]); 2 from Alagoas (*Trichophoromyia viannamartinsi*); 2 from Roraima (*Psychodopygus squamiventris* [n = 1]; *Psychodopygus ayrozai* [n = 1]); 1 from Bahia (*Trichopygomyia longispina*); 1 from Ceará (*Lutzomyia longipalpis*); and 1 from Pará (*Psychodopygus paraensis*) (Figure 1). The range of Cq values of positive samples was 30.1–41.8. We selected 16 of those samples (based on the lowest PCR Cq values) and obtained 7 readable sequences. On the basis of BLASTn analysis, we confirmed that all 7 sequences corresponded to a *Bartonella* sp. (Appendix Table 2). However, the sequences were too short (179–222 bp) to be used for phylogenetic inferences. The value of the qPCR efficiency fell in the range of 98.7%–104.8% (mean 102.3, SD 2.29). The R^2 value was 0.834–0.986 (mean 0.978, SD 0.05), the Y-intercept range was 34.429–42.318 (mean 37.97, SD, 2.75), and the slope was −3.22 to −3.35 (mean −3.27; SD, 0.05). We were unable to measure the DNA load of positive samples because the Cq difference between replicates was >0.5, possibly because of the Monte Carlo effect (*31*).

We performed further molecular characterization (by conventional PCR) of samples that tested positive in the ITS screening qPCR assay and generated amplicons for the following genes: 4 for the *gltA*, 4 for the ITS, 2 for the *ftsZ*, 2 for the *pap31*, 1 for the *rpoB*, and 1 for the *nuoG*. Of those, we obtained 2 readable sequences: one 377-bp *gltA* sequence (GenBank accession no. PP421218) from a *L. longipalpis* sand fly captured in the state of Ceará, and one 345-bp *nuoG* sequence from a *N. antunesi* sand fly from Acre.

The BLASTn analysis demonstrated that the *gltA* sequence obtained from *L. longipalpis* sand flies demonstrated >96% identity with *B. ancashensis* sequences previously obtained from infected humans (GenBank accession nos. CP010401.1, KC886736.1, and KC178618.1). Phylogenetic analyses positioned this sequence in the same subclade as *B. ancashensis* sequences and with a *Bartonella* sp. sequence detected in a *Dampfomyia beltrani* sand fly from Mexico (GenBank accession no. OQ343492.1), with a bootstrap clade support value of 95 (Figure 2).

The BLASTn analysis of the *nuoG* sequence from an *N. antunesi* sand fly indicated a 94.04%–94.47% identity with 2 *Bartonella* sp. sequences obtained from *Pteronotus davyi* bats from Guatemala (GenBank accession nos. MN270091.1 and MN270098.1). The few

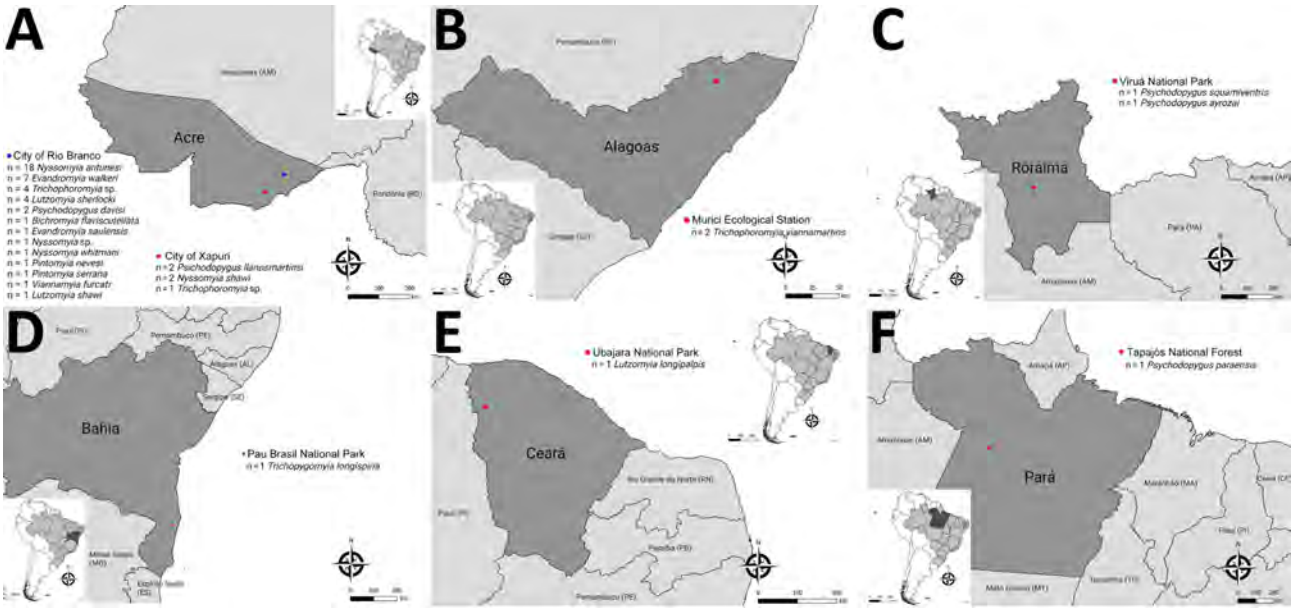

Figure 1. Sampling locations for sand flies that were qPCR positive in the screening for *Bartonella* spp. DNA from specimens collected in Brazil. A) State of Acre, northern Brazil; B) State of Alagoas, northeastern Brazil; C) State of Roraima, northern Brazil; D) State of Bahia, northeastern Brazil; E) State of Ceará, northeastern Brazil; F) State of Pará, northern Brazil. Dark gray indicates states with positive specimens, and red and blue dots representing the geographic location or city of sampling site. Inset maps show locations of each state in South America.

Bartonella nuoG sequences in GenBank and low values of bootstrap clades hampered robust phylogenetic inference by using this molecular marker.

Discussion

We documented the presence of *Bartonella* spp. DNA in phlebotomine sand flies from Brazil. The occurrence rate observed in this study (55/634 specimens; 8.67%) is similar that reported in southern Mexico, where 2 (8.69%) of 23 specimens were positive (*32*). Other investigations have reported a range of rates; 2 studies in Peru found positive results in 17 (6.02%) of 228 pools (*27*) and 2 (2.63%) of 76 pools (*20*), whereas 2 other studies in Mexico found positive results in 27 (5.08%) of 531 specimens (*33*) and 11 (2.06%) of 532 specimens (*28*). Differences in lower occurrence rates can be explained by the wide diversity of sand fly species present in different countries, the method of molecular analysis employed for DNA amplification, and, as illustrated in this study, technical limitations in obtaining phylogenetically relevant *Bartonella* DNA sequences from these small insects. Although the phlebotomine vectors of *Bartonella* spp. are very restricted to defined geographic areas, there have been minimal efforts to investigate the prevalence of this bacterial genus in sand flies from regions other than Peru. In our study, the selection of a broad diversity of sand fly species for *Bartonella* detection can be misleading, since most of the species are not confirmed to be carriers of these bacteria. In this context, we can assume that sand flies that were negative for the *Bartonella* sp. detection are either unable to host the bacteria or can be considered infrequent vectors. Further studies are necessary to elucidate the role of different sand fly species in the *Bartonella* epidemiologic cycles.

Although pooling specimens for analysis might have yielded a higher quantity of DNA (ng/μL), we would not have been able to accurately quantify the number of specimens that contained *Bartonella* sp. DNA, potentially leading to an underrepresentation of PCR-positive sand flies. Therefore, we opted to individually extract the DNA from the specimens by using the TRIzol reagent (Thermo Fisher Scientific), which resulted in satisfactory DNA quality, with concentrations of 1–15 ng/μL, and provided enough volume to perform the molecular detection and characterization. We confirmed the absence of PCR inhibitors by successfully amplifying the invertebrate *cox*1 gene in all samples.

Our detection of *Bartonella* sp. in *L. longipalpis* sand flies from Ceará state in northeastern Brazil corroborates previous findings. Our obtained 377-bp *Bartonella gltA* sequence clustered in the same subclade as *B. ancashensis* sequences obtained from humans with verruga peruana and a genotype recently detected in pools of *Dampfomyia beltrani* sand flies from Mexico (*34*). Of interest, genotypes closely related to

B. bacilliformis were previously detected in *Psathyromyia* sand flies from Mexico, a nonendemic country for Carrion's disease (*28*). Collectively, findings to date highlight the occurrence of putative novel genotypes belonging to ancient *Bartonella* lineages in sand flies from Brazil and Mexico, whose zoonotic potential remains unknown.

Although natural *Bartonella* sp. infections have not been previously reported in *L. longipalpis* sand flies, experimental studies of this species demonstrated infection with *B. ancashensis*, which remained viable in the anterior midgut for up to 7 days (*4*). A subsequent report describing the experimental infection of *L. longipalpis* sand flies with *B. bacilliformis* noted similar bacterial viability results (*35*). Although the *L. longipalpis* species has been used as a model for sand fly infection with *B. bacilliformis*, there are no reports of this species in Peru, where Carrion's disease is endemic (*36*). Prior investigators have suggested *L. longipalpis* sand flies might play a short-term role in the maintenance of *Bartonella* and potentially serve as a vector during that time (*4*,*35*). Our data further reinforce the need for additional investigation into the potential role of various sand flies for transmission of *Bartonella* spp. to human patients and sick animals. Future research specifically focusing on *L. longipalpis* sand flies is of particular importance because the species is the main vector of *Leishmania infantum* and is widely distributed in Brazil and throughout Central and South America (*37*). Although absent from Peru, the *L. longipalpis* sand fly belongs to the same genus, albeit from different subgenus, as the primary vector of *Bartonella bacilliformis* in Peru, namely the *Lutzomyia (Helcocyrtomyia) peruensis* sand fly. Furthermore, the *L. longipalpis* sand fly is related to sand fly species in which *Bartonella* DNA have already been detected, namely *Lutzomyia (Tricholateralis) gomezi*, *Lutzomyia (Tricholateralis) cruciata*, *Lutzomyia (Tricholateralis) sherlocki*, or to species that have been incriminated as additional putative vectors for *B. bacilliformis*, namely *Lutzomyia (Helcocyrtomyia) pescei*, *Lutzomyia (Helcocyrtomyia) noguchii*, and *Lutzomyia (Helcocyrtomyia) ayacuchensis* (*7*,*19*,*22*,*23*,*29;* A.R. Carrazco-Montalvo, unpub. data. Those findings highlight the importance of the sand fly genus *Lutzomyia* sensu stricto in the transmission cycles of *Bartonella* in South America.

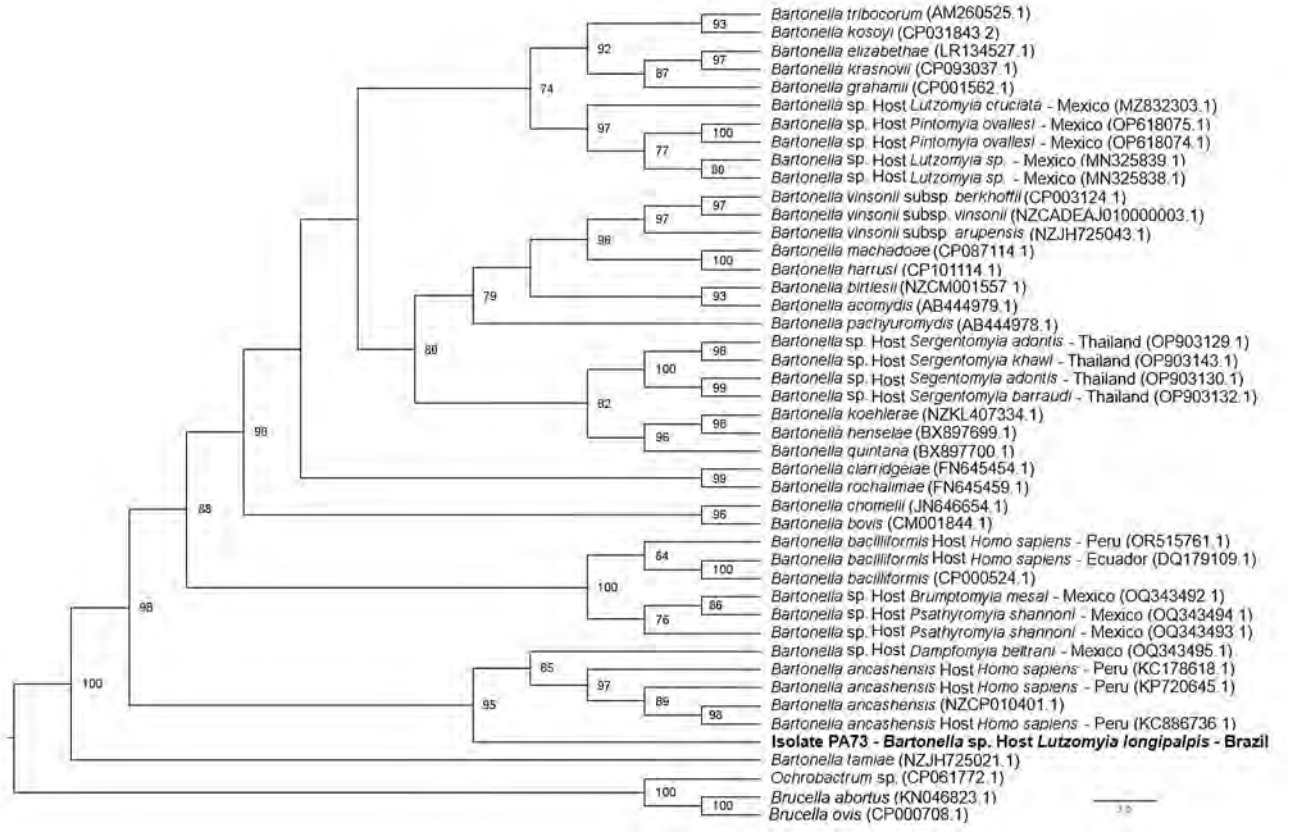

Figure 2. Phylogenetic tree based on an alignment of 380 bp-length of the *gltA* sequences obtained from phlebotomine sand flies collected in Brazil (bold) and reference sequences. Tree was created using the maximum-likelihood method and generalized time reversible plus invariate sites plus gamma as the evolutionary model. *Ochrobactrum* sp., *Brucella ovis*, and *Brucella abortus* were used as outgroups. Only bootstrap values >70 are shown. GenBank accession numbers are provided in parentheses.

Our investigation also revealed the amplification of a *Bartonella* sp. *nuoG* sequence with ≈94% identity to sequences previously detected in insectivorous *P. davyi* bats from Guatemala. The obtained genotype (detected in a *Nyssomyia antunesi* specimen captured in the state of Acre) shared 88%–91% identity with other *Bartonella* sp. sequences previously detected in bats and their associated ectoparasites from Brazil, including sequences amplified from *Diphylla ecaudata* and *Desmodus rotundus* vampire bats (*38*) and *Trichobius dugesii* flies (*39*). Despite the diverse phlebotomine sand fly fauna found across many Brazil biomes (≈370 species) and the country's proximity to regions reporting cases of Carrion's disease and *Bartonella* sp. in sand flies, the occurrence of *Bartonella* in those dipterans in Brazil has been unconfirmed. However, based on phlebotomine sand fly feeding habits (*40*), many studies have reported the occurrence of *Bartonella* sp. in vertebrates that act as hosts for sand fly blood meals, including rodents (*41*,*42*), marsupials *43*), bats (*38*,*39*,*42*), and xenarthrans (*44*). Although Streblidae and Nycteribiidae flies act as the main putative vectors of *Bartonella* species transmission among bats (*39*,*45*), many sand fly species that feed on bats (and other hosts) can acquire *Bartonella* spp. infections during blood-feeding. We believe that sand fly feeding habits and the high prevalence of *Bartonella* infection in many reservoir mammal hosts indicates a potential relationship and involvement of sand flies in the epidemiologic cycles of these bacteria.

In conclusion, we amplified *Bartonella* spp. DNA and successfully sequenced from *L. longipalpis* and *Ny. antunesi* sand flies, indicating possible involvement of these phlebotomine species in the maintenance or transmission cycle of *Bartonella* spp. The *Bartonella gltA* genotype was closely related to *B. ancashensis*, and the *nuoG* genotype was most closely related to a bat-associated *Bartonella* sp. Determining the epidemiologic cycle of these agents in Brazil will require elucidating the species and lineages of *Bartonella* spp. circulating among sand flies and determining whether sand flies in Brazil are capable of *Bartonella* spp. transmission to animals, including humans.

The dataset for this study is publicly available in the Sistema de Informação sobre a Biodiversidade Brasileira (SiBBr) and the Global Biodiversity Facility Information (GBIF) (https://doi.org/10.15468/3cnmuw).

This study was supported by Fundação de Amparo à Pesquisa do Estado de São Paulo (FAPESP process nos. 2022/07008-6 and 2022/08543-2), and CNPq (Conselho Nacional de Desenvolvimento Científico e Tecnológico–Productivity Grant for MRA, CNPq process no. 303701/2021-8). P.H.F.S. recieved financial support from Fundação de Amparo à Pesquisa do Estado de Minas Gerais (PPM-00676-18).

About the Author

Dr. Lee is a veterinarian and currently a PhD student at São Paulo State University in Brazil. His research is focused on the molecular detection of bloodborne agents in ectoparasites and wild and domestic animals.

References

1. Okaro U, Addisu A, Casanas B, Anderson B. *Bartonella* species, an emerging cause of blood-culture-negative endocarditis. Clin Microbiol Rev. 2017;30:709–46. https://doi.org/10.1128/CMR.00013-17
2. Breitschwerdt EB. Bartonellosis: one health perspectives for an emerging infectious disease. ILAR J. 2014;55:46–58. https://doi.org/10.1093/ilar/ilu015
3. Garcia-Quintanilla M, Dichter AA, Guerra H, Kempf VAJ. Carrion's disease: more than a neglected disease. Parasit Vectors. 2019;12:141. https://doi.org/10.1186/s13071-019-3390-2
4. Minnick MF, Robinson AJ, Powell RD, Rowland TE. Experimental colonization of sand flies (*Lutzomyia longipalpis*; Diptera: Psychodidae) by *Bartonella ancashensis*. Vector Borne Zoonotic Dis. 2023;23:324–30. https://doi.org/10.1089/vbz.2022.0087
5. Regier Y, O Rourke F, Kempf VAJ. *Bartonella* spp. - a chance to establish One Health concepts in veterinary and human medicine. Parasit Vectors. 2016;9:261. https://doi.org/10.1186/s13071-016-1546-x
6. Lin EY, Tsigrelis C, Baddour LM, Lepidi H, Rolain JM, Patel R, et al. Candidatus *Bartonella mayotimonensis* and endocarditis. Emerg Infect Dis. 2010;16:500–3. https://doi.org/10.3201/eid1603.081673
7. Gomes C, Ruiz J. Carrion's disease: the sound of silence. Clin Microbiol Rev. 2017;31:e00056–17.
8. Chomel BB, Boulouis HJ, Breitschwerdt EB, Kasten RW, Vayssier-Taussat M, Birtles RJ, et al. Ecological fitness and strategies of adaptation of *Bartonella* species to their hosts and vectors. Vet Res. 2009;40:29. https://doi.org/10.1051/vetres/2009011
9. Rudolf I, Blažejová H, Mendel J, Straková P, Šebesta O, Rettich F, et al. *Bartonella* species in medically important mosquitoes, Central Europe. Parasitol Res. 2020;119:2713–7. https://doi.org/10.1007/s00436-020-06732-1
10. Sacristán C, das Neves CG, Suhel F, Sacristán I, Tengs T, Hamnes IS, et al. *Bartonella* spp. detection in ticks, *Culicoides* biting midges and wild cervids from Norway. Transbound Emerg Dis. 2021;68:941–51. https://doi.org/10.1111/tbed.13762
11. Laroche M, Berenger J-M, Mediannikov O, Raoult D, Parola P. Detection of a potential new *Bartonella* species "Candidatus *Bartonella rondoniensis*" in human biting kissing bugs (Reduviidae; Triatominae). PLoS Negl Trop Dis. 2017;11:e0005297. https://doi.org/10.1371/journal.pntd.0005297
12. Melter O, Arvand M, Votýpka J, Hulínská D. *Bartonella quintana* transmission from mite to family with high socioeconomic status. Emerg Infect Dis. 2012;18:163–5. https://doi.org/10.3201/eid1801.110186

13. Loan HK, Cuong NV, Takhampunya R, Klangthong K, Osikowicz L, Kiet BT, et al. *Bartonella* species and trombiculid mites of rats from the Mekong Delta of Vietnam. Vector Borne Zoonotic Dis. 2015;15:40–7. https://doi.org/10.1089/vbz.2014.1604
14. Han HJ, Li ZM, Li X, Liu JX, Peng QM, Wang R, et al. Bats and their ectoparasites (Nycteribiidae and Spinturnicidae) carry diverse novel Bartonella genotypes, China. Transbound Emerg Dis. 2022;69:e845–58. https://doi.org/10.1111/tbed.14357
15. Billeter SA, Levy MG, Chomel BB, Breitschwerdt EB. Vector transmission of *Bartonella* species with emphasis on the potential for tick transmission. Med Vet Entomol. 2008;22:1–15. https://doi.org/10.1111/j.1365-2915.2008.00713.x
16. Król N, Militzer N, Stöbe E, Nijhof AM, Pfeffer M, Kempf VAJ, et al. Evaluating transmission paths for three different *Bartonella* spp. in *Ixodes ricinus* ticks using artificial feeding. Microorganisms. 2021;9:5:901.
17. Shimabukuro PHF, de Andrade AJ, Galati EAB. Checklist of American sand flies (Diptera, Psychodidae, Phlebotominae): genera, species, and their distribution. ZooKeys. 2017;660:67–106. https://doi.org/10.3897/zookeys.660.10508
18. Jancarova M, Polanska N, Volf P, Dvorak V. The role of sand flies as vectors of viruses other than phleboviruses. J Gen Virol. 2023;104:001837. https://doi.org/10.1099/jgv.0.001837
19. Lydy SL, Lascano MS, Garcia-Perez JE, Williams-Newkirk AJ, Grijalva MJ. Seroprevalence and risk factors for infection with *Bartonella bacilliformis* in Loja province, Ecuador. Emerg Microbes Infect. 2018;7:115. https://doi.org/10.1038/s41426-018-0110-5
20. Ulloa GM, Vásquez-Achaya F, Gomes C, Del Valle LJ, Ruiz J, Pons MJ, et al. Molecular detection of *Bartonella bacilliformis* in *Lutzomyia maranonensis* in Cajamarca, Peru: a new potential vector of carrion's disease in Peru? Am J Trop Med Hyg. 2018;99:1229–33. https://doi.org/10.4269/ajtmh.18-0520
21. Alexander B. A review of bartonellosis in Ecuador and Colombia. Am J Trop Med Hyg. 1995;52:354–9. https://doi.org/10.4269/ajtmh.1995.52.354
22. Minnick MF, Anderson BE, Lima A, Battisti JM, Lawyer PG, Birtles RJ. Oroya fever and verruga peruana: bartonelloses unique to South America. PLoS Negl Trop Dis. 2014;8:e2919. https://doi.org/10.1371/journal.pntd.0002919
23. Noguchi H, Shannon RC, Tilden EB, Tyler JR. Etiology of Oroya fever: XIV. The insect vectors of Carrion's disease. J Exp Med. 1929;49:993–1008. https://doi.org/10.1084/jem.49.6.993
24. Mullins KE, Hang J, Jiang J, Leguia M, Kasper MR, Ventosilla P, et al. Description of *Bartonella ancashensis* sp. nov., isolated from the blood of two patients with verruga peruana. Int J Syst Evol Microbiol. 2015;65:3339–43. https://doi.org/10.1099/ijsem.0.000416
25. Mullins KE, Hang J, Clifford RJ, Onmus-Leone F, Yang Y, Jiang J, et al. Whole-genome analysis of *Bartonella ancashensis*, a novel pathogen causing verruga peruana, rural Ancash region, Peru. Emerg Infect Dis. 2017;23:430–8. https://doi.org/10.3201/eid2303.161476
26. Shimabukuro PHF, Andrade AJ, Galati EAB. Phlebotominae in Catálogo Taxonômico da Fauna do Brasil. PNUD. 2024 [cited 2024 Feb 14]. http://fauna.jbrj.gov.br/fauna/faunadobrasil/3297
27. Zorrilla VO, Lozano ME, Espada LJ, Kosoy M, McKee C, Valdivia HO, et al. Comparison of sand fly trapping approaches for vector surveillance of *Leishmania* and *Bartonella* species in ecologically distinct, endemic regions of Peru. PLoS Negl Trop Dis. 2021;15:e0009517. https://doi.org/10.1371/journal.pntd.0009517
28. Lozano-Sardaneta YN, Soto-Olguín NJ, Rodríguez-Rojas JJ, Sánchez-Montes S, Rebollar-Téllez EA, Becker I. Molecular detection of *Bartonella* sp. in *Psathyromyia shannoni* and *Lutzomyia cruciata* from northeastern Mexico. Front Trop Dis. 2021;2:780808. https://doi.org/10.3389/fitd.2021.780808
29. Galati EAB. Phlebotominae (Diptera, Psychodidae) classificação, morfologia, terminologia e identificação de adultos. Apostila. Bioecologia e Identificação de Phlebotominae. 2016;1:131.
30. Hall TA. BioEdit: a user-friendly biological sequence alignment editor and analysis program for Windows 95/98/NT. Nucleic Acids Symp Ser. 1999;41:95–8.
31. Bustin SA, Nolan T. Pitfalls of quantitative real-time reverse-transcription polymerase chain reaction. J Biomol Tech. 2004;15:155–66.
32. Lozano-Sardaneta YN, Colunga-Salas P, Sánchez-Montes S, Cáceres AG, Becker I. First report of *Bartonella* sp. in sand flies (Diptera: Psychodidae: Phlebotominae) from southern Mexico. J Am Mosq Control Assoc. 2019;35:224–7. https://doi.org/10.2987/19-6854.1
33. Lozano-Sardaneta YN, Marina CF, Torres-Monzón JA, Sánchez-Cordero V, Becker I. Molecular detection of *Wolbachia* and *Bartonella* as part of the microbiome of phlebotomine sand flies from Chiapas, Mexico. Parasitol Res. 2023;122:1293–301. https://doi.org/10.1007/s00436-023-07829-z
34. Martínez-Burgos M, Lozano-Sardaneta YN, Rodríguez-Rojas JJ, Gómez-Rivera AS, Canto-Mis KL, Flores-Escobar E, et al. Species diversity and detection of pathogens in phlebotomine sand flies collected from forest management areas of Quintana Roo, Mexico. Med Vet Entomol. 2023;37:845–58. https://doi.org/10.1111/mve.12691
35. Battisti JM, Lawyer PG, Minnick MF. Colonization of *Lutzomyia verrucarum* and *Lutzomyia longipalpis* sand flies (Diptera: Psychodidae) by *Bartonella bacilliformis*, the etiologic agent of Carrión's disease. PLoS Negl Trop Dis. 2015;9:e0004128. https://doi.org/10.1371/journal.pntd.0004128
36. Sousa-Paula LC, Otranto D, Dantas-Torres F. *Lutzomyia longipalpis* (sand fly). Trends Parasitol. 2020;36:796–7. https://doi.org/10.1016/j.pt.2020.05.007
37. Lainson R, Rangel EF. Lutzomyia longipalpis and the eco-epidemiology of American visceral leishmaniasis, with particular reference to Brazil: a review. Mem Inst Oswaldo Cruz. 2005;100:811–27. https://doi.org/10.1590/S0074-02762005000800001
38. André MR, Gutiérrez R, Ikeda P, do Amaral RB, de Sousa KCM, Nachum-Biala Y, et al. Genetic diversity of *Bartonella* spp. in vampire bats from Brazil. Transbound Emerg Dis. 2019;66:2329–41. https://doi.org/10.1111/tbed.13290
39. Ikeda P, Marinho Torres J, Perles L, Lourenço EC, Herrera HM, de Oliveira CE, et al. Intra- and inter-host assessment of *Bartonella* diversity with focus on non-hematophagous bats and associated ectoparasites from Brazil. Microorganisms. 2020;8:1822. https://doi.org/10.3390/microorganisms8111822
40. Sousa RLT, Vasconcelos SA, Santos-Mallet JR, Nascimento EF, Teixeira CR, Silva CLM, et al. Padrões de fonte alimentar dos Flebotomíneos (Diptera: Psychodidae) vetores das Leishmanioses: uma revisão bibliográfica. Revista Eletrônica Acervo Saúde. 2021;13:e8567. https://doi.org/10.25248/reas.e8567.2021
41. do Amaral RB, Cardozo MV, Varani AM, Gonçalves LR, Furquim MEC, Dias CM, et al. *Bartonella machadoae* sp. nov.

isolated from wild rodents in the Pantanal wetland. Acta Trop. 2022;229:106368. https://doi.org/10.1016/j.actatropica.2022.106368
42. Pacheco TDA, Amaral RBD, Ikeda P, Maia MO, Lee DAB, Semedo TBF, et al. Molecular detection and characterization of *Bartonella* spp. in small mammals in the Amazonia and Cerrado biomes, midwestern Brazil. Acta Trop. 2024; 251:107129. https://doi.org/10.1016/j.actatropica.2024.107129
43. Braga MDSCO, Costa FB, Calchi AC, de Mello VVC, Mongruel ACB, Dias CM, et al. Molecular detection and characterization of vector-borne agents in common opossums (*Didelphis marsupialis*) from northeastern Brazil. Acta Trop. 2023;244:106955. https://doi.org/10.1016/j.actatropica.2023.106955
44. Calchi AC, Vultão JG, Alves MH, Yogui DR, Desbiez ALJ, do Amaral RB, et al. Multi–locus sequencing reveals a novel *Bartonella* in mammals from the Superorder Xenarthra. Transbound Emerg Dis. 2020;67:tbed.13545. https://doi.org/10.1111/tbed.13545
45. do Amaral RB, Lourenço EC, Famadas KM, Garcia AB, Machado RZ, André MR. Molecular detection of Bartonella spp. and Rickettsia spp. in bat ectoparasites in Brazil. PLoS One. 2018;13:e0198629. https://doi.org/10.1371/journal.pone.0198629

Address for correspondence: Marcos Rogério André, Vector-Borne Bioagents Laboratory, Department of Pathology, Reproduction and One Health, Faculty of Agrarian and Veterinary Sciences, São Paulo State University, Via de Acesso Prof. Paulo Donato Castellane s/n, CEP 14884-900, Bairro Rural, Jaboticabal-SP, Brazil; email: mr.andre@unesp.br

Early Introductions of *Candida auris* Detected by Wastewater Surveillance, Utah, USA, 2022–2023

Jorge Chavez,[1,2] Katherine Crank,[1] Casey Barber, Daniel Gerrity, Thomas Iverson, Joshua Mongillo,[3] Angela Weil, Linda Rider, Nathan Lacross, Kelly Oakeson, Alessandro Rossi

Candida auris is considered a nosocomial pathogen of high concern and is currently spreading across the United States. Infection control measures for *C. auris* focus mainly on healthcare facilities, yet transmission levels may already be significant in the community before outbreaks are detected in healthcare settings. Wastewater-based epidemiology (culture, quantitative PCR, and whole-genome sequencing) can potentially gauge pathogen transmission in the general population and lead to early detection of *C. auris* before it is detected in clinical cases. To learn more about the sensitivity and limitations of wastewater-based surveillance, we used wastewater-based methods to detect *C. auris* in a southern Utah jurisdiction with no known clinical cases before and after the documented transfer of colonized patients from bordering Nevada. Our study illustrates the potential of wastewater-based surveillance for being sufficiently sensitive to detect *C. auris* transmission during the early stages of introduction into a community.

Candida auris is an antifungal-resistant yeast that leads to high mortality rates among patients with underlying conditions and displays a formidable persistence in healthcare settings because of its biofilm-forming potential and resistance to some commonly used disinfectants (*1*–*3*). Circulating strains are classified into 5 genomic clades linked to their geographic area of origin: clade I (southern Asia), clade II (eastern Asia), clade III (Africa), clade IV (South America), and clade V (Iran) (*4*,*5*). Since *C. auris* introduction into the United States was documented in 2013 (*6*), prevalence has increased rapidly and the organism has become endemic to many jurisdictions (*7*). The strain exerted by the COVID-19 pandemic on infection control practices and public health resources in general is thought to have contributed to *C. auris* expansion (*8*).

Despite the widespread prevalence of *C. auris* in the United States, its effect on healthcare facilities should be limited, and jurisdictions that have not yet experienced sustained transmission should be protected. In addition to classic infection prevention strategies focused on admission screenings, point prevalence surveys (PPSs), and interfacility communication (*9*,*10*), wastewater-based surveillance could help control the spread of emerging pathogens by providing opportunities for early detection and management of outbreak responses (*11*–*13*).

We and others have previously shown the feasibility of community-scale wastewater surveillance for *C. auris* in high disease prevalence settings, specifically Nevada and Florida (*14*–*16*). We monitored the influent of the only wastewater treatment plant (WWTP) in St. George, Utah, before and after the transfer of a *C. auris*–positive patient into that community. On the basis of available epidemiologic information and modeling, we propose that wastewater surveillance could be a sufficiently sensitive strategy for early detection of *C. auris*, before it is detected in clinical surveillance efforts. In addition, we report improvements to the culture method that we originally used to recover *C. auris* isolates from wastewater and demonstrate the utility of organism isolation in providing high-quality genomic data for investigations. Our

Author affiliations: Utah Department of Health and Human Services, Salt Lake City, Utah, USA (J. Chavez, T. Iverson, J. Mongillo, A. Weil, L. Rider, N. Lacross, K. Oakeson, A. Rossi); Southern Nevada Water Authority, Las Vegas, Nevada, USA (K. Crank, C. Barber, D. Gerrity)

DOI: https://doi.org/10.3201/eid3010.240173

[1]These first authors contributed equally to this article.

[2]Current affiliation: Center for Disease Control and Prevention, Atlanta, Georgia, USA.

[3]Current affiliation: North Carolina Department of Health and Human Services, Wilmington, North Carolina, USA.

study was performed under Utah Department of Health and Human Services (DHHS) Institutional Review Board protocol no. 651 ("Community and facility level surveillance for multidrug resistant organisms using wastewater samples").

Materials and Methods

Wastewater Sample Collection and Transport

During November 2022–June 2023, we collected 24-hour composite influent wastewater samples from 3 WWTPs in southwestern Utah, near the border with Nevada: St. George (population ≈92,000), Ash Creek (≈25,000), and Cedar City (≈32,000) (Table 1; Figure 1, panel A). The St. George WWTP served as the primary experimental site, and the Ash Creek and Cedar City WWTPs served as presumptive negative control sites (Table 1). The average flow rate for the St. George WWTP during this study was 12.73 million gallons per day (mgd), which corresponds to 138 gallons per capita per day (gpcd). The per capita wastewater generation rate is similar to the national average of 132 gpcd (*17*). Each sample consisted of 250 mL of influent wastewater collected in polypropylene bottles and transported on ice (≈24 hours) to the Utah Public Health Laboratory (UPHL). Subsequently, 150-mL aliquots of each sample were shipped on ice with an overnight priority service (≈24 hours) to the Southern Nevada Water Authority laboratory.

Quantitative Real-Time PCR Monitoring and Performance Characteristics

To perform wastewater surveillance of *C. auris*, the Southern Nevada Water Authority used quantitative PCR (qPCR) as previously described (*15*). In the earlier study, the statistical limit of quantification was determined to be a quantification cycle (Cq) of 33.03 (*15*), which equated to an average of 7 gene copies (gc) across all study-specific standard curves, and the theoretical limit of detection was assumed to correspond to 1 gc. Across 18 samples in our study, the average equivalent sample volume (ESV) for each qPCR reaction was 1.07 ± 0.81 mL of influent wastewater, yielding an average limit of detection of 2.97 $\log_{10}$ gc/L. Limits of quantification ranged

Table 1. *Candida auris* qPCR and culture results from St. George, Ash Creek, and Cedar City, Utah, USA, 2022–2023*

Site	Sample date	qPCR Cq	No. qPCR amplifications (of 3 reps)	Quantifiable (LoQ = 33.03)	qPCR ESV, mL/reaction	qPCR concentration, $\log_{10}$ gc/L†	Culture results	Avg. WWTP flow, mgd
St. George	2022 Nov 8	‡	0	‡	1.13	<2.95‡§	Neg¶	11.67
	2022 Nov 15	‡	0	‡	1.13	<2.95‡§	Neg¶	11.55
	2022 Nov 29	33.42	3	No	3.75	4.22#	Neg¶	12.21
	2022 Dec 6	34.85	2	No	1.00	4.40#	Neg¶	11.89
	2022 Dec 13	34.78	2	No	0.75	4.61#	Neg¶	11.84
	2023 Jan 10	33.74	3	No	0.50	5.12#	Neg¶	12.47
	2023 Jan 24	30.96	3	Yes	1.50	4.91	NP	12.81
	2023 Jan 31	31.58	2	Yes	0.25	5.51	NP	12.75
	2023 Feb 7	33.53	3	No	0.75	4.49#	NP	12.67
	2023 Mar 28	NA	NA	NA	NA	NA	Pos**	14.08
	2023 Apr 4	NA	NA	NA	NA	NA	Pos**	14.06
	2023 Apr /6	31.70	3	Yes	0.38	4.81	NP	14.65
	2023 Apr 11	29.59	3	Yes	0.30	5.51	NP	13.98
	2023 Apr 18	29.22	3	Yes	1.50	4.92	Neg**	13.58
	2023 Apr 20	NA	NA	NA	NA	NA	Neg**	13.30
	2023 Apr 25	29.26	3	Yes	0.75	5.20	NP	13.17
	2023 May 2	30.38	3	Yes	0.38	5.17	NP	12.99
	2023 May 9	30.95	3	Yes	1.88	4.32	NP	12.53
	2023 May 16	31.21	3	Yes	1.13	4.47	NP	12.32
	2023 May 23	NA	NA	NA	NA	NA	Neg**	11.92
	2023 May 30	32.53	3	Yes	1.13	4.34	Neg**	11.87
	2023 Jun 13	32.18	3	Yes	1.13	4.44	Neg**	11.81
Cedar City	2023 Jan 24	‡	0	‡	1.50	<2.82‡§	Neg¶	3.26
	2023 Feb 7	‡	0	‡	0.37	<3.43‡§	NP	3.39
	2023 Jun 13	‡	0	‡	0.25	<3.60‡§	NP	2.99
Ash Creek	2023 Jun 13	‡	0	‡	0.75	<3.12‡§	NP	1.70

*Cq, quantification cycle; ESV, equivalent sample volume; gc, gene copies; LoD, limit of detection; LoQ, limit of quantification; mgd, million gallons/day; NA, samples not analyzed by qPCR; neg, negative; NP, not performed; pos, positive; qPCR, quantitative PCR; WWTP, wastewater treatment plant.
†Concentration calculations were based on the average Cq of positive qPCR replicates.
‡Not detectable.
§Left-censored concentrations are based on the theoretical LoD of 1 gene copy.
¶Culture performed via centrifugation method.
#Reported concentrations are technically below the LoQ.
**Culture performed via filtration method.

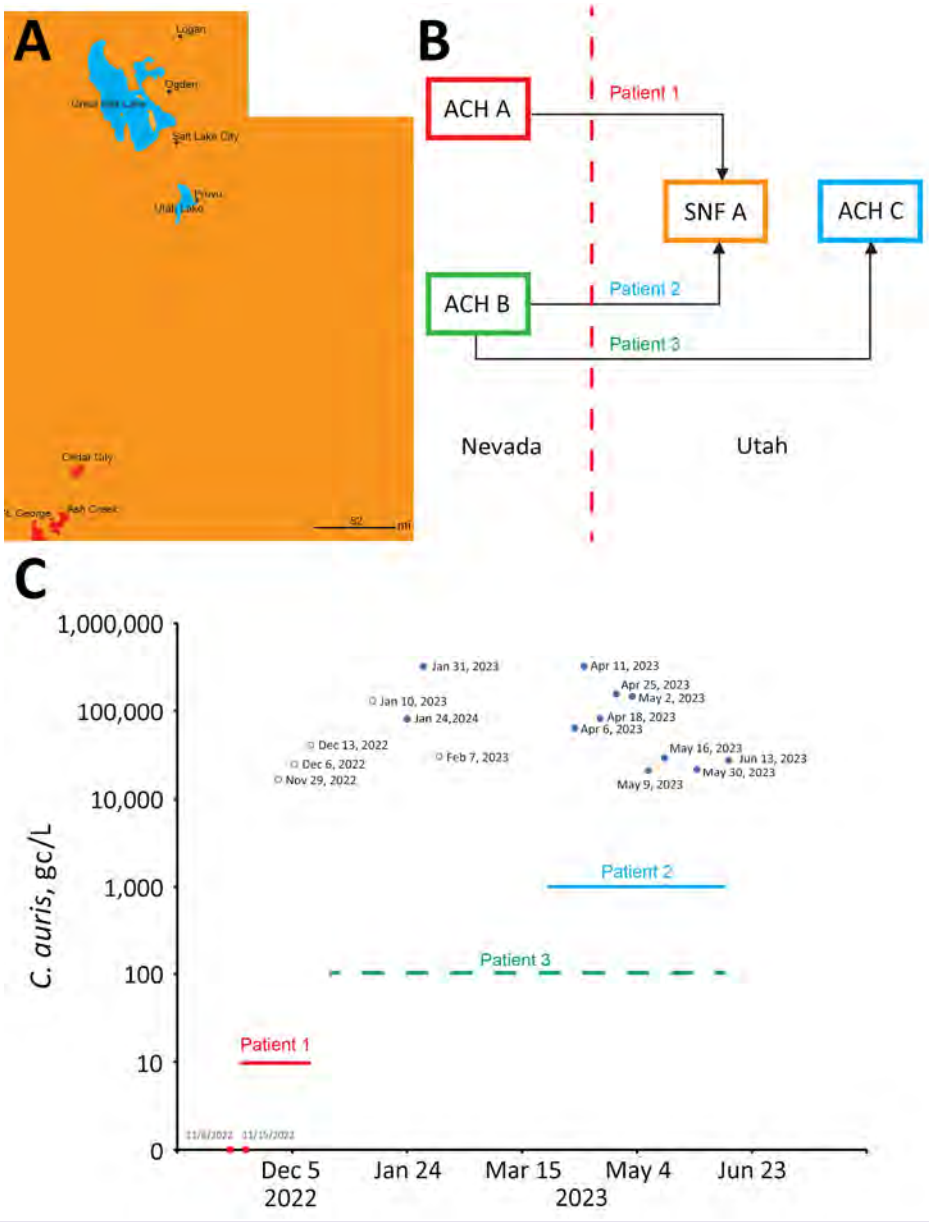

Figure 1. Transfer of *Candida auris* cases from Nevada to St. George, Utah, USA, and quantitative PCR monitoring of *C. auris* concentrations at the St. George wastewater treatment plant. A) Locations of sewersheds of St. George, Ash Creek, and Cedar City (red) in Utah. The western border of Utah is adjacent to Nevada. Scale bar indicates 52 miles. B) Interstate transfers from Nevada to Utah of 3 patients with *C. auris* infection (red dash line represents the state border). C) Sampling dates and corresponding *C. auris* concentrations in wastewater treatment plant influent samples expressed as gc/L, over the time of the study. Nondetected samples are indicated as solid red dots, positive samples with concentrations less than the limit of quantification are indicated as empty blue dots, and positive samples with concentration at or equal to the limit of quantification are indicated as solid blue dots. The patient time frames are indicated by horizontal lines. The line for patient 3 is dashed to indicated that the person commuted continuously between Nevada and Utah. ACH, acute-care hospital; gc, gene copies; SNF, skilled nursing facility.

from 3.95 to 4.47 $\log_{10}$ gc/L based on variability in run-specific standard curves and an assumed average ESV of 1.07 mL (Appendix, https://wwwnc.cdc.gov/EID/article/30/10/24-0173-App1.pdf).

C. auris Isolation by Culture of Filter-Based Concentration

We vacuum filtered ≤50 mL of influent wastewater through 0.45-µm cellulose nitrate analytical filters (ThermoFisher Scientific, https://www.thermofisher.com). We removed the filters from the vacuum unit by using forceps, placed the filters in a 50-mL conical tube, and submerged them in 12 mL of Salt Sabouraud Dulcitol Broth (2) (Thomas Scientific, https://www.thomassci.com) supplemented with 32 µg/mL fluconazole (*14*). The submerged filters were incubated at 42°C for up to 5 days with vigorous agitation at 250 rpm. We performed plating of the broth after incubation on chromogenic media and species identification of presumptive colonies as previously described (*14*).

Whole-Genome Sequencing and Bioinformatics

We sequenced *C. auris* genomes by using a NextSeq platform (Illumina, https://www.illumina.com). We performed single-nucleotide polymorphism (SNP) distance analyses by using the MycoSNP pipeline (*18*), as previously described (*14*).

Monte Carlo Modeling

We created a model to assess the theoretical sensitivity of the wastewater qPCR method for detecting *C. auris* from 1 shedding person in the sewershed. The model predicts the concentration of *C. auris* in wastewater (in gc/L) from 1 shedder (Table 2). We performed a Monte Carlo simulation by using 10,000 random samplings of the parameter distributions to characterize the distribution of possible *C. auris* concentrations with 1 *C. auris* shedder contributing urine and feces to the wastewater (Appendix).

Epidemiology Data and Infection Control Practices

C. auris reporting and submission of isolates or residual primary specimens is regulated by the Utah Communicable Disease Rule R386-702. The Utah DHHS uses EpiTrax as the centralized reportable disease database (*25*). Reports are filed electronically or via manual entry after notification to Utah DHHS by fax. Federal regulations recommend transfer notifications of patients colonized or infected with *C. auris*; however, compliance is seldom enforced, and effective interfacility communication relies on good infection prevention stewardship.

PPSs were conducted via composite axilla/groin swabbing (*26*) with nylon swabs, and samples were transported in liquid Amies (Eswab system; Copan, https://www.copanusa.com). We processed 200 µL of Amies media by using the on-board extraction PCR system BDMax (Becton, Dickinson and Company, https://www.bd.com) (*27*).

Results

Introduction of *C. auris* into St. George

In November 2022, the Utah DHHS was notified about the upcoming transfer of a patient with an active *C. auris* infection from Nevada to St. George, Utah (patient 1). Before patient 1 was transferred, no *C. auris* case or colonized person had been recorded in Utah. On November 10, 2022, patient 1 was transferred from an acute-care hospital (ACH A) in Nevada to a skilled nursing facility (SNF A) in St. George (Figure 1, panels B, C). Patient 1 was highly debilitated and while in St. George had a *C. auris*–positive urine culture (>10^5 CFU/mL); the patient died after the transfer (December 2022) (Figure 1, panel C). No additional colonized persons were discovered at SNF A through a PPS evaluating 40 persons.

In March 2023, Utah DHHS was notified about the transfer of a second *C. auris*–colonized person from Nevada (patient 2). Patient 2 had been hospitalized in a different acute-care hospital in Nevada (ACH B) and was admitted to SNF A in St. George on March 23, 2023; the patient remained there for the duration of our wastewater surveillance study (Figure 1, panels B, C).

We discovered a third patient from Nevada (patient 3) retrospectively. Patient 3 previously resided at ACH B in Nevada (similar to patient 2) but was not found to be colonized with *C. auris* before being transferred to St. George in December 2022 (Figure 1, panels B, C). Because of the risk factor associated with patient 3 being transferred from a healthcare facility with an ongoing outbreak (i.e., ACH B in Nevada), the acute-care hospital in St. George (ACH C) ordered an admission screening, which led to confirmation of *C. auris* colonization on December 28, 2022 (Figure 1, panels B, C). The colonization status of patient 3 was communicated via fax to the Utah DHHS according to Utah communicable diseases rules; however, the alert was overlooked because of human error. After 2 days at ACH C, patient 3 was discharged and continued to receive dialysis in an outpatient setting in St. George until June 2023, albeit by commuting between his residence in Nevada and St. George (Figure 1, panel C).

Collectively, the 3 patient transfers potentially resulted in nearly continuous shedding of *C. auris* into St. George wastewater during November 2022–June 2023, which coincided with the duration of our wastewater surveillance study. Moreover, patients 2 and 3 simultaneously resided or spent a substantial amount of time in St. George during March–June 2023 (Figure 1, panel C), potentially increasing *C. auris* loading in local wastewater.

Detection of *C. auris* in St. George Wastewater

After being notified of the pending transfer of patient 1 to St. George, we identified a unique opportunity to assess the sensitivity of wastewater surveillance for the early detection of *C. auris*. On November 8, 2022 (2 days before the transfer), we initiated qPCR-based wastewater surveillance at the St. George WWTP (Figure 1, panel C), which continued at irregular intervals until June 13, 2023 (Table 1; Figure 1, panel C). *C. auris* was not detected (i.e., below the limit of detection) in the first 2 samples collected for the study (November 8 and 15), which straddled the transfer date of patient 1 (Table 1; Figure 1, panel C). However, *C. auris* was detected, albeit below the limit of quantification, in a sample collected on November 29 and was detected in every sample thereafter (Table 1; Figure 1, panel C). Before March 2023, only 2 of 7 samples were above the limit of quantification, but starting in April 2023, when patients 2 and 3 were potentially contributing

to the St. George WWTP, all samples were above the limit of quantification (Table 1; Figure 1, panel C).

To assess potential transmission in areas near St. George, we also analyzed 4 influent wastewater samples from WWTPs in Ash Creek and Cedar City (Figure 1, panel A). *C. auris* was not detected in those presumptive negative control samples (Table 1).

Modeled Sensitivity of qPCR-Based, Community-Scale Wastewater Surveillance

Given the available epidemiologic data and the fact that *C. auris* was not detected in the sample collected before the initial transfer of patient 1, the subsequent *C. auris*–positive wastewater could represent detection of its initial introduction in St. George. If true, that finding indicates that qPCR-based wastewater surveillance may be sufficiently sensitive to detect a single *C. auris* shedder in a sewershed serving ≈100,000 inhabitants.

To gauge the plausibility of that statement, we used a Monte Carlo simulation model previously used for SARS-CoV-2 but adapted to *C. auris* (*28*). The model considers the following parameters: *C. auris* concentration ranges for urine and feces (based on a neutropenic mouse model and quantitative analyses of urine clinical cultures [*19*,*22*]); urine and feces production rates in healthy humans (*20*,*21*,*23*); variable gc numbers of the qPCR target (internal transcribed spacer 2) across *C. auris* strains (based on a nucleotide BLAST analysis in which the sequence of the qPCR probe was searched in various *C. auris* genomes, as well as the number of rRNA genes reported in *C. albicans* as an upper hypothetical value [*24*,*29*,*30*]); and average daily wastewater flow rate (Table 2).

The primary site of *C. auris* colonization is skin (*31*), and routine hygiene practices (e.g., handwashing, showering, laundering) should also represent a major route for release of organisms into the sewer system. However, we did not incorporate that shedding mode in our model because it would entail assumptions with considerable uncertainty (e.g., affected water volumes, affected skin surface area, skin mobilization rate, frequency of handwashing/showering/laundering).

Our model indicates that 97% of the predicted *C. auris* wastewater concentrations resulting from 1 person shedding the pathogen in urine and feces were above the average limit of detection for our study (2.97 $\log_{10}$ gc/L; assumes a limit of 1 gc and the average of all sample-specific ESVs for our study) (Figure 2, panels A, B). The median predicted concentration from the Monte Carlo simulation was 3.90 $\log_{10}$ gc/L, a value greater than the upper limit of observed limits of detection (i.e., 3.60 $\log_{10}$ gc/L; assumes a limit of 1 gc and the average of all sample-specific ESVs for our study) (Figure 2, panel A). The upper-bound probability of detection increases to 99.9% when the lowest limit of detection is considered (Figure 2, panel B). If shedding is modeled through either urine or feces alone, the probability of detection decreases to ≈85% when the average limit of detection is considered (Figure 2, panel B).

To determine the effect of each stochastic parameter on the final predicted wastewater concentrations, we used the Spearman correlation coefficient to perform a sensitivity analysis on the Monte Carlo model (*28*) (Figure 2, panel C). The parameter with the strongest correlation was the number of genome copies per CFU, followed by the rate of *C. auris* shedding in urine (and to a slightly lesser extent, feces).

Table 2. *Candida auris* shedding model parameters and distributions*

Parameter	Unit	Reported value	Assumed distribution	Reference	Assumption
C. auris fecal shedding rate	CFU/μL	10^4–10^5	Uniform: min = 10^4, max = 10^5	(*19*)	Based on neutropenic mouse model
Daily wet stool production	g/day		Truncated: log-normal (base *e*): μ = 4.763, σ = 0.471, min = 0, max = 520	(*20*)	Based on healthy persons
Wet fecal density	g/mL	1.06	Point value: 1.06	(*21*)	NA
C. auris urine shedding rate	CFU/μL	10^2–10^4	Uniform: min = 10^2, max = 10^4	(*22*)	Based on the clinical definition of UTI for clean catch collection (e.g., ≥10^2 CFU/μL)
Daily urine production	L/day		Gamma: shape = 5.315, scale = 0.25, offset = +0.5	(*23*)	Based on healthy persons
C. auris qPCR:culture (GC:CFU)	unitless	3–50	Uniform: min = 3, max = 50	(*24*)	Based on the analysis of several NCBI deposited *C. auris* genomes and a value reported for *C. albicans*
Average WWTP flow rate	mgd	12.73 ± 0.87	Normal: μ = 12.73, σ = 0.87	NA	NA

*GC, gene copies; mgd, million gallons/day; NA, no assumption made; NCBI, National Center for Biotechnology Information; qPCR, quantitative PCR; UTI, urinary tract infection; WWTP, wastewater treatment plant.

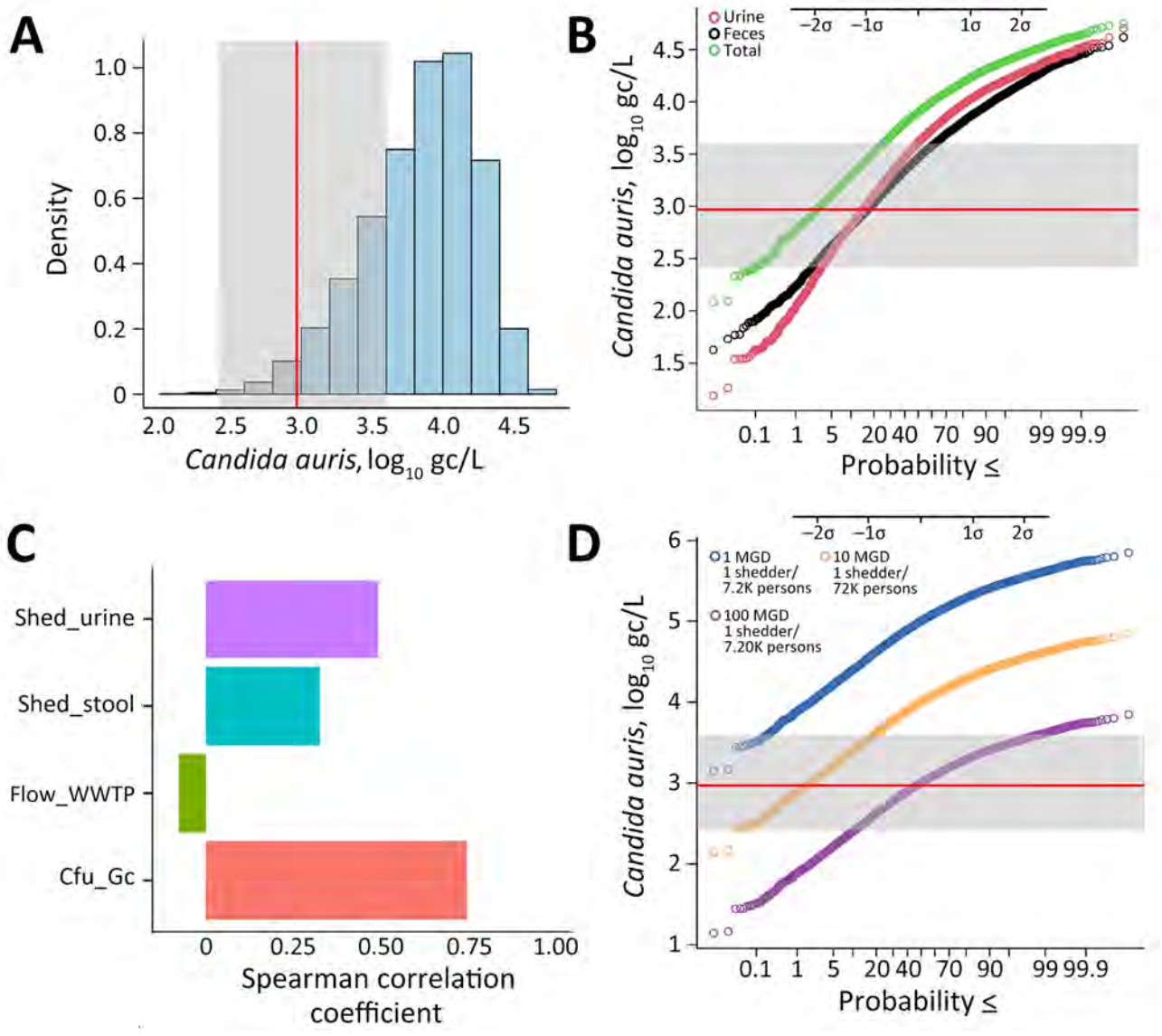

Figure 2. Monte Carlo simulation model forecasting *Candida auris* concentrations as a function of variable shedding levels in urine and feces, organism gene copy numbers, and WWTP flow rate (Table 2) as part of a study of *Candida auris* detection by wastewater surveillance, Utah, USA. A) Density plot of computed *C. auris* concentrations in wastewater resulting from 1 person shedding the organism in urine and feces. B) Probability plot showing the probability of detection at different organism concentrations. C) Sensitivity analysis, showing the correlation between individual parameters and their effect on predicted *C. auris* concentrations (i.e., the strength of the effect of each parameter on the model). D) Probability plot showing the effect of the magnitude of hypothetical flow rate (or sewershed size) on the likelihood of detecting the organism by quantitative PCR; infection prevalence metrics assume a St. George wastewater generation rate of 138 gpcd. In panels A, B, and D, the average limit of detection of the quantitative PCR is shown as a red line, and the minimum and maximum limits of detection observed in the study resulting from variation in sample-specific ESV are delineated by the gray area. Probabilities are less than or equal to the values indicated. ESV, equivalent sample volume; gc, gene copies; gcpd, gallons per capita per day; mgd, million gallons per day; WWTP, wastewater treatment plant.

The flow rate had a moderate negative correlation, indicating that an increased flow rate results in a decreased probability of detection in wastewater from 1 shedder. To better illustrate this effect, we generated probability plots for 3 hypothetical WWTP flow rates: 1, 10, and 100 mgd. Assuming the St. George per capita wastewater generation rate of 138 gpcd, those flow rates represent *C. auris* infection prevalences of 1 in 7,200 (flow rate 1 mgd), 1 in 72,000 (flow rate 10 mgd), and 1 in 720,000 (flow rate 100 mgd) persons. At the average limit of detection, the detection probability relative to a single shedder was almost 100% at a flow rate of 1 mgd, ≈97.5% at 10 mgd, and 50% at 100 mgd (Figure 2, panel D). Altogether, our modeled

and observed results support the hypothesis that use of qPCR-based wastewater surveillance for *C. auris* can achieve sensitivity on the order of 1 in 100,000.

Isolation of *C. auris* from the St. George Sewershed and Genetic Relatedness to Clinical Isolates

We complemented qPCR-based wastewater surveillance with culturing and subsequent whole-gene sequencing of recovered isolates. Initial attempts with the centrifugation-based method previously used for southern Nevada wastewater (*14*) were unsuccessful (Table 1). As such, we explored a filtration-based alternative that was observed to be superior to our original method across 2 split samples from Nevada (Appendix Figure 1). Using that improved method, we were able to recover 15 *C. auris* isolates from 2 samples consecutively collected on March 28, 2023, and April 4, 2023 (Table 1). All wastewater isolates belonged to clade III and segregated topologically into 2 individual subgroups distinctly separated by collection date (Figure 3). Isolates within the subgroup linked to the March 28 wastewater sample were highly related to the clinical isolate available for patient 2 (0–6 SNPs), who was transferred to St. George on March 23. The isolates within the subgroup linked to the April 4 sample displayed ≈12 SNP differences from the patient 2 isolate (Figure 3). Unfortunately, no clinical whole-genome sequencing (WGS) data were available for patient 3 because the patient's colonization status was not determined in Nevada and the positive clinical sample collected in Utah was not submitted to UPHL. Patient 1 was infected with a clade I strain, but we were unable to culture *C. auris* in any wastewater samples collected during the time of the patient's stay at SNF A or before March 28, 2023 (Table 1). As such, we were unable to study the contribution of clade I isolates to the overall *C. auris* signal in the St. George sewershed.

Discussion

The recent history of *C. auris* in the United States highlighted the challenges in controlling the pathogen after it becomes established in an area (*7*). Early detection strategies coupled with aggressive infection

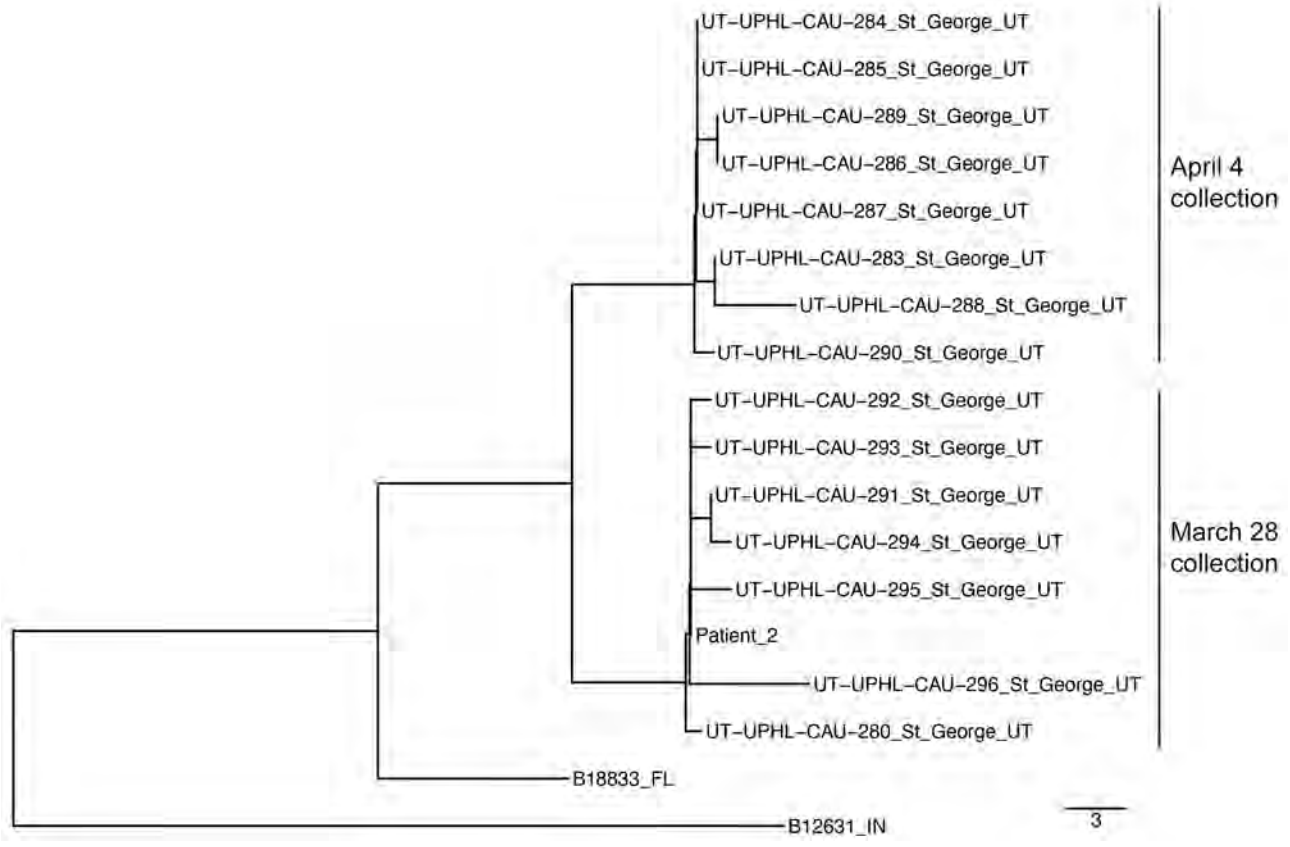

Figure 3. Neighbor-joining phylogenetic tree including clade III *Candida auris* isolates recovered from the St. George, Utah, USA, wastewater treatment plant on 2 collection dates (March 28 and April 4, 2023) and from a second patient. National Center for Biotechnology Information Sequence Read Archive accessions for all isolates are listed in the Appendix (https://wwwnc.cdc.gov/EID/article/30/10/24-0173-App1.pdf). Scale bar indicates single-nucleotide polymorphisms.

control measures could reduce its effect on healthcare facilities and the general population. In that respect, wastewater-based surveillance is a promising tool for detecting pathogens that are circulating in the population at very low prevalence and have not been overtly manifested at the clinical level (*12*).

The application of wastewater-based surveillance to the *C. auris* problem is in its infancy (*14*–*16*), so fundamental parameters that will guide its use have not yet been studied in detail. For example, levels of *C. auris* shedding in human excreta and body site densities during colonization have not yet been adequately characterized. *C. auris* effectively colonizes skin and nares (*26*,*31*) but is not typically recovered from the buccal mucosa (*31*,*32*). A regular nylon swab can usually recover 10^2–10^{10} CFU of *C. auris* from various skin sites (e.g., palms/fingertips, toe web, perianal skin, axilla, inguinal crease, neck) and nares (*31*). As such, it is conceivable that the organism could be released in great numbers into the sewershed via skin shedding during routine hygiene practices or even when laundering items that have been in contact with a colonized person. Because skin is the primary *C. auris* colonization site, clinical studies aimed at determining the actual bioburden released through hygiene practices (*33*) will be essential for assessing quantitative measurements in wastewater. *C. auris* is also commonly recovered from urine (*4*,*26*) of patients with candiduria (*34*), as well as from asymptomatic persons (*35*). *C. auris* is less frequently recovered from fecal samples but has been recovered via rectal swabbing (*26*,*32*,*36*). Of note, a correlation between gut colonization and urinary tract infections has been observed in cohorts of patients affected by *C. auris* (*36*).

As has been accomplished for wastewater-based surveillance of SARS-CoV-2, additional modeling and parameterization are needed to fully characterize relationships between incidence/prevalence and expected wastewater concentrations (*28*,*37*). Early attempts to establish those correlations for *C. auris* have been extremely challenging (*16*). Nevertheless, the qPCR data and the excreta-only model used in our study fit very well with the clinical course of patient 1 (the putative introduction event in St. George) and indicate that detecting 1 *C. auris* shedder to a community-scale wastewater system of moderate size is plausible (Figure 2). Although our study focused on early detection of pathogen introduction, future studies should consider monitoring wastewater *C. auris* loads after the population presumably returns to a zero-infection status.

Recovery of *C. auris* in culture has been instrumental in obtaining isolates for molecular epidemiology analyses by WGS (*14*). The incorporation of WGS into wastewater-based surveillance systems for *C. auris* should be universally adopted to understand the origin of introduction events as well as the evolving diversity of contributions to sewersheds. Motivated by the initial inability to recover *C. auris* isolates in St. George (Table 1), we worked at improving our original culture method by changing the sample concentration step from centrifugation to membrane filtration (Appendix Figure 1), an approach also recently used by Babler et al. (*16*). Yet, culture from wastewater samples remains a highly variable endeavor, possibly because of variable competition from other species of fungi or fluctuations in environmental factors within the sewer environment affecting the growth of *C. auris*, such as dissolved oxygen concentration (*38*,*39*). In addition, our broth enrichment approach remains unsuitable for isolating fluconazole-susceptible isolates (*14*).

WGS analysis indicated a close relationship between *C. auris* wastewater isolates and 1 isolate from patient 2 (Figure 3). When those wastewater samples were collected, both patients 2 and 3 were potentially contributing *C. auris* to the St. George WWTP (Figure 1, panel C). With the data available, we cannot discriminate whether the genetic diversity of the wastewater isolates collected on 2 separate dates encompasses shedding from patient 3 or other unidentified colonized persons. Moreover, mixed colonization consisting of clones separated by SNP distances greater than those displayed in Figure 3 is not unusual (*40*,*41*) and represents another layer of complexity in the interpretation of molecular epidemiology analyses for *C. auris* (*42*). However, incorporating WGS analyses into *C. auris* wastewater surveillance would still be invaluable for detecting contributions from strains belonging to different clades or displaying very large SNP distances. In addition, if *C. auris* strains can persist in sewer pipes as biofilm (a phenomenon not yet investigated for this organism) (*38*), WGS could potentially distinguish persistent signals from a new shedding event.

In conclusion, we used a holistic approach to *C. auris* wastewater-based surveillance that entailed using qPCR as the main testing method, as well as culture and WGS to better characterize the source of the molecular signals. After being proven effective, metagenomic approaches could potentially bypass the need for culture (*43*). We believe that our case study illustrates the potential of wastewater-based surveillance to be a sufficiently sensitive method for discovering *C. auris* transmission at early stages of introduction into a community.

Acknowledgments

We thank Andrew Gorzalski for sharing clinical isolates sequences. We are grateful for the support and contributions of many groups: the Healthcare-associated Infections and Antimicrobial Resistance team at Utah DHHS and the Antimicrobial Resistance Laboratory Network, NGS, and wastewater testing teams at UPHL.

J.C. was supported by an Association of Public Health Laboratories Fellowship in Antibiotic Resistance (cooperative agreement no. NU60OE000104, funded by the Centers for Disease Control and Prevention [CDC] through the Association of Public Health Laboratories). Southern Nevada wastewater sample collection was supported by CDC grant NH75OT000057-01-00.

About the Author

Mr. Chavez is an ORISE (Oak Ridge Institute for Science and Education) Fellow at CDC. His research expertise encompasses environmental microbiology, wastewater surveillance, and mycotic diseases. Dr. Crank is a research microbiologist at the Southern Nevada Water Authority. Her research expertise encompasses environmental health engineering, environmental microbiology, and wastewater surveillance.

References

1. Lone SA, Ahmad A. *Candida auris*—the growing menace to global health. Mycoses. 2019;62:620–37. https://doi.org/10.1111/myc.12904
2. Welsh RM, Bentz ML, Shams A, Houston H, Lyons A, Rose LJ, et al. Survival, persistence, and isolation of the emerging multidrug-resistant pathogenic yeast *Candida auris* on a plastic health care surface. J Clin Microbiol. 2017;55:2996–3005. https://doi.org/10.1128/JCM.00921-17
3. Ku TSN, Walraven CJ, Lee SA. *Candida auris*: disinfectants and implications for infection control. Front Microbiol. 2018;9:726. https://doi.org/10.3389/fmicb.2018.00726
4. Lockhart SR, Etienne KA, Vallabhaneni S, Farooqi J, Chowdhary A, Govender NP, et al. Simultaneous emergence of multidrug-resistant *Candida auris* on 3 continents confirmed by whole-genome sequencing and epidemiological analyses. Clin Infect Dis. 2017;64:134–40. https://doi.org/10.1093/cid/ciw691
5. Chow NA, de Groot T, Badali H, Abastabar M, Chiller TM, Meis JF. Potential fifth clade of *Candida auris*, Iran, 2018. Emerg Infect Dis. 2019;25:1780–1. https://doi.org/10.3201/eid2509.190686
6. Vallabhaneni S, Kallen A, Tsay S, Chow N, Welsh R, Kerins J, et al.; MSD. Investigation of the first seven reported cases of *Candida auris*, a globally emerging invasive, multidrug-resistant fungus—United States, May 2013–August 2016. MMWR Morb Mortal Wkly Rep. 2016;65:1234–7. https://doi.org/10.15585/mmwr.mm6544e1
7. Lyman M, Forsberg K, Sexton DJ, Chow NA, Lockhart SR, Jackson BR, et al. Worsening spread of *Candida auris* in the United States, 2019 to 2021. Ann Intern Med. 2023;176:489–95. https://doi.org/10.7326/M22-3469
8. Thoma R, Seneghini M, Seiffert SN, Vuichard Gysin D, Scanferla G, Haller S, et al. The challenge of preventing and containing outbreaks of multidrug-resistant organisms and *Candida auris* during the coronavirus disease 2019 pandemic: report of a carbapenem-resistant *Acinetobacter baumannii* outbreak and a systematic review of the literature. Antimicrob Resist Infect Control. 2022;11:12. https://doi.org/10.1186/s13756-022-01052-8
9. Saleem Z, Godman B, Hassali MA, Hashmi FK, Azhar F, Rehman IU. Point prevalence surveys of health-care-associated infections: a systematic review. Pathog Glob Health. 2019;113:191–205. https://doi.org/10.1080/20477724.2019.1632070
10. Wang TZ, White KN, Scarr JV, Simon MS, Calfee DP. Preparing your healthcare facility for the new fungus among us: an infection preventionist's guide to *Candida auris*. Am J Infect Control. 2020;48:825–7. https://doi.org/10.1016/j.ajic.2020.01.021
11. Vo V, Tillett RL, Papp K, Shen S, Gu R, Gorzalski A, et al. Use of wastewater surveillance for early detection of Alpha and Epsilon SARS-CoV-2 variants of concern and estimation of overall COVID-19 infection burden. Sci Total Environ. 2022;835:155410. https://doi.org/10.1016/j.scitotenv.2022.155410
12. Gupta P, Liao S, Ezekiel M, Novak N, Rossi A, LaCross N, et al. Wastewater genomic surveillance captures early detection of omicron in Utah. Microbiol Spectr. 2023;11:e0039123. https://doi.org/10.1128/spectrum.00391-23
13. Ryerson AB, Lang D, Alazawi MA, Neyra M, Hill DT, St George K, et al.; 2022 U.S. Poliovirus Response Team. Wastewater testing and detection of poliovirus type 2 genetically linked to virus isolated from a paralytic polio case—New York, March 9–October 11, 2022. MMWR Morb Mortal Wkly Rep. 2022;71:1418–24. https://doi.org/10.15585/mmwr.mm7144e2
14. Rossi A, Chavez J, Iverson T, Hergert J, Oakeson K, LaCross N, et al. *Candida auris* discovery through community wastewater surveillance during healthcare outbreak, Nevada, USA, 2022. Emerg Infect Dis. 2023;29:422–5. https://doi.org/10.3201/eid2902.221523
15. Barber C, Crank K, Papp K, Innes GK, Schmitz BW, Chavez J, et al. Community-scale wastewater surveillance of *Candida auris* during an ongoing outbreak in southern Nevada. Environ Sci Technol. 2023;57:1755–63. https://doi.org/10.1021/acs.est.2c07763
16. Babler K, Sharkey M, Arenas S, Amirali A, Beaver C, Comerford S, et al. Detection of the clinically persistent, pathogenic yeast spp. *Candida auris* from hospital and municipal wastewater in Miami-Dade County, Florida. Sci Total Environ. 2023;898:165459. https://doi.org/10.1016/j.scitotenv.2023.165459
17. Chini CMS, Stillwell AS. The state of U.S. urban water: data and the energy-water nexus. Water Resour Res. 2018;54:1796–811. https://doi.org/10.1002/2017WR022265
18. Bagal UR, Phan J, Welsh RM, Misas E, Wagner D, Gade L, et al. MycoSNP: A portable workflow for performing whole-genome sequencing analysis of *Candida auris*. Methods Mol Biol. 2022;2517:215–28. https://doi.org/10.1007/978-1-0716-2417-3_17
19. Torres SR, Pichowicz A, Torres-Velez F, Song R, Singh N, Lasek-Nesselquist E, et al. Impact of *Candida auris* infection in a neutropenic murine model. Antimicrob Agents Chemother. 2020;64:e01625-19. https://doi.org/10.1128/AAC.01625-19
20. Rose C, Parker A, Jefferson B, Cartmell E. The characterization of feces and urine: a review of the literature to inform advanced treatment technology. Crit Rev Environ

Sci Technol. 2015;45:1827–79. https://doi.org/10.1080/10643389.2014.1000761
21. Penn R, Ward BJ, Strande L, Maurer M. Review of synthetic human faeces and faecal sludge for sanitation and wastewater research. Water Res. 2018;132:222–40. https://doi.org/10.1016/j.watres.2017.12.063
22. Croxatto A, Dijkstra K, Prod'hom G, Greub G. Comparison of inoculation with the InoqulA and WASP automated systems with manual inoculation. J Clin Microbiol. 2015;53:2298–307. https://doi.org/10.1128/JCM.03076-14
23. Rauch W, Brockmann D, Peters I, Larsen TA, Gujer W. Combining urine separation with waste design: an analysis using a stochastic model for urine production. Water Res. 2003;37:681–9. https://doi.org/10.1016/S0043-1354(02)00364-0
24. Jones T, Federspiel NA, Chibana H, Dungan J, Kalman S, Magee BB, et al. The diploid genome sequence of *Candida albicans*. Proc Natl Acad Sci U S A. 2004;101:7329–34. https://doi.org/10.1073/pnas.0401648101
25. Whipple A, Jackson J, Ridderhoff J, Nakashima AK. Piloting electronic case reporting for improved surveillance of sexually transmitted diseases in Utah. Online J Public Health Inform. 2019;11:e7. https://doi.org/10.5210/ojphi.v11i2.9733
26. Zhu Y, O'Brien B, Leach L, Clarke A, Bates M, Adams E, et al. Laboratory analysis of an outbreak of *Candida auris* in New York from 2016 to 2018: impact and lessons learned. J Clin Microbiol. 2020;58:e01503-19. https://doi.org/10.1128/JCM.01503-19
27. Leach L, Russell A, Zhu Y, Chaturvedi S, Chaturvedi V. A rapid and automated sample-to-result *Candida auris* real-time PCR assay for high-throughput testing of surveillance samples with the BD Max Open System. J Clin Microbiol. 2019;57:e00630-19. https://doi.org/10.1128/JCM.00630-19
28. Crank K, Chen W, Bivins A, Lowry S, Bibby K. Contribution of SARS-CoV-2 RNA shedding routes to RNA loads in wastewater. Sci Total Environ. 2022;806:150376. https://doi.org/10.1016/j.scitotenv.2021.150376
29. Altschul SF, Gish W, Miller W, Myers EW, Lipman DJ. Basic Local Alignment Search Tool. J Mol Biol. 1990;215:403–10. https://doi.org/10.1016/S0022-2836(05)80360-2
30. Leach L, Zhu Y, Chaturvedi S. Development and validation of a real-time PCR assay for rapid detection of *Candida auris* from surveillance samples. J Clin Microbiol. 2018;56:e01223-17. https://doi.org/10.1128/JCM.01223-17
31. Proctor DM, Dangana T, Sexton DJ, Fukuda C, Yelin RD, Stanley M, et al.; NISC Comparative Sequencing Program. Integrated genomic, epidemiologic investigation of *Candida auris* skin colonization in a skilled nursing facility. Nat Med. 2021;27:1401–9. https://doi.org/10.1038/s41591-021-01383-w
32. Du H, Bing J, Hu T, Ennis CL, Nobile CJ, Huang G. *Candida auris*: epidemiology, biology, antifungal resistance, and virulence. PLoS Pathog. 2020;16:e1008921. https://doi.org/10.1371/journal.ppat.1008921
33. Plano LR, Garza AC, Shibata T, Elmir SM, Kish J, Sinigalliano CD, et al. Shedding of *Staphylococcus aureus* and methicillin-resistant *Staphylococcus aureus* from adult and pediatric bathers in marine waters. BMC Microbiol. 2011;11:5. https://doi.org/10.1186/1471-2180-11-5
34. Griffith N, Danziger L. *Candida auris* urinary tract infections and possible treatment. Antibiotics (Basel). 2020;9:898. https://doi.org/10.3390/antibiotics9120898
35. Sayeed MA, Farooqi J, Jabeen K, Awan S, Mahmood SF. Clinical spectrum and factors impacting outcome of *Candida auris*: a single center study from Pakistan. BMC Infect Dis. 2019;19:384. https://doi.org/10.1186/s12879-019-3999-y
36. Piatti G, Sartini M, Cusato C, Schito AM. Colonization by *Candida auris* in critically ill patients: role of cutaneous and rectal localization during an outbreak. J Hosp Infect. 2022;120:85–9. https://doi.org/10.1016/j.jhin.2021.11.004
37. Gerrity D, Papp K, Stoker M, Sims A, Frehner W. Early-pandemic wastewater surveillance of SARS-CoV-2 in southern Nevada: methodology, occurrence, and incidence/prevalence considerations. Water Res X. 2021;10:100086. https://doi.org/10.1016/j.wroa.2020.100086
38. McLellan SL, Roguet A. The unexpected habitat in sewer pipes for the propagation of microbial communities and their imprint on urban waters. Curr Opin Biotechnol. 2019;57:34–41. https://doi.org/10.1016/j.copbio.2018.12.010
39. Day AM, McNiff MM, da Silva Dantas A, Gow NAR, Quinn J. Hog1 regulates stress tolerance and virulence in the emerging fungal pathogen *Candida auris*. MSphere. 2018;3:e00506-18. https://doi.org/10.1128/mSphere.00506-18
40. Eyre DW, Sheppard AE, Madder H, Moir I, Moroney R, Quan TP, et al. A *Candida auris* outbreak and its control in an intensive care setting. N Engl J Med. 2018;379:1322–31. https://doi.org/10.1056/NEJMoa1714373
41. Roberts SC, Zembower TR, Ozer EA, Qi C. Genetic evaluation of nosocomial *Candida auris* transmission. J Clin Microbiol. 2021;59:e02252-20. https://doi.org/10.1128/JCM.02252-20
42. Chow NA, Gade L, Tsay SV, Forsberg K, Greenko JA, Southwick KL, et al.; US Candida auris Investigation Team. Multiple introductions and subsequent transmission of multidrug-resistant *Candida auris* in the USA: a molecular epidemiological survey. Lancet Infect Dis. 2018;18:1377–84. https://doi.org/10.1016/S1473-3099(18)30597-8
43. Huang X, Welsh RM, Deming C, Proctor DM, Thomas PJ, Gussin GM, et al.; NISC Comparative Sequencing Program. Skin metagenomic sequence analysis of early *Candida auris* outbreaks in U.S. nursing homes. MSphere. 2021;6:e0028721. https://doi.org/10.1128/mSphere.00287-21

Address for correspondence: Alessandro Rossi, Utah Public Health Laboratory, 4431 S 2700 West, Taylorsville, UT 84129, USA; email: arossi@utah.gov

Temporal Characterization of Prion Shedding in Secreta of White-Tailed Deer in Longitudinal Study of Chronic Wasting Disease, United States

Nathaniel D. Denkers, Erin E. McNulty, Caitlyn N. Kraft, Amy V. Nalls, Joseph A. Westrich, Edward A. Hoover, Candace K. Mathiason

Chronic wasting disease (CWD) affects cervids in North America, Asia, and Scandinavia. CWD is unique in its efficient spread, partially because of contact with infectious prions shed in secreta. To assess temporal profiles of CWD prion shedding, we collected saliva, urine, and feces from white-tailed deer for 66 months after exposure to low oral doses of CWD-positive brain tissue or saliva. We analyzed prion seeding activity by using modified amyloid amplification assays incorporating iron oxide bead extraction, which improved CWD detection and reduced false positives. CWD prions were detected in feces, urine, and saliva as early as 6 months postinfection. More frequent and consistent shedding was observed in deer homozygous for glycine at prion protein gene codon 96 than in deer expressing alternate genotypes. Our findings demonstrate that improved amplification methods can be used to identify early antemortem CWD prion shedding, which might aid in disease surveillance of cervids.

Chronic wasting disease (CWD) has been identified in North America, Asia, and Scandinavia (*1*–*4*) and is the only known prion disease in wildlife. CWD is often considered the most infectious of all prion diseases, but how CWD spreads so efficiently remains unclear. It is generally accepted that facile CWD transmission results from robust prion replication in target tissues, leading to shedding of infectious prions into saliva, urine, and feces (i.e., secreta). Cervids are likely exposed to infectious prions via direct animal-to-animal contact or indirect contact with the agent shed into the environment.

Author affiliation: Colorado State University, Fort Collins, Colorado, USA

DOI: https://doi.org/10.3201/eid3010.240159

Landscapes previously housing CWD-infected cervids are contaminated with sufficient infectious prions to initiate subsequent infections (*5*,*6*). Fomite-only exposure of uninfected deer to buckets and bedding from suites housing CWD-positive animals resulted in CWD infections in disease-naive deer within 19 months after exposure (*7*). Studies in white-tailed deer (WTD; *Odocoileus virginianus*) also revealed that large oral doses of saliva, urine, or feces contained adequate concentrations of the CWD agent to initiate infections (*8*,*9*). Additional studies in WTD established a minimum oral CWD infectious dose equivalent to 100–300 ng CWD-positive brain tissue (*10*). Yet, equivalent saliva doses (16.5–30 mL) seem large compared with a dose expected in nature. Nevertheless, taken together, those studies indicate doses of CWD prions in saliva and exposure to shed prions in the environment are sufficient for CWD transmission.

The temporal shedding profile of CWD prions in secreta remains poorly understood. Little is known about the onset and duration of the complete prion shedding profile during the asymptomatic phase of CWD infection. It is suspected that prion levels in shed secreta are low, and inhibitors or nonspecific substrate activators in secreta can constrain the use of sensitive in vitro amplification assays, such as serial protein misfolding amplification (sPMCA) and real-time quaking-induced conversion (RT-QuIC) (*11*–*14*). To enhance detection capabilities of those assays, sodium phosphotungstic acid or iron oxide bead capture techniques have been used to concentrate prions and reduce or bypass interfering factors (*15*–*26*). Thus, continued in vitro assay optimization has improved CWD antemortem detection.

In addition to the route and dose by which CWD prions are transmitted, the sequence of the prion protein gene *PRNP* is another factor affecting disease pathogenesis. The prion protein is highly conserved between cervids (*27*), although single-nucleotide polymorphisms within the gene sequence can lead to reduced susceptibility (*28*), slower disease progression (*29*,*30*), and prolonged survival (*31*,*32*), all of which might affect prion shedding (*18*,*33*). Specific codon polymorphisms known to influence cervid CWD susceptibility are codons 132 in elk (M→L) (*28*), 225 in mule deer (S→F) (*31*), and 96 in WTD (G→S) (*34*). As additional polymorphisms are identified (*35*), the role they play in CWD susceptibility, pathogenesis, and shedding will need to be explored.

We used iron oxide bead (IOB) capture in combination with sPMCA and RT-QuIC to profile longitudinal (66 months) prion shedding in urine, saliva, and feces collected from WTD exposed to low oral doses of CWD prions. Because dose and *PRNP* genotype affect initial detection of infection and disease onset, we correlated those factors with prion shedding consistency and duration. Our goal was to provide a more complete understanding of prion shedding onset and duration that contributes to CWD pathogenesis and transmission and aid in early antemortem detection by using minimally invasive methods.

Methods

Animals

We obtained CWD-free WTD fawns from the University of Georgia Warnell School of Forestry and Natural Resources (Athens, GA, USA). At 4 months of age, the fawns were transported to the indoor CWD research facility at Colorado State University (Fort Collins, CO, USA), where we conducted studies under strict guidelines according to protocols approved by the Institutional Animal Care and Use Committee (protocol nos. 18-8396A and 1242). We housed cohorts of deer in separate suites. We housed mock-infected control deer in different suites within the same facility; they served as sentinels to ensure that no unexpected pathogen exposures occurred during the long course of CWD prion infections.

Inoculations

We exposed 12 WTD to low oral doses of CWD-positive brain tissue (n = 8) or saliva (n = 4); seeding activities were equivalent to 1 mg (n = 4) or 300 ng (n = 4) CWD-positive brain tissue or 300 ng (n = 4) CWD-positive saliva. Deer number, inoculum source, dose, regimen, and genotypes were described previously (*10*,*36*). Because access to WTD is limited and to conserve animals, 2 sham-inoculated deer served as negative controls. Each sham-inoculated deer received a total of 300 ng CWD-negative brain material and 300 ng CWD-negative saliva that had been preincubated with 600 mg of montmorillonite clay. We administered the sham inocula as 3 doses of 200 ng CWD-negative material (100 ng brain + 100 ng saliva + 200 mg montmorillonite clay) 1 time/week for 3 consecutive weeks.

PRNP Genotype

We determined the *PRNP* genotype of the deer at codon 96 before beginning the study; 7 deer expressed 96GG and 5 expressed 96GS polymorphisms. The negative control deer were both 96GG. One 96GG deer also had a rare polymorphism at codon 103 (103NT). In an unrelated study (N.D. Denkers, unpub. data), we identified another deer expressing codon 103NT; both deer had disease courses similar to deer expressing the 96GS polymorphism. Because a previous low-dose study demonstrated no observable clinical differences (*10*), we compared animals with wild-type codon 96GG genotypes (cohort 1; n = 6) with deer expressing *PRNP* gene polymorphisms 96GS or 103NT that delayed CWD infection (cohort 2; n = 6). Cohort 1 consisted of 5 male and 1 female deer; cohort 2 had 3 male and 3 female deer.

Sample Collections

We performed tonsil and recto-anal mucosa-associated lymphoid tissue biopsies at 3 months postinoculation (mpi) and analyzed the tissue for amyloid seeding activity by using RT-QuIC and for CWD prion protein (PrP^{cwd}) deposition by using immunohistochemistry. We considered deer to be infected with CWD prions when 2 consecutive tonsil biopsies were RT-QuIC positive (*36*).

We collected saliva, urine, and feces in conjunction with lymphoid biopsy tissue (Table 1). We collected urine from male deer for 21 months by free catch, then manually by bladder expression. We catheterized female deer and obtained urine via syringe aspiration. We collected saliva by syringe aspiration of the buccal pouch. We collected feces directly from the rectum and placed it into specimen cups. We collected all samples by using clean single-use syringes or containers, which we then aliquoted and stored at –80°C until analysis.

Sample Preparation and CWD Status Analysis

We subjected fecal samples to IOB capture before 4 rounds of sPMCA. We used RT-QuIC as a readout for the sPMCA product; that procedure is hereafter

Table 1. Summary of collected tissues and secreta in longitudinal study of temporal characterization of prion shedding in white-tailed deer with chronic wasting disease, United States*

	96GG genotype						96GS/103NT genotypes					
mpi	No. deer	Tonsil	RAMALT	Urine	Saliva	Feces	No. deer	Tonsil	RAMALT	Urine	Saliva	Feces
6	6	1/6	0/6	ND	0/6	1/5	6	0/6	0/6	ND	0/6	1/2
9	6	3/6	2/6	0/1	2/6	1/4	6	0/6	1/6	0/3	0/6	0/3
12	6	3/6	3/6	0/3	2/6	2/5	6	0/6	1/6	0/6	0/6	0/5
15	6	4/6	4/6	0/1	1/6	4/6	6	1/6	0/6	0/4	0/6	0/4
18	6	6/6	5/6	1/2	1/6	4/5	6	1/6	1/6	0/3	0/6	0/5
21	6	6/6	6/6	1/1	2/5	5/5	6	3/6	1/6	0/5	1/6	0/6
24	5	5/5	5/5	3/4	2/4	4/5	6	5/5	4/6	0/5	1/6	1/4
27	3	3/3	3/3	1/1	1/3	2/3	6	6/6	5/6	1/5	1/6	1/4
29	2	2/2	2/2	1/1	2/2	1/1	6	6/6	6/6	0/5	3/6	1/4
32	1	1/1	1/1	0/0	1/1	1/1	3	3/3	3/3	0/2	0/3	0/2
35	1	1/1	1/1	1/1	1/1	1/1	3	3/3	3/3	0/2	0/3	1/2
39	1	1/1	1/1	1/1	0/1	1/1	3	3/3	3/3	0/3	0/3	2/3
42	0	0	0	0	0	0	2	2/2	2/2	0/2	0/2	1/2
45	0	0	0	0	0	0	2	2/2	2/2	0/2	1/2	1/2
48	0	0	0	0	0	0	2	2/2	2/2	0/2	1/2	1/2
66	0	0	0	0	0	0	1	1/1	1/1	0/1	0/1	0/1

*Values are number of positive samples over total number of samples collected at each timepoint. Tissues and secreta from deer with wild-type genotype 96GG or alternative genotypes 96GS or 103NT of the prion protein gene were compared. mpi, months postinoculation; ND, not done; RAMALT, recto-anal mucosa-associated lymphoid tissue.

designated as IPQ. In brief, we prepared fecal samples as 10% wt/vol homogenates in 1× phosphate-buffered saline (PBS; 20 mmol/L $NaPO_4$, 150 mmol/L NaCl; Sigma-Aldrich, https://www.sigmaaldrich.com). We diluted the homogenates 1:10 to a final volume of 1 mL (100 µL sample:900 µL 1× PBS) and added 2 µL IOB suspension (Bangs Laboratories, Inc., https://www.bangslabs.com) directly to each sample. We incubated the tubes containing the feces/bead mixture by using end-over-end rotation for 30 minutes at room temperature. We transferred each tube to a magnetic separator for 5 minutes, removed the supernatants, and resuspended the demagnetized beads in 10 µL 1× PBS. We added resuspended beads to 90 µL of Tg(CerPrP-E226)5037$^{+/-}$ normal brain homogenate (*37*) and performed 4 rounds of sPMCA. After each round, we froze the sPMCA sample at –20°C until analysis. We prepared 1:100 dilutions of sPMCA samples from rounds 2–4 in 0.1% sodium dodecyl sulfate (SDS; Sigma-Aldrich) and assayed them in quadruplicate (2 µL/well) by using RT-QuIC in ≥2 plates/sample to achieve a minimum of 8 replicates/sample. We used this method to monitor sequential amplification in each round. We only analyzed round 4 products to determine statistical significance for amyloid seeding activity.

We processed individual saliva and urine samples by using IOB capture and subsequent RT-QuIC, hereafter abbreviated as IQ (*23*). In brief, we added 2 µL IOB suspension to 1 mL of saliva diluted 1:20 in 1× PBS (50 µL saliva:950 µL PBS) or to 1 mL undiluted urine. We placed samples on an end-over-end rotator for 30 minutes at room temperature, transferred the tubes to a magnetic separator for 5 minutes, removed supernatants, and resuspended the demagnetized beads in 10 µL of 0.1% SDS. We added 2 µL of each bead/sample suspension into Greiner Bio-One black optical-bottom microtiter plate wells (VWR, https://www.vwr.com) containing 96 µL RT-QuIC master mix. We assayed a total of 8 replicates/sample in ≥2 microtiter plates.

sPMCA

We performed sPMCA as previously described (*13*). In brief, we combined 90 µL of 10% (wt/vol) Tg(CerPrP-E226)5037$^{+/-}$ normal brain homogenate in 1× PBS containing 1% Triton X-100 (*37*) with 10 µL of each IOB-captured sample in 0.2 mL PCR tubes (ThermoFisher Scientific, https://www.thermofisher.com) containing 2.38 mm and 1.59 mm polytetrafluoroethylene beads (McMaster-Carr, https://www.mcmaster.com). We exposed round 1 sPMCA samples to 30 second pulse sonication followed by 29.5 minutes of rest (1 cycle) for 72 hours (144 cycles total). For rounds 2–4, we added 30 µL of sPMCA product from the previous round to 60 µL of 10% normal brain homogenate and exposed those samples to 24 hours (48 cycles) of the same pulse sonication conditions used for round 1.

RT-QuIC

We produced, purified, and refolded truncated Syrian hamster recombinant prion protein (rPrP; codons 90–231) as previously described with minor modifications (*15*,*38*,*39*). In brief, we expressed rPrP in *Escherichia coli* BL21-Star cells, harvested inclusion bodies, and solubilized the protein before binding to Ni-agarose resin (GE Healthcare, https://www.gehealthcare.com).

We refolded, eluted, and dialyzed the rPRP before aliquoting and storing at 4°C until use.

For RT-QuIC reactions, we loaded each well of a 96-well plate with 96 μL substrate master mix (0.10 mg/mL rPrP, 10 μmol/L thioflavin T [Sigma], 320 mmol/L NaCl [Sigma], 1 mmol/L EDTA [Sigma], and 1× PBS). We diluted each sample in 0.1% SDS and then added 2 μL of the sample to each well. We performed RT-QuIC reactions in a FLUOstar Omega microplate reader (BMG Labtech, https://www.bmglabtech.com) programmed to alternate between 1 minute shaking (double-orbital program at 700 rpm) and 1 minute rest cycles. We measured thioflavin T fluorescence every 15 minutes at 450-nm excitation and 480-nm emission wavelengths and used a fluorescence gain of 1,700. We conducted RT-QuIC experiments at 42°C for 62.5 hours for all IQ studies and 36 hours for all IPQ studies. We displayed RT-QuIC data as 1/lag phase; we defined lag phase as the time (hours) when each replicate fluorescence reached 5 SD above the average baseline fluorescence. We considered samples to be positive if total reaction rate–positive replicates were significantly different ($p<0.05$) compared with total reaction rate replicates from negative controls by using Mann-Whitney U tests.

Immunohistochemistry

We confirmed CWD status by using immunohistochemical detection of PrP^{CWD} deposition in tonsil and recto-anal mucosa-associated lymphoid tissue biopsy samples as previously described (*40*). In brief, we treated rehydrated 5 μm tissue sections with 88% formic acid, then citrate buffer for heat-induced epitope retrieval, and blocked with 3% hydrogen peroxide in methanol followed by TNB buffer (0.5% blocking powder; Perkin Elmer, https://www.perkinelmer.com). We incubated slides overnight with monoclonal antibody BAR-224 (1 mg/mL; Cayman Chemical, https://www.caymanchem.com) diluted 1:750 in TNB buffer, followed by Dako Envision+ System horseradish peroxidase–labeled secondary antibody (Agilent, https://www.agilent.com) and 3-amino-9-ethylcarbazole substrate (Abcam, https://www.abcam.com) for visualization. We tested negative control tissues simultaneously in each experiment.

Results

We report temporal shedding profiles in secreta collected from WTD exposed orally to CWD prion concentrations that might more closely resemble those experienced in nature (*10*). We correlated the shedding profiles with *PRNP* polymorphisms known to modulate CWD infection and disease progression (*34*,*41*).

Prion Extraction Approach for Feces, Saliva, and Urine

Amplification assays continue to be modified to overcome assay inhibitors or spurious constituents in secreta (*18*,*19*,*21*,*22*). We found that enriching for prions in fecal samples by incorporating IOB capture or phosphotungstic acid precipitation alone often resulted in high nonspecific seeding background in known CWD-negative controls (Figure 1, panel A). To eliminate false-positive backgrounds, fecal samples underwent dilution and IOB capture followed by 4 rounds of sPMCA. The sPMCA products were read out by using RT-QuIC rather than Western blot analysis, thus building upon previous in vitro amplification assay modifications (*13*,*24*). The combination of sPMCA and RT-QuIC readout eliminated false positives in fecal samples and led to enhanced prion seeding activity detection in feces, indicated by higher reaction rates (Figure 1, panel B).

We assayed prion seeding activity in urine and saliva by using IQ and detected positive seeding activity in infected deer compared with negative controls (Figure 2, panel A). Because enhanced detection sensitivity was observed in feces by incorporating IPQ, we used IPQ to measure seeding activity in urine and saliva samples. IQ-positive urine and saliva samples were strongly amplified by using IPQ (Figure 2, panel B). In a separate subset of urine and saliva longitudinal samples, IPQ identified only 1 additional positive saliva sample; the remaining sample results were concordant with IQ results. IPQ did not appreciably increase sensitivity and sPMCA adds 7 days to the analysis protocol. Therefore, we completed analysis of all urine and saliva samples by using IQ.

Temporal Detection of CWD Shedding in Feces

We observed CWD prion shedding in feces collected from all 6 deer expressing the 96GG genotype. The earliest detection was at 6 mpi, coinciding with the first positive tonsil biopsy (Table 1; Figure 3). Detectable shedding occurred in all deer within 6 months of the initial RT-QuIC–positive tonsil biopsy (Figure 3). Seeding activity was consistently detected (≥4 consecutive positive timepoints) in 4 (66%) of 6 deer and infrequently detected (≤3 consecutive positive timepoints) in 2 (33%) of 6 deer. For deer with alternate polymorphisms (96GS or 103NT), ≥1 positive fecal result was recorded in 4 (66%) of 6 deer during 9–15 months after the first RT-QuIC–positive tonsil biopsy (Table 1; Figure 4). In 1 (17%) of 6 deer, seeding activity was detected in 3 consecutive fecal samples.

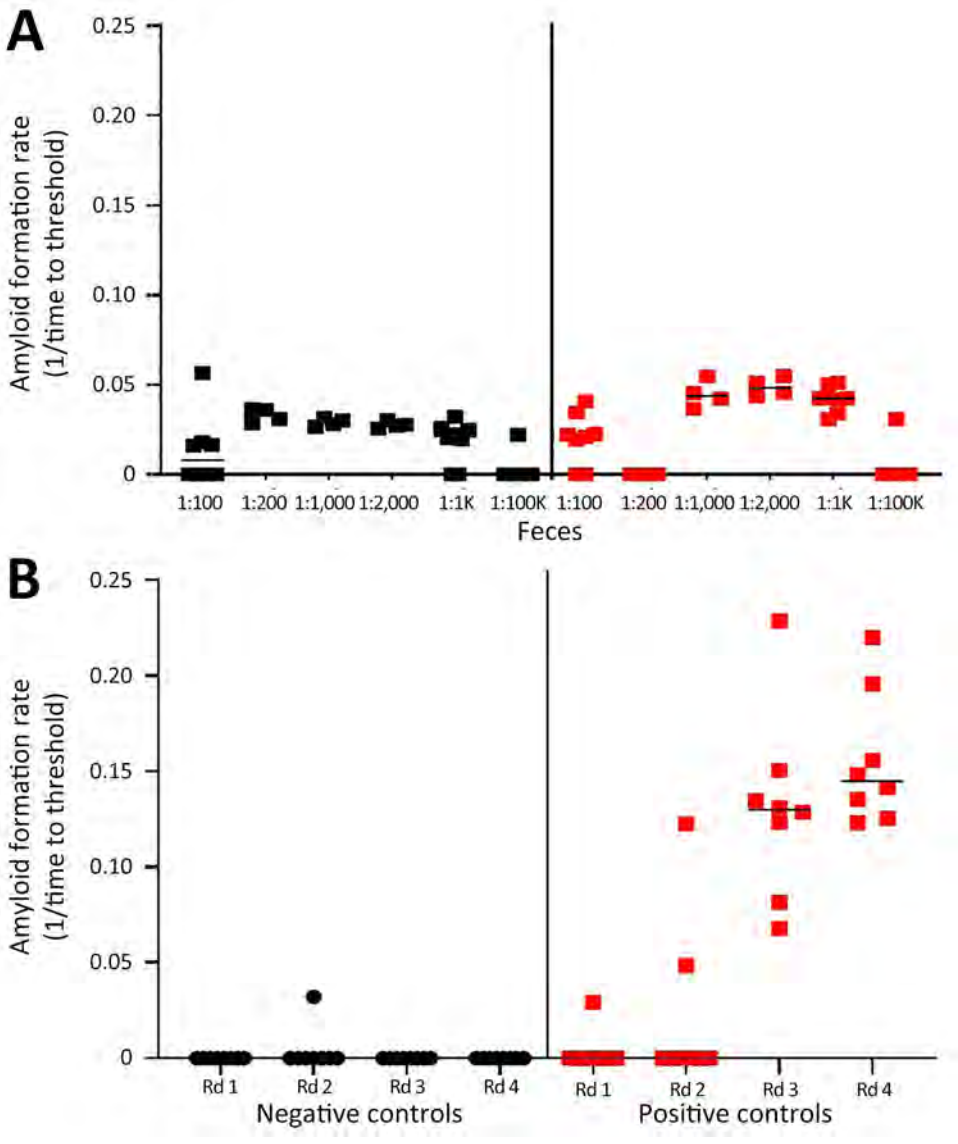

Figure 1. Amyloid formation rates in fecal samples from white-tailed deer with chronic wasting disease in longitudinal study of temporal characterization of prion shedding in secreta, United States. A) Amyloid formation rates measured by using iron oxide bead capture and subsequent real-time quaking-induced conversion. Rates were measured for serial dilutions of fecal samples. B) Amyloid formation rates measured by using iron oxide bead capture, 4 rounds of serial protein misfolding amplification, and subsequent real-time quaking-induced conversion. Rates were measured for 1:100 dilutions of fecal samples from each round of amplification. Black indicates prion-negative feces; red indicates prion-positive feces. Horizontal lines in each grouping indicate median values. Rd, round.

Overall, prion shedding was detected in 27 (64%) of 42 fecal samples from the 96GG cohort (Table 2) and 10 (19%) of 52 fecal samples collected from the 96GS/103NT cohort. All 21 fecal samples from sham-inoculated control deer remained negative. Thus, CWD shedding in feces was more frequently detected by IPQ in deer expressing the 96GG genotype than in those expressing alternate polymorphisms (96GS or 103NT).

Temporal Detection of CWD Shedding in Urine

CWD prion shedding was observed in urine samples collected from 1 (50%) of 2 deer expressing the 96GG genotype at 18 mpi, 9 months after the first RT-QuIC–positive tonsil biopsy (Table 1; Figure 3). Shedding persisted in 3 (50%) of 6 deer from 18 months until deer were euthanized; 2 (33%) of 6 were positive only at the terminal sample collection. One (17%) of 6 deer had CWD prion–negative urine throughout disease course. Among deer in the 96GS/103NT cohort, CWD prion seeding activity was detected in urine from only 1 (17%) of 6 deer at 27 mpi, coinciding with the first RT-QuIC–positive tonsil biopsy (Table 1; Figure 4).

In total, CWD prion shedding was detected in 9 (56%) of 16 urine samples collected from deer in the 96GG cohort and in 1 (2%) of 50 urine samples collected from deer in the 96GS/103NT cohort (Table 2). All 28 urine samples collected from sham-inoculated control deer remained negative. We show that CWD-infected deer expressing the 96GG genotype shed prions in their urine during later disease stages and did so more frequently and consistently than deer expressing alternate polymorphisms.

Temporal Detection of CWD Shedding in Saliva

CWD prion shedding occurred in saliva as early as 9 mpi in 2 (33%) of 6 deer expressing the 96GG genotype, coinciding with the first RT-QuIC–positive tonsil biopsy (Table 1; Figure 3). Intermittent shedding occurred throughout the disease course in 5 (83%) of 6 deer during 0–6 months after the first positive tonsil biopsy. In the 96GS/103NT cohort, prion shedding was detected in 3 (50%) of 6 deer starting at 21 mpi, ranging from 3 to 9 months after the first positive tonsil biopsy. Prion detection was infrequent in saliva throughout the disease course (Table 1; Figure 4).

Seeding activity was detected in 15 (32%) of 47 saliva samples collected from deer expressing the 96GG genotype and 8 (11%) of 70 saliva samples collected from deer expressing the 96GS or 103NT genotypes (Table 2). No seeding activity was detected in any of the 28 saliva samples from sham-inoculated control deer. Prion shedding in saliva occurred more frequently than in urine throughout the disease course.

CWD Initiation and Progression According to WTD *PRNP* Polymorphism

PRNP codon 96 polymorphisms are known to affect relative CWD susceptibility and the rate of disease progression in WTD (*10*,*29*,*30*,*42*–*44*). After low-dose oral CWD prion exposure, deer expressing the 96GG genotype had RT-QuIC–positive lymphoid biopsies at 6 (1/6; 17%) to 18 (6/6; 100%) mpi (Table 1; Figure 3). In contrast, deer expressing 96GS or 103NT polymorphisms had delayed CWD-positive status by an additional 9 months; the first RT-QuIC–positive tonsil biopsies occurred at 15–27 mpi (Table 1; Figure 4). Differences in clinical disease kinetics were also

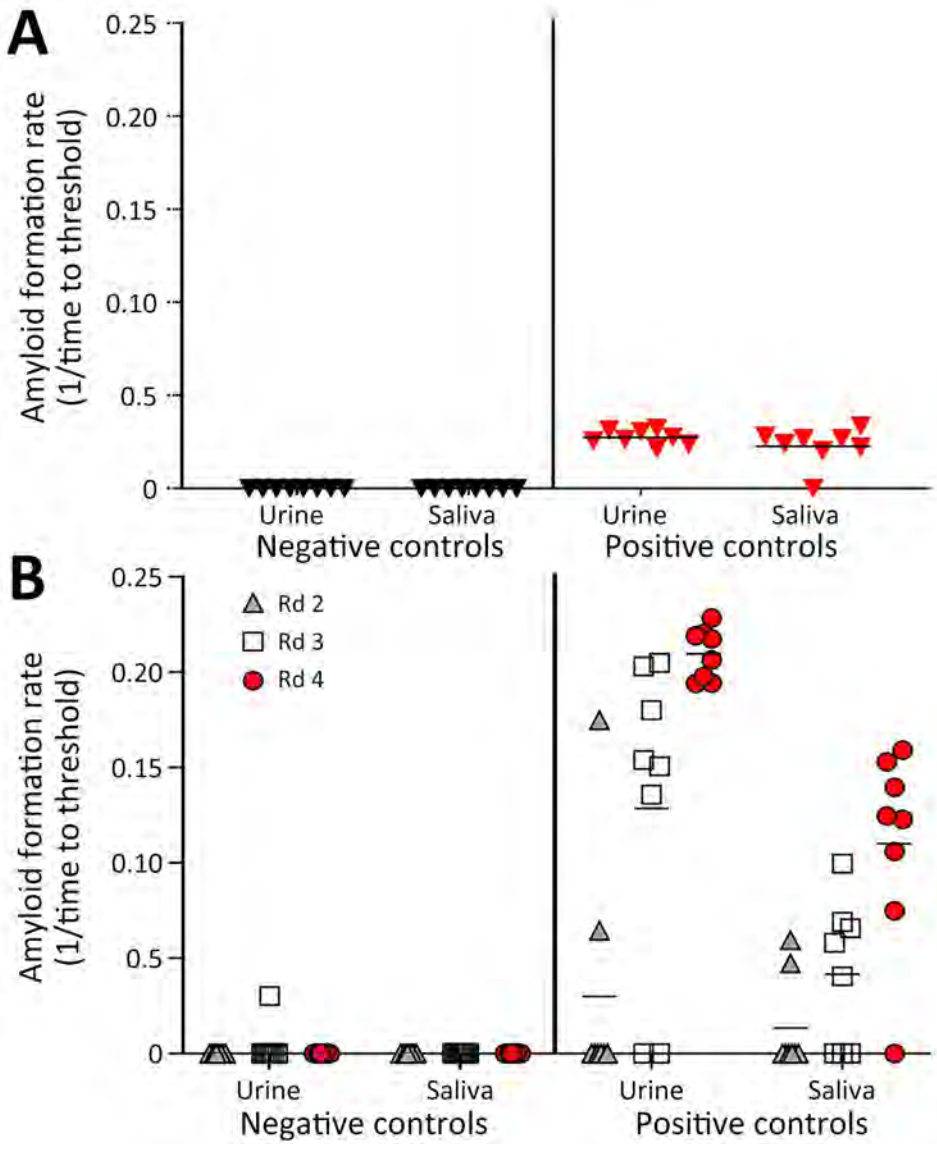

Figure 2. Amyloid formation rates in urine and saliva samples from white-tailed deer with chronic wasting disease in longitudinal study of temporal characterization of prion shedding in secreta, United States. A) Amyloid formation rates measured by using iron oxide bead capture and subsequent real-time quaking-induced conversion. Black indicates prion-negative samples; red indicates prion-positive samples. B) Amyloid formation rates measured by using iron oxide bead capture, 4 rounds of serial protein misfolding amplification, and subsequent real-time quaking-induced conversion in the same samples as those in panel A. Rates were measured for samples after amplification rounds 2–4. Horizontal lines in each grouping indicate median values. Rd, round.

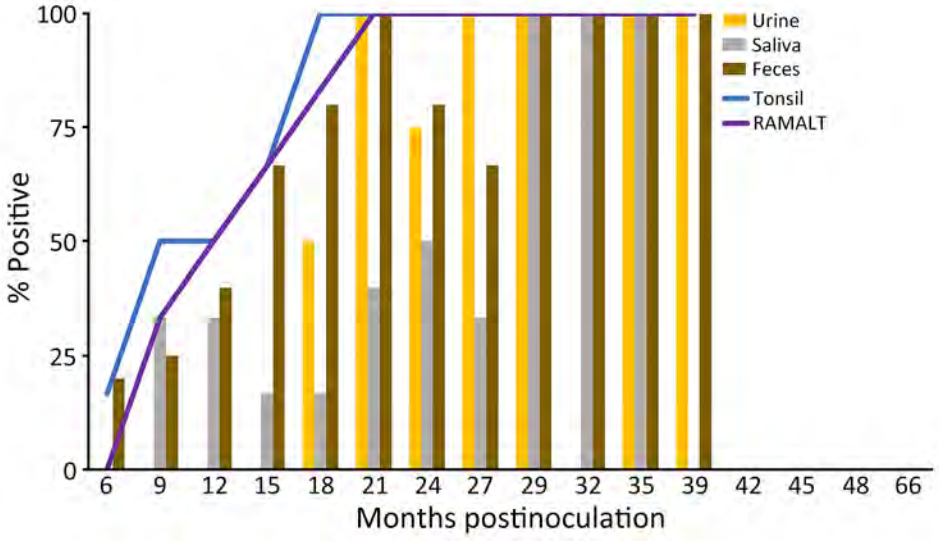

Figure 3. Percentage of prion-positive samples from white-tailed deer with chronic wasting disease that had the prion protein genotype 96GG in study of prion shedding in secreta, United States. Tissue samples and secreta were collected from deer after exposure to low oral doses of chronic wasting disease–positive brain tissue or saliva. RAMALT, recto-anal mucosa-associated lymphoid tissue.

observed between the 2 cohorts. All deer with the 96GG genotype were euthanized by 39 mpi because of progressive clinical CWD, whereas 3 (50%) of 6 deer with 96GS or 103NT genotypes remained asymptomatic when euthanized at 48 (n = 2; 96GS) and 66 (n = 1; 103NT) mpi (Table 1). Those results support both slower disease kinetics and reduced prion shedding for WTD expressing the *PRNP* gene encoding 96GS or 103NT polymorphisms.

Discussion

CWD continues to affect cervid populations in North America, Asia, and Europe (*1*–*4*). The extended asymptomatic phase of disease, during which the infectious CWD prion is shed, appears to be central to environmental contamination and efficient transmission. Yet, little is known about the temporal profiles of CWD shedding in secreta or the role *PRNP* might play in prion shedding. We found consistent prion shedding profiles throughout the disease course (39 mpi) in WTD that had a wild-type *PRNP* genotype at codon 96 (96GG). CWD shedding in secreta was less frequent during the disease course (66 mpi) in deer with alternate polymorphisms (96GS or 103NT), factors that delay CWD infection and progression. Ongoing efforts to establish breeding programs for farmed WTD that have alternate *PRNP* polymorphisms have been initiated (*45*). Our findings suggest that deer expressing alternative *PRNP* polymorphisms might live longer and, although they shed fewer prions throughout CWD course, might over their extended lifespan increase CWD prions in the environment.

We pursued options to improve prion seeding activity detection in fecal samples by combining IOB capture with sPMCA and RT-QuIC readout (IPQ). High-speed centrifugation, sodium phosphotungstic

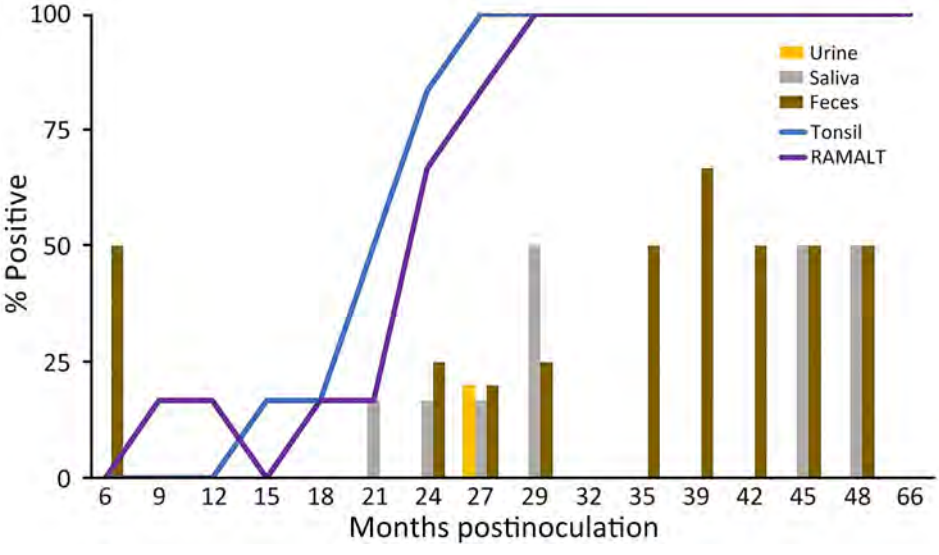

Figure 4. Percentage of prion-positive samples from white-tailed deer with chronic wasting disease that had prion protein genotypes 96GS or 103NT in study of prion shedding in secreta, United States. Tissue samples and secreta were collected from deer after exposure to low oral doses of chronic wasting disease–positive brain tissue or saliva. RAMALT, recto-anal mucosa-associated lymphoid tissue.

acid, or IOB have previously been used in combination with either PMCA or RT-QuIC to detect prions in feces of CWD-infected animals (*14*,*17*–*23*). However, those using PMCA analyzed products by Western blots rather than RT-QuIC. IPQ eliminated spurious nonspecific amplification that has been noted with fecal samples (*17*,*20*,*22*), providing a much clearer longitudinal CWD fecal shedding profile. We found that the incorporation of IPQ to enhance prion detection sensitivity in urine and saliva samples was not advantageous over the use of IQ.

Feces have been shown to contain low yet sufficient CWD infectivity to initiate infection (*9*,*46*). We observed higher prion concentrations in fecal samples collected from deer expressing the wild-type 96GG genotype than deer expressing alternate polymorphisms. Fecal prions were detected in wild-type deer shortly after biopsy positivity and were consistent throughout disease course, whereas shedding was delayed and inconsistent in deer expressing the alternate polymorphisms. We observed higher prion concentrations in feces than in saliva or urine collected from the 2 deer cohorts, possibly suggesting the prion load in feces is higher than previously recognized (*18*,*21*) or IPQ removes inhibitors that permit enhanced detection in feces not attained in urine or saliva samples Further assay development will be needed to address this question and to establish prion titers across all 3 secreta types.

Bioassay studies in WTD and cervid PrP–expressing transgenic mice have revealed low levels of prion infectivity in urine and saliva collected at various stages of CWD (*8*–*10*,*47*). In vitro detection has been challenging, presumably because of low concentrations or inhibitors in those bodily secretions (*11*–*13*,*15*,*16*,*23*). By combining IOB capture and RT-QuIC amplification, we found consistent CWD prion shedding in urine and saliva collected from WTD expressing wildtype *PRNP* compared with those expressing alternate *PRNP* polymorphisms. Our findings support an earlier study that showed CWD shedding in urine occurred less frequently in deer with more CWD-resistant genotypes (*18*).

Overall, our results support the tenet that prion shedding in secreta occurs more frequently and consistently in WTD expressing *PRNP* genotype 96GG and less frequently in deer with *PRNP* 96GS or 103NT polymorphisms. We also found more consistent CWD prion shedding in saliva than urine for both cohorts, suggesting that saliva might be a plausible vector for efficient disease transmission. This finding reinforces previous studies reporting that saliva is more infectious than urine or feces after experimental CWD prion inoculation (*8*,*10*,*47*,*48*). It would be advantageous to determine which secreta is responsible for the efficient CWD transmission dynamics. However, many variables exist that might influence infection, such as infection route, genotype, environmental/soil factors, CWD prion strain, and dose, and it might be misleading to suggest one secretum contributes more to CWD spread than another.

Table 2. Total prion seeding activity detected in each sample type in longitudinal study of temporal characterization of prion shedding in secreta of white-tailed deer with chronic wasting disease, United States*

Sample	96GG genotype	96GS/103NT genotype	Negative controls
Urine	9/16 (56)	1/50 (2)	0/28 (0)
Saliva	15/47 (32)	8/70 (11)	0/28 (0)
Feces	27/42 (64)	10/52 (19)	0/21 (0)

*Values are number of positive samples over total number of samples (%). Secreta from deer with wild-type genotype 96GG or alternative genotypes 96GS or 103NT of the prion protein gene were compared.

In conclusion, our findings indicate the role prion shedding might have on CWD transmission, particularly given the presumed low prion content in secreta. We conducted our study with an overarching eye on the potential advances, limitations, and opportunities that remain to fully exploit ultrasensitive prion seeding assays used to examine amyloid development in complex milieus and matrices. Our findings demonstrate improved amplification methods can be used to identify early antemortem CWD prion shedding in cervids that might aid in disease surveillance.

Acknowledgments

We thank David Osborn, Carl Miller, Gino D'Angelo, and Sallie Dahmes for providing the hand-raised, indoor-adapted fawns for this study.

This manuscript is devoted to Edward A. Hoover, deceased, whose dedication and contributions to the field of prion research spanned >25 years. His knowledge and guidance bolstered everyone in his presence and pioneered our current understanding of CWD transmission, pathogenesis, and assay development. His presence will be greatly missed by many throughout the scientific community.

Funding for this study was awarded to C.K.M. through the US National Institutes of Health (grant nos. RO1-NS061902-09R, PO1-AI077774, and RO1-AI112956-06).

About the Author

Dr. Denkers is a pathologist at Colorado State University. His research interests focus on transmission mechanisms and pathogenesis of CWD in natural hosts, CWD surveillance in wild cervid populations, vaccine trials, and prion diagnostics development.

References

1. Sohn HJ, Kim JH, Choi KS, Nah JJ, Joo YS, Jean YH, et al. A case of chronic wasting disease in an elk imported to Korea from Canada. J Vet Med Sci. 2002;64:855–8. https://doi.org/10.1292/jvms.64.855
2. Benestad SL, Mitchell G, Simmons M, Ytrehus B, Vikøren T. First case of chronic wasting disease in Europe in a Norwegian free-ranging reindeer. Vet Res. 2016;47:88. https://doi.org/10.1186/s13567-016-0375-4
3. Pirisinu L, Tran L, Chiappini B, Vanni I, Di Bari MA, Vaccari G, et al. Novel type of chronic wasting disease detected in moose (*Alces alces*), Norway. Emerg Infect Dis. 2018;24:2210–8. https://doi.org/10.3201/eid2412.180702
4. US Geological Survey, National Wildlife Health Center. Expanding distribution of chronic wasting disease. 2022 [cited 2024 Jun 1]. https://www.usgs.gov/centers/nwhc/science/expanding-distribution-chronic-wasting-disease
5. Miller MW, Williams ES. Prion disease: horizontal prion transmission in mule deer. Nature. 2003;425:35–6. https://doi.org/10.1038/425035a
6. Miller MW, Williams ES, Hobbs NT, Wolfe LL. Environmental sources of prion transmission in mule deer. Emerg Infect Dis. 2004;10:1003–6. https://doi.org/10.3201/eid1006.040010
7. Mathiason CK, Hays SA, Powers J, Hayes-Klug J, Langenberg J, Dahmes SJ, et al. Infectious prions in pre-clinical deer and transmission of chronic wasting disease solely by environmental exposure. PLoS One. 2009;4:e5916. https://doi.org/10.1371/journal.pone.0005916
8. Mathiason CK, Powers JG, Dahmes SJ, Osborn DA, Miller KV, Warren RJ, et al. Infectious prions in the saliva and blood of deer with chronic wasting disease. Science. 2006;314:133–6. https://doi.org/10.1126/science.1132661
9. Haley NJ, Mathiason CK, Zabel MD, Telling GC, Hoover EA. Detection of sub-clinical CWD infection in conventional test-negative deer long after oral exposure to urine and feces from CWD+ deer. PLoS One. 2009;4:e7990. https://doi.org/10.1371/journal.pone.0007990
10. Denkers ND, Hoover CE, Davenport KA, Henderson DM, McNulty EE, Nalls AV, et al. Very low oral exposure to prions of brain or saliva origin can transmit chronic wasting disease. PLoS One. 2020;15:e0237410. https://doi.org/10.1371/journal.pone.0237410
11. John TR, Schätzl HM, Gilch S. Early detection of chronic wasting disease prions in urine of pre-symptomatic deer by real-time quaking-induced conversion assay. Prion. 2013;7:253–8. https://doi.org/10.4161/pri.24430
12. Rubenstein R, Chang B, Gray P, Piltch M, Bulgin MS, Sorensen-Melson S, et al. Prion disease detection, PMCA kinetics, and IgG in urine from sheep naturally/experimentally infected with scrapie and deer with preclinical/clinical chronic wasting disease. J Virol. 2011;85:9031–8. https://doi.org/10.1128/JVI.05111-11
13. Davenport KA, Hoover CE, Denkers ND, Mathiason CK, Hoover EA. Modified protein misfolding cyclic amplification overcomes real-time quaking-induced conversion assay inhibitors in deer saliva to detect chronic wasting disease prions. J Clin Microbiol. 2018;56:e00947-18. https://doi.org/10.1128/JCM.00947-18
14. Pulford B, Spraker TR, Wyckoff AC, Meyerett C, Bender H, Ferguson A, et al. Detection of PrP^{CWD} in feces from naturally exposed Rocky Mountain elk (*Cervus elaphus nelsoni*) using protein misfolding cyclic amplification. J Wildl Dis. 2012;48:425–34. https://doi.org/10.7589/0090-3558-48.2.425
15. Henderson DM, Manca M, Haley NJ, Denkers ND, Nalls AV, Mathiason CK, et al. Rapid antemortem detection of CWD prions in deer saliva. PLoS One. 2013;8:e74377. https://doi.org/10.1371/journal.pone.0074377
16. Henderson DM, Denkers ND, Hoover CE, Garbino N, Mathiason CK, Hoover EA. Longitudinal detection of prion shedding in saliva and urine by chronic wasting disease–infected deer by real-time quaking-induced conversion. J Virol. 2015;89:9338–47. https://doi.org/10.1128/JVI.01118-15
17. Henderson DM, Tennant JM, Haley NJ, Denkers ND, Mathiason CK, Hoover EA. Detection of chronic wasting disease prion seeding activity in deer and elk feces by real-time quaking-induced conversion. J Gen Virol. 2017;98:1953–62. https://doi.org/10.1099/jgv.0.000844
18. Plummer IH, Wright SD, Johnson CJ, Pedersen JA, Samuel MD. Temporal patterns of chronic wasting disease prion excretion in three cervid species. J Gen Virol. 2017;98:1932–42. https://doi.org/10.1099/jgv.0.000845
19. Cheng YC, Hannaoui S, John TR, Dudas S, Czub S, Gilch S. Real-time quaking-induced conversion assay for detection of CWD prions in fecal material. J Vis Exp. 2017;127:56373. https://doi.org/10.3791/56373
20. Cheng YC, Hannaoui S, John TR, Dudas S, Czub S, Gilch S. Early and non-invasive detection of chronic wasting disease prions in elk feces by real-time quaking induced conversion. PLoS One. 2016;11:e0166187. https://doi.org/10.1371/journal.pone.0166187
21. Tennant JM, Li M, Henderson DM, Tyer ML, Denkers ND, Haley NJ, et al. Shedding and stability of CWD prion seeding activity in cervid feces. PLoS One. 2020;15:e0227094. https://doi.org/10.1371/journal.pone.0227094
22. Hwang S, Greenlee JJ, Nicholson EM. Real-time quaking-induced conversion detection of PrP^{Sc} in fecal samples from chronic wasting disease infected white-tailed deer using bank vole substrate. Front Vet Sci. 2021;8:643754. https://doi.org/10.3389/fvets.2021.643754
23. Denkers ND, Henderson DM, Mathiason CK, Hoover EA. Enhanced prion detection in biological samples by magnetic particle extraction and real-time quaking-induced conversion. J Gen Virol. 2016;97:2023–9. https://doi.org/10.1099/jgv.0.000515
24. McNulty EE, Nalls AV, Xun R, Denkers ND, Hoover EA, Mathiason CK. In vitro detection of haematogenous prions in white-tailed deer orally dosed with low concentrations of chronic wasting disease. J Gen Virol. 2020;101:347–61. https://doi.org/10.1099/jgv.0.001367
25. Henderson DM, Davenport KA, Haley NJ, Denkers ND, Mathiason CK, Hoover EA. Quantitative assessment of prion infectivity in tissues and body fluids by real-time quaking-induced conversion. J Gen Virol. 2015;96:210–9. https://doi.org/10.1099/vir.0.069906-0
26. Ferreira NC, Charco JM, Plagenz J, Orru CD, Denkers ND, Metrick MA 2nd, et al. Detection of chronic wasting disease in mule and white-tailed deer by RT-QuIC analysis of outer ear. Sci Rep. 2021;11:7702. https://doi.org/10.1038/s41598-021-87295-8
27. Arifin MI, Hannaoui S, Chang SC, Thapa S, Schatzl HM, Gilch S. Cervid prion protein polymorphisms: role in chronic wasting disease pathogenesis. Int J Mol Sci. 2021;22:2271. https://doi.org/10.3390/ijms22052271
28. O'Rourke KI, Besser TE, Miller MW, Cline TF, Spraker TR, Jenny AL, et al. PrP genotypes of captive and free-ranging Rocky Mountain elk (*Cervus elaphus nelsoni*) with chronic wasting disease. J Gen Virol. 1999;80:2765–9. https://doi.org/10.1099/0022-1317-80-10-2765
29. Johnson C, Johnson J, Vanderloo JP, Keane D, Aiken JM, McKenzie D. Prion protein polymorphisms in white-tailed deer influence susceptibility to chronic wasting disease.

J Gen Virol. 2006;87:2109–14. https://doi.org/10.1099/vir.0.81615-0
30. Johnson CJ, Herbst A, Duque-Velasquez C, Vanderloo JP, Bochsler P, Chappell R, et al. Prion protein polymorphisms affect chronic wasting disease progression. PLoS One. 2011;6:e17450. https://doi.org/10.1371/journal.pone.0017450
31. Jewell JE, Conner MM, Wolfe LL, Miller MW, Williams ES. Low frequency of PrP genotype 225SF among free-ranging mule deer (*Odocoileus hemionus*) with chronic wasting disease. J Gen Virol. 2005;86:2127–34. https://doi.org/10.1099/vir.0.81077-0
32. Hamir AN, Gidlewski T, Spraker TR, Miller JM, Creekmore L, Crocheck M, et al. Preliminary observations of genetic susceptibility of elk (*Cervus elaphus nelsoni*) to chronic wasting disease by experimental oral inoculation. J Vet Diagn Invest. 2006;18:110–4. https://doi.org/10.1177/104063870601800118
33. Kraft CN, Denkers ND, Mathiason CK, Hoover EA. Longitudinal detection of prion shedding in nasal secretions of CWD-infected white-tailed deer. J Gen Virol. 2023;104:001825. https://doi.org/10.1099/jgv.0.001825
34. Johnson C, Johnson J, Clayton M, McKenzie D, Aiken J. Prion protein gene heterogeneity in free-ranging white-tailed deer within the chronic wasting disease affected region of Wisconsin. J Wildl Dis. 2003;39:576–81. https://doi.org/10.7589/0090-3558-39.3.576
35. Robinson SJ, Samuel MD, O'Rourke KI, Johnson CJ. The role of genetics in chronic wasting disease of North American cervids. Prion. 2012;6:153–62. https://doi.org/10.4161/pri.19640
36. Henderson DM, Denkers ND, Hoover CE, McNulty EE, Cooper SK, Bracchi LA, et al. Progression of chronic wasting disease in white-tailed deer analyzed by serial biopsy RT-QuIC and immunohistochemistry. PLoS One. 2020;15:e0228327. https://doi.org/10.1371/journal.pone.0228327
37. Angers RC, Seward TS, Napier D, Green M, Hoover E, Spraker T, et al. Chronic wasting disease prions in elk antler velvet. Emerg Infect Dis. 2009;15:696–703. https://doi.org/10.3201/eid1505.081458
38. Wilham JM, Orrú CD, Bessen RA, Atarashi R, Sano K, Race B, et al. Rapid end-point quantitation of prion seeding activity with sensitivity comparable to bioassays. PLoS Pathog. 2010;6:e1001217. https://doi.org/10.1371/journal.ppat.1001217
39. Atarashi R, Sano K, Satoh K, Nishida N. Real-time quaking-induced conversion: a highly sensitive assay for prion detection. Prion. 2011;5:150–3. https://doi.org/10.4161/pri.5.3.16893
40. Denkers ND, Hayes-Klug J, Anderson KR, Seelig DM, Haley NJ, Dahmes SJ, et al. Aerosol transmission of chronic wasting disease in white-tailed deer. J Virol. 2013;87:1890–2. https://doi.org/10.1128/JVI.02852-12
41. O'Rourke KI, Spraker TR, Hamburg LK, Besser TE, Brayton KA, Knowles DP. Polymorphisms in the prion precursor functional gene but not the pseudogene are associated with susceptibility to chronic wasting disease in white-tailed deer. J Gen Virol. 2004;85:1339–46. https://doi.org/10.1099/vir.0.79785-0
42. Otero A, Duque Velásquez C, Johnson C, Herbst A, Bolea R, Badiola JJ, et al. Prion protein polymorphisms associated with reduced CWD susceptibility limit peripheral PrP^{CWD} deposition in orally infected white-tailed deer. BMC Vet Res. 2019;15:50. https://doi.org/10.1186/s12917-019-1794-z
43. Race B, Meade-White K, Miller MW, Fox KA, Chesebro B. In vivo comparison of chronic wasting disease infectivity from deer with variation at prion protein residue 96. J Virol. 2011;85:9235–8. https://doi.org/10.1128/JVI.00790-11
44. Hoover CE, Davenport KA, Henderson DM, Denkers ND, Mathiason CK, Soto C, et al. Pathways of prion spread during early chronic wasting disease in deer. J Virol. 2017;91:e00077-17. https://doi.org/10.1128/JVI.00077-17
45. Haley N, Donner R, Merrett K, Miller M, Senior K. Selective breeding for disease-resistant *PRNP* variants to manage chronic wasting disease in farmed whitetail deer. Genes (Basel). 2021;12:1396. https://doi.org/10.3390/genes12091396
46. Tamgüney G, Miller MW, Wolfe LL, Sirochman TM, Glidden DV, Palmer C, et al. Asymptomatic deer excrete infectious prions in faeces. Nature. 2009;461:529–32. https://doi.org/10.1038/nature08289
47. Haley NJ, Seelig DM, Zabel MD, Telling GC, Hoover EA. Detection of CWD prions in urine and saliva of deer by transgenic mouse bioassay. PLoS One. 2009;4:e4848. https://doi.org/10.1371/journal.pone.0004848
48. Tamgüney G, Richt JA, Hamir AN, Greenlee JJ, Miller MW, Wolfe LL, et al. Salivary prions in sheep and deer. Prion. 2012;6:52–61. https://doi.org/10.4161/pri.6.1.16984

Address for correspondence: Candace K. Mathiason, Prion Research Center, Department of Microbiology, Immunology, and Pathology, College of Veterinary Medicine and Biological Sciences, 1619 Campus Delivery, Colorado State University, Fort Collins, CO 80523, USA; email: candace.mathiason@colostate.edu

Presumed Transmission of 2 Distinct Monkeypox Virus Variants from Central African Republic to Democratic Republic of the Congo

Emmanuel Hasivirwe Vakaniaki, Eddy Kinganda-Lusamaki, Sydney Merritt, Francois Kasongo, Emile Malembi, Lygie Lunyanga, Sylvie Linsuke, Megan Halbrook, Ernest Kalthan, Elisabeth Pukuta, Adrienne Amuri Aziza, Jean Claude Makangara Cigolo, Raphael Lumembe, Gabriel Kabamba, Yvon Anta, Pierrot Bolunza, Innocent Kanda, Raoul Ngazobo, Thierry Kalonji, Justus Nsio, Patricia Matoka, Dieudonné Mwamba, Christian Ngandu, Souradet Y. Shaw, Robert Shongo, Joule Madinga, Yap Boum, Laurens Liesenborghs, Eric Delaporte, Ahidjo Ayouba, Nicola Low, Steve Ahuka Mundeke, Lisa E. Hensley, Jean-Jacques Muyembe Tamfum, Emmanuel Nakoune, Martine Peeters, Nicole A. Hoff, Jason Kindrachuk, Anne W. Rimoin,[1] Placide Mbala-Kingebeni[1]

We linked 4 mpox cases in South Ubangi, Democratic Republic of the Congo, to transboundary transmission from Central African Republic. Viral genome sequencing demonstrated that the monkeypox virus sequences belonged to distinct clusters of subclade Ia. This finding demonstrates the borderless nature of mpox and highlights the need for vigilant regional surveillance.

Mpox is a zoonotic viral infectious disease first identified in humans in the Democratic Republic of the Congo (DRC) in 1970 (*1*). Monkeypox virus (MPXV) is endemic to forested regions of Central and West Africa (*2*) and is subclassified into clade I and clade II; subclade IIb was responsible for a global epidemic in 2022 (*3*). We have recommended subdivision of clade I into subclades Ia and Ib, where subclade Ib is associated with sustained human-to-human transmission in the DRC (*4*). Clade I is endemic to Central Africa, particularly in the DRC, and infections are associated with greater disease severity than for clade II infection (*5*,*6*). Zoonotic spillover has been the primary driver of clade I MPXV

Author affiliations: Institut National de Recherche Biomédicale, Kinshasa, Democratic Republic of the Congo (E.H. Vakaniaki, E. Kinganda-Lusamaki, F. Kasongo, L. Lunyanga, S. Linsuke, E. Pukuta, A.A. Aziza, J.C. Makangara Cigolo, R. Lumembe, G. Kabamba, Y. Anta, J. Madinga, S.A. Mundeke, J.-J. Muyembe Tamfum, P. Mbala-Kingebeni); Institute of Tropical Medicine, Antwerp, Belgium (E.H. Vakaniaki, L. Liesenborghs); Cliniques Universitaires de Kinshasa, Kinshasa University, Kinshasa (E. Kinganda-Lusamaki, J.C. Makangara Cigolo, R. Lumembe, G. Kabamba, S.A. Mundeke, J.-J. Muyembe Tamfum, P. Mbala-Kingebeni); Université de Montpellier, French National Research Institute for Sustainable Development, INSERM, Montpellier, France (E. Kinganda-Lusamaki, E. Delaporte, A. Ayouba, M. Peeters); University of California, Los Angeles, California, USA (S. Merritt, M. Halbrook, N.A. Hoff, A.W. Rimoin); Hemorrhagic Fevers and Monkeypox Program, Ministry of Health, Kinshasa (E. Malembi, T. Kalonji, R. Shongo); Ministry of Health and Populations, Bangui, Central African Republic (E. Kalthan); University of Bern, Bern, Switzerland (J.C. Makangara Cigolo, N. Low); Provincial Health Division, South Ubangi, Democratic Republic of the Congo (P. Bolunza, I. Kanda); Mbaya Health Zone, South Ubangi (R. Ngazobo); National Border Hygiene Program, Ministry of Health, Kinshasa (J. Nsio, P. Matoka); National Institute of Public Health, Ministry of Health, Kinshasa (D. Mwamba, C. Ngandu); University of Manitoba, Winnipeg, Manitoba, Canada (S.Y. Shaw, J. Kindrachuk); Pasteur Institute of Bangui, Bangui, Central African Republic (Y. Boum, E. Nakoune); USDA Agricultural Research Service, Manhattan, Kansas, USA (L.E. Hensley)

DOI: https://doi.org/10.3201/eid3010.241118

[1]These authors equally cosupervised this work.

infections; however, sustained human-to-human transmission is increasing, and spread of clade I MPXV through sexual contact has been reported in multiple regions of the DRC (*4*,*7*).

Among mpox-endemic regions, the DRC has been the most severely affected. The number of reported cases has increased since the cessation of smallpox vaccination campaigns in 1980 (*8*). This increase accelerated from 2022 onward (*9*), including into regions with no previously reported cases (*10*). Cross-border travel has been demonstrated as a factor in transmission of clade II MPXV, but less is known for clade I cases in regional settings. Given the recent geographic expansion for clade I MPXV and increasing observation of sustained human-to-human transmission, considerable concerns exist about geographic expansion of mpox through cross-border transmission (*10*).

The Central African Republic (CAR) shares a >1,000-mile border with the DRC. CAR has reported 40 confirmed mpox outbreaks (95 suspected cases during 2001–2021), increasing from 0–2 annually during 2001–2017 to 9 annually since 2018 (*11*). Most of those outbreaks occurred in 2 regions along the border with the DRC. Here, we report suspected cross-border transmission of mpox between CAR and the DRC in 2023 and potential links to MPXV circulation in DRC.

The Study

The South Ubangi Provincial Health Division in the DRC issued an alert for a suspected mpox case in January 2023 after the death of a fisherman displaying respiratory distress and skin lesions in Mbaya Health Zone. South Ubangi directly borders CAR, separated by the Ubangi River. The National Programme for Control of Mpox and Viral Hemorrhagic Fevers and the National Institute for Biomedical Research deployed a multidisciplinary team to investigate the case with the Provincial Health Division. As part of the investigation, the national and provincial health teams conducted supplemental training sessions to raise awareness of the clinical signs and transmission modes for mpox.

The index case was an adult man residing in Bangui, CAR, who moved frequently between

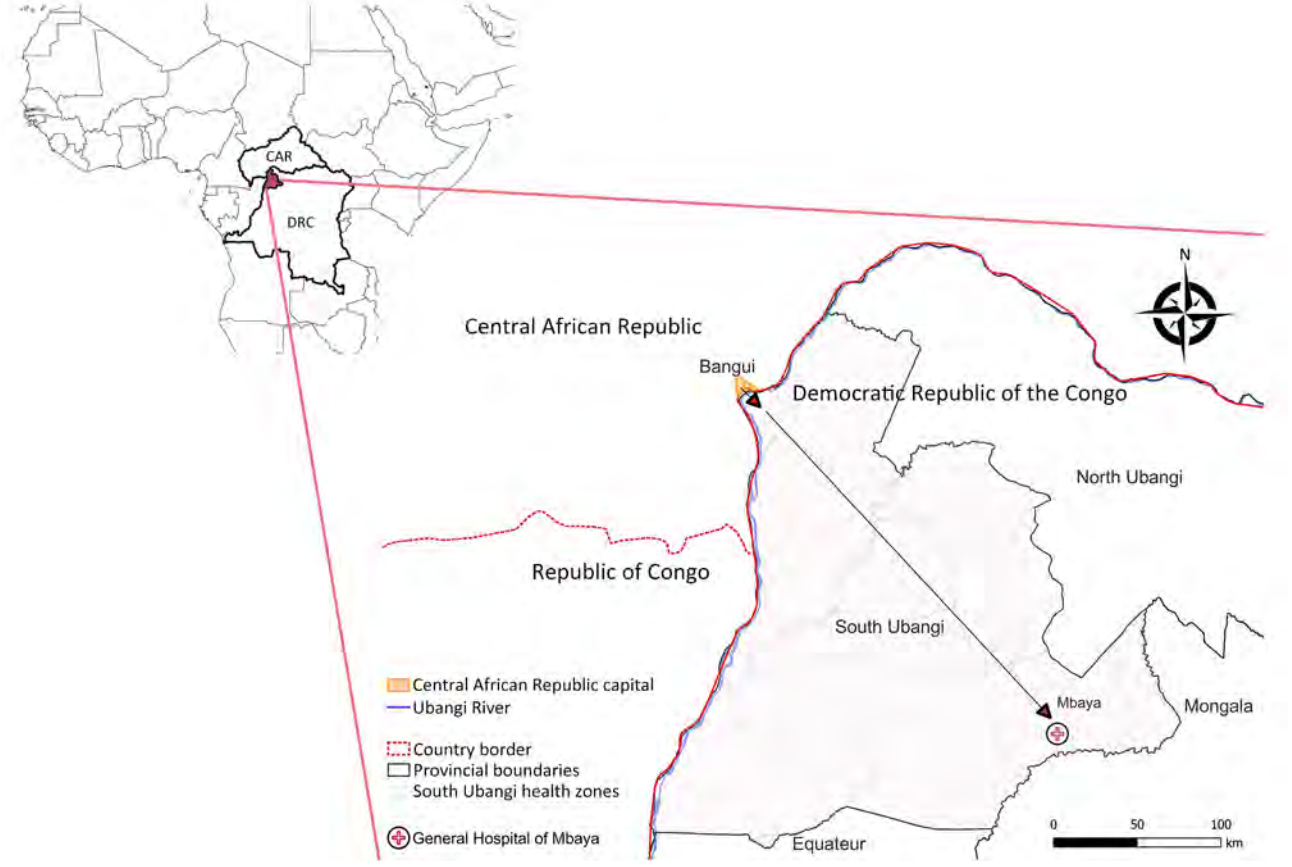

Figure 1. Possible transmission route of monkeypox virus between Bangui, Central African Republic, and Mbaya Health Zone, South Ubangi Province, Democratic Republic of the Congo, January 2023. Inset map shows location of countries and study area within Africa. Created with BioRender.com.

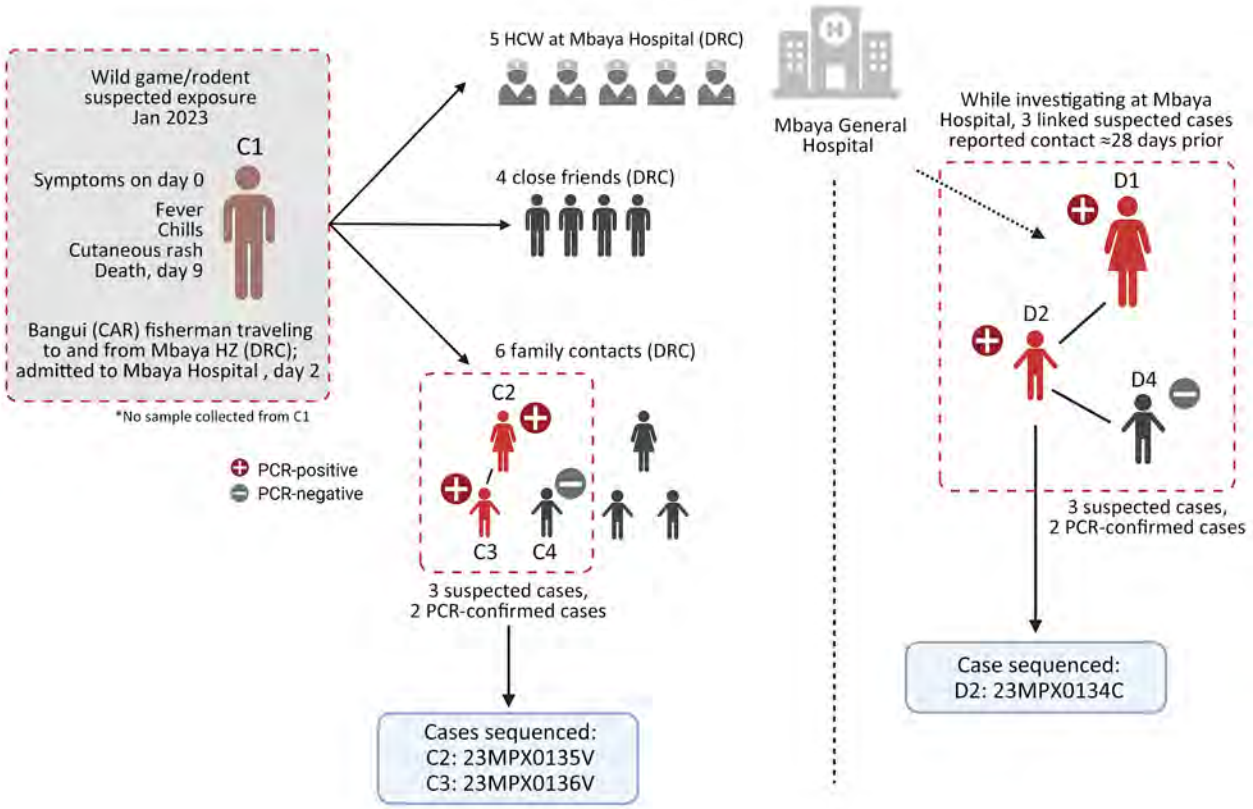

Figure 2. Possible transmission chain of monkeypox virus from CAR to the DRC and second identified chain at Mbaya General Reference Hospital, Mbaya, DRC. CAR, Central African Republic; DRC, Democratic Republic of the Congo; HCW, healthcare workers; HZ, health zone. Created with BioRender.com.

CAR and the DRC by the Ubangi River (cluster 1, case 1: C1) (Figure 1). After suspected exposure to wildlife meat and the potential consumption of rodents in CAR in early January 2023, symptom onset began shortly after (day 0); symptoms were fever, headache, chills, and cutaneous rash. After traveling to the DRC, he was admitted to Mbaya General Reference Hospital 2 days later, where he died on day 9 after symptom onset, after experiencing respiratory distress. No samples or information on his immune status were collected from this probable mpox case-patient.

We identified 15 contacts of the patient in Mbaya Health Zone, consisting of 5 healthcare workers and 10 close contacts (4 close friends and 6 family contacts). The investigation revealed a cluster of 3 symptomatic family contacts. Of those, 2 contacts had samples taken, and both tested positive for MPXV by PCR; those contacts were the adult female partner of C1 (C2) and their child (C3). A second child of C1 and C2 (C4) was treated locally for suspected mpox using traditional methods and was not investigated further. No suspected mpox cases were identified among family or close contacts of C1 in Bangui.

During the investigation, we identified a distinct second mpox cluster, which likely originated from a different source. We identified 3 suspected mpox cases in the same hospital at the same time as the first cluster that had no known epidemiologic link. An adult woman (cluster 2, case 1: D1) was hospitalized for nonspecific signs of mpox at the same time as C1 and reported contact with a child with mpox symptoms ≈28 days before. The 2 additional suspected cases were the child of D1 (D2), in whom mpox was subsequently confirmed by PCR, and a contact of D2 (D3), who tested negative by PCR (Figure 2). Confirmed mpox clinical symptoms included multiple pustular and papular lesions (C2); disseminated pustules (C3); discreet lacrimation in the left eye and postinflammatory hyperpigmentation (D1); and hyperpigmented, disseminated macules and steep-edged ulcerations (D2) (Figure 3).

We subsequently performed viral genome sequencing on 3 PCR-positive samples: 2 from the first mpox cluster (C2 and C3) and 1 from the second cluster (D2) (Figure 4). Phylogenetic analysis included 98 clade I MPXV previously published genomes. We generated the phylogenetic tree by maximum-

likelihood using the Kimura 3-parameter model with unequal base frequencies plus gamma distribution plus invariable sites (*12*,*13*). The 3 sequences, all clade Ia, clustered with MPXV genome sequences isolated from CAR. The genetic distance between the new cases and the date between the CAR and DRC samples are too long to conclude direct links between the 2 countries. Nevertheless, the new samples from South-Ubangi clustered in the same subgroup (group II) according to previous classification of MPXV sequences in clade Ia (*14*).

Further, the National Programme for Control of Mpox and Viral Hemorrhagic Fevers investigated 109 suspected mpox cases from 15 health zones in South Ubangi during January–November 2023. Case-patients were predominantly male (60 male and 46 female; data were unavailable for 3 cases); the average age was 21 years (range 35 months–63 years). Of those, 61 cases (56%) were confirmed positive by PCR at National Institute for Biomedical Research. Three of the 46 mpox-negative cases (6%) were confirmed as positive for varicella zoster virus.

Conclusions

This investigation describes 2 distinct clusters of mpox cases in Mbaya Health Zone in South Ubangi Province in the DRC, presumably resulting from 2 different introductions. We identified epidemiologic links to cross-border travel from CAR for the first cluster and identified genomic links with historic CAR cases for both clusters. MPXV transmission in the DRC is currently driven by both zoonotic and human-to-human contact, thus increasing the complexity of containment and mitigation efforts. Wider regional and international expansion of mpox, specifically, the concentration of MPXV outbreaks in CAR and the

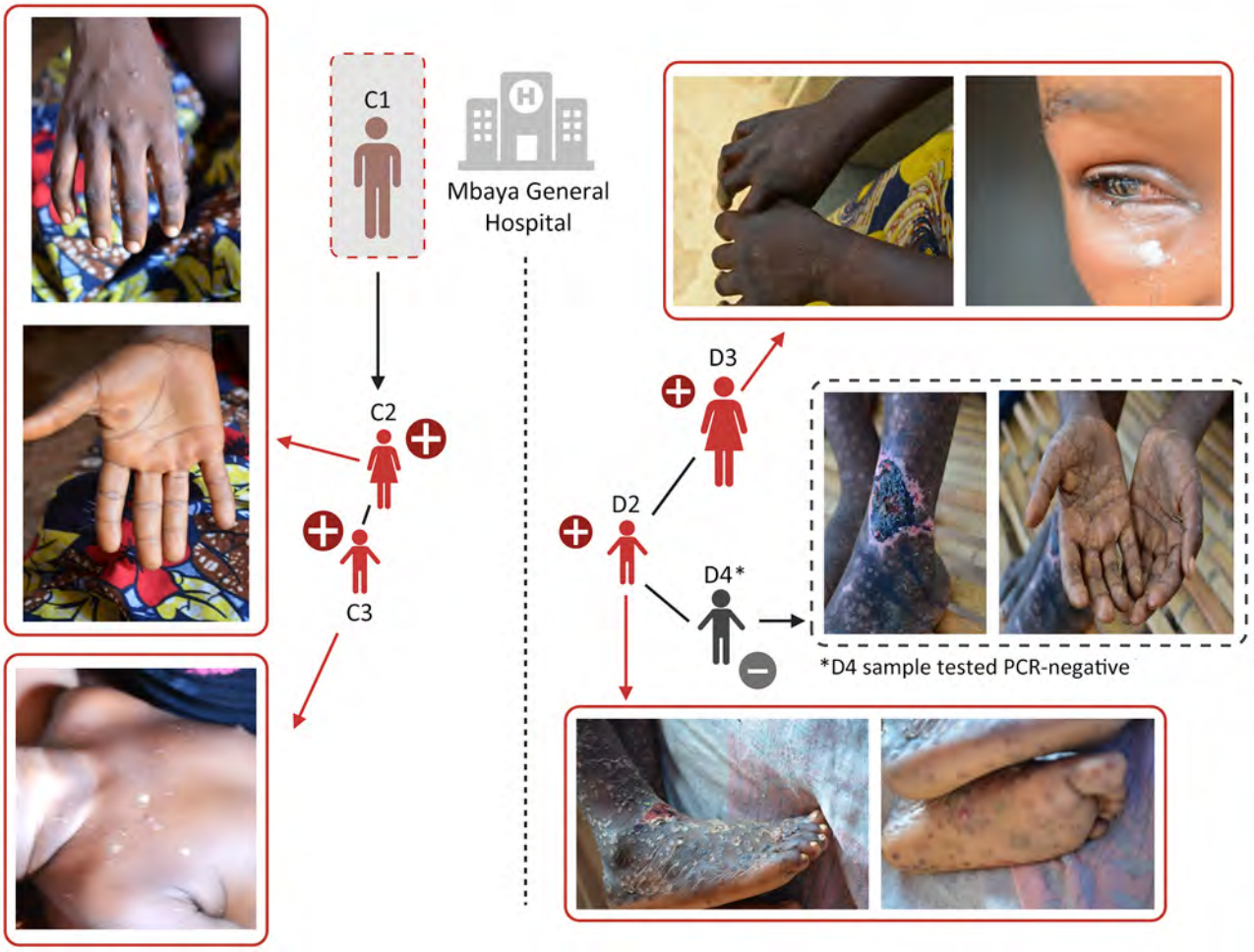

Figure 3. Clinical manifestations of suspected mpox from 2 mother-child pairs in study of presumed transmission of monkeypox virus variants from Central African Republic to Democratic Republic of the Congo. One mother-child pair was linked to the deceased fisherman in Mbaya Health Zone, and the other pair were identified at Mbaya Hospital, Mbaya, Democratic Republic of the Congo. Created with BioRender.com.

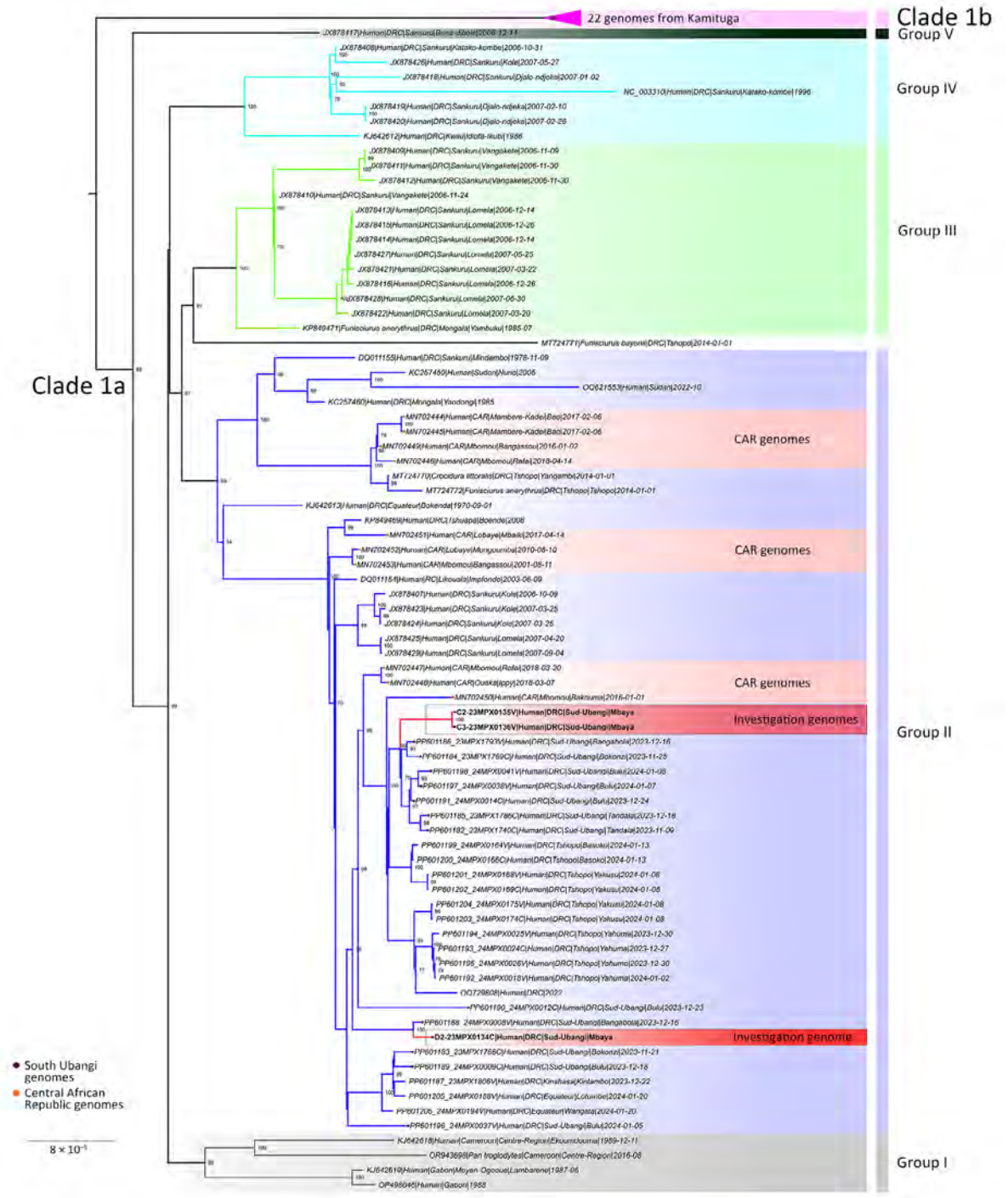

Figure 4. Phylogenetic analysis of monkeypox virus (MPXV) sequences from Mbaya Health Zone in study of presumed transmission of MPXV variants from Central African Republic to Democratic Republic of the Congo. Phylogenetic analysis of MPXV genome sequences are from samples described in this study and clade I MPXV sequences from Central Africa. Bootstrap support values are shown at branch points. DNA was extracted at the National Institute for Biomedical Research using a QIAGEN DNA Mini Kit (https://www.qiagen.com) from blood samples and subsequently screened for MPXV with an orthopoxvirus-specific real-time PCR assay. Whole-genome sequencing was attempted on samples from the index case by next-generation sequencing. Library preparation was performed using Illumina DNA Prep with Enrichment (https://www.illumina.com), and libraries were enriched for MPXV using biotinylated custom probes synthesized by Twist Biosciences (https://www.twistbioscience.com). Note that 23MPX0134C(D2), 23MPX0135V(C2), and 23MPX0136V(C3) are samples from crust or vesicles from separate individuals. Sequences can be accessed with the following GISAID (https://www.gisaid.org) accession nos.: EPI_ISL_19287107 (D2), EPI_ISL_19287108 (C2), EPI_ISL_19287109 (C3). Scale bar indicates number of substitutions per site.

DRC along the Ubangi River, recent sustained human-to-human transmission, resource limitations for identifying and treating mpox, disease stigma, population displacement because of conflict, and transient cross-border transit are serious concerns.

In August 2022, a first regional meeting involving 6 neighboring countries of Central and West Africa was held in Kinshasa, the DRC, to establish a regional mpox surveillance network, the Mpox Threat Reduction Network. Through this network, multiple teams including experts from the Health Ministries of the DRC and CAR were able to communicate rapidly on suspected cases crossing borders in South Ubangi while also reporting to International Health Regulations focal points. Considering the relatively porous borders in the Central African region and continuing increases in reported mpox cases, documenting transboundary mpox transmission is critical. This investigation highlights the importance of long-term collaborative partnerships for sustained mpox surveillance and containment in endemic regions.

This article was published as a preprint at https://www.medrxiv.org/content/10.1101/2024.08.13.24311555v1.

Acknowledgments

We thank Gradi Luakanda for his continued support of this work. All maps were generated using qGIS version 3.30. All efforts presented in this work are part of regular public health surveillance conducted by the Ministry of Health and partners in the DRC and CAR.

The project or effort depicted is sponsored by the Department of Defense Threat Reduction Agency (HDTRA1-21-1-0040) and US Department of Agriculture (USDA) Agriculture Research Service (ARS) (USDA ARS NACA no. 20230048, grant no. 58-30.22-2-020). The content of the information does not necessarily reflect the position or the policy of the US federal government, and no official endorsement should be inferred. This work was also supported by the International Mpox Research Consortium (IMReC) through funding from the Canadian Institutes of Health Research and International Development Research Centre (grant no. 202209MRR-489062-MPX-CDAA-168421) and the Agence Française de Développement through the PANAFPOX and AFROSCREEN project (grant agreement CZZ3209), coordinated by ANRS Maladies infectieuses émergentes in partnership with Institut de Recherche pour le Développement (IRD). E.L. received a PhD grant from the French Foreign Office.

About the Author

Dr. Vakaniaki is a medical researcher and ecoepidemiologist at the Institut National de Recherche Biomédicale and a predoctoral fellow at the Antwerp Institute of Tropical Medicine. His research focuses on emerging and reemerging infectious diseases, the contribution of vaccination to the control of vaccine-preventable diseases, and health risks in the context of One Health.

References

1. Ladnyj ID, Ziegler P, Kima E. A human infection caused by monkeypox virus in Basankusu Territory, Democratic Republic of the Congo. Bull World Health Organ. 1972;46:593–7.
2. Titanji BK, Tegomoh B, Nematollahi S, Konomos M, Kulkarni PA. Monkeypox: a contemporary review for healthcare professionals. Open Forum Infect Dis. 2022;9:ofac310. https://doi.org/10.1093/ofid/ofac310
3. Happi C, Adetifa I, Mbala P, Njouom R, Nakoune E, Happi A, et al. Urgent need for a non-discriminatory and non-stigmatizing nomenclature for monkeypox virus. PLoS Biol. 2022;20:e3001769. https://doi.org/10.1371/journal.pbio.3001769
4. Vakaniaki EH, Kacita C, Kinganda-Lusamaki E, O'Toole Á, Wawina-Bokalanga T, Mukadi-Bamuleka D, et al. Sustained human outbreak of a new MPXV clade I lineage in eastern Democratic Republic of the Congo. Nat Med. 2024. https://doi.org/10.1038/s41591-024-03130-3
5. Weaver JR, Isaacs SN. Monkeypox virus and insights into its immunomodulatory proteins. Immunol Rev. 2008; 225:96–113. https://doi.org/10.1111/j.1600-065X.2008.00691.x
6. McCollum AM, Damon IK. Human monkeypox. Clin Infect Dis. 2014;58:260–7. https://doi.org/10.1093/cid/cit703
7. Kibungu EM, Vakaniaki EH, Kinganda-Lusamaki E, Kalonji-Mukendi T, Pukuta E, Hoff NA, et al.; International Mpox Research Consortium. Clade I–associated mpox cases associated with sexual contact, the Democratic Republic of the Congo. Emerg Infect Dis. 2024;30:172–6. https://doi.org/10.3201/eid3001.231164
8. Ministry of Public Health, Hygiene and Prevention of the Democratic Republic of the Congo. Report on the epidemiological situation of monkeypox virus—S1–S6 2024. Kinshasa: The Ministry; 2024.
9. World Health Organization. Disease Outbreak News: mpox—Democratic Republic of the Congo; 2024 Jun 14 [cited 2024 Jun 25]. https://www.who.int/emergencies/disease-outbreak-news/item/2024-DON522
10. Mbala-Kingebeni P, Rimoin AW, Kacita C, Liesenborghs L, Nachega JB, Kindrachuk J. The time is now (again) for mpox containment and elimination in Democratic Republic of the Congo. PLOS Glob Public Health. 2024;4:e0003171. https://doi.org/10.1371/journal.pgph.0003171
11. Besombes C, Mbrenga F, Schaeffer L, Malaka C, Gonofio E, Landier J, et al. National monkeypox surveillance, Central African Republic, 2001–2021. Emerg Infect Dis. 2022;28:2435–45. https://doi.org/10.3201/eid2812.220897
12. Kalyaanamoorthy S, Minh BQ, Wong TKF, von Haeseler A, Jermiin LS. ModelFinder: fast model selection for accurate

phylogenetic estimates. Nat Methods. 2017;14:587–9. https://doi.org/10.1038/nmeth.4285
13. Minh BQ, Schmidt HA, Chernomor O, Schrempf D, Woodhams MD, von Haeseler A, et al. IQ-TREE 2: new models and efficient methods for phylogenetic inference in the genomic era. Mol Biol Evol. 2020;37:1530–4. https://doi.org/10.1093/molbev/msaa015
14. Berthet N, Descorps-Declère S, Besombes C, Curaudeau M, Nkili Meyong AA, Selekon B, et al. Genomic history of human monkey pox infections in the Central African Republic between 2001 and 2018. Sci Rep. 2021;11:13085. https://doi.org/10.1038/s41598-021-92315-8

Address for correspondence: Anne W. Rimoin, Department of Epidemiology, Gordon-Levin Endowed Chair in Infectious Diseases and Public Health, UCLA Fielding School of Public Health, 650 Charles E. Young Dr, CHS 41-275, Los Angeles, CA 90095, USA; email: arimoin@ucla.edu; Placide Mbala-Kingebeni, School of Medicine, University of Kinshasa (UNIKIN), Department of Epidemiology and Global Health, Institute National de la Recherche Biomédicale (INRB), Kinshasa, Democratic Republic of the Congo; email: mbalaplacide@gmail.com

Highly Pathogenic Avian Influenza A Virus in Wild Migratory Birds, Qinghai Lake, China, 2022

Xiaoqing Zhang,[1] Jiaying Wu,[1] Yanhai Wang, Mengchan Hao, Haizhou Liu, Sanling Fan, Juan Li, Jianqing Sun, Yubang He, Yuan Zhang, Jianjun Chen

In July 2022, an outbreak of highly pathogenic avian influenza A(H5N1) virus clade 2.3.4.4b occurred among migratory birds at Qinghai Lake in China. The virus circulated in June, and reassortants emerged after its introduction into the area. Surveillance in 2023 showed that the virus did not establish a stable presence in wild waterfowl.

Qinghai Lake in China, situated at the intersection of the Central Asian and East Asian–Australasian Flyways, is the largest lake in the Qinghai–Tibet Plateau (*1*). This breeding and stopover area for migratory birds supports ≥200,000 waterfowl each year (*2*). Historically, 4 outbreaks of highly pathogenic avian influenza viruses (HPAIVs) at Qinghai Lake occurred in 2005 (*3*), 2009 (*4*), 2015 (*5*), and 2016 (*6*) during the breeding season (May–August). Since 2015, we have performed long-term avian influenza surveillance at Qinghai Lake during the breeding season. Our previous studies have reported HPAIV outbreaks of H5N1 clade 2.3.2.1c in 2015 and H5N8 clade 2.3.4.4b in 2016 at Qinghai Lake (*5*–*7*). Since late 2020, H5N1 clade 2.3.4.4b viruses, which are descendant of H5N8 clade 2.3.4.4b viruses, have emerged and become the dominant HPAIVs and caused outbreaks worldwide (*8*). We describe data collected from our ongoing surveillance of avian influenza in the Qinghai Lake area and record the introduction of clade H5N1 2.3.4.4b to Qinghai Lake birds in 2022.

Author affiliations: Wuhan Institute of Virology, Wuhan, China (X. Zhang, J. Wu, Y. Wang, M. Hao, H. Liu, S. Fan, Y. Zhang, J. Chen); University of Chinese Academy Sciences, Beijing, China (X. Zhang, J. Wu, Y. Wang, M. Hao, S. Fan); Shandong First Medical University & Shandong Academy of Medical Sciences, Taian, China (J. Li); Qinghai Lake National Nature Reserve, Qinghai, China (J. Sun, Y. He)

DOI: https://doi.org/10.3201/eid3010.240460

The Study

During 2019–2021, we collected fresh fecal samples annually from the wetlands around Qinghai Lake during the avian breeding season (Figure 1). No HPAIV was detected in 2019–2021, and only 8 strains of low pathogenic avian influenza viruses (LPAIVs) were isolated (Appendix Table 1, https://wwwnc.cdc.gov/EID/article/30/10/24-0460-App1.pdf). In June 2022, a highly pathogenic H5N1 virus emerged, and 8 strains were isolated from 726 fresh fecal samples (1.1%) (Figure 2). In addition, 5 decomposed bird carcasses were found at the sampling sites in June 2022, and H5N1 virus was isolated from a swab sample of a bar-headed goose (*Anser indicus*) carcass. In July 2022, an outbreak occurred, and ≥200 birds died. Our surveillance data showed the positivity rate of H5N1 virus in fecal samples was 0.68% (5/730) in July 2022 (Figure 2). H5N1 viruses were also isolated from tissue samples of the carcasses of 12 birds (Appendix Table 2).

In 2023, we collected 3,481 fecal samples during May–September and obtained tissue samples from 9 wild bird carcasses (Appendix Table 2). No highly pathogenic H5 viruses were isolated from fecal or tissue samples in 2023, although several strains of low pathogenicity avian influenza viruses (LPAIVs) were isolated (Appendix Table 1). By using next-generation sequencing, we performed whole-genome sequencing of 25 H5N1 and other subtypes of avian influenza viruses isolated during 2022 and 2023 (Appendix).

To understand the genetic relationship between the Qinghai Lake H5N1 viruses and other viruses, we performed phylogenetic analysis of the 25 H5N1 strains and relevant sequences from public databases. The phylogenetic analysis of hemagglutinin (HA) showed that Qinghai Lake H5N1 belonged to clade 2.3.4.4b (Appendix Figure 1). Moreover, examination

[1]These authors contributed equally to this article.

Figure 1. Fecal sample collection for the surveillance of avian influenza viruses at Qinghai Lake, China. Sampling sites in Qinghai Lake during the breeding season are shown. Inset map shows location of Qinghai Lake (blue) and the surrounding area in China.

of the phylogenetic evolution trees of neuraminidase, polymerase basic 1 and 2, polymerase acidic (PA), nucleoprotein, matrix, and nonstructural protein genes indicated that Qinghai Lake H5N1 viruses clustered together with H5N1 strains isolated from wild birds and poultry in China (*9*), Japan (*10*), South Korea (*11*), Bangladesh (*12*), and Malaysia from the end of 2021 through the first half of 2023 (Appendix Figure 2). Those findings suggest a close genetic relationship between Qinghai Lake H5N1 viruses and strains from countries or regions along the East Asian–Australasian and Central Asian migration flyways.

In the phylogenetic tree of the PA gene (Appendix Figure 2), the Qinghai Lake strains fell into 2 branches and only 1 strain (A/Bar-headed goose/Qinghai/06-225-2/2022 [H5N1]) clustered together with the LPAIV H10 strain isolated from Qinghai Lake in the same month, forming a separate monocluster with LPAIVs from China, Japan, South Korea, and Bangladesh. Analysis on the basis of the different sources of the PA gene revealed 2 genotypes among the 25 H5N1 strains (Figure 3); most H5N1 strains belonged to genotype G1 (n = 24) and only A/Bar-headed goose/Qinghai/06-225-2/2022 (H5N1) strains

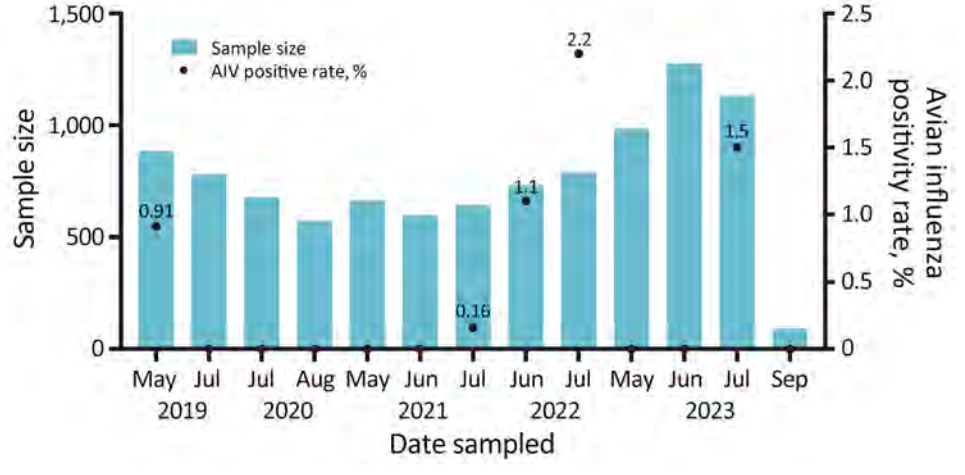

Figure 2. Monthly sample sizes and positivity rates from fecal sample collection for surveillance of AIVs at Qinghai Lake, China. AIV, avian influenza virus.

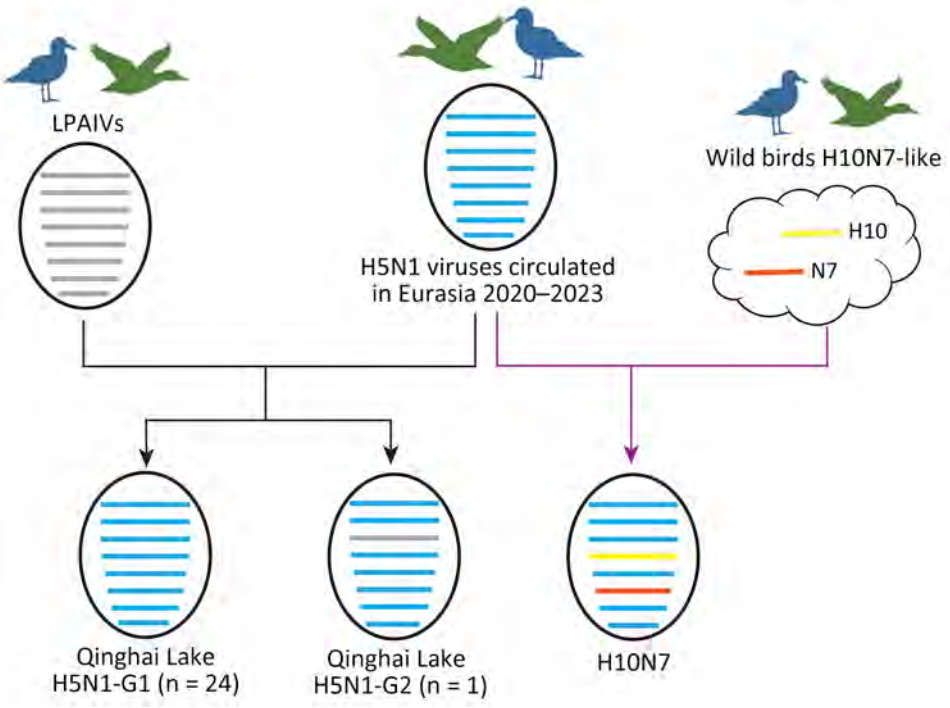

Figure 3. Hypothetical reassortment pathway of avian influenza virus H5N1 and H10N7 isolates collected at Qinghai Lake, China, in 2022. Virus particles are shown as ovals containing horizontal bars representing 8 gene segments (top to bottom: polymerase basic 1 and 2, polymerase acidic, hemagglutinin, nucleoprotein, neuraminidase, matrix, and nonstructural). The colors represent the genetic origin of reassortments found. G1, genotype 1; G2, genotype 2; LPAIVs, low pathogenic avian influenza viruses.

belonging to genotype G2 (n = 1). In the phylogenetic trees of 6 internal protein genes, H10N7 strain A/Bar-headed goose/Qinghai/06-JXG-1/2022, isolated from Qinghai Lake in June 2022, clustered together with the Qinghai Lake H5N1 strains (Appendix Figure 2), indicating reassortment between H5N1 and H10N7 viruses. The phylogenetic results showed that, after H5N1 virus was introduced into Qinghai Lake, reassortment occurred with LPAIVs in local wild birds. Of note, H5N1 acquired the PA gene from the low pathogenicity strain, leading to the emergence of a new genotype strain. The H10N7 strain obtained all 6 internal genes from H5N1 through reassortment (Figure 3).

Amino acid sequence analysis showed that all the 25 H5N1 viruses isolated in June and July 2022

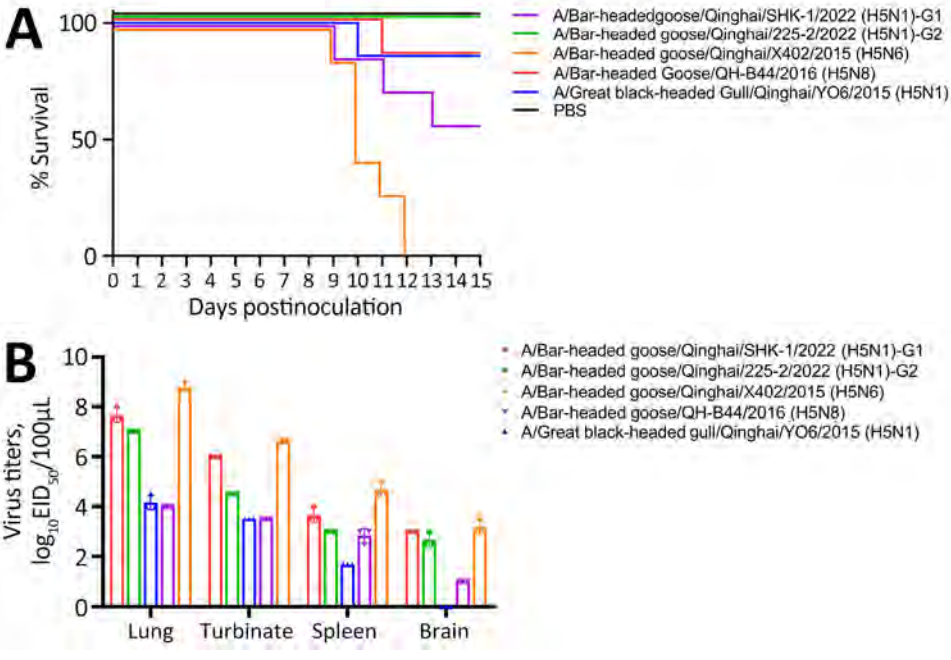

Figure 4. Mouse models of replication and pathogenicity of highly pathogenic H5 avian influenza viruses isolated from wild birds at Qinghai Lake, China. Each group of mice was inoculated intranasally at a dose of 10^6 EID_{50} of H5N1 (3 strains), H5N8, and H5N6 viruses. Mice in the control group were inoculated with PBS. A) Kaplan–Meier survival curve. B) Organ viral titers determined at 3 days postinoculation by measuring EID_{50} in organ tissue from infected mice. Three mice from each group were euthanized for organ tissue collection. EID_{50}, 50% egg infectious dose; PBS, phosphate-buffered saline.

were HPAIVs (Appendix Table 3). Those viruses contain multiple basic amino acids (REKRRKR/G) at the HA protein cleavage site. The HA proteins of those viruses had T160A mutations that were associated with enhanced binding ability to the α-2,6 receptor (*13*). In addition, amino acid mutations associated with increased virulence and replication in mammals have been identified in multiple proteins (Appendix Table 3).

We evaluated the pathogenicity of Qinghai Lake isolates in BALB/c mice. The isolates included were 2022 H5N1 (clade 2.3.4.4b), 2015 H5N1 (clade 2.3.2.1c), 2015 H5N6 (clade 2.3.4.4), and 2016 H5N8 (clade 2.3.4.4) strains isolated by our group during surveillance and previous outbreaks. Inoculation with the Qinghai Lake genotype G1 H5N1 strain from 2022 resulted in a ≈43% mortality rate (3/7) in mice, whereas all mice in the genotype G2 infection group survived (Figure 4, panel A), indicating differences in the pathogenicity of G1 and G2 genotype strains. After inoculation with the 2016 H5N8 and 2015 H5N1 strains, 1/7 mice died, whereas the 2015 H5N6 strain caused death in all inoculated mice (Figure 4, panel A). We performed a virus titer analysis of multiple organs and found the Qinghai Lake viruses could replicate in the lungs, nasal turbinates, and spleens of mice. The viruses could also replicate in mouse brains, except for the 2015 H5N1 (clade 2.3.2.1c) strain (Figure 4, panel B).

Conclusions

Our surveillance data showed H5N1 clade 2.3.4.4b virus emerged in summer 2022 in the Qinghai Lake area. Because there is no poultry in the vicinity of Qinghai Lake, the virus was likely spread because of migratory birds, similar to the case for H5N8 in 2016 (*6*). In 2023, the H5N1 clade 2.3.4.4b virus was not detected, suggesting that this virus does not exhibit sustained circulation among wild birds at Qinghai Lake. Because the H5N1 clade 2.3.4.4b virus continues to circulate in other regions (*14*), it is possible for reintroduction to Qinghai Lake to cause an outbreak. Therefore, continuous surveillance of avian influenza virus in wild birds at Qinghai Lake is necessary.

The H5N1 clade 2.3.4.4b viruses isolated in this study had amino acid mutations associated with increased virulence and replication in mammals. Our animal experiment also demonstrated that genotype G1 of the H5N1 strain resulted in death in mice, suggesting that the virus has the potential to spill over to nonhuman mammals. Many livestock (mainly sheep, goats, and yaks) graze around Qinghai Lake, and wild birds and livestock often graze on the same grassland. A risk for transmission of H5N1 clade 2.3.4.4b virus from infected birds to livestock at Qinghai Lake exists, similar to bird-to-cow transmission of H5N1 clade 2.3.4.4b previously reported in the United States (*15*). Avian influenza virus surveillance should include livestock around Qinghai Lake.

Acknowledgments

We thank those who have submitted avian influenza virus sequences to the GISAID (http://platform.gisaid.org) and GenBank databases. We also thank Hao Tang, Jun Liu, Jia Wu, and Li Li.

This work was supported by the National Key R&D Program of China (2023YFC260550), National Natural Science Foundation of China (31970174), and Major Project of Guangzhou National Laboratory (GZNL2023A01001).

About the Author

Ms. Zhang is a postundergraduate student of the Wuhan Institute of Virology, Chinese Academic Sciences. Her research interests include molecular virology, evolution, and emerging influenza viruses at the animal–human interface.

References

1. Prosser DJ, Cui P, Takekawa JY, Tang M, Hou Y, Collins BM, et al. Wild bird migration across the Qinghai-Tibetan plateau: a transmission route for highly pathogenic H5N1. PLoS ONE. 2011;6:e17622.
2. Reserve QLNN. Qinghai Lake home to 200,000 migratory birds. 2018 [cited 2023 Aug 20] http://www.ecns.cn/hd/2018-08-20/detail-ifyxccrz0968790.shtml
3. Liu J, Xiao H, Lei F, Zhu Q, Qin K, Zhang XW, et al. Highly pathogenic H5N1 influenza virus infection in migratory birds. Science. 2005;309:1206. https://doi.org/10.1126/science.1115273
4. Hu X, Liu D, Wang M, Yang L, Wang M, Zhu Q, et al. Clade 2.3.2 avian influenza virus (H5N1), Qinghai Lake region, China, 2009–2010. Emerg Infect Dis. 2011;17:560–2. https://doi.org/10.3201/eid1703.100948
5. Bi Y, Chen J, Zhang Z, Li M, Cai T, Sharshov K, et al. Highly pathogenic avian influenza H5N1 clade 2.3.2.1c virus in migratory birds, 2014–2015. Virol Sin. 2016;31:300–5. https://doi.org/10.1007/s12250-016-3750-4
6. Li M, Liu H, Bi Y, Sun J, Wong G, Liu D, et al. Highly pathogenic avian influenza A(H5N8) virus in wild migratory birds, Qinghai Lake, China. Emerg Infect Dis. 2017;23:637–41. https://doi.org/10.3201/eid2304.161866
7. Chen J, Liang B, Hu J, Liu H, Sun J, Li M, et al. Circulation, evolution and transmission of H5N8 virus, 2016-2018. J Infect. 2019;79:363–72. https://doi.org/10.1016/j.jinf.2019.07.005
8. Xie R, Edwards KM, Wille M, Wei X, Wong SS, Zanin M, et al. The episodic resurgence of highly pathogenic avian influenza H5 virus. Nature. 2023;622:810–7. https://doi.org/10.1038/s41586-023-06631-2
9. Cui P, Shi J, Wang C, Zhang Y, Xing X, Kong H, et al. Global dissemination of H5N1 influenza viruses bearing the clade 2.3.4.4b HA gene and biologic analysis of the ones

detected in China. Emerg Microbes Infect. 2022;11:1693–704. https://doi.org/10.1080/22221751.2022.2088407
10. Soda K, Mekata H, Usui T, Ito H, Matsui Y, Yamada K, et al. Genetic and antigenic analyses of H5N8 and H5N1 subtypes high pathogenicity avian influenza viruses isolated from wild birds and poultry farms in Japan in the winter of 2021-2022. J Vet Med Sci. 2023;85:1180–9. https://doi.org/10.1292/jvms.23-0121
11. Cha RM, Lee YN, Park MJ, Baek YG, Shin JI, Jung CH, et al. Genetic characterization and pathogenesis of H5N1 high pathogenicity avian influenza virus isolated in South Korea during 2021–2022. Viruses. 2023;15:1403. https://doi.org/10.3390/v15061403
12. Barman S, Turner JCM, Kamrul Hasan M, Akhtar S, Jeevan T, Franks J, et al. Emergence of a new genotype of clade 2.3.4.4b H5N1 highly pathogenic avian influenza A viruses in Bangladesh. Emerg Microbes Infect. 2023;12:e2252510. https://doi.org/10.1080/22221751.2023.2252510
13. Linster M, van Boheemen S, de Graaf M, Schrauwen EJA, Lexmond P, Mänz B, et al. Identification, characterization, and natural selection of mutations driving airborne transmission of A/H5N1 virus. Cell. 2014;157:329–39. https://doi.org/10.1016/j.cell.2014.02.040
14. Adlhoch C, Fusaro A, Gonzales JL, Kuiken T, Mirinavičiūtė G, Niqueux É, et al.; European Food Safety Authority; European Center for Disease Prevention and Control; European Union Reference Laboratory for Avian Influenza. Avian influenza overview September–December 2023. EFSA J. 2023;21:e8539.
15. Oguzie JU, Marushchak LV, Shittu I, Lednicky JA, Miller AL, Hao H, et al. Avian influenza A(H5N1) virus among dairy cattle, Texas, USA. Emerg Infect Dis. 2024;30:1425–9. https://doi.org/10.3201/eid3007.240717

Address for correspondence: Jianjun Chen, Wuhan Institute of Virology, 44 Xiaohongshan, Wuhan 430071, China: email: chenjj@wh.iov.cn

Circovirus Hepatitis in Immunocompromised Patient, Switzerland

Baptiste Hamelin,[1] Philippe Pérot,[1] Ian Pichler,[1] Jasmin D. Haslbauer, David Hardy, David Hing, Sarra Loulizi, Béatrice Regnault, Anouk Pieters, Ingmar Heijnen, Caroline Berkemeier, Maria Mancuso, Verena Kufner, Niels Willi, Anne Jamet, Nolwenn Dheilly, Marc Eloit, Mike Recher, Michael Huber,[2] Kirsten D. Mertz[2]

We identified a novel human circovirus in an immunocompromised 66-year-old woman with sudden onset of self-limiting hepatitis. We detected human circovirus 1 (HCirV-1) transcripts in hepatocytes and the HCirV-1 genome long-term in the patient's blood, stool, and urine. HCirV-1 is an emerging human pathogen that persists in susceptible patients.

Circoviruses are an emerging group of DNA viruses with largely unknown pathogenicity in humans (*1*,*2*). The best-studied circovirus is porcine circovirus 2, which causes hepatitis in pigs, among other diseases (*3*,*4*). Novel human circovirus 1 (HCirV-1) was recently linked to chronic infection and liver damage in an immunosuppressed patient (*5*).

The Study

A 66-year-old woman who sought care at a regional hospital in Switzerland had sudden elevation of hepatic transaminases in July 2022. Transaminases reached peak values in September 2022, without concurrent elevation of autoantibody in serologic tests (Figure 1). Results of serologic tests for hepatitis viruses A, B, C, and E were negative. When cytolytic hepatitis was diagnosed, the patient had had rheumatoid arthritis for 20 years, which had been treated with a daily dose of prednisolone (5 mg), intravenous rituximab (1,000 mg at 6-month intervals), and intermittent methotrexate. The most recent rituximab was given in June 2022, and methotrexate had been paused. Eight months before onset of hepatitis, the patient had been hospitalized for 2 months with SARS-CoV-2–associated acute respiratory distress syndrome (November–December 2021). During that hospitalization, she had a small intestine diverticular perforation, which required surgery, and macrocytic anemia, for which she received a blood transfusion. Throughout hospitalization, she received additional corticosteroids.

The patient lives alone in rural Switzerland, without direct contact with animals. She had not traveled outside Switzerland during the past 8 years. Her dietary habits were unremarkable except for sporadic consumption of raw calf liver, which she most recently consumed before 2018. She eats cured pork and beef products and gets milk from the supermarket.

Because of the unclear increase in liver enzymes, the treating physician performed a liver biopsy in October 2022 (Figure 1). Histologic analysis revealed acute and subacute hepatitis with a periportal mixed inflammatory infiltrate consisting of lymphocytes, histiocytes, plasma cells, and neutrophilic and eosinophilic granulocytes (Appendix Figure 1, https://wwwnc.cdc.gov/EID/article/30/10/24-0678-App1.pdf). Necroinflammatory foci associated with fat droplets, fibrin, or both were reported. The pathologist categorized the changes most likely as infectious hepatitis. Histologic differential diagnoses included drug-related hepatitis and autoimmune hepatitis,

Author affiliations: Cantonal Hospital Baselland, Liestal, Switzerland (B. Hamelin, M. Mancuso, N. Willi, K.D. Mertz); University Hospital Basel, Basel, Switzerland (B. Hamelin, J.D. Haslbauer, I. Heijnen, C. Berkemeier, M. Mancuso, N. Willi, M. Recher, K.D. Mertz); Institut Pasteur, Paris, France (P. Pérot, D. Hardy, D. Hing, S. Loulizi, B. Regnault, N. Dheilly, M. Eloit); University of Zurich, Zurich, Switzerland (I. Pichler, V. Kufner, M. Huber); University of Basel Department of Biomedicine, Basel (A. Pieters, M. Recher, K.D. Mertz); Assistance Publique–Hôpitaux de Paris Centre Université de Paris Cité Necker-Enfants Malades Hospital, Paris (A. Jamet)

DOI: https://doi.org/10.3201/eid3010.240678

[1]These first authors contributed equally to this article.

[2]These senior authors contributed equally to this article.

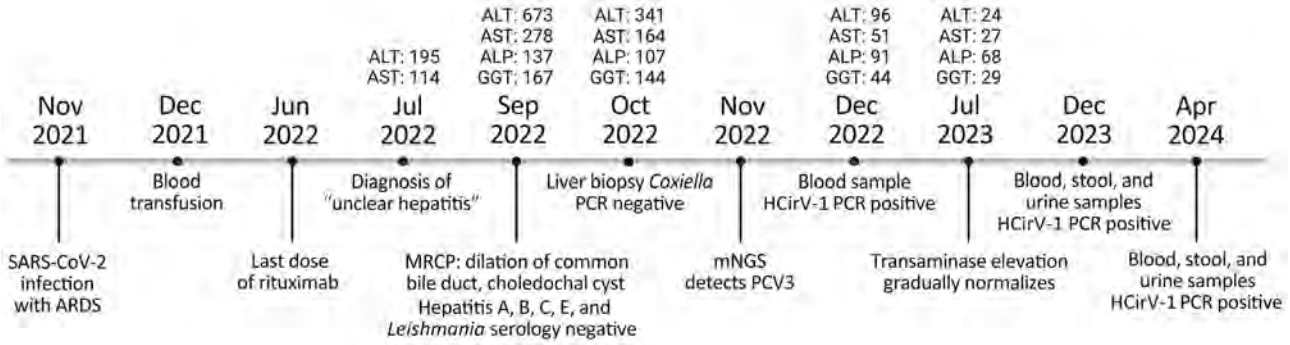

Figure 1. Clinical course of patient with hepatitis of unknown origin, Switzerland, November 2021–April 2024. Top of timeline shows results of enzyme level testing, expressed as units per liter; bottom of timeline shows clinical course. ALP, alkaline phosphatase; ALT, alanine aminotransferase; ARDS, acute respiratory distress syndrome; AST, aspartate aminotransferase; GGT, gammaglutamyl transferase; HCirV-1, human circovirus; mNGS, metagenomic next-generation sequencing; MRCP, magnetic resonance cholangiopancreatography; PCV3, porcine circovirus 3.

both of which seemed highly unlikely (i.e., no change in medication and no autoantibodies in serologic tests). Several pathogens, including *Coxiella burnetii* bacteria, cytomegalovirus, Epstein-Barr virus, and *Leishmania*, were ruled out by laboratory testing ordered by the treating physician. Transaminase levels gradually decreased and eventually normalized in July 2023.

To clarify the origin of the hepatitis, we analyzed the liver biopsy with a metagenomic next-generation sequencing workflow to identify pathogens (*6*–*8*). We identified some reads that were initially assigned to porcine circovirus 3 (PCV3) (Appendix Table 1). After publication of the HCirV-1 genome (HCirV-1-FR), we incorporated the HCirV-1 genome sequence into our taxonomic profiling index, reanalyzed our sequencing data, and found greater sequence identity with HCirV-1 than with PCV3 or any other circovirus (Appendix Table 2). We analyzed sequencing data by using Microseek to help identify more distant sequences (*9*). We deposited the full-length genome sequence of the HCirV-1 strain from Switzerland (HCirV-1-CH) into GenBank (accession no. OR905605).

The nucleotide identities of HCirV-1-FR and HCirV-1-CH at the full-genome level were 83.6% similar, higher for the polymerase gene (91.2% nucleotide identity, 95.6% amino acid identity) and lower for the capsid gene (69.4% nucleotide identity; 64.1% amino acid identity). Phylogenetic analysis based on the capsid protein clustered HCirV-1-FR and HCirV-1-CH together and indicated that our patient had a novel strain of HCirV-1. HCirV-1-FR and HCirV-1-CH cluster closely with the circovirus sequence recently described in drug users in China (*10*). HCirV-1-FR, HCirV-1-CH, and the strains from China form a new phylogenetic clade distinct from other animal circoviruses (Figure 2).

We confirmed the presence of HCirV-1 in the liver biopsy by using HCirV-1–specific PCRs. We used HCirV-1-FR–specific primers and a second pair of primers adapted to target the broadening clade of human circoviruses, including the strains from China, but not any animal strains (Figure 3; Appendix Figure 2) (*5*,*11*). Although both primer sets successfully amplified the HCirV-1-CH strain despite several mismatches between HCirV-1-FR primers and HCirV-1-CH, the second pair of primers led to more efficient amplification, so we used them for subsequent quantification. We found HCirV-1 viral load to be high in the liver biopsy (3.39×10^9 genome copies/g or 3.63×10^9 genome copies/mL) (Figure 4; Appendix Table 3).

Archival formalin-fixed paraffin-embedded tissues of the patient were available, including biopsies from the gastrointestinal tract taken before the diagnosis of circovirus hepatitis. We tested all of those tissue samples with HCirV-1–specific PCRs, and the results were negative (i.e., we did not detect HCirV-1 before hepatitis nor outside the liver) (Appendix Table 4).

We retrospectively analyzed an archival blood sample from the period when the patient had hepatitis (December 2022) by using HCirV-1–specific PCRs; results were positive, indicating viremia (Figure 4; Appendix Table 3). In more recent blood, stool, and urine samples (taken December 2023–April 2024 [i.e., 17–21 months after the hepatitis diagnosis]), we still detected HCirV-1 in blood; viral loads remained high. We detected HCirV-1, albeit with lower viral loads, in urine and stool (Figure 4; Appendix Table 3). We also detected HCirV-1 in a saliva sample (April 2024), albeit with a low viral load. Those data confirm HCirV-1 persistence in this patient for ≥21 months and that the patient

continuously shed the virus. We re-sequenced HCirV-1-CH in the most recently collected blood and could not detect notable changes in the genome, meaning that the virus has not mutated over time, which was consistent with low selection pressure from a suppressed immune system. Because the patient had been transfused with an erythrocyte concentrate (December 2021), we analyzed the

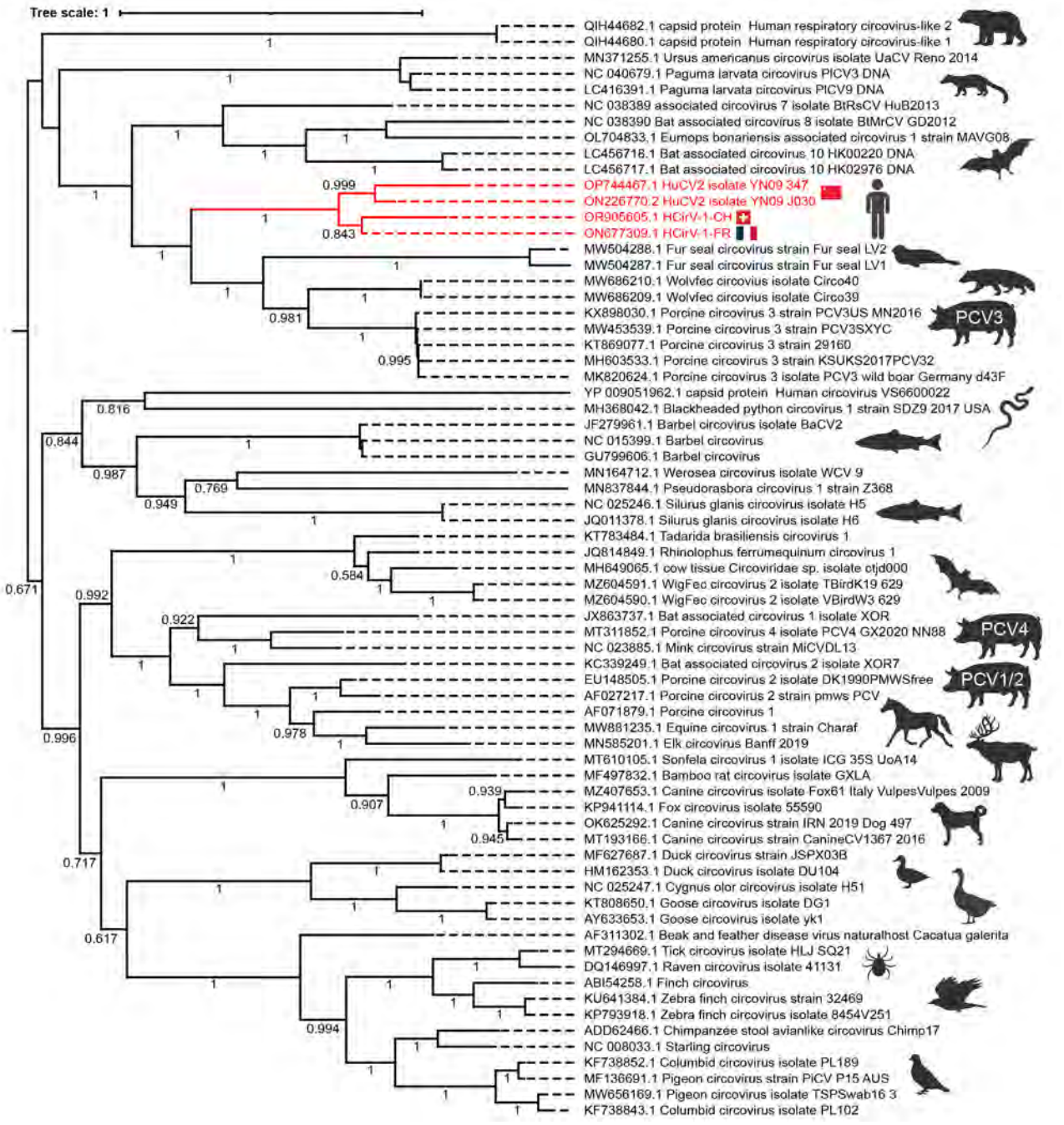

Figure 2. Phylogenetic analysis of the circovirus isolate from a patient with hepatitis of unknown origin, Switzerland (HCirV-1-CH). Capsid protein sequences representative of human and animal circovirus strains are shown. We aligned sequences by using MAFFT (https://mafft.cbrc.jp/alignment/software) under the L-INS-I parameter and performed maximum-likelihood phylogenetic reconstruction through the IQ-Tree portal (http://www.iqtree.org). Red indicates HCirV-1-FR, HCirV-1-CH, and HuCV2 sequences. Tree scale indicates the number of amino acid substitutions per site. Display range for bootstraps is 0.5–1.0. GenBank accession numbers are provided. HCirV-1-CH, human circovirus 1 from patient in Switzerland; HCirV-1-FR, published human circovirus 1 genome from France; HuCV2, human circovirus sequence detected in injection drug users in China (*10*); PCV, porcine circovirus.

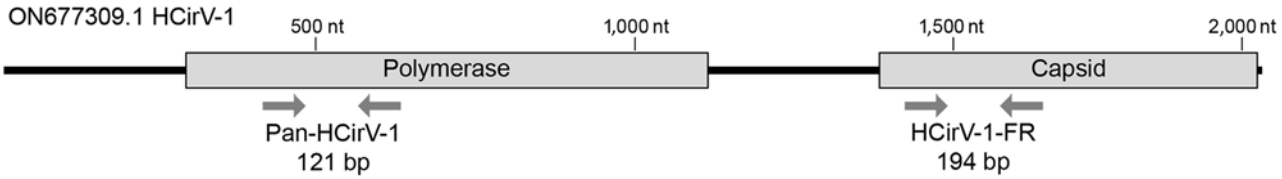

Figure 3. Nonhuman metagenomic next-generation sequencing reads from liver biopsy of hepatitis patient in Switzerland mapped against the human circovirus genome (Appendix Tables 1, 2, https://wwwnc.cdc.gov/EID/article/30/10/24-0678-App1.pdf). Positions of the putative sequences for polymerase and capsid proteins and the 2 primer pairs (HCirV-1-FR, Pan-HCirV-1) used for the PCRs are indicated. HCirV-1-FR, published human circovirus 1 genome from France (GenBank accession no. ON677309.1); Pan-HCirV-1, primers adapted to target the broadening clade of human circoviruses.

donor's serum by using HCirV-1–specific PCRs, which were negative, showing that the virus had not been acquired during blood transfusion.

To characterize the tropism of HCirV-1-CH, we used RNAscope in situ hybridization (Bio-Techne, https://www.bio-techne.com) to localize the HCirV-1-CH nucleic acids in the patient's liver tissue. The probes targeting HCirV-1-CH stained ≈40% of the hepatocytes (Appendix Figure 3), whereas no staining of normal liver tissues (n = 3) or of liver tissues from patients infected with hepatitis viruses B or C (n = 4) occurred (Appendix Table 5). The areas with the strongest positivity co-localize with the nuclei, which is consistent with nuclear replication of circoviruses and therefore supports the assumption of replicative activity of the virus, even if the RNA cannot be quantified.

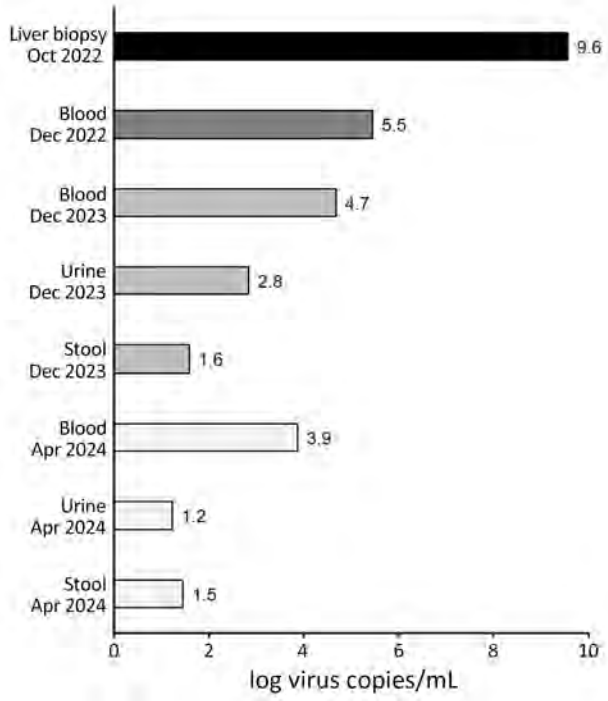

Figure 4. Human circovirus 1 viral loads in recently collected and archival samples (2023 and 2024) compared with viral load in initial liver biopsy (2022) from a hepatitis patient, Switzerland. Virus copies and log virus copies were also tabulated (Appendix Table 3, https://wwwnc.cdc.gov/EID/article/30/10/24-0678-App1.pdf).

This patient had a moderately severe antibody deficiency and missing B cells consistent with years of immunosuppressive therapy (Appendix, Appendix Table 6). She also had a dysfunction in the activation of the complement system through the mannose-binding lectin pathway. Low numbers of B cells and immunoglobulins probably contributed to the persistence of HCirV-1-CH in this patient.

Conclusions

We report a case of HCirV-1–associated hepatitis (*5*) that strengthens the assumption that circoviruses are emerging new pathogens in humans, particularly among immunosuppressed patients (*5*,*10*). Our study provides clues to the understanding of HCirV-1 pathobiology and transmission. We ruled out human-to-human transmission through blood transfusion. We show that the virus can persist in humans for a prolonged period and that it is shed in body fluids, thus posing a risk for horizontal transmission in human populations. Of note, parallels can be drawn with porcine circoviruses, which also have an exceptional ability to cause persistent infections and to be shed in fluids, enabling them to spread rapidly in pig populations worldwide after their initial emergence (*12*). In tandem with testing more donor plasma pools, wastewater testing for HCirV-1 could elucidate the regional distribution and prevalence of HCirV-1 infections.

About the Author

Dr. Hamelin is a molecular biologist supervising the molecular infectious pathology laboratory at the Cantonal Hospital Baselland and the University Hospital Basel, Switzerland. His primary research interests include clinical metagenomics and next-generation sequencing of formalin-fixed paraffin-embedded human tissues.

Acknowledgments

The authors thank the patient who participated in this study and her general practitioner.

This work was supported at the University of Zurich by the Clinical Research Priority Program titled Comprehensive Genomic Pathogen Detection. The funding body did not have any role in the design of the study, in the collection, analysis, and interpretation of data, or in the writing of the manuscript.

The high-throughput sequencing data acquired for this study are accessible through the European Nucleotide Archive (https://www.ebi.ac.uk) (accession no. PRJEB75433). The HCirV1-CH genome is available on GenBank (accession no. OR905605).

Author contributions: data acquisition, including histologic analysis (B.H., P.P., I.P., J.D.H., B.R., A.P., I.H., C.B., M.M., V.K., N.W., N.D., M.R., M.H., and K.D.M.); PCR and metagenomic next-generation sequencing assays (B.H., P.P., I.P., and M.M.); clinical information (J.D.H., N.W., M.R., M.H., and K.D.M.); in situ hybridization (D.H., D.H., and S.L.); and manuscript, including critical appraisal (B.H., P.P., I.P., J.D.H., N.W., A.J., N.D., M.E., M.H., and K.D.M.).

References

1. Opriessnig T, Xiao CT, Mueller NJ, Denner J. Emergence of novel circoviruses in humans and pigs and their possible importance for xenotransplantation and blood transfusions. Xenotransplantation. 2024;31:e12842. https://doi.org/10.1111/xen.12842
2. Kroeger M, Temeeyasen G, Piñeyro PE. Five years of porcine circovirus 3: what have we learned about the clinical disease, immune pathogenesis, and diagnosis. Virus Res. 2022;314:198764. https://doi.org/10.1016/j.virusres.2022.198764
3. Niu G, Chen S, Li X, Zhang L, Ren L. Advances in crosstalk between porcine circoviruses and host. Viruses. 2022;14:1419. https://doi.org/10.3390/v14071419
4. Rosell C, Segalés J, Domingo M. Hepatitis and staging of hepatic damage in pigs naturally infected with porcine circovirus type 2. Vet Pathol. 2000;37:687–92. https://doi.org/10.1354/vp.37-6-687
5. Pérot P, Fourgeaud J, Rouzaud C, Regnault B, Da Rocha N, Fontaine H, et al. Circovirus hepatitis infection in heart-lung transplant patient, France. Emerg Infect Dis. 2023;29:286–93. https://doi.org/10.3201/eid2902.221468
6. Nienhold R, Mensah N, Frank A, Graber A, Koike J, Schwab N, et al. Unbiased screen for pathogens in human paraffin-embedded tissue samples by whole genome sequencing and metagenomics. Front Cell Infect Microbiol. 2022;12:968135. https://doi.org/10.3389/fcimb.2022.968135
7. Fourgeaud J, Regnault B, Ok V, Da Rocha N, Sitterlé É, Mekouar M, et al. Performance of clinical metagenomics in France: a prospective observational study. Lancet Microbe. 2024;5:e52–61. https://doi.org/10.1016/S2666-5247(23)00244-6
8. Chiu CY, Miller SA. Clinical metagenomics. Nat Rev Genet. 2019;20:341–55. https://doi.org/10.1038/s41576-019-0113-7
9. Pérot P, Bigot T, Temmam S, Regnault B, Eloit M. Microseek: a protein-based metagenomic pipeline for virus diagnostic and discovery. Viruses. 2022;14:1990. https://doi.org/10.3390/v14091990
10. Li Y, Zhang P, Ye M, Tian RR, Li N, Cao L, et al. Novel circovirus in blood from intravenous drug users, Yunnan, China. Emerg Infect Dis. 2023;29:1015–9. https://doi.org/10.3201/eid2905.221617
11. Pérot P, Da Rocha N, Farcet MR, Kreil TR, Eloit M. Human circovirus is not detected in plasma pools for fractionation. Transfusion. 2024;64:16–8. https://doi.org/10.1111/trf.17604
12. Turlewicz-Podbielska H, Augustyniak A, Pomorska-Mól M. Novel porcine circoviruses in view of lessons learned from porcine circovirus type 2-epidemiology and threat to pigs and other species. Viruses. 2022;14:261. https://doi.org/10.3390/v14020261

Address for correspondence: Kirsten D. Mertz, Chefärztin Pathologie, Universitätsspital Basel, Institut für Medizinische Genetik und Pathologie, Schönbeinstrasse 40, CH-4031 Basel, Switzerland; email: kirsten.mertz@usb.ch

Mpox Epidemiology and Vaccine Effectiveness, England, 2023

Hannah Charles, Katie Thorley, Charlie Turner, Kirsty F. Bennet, Nick Andrews, Marta Bertran, Sema Mandal, Gayatri Amirthalingam, Mary E. Ramsay, Hamish Mohammed, Katy Sinka

Reported mpox cases in England continued at a low but steady frequency during 2023. Of 137 cases reported in 2023, approximately half were acquired overseas and half were in vaccinated persons. Estimated effectiveness of 2-dose vaccine was 80%, and no vaccinated mpox patient was hospitalized.

In England, after the July 2022 peak in the mpox outbreak (*1*), which affected primarily gay, bisexual, and other men who have sex with men (GBMSM), cases declined and remained low into 2023 (*2*). We analyzed the epidemiology of postpeak mpox cases in 2023 in England, describing case-patient characteristics including vaccination status and providing an updated estimate of Modified Vaccinia Ankara–Bavarian Nordic (MVA-BN) vaccine effectiveness (VE).

The Study

We extracted records of confirmed and highly probable mpox diagnoses reported during January 1–December 31, 2023, from the UK Health Security Agency (UKHSA) Second Generation Surveillance System (SGSS) and deduplicated them by using specimen and patient identifiers. We defined a confirmed case as a positive monkeypox virus–specific PCR result and a highly probable case as a positive *Orthopoxvirus* PCR result (*3*). SGSS receives positive test results from all diagnostic laboratories in England (*4*). Because mpox is notifiable in England (*5*), reporting to SGSS is probably complete. UKHSA local Health Protection Teams collected self-reported epidemiologic and behavioral information (including vaccination status). NHS England provided aggregate data for mpox vaccinations administered in 2022 and 2023. We estimated overall VE by using the screening method (*6*). For the primary VE analysis, the eligible GBMSM denominator was 89,240 and was 20% higher at 107,088 according to a sensitivity analysis, similar to previous analyses (*7*). We estimated the proportion of GBMSM vaccinated by matching each case to the 1- and 2-dose coverage at the time, 2 weeks before persons became case-patients, then averaging the matched coverage across cases. For the 22 case-patients for whom vaccination status was unknown, we assumed that they would be distributed among those with 0, 1, and 2 doses in the same ratio as the observed ratio for these groups, to give a corrected value. We tested the difference between 1-dose and 2-dose VE estimates by using the Pearson χ^2 test at 5% significance.

During January 1–December 31, 2023, a total of 137 mpox cases were reported (Appendix Figure, https://wwwnc.cdc.gov/EID/article/30/10/24-0292-App1.pdf), 135 confirmed and 2 highly probable. Most case-patients (105/137 [77%]) were London residents, comparable to case-patients in 2022 (Table 1). Of the 137 case-patients, 64 (47%) reported no travel outside the United Kingdom in the 21 days before symptom onset, indicating probable acquisition in the United Kingdom; 58 (91%) of the 64 identified as GBMSM. Of the 137 case-patients, 53 (39%) reported international travel, among which 43 (81%) identified as GBMSM and reported traveling to Europe, the Middle East, Asia Pacific region, and North America.

Most case-patients identified as GBMSM (107/137 [78%]); another 21 were adult men without recorded information about sexual orientation and no travel to the mpox-endemic countries in Central or West Africa. We included all of them as part of the 2022–2023 global clade IIb mpox outbreak, totaling 128 case-patients. Of the 9 case-patients excluded from the subsequent analysis, 8 were directly or indirectly linked to an mpox-endemic country; sporadic cases were distributed across time, and case-patients were heterosexual persons or children.

Most case-patients associated with the outbreak were HIV negative (69/128 [54%]), of whom most (51/69 [74%]) were taking HIV preexposure

Author affiliation: UK Health Security Agency, London, UK

DOI: https://doi.org/10.3201/eid3010.240292

Table 1. Available demographic characteristics of mpox case-patients, England, 2022 and 2023*

Variable	Year, no, (%)	
	2022, n = 3,412†	2023, n = 137
Region		
London	2,359 (69)	105 (77.0)
Outside London	1,040 (30)	32 (23.0)
Unknown	13 (0.4)	0
Sex		
M	3,345 (98)	135 (99.0)
F	45 (1.3)	1 (0.7)
Unknown	22 (0.6)	1 (0.7)
Sexual orientation GBMSM	983 (97)‡	128 (93)§

*Patients were median 36 years of age for both years (IQR 30–44 y in 2022 and 29–43 y in 2023). IQR, interquartile range; GBMSM, gay, bisexual, and other men who have sex with men.
†May 6–Sep 16, 2022 (*1*).
‡Obtained via enhanced surveillance questionnaires, which were complete for 31% of case-patients by September 18, 2022.
§107 case-patients self-identified identifying as GBMSM plus 21 who were adult men without recorded information on sexual orientation and no travel to mpox-endemic countries in Central or West Africa but were presumed to be part of the outbreak.

prophylaxis. Of the 128 HIV-negative case-patients, 28 (22%) reported attending an event involving sexual contact with multiple partners, and 24 (19%) had received a concurrent diagnosis of a sexually transmitted infection (Table 2).

Almost half of the case-patients with known vaccination status were fully or partially vaccinated (≥1 dose) (52/106 [49%]), among whom 30 received ≥2 doses, 20 received 1 dose, and 2 did not report the number of doses. Among vaccinated case-patients, 20 (38%) reported attending an event involving sexual contact with multiple partners.

During July 2022–December 2023, a total of 77,543 GBMSM in England were vaccinated against mpox, 32,983 with 1 dose and 44,560 with 2 doses. MVA-BN vaccine coverage at the end of December 2023 was estimated at 37% for 1 dose and 50% for 2 doses (87% for 1 or 2 doses). Most vaccines had been given by March 2023 (91% first doses and 76% second doses).

VE of 1 dose was estimated at 84% (95% CI 74%–91%) (Table 3), comparable to the previous estimate of 78% (*7*). The VE of 2 doses was marginally, but not statistically significantly, lower than 1 dose, at 80% (95% CI 69%–83%) (p = 0.40). Overall VE of 1 or 2 doses was 82% (95% CI 74%–88%). Sensitivity analysis resulted in VE estimates that were markedly lower (Table 3), demonstrating that the method is affected by the estimated GBMSM population size.

Table 2. Characteristics and risk factors for case-patients with mpox confirmed or highly probable according to specimens collected in 2023, England*

Variable	No. (%), n = 128†
HIV status	
Living with HIV	13 (10)
HIV negative	69 (54)
Taking HIV PrEP‡	51 (74)
Not taking PrEP‡	18 (26)
Unknown	46 (36)
Modified Vaccinia Ankara–Bavarian Nordic vaccination status§	
Vaccinated: ≥2 doses¶	30 (23)
Vaccinated: 1 dose	20 (16)
Vaccinated: no. doses unknown	2 (2)
Unvaccinated	54 (42)
Unknown	22 (17)
Childhood smallpox vaccination status	
Vaccinated	4 (3)
Unknown	124 (97)
Hospital admission	
Yes	11 (9)
No	117 (91)
Unknown	
Reporting attending events involving multiple sex partners	
Yes	28 (22)
No	17 (13)
Unknown	83 (65)
Concurrent STI	
Yes	24 (19)
No	28 (22)
Unknown	76 (59)

*Patients were median 36 years of age, range 19–70 years, interquartile range 29–24 years. PrEP, preexposure prophylaxis; STI, sexually transmitted infection.
†Unless otherwise stated, denominators are 128; denominators for percentage calculations are HIV-negative persons.
‡We do not have information on HIV treatment or outcomes of treatment for these cases. Nevertheless, most people living with HIV in England take antiretroviral therapy and have an undetectable viral load (*8*).
§Estimated date of vaccination was available for 33 out of 52 vaccinated cases, all of whom received the Modified Vaccinia Ankara–Bavarian Nordic vaccine ≤2 weeks before infection.
¶Includes 1 person who reported receiving 3 doses.

Table 3. Vaccination status of mpox case-patients used to estimate vaccine effectiveness of various doses of Modified Vaccinia Ankara–Bavarian Nordic vaccine by using the screening method, England, 2023*

Doses	Cases in 2023	Corrected cases†	PCV, %	PPV, %	PPV, sensitivity, %‡	VE, % (95% CI)	VE sensitivity, % (95% CI)‡
0	54	65.4	52	16	30		
1	20	24.2	19	38	32	84 (74–91)	65 (42–79)
2	30	36.4	29	45	38	80 (69–83)	56 (31–72)
Unknown	22						
1 or 2	50	60.6	48	84	70	82 (74–88)	60 (41–73)
Total	126	126					

*PCV, percentage of case-patients with the given number of doses; PPV, percentage of the population with the given number of doses obtained by matching each case to the population uptake 14 d before onset and averaging this across cases; VE, vaccine effectiveness.
†22 case-patients with unknown vaccination status distributed among 0, 1, and 2 doses.
‡Based on the higher estimated denominator for gay, bisexual, men who have sex with men (107,088).

Among known vaccinated case-patients in 2023, none were hospitalized. Of 11 (9%) persons who required hospital treatment for mpox, 9 were unvaccinated and vaccination status was unknown for 2.

Conclusions

The low numbers of mpox cases in 2023 were initially interpreted as the final few cases of the 2022 outbreak (*1*). However, throughout the year, cases continued steadily, split evenly between imported infections and community transmission. The demographic and behavioral characteristics of mpox case-patients in 2023 remained comparable to those in 2022 (Table 1), indicating that mpox continues to circulate predominately within GBMSM sexual networks.

Nearly half of outbreak case-patients in 2023 were vaccinated, and there were more cases among those who had received 2 doses of MVA-BN vaccine than among those who had received 1 dose. Our analysis, based on full-year data from 2023, demonstrates that VE of 1 or 2 doses remains high (82%). The estimated VE for 2 doses compared with 1 dose was marginally lower, but the difference was not statistically significant. Considering that first doses will have been given farther in the past than second doses and that 2 doses would be expected to confer more protection, that finding is counterintuitive and may reflect differences in risk behavior among those who came forward for a second dose because they may also be at greater risk for exposure to monkeypox virus. Our observation is consistent with reports from other high-income countries with outbreaks predominantly among GBMSM. In May 2023, the Chicago Department of Public Health (Chicago, IL, USA) noted that most of the cases reported since mid-April were among men who had received 2 doses of MVA-BN vaccine (*9*), yet a higher number of first doses had been given compared with second doses overall (*10*).

We found that no vaccinated persons had been hospitalized for mpox in 2023, indicating that the MVA-BN vaccine probably protects against severe disease requiring hospitalization. Our finding is corroborated by a global case series that found illness among vaccinated persons to be less severe (*11*).

Among the limitations of our analysis, we were unable to examine VE in different population groups, because of unavailability of corresponding disaggregated coverage data. In addition, hospitalization resulting from clinical need was used as a proxy for severity, a pragmatic decision based on the unavailability of data using an objective measure.

Overall, the experience in England during 2023 was of continued low-level community transmission among GBMSM, as well as imported infections, which will probably continue. Given that ≈20 countries continued to report mpox cases in December 2023 and the World Health Organization assessment that the overall global risk for GBMSM remains moderate (*12*), continued low-level transmission is likely before elimination is reached. Our findings highlight the value of continued active prevention through vaccination and health promotion to persons at higher risk and ongoing surveillance to examine factors that contribute to continued transmission.

Acknowledgments

We thank NHS England for their collection and sharing of vaccination data for the mpox vaccination program and sexual health services for delivering the vaccines. We also thank the UKHSA Health Protection Teams for collecting epidemiologic information during public health management of cases.

No external funding was received for this work.

H.C. led the epidemiologic analysis and drafted the manuscript. K.T. and K.F.B. validated the epidemiologic data analysis. N.A. led the VE analysis. All co-authors contributed to interpretation of the findings and to revision of the manuscript.

Our analysis was undertaken for health protection purposes under permissions granted to the UKHSA to collect and process confidential patient data under Regulation 3 of The Health Service (Control of Patient Information) Regulations 2020 and Section 251 of the National Health Service (NHS) Act 2006.

About the Author

Ms. Charles is a principal epidemiologist at the UKHSA and was involved in the UK response to the global 2022 mpox outbreak. Her particular interest is outbreak investigation and real-time surveillance of sexually transmitted infections.

References

1. UK Health Security Agency. Monkeypox outbreak: technical briefing 8 [cited 2024 Feb 14]. https://www.gov.uk/government/publications/monkeypox-outbreak-technical-briefings/investigation-into-monkeypox-outbreak-in-england-technical-briefing-8
2. UK Health Security Agency. Mpox (monkeypox) outbreak: epidemiological overview [cited 2024 Feb 14]. https://www.gov.uk/government/publications/monkeypox-outbreak-epidemiological-overview
3. UK Health Security Agency. Mpox (monkeypox): case definitions [cited 2024 Feb 14]. https://www.gov.uk/guidance/monkeypox-case-definitions
4. UK Health Security Agency. Reporting to UKHSA: a guide for diagnostic laboratories [cited 2024 Feb 14]. https://assets.publishing.service.gov.uk/government/uploads/system/uploads/attachment_data/file/1159953/UKHSA_Laboratory_reporting_guidelines_May_2023.pdf
5. UK Health Security Agency. Notifiable diseases and causative organisms: how to report [cited 2024 Feb 14]. https://www.gov.uk/guidance/notifiable-diseases-and-causative-organisms-how-to-report
6. Flannery B, Andrews N, Feikin D, Patel MK. Commentary: estimation of vaccine effectiveness using the screening method. Int J Epidemiol. 2023;52:19–21. https://doi.org/10.1093/ije/dyac013
7. Bertran M, Andrews N, Davison C, Dugbazah B, Boateng J, Lunt R, et al. Effectiveness of one dose of MVA-BN smallpox vaccine against mpox in England using the case-coverage method: an observational study. Lancet Infect Dis. 2023;23:828–35. https://doi.org/10.1016/S1473-3099(23)00057-9
8. UK Health Security Agency. HIV action plan monitoring and evaluation framework [cited 2024 Apr 25]. https://www.gov.uk/government/publications/hiv-monitoring-and-evaluation-framework
9. Chicago Health Alert Network. Potential risk for new mpox cases—provider update: May 9, 2023 [cited 2024 Feb 14]. https://emergency.cdc.gov/han/2023/han00490.asp
10. Chicago Department of Public Health. Mpox dashboard [cited 2024 Feb 14]. https://www.chicago.gov/city/en/depts/cdph/provdrs/infectious_disease/supp_info/mpox-home/mpox-dashboard.html
11. Hazra A, Zucker J, Bell E, Flores J, Gordon L, Mitjà O, et al. Mpox in people with past infection or a complete vaccination course: a global case series. Lancet Infect Dis. 2023.
12. World Health Organization. Multi-country outbreak of mpox: external situation report #31—22 December 2023 [cited 2024 Feb 14]. https://www.who.int/publications/m/item/multi-country-outbreak-of-mpox--external-situation-report-31---22-december-2023

Address for correspondence: Hannah Charles, UK Health Security Agency, 61 Colindale Ave, London NW9 5EQ, UK; email: hannah.charles@ukhsa.gov.uk

Dengue Virus Serotype 3 Origins and Genetic Dynamics, Jamaica

Shanice A. Redman,[1] Lester J. Perez,[1] Kenn Forberg, Keisha Francis, Jerome P. Walker, Tamara K. Thompson, Heather Phillips, Gavin A. Cloherty, Michael G. Berg, Joshua J. Anzinger

We identified 3 clades of dengue virus serotype 3 belonging to genotype III isolated during 2019–2020 in Jamaica by using whole-genome sequencing and phylogenomic and phylogeographic analyses. The viruses likely originated from Asia in 2014. Newly expanded molecular surveillance efforts in Jamaica will guide appropriate public health responses.

An estimated 390 million dengue virus (DENV) infections occur each year worldwide (*1*), and cases are expected to increase because of vector expansion (*2*). In the Americas, dengue incidence has increased dramatically since the 1990s (*3*), yet molecular epidemiologic investigations of DENV have remained uncommon for many countries in the region.

Molecular surveillance of DENV in Jamaica has been limited, and serotype testing has been typically performed only for select samples during epidemics. DENV genomic sequencing has rarely been performed in the Caribbean and almost never in Jamaica; only 1 published study from Jamaica analyzed sequences of patient samples collected in 2007 (*4*). Jamaica was established as an Abbott Pandemic Defense Coalition site in 2022 (*5*) and next-generation sequencing (NGS) was introduced in response to the COVID-19 pandemic, so NGS virus surveillance is becoming routine.

Author affiliations: Abbott Pandemic Defense Coalition, Kingston, Jamaica (S.A. Redman, K. Francis, J.P. Walker, T.K. Thompson, H. Phillips, J.J. Anzinger); The University of the West Indies, Kingston (S.A. Redman, K. Francis, J.P. Walker, T.K. Thompson, H. Phillips, J.J. Anzinger); Abbott Laboratories, Abbott Park, Illinois, USA (L.J. Perez, K. Forberg, G.A. Cloherty, M.G. Berg); Abbott Pandemic Defense Coalition, Abbott Park (L.J. Perez, K. Forberg, G.A. Cloherty, M.G. Berg); Global Virus Network, Baltimore, Maryland, USA (J.J. Anzinger)

DOI: https://doi.org/10.3201/eid3010.240170

In 2019, after a brief lull in dengue cases in the Americas after the introduction of Zika virus (ZIKV) in 2015–2016, a massive surge in dengue cases occurred throughout the region (*3*,*6*), at which time Jamaica recorded its greatest number of dengue cases (*6*). We describe DENV whole-genome NGS results for patients who sought clinical care in Jamaica for dengue during the 2018–2020 epidemic and examine DENV transmission dynamics by using phylogenetics and phylogeography.

The Study

We obtained residual diagnostic serum samples positive for DENV nonstructural (NS) protein 1 that were collected from patients at the University Hospital of the West Indies in Kingston, Jamaica, during December 2019–September 2020. Fourteen of 15 total samples were collected during December 2019–January 2020, when cases exceeded the Jamaica Ministry and Health and Wellness's epidemic threshold; the additional serum sample was collected at the end of the epidemic during September 2020 (*7*). We extracted total nucleic acids from samples by using the Abbott Diagnostics *m*2000sp instrument (Abbott, https:/www.abbott.com) and performed virus RNA enrichment by using the Comprehensive Viral Research Panel probe set (Twist Bioscience, https://www.twistbioscience.com).

We obtained 5 whole (100% coverage), 7 near-whole (91%–99% coverage), and 3 partial (28%–65% coverage) genome sequences (Appendix Table 1, https://wwwnc.cdc.gov/EID/article/30/10/24-0170-App1.pdf); all were DENV serotype 3 (DENV-3). We retrieved all DENV-3 sequences available in Nextstrain (https://nextstrain.org) and aligned them with sequences and metadata from this study (https://github.com/LesterJP/Dengue_Jamaica_Study) by using MAFFT (*8*). We inferred

[1]These first authors contributed equally to this article.

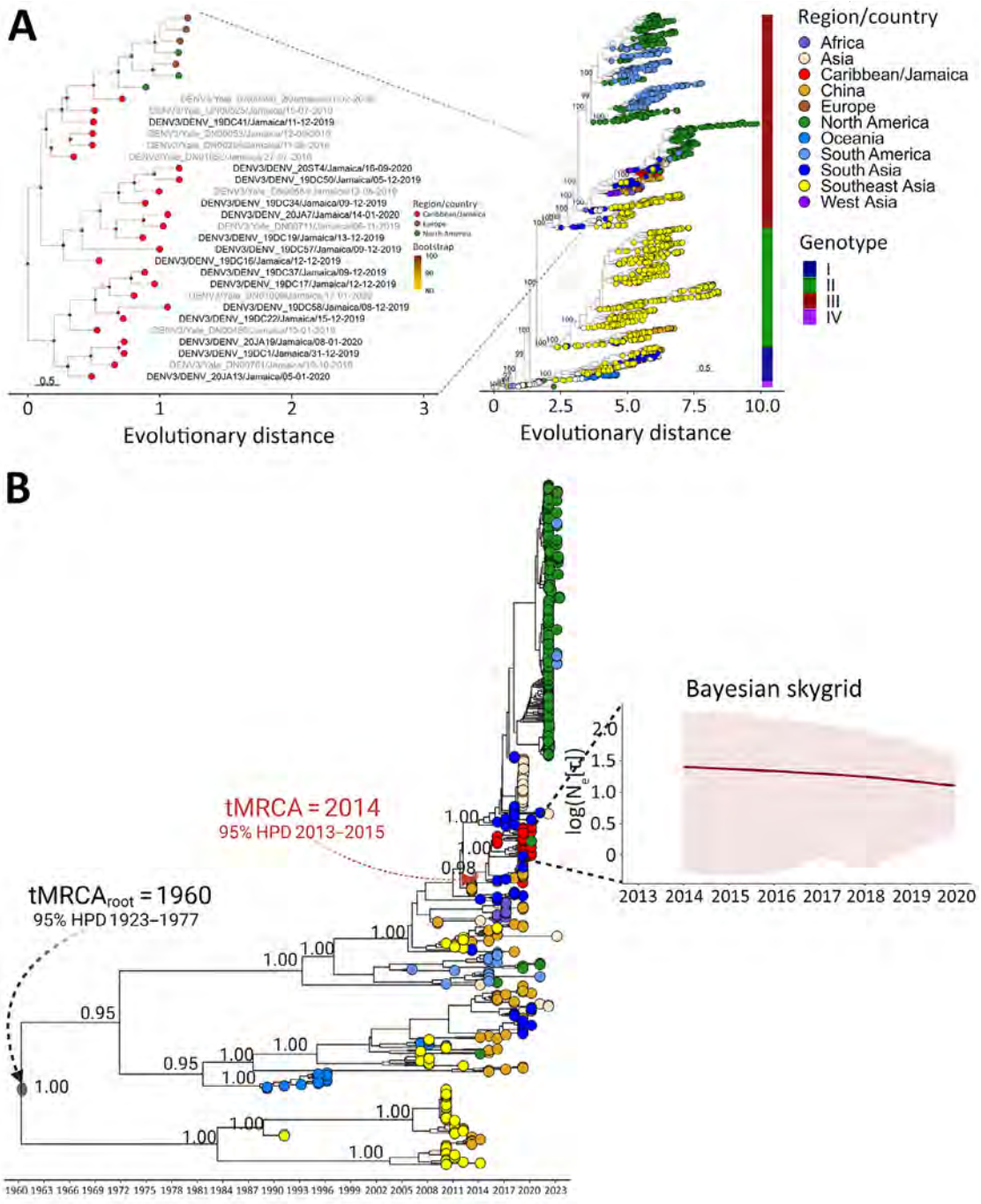

Figure 1. Phylogenetic analysis, temporal emergence, and demographic characterization of DENV-3 in study of origins and genetic dynamics, Jamaica. A) Maximum-likelihood phylogenetic trees of global DENV-3 sequences indicate the strains circulating in Jamaica belong to genotype III and are organized into 3 independent clades (left tree). The sequences were mapped according to the country of sampling and their genotypes (right tree) by using the *ggtreeExtra* R package (The R Project for Statistical Computing, https://www.r-project.org). Bootstrap values >80% are displayed for all nodes in the left tree (colored circles at nodes) and only for external nodes and main clade of interest in the main tree (right side). All bootstrap values are shown in Appendix Figure 1 (https://wwwnc.cdc.gov/EID/article/30/10/24-0170-App1.pdf). Scale bars indicate nucleotide substitutions per site. B) Time-scaled maximum clade credibility tree of DENV-3 sequences indicates the temporal emergence of DENV-3 strains in Jamaica starting in 2014. tMRCA and 95% HPD intervals for the tree root and the clade containing the sequences from Jamaica are indicated. Confidence values, determined by posterior probabilities, are indicated for external nodes and the node of interest. Full node support for the tree is indicated in Appendix Figure 2, panel A. Bayesian skygrid plot of the effective population size (Ne[τ]) over time indicates median values and 95% HPD intervals. DENV-3, dengue virus serotype 3; HPD, highest posterior density; tMRCA, time to most recent common ancestor.

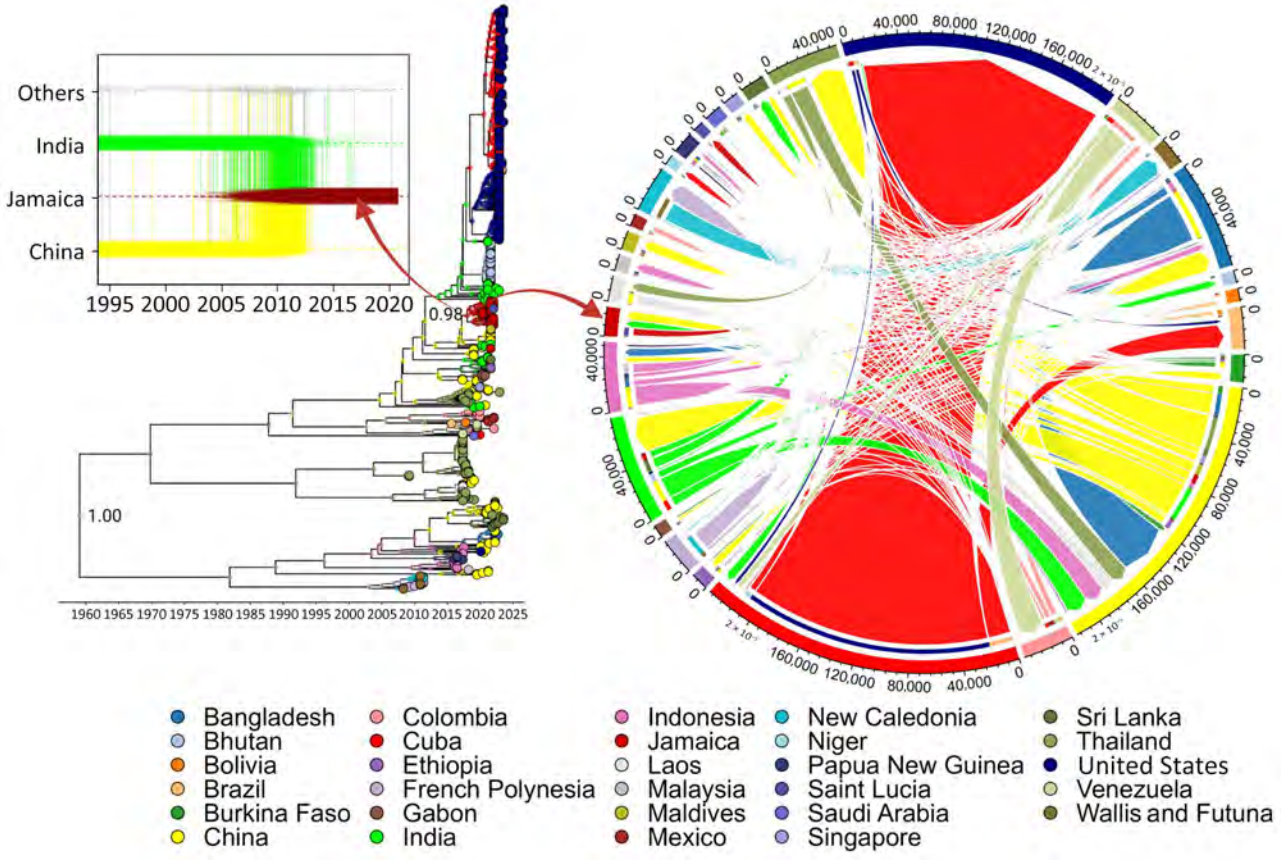

Figure 2. Time-scaled explicit discrete phylogeographic analysis of dengue virus serotype 3 (DENV-3) spread in Jamaica. Relationship between the dispersal trajectory of DENV-3 in the maximum clade credibility tree and the specific DENV-3 migration patterns into Jamaica over time (box) is indicated. Nodes of the tree represent the inferred country of origin for sampled strains. Arrows indicate the nodes from which taxa were selected for analysis by using the TaxaMarkovJumpHistoryAnalyzer (https://github.com/beast-dev/beast-mcmc). Only values of discrete state probability for the root and the node of interest are shown in the tree; complete state probability values of the nodes are indicated in Appendix Figure 2, panel B (https://wwwnc.cdc.gov/EID/article/30/10/24-0170-App1.pdf). Dynamic pathways of DENV-3 geographic movement are indicated by Markov jump mappings (right circular map). Transmission network of DENV-3 is summarized by Markov jump events, analyzed using TreeMarkovJumpHistoryAnalyzer and visualized in a circular layout by using the circlize package in R (The R Project for Statistical Computing, https://www.r-project.org). The width of each link reflects the frequency of virus movement; quantitative estimates were provided by using the TreeMarkovJumpHistoryAnalyzer. Tick marks on the outside of the circle's segments indicate virus movement frequencies.

maximum-likelihood phylogenetic reconstructions by using IQ-TREE2 (Appendix). Sequences from Jamaica formed a monophyletic clade within DENV-3 genotype III (GIII), which was further divided into 3 monophyletic subclades: 2 exclusively containing sequences from Jamaica and 1 containing sequences from Jamaica, North America, and Europe (Figure 1, panel A). Those results suggested DENV-3 circulation in Jamaica might have been either from multiple introductions or from endemic evolution that later mirrored the genetics of other DENVs in global circulation. A temporal analysis traced the emergence of DENV-3 to 1960, which had an evolutionary rate of 3.96×10^{-3} substitutions/site/year; DENV-3 GIII was most likely introduced into Jamaica during 2014 (Figure 1, panel B). A Bayesian skygrid reconstruction of the DENV-3 monophyletic clade from Jamaica (Appendix) revealed that genetic diversity remained stable, and the evolutionary rate was 1.78×10^{-3} substitutions/site/year.

We conducted discrete phylogeographic analyses to determine whether DENV-3 genetic diversification in Jamaica arose from external introductions or endemic circulation (Figure 2). Integrating country-specific data with virus dispersal trajectories identified Indonesia as the putative origin of DENV-3 (i.e., the tree root) and showed a clear pattern of intercountry virus spread. A Markov jump reward plot showed the intracountry and intercountry dynamics of DENV-3 globally, indicating China, India, Thailand, and Bangladesh were key virus exporters with high interconnectivity.

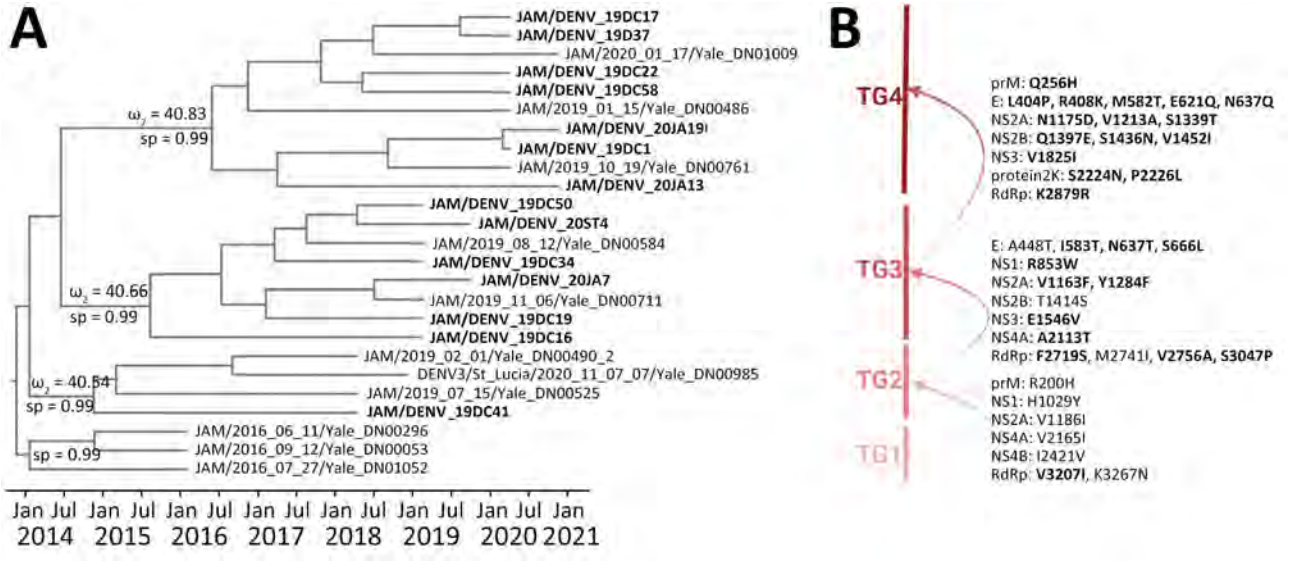

Figure 3. Time-scaled phylogenetic analysis, molecular characterization, dynamics, and natural selection of dengue virus serotype 3 in Jamaica. A) Phylogenetic tree indicates monophyletic clusters of strains from Jamaica (bold text) extracted from the discrete phylogeographic analysis (Figure 2). Discrete sp values (ω) for nodes evaluated for episodic selection are shown. Full sp values for nodes are shown in Appendix Figure 2, panel B (https://wwwnc.cdc.gov/EID/article/30/10/24-0170-App1.pdf). B) Strains were evaluated for amino acid replacements according to each TG. Arrows indicate episodic selection of each main TG clade. Bold text indicates positively selected mutations. sp, state probability; TG, temporal group.

In the Caribbean, Cuba was a primary source for regional DENV-3 spread and introduction into the United States. For Jamaica specifically, this analysis and the TaxaMarkovJump history reconstruction method (*9*) indicated 2 major concurrent importation events from Asia; strains from Jamaica were subsequently transmitted to Saint Lucia and other potentially unsampled Caribbean countries. Further intracountry diversification likely led to the 2018–2020 dengue epidemic.

To analyze mutation signatures associated with temporal clades, we extracted strains from Jamaica from the discrete phylogeographic tree and categorized them into temporal groups (TGs) (Figure 3, panel A). Initially (TG1→TG2), amino acid replacements were infrequent and dispersed throughout NS genes. Over time (TG2→TG3), an accumulation of mutations was concentrated in the RNA-dependent RNA polymerase and envelope (E) genes. This trend continued (TG3→TG4) with additional mutations in E and NS2 genes. Mutations in the E gene were located within the lateral ridge and hinge epitopes of strains in TG3 and in the lateral ridge epitope for TG4 (Figure 3, panel B; Figure 4). This pattern of mutations, particularly in the E gene that encodes the most critical protein target of neutralizing antibodies (*10*), suggests that immune evasion contributed to selection of those mutations. In contrast, we found no indication of immune evasion for E gene domain III (receptor-binding protein) and fusion peptide sequences; those regions were not identified under positive selection.

Episodic and pervasive selection analyses to assess sudden and consistent positive selection were performed to determine which DENV-3 strains and mutations were evolutionarily favored. Branch-site models applied to the complete DENV-3 coding sequence indicated the emergence of each successive time-epoch lineage was under positive, episodic selection (Appendix Table 2). This selection was the predominant force driving retention of numerous mutations within key functional domains for virus replication and structural proteins and determining the evolutionary trajectory of those strains (Figure 3, panel A). We applied site models for the E protein to ascertain which mutations were subject to positive, pervasive selection (Appendix Tables 3, 4) and were likely causes of immune escape. Domain III mutations S666L in TG3 and M582T in TG4 and domain I/II mutation R408K in TG4 strains located at the hinge region were positively selected residues (Figure 3, panel B; Figure 4).

Introductions from Asia most likely brought DENV-3 to Jamaica in 2014, and it was first detected in the country in 2016 (https://www.who.int/emergencies/disease-outbreak-news/item/4-february-2019-dengue-jamaica-en). A mixed outbreak of DENV-3 and DENV-4 infections occurred in 2016 when ZIKV was detected (*11*). Our findings

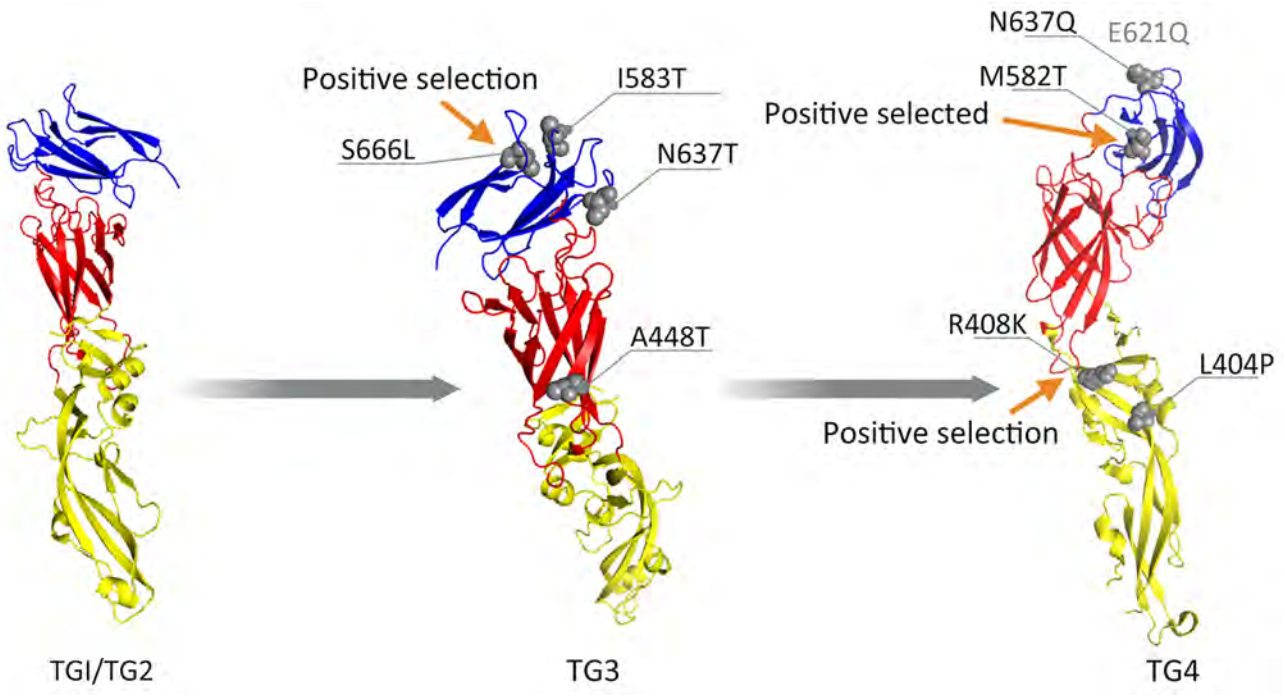

Figure 4. Envelope glycoprotein 3-dimensional structures (structure 7a3s; RCSB Protein Data Bank, https://www.rcsb.org) from dengue virus serotype 3 strains in Jamaica. Red indicates protein domain I, yellow indicates domain II, and blue indicates domain III. Gray spheres indicate mutations identified across various TGs. Arrows indicate mutations detected by site models. E621Q (faded text) is in the loop region not visible in the crystal structure. TG, temporal group.

show that DENV-3 GIII continued to circulate at low levels in Jamaica after 2016, which then led to an explosive DENV-3 GIII disease epidemic during November 2018–March 2020. It remains inconclusive why a period of low-level DENV circulation occurred in the Americas after the introduction of ZIKV in 2015–2016, although ZIKV cross-immunity with DENV and public health interventions and behavioral changes in response to ZIKV might have contributed (*3*,*12*).

The E glycoprotein is a critical target of neutralizing antibodies (*10*). Our findings indicated E glycoprotein mutations were positively selected, underscoring their relevance for adaptive evolutionary responses that might have influenced strain prevalence and virulence. Neutralizing antibodies against E protein domain III of DENV-3 GIII are typically weaker than those against other domains (*13*), which might explain why domain III mutations were observed over time in our study; subneutralizing antibodies would enable continued virus circulation. Those mutations are not expected to have a large effect on circulation because DENV immunity usually protects from homotypic reinfection; however, breakthrough infections have been described and could contribute to sustained DENV circulation (*14*).

Conclusions

The circulation of DENV-3 during 2014–2020, a dengue outbreak in 2016, and a large dengue epidemic during 2018–2020 likely produced substantial population immunity to DENV-3 in Jamaica, which might have led to the introduction of a new DENV serotype(s), a well-described risk factor for severe dengue (*15*). Newly expanded molecular surveillance efforts in Jamaica will enable whole-genome NGS of DENV in clinical samples collected after 2020 to determine ongoing circulation patterns and guide appropriate public health responses.

Ethics approval for this study was granted through the University of the West Indies Mona Campus Research Committee with yearly extensions (reference code CREC-MN.150 2020/21). Access and use of patient samples was in accordance with policies of the University Hospital of the West Indies.

This work was funded by the National Health Fund Jamaica and Abbott Laboratories.

S.R. is a global infectious diseases scholar who received mentored research training in work leading to the development of this manuscript. This training was supported in part by the University of Buffalo Clinical and Translational Science Institute (award no. UL1TR001412) and the Global Infectious Diseases Research Training Program (award no. D43TW010919).

About the Author

Ms. Redman is an MSc student in biomedical research at The University of the West Indies, Mona Campus, Jamaica. Her research interests focus on molecular virology, especially arboviruses.

References

1. Guzman MG, Gubler DJ, Izquierdo A, Martinez E, Halstead SB. Dengue infection. Nat Rev Dis Primers. 2016;2:16055. https://doi.org/10.1038/nrdp.2016.55
2. Kraemer MUG, Reiner RC Jr, Brady OJ, Messina JP, Gilbert M, Pigott DM, et al. Publisher correction: past and future spread of the arbovirus vectors *Aedes aegypti* and *Aedes albopictus*. Nat Microbiol. 2019;4:901. https://doi.org/10.1038/s41564-019-0440-7
3. Perez F, Llau A, Gutierrez G, Bezerra H, Coelho G, Ault S, et al. The decline of dengue in the Americas in 2017: discussion of multiple hypotheses. Trop Med Int Health. 2019;24:442–53. https://doi.org/10.1111/tmi.13200
4. Brown MG, Salas RA, Vickers IE, Heslop OD, Smikle MF. Molecular epidemiology of dengue in Jamaica dengue virus genotypes in Jamaica, 2007. West Indian Med J. 2011;60:120–5.
5. Averhoff F, Berg M, Rodgers M, Osmanov S, Luo X, Anderson M, et al. The Abbott Pandemic Defense Coalition: a unique multisector approach adds to global pandemic preparedness efforts. Int J Infect Dis. 2022;117:356–60. https://doi.org/10.1016/j.ijid.2022.02.001
6. Lue AM, Richards-Dawson MEH, Gordon-Strachan GM, Kodilinye SM, Dunkley-Thompson JAT, James-Powell TD, et al. Severity and outcomes of dengue in hospitalized Jamaican children in 2018–2019 during an epidemic surge in the Americas. Front Med (Lausanne). 2022;9:889998. https://doi.org/10.3389/fmed.2022.889998
7. Ministry of Health and Wellness, National Epidemiology Unit, Jamaica. Weekly epidemiology bulletin. December 12, 2020 [cited 2024 Jan 19]. https://www.moh.gov.jm/wp-content/uploads/2020/12/Weekly-Bulletin-EW-50_2020-.pdf
8. Rozewicki J, Li S, Amada KM, Standley DM, Katoh K. MAFFT-DASH: integrated protein sequence and structural alignment. Nucleic Acids Res. 2019;47:W5–10. https://doi.org/10.1093/nar/gkz342
9. Hong SL, Lemey P, Suchard MA, Baele G. Bayesian phylogeographic analysis incorporating predictors and individual travel histories in BEAST. Curr Protoc. 2021;1:e98. https://doi.org/10.1002/cpz1.98
10. Gallichotte EN, Baric RS, de Silva AM. The molecular specificity of the human antibody response to dengue virus infections. Adv Exp Med Biol. 2018;1062:63–76. https://doi.org/10.1007/978-981-10-8727-1_5
11. Anzinger JJ, Mears CD, Ades AE, Francis K, Phillips Y, Leys YE, et al.; ZIKAction Consortium1,2. Antenatal seroprevalence of Zika and chikungunya viruses, Kingston Metropolitan Area, Jamaica, 2017–2019. Emerg Infect Dis. 2022;28:473–5. https://doi.org/10.3201/eid2802.211849
12. Pan American Health Organization. Response to the epidemic of Zika virus in the Americas [cited 2024 Jan 19]. https://www.paho.org/sites/default/files/2019-04/Zika-Annual-Report-Dec-2015-2016.pdf
13. Young E, Carnahan RH, Andrade DV, Kose N, Nargi RS, Fritch EJ, et al. Identification of dengue virus serotype 3 specific antigenic sites targeted by neutralizing human antibodies. Cell Host Microbe. 2020;27:710–724.e7. https://doi.org/10.1016/j.chom.2020.04.007
14. Waggoner JJ, Balmaseda A, Gresh L, Sahoo MK, Montoya M, Wang C, et al. Homotypic dengue virus reinfections in Nicaraguan children. J Infect Dis. 2016;214:986–93. https://doi.org/10.1093/infdis/jiw099
15. Guzman MG, Alvarez M, Halstead SB. Secondary infection as a risk factor for dengue hemorrhagic fever/dengue shock syndrome: an historical perspective and role of antibody-dependent enhancement of infection. Arch Virol. 2013;158:1445–59. PubMed https://doi.org/10.1007/s00705-013-1645-3

Address for correspondence: Joshua J. Anzinger, The University of the West Indies, Ring Rd, Kingston KGN7, Jamaica; email: joshua.anzinger@uwimona.edu.jm

Oropouche Fever, Cuba, May 2024

Ana Julia Benitez,[1] Mayling Alvarez,[1] Lissette Perez, Rosario Gravier, Silvia Serrano, Denelsys Milagro Hernandez, Melissa Maria Perez, Gladys Gutierrez-Bugallo, Yanet Martinez, Ariamys Companioni, Carilda Peña, Jose Raul de Armas, Dayana Couto, Iliovanys Betancourt I, Madelaine Rivera Sanchez, Sonia Resik, Vivian Kouri, Maria G. Guzman

Phylogenetic analyses showed that the virus responsible for a May 2024 Oropouche fever outbreak in Cuba was closely related to viruses from Brazil in 2023. Pools of *Ceratopogonidae* spp. biting midges and *Culex quinquefasciatus* mosquitoes were positive for Oropouche viral RNA. No cases were severe. Virus extension to new areas may increase case numbers and severity.

On May 9, 2024, the Pan American Health Organization reported 5,193 cases of Oropouche fever (also called Oropouche virus disease) in Bolivia, Brazil, Colombia, and Peru and sent an alert with regard to autochthonous cases in areas of Brazil and Bolivia, where the disease had not been previously reported (*1*). During the past decade, Oropouche fever has been reported mainly in the Amazon region. However, in 2014, the first case outside that region was registered in Haiti, raising concerns about its geographic extension (*2*). The virus has been detected in Central and South America (e.g., Bolivia, Brazil, Colombia, Peru, and Panama); ≈500,000 cases have been diagnosed. Given the clinical picture of Oropouche fever (fever, headache, arthralgia, myalgia), the disease can be confused with dengue, Zika, or other febrile illnesses.

Oropouche virus (OROV) is a member of the family *Peribunyaviridae*, genus *Orthobunyavirus*, and was first identified in Trinidad and Tobago. OROV is maintained in nature through sylvatic and urban cycles. The urban cycle is thought to mainly involve the bite of the *Culicoides paraensis* midge. Another urban vector in tropical regions, where it feeds on both humans and animals, is the *Culex quinquefasciatus* mosquito (*3*). The OROV genome comprises 3 single-stranded negative-sense RNA segments (large, medium, and small). Sequencing studies of the small segment suggest the existence of 4 genotypes (I–IV) (*4*,*5*).

The source of patients for dengue surveillance in Cuba is the primary healthcare level search, clinical management, and notification of acute febrile illness (AFI) cases of unknown etiology or cases suspected of being dengue. A network of 30 laboratories with capacity for dengue IgM detection guarantees serologic surveillance conducted on samples collected at day 6 of fever onset. Positive samples are confirmed at the National Reference Laboratory of the Institute "Pedro Kouri" (NRL-IPK). Molecular surveillance at the NRL-IPK enables real-time PCR identification of dengue viruses in acute-phase samples from patients with suspected cases. Negative samples are tested for Zika, chikungunya, and yellow fever viruses. The NRL-IPK is also in charge of virus genetic surveillance (*6*). Environmental and entomologic surveillance complement the national integrated arbovirus surveillance system.

The Study

On May 20, 2024, the NRL-IPK received samples from 89 patients with AFI of unknown etiology in Santiago de Cuba and Cienfuegos Provinces, Cuba, where an increase of similar cases had been reported, most negative for dengue IgM. Patients reported acute fever onset with headache and joint pain for 2–3 days and rapid recovery. Median patient age was 35 years (interquartile range [IQR] 19–50); 49.4% of patients were female and 51.6% male. Of the 89 serum samples received, 69 were from Santiago de Cuba (Boniato, n = 39; Songo la Maya, n = 30) and 20 from Cienfuegos (Abreu, n = 4; Cienfuegos, n = 11; and Rodas, n = 5). Urine (n = 6) and feces (n = 30) samples were also collected from the 89 patients.

Author affiliations: Pedro Kouri Tropical Medicine Institute, Havana, Cuba (A.J. Benitez, M. Alvarez, L. Perez, R. Gravier, S. Serrano, D.M. Hernandez, M. Perez, G. Gutierrez-Bugallo Y. Martinez, A. Companioni, S. Resik, V. Kouri, M.G. Guzman); Cuban Ministry of Health, Havana (C. Peña, J.R. de Armas, D. Couto, I. Betancourt, M. Rivera)

DOI: https://doi.org/10.3201/eid3010.240900

[1]These authors contributed equally to this article.

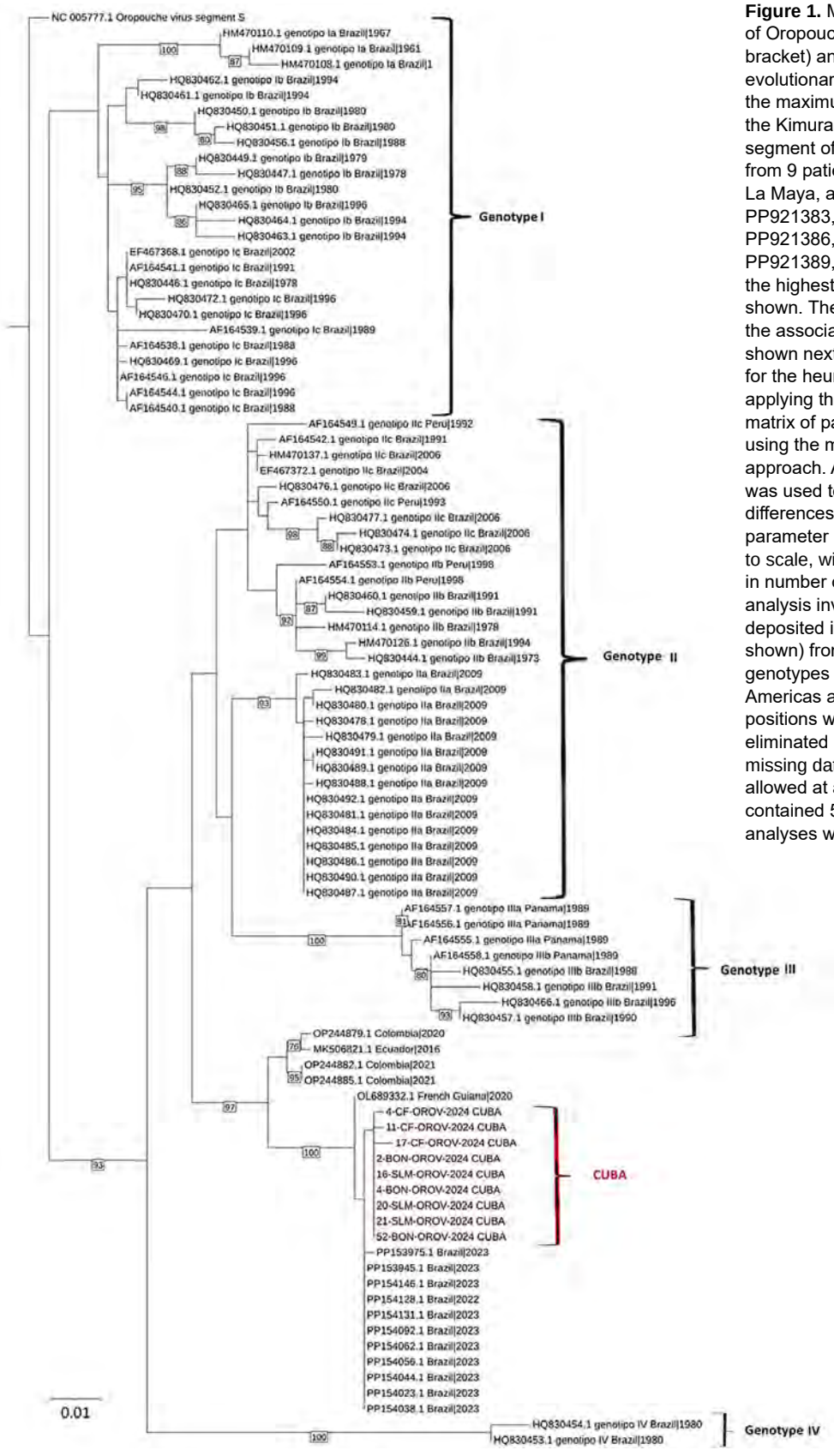

Figure 1. Molecular phylogenetic analysis of Oropouche viruses isolated in Cuba (red bracket) and reference sequences. The evolutionary history was inferred by using the maximum-likelihood method based on the Kimura 2-parameter model to the small segment of Oropouche orthobunyavirus from 9 patients from Boniato, Songo La Maya, and Cienfuegos (PP921382, PP921383, PP921384, PP921385, PP921386, PP921387, PP921388, PP921389, PP921390) (*14*). The tree with the highest log likelihood (−2,403.4997) is shown. The percentage of trees in which the associated taxa clustered together is shown next to the branches. Initial tree(s) for the heuristic search were obtained by applying the neighbor-joining method to a matrix of pairwise distances estimated by using the maximum composite likelihood approach. A discrete gamma distribution was used to model evolutionary rate differences among sites (5 categories [+G, parameter = 0.1407]). The tree is drawn to scale, with branch lengths measured in number of substitutions per site. The analysis involved 101 nt sequences deposited in GenBank (accession numbers shown) from the different outbreaks and genotypes of Oropouche virus in the Americas and the Caribbean region. All positions with <95% site coverage were eliminated (i.e., <5% alignment gaps, missing data, and ambiguous bases were allowed at any position) The final dataset contained 521 positions. Evolutionary analyses were conducted in MEGA6 (*13*).

We extracted RNA by using the commercial QIAamp Viral RNA Mini Kit (QIAGEN, https://www.qiagen.com) according to the manufacturer's instructions. We processed extracted RNA for dengue, Zika and chikungunya viruses by using by real-time PCR (*7*–*9*), and all serum samples were negative. Rapid test results for dengue nonstructural protein 1 (Bioline Dengue Duo; Abbott Laboratories, https://www.abbott.com) and chikungunya IgM (Kabla Diagnósticos, https://www.biodiagnosticos.com) were also negative. Fecal samples were negative for enterovirus (*10*).

We examined 89 serum and 6 urine samples for Oropouche and Mayaro viruses by using real-time PCR (*11*). All samples were negative for Mayaro virus, and 74 (83. 1%) serum samples (54 from Santiago de Cuba and 20 from Cienfuegos) and 5 (83.3%) urine samples were positive for OROV.

For the viral genetic characterization, we studied 9 serum samples (3 from Boniato, 3 from Songo La Maya, and 3 from Cienfuegos). We subjected extracted RNA to reverse transcription by PCR using the QIAGEN OneStep RT-PCR Kit system and primers NORO5 (5′-AAAGAGGATCCAATAATGTCAGAGTTCATTT-3′) and ORON3 (5′-AATTCGGAATTGGCATATAGTGGAATTCAC-3′) (*12*). We purified the 626-bp fragments obtained, which encode for the viral nucleocapsid (positions 85–718), by using the QIAquick PCR Purification Kit (QIAGEN), followed by sequencing with the Dye Terminator Cycle Sequencing Quick Start Kit (Analis, https://www.analis.com) and primers NORO5, ORON3, OROV-F (5′-TCCGGAGGCAGCATATGTG-3′), and OROV-R (5′-AAGTGCTCAATGCTGGTGTTGT-3′) (donated by the Pan American Health Organization). We purified the sequencing products and then separated the generated fragments on a CEQ 8800 Genetic Analysis System sequencer (Analis). We edited and assembled the electropherograms by using Sequencher version 4.10.1 software (Gene Codes Corporation, https://www.genecodes.com). As a reference, we used the complete sequence of the small segment of the Oropouche orthobunyavirus strain (GenBank accession no. OP244879.1, Oropouche orthobunyavirus isolate 0200178W, small segment, complete sequence). Phylogenetic analyses (MEGA version 6) (*13*) revealed that the isolated viruses clustered in a separate branch, closely related to those reported from Brazil in 2023 (Figure 1).

Table 1. Epidemiologic characteristics of confirmed cases of Oropouche fever, Cuba, 2024*

Data	Values
M:F ratio	51/48 (1.1)
Median days of sample collection according to illness onset (range)	2 (0–4)
Median age, y (range) [IQR]	34.5 (4–83) [18–50.5]

*IQR, interquartile range.

After we had identified OROV transmission, national surveillance for dengue and Oropouche fever was intensified (active AFI case search). In addition, vector control intervention (adulticide treatment, source reduction, environmental management, biolarvicide application on permanent breeding sites) was applied in the areas with confirmed transmission.

During May 28–June 3, 2024, we processed 31 serum samples collected from locations with increased

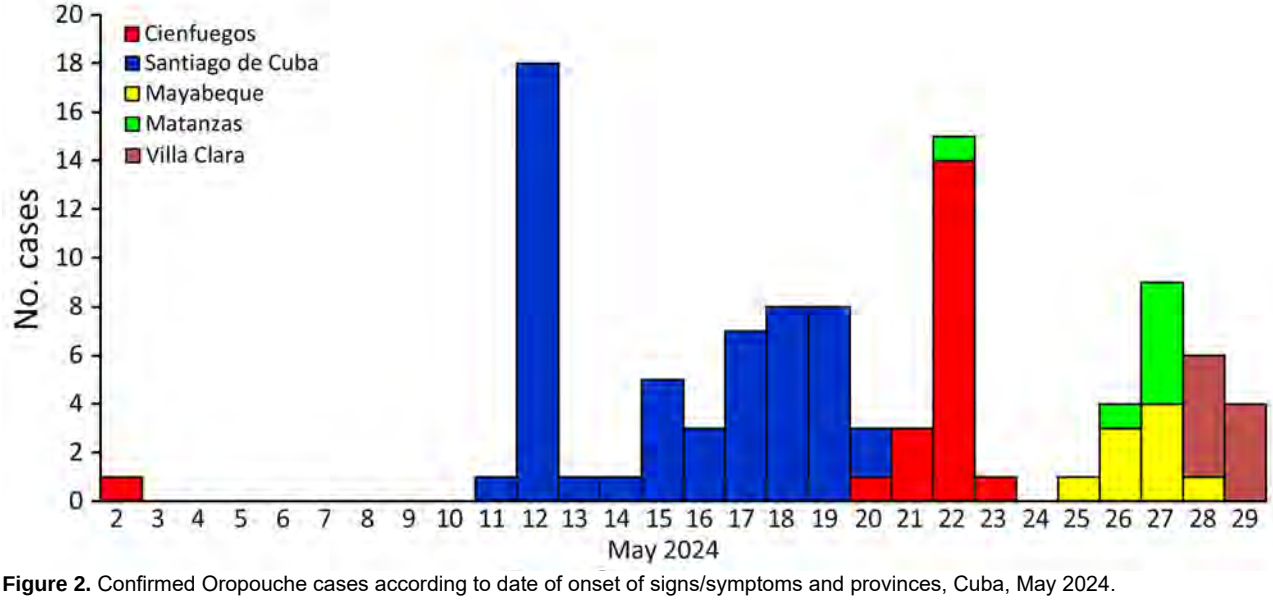

Figure 2. Confirmed Oropouche cases according to date of onset of signs/symptoms and provinces, Cuba, May 2024.

Table 2. Clinical characteristics of patients with confirmed Oropouche fever, Cuba, 2024

Clinical signs/symptoms	No. (%) patients
Fever	86 (86.9)
Headache	71 (71.7)
General malaise	51 (51.5)
Arthralgia	22 (22.2)
Asthenia	18 (18.1)
Anorexia	16 (16.2)
Retroocular pain	14 (14.1)
Abdominal pain	8 (8)
Vomiting	7 (7)
Diarrhea	7 (7)
Chills	4 (4)
Lumbar pain	3 (3)

AFI cases (San Nicolas de Bari in Mayabeque; Perico, Cienaga de Zapata, and Jovellanos in Matanzas; and Ranchuelo in Villa Clara). OROV infection was confirmed in 25 (80.6%) samples: 7 from Matanzas, 9 from Mayabeque, and 9 from Villa Clara Provinces (Table 1). Median patient age was 34.5 years (range 4–83 years), male:female ratio was 1.1. Signs and symptoms by order of frequency were fever, headache, general malaise, myalgia, and arthralgia (Table 2; Figure 2; Appendix Table, https://wwwnc.cdc.gov/EID/article/30/10/24-0900-App1.pdf). No serious or fatal cases were reported.

To investigate the vector involved with OROV transmission in Cuba, we collected 156 *C. quinquefasciatus* mosquitoes and 49 *Ceratopogonidae* spp. from suspected areas of transmission in 5 blocks of houses in Boniato. After potential vector identification, we grouped not visibly engorged female *C. quinquefasciatus* mosquitoes into 9 pools (10–20/pool) and *Ceratopogonidae* spp. specimens into 2 pools (7–19/pool). We extracted RNA and conducted real-time PCR. Positive samples were attributed to 5 (56%) pools of *C. quinquefasciatus* mosquitoes and 1 (50%) pool of *Ceratopogonidae* biting midges.

Among our study limitations was collection of signs/symptoms by using a standardized form for AFI or dengue cases; consequently, we might have missed less common presentations such as meningitis. In addition, the presence of viral RNA does not confirm the vector role in virus transmissibility. More work is needed to determine the primary vectors responsible for the current outbreak.

Conclusions

Oropouche fever is an emerging disease of concern in South and Central America. Transmission outside of the Amazon region is probably silent and not detected by public health surveillance systems. Our results confirm an outbreak of OROV in Cuba. Transmission was detected in semi-urban localities of 5 of 16 provinces located in the western, central, and eastern parts of the country. Dengue surveillance enabled us to identify cases with nondengue AFI. As of August 2024, OROV transmission had been confirmed in 7 provinces. The outbreak in Cuba alerts the Americas and the world of the need for integrated dynamic surveillance systems to detect the introduction and early transmission of OROV and consequently implement effective measures for its control.

Acknowledgments

We thank Jairo Mendez, Leticia Franco, Felipe Naveca, and Yosiel Molina for their useful comments and recommendations.

This work was funded by the Cuban Ministry of Health. Real-time PCR reagents were provided by the Pan American Health Organization.

M.G.G., S.R., and V.K. coordinated and designed the study, analyzed the results, and drafted and reviewed the manuscript; M.A. conducted the laboratory work, analyzed the results, and cleaned the data; A.J.B., S.S., and M.P. performed all real-time PCRs; L.P., R.G., and M.P. performed the genetic characterization; G.G., Y.M., and A.C. performed the vector studies; and C.P., J.R.A., and M.R. coordinated the epidemiologic and field studies; and D.C. and I.B. collected the clinical and epidemiologic data. All authors reviewed the draft and approved the final version.

About the Author

Ms. Benitez is a microbiologist at the Institute of Tropical Medicine "Pedro Kouri" in Havana, Cuba, pursuing a master's degree in virology. Her primary research interests are the arboviral infections, including viral molecular diagnosis.

References

1. Pan American Health Organization/World Health Organization. Alerta Epidemiológica: oropouche en la región de las Américas, 9 de mayo del 2024 [cited 2024 May 12]. https://www.paho.org/es/documentos/alerta-epidemiologica-oropouche-region-americas-9-mayo-2024
2. Elbadry MA, Durães-Carvalho R, Blohm GM, Stephenson CJ, Loeb JC, et al. Orthobunyaviruses in the Caribbean: Melao and Oropouche virus infections in school children in Haiti in 2014. PLoS Negl Trop Dis. 2021;15:e0009494. https://doi.org/10.1371/journal.pntd.0009494
3. Cardoso BF, Serra OP, Heinen LB, Zuchi N, Souza VC, Naveca FG, et al. Detection of Oropouche virus segment S in patients and in *Culex quinquefasciatus* in the state of Mato Grosso, Brazil. Mem Inst Oswaldo Cruz. 2015;110:745–54. https://doi.org/10.1590/0074-02760150123

4. Travassos da Rosa JF, de Souza WM, Pinheiro FP, Figueiredo ML, Cardoso JF, Acrani GO, et al. Oropouche virus: clinical, epidemiological, and molecular aspects of a neglected orthobunyavirus. Am J Trop Med Hyg. 2017;96:1019–30. https://doi.org/10.4269/ajtmh.16-0672
5. Files MA, Hansen CA, Herrera VC, Schindewolf C, Barrett ADT, Beasley DWC, et al. Baseline mapping of Oropouche virology, epidemiology, therapeutics, and vaccine research and development. NPJ Vaccines. 2022;7:38. https://doi.org/10.1038/s41541-022-00456-2
6. Guzmán MG, Vázquez S, Álvarez M, Pelegrino JL, Ruiz Amores D, Martínez PA, et al. Vigilancia de laboratorio de dengue y otros arbovirus en Cuba, 1970–2017. Rev Cubana Med Trop. 2019;71.
7. Santiago GA, Vergne E, Quiles Y, Cosme J, Vazquez J, Medina JF, et al. Analytical and clinical performance of the CDC real time RT-PCR assay for detection and typing of dengue virus. PLoS Negl Trop Dis. 2013;7:e2311. https://doi.org/10.1371/journal.pntd.0002311
8. Lanciotti RS, Kosoy OL, Laven JJ, Velez JO, Lambert AJ, Johnson AJ, et al. Genetic and serologic properties of Zika virus associated with an epidemic, Yap State, Micronesia, 2007. Emerg Infect Dis. 2008;14:1232–9. https://doi.org/10.3201/eid1408.080287
9. Johnson BW, Russell BJ, Goodman CH. Laboratory diagnosis of chikungunya virus infections and commercial sources for diagnostic assays. J Infect Dis. 2016;214(suppl 5):S471–4. https://doi.org/10.1093/infdis/jiw274
10. Nijhuis M, van Maarseveen N, Schuurman R, Verkuijlen S, de Vos M, Hendriksen K, et al. Rapid and sensitive routine detection of all members of the genus *Enterovirus* in different clinical specimens by real-time PCR. J Clin Microbiol. 2002;40:3666–70. https://doi.org/10.1128/JCM.40.10.3666-3670.2002
11. Naveca FG, Nascimento VAD, Souza VC, Nunes BTD, Rodrigues DSG, Vasconcelos PFDC. Multiplexed reverse transcription real-time polymerase chain reaction for simultaneous detection of Mayaro, Oropouche, and Oropouche-like viruses. Mem Inst Oswaldo Cruz. 2017;112:510–3. https://doi.org/10.1590/0074-02760160062
12. Vasconcelos HB, Nunes MRT, Casseb LMN, Carvalho VL, Pinto da Silva EV, Silva M, et al. Molecular epidemiology of Oropouche virus, Brazil. Emerg Infect Dis. 2011;17:800–6. https://doi.org/10.3201/eid1705.101333
13. Tamura K, Stecher G, Peterson D, Filipski A, Kumar S. MEGA6: Molecular Evolutionary Genetics Analysis version 6.0. Mol Biol Evol. 2013;30:2725–9. https://doi.org/10.1093/molbev/mst197
14. Kimura M. A simple method for estimating evolutionary rates of base substitutions through comparative studies of nucleotide sequences. J Mol Evol. 1980;16:111–20. https://doi.org/10.1007/BF01731581

Address for correspondence: Maria G. Guzman, Instituto Medicina Tropical Pedro Kouri, Autopista Novia del Mediodía Km 6 1/2, Havana Lisa 11600, Cuba; email: lupe@ipk.sld.cu

etymologia revisited

Malaria

[mə-lar′e-ə]

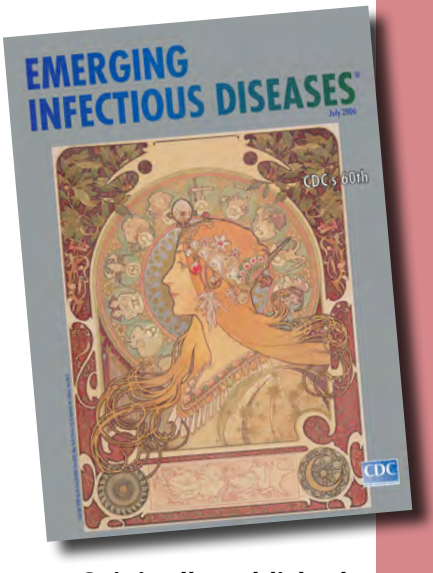

Originally published in July 2006

Malaria, "bad air" in Italian, was blamed for the deaths of >1,000 workers digging the Erie Canal in 1819. Work on the canal continued in winter, when the swamp was frozen over (and, although the vector was not known at the time, mosquitoes were dormant). Malaria, caused by parasites of the genus *Plasmodium* and usually transmitted by the bite of infected *Anopheles* mosquitoes, is endemic in many warm regions. Charles Louis Alphonse Laveran discovered the protozoan cause of malaria in 1880. The Office of Malaria Control in War Areas, which was established in 1942 to control malaria and other vectorborne diseases in the southern United States, evolved into what is today the Centers for Disease Control and Prevention.

Source:

Dorland's illustrated medical dictionary. 30th ed. Philadelphia: Saunders; 2003; cdc.gov; and wikipedia.org

https://wwwnc.cdc.gov/eid/article/12/7/ET-1207_article

Highly Pathogenic Avian Influenza A(H5N1) Virus Clade 2.3.4.4b Infections in Seals, Russia, 2023

Ivan Sobolev, Alexander Alekseev, Kirill Sharshov, Maria Chistyaeva, Alexander Ivanov, Olga Kurskaya, Olesia Ohlopkova, Alexey Moshkin, Anastasiya Derko, Arina Loginova, Mariya Solomatina, Alimurad Gadzhiev, Yuhai Bi, Alexander Shestopalov

Highly pathogenic avian influenza A(H5N1) virus was detected in dead seals on Tyuleniy Island in eastern Russia, in the Sea of Okhotsk. Viruses isolated from dead northern fur seals belong to clade 2.3.4.4b and are closely related to viruses detected predominantly in the Russian Far East and Japan in 2022–2023.

In July 2023, the deaths of northern fur seals (*Callorhinus ursinus*) and Steller sea lions (*Eumetopias jubatus*) were noted in the Far East region of the Russian Federation on Tyuleniy Island (Figure 1). The island is situated in the southwestern part of the Sea of Okhotsk, the northern part of the Pacific Ocean, close to Sakhalin Island. Tyuleniy Island has an area of 0.054 km^2 and is devoid of water, woody vegetation, terrestrial predators, and permanent human settlements. Its unique environment enables marine mammals to form extensive rookeries and seabirds to establish nesting colonies (*1*), reaching extremely high densities of animals of different ages (Appendix 1 Figures 1–3, https://wwwnc.cdc.gov/EID/article/30/10/23-1728-App1.pdf). The population size of the northern fur seal on Tyuleniy Island in 2022 was ≈55,221 (*2*).

The Study

We detected the first seal death on July 15, 2023, and a mass death of seals during July 15–August 15, 2023; a total of 3,500 northern fur seals and 1 Steller sea lion died. Many adult animals died in the surf or water; thus, it is likely that the actual number of animal deaths exceeds the number we counted. We found dead pups (1–5 weeks old) on August 4; pup deaths became widespread. In observing diseased animals, we identified 2 stages of disease progression from the onset of symptoms. In stage 1, lasting 6–8 hours, animals experienced fever, lethargy, confusion, and disorientation, and in stage 2, lasting 2–4 hours, they experienced convulsions and death.

We took samples from the lungs, small intestine, and liver of 2 deceased northern fur seals. We detected influenza A virus (IAV) of the H5 subtype in the lungs and small intestine of 1 animal and in the lungs and liver of the other animal by real-time PCR. We isolated IAV from the PCR-positive organs in embryonated chicken eggs. We sequenced whole genomes of 3 viruses isolated from the small intestine and lungs of the first animal and from the lungs of the second animal (Table) using Illumina MiSeq (https://www.illumina.com). We identified all isolates as highly pathogenic avian influenza (HPAI) viruses on the basis of the amino acid sequence of the hemagglutinin (HA) polybasic proteolytic cleavage site (PLREKRRKR/G) and intravenous pathogenicity index values of 2.90 in chickens. We determined the subtype of the HPAI virus neuraminidase (NA) through NA sequence analysis as N1.

Phylogenetic analysis of the HA segment revealed that the strains isolated from northern fur seals on Tyuleniy Island belonged to HPAI H5N1 virus clade 2.3.4.4.b of the A/goose/Guangdong/1/96-like (Gs/GD) lineage (Figure 2). We found the HA segments of the viruses isolated from northern fur seals on Tyuleniy Island belonged to G2 group of clade 2.3.4.4b (Figure 2). Clade 2.3.4.4.b was divided into groups G1 and G2. Subsequently, several subgroups were identified in group G2: G2a–G2e (*3*,*4*). The G2 group comprises

Author affiliations: Federal Research Center of Fundamental and Translational Medicine, Novosibirsk, Russia (I. Sobolev, A. Alekseev, K. Sharshov, M. Chistyaeva, O. Kurskaya, O. Ohlopkova, A. Moshkin, A. Derko, A. Loginova, M. Solomatina, A. Shestopalov); Green Sakhalin Nature and Environment Protection Fund, Kholmsk, Russia (A. Ivanov); Dagestan State University, Makhachkala, Russia (A. Gadzhiev); Chinese Academy of Sciences, Beijing, China (Y. Bi)

DOI: http://doi.org/10.3201/eid3010.231728

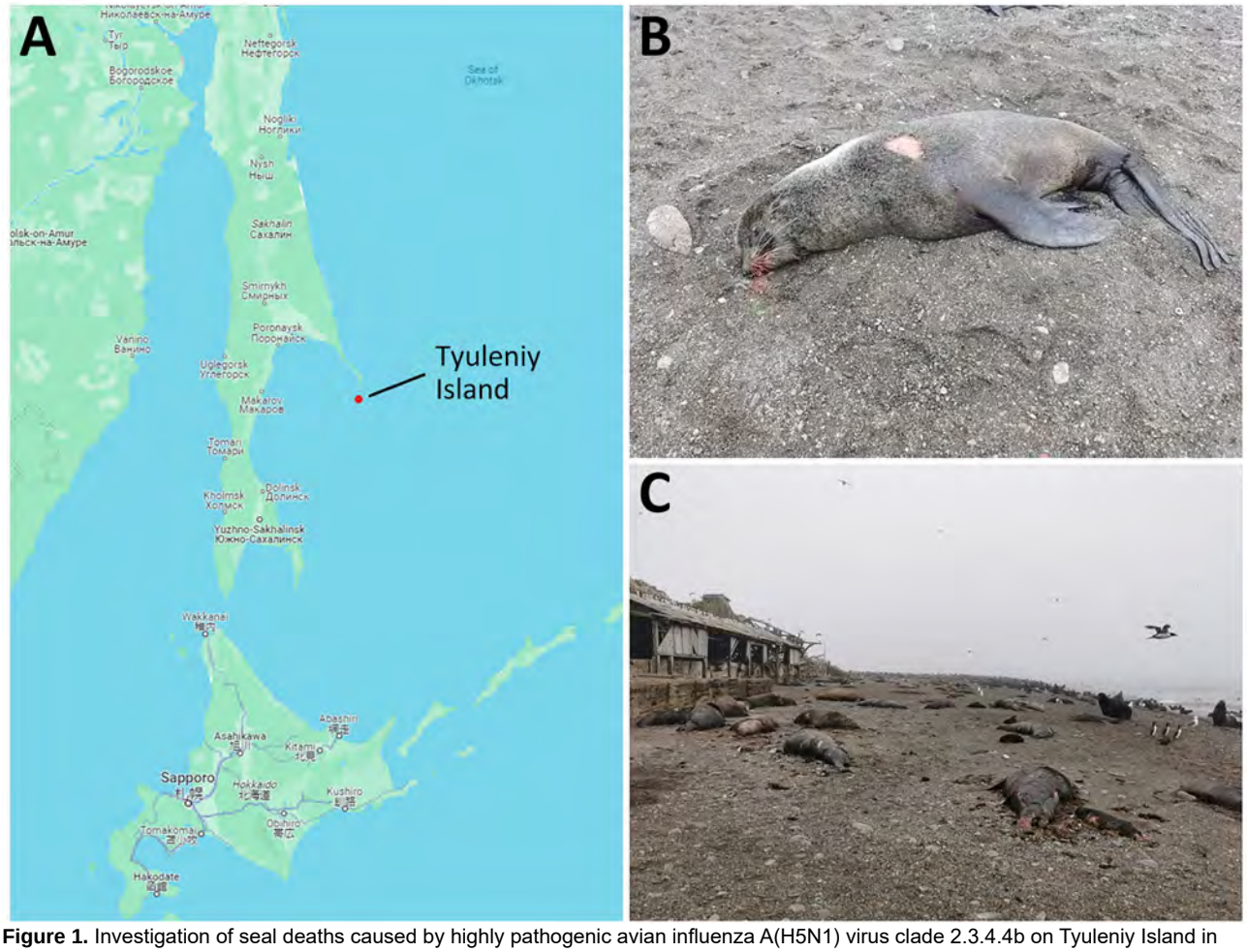

Figure 1. Investigation of seal deaths caused by highly pathogenic avian influenza A(H5N1) virus clade 2.3.4.4b on Tyuleniy Island in eastern Russia. A) Location of Tyuleniy Island in the Sea of Okhotsk. B, C) Deceased seals infected with the virus.

viruses detected in Egypt during 2017–2019, in Iraq in May 2020, in Russia, Kazakhstan, and Europe in July–November 2020 (*5*–*8*) and subsequently spread throughout Eurasia (*3*,*4*).

Whole-genome phylogenetic analysis (Figure 2; Appendix 1 Figures 4–10) revealed that viruses from northern fur seals are closely related to HPAI viruses circulating predominantly in Japan (in January–March 2022, October–December 2022, and January–April 2023) and to viruses detected in the Far East of Russia in April and October–November 2022. HPAI viruses circulating in Japan (September 2022–April 2023 and November 2023) and in the Far East of Russia, Khabarovsk and Magadan, in April 2022 and in October 2022, belong to 3 genetic subgroups (G2b, G2c, and G2d) of clade 2.3.4.4b (*9*). Viruses from Tyuleniy Island clustered with G2d subgroup viruses described earlier by Hew et al. (*9*). Phylogenetic and BLAST analysis (https://blast.ncbi.nlm.nih.gov) of HA sequences of H5Nx influenza viruses detected in mammals indicated that the viruses from seals from Tyuleniy Island are related to other mammal viruses isolated from raccoon dogs and Ezo red foxes in Japan in 2022, as well as from red foxes in Estonia in 2021 and Alaska in 2022. Previously published literature and information from GISAID EpiFlu (https://www.gisaid.org) showed multiple instances of HPAI H5Nx clade 2.3.4.4b virus infection in mammals, including marine mammals (*10*–*14*).

Table. Highly pathogenic avian influenza viruses isolates from 2 northern fur seals on Tyuleniy Island, Russia, 2023*

Isolate name	Host	Source	GISAID ID
A/Northern_fur_seal/Russia_Tyuleniy/74/2023	Seal 1	Small intestine	EPI_ISL_18554237
A/Northern_fur_seal/Russia_Tyuleniy/74-2/2023	Seal 1	Lung	EPI_ISL_19080209
A/Northern_fur_seal/Russia_Tyuleniy/75/2023	Seal 2	Lung	EPI_ISL_19080210

*Samples were collected on August 10, 20203. GISAID, https://www.gisaid.org; ID, identification.

Figure 2. Maximum-likelihood phylogenetic tree of the hemagglutinin segment of HPAI A(H5N1) from northern fur seals on Tyuleniy Island in eastern Russia (red) and in other marine mammals, by clade group. Black dots indicate HA of viruses isolated from other mammals, and blue text indicates HPAI viruses isolated in Japan during January–April 2023. GISAID accession numbers are shown for reference sequences (https://www.gisaid.org). Note that dates are shown in DD.MM.YYYY format. Scale bar indicates number of substitutions per site. HA, hemagglutinin; HPAI, highly pathogenic avian influenza.

During 2022–2023, the HPAI H5 virus spread extensively throughout Japan, affecting a wide range of hosts, including not only wild waterfowl but also poultry and birds of prey. The virus was also detected in the Russian Far East, particularly in Magadan and Sakhalin. Data obtained from satellite tracking (*15*) showed that birds wintering in Japan mainly migrate in the spring to Kamchatka, often via Sakhalin, and then further to Chukotka. Some birds remain on Sakhalin, and a small number migrate to the Kuril Islands and Kolyma (and further to Chukotka).

The coexistence of birds and marine mammals on Tyuleniy Island creates favorable conditions for the spread of viruses, not only among birds but also for their transmission to seals during the breeding season (April–August). On the basis of phylogenetic analysis, the timing of outbreak, and data on bird migration in the Pacific region, we suggest the virus that caused the deaths of marine mammals on Tyuleniy Island near Sakhalin in 2023 likely entered their populations as a result of spring bird migration from Japan. Viruses isolated from 2 northern fur seals on Tyuleniy Island are closely related but not completely identical. They differed by several amino acid substitutions, including the E627K mutation in PB2 of strains A/Northern fur seal/Russia_Tyuleniy74/2023 and A/Northern fur seal/Russia_Tyuleniy74-2/2023 isolated from the small intestine and lungs of 1 animal. That mutation is known to be associated with a shift in virus host specificity from birds to mammals and has been repeatedly detected, including in viruses isolated from marine mammals (*13*,*14*).

Conclusions

The results of our study, combined with information from databases and data published in the literature, show that HPAI viruses have been repeatedly detected in mammals, including marine mammals, for several years. GISAID contains the nucleotide sequences of 84 strains of HPAI virus isolated from seals and sea lions. Most of the reported cases were identified during 2021–2023 and were caused by HPAI H5Nx viruses of clade 2.3.4.4.b.

The widespread distribution of this relatively new variant of the influenza virus has resulted in cases of transmission from birds to mammals. It is likely that the high population density of birds and marine mammals on the small Tyuleniy Island, as well as their close proximity, contributed to the widespread infection of seals with HPAI virus. Transmission from birds probably occurred in 2 ways: through adult seals eating sick or dead birds, and through seal adults' and pups' contact with feces from infected birds. Unfortunately, the variability and transmission of the detected virus cannot be traced without a long-term study of the virus in parallel in the Tyuleniy Island bird population and in the seal population, starting from the beginning of spring bird migration. Even so, the number of seal deaths, mass mortality of pups, phylogenetic differences with viruses circulating in October–December 2022 and January–April 2023, and the detection of the E627K substitution indicate the possibility of adaptation and transmission from seal to seal.

Acknowledgments

We thank those who provided sequence information through the GISAID EpiFlu database (Appendix 2, https://wwwnc.cdc.gov/EID/article/30/10/23-1728-App1.xlsx). We also thank Tourist and Ecological Club 'Boomerang' in Yuzhno-Sakhalinsk, Russia.

This study was supported by state Russian Science Foundation (project no. 23-64-00005).

About the Author

Dr. Sobolev is a researcher at the Research Institute of Virology, Federal Research Center of Fundamental and Translational Medicine, Siberian Branch, Russian Academy of Sciences, Russia. His primary research interest is the molecular diagnosis and epidemiology of avian influenza viruses.

References

1. Kondratyev AY, Litvinenko NM, Kaiser GW. Seabirds of the Russian Far East. Canadian Wildlife Service. 2000 [cited 2024 Apr 29]. https://publications.gc.ca/collections/Collection/CW69-15-4-2000E.pdf
2. Main results of fulfillment of the state task and plan of financial and economic activities of the Pacific branch of VNIRO ("TINRO") in 2022 [in Russian]. 2022 [cited 2024 Apr 29]. http://tinro.vniro.ru/ru/tinro/rezul-taty-nauchno-proizvodstvennoj-deyatel-nosti
3. Baek YG, Lee YN, Lee DH, Shin JI, Lee JH, Chung DH, et al. Multiple reassortants of H5N8 clade 2.3.4.4b highly pathogenic avian influenza viruses detected in South Korea during the winter of 2020-2021. Viruses. 2021;13:490. https://doi.org/10.3390/v13030490
4. Okuya K, Mine J, Tokorozaki K, Kojima I, Esaki M, Miyazawa K, et al. Genetically diverse highly pathogenic avian influenza A(H5N1/H5N8) viruses among wild waterfowl and domestic poultry, Japan, 2021. Emerg Infect Dis. 2022;28:1451–5. https://doi.org/10.3201/eid2807.212586
5. Beerens N, Heutink R, Harders F, Roose M, Pritz-Verschuren SBE, Germeraad EA, et al. Incursion of novel highly pathogenic avian influenza A(H5N8) virus, the Netherlands, October 2020. Emerg Infect Dis. 2021;27:1750–3. https://doi.org/10.3201/eid2706.204464
6. Lewis NS, Banyard AC, Whittard E, Karibayev T, Al Kafagi T, Chvala I, et al. Emergence and spread of novel H5N8, H5N5 and H5N1 clade 2.3.4.4 highly pathogenic avian influenza in 2020. Emerg Microbes Infect. 2021;10:148–51. https://doi.org/10.1080/22221751.2021.1872355

7. Verhagen JH, Fouchier RAM, Lewis N. Highly pathogenic avian influenza viruses at the wild-domestic bird interface in Europe: future directions for research and surveillance. Viruses. 2021;13:212. https://doi.org/10.3390/v13020212
8. Sobolev I, Sharshov K, Dubovitskiy N, Kurskaya O, Alekseev A, Leonov S, et al. Highly pathogenic avian influenza A(H5N8) virus clade 2.3.4.4b, western Siberia, Russia, 2020. Emerg Infect Dis. 2021;27:2224–7. https://doi.org/10.3201/eid2708.204969
9. Hew L, Isoda N, Takaya F, Ogasawara K, Kobayashi D, Huynh L, et al. Continuous introduction of H5 high pathogenicity avian influenza viruses in Hokkaido, Japan: characterization of viruses isolated in winter 2022–2023 and early winter 2023–2024. Transbound Emerg Dis. 2024;2024:1–18. https://doi.org/10.1155/2024/1199876
10. Shin DL, Siebert U, Lakemeyer J, Grilo M, Pawliczka I, Wu NH, et al. Highly pathogenic avian influenza A(H5N8) virus in gray seals, Baltic Sea. Emerg Infect Dis. 2019;25:2295–8. https://doi.org/10.3201/eid2512.181472
11. Leguia M, Garcia-Glaessner A, Muñoz-Saavedra B, Juarez D, Barrera P, Calvo-Mac C, et al. Highly pathogenic avian influenza A (H5N1) in marine mammals and seabirds in Peru. Nat Commun. 2023;14:5489. https://doi.org/10.1038/s41467-023-41182-0
12. Rimondi A, Vanstreels RET, Olivera V, Donini A, Lauriente MM, Uhart MM. Highly pathogenic avian influenza A(H5N1) viruses from multispecies outbreak, Argentina, August 2023. Emerg Infect Dis. 2024;30:812–4. https://doi.org/10.3201/eid3004.231725
13. Mirolo M, Pohlmann A, Ahrens AK, Kühl B, Rubio-Garcìa A, Kramer K, et al. Highly pathogenic avian influenza A virus (HPAIV) H5N1 infection in two European grey seals (*Halichoerus grypus*) with encephalitis. Emerg Microbes Infect. 2023;12:e2257810. https://doi.org/10.1080/22221751.2023.2257810
14. Bordes L, Vreman S, Heutink R, Roose M, Venema S, Pritz-Verschuren SBE, et al. Highly pathogenic avian influenza H5N1 virus infections in wild red foxes (*Vulpes vulpes*) show neurotropism and adaptive virus mutations. Microbiol Spectr. 2023;11:e0286722. https://doi.org/10.1128/spectrum.02867-22
15. Hupp JW, Yamaguchi N, Flint PL, Pearce JM, Tokita K-i, Shimada T, et al. Variation in spring migration routes and breeding distribution of northern pintails Anas acuta that winter in Japan. J Avian Biol. 2011;42:289–300. https://doi.org/10.1111/j.1600-048X.2011.05320.x

Address for correspondence: Ivan Sobolev, Research Institute of Virology, Federal Research Center of Fundamental and Translational Medicine, 2 Timakov St, Novosibirsk, Russia 630117; email: sobolev_i@hotmail.com

etymologia revisited

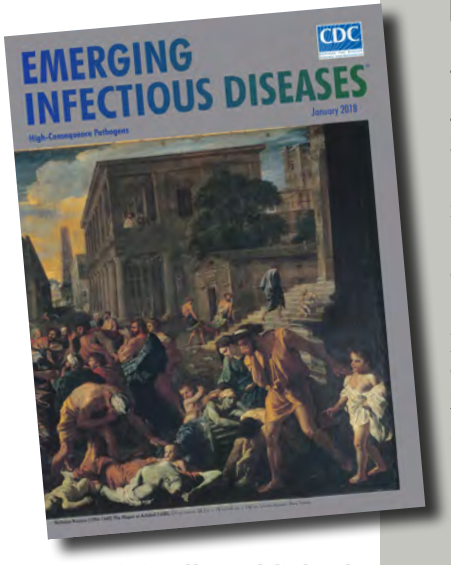

Originally published in January 2018

Plague

[plāg]

Plague (from the Latin *plaga*, "stroke" or "wound") infections are believed to have been common since at least 3000 BCE. Plague is caused by the ancestor of current *Yersinia* (named for Swiss bacteriologist Alexandre Yersin, who first isolated the bacterium) *pestis* strains. However, this ancestral *Y. pestis* lacked the critical *Yersinia* murine toxin (*ymt*) gene that enables vectorborne transmission. After acquiring this gene (sometime during 1600–950 BCE), which encodes a phospholipase D that protects the bacterium inside the flea gut, *Y. pestis* evolved the ability to cause pandemics of bubonic plague. The first recoded of these, the Justinian Plague, began in 541 ACE and eventually killed more than 25 million persons.

References:

1. Alexandre Yersin BW. Etymologia: yersinia. Emerg Infect Dis. 2010;16:496.
2. Centers for Disease Control and Prevention. History of plague [cited 2017 Oct 19]. https://www.cdc.gov/plague/history/index.html.
3. Rasmussen S, Allentoft ME, Nielsen K, Orlando L, Sikora M, Sjögren K-G, et al. Early divergent strains of Yersinia pestis in Eurasia 5,000 years ago. Cell. 2015;163:571–82.

https://wwwnc.cdc.gov/eid/article/24/1/et-2401_article

Autochthonous Human *Babesia divergens* Infection, England

Guillermo A. Zabala, Robert Lever, Xin Hui Chan, Henrietta Bristowe, Emer Kilbride, David Richards, Mark Daly, Michael Brown, Nick Johnson, Laura Eve Nabarro, Hanif Esmail, Gauri Godbole, Peter L. Chiodini

We describe a case of autochthonous human *Babesia divergens* infection in an immunocompetent woman in England. The patient had fever, hemolysis, multiorgan failure, and 18% parasitemia. We confirmed *B. divergens* by 18S rDNA PCR and sequencing. Clinicians should consider babesiosis as a differential diagnosis in patients with unexplained hemolysis.

Babesiosis is caused by intraerythrocytic protozoa from the genus *Babesia*. First reported in 1957 (*1*), babesiosis is now described worldwide. *Babesia* infecting humans come from 4 clades (*2*): 3 clades of small *Babesia*, 1 including *B. microti*, which exists as a species complex; 1 including *B. duncani*; and 1 including *B. divergens*, which, despite being small, is related to the 1 clade of large *Babesia* spp., which infects ungulates. *Ixodes* spp. ticks transmit *Babesia* between animal hosts. Each *Babesia*–vector–mammal host system has its own characteristics, and the ecology and bionomics of the vector tick define the pattern of risk for the human population. Humans are accidental hosts and can also acquire babesiosis by horizontal transmission in blood products and, in rare instances, via transplacental transmission (*3*).

Most human babesiosis cases are caused by *B. microti* species complex or *B. divergens*, but as recognition of human cases increases, other species, some newly described, have been found in humans. *B. microti* is endemic in the Northeast and northern Midwest United States, and ≈2,000 human *B. microti* babesiosis cases are reported annually (*4*). However, cases of *B. divergens* infections are rare, ≈50 reports in the literature, and often cause more severe illness (*5*).

In the United Kingdom, increasing *Babesia* spp. prevalence in *Ixodes* ticks has been noted (*6*), but only 1 human case of *B. divergens* babesiosis has been reported, from Scotland in 1979 (*7*). We describe a case of autochthonous *B. divergens* infection in England.

The Study

A 72-year-old retired nurse was admitted to a hospital in southwest England after 4 days of fever, body aches, loin pain, and frank hemoglobinuria. She received ciprofloxacin in primary care the preceding day for presumed urinary tract infection, but vomiting and jaundice subsequently developed. Physical examination confirmed fever (>40°C), tachycardia, and jaundice, but no other findings. Hemoglobin was 75 g/L and bilirubin 190 μmol/L.

Blood film showed intraerythrocytic parasites with the Maltese cross formation, pathognomonic for *Babesia* spp. (Figure 1). We published that morphology as an update to raise awareness in hematology laboratories (*8*). Peripheral parasitemia in erythrocytes was 18% at diagnosis (Table). After consulting the Hospital for Tropical Diseases (HTD), we began treatment with intravenous clindamycin (600 mg every 6 h) and quinine (10 mg/kg every 8 h). One day into admission the patient deteriorated, had severe hypoxia requiring intubation, and was transferred by helicopter to the HTD intensive care unit (ICU).

The patient had no underlying immunosuppressive conditions and no history of splenectomy or reduced splenic function. She lived in a coastal town in Devon, UK; her only travel abroad in the preceding 12 months was a vacation in Tenerife, Spain, 5

Author affiliations: Infectious Diseases Data Observatory, Oxford, UK (G.A. Zambala); Hospital for Tropical Diseases, University College Hospital, London, UK (G.A. Zabala, R. Lever, X.H. Chan, H. Bristowe, E. Kilbride, M. Brown, L.E. Nabarro, H. Esmail, G. Godbole, P.L. Chiodini); London School of Hygiene and Tropical Medicine, London (R. Lever, M. Brown, G. Godbole, P.L. Chodini); Centre for Tropical Medicine and Global Health, University of Oxford, Oxford (X.H Chan); North Devon District Hospital, Barnstaple, UK (D. Richards, M. Daly); Animal and Plant Health Agency, Surrey, UK (N. Johnson); Institute for Global Health and Medical Research Council Clinical Trials Unit, University College London, London (H. Esmail)

DOI: https://doi.org/10.3201/eid3010.240866

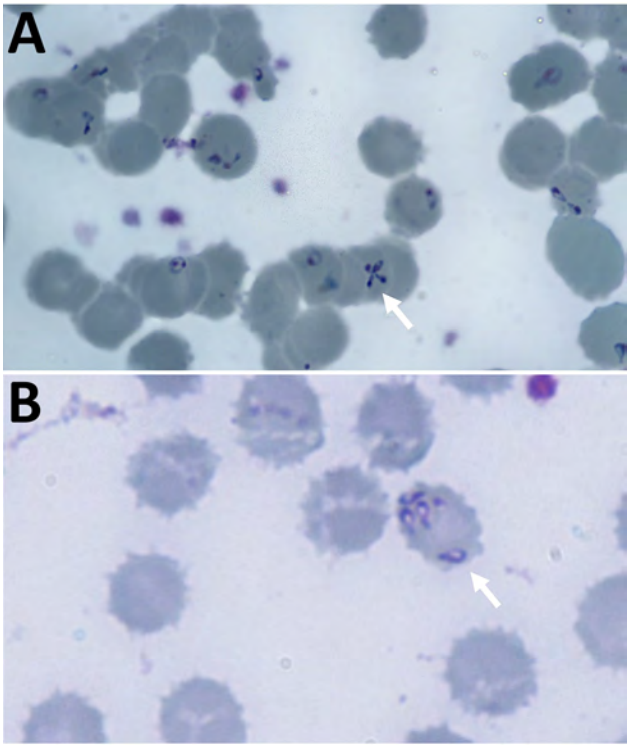

Figure 1. Giemsa-stained thin blood film from a case of autochthonous human *Babesia divergens* infection, England. A) Stains show characteristic Maltese cross form (arrow) and erythrocytes containing 5 pyriform rings. Original magnification ×1,000. B) Absence of pigment in erythrocytes (arrow). Original magnification ×1,000.

months earlier. In the weeks before admission, she took walks along the coast, where cattle (the mammal host of *B. divergens*) grazed. Although ticks were in the area, she had not noticed any bites. She had no companion animals, but her daughter had a dog. She had never received blood products.

The patient's illness was complicated by anuric acute kidney injury and fluid-refractory hypotension requiring renal dialysis and vasopressor support. Bilateral exudative pleural effusions developed (Figure 2), and she had hospital-acquired pneumonia. Severe intravascular hemolysis and black urine continued (Figure 3), which later showed evidence of hypersplenism, extravascular hemolysis, and thrombocytopenia. Her direct antiglobulin test remained negative throughout hospitalization. She underwent manual exchange transfusion with 4 units of O-negative blood and subsequent transfusion with 2 units of M- and S-antigen–negative erythrocytes on day 9 (Table). Because her recovery was protracted and thrombocytopenia was evolving, we added intravenous doxycycline (200 mg every 24 h) for possible *Anaplasma* co-infection.

Despite good parasitological response to treatment, the patient suffered a prolonged period of encephalopathy during convalescence. Magnetic resonance imaging of the brain showed an old cerebellar infarct, cerebrospinal fluid analysis was unremarkable, and an electroencephalogram showed nonspecific cerebral dysfunction.

Results of testing for immunoglobulins, complement blood tests, lymphocyte subsets, nuclear antibodies, tissue-transglutaminase antibodies, pneumococcal antibodies, and serum protein electrophoresis were all within reference ranges. Results of HIV serology and markers for hepatitis B and C viruses were negative; abdominal ultrasonography ruled out anatomic hyposplenia.

The patient's encephalopathy gradually resolved, and she was extubated on day 13 of her ICU stay. Blood films on day 14 of treatment were negative, and antiparasitic agents were discontinued 24 hours later (Table). She subsequently recovered renal function and no longer required dialysis.

B. divergens infection was confirmed by 18S PCR and genomic sequencing from a blood sample drawn shortly after ICU admission (Appendix, https://wwwnc.cdc.gov/EID/article/30/10/24-0866-App1.pdf). Acute-phase serology was negative for tick-borne encephalitis, *Rickettsia*, *Borrelia*, and *Anaplasma*. Convalescent serology for *Anaplasma* gave a weak, nonspecific reaction.

Conclusions

B. divergens, transmitted by *Ixodes ricinus*, has been in England, including Devon, for >100 years (*9*). In

Table. Course of parasitemia during admission and interventions used in a case of autochthonous human *Babesia divergens* infection, England*

Days after admission	% Parasitemia†	Intervention
0	18	IV quinine, 10 mg/kg every 8 h; IV clindamycin, 600 mg every 6 h
1	9	
2	2.4	IV quinine, 10 mg/kg every 8 h; IV clindamycin, 600 mg every 6 h; nasogastric atovaquone, 750 mg every 12 h
3	1.3	4 units red blood cells via manual exchange transfusion
4	0.9	
5	0.07	IV azithromycin, 250 mg every 24 h; IV clindamycin, 600 mg every 6 h; nasogastric atovaquone 750 mg every 12 h
6	0.1	
7	0.08	
8	0.05	IV doxycycline, 200 mg every 24 h
9	0.03	
10	0.03	
11	0.02	2 units of M- and S-antigen–negative red blood cells
12	0.01	
13	0.01	
14	0	
15	0	Antiparasitic agents discontinued

*IV, intravenous.
†Percentage of parasitized erythrocytes detected by light microscopy of thin blood films.

Figure 2. Axial computed tomography image from a case of autochthonous human *Babesia divergens* infection, England. Image shows bilateral pleural effusions.

Figure 3. Urometer from a case of autochthonous human *Babesia divergens* infection, England. Black urine can be noted in the collection bag.

mild bovine cases, babesiosis (also called Redwater fever) causes fever and anorexia; severe cases result in fatal hemolytic anemia with hemoglobinuria. This case documents emergence of autochthonous human babesiosis in England. Public health conducted a tick survey in the patient's local area but found no ticks carrying *Babesia* spp. (*10*). Serologic surveys were not possible because *B. divergens* serology is unavailable in the United Kingdom; whether subclinical human *B. divergens* infections occurred in the locality at the time is unknown, but clinicians and veterinarians in England were notified of the case to raise awareness.

This case highlights the potential for severe *B. divergens* infection in the absence of depressed immunity. Severe *B. divergens* infection causes influenza-like illness and hemolysis, after which ≈40% of patients have multiorgan failure and die (*5*). In a case series in Europe, 84% of *B. divergens* infections were in patients with previous splenectomy (*3*). However, PCR-confirmed *B. divergens* infection was found in an immunocompetent adult in France, demonstrating the parasite's ability to cause illness in previously healthy persons (*11*), as in our case. We considered whether *Anaplasma* co-infection increased illness severity in our patient, but that was not proven. For *B. microti*, patients with *B. burgdorferi* co-infection reportedly have more symptoms and longer illness than patients with either infection alone, although no uniform agreement exists between studies on co-infection, neither in humans nor animal models (*12*). Nevertheless, dual infections are increasingly seen, as have triple diagnoses with babesiosis, Lyme disease, and anaplasmosis (*13*). Thus, clinicians should suspect multi-infection in patients with an initial babesiosis diagnosis.

Clinical laboratories diagnose *B. divergens* via blood film identification and PCR confirmation (*13*). Babesiosis treatment options include oral atovaquone and azithromycin in mild disease or intravenous clindamycin and quinine in severe cases (*13*). Extrapolating from *B. microti* treatment, oral atovaquone plus intravenous azithromycin is an option in *B. divergens* cases, but no randomized controlled trials or pharmacokinetic studies on *B. divergens* in humans are available. Exchange transfusion is recommended for parasitemia >10%, or moderate parasitemia with severe hemolytic anemia or organ dysfunction (*13*), and novel approaches to exchange transfusion have been suggested (*14*). No published trials are available, but to reduce parasitic invasion of additional erythrocytes in our patient, we administered 2 units of M- and S-antigen–negative erythrocytes, which are resistant to *B. divergens* invasion, during the second transfusion (*14*).

In summary, the clinical and laboratory features of babesiosis and its rarity could lead clinicians to misdiagnose babesiosis as leptospirosis, urosepsis, or biliary sepsis and thus cause delays in appropriate therapy. *Babesia* also can be morphologically misidentified as *Plasmodium*. Furthermore, *Borrelia*, *Anaplasma*, or *Ehrlichia* co-infection can complicate the illness. Physicians should consider babesiosis as a differential diagnosis in patients with unexplained intravascular hemolysis, especially in rural areas.

About the Author

Dr. Zabala is a senior clinical fellow in Infectious Diseases and Internal Medicine at University College Hospital in London, UK, and a research scientist at the Infectious Diseases Data Observatory in Oxford, UK. His research interests are emerging infectious diseases and the pharmacoepidemiology of poor-quality antibiotics.

References

1. Skrabalo Z, Deanovic Z. Piroplasmosis in man; report of a case. Doc Med Geogr Trop. 1957;9:11–6.
2. Vannier E, Krause PJ. Human babesiosis. N Engl J Med. 2012;366:2397–407. https://doi.org/10.1056/NEJMra1202018
3. Kjemtrup AM, Conrad PA. Human babesiosis: an emerging tick-borne disease. Int J Parasitol. 2000;30:1323–37. https://doi.org/10.1016/S0020-7519(00)00137-5
4. Krause PJ. Human babesiosis. Int J Parasitol. 2019;49:165–74. https://doi.org/10.1016/j.ijpara.2018.11.007
5. Hildebrandt A, Gray JS, Hunfeld KP. Human babesiosis in Europe: what clinicians need to know. Infection. 2013;41:1057–72. https://doi.org/10.1007/s15010-013-0526-8
6. Abdullah S, Helps C, Tasker S, Newbury H, Wall R. Prevalence and distribution of *Borrelia* and *Babesia* species in ticks feeding on dogs in the U.K. Med Vet Entomol. 2018;32:14–22. https://doi.org/10.1111/mve.12257
7. Entrican JH, Williams H, Cook IA, Lancaster WM, Clark JC, Joyner LP, et al. Babesiosis in man: report of a case from Scotland with observations on the infecting strain. J Infect. 1979;1:227–34. https://doi.org/10.1016/S0163-4453(79)91219-2
8. Chan WY, MacDonald C, Keenan A, Xu K, Bain BJ, Chiodini PL. Severe babesiosis due to *Babesia divergens* acquired in the United Kingdom. Am J Hematol. 2021;96:889–90. https://doi.org/10.1002/ajh.26097
9. McFadzean H, Johnson N, Phipps LP, Swinson V, Boden LA. Surveillance and risk analysis for bovine babesiosis in England and Wales to inform disease distribution. Animals (Basel). 2023;13:2118. https://doi.org/10.3390/ani13132118
10. Johnson N, Phipps P, Godbole G, Hansford K, Johnston C, White M, et al. Preventing tick exposure in vets and farmers. Vet Rec. 2020;187:195. https://doi.org/10.1136/vr.m3334
11. Martinot M, Zadeh MM, Hansmann Y, Grawey I, Christmann D, Aguillon S, et al. Babesiosis in immunocompetent patients, Europe. Emerg Infect Dis. 2011;17:114–6. https://doi.org/10.3201/eid1701.100737
12. Krause PJ, McKay K, Thompson CA, Sikand VK, Lentz R, Lepore T, et al.; Deer-Associated Infection Study Group. Disease-specific diagnosis of coinfecting tickborne zoonoses: babesiosis, human granulocytic ehrlichiosis, and Lyme disease. Clin Infect Dis. 2002;34:1184–91. https://doi.org/10.1086/339813
13. Smith RP, Hunfeld K-P, Krause PJ. Management strategies for human babesiosis. Expert Rev Anti Infect Ther. 2020;18:625–36. https://doi.org/10.1080/14787210.2020.1752193
14. Jajosky RP, Jajosky AN, Jajosky PG. Optimizing exchange transfusion for patients with severe *Babesia divergens* babesiosis: therapeutically-rational exchange (T-REX) of M antigen-negative and/or S antigen-negative red blood cells should be evaluated now. Transfus Clin Biol. 2019;26:76–9. https://doi.org/10.1016/j.tracli.2018.10.001

Address for correspondence: Peter L. Chiodini, UKHSA Malaria Reference Laboratory, The London School of Hygiene and Tropical Medicine, London WC1E 7HT, UK; email: p.chiodini@nhs.net

Bluetongue Virus in the Iberian Lynx (*Lynx pardinus*), 2010–2022

Javier Caballero-Gómez, Marta Sánchez-Sánchez, Cristina Lorca-Oró, Isabel G. Fernández de Mera, Irene Zorrilla, Guillermo López, Rosa Rosell, Rebeca Grande-Gómez, Juan I. Montoya-Oliver, Javier Salcedo, Jorge Paniagua, Cristina Cano-Gómez, Moisés Gonzálvez, Ignacio García-Bocanegra

Clinical infection and death caused by bluetongue virus infection has been reported in the Eurasian lynx. Bluetongue virus surveillance in the Iberian lynx revealed widespread and repeated exposure to serotypes 1 and 4 in wild and captive populations of this species. This exposure is possibly from a spillover event from sympatric ruminants.

Bluetongue virus (BTV) is a reemerging, multihost orbivirus of animal health concern. Although the disease is subject to eradication in some regions of Europe, BTV continues to circulate and spread to new areas of the continent (*1*,*2*). Wild ruminants play a role in the continued presence and dissemination of BTV in Iberian ecosystems (*3*), where they share habitats and natural resources with other wildlife species such as the Iberian lynx (*Lynx pardinus*). The Iberian lynx, endemic to the Iberian Peninsula, is one of the most vulnerable felids in the world (*4*). In recent decades, shared pathogens with sympatric species, including ruminants, have caused clinical disease and death in the Iberian lynx (*5*). Although exposure, clinical infection, and death because of BTV infection have been reported in the Eurasian lynx (*L. lynx*) (*6*,*7*), the susceptibility of Iberian lynxes to BTV is unknown. The objectives of our research were to determine BTV exposure in Iberian lynx populations, to assess potential risk factors associated with viral exposure in this species, and to evaluate the dynamics of seropositivity to BTV in longitudinally sampled animals.

The Study

We collected blood, serum, and spleen samples from 340 Iberian lynxes (229 free-ranging and 111 captive) throughout the Iberian Peninsula during 2010–2022 (Table; Figure 1). In addition, longitudinal surveillance was conducted on 50 of the 340 Iberian lynxes during the study period.

We tested serum samples for BTV antibodies by using a double recognition ELISA (Gold Standard Diagnostics, https://www.goldstandarddiagnostics.com). Whenever possible, we tested ELISA-positive serum by using a virus neutralization test (VNT) to detect specific antibodies against BTV-1 and BTV-4 serotypes (Appendix, https://wwwnc.cdc.gov/EID/article/30/10/24-0235-App1.pdf). We assessed the presence of viral RNA in blood and spleen samples from ELISA-seropositive lynxes with available samples (n = 30) and a subset of randomly selected seronegative animals (n = 69) by molecular analyses (Appendix) (*8*–*10*). We analyzed associations between the seropositivity to BTV detected by ELISA and explanatory variables by using Pearson χ^2 or Fisher exact tests, considering differences significant at $p \leq 0.05$.

ELISA testing found that 39 (11.5%; 95% CI 8.5–15.3) of the 340 Iberian lynxes were positive for BTV antibodies (Table; Figure 1). We detected significant differences in the ages, sexes, life condition, and sampling region of the animals (Table). Of the 50 longitudinally sampled animals, 4 were seropositive at all samplings, whereas seroconversions were

Author affiliations: University of Cordoba, Cordoba, Spain (J. Caballero-Gómez, I. García-Bocanegra, J. Paniagua, M. Gonzálvez, I. García-Bocanegra); Carlos III Health Institute, Madrid, Spain (J. Caballero-Gómez); Institute for Game and Wildlife Research, Ciudad Real, Spain (M. Sánchez-Sánchez, I.G. Fernández de Mera); Campus de la Universitat Autònoma de Barcelona, Bellaterra, Spain (C. Lorca-Oró, R. Rosell); Junta de Andalucía, Malaga, Spain (I. Zorrilla, G. López); Generalitat de Catalunya, Barcelona, Spain (R. Rosell); Technical Assistance from the General Direction of the Natural Environment and Sustainable Development of the Board of Communities of Castilla La Mancha, Toledo, Spain (R. Grande-Gómez); Ministry for the Ecological Transition and the Demographic Challenge, Madrid (J.I. Montoya-Oliver); Junta de Andalucía, Seville, Spain (J. Salcedo); Spanish Ministry of Agriculture, Food and Fisheries, Madrid (C. Cano-Gómez); University of Murcia, Murcia, Spain (M. Gonzálvez).

DOI: https://doi.org/10.3201/eid3010.240235

Table. Bluetongue virus seropositivity in Iberian lynxes (*Lynx pardinus*) sampled in the Iberian Peninsula during 2010–2022 by age, sex, life condition, sampling period, and region

Variable	Seroprevalence, % (95% CI)	No. positives/no. analyzed*	p value†
Age			
Yearling	4.5 (1.9–10.0)	5/112	<0.001
Subadult	6.0 (2.5–13.2)	5/83	
Adult	20.6 (14.7–28.0)	29/141	
Sex			
F	7.5 (4.3–12.6)	12/161	0.016
M	15.6 (10.1–21.8)	26/167	
Life condition			
Captive	6.3 (3.1–12.5)	7/111	0.025
Free ranging	14.0 (10.1–19.1)	32/229	
Sampling period‡			
2010–2016	12.4 (7.8–19.2)	16/129	0.128
2017–2020	7.3 (3.9–13.2)	9/124	
2021–2022	16.1 (9.8–25.2)	14/87	
Sampling region			
Central	6.8 (2.9–14.9)	5/74	0.009
South	17.8 (12.5–24.6)	27/152	
Southwest	6.8 (3.3–13.4)	7/103	

*Missing values excluded.
†p≤0.5 significant.
‡The frequency of seropositivity by sampling year was 16.7% (2/12) in 2010, 0% (0/1) in 2011, 11.1% (2/18) in 2012, 13.3% (2/15) in 2013, 0% (0/2) in 2014, 12.5% (3/24) in 2015, 12.3% (7/57) in 2016, 11.8% (4/34) in 2017, 13.3% (2/15) in 2018, 6.5% (2/31) in 2019, 2.3% (1/44) in 2020, 11.7% (9/77) in 2021, and 50.0% (5/10) in 2022.

found in 9 animals and seroreversions in 3 animals (Appendix Table 1).

Of the ELISA-seropositive samples, 7 could not be analyzed by using VNT because of cytotoxicity or insufficient sample volume, and 13 of the ELISA-seropositive samples were negative by using VNT (Appendix Table 2). Of the Iberian lynxes analyzed, 19 (59.4%) had antibodies against BTV by both ELISA and VNT. Specific antibodies against serotype BTV-1 were detected in 10 samples (3.0%, 95% CI 1.6%–5.4%) and against BTV-4 were detected in 9 samples (2.7%, 95% CI 1.4%–5.1%). Of note, 2/10 animals with BTV-1 antibodies also showed neutralizing activity to BTV-4. Despite having 4-fold lower titers,

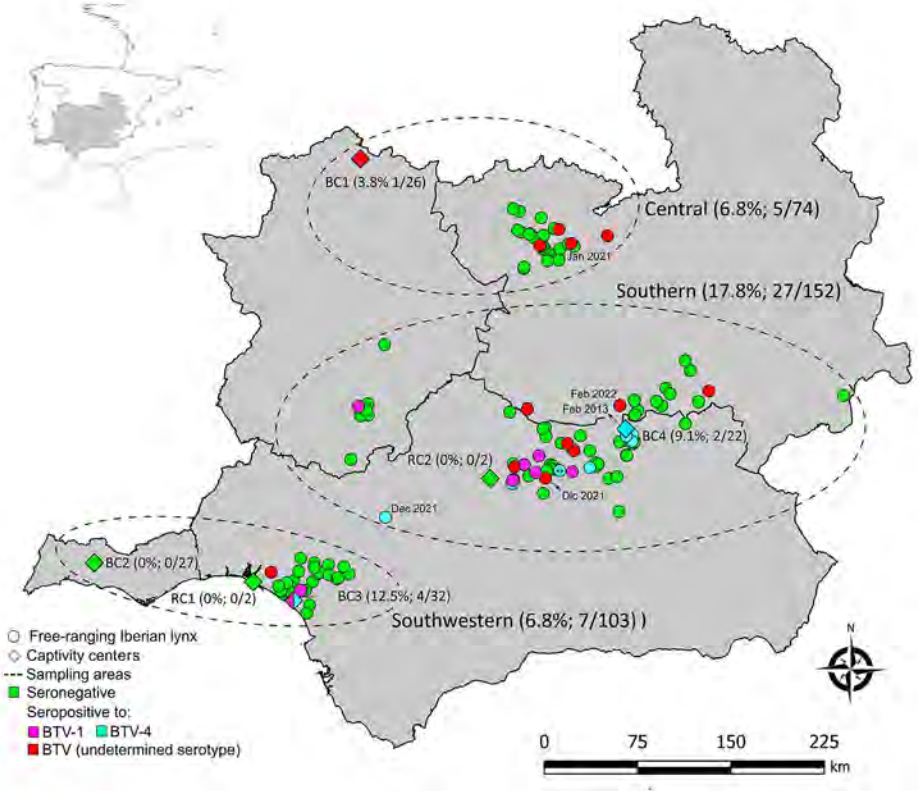

Figure 1. Spatial distribution and BTV serologic results of the Iberian lynxes (*Lynx pardinus*) sampled in the Iberian Peninsula during 2010–2022. The frequency of seropositivity and the numbers of seropositive and total of animals analyzed by ELISA at each sampling region and captivity center are shown in parentheses. Inset map shows location of study area on the Iberian Peninsula. **Animal tested positive for BTV RNA. BC, breeding center; BTV, bluetongue virus; RC, recovery center of threatened species.

co-exposure to both serotypes in these animals cannot be ruled out. BTV RNA was detected in the blood of 1 Iberian lynx (1.0%, 95% CI 0.2%–5.5%), which also had specific neutralizing antibodies against BTV-4. Phylogenetic analysis of segments 2, 5, and 10 confirmed the presence of BTV-4 RNA (GenBank accession nos. PP319976–319978) and showed high similarity (≥99%) with BTV-4 sequences obtained during the study period from cattle, goats, sheep, and Iberian ibexes in southern Spain (Figure 2).

Our study confirms the exposure of Iberian lynx populations to BTV, increasing the number of wildlife species susceptible to this virus. Although BTV was thought to be transmitted to carnivores through *Culicoides* biting midges, BTV infection in carnivores appears to occur primarily through the ingestion of infected animals (*11*). Because of this transmission, the higher seropositivity found in free-ranging animals (14.0%) compared with captive animals (6.3%) might be explained by the trophic behavior of free-ranging Iberian lynxes on wild ungulates (*12*), which is further supported by the high homology (≥99%) of the BTV-4 sequence with those found in wild ungulates from Spain. However, it is also possible that free-ranging lynxes are more frequently exposed to *Culicoides* because of their larger home range and the lack of periodic cleaning and disinfestation procedures used in captivity centers (*13*), which could interfere with the breeding cycle of *Culicoides*.

The higher seroprevalence detected in male compared with female animals aligns with findings in wild ruminants, where male animals' larger home ranges and body mass increase their risk for contact with *Culicoides* midges (*14*). The higher frequency of seropositivity detected in adults (20.6%) compared with that for subadults (6.0%) and yearlings (4.5%) might be associated with a higher likelihood of cumulative exposure to BTV and lifelong persistence of antibodies in Iberian lynxes (*3*). Of note, 1 yearling sampled in 2013, 3 yearlings sampled in 2021, and 1

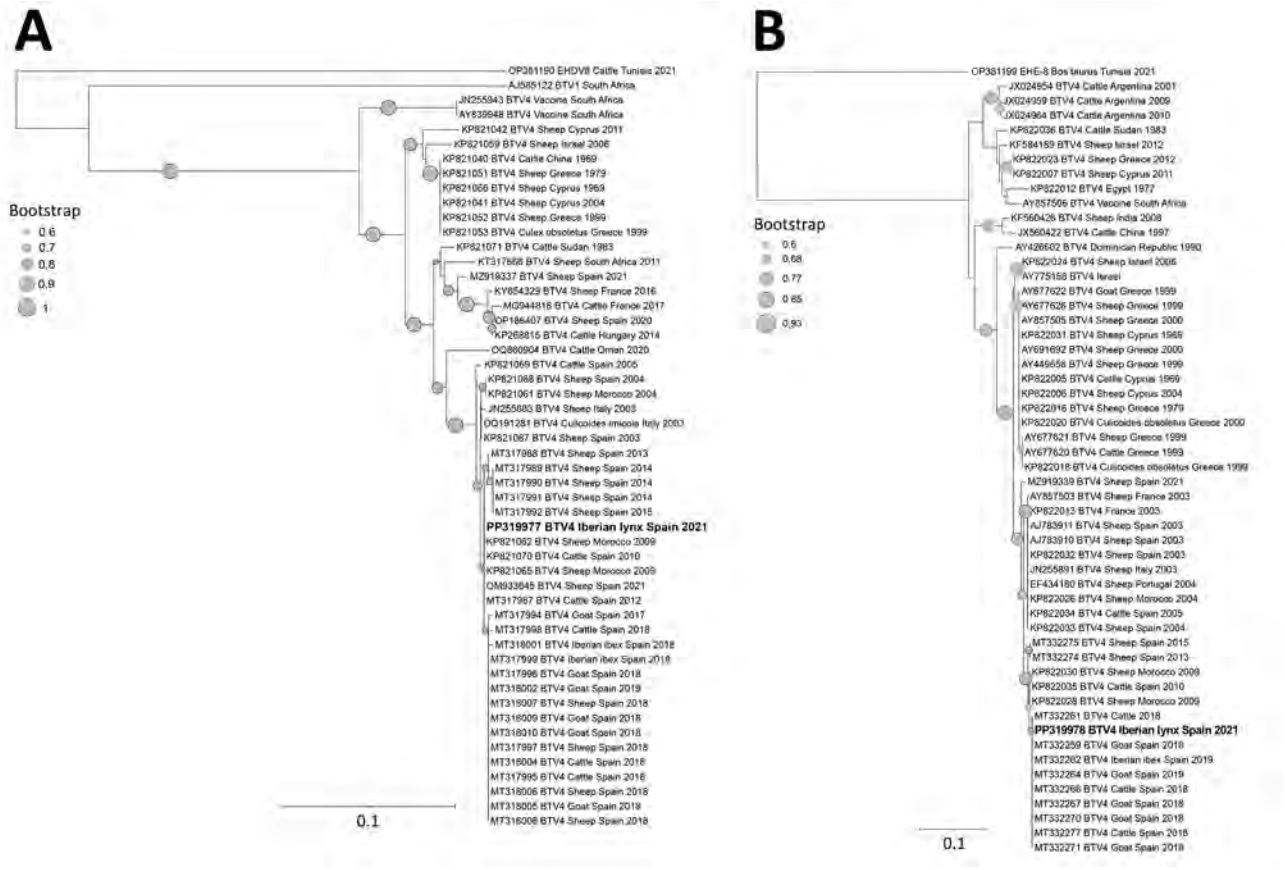

Figure 2. Phylogenetic tree of BTV from Iberian lynxes (*Lynx pardinus*) sampled in the Iberian Peninsula during 2010–2022 (bold) and reference sequences. Tree was constructed by the neighbor-joining method (1,000 bootstraps). A) Segment 2 tree, based on 393 nucleotides of 52 sequences. BTV-1 serotype and epizootic hemorrhagic disease virus serotype 8 reference strains were included to root the tree. B) Segment 10 tree, based on 216 nucleotides of 54 sequences. Epizootic hemorrhagic disease virus serotype 8 reference strain was included to root the tree. Gray circles indicate bootstrap values; only values ≥60 are shown. GenBank accession numbers are provided. Scale bars indicate number of substitutions per site. BTV, bluetongue virus.

yearling sampled in 2022 were positive for BTV antibodies, suggesting recent exposure to BTV in Iberian lynx populations during these years. This hypothesis is supported by concurrent outbreaks of BTV infection in livestock (*15*). Furthermore, the 4 BTV-1 seroconversions overlap spatiotemporally with outbreaks of this serotype reported in livestock (*15*). This finding, together with the higher seroprevalence observed in lynxes from the southern region, which is consistent with the higher number of BTV outbreaks reported in livestock in this area (*15*), suggests a common epidemiologic pattern of BTV in domestic and wild species. However, 2/5 seropositive yearlings were sampled in the provinces of Jaen and Toledo (southern and central Spain) in February 2013 and January 2021, whereas the previous BTV outbreaks reported in livestock in these provinces occurred in 2010 and 2014 (*15*). Those findings are consistent with previous reports of BTV circulating in wild ruminants in the absence of BTV outbreaks in livestock in Spain (*3*) and highlight the importance of wildlife in the epidemiology of this virus in the study area, especially in areas where livestock vaccination has been implemented.

Conclusions

We confirmed the presence of BTV-1 and BTV-4 serotype neutralizing antibodies in both free-ranging and captive Iberian lynxes. This result is consistent with the BTV outbreaks detected in livestock in Spain during the study period, where cases of BTV-1 and BTV-4 were reported (*15*). The detection of BTV-4 RNA in an Iberian lynx confirms the susceptibility of the species to BTV infection. The infected lynx was a BTV-4–seropositive, free-ranging lynx sampled in southern Spain (municipality of Marmolejo) on November 31, 2021. Exposure to BTV was also detected in a yearling sampled close to this municipality on December 3, 2021, and outbreaks of BTV-4 serotype were reported in domestic ruminants close to this location during this period (*15*). This finding, together with the high similarity with other sequences obtained from domestic and wild ruminants in Spain, provides evidence that the exposure of Iberian lynxes to BTV could be the result of spillover from domestic or wild sympatric ruminants, indicating a common epidemiologic cycle of BTV among ruminants and Iberian lynxes.

In summary, we report evidence of widespread and repeated exposure to BTV in Iberian lynx populations. Further studies are needed to determine the effects of BTV on the health of Iberian lynx populations, but the low prevalence of infection suggests that this species may be considered a spillover host, rather than a true reservoir of BTV.

Acknowledgments

We thank the regional governments of Junta de Andalucía and Junta de Castilla-La Mancha for allowing us to carry out this study. We thank the conservation programs of the Iberian lynx. We thank the Laboratorio Regional Agroalimentario y Ambiental de Castilla-La Mancha, especially Sonia Lázaro, for their support.

This study is part of the TED2021-132599B-C22 project, funded by MCIN/AEI/10.13039/501100011033 and the Recovery, Transformation and Resilience Plan, funded by the European Union (Next Generation EU). J.C-G. was supported by the CIBER-Consorcio Centro de Investigación Biomédica en Red-(CB21/13/00083), Instituto de Salud Carlos III, Ministerio de Ciencia e Innovación and the European Union (Next Generation EU). M.G. was supported by a postdoctoral contract Margarita Salas (University of Murcia) from the Program of Requalification of the Spanish University System (Spanish Ministry of Universities) financed by the European Union-NextGenerationEU. M.S-S. was supported by Investigo Program, funded by European Union (Next Generation EU).

About the Author

Dr. Caballero-Gómez is a postdoctoral researcher at the Maimonides Biomedical Research Institute of Cordoba. His research interests include the epidemiology and diagnosis of emerging and reemerging diseases of public and animal health concerns.

References

1. European Commission. About bluetongue. 2023 [cited 2024 Jan 22]. https://food.ec.europa.eu/animals/animal-diseases/surveillance-eradication-programmes-and-disease-free-status/bluetongue_en
2. World Animal Health Information System. 2023 [cited 2024 Jan 20]. https://www.woah.org/es/que-hacemos/sanidad-y-bienestar-animal/recopilacion-de-datos-sobre-enfermedades/sistema-mundial-de-informacion-sanitaria
3. García-Bocanegra I, Arenas-Montes A, Lorca-Oró C, Pujols J, González MÁ, Napp S, et al. Role of wild ruminants in the epidemiology of bluetongue virus serotypes 1, 4 and 8 in Spain. Vet Res. 2011;42:88. https://doi.org/10.1186/1297-9716-42-88
4. International Union for Conservation of Nature. The IUCN red list of threatened species. 2023 [cited 2024 Feb 10]. https://www.iucnredlist.org
5. Millán J, Candela MG, Palomares F, Cubero MJ, Rodríguez A, Barral M, et al. Disease threats to the endangered Iberian lynx (*Lynx pardinus*). Vet J. 2009;182:114–24. https://doi.org/10.1016/j.tvjl.2008.04.005
6. Jauniaux TP, De Clercq KE, Cassart DE, Kennedy S, Vandenbussche FE, Vandemeulebroucke EL, et al. Bluetongue in Eurasian lynx. Emerg Infect Dis. 2008;14:1496–8. https://doi.org/10.3201/eid1409.080434
7. Caballero-Gómez J, Cano Terriza D, Pujols J, Martínez-Nevado E, Carbonell MD, Guerra R, et al.

Monitoring of bluetongue virus in zoo animals in Spain, 2007–2019. Transbound Emerg Dis. 2022;69:1739–47. https://doi.org/10.1111/tbed.14147
8. Toussaint JF, Sailleau C, Breard E, Zientara S, De Clercq K. Bluetongue virus detection by two real-time RT-qPCRs targeting two different genomic segments. J Virol Methods. 2007;140:115–23. https://doi.org/10.1016/j.jviromet.2006.11.007
9. Gómez-Guillamón F, Caballero-Gómez J, Agüero M, Camacho-Sillero L, Risalde MA, Zorrilla I, et al. Reemergence of bluetongue virus serotype 4 in Iberian ibex (*Capra pyrenaica*) and sympatric livestock in Spain, 2018–2019. Transbound Emerg Dis. 2021;68:458–66. https://doi.org/10.1111/tbed.13696
10. Hofmann MA, Renzullo S, Mader M, Chaignat V, Worwa G, Thuer B. Genetic characterization of toggenburg orbivirus, a new bluetongue virus, from goats, Switzerland. Emerg Infect Dis. 2008;14:1855–61. https://doi.org/10.3201/eid1412.080818
11. More S, Bicout D, Bøtner A, Butterworth A, Depner K, Edwards S, et al.; EFSA Panel on Animal Health and Welfare (AHAW). Assessment of listing and categorization of animal diseases within the framework of the Animal Health Law (Regulation (EU) No 2016/429): bluetongue. EFSA J. 2017;15:e04957.
12. Gonzálvez M, Jiménez-Ruiz S, Paniagua J, Rouco C, García-Bocanegra I. Vulture feeding stations threaten Iberian lynx. Biol Conserv. 2023;281:109960. https://doi.org/10.1016/j.biocon.2023.109960
13. Rivas A, Boixader J, Vargas A, Pérez MJ, Serra R, Asensio V, et al. Manual del manejo del lince ibérico en cautividad. Programa de conservación ex-situ del Lin ce Ibérico. 2016 [cited 2024 Jan 22] https://www.lynxexsitu.es/ficheros/documentos_pdf/84/Manual_Manejo_Lince_Iberico_2016.pdf
14. Ruiz-Fons F, Sánchez-Matamoros A, Gortázar C, Sánchez-Vizcaíno JM. The role of wildlife in bluetongue virus maintenance in Europe: lessons learned after the natural infection in Spain. Virus Res. 2014;182:50–8. https://doi.org/10.1016/j.virusres.2013.12.031
15. Red de Alerta SV. Ministerio de agricultura pesca y alimentación. 2023 [cited 2024 Feb 10]. https://servicio.mapama.gob.es/rasve/Acceso.aspx

Address for correspondence: Moisés Gonzálvez, Department of Animal Health, Road Madrid-Cadiz Km 396, University of Cordoba, 14014 Cordoba, Spain; email: sa2gojum@uco.es

etymologia revisited

Zika [zēkə] Virus

Originally published in June 2014

Zika virus is a mosquito-borne positive-sense, single-stranded RNA virus in the family *Flaviviridae*, genus *Flavivirus,* that causes a mild, acute febrile illness similar to dengue. In 1947, scientists researching yellow fever placed a rhesus macaque in a cage in the Zika Forest (*zika* meaning "overgrown" in the Luganda language), near the East African Virus Research Institute in Entebbe, Uganda. A fever developed in the monkey, and researchers isolated from its serum a transmissible agent that was first described as Zika virus in 1952. It was subsequently isolated from a human in Nigeria in 1954. From its discovery until 2007, confirmed cases of Zika virus infection from Africa and Southeast Asia were rare. In 2007, however, a major epidemic occurred in Yap Island, Micronesia. More recently, epidemics have occurred in Polynesia, Easter Island, the Cook Islands, and New Caledonia.

References

1. Dick GW, Kitchen SF, Haddow AJ. Zika virus. I. Isolations and serological specificity. Trans R Soc Trop Med Hyg. 1952;46:509–20. http://dx.doi.org/10.1016/ 0035-9203 (52)90042-4
2. Hayes EB. Zika virus outside Africa. Emerg Infect Dis. 2009; 15:1347–50. http://dx.doi.org/10.3201/eid1509.090442
3. MacNamara FN. Zika virus: a report on three cases of human infection during an epidemic of jaundice in Nigeria. Trans R Soc Trop Med Hyg. 1954;48:139–45. http://dx.doi.org/10.1016/0035-9203(54)90006-1
4. Murphy JD. Luganda–English dictionary. Washington (DC): The Catholic University of America Press; 1972.

https://wwwnc.cdc.gov/eid/article/20/6/et-2014_article

Chlorine Inactivation of *Elizabethkingia* spp. in Water

David A. Holcomb, Diana Riner, Benjamin Cowan, Zainab Salah, Wiley C. Jennings, Mia C. Mattioli, Jennifer L. Murphy

We performed chlorine inactivation experiments for *Elizabethkingia anophelis* and *E. meningoseptica* bacterial strains from clinical and environmental sources. Free chlorine concentration × contact time values ≤0.04 mg·min/L achieved 99.9% inactivation of *Elizabethkingia* species, indicating chlorine susceptibility. Measures to control biofilm producing pathogens in plumbing are needed to prevent *Elizabethkingia* bacterial infections.

Elizabethkingia spp. are widely distributed environmental bacteria and opportunistic pathogens that can cause sepsis and meningitis, particularly in neonates (*1*,*2*). At least 3 phenotypically similar species (*E. anophelis*, *E. meningoseptica*, and *E. miricola*) are intrinsically resistant to multiple antimicrobial classes and have been implicated in fatal healthcare-associated outbreaks (*3*). The largest reported United States outbreak was an *E. anophelis* strain that caused 66 laboratory-confirmed infections in Wisconsin and neighboring states in 2015–2016, for which the infection source was never identified. That outbreak was unusual for primarily consisting of community-acquired infections (*4*). Plumbing fixtures such as taps and sink drains, which *Elizabethkingia* bacteria readily colonize in biofilms, are common exposure vehicles in healthcare settings (*2*,*5*,*6*). Transmission from handwashing in contaminated sinks is of particular concern and has been shown to contaminate health worker hands with *E. anophelis*, even with the use of chlorhexidine soap (*5*).

Chlorination is the most common disinfection method for public water supplies. When used at the end of the treatment chain, chlorination provides residual disinfection during distribution and storage. Reports of *Elizabethkingia* bacterial persistence in chlorinated water supplies and plumbing fixtures cleaned with sodium hypochlorite have raised concerns of chlorine tolerance (*2*,*6*,*7*), but no data have been published. We conducted disinfection experiments with a free chlorine residual (FCR) dose of 0.2 mg/L, the minimum disinfectant residual for treated surface water entering distribution systems in the United States, to assess inactivation of 2 *Elizabethkingia* spp. isolated from clinical and environmental samples (*8*). We fit inactivation kinetics models to estimate the product of FCR dose (C; mg/L) and contact time (T; minutes) required to reduce *Elizabethkingia* bacterial concentrations by 99.9% ($CT_{99.9\%}$).

The Study

We performed disinfection experiments in triplicate for 6 *E. anophelis* and 5 *E. meningoseptica* strains from clinical and environmental sources (Table 1). We prepared bacterial stocks by incubating cultures in tryptic soy broth overnight at 37°C, followed by subculture into tryptic soy broth at 37°C for ≈5 hours (*9*). We pelleted the log phase cultures, washed with sterile phosphate-buffered saline (PBS), repelleted, and resuspended in 5 ml PBS. We prepared 50-mL glass flasks with 25 mL of sterile oxidant demand–free water buffered at pH 7.5, dosed to 0.2 mg/L FCR with 5.25% sodium hypochlorite, and maintained in a water bath at 25°C. We seeded flasks with 0.1 mL bacterial stock and extracted 10 mL aliquots from 3 flasks after 15, 30, and 60 seconds, immediately quenching the aliquots with 100 µL of 10% sodium thiosulfate (Fisher Scientific, https://www.fishersci.com). We extracted triplicate aliquots from 3 chlorine-free flasks at 60 seconds to examine dieoff with no disinfectant exposure. We also measured FCR in aliquots removed at 30 and 60 seconds from a final seeded flask to assess disinfectant decay. We serially diluted the initial bacterial stocks and experimental aliquots with sterile PBS and enumerated by using membrane filtration plated onto tryptic soy agar containing 5% rabbit blood, incubated at 37°C, and counted after 24–36 hours.

Author affiliation: Centers for Disease Control and Prevention, Atlanta, Georgia, USA

DOI: https://doi.org/10.3201/eid3010.240917

Table 1. *Elizabethkingia* strains from environmental and clinical sources provided by the Centers for Disease Control and Prevention used for study of chlorine inactivation of *Elizabethkingia* spp. in water

Species	Strain	Accession no.	Year	Location	Source	Origin
E. anophelis	DSM 23781	FLST00000000	2009	The Gambia	Insect*	Midgut
	CSID_3015183678	MAFY00000000	2016	Wisconsin, USA	Clinical	Blood
	CSID_3015183679	MAHO00000000	2016	Wisconsin, USA	Clinical	Blood
	CSID_3015183681	GCA_001618545.2	2016	Wisconsin, USA	Clinical	Blood
	17-336	NA	2017	Oklahoma, USA	Environmental	Sink drain swab
	17-337	NA	2017	Oklahoma, USA	Environmental	Sink drain swab
E. meningoseptica	KC1913 (ATCC 13253)	LNOH00000000	1959	Massachusetts, USA	Clinical	Spinal fluid
	16-062	NA	2016	Minnesota, USA	Clinical	Bronchial wash
	16-148	NA	2016	Florida, USA	Clinical	Blood
	17-276	NA	2016	Michigan, USA	Clinical	Sputum
	2016-08-103-03	NA	2016	NA	Environmental	NA

*DSM 23781 was isolated from the *Anopheles gambiae* mosquito midgut and was excluded from comparisons between clinical and environmental sources. NA, not available.

We analyzed inactivation kinetics by modeling the natural log-survival, the ratio of the bacterial concentration at contact time T to the initial concentration, as a function of time and FCR dose governed by an inactivation rate constant *k*. We estimated *k* by using the pseudo-first order Chick-Watson model and the nonlinear generalization, the Hom model, assuming first-order disinfectant decay and excluding samples for which the concentration was too low to detect (*10*). We used R version 4.3.2 (The R Project for Statistical Computing, https://www.R-project.org) to fit inactivation models by nonlinear least squares; estimate disinfectant decay rates, *k'*, with linear regression; calculate CT values from the fitted kinetic models; and perform z-tests (5% significance level) to compare rate constant estimates between species and between strain sources (*11*,*12*). Both inactivation kinetic models provided comparable fits to the experimental data that were indicated by similar values of the Akaike information criterion and root mean square error (Table 2). However, the Hom model was computationally unstable and produced rate constant estimates with larger SEs. Because of the larger SEs, we used only the Chick-Watson model to compare rate constants of different species and between clinical and environmental strains. Sensitivity analyses that accounted for potential correlation between replicates by using the geometric mean concentration to calculate strain-specific log-survival at each time point produced comparable rate constant estimates and CT values.

Both models indicated a free chlorine CT of ≈0.03 milligram-minutes per liter (mg · min/L) inactivated 99.9% of *Elizabethkingia* bacteria (Table 2). In stratified Chick-Watson analyses, both species demonstrated $CT_{99.9\%}$ ≤0.04 mg · min/L and rate constant estimates that were not statistically different (p = 0.92). However, *E. anophelis* was reduced to undetectable concentrations at 1 minute of exposure in 30% (n = 15) of samples, whereas *E. meningoseptica* was not detected at 1 minute of exposure in only 11% (n = 6) of samples. Environmental strains displayed less variable log-survival than clinical strains (Figure), but the rate constant estimates were not statistically different (p = 0.37). Both strains produced similar $CT_{99.9\%}$ values of 0.04 mg·min/L (environmental) and 0.03 mg · min/L (clinical). All environmental strains were still detectable after 1 minute of exposure, whereas clinical strains were not detected in 18 samples (26%).

Table 2. Inactivation kinetic model performance metrics, rate constant estimates, and disinfectant CT values needed to achieve a 99%–99.99% reduction in *Elizabethkingia* detection in study of chlorine inactivation of *Elizabethkingia* spp. in water*

Comparison	N	No. (%) ND	AIC	RMSE	Rate constant (SE),† min^{-1} *k'*	Rate constant (SE),† min^{-1} ln(*k*)	Pooled SE‡	z-score (p value)	CT value, mg·min/L 99%	CT value, mg·min/L 99.9%	CT value, mg·min/L 99.99%
Model, all data											
Chick-Watson	83	21 (20)	430	3.1	0.89 (0.08)	10.4 (1.3)	NA	NA	0.021	0.031	0.042
Hom			431	3.0		22.1 (18.4)			0.021	0.026	0.029
Species, Chick-Watson model											
E. anophelis	35	15 (30)	183	3.0	0.90 (0.13)	10.3 (1.8)	2.5	0.10	0.019	0.029	0.039
E. meningoseptica	48	6 (11)	248	3.0	0.88 (0.11)	10.0 (1.8)		(0.92)	0.023	0.035	0.047
Source,§ Chick-Watson model											
Clinical	51	18 (26)	280	3.5	0.90 (0.09)	10.0 (1.9)	2.2	0.90	0.021	0.032	0.043
Environmental	27	0 (0)	120	2.0	1.09 (0.13)	8.1 (1.1)		(0.37)	0.025	0.037	0.050

*AIC, Akaike information criterion; CT value, product of concentration and contact time required to achieve specified reduction; N, number of observations (out of 104 total) with detectable *Elizabethkingia* used to fit model; ND, not detected; RMSE, root mean square error.
†Point estimates and SEs of the disinfectant decay rate constant *k'* and natural logarithm of the inactivation rate constant *k*.
‡Pooled SE for z-test of the equality of rate constants for each subset, obtained as the square root of the sum of the squared standard errors of both rate constant estimates.
§The *E. anophelis* type strain DSM 23781 was isolated from an insect host and thus excluded from the comparison of clinical and environmental sources.

The initial FCR dose was reduced by approximately two thirds after 1 minute. The median reduction in *Elizabethkingia* after 1 minute with no chlorine exposure was 0.13 $\log_{10}$ (26%). In contrast, the Chick-Watson model predicted ≈5 $\log_{10}$ (99.999%) inactivation in 1 minute for a 0.2 mg/L FCR dose (Figure). Model 95% prediction intervals indicated a minimum expected inactivation of ≈2 $\log_{10}$ after 1 minute at the experimental conditions (Figure). Of the 1-minute samples, ≥3 $\log_{10}$ inactivation was observed for 32 of the 35. The 3 samples below the 3 $\log_{10}$ inactivation threshold were replicates of the same clinical strain and experienced 2.6–2.9 $\log_{10}$ inactivation.

Conclusions

Contrary to the chlorine tolerance hypothesized in the literature, we observed rapid inactivation of *Elizabethkingia* at typical point-of-use free-chlorine concentrations (≈0.2 mg/L). Across species and sources, *Elizabethkingia* strains demonstrated greater chlorine susceptibility ($CT_{99.9\%}$; <0.04 mg · min/L) than a reported *Escherichia*

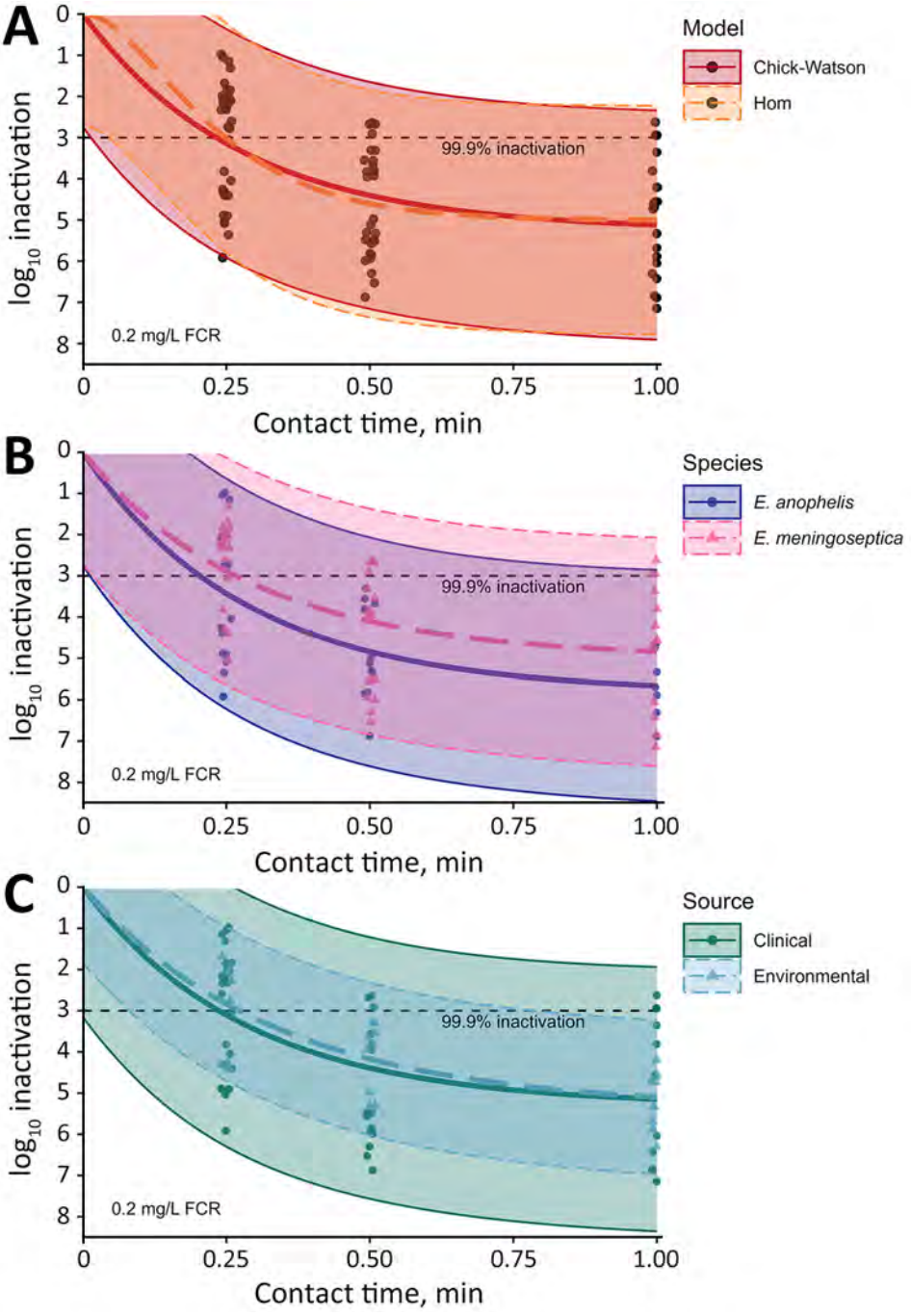

Figure. Observed and model-predicted $\log_{10}$ inactivation in study of chlorine inactivation of *Elizabethkingia* spp. in water. Samples from environmental and clinical sources were exposed to chlorine in water with increasing contact time at an initial dose of 0.2 mg/L FCR. Panels show comparisons in modeled inactivation by model specification. A) All data used for both models. B) Stratified by species, Chick-Watson model. C) Strain source, Chick-Watson model. Curved lines indicate model-predicted inactivation; dots, observed inactivation; and shaded regions, model 95% prediction intervals. FCR, free chlorine residual.

coli reference strain ($CT_{99.9\%}$; 0.09 mg · min/L) that was used to benchmark disinfectant susceptibility of waterborne pathogens (*13*). However, we also observed cells persisting at detectable concentrations after 1 minute of contact time, particularly among environmental strains. The more persistent subpopulations could seed biofilms, which *Elizabethkingia* bacteria readily form in plumbing fixtures, and have been shown to rapidly recolonize sink drains within days of seemingly effective disinfection (*2*,*14*), possibly accounting for the reported survival of *Elizabethkingia* spp. after chlorination in healthcare settings. Biofilms can protect embedded organisms from disinfection through multiple mechanisms, including oxidant demand exerted by the extracellular matrix, limited diffusion of the disinfectant to inner layers, and phenotypic adaptations in response to sublethal disinfectant doses and the biofilm environment itself (*15*). A review of 6 bacteria species reported biofilm-embedded cells required 2–600 times the chlorine dose or contact time for inactivation than their planktonic (free-swimming) counterparts (*15*). Prevention of *Elizabethkingia* infections, as with other opportunistic biofilm pathogens, may be most readily accomplished by limiting the environments in which biofilms can form and reducing exposure to potentially contaminated sources (*5*–*7*). Building managers should adopt water management programs to limit the growth and transmission of opportunistic pathogens of plumbing.

Acknowledgments

We thank John McQuiston, Melissa Bell, Ainsley Nicholson, Charles Haas, and Helen Keevy.

All the code and data used to produce this analysis are available at https://cdcgov.github.io/WDPB_EMEL/manuscripts/elizabethkingia.

About the Author

Dr. Holcomb is a microbiologist in the Division of Foodborne, Waterborne, and Environmental Diseases, National Center for Emerging and Zoonotic Infectious Diseases, Centers for Disease Control and Prevention, Atlanta, Georgia, USA. His research interests include environmental transmission and control of antimicrobial-resistant pathogens.

References

1. Dziuban EJ, Franks JL, So M, Peacock G, Blaney DD. *Elizabethkingia* in children: a comprehensive review of symptomatic cases reported from 1944 to 2017. Clin Infect Dis. 2018;67:144–9. https://doi.org/10.1093/cid/cix1052
2. Lin P-Y, Chen H-L, Huang C-T, Su L-H, Chiu C-H. Biofilm production, use of intravascular indwelling catheters and inappropriate antimicrobial therapy as predictors of fatality in *Chryseobacterium meningosepticum* bacteraemia. Int J Antimicrob Agents. 2010;36:436–40. https://doi.org/10.1016/j.ijantimicag.2010.06.033
3. Han M-S, Kim H, Lee Y, Kim M, Ku NS, Choi JY, et al. Relative prevalence and antimicrobial susceptibility of clinical isolates of *Elizabethkingia* species based on 16s rRNA gene sequencing. J Clin Microbiol. 2016;55:274–80. https://doi.org/10.1128/JCM.01637-16
4. Perrin A, Larsonneur E, Nicholson AC, Edwards DJ, Gundlach KM, Whitney AM, et al. Evolutionary dynamics and genomic features of the *Elizabethkingia anophelis* 2015 to 2016 Wisconsin outbreak strain. Nat Commun. 2017;8:15483. https://doi.org/10.1038/ncomms15483
5. Yung C-F, Maiwald M, Loo LH, Soong HY, Tan CB, Lim PK, et al. *Elizabethkingia anophelis* and association with tap water and handwashing, Singapore. Emerg Infect Dis. 2018;24:1730–3. https://doi.org/10.3201/eid2409.171843
6. Balm MND, Salmon S, Jureen R, Teo C, Mahdi R, Seetoh T, et al. Bad design, bad practices, bad bugs: frustrations in controlling an outbreak of *Elizabethkingia meningoseptica* in intensive care units. J Hosp Infect. 2013;85:134–40. https://doi.org/10.1016/j.jhin.2013.05.012
7. Mallinckrodt L, Huis In 't Veld R, Rosema S, Voss A, Bathoorn E. Review on infection control strategies to minimize outbreaks of the emerging pathogen *Elizabethkingia anophelis*. Antimicrob Resist Infect Control. 2023;12:97. https://doi.org/10.1186/s13756-023-01304-1
8. United States Environmental Protection Agency. The effectiveness of disinfectant residuals in the distribution system. 2007 [cited 2024 Jun 7]. https://www.epa.gov/dwreginfo/effectiveness-disinfectant-residuals-distribution-system
9. American Public Health Association, American Water Works Association, Water Environment Federation. Standard methods for the examination of water and wastewater. 24th edition. Lipps WC, Braun-Howland EB, Baxter TE, editors. Washington: APHA Press; 2023.
10. Haas CN, Kaymak B. Effect of initial microbial density on inactivation of *Giardia muris* by ozone. Water Res. 2003; 37:2980–8. https://doi.org/10.1016/S0043-1354(03)00112-X
11. Murphy JL, Haas CN, Arrowood MJ, Hlavsa MC, Beach MJ, Hill VR. Efficacy of chlorine dioxide tablets on inactivation of *Cryptosporidium* oocysts. Environ Sci Technol. 2014;48:5849–56. https://doi.org/10.1021/es500644d
12. Mattioli MC, Sassoubre LM, Russell TL, Boehm AB. Decay of sewage-sourced microbial source tracking markers and fecal indicator bacteria in marine waters. Water Res. 2017;108:106–14. https://doi.org/10.1016/j.watres.2016.10.066
13. Falkinham JO III. Common features of opportunistic premise plumbing pathogens. Int J Environ Res Public Health. 2015;12:4533–45. https://doi.org/10.3390/ijerph120504533
14. Ledwoch K, Robertson A, Lauran J, Norville P, Maillard J-Y. It's a trap! The development of a versatile drain biofilm model and its susceptibility to disinfection. J Hosp Infect. 2020;106:757–64. https://doi.org/10.1016/j.jhin.2020.08.010
15. Bridier A, Briandet R, Thomas V, Dubois-Brissonnet F. Resistance of bacterial biofilms to disinfectants: a review. Biofouling. 2011;27:1017–32. https://doi.org/10.1080/08927014.2011.626899

Address for correspondence: Jennifer Murphy, Centers for Disease Control and Prevention, 1600 Clifton Rd NE, Mailstop H23-9, Atlanta, GA 30329-4027, USA; email: iod7@cdc.gov

Oxacillinase-484–Producing Enterobacterales, France, 2018–2023

Cécile Emeraud, Sandrine Bernabeu, Delphine Girlich, Inès Rezzoug, Agnès B. Jousset, Aurélien Birer, Thierry Naas, Rémy A. Bonnin, Laurent Dortet

We examined the emergence and characteristics of oxacillinase-484–producing Enterobacterales in France during 2012–2023. Genomic analysis identified 2 predominant sequence types in *Escherichia coli*: ST410 and ST1722. Plasmid analysis revealed that $bla_{OXA-484}$ genes were carried mostly on an IncX3-type plasmid associated with genetic elements including insertion sequences IS*3000* and IS*Kpn19*.

Carbapenemase-producing Enterobacterales (CPEs) pose a considerable threat to public health because of antimicrobial resistance. In France, the most prevalent carbapenemases are OXA-48–like type. More than 55 variants of OXA-48–like enzymes have been identified (*1*); OXA-48, OXA-181, and OXA-244 are most prevalent, but OXA-484 has been increasingly identified. OXA-484 differs from OXA-48 by 5 amino acid substitutions (Thr104Ala, Asn110Asp, Glu168Gln, Ser171Ala, Arg214Gly) and from OXA-181 by a single amino acid at position 214 within the β5-β6 loop (*2*). Most prior reports have described OXA-484 in *Escherichia coli* (*3*–*6*), but some reports also have identified it in *K. pneumoniae* (*2*,*7*), *K. aerogenes* (*6*), and *K. variicola* (*8*). Reported OXA-484–producing *E. coli* was noted to belong mainly to the sequence type (ST) 410 (*3*,*5*,*6*), and $bla_{OXA-484}$ genes were carried mainly on 51-kb IncX-type plasmids (*3*,*4*,*6*). Given the similar genetic background of $bla_{OXA-484}$ and $bla_{OXA-181}$, several studies suggested that $bla_{OXA-484}$ could directly derive from $bla_{OXA-181}$ (*3*,*8*). We used whole-genome sequencing to decipher the epidemiology of OXA-484–producing Enterobacterales in France during 2012–2023.

Author affiliations: Bicêtre Hospital, Le Kremlin-Bicetre, France (C. Emeraud, S. Bernabeu, I. Rezzoug, A.B. Jousset, T. Naas, R.A. Bonnin, L. Dortet); INSERM, Paris, France (D. Girlich); Centre National de Référence de la Résistance aux Antibiotiques, Clermont-Ferrand, France (A. Birer)

DOI: http://doi.org/10.3201/eid3010.240814

The Study

The French National Reference Center (Le Kremlin-Bicêtre, France) receives bacterial strains sent by microbiology laboratories throughout France to analyze for suspected carbapenemase production. The center received 64 clinical, nonduplicate OXA-484–producing isolates during 2012–2023 (Appendix 1 Table 1, https://wwwnc.cdc.gov/EID/article/30/10/24-0814-App1.xlsx). We identified OXA-484 producers in 3 isolates from 2018 (0.11% of CPEs, 0.16% of OXA-48–like), 6 from 2021 (0.24% of CPEs, 0.38% of OXA-48–like), 16 from 2022 (0.41% of CPEs, 0.68% of OXA-48–like), and 39 from 2023 (0.77% of CPEs, 1.24% of OXA-48–like) (Figure 1). All OXA-484 producers were *E. coli*, except 1 *K. pneumoniae* and 1 *Citrobacter youngae*. Short-read next-generation sequencing (Appendix 2, https://wwwnc.cdc.gov/EID/article/30/10/24-0814-App1.pdf) showed that the *C. youngae* isolate belonged to ST491 and the *K. pneumoniae* isolate to ST268. We identified 10 single STs among the 62 *E. coli* isolates; most were ST410 (n = 29) and ST1722 (n = 23).

To compare strains belonging to the 2 predominant sequence types (ST410 and ST1722), we constructed a matrix of single-nucleotide polymorphisms (SNPs) in SNIppy version 4.6.0 (ILRI-CGIAR, https://hpc.ilri.cgiar.org). We found 2 ST410 strains (399A8 and 415H3), isolated in the same region, were notably distinct from the others (>1,000 SNPs with the remaining strains) (Appendix 2 Figure 1, panel A). For the other strains, all isolated from different areas, we observed a maximum of 57 SNPs between any 2 strains. We constructed a phylogenetic tree that included all *E. coli* ST410 strains received at the F-NRC (n = 459). Except for 399A8 and 415H3, the OXA-484– producers formed a distinct cluster among *E. coli* ST410 (Figure 2).

We observed a maximum of 35 SNPs among the OXA-484–producing *E. coli* ST1722 (Appendix

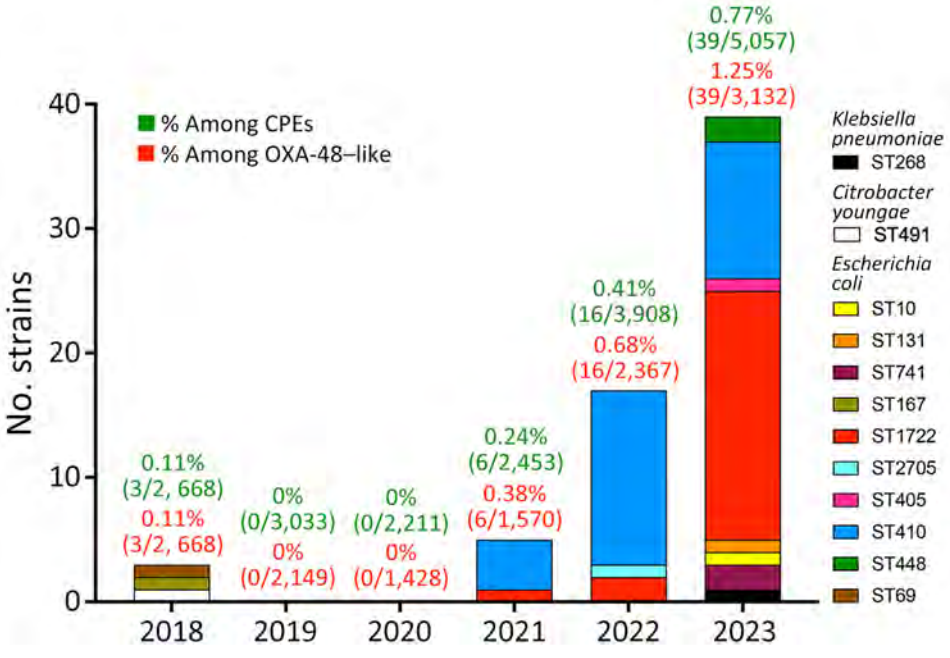

Figure 1. Evolution of number of OXA-484–producing CPE isolates received at the French National Reference Center for Carbapenem-Resistant Enterobacterales, France, 2012–2023. No OXA-484–producing isolate was received before 2018. Colors indicate species and STs. CPE, carbapenem-resistant Enterobacterales; OXA, oxacillinase; ST, sequence type.

2 Figure 1, panel B); all OXA-484 producers clustered inside *E. coli* ST1722 (n = 43) (Appendix 2 Figure 2). Mapping of short-read data by using CLC Genomics Workbench (QIAGEN, https://www.qiagen.com) onto previously published plasmids (GenBank accession nos. NZ_OP594535, CP058621, CP076530, OP594534, NZ_JANQAU010000004, and CP076530) revealed a high nucleotide identity in most strains. In *E. coli*, plasmids harboring $bla_{OXA-484}$ appeared similar to the IncX3 described by Moser et al. (*3*), with the exception of 2 strains belonging to ST1722, in which plasmids were closed to the IncFIA-like/IncFIB-like/IncFII-type plasmid reported by Findlay (*5*) (Appendix 1 Table 2). In addition, in *C. youngae* and *E. coli* 172D10 strains, the $bla_{OXA-484}$ gene was located on a new 58,440 pb IncP1 plasmid. For strains having short reads that did not map accurately to described plasmids (query cover <90%, n = 10; Appendix 1 Table 2), we performed long-read sequencing as previously described (*9*) to reconstruct these plasmids using MinION technology (Oxford Nanopore Technologies, https://nanoporetech.com). The sizes of $bla_{OXA-484}$–carrying plasmids were 18,731–162,425 bp; 7/10 possessed replicases close to colKP3-like, IncFIA-like, IncFIB-like, and IncFII, and 3 contained only colKP3-like. Some plasmids carried other resistance genes, notably *qnrS1* (9/10 plasmids) and *mph(A)* (4/10 plasmids) (Appendix 1 Table 3).

We analyzed the close genetic context of $bla_{OXA-484}$ and found the same genetic environment for 62/64 strains (Figure 3). For strain 346D9, the close genetic environment was slightly smaller, with the IS*3000* upstream and the truncated ColKP3 replicase downstream and an IS*26* instead of the IS*Kpn19*. For the $bla_{OXA-484}$ carried by the IncP1-type plasmid, the genetic environment was totally different, with various truncated IS elements (Figure 3). We found no homologous sequences associated with OXA-48–like or any other carbapenemase-encoding gene.

We determined MICs of various antimicrobial drugs for the entire collection (Table 1; Appendix 1 Table 4). As expected, OXA-484 producers exhibited low MICs for the 3 carbapenems and were susceptible to imipenem/relebactam and meropenem/vaborbactam combinations (with no inhibitory role of relebactam and vaborbactam). Given that most OXA-484 producers coproduce an extended-spectrum β-lactamase (CTX-M-14 or CTX-M-15) or an acquired cephalosporinase (mostly CMY-42), those we analyzed were found to be resistant to third- and fourth-generation cephalosporins and to aztreonam, but they remained susceptible to ceftazidime/avibactam and aztreonam/avibactam. All strains were susceptible to colistin (Table).

ST410 *E. coli* strains possess a 4-aa insertion in penicillin-binding protein 3 (e.g., YRIN motif) (*10*) that confers decreased susceptibility to certain antibiotics (e.g., ceftazidime and aztreonam). In our collection, all OXA-484–producing ST410 *E. coli* strains possessed the YRIN insertion in penicillin-binding

protein 3 (Figure 2) and exhibited higher MICs for aztreonam/avibactam and ceftazidime/avibactam compared with strains belonging to other sequence types (Appendix 2 Figure 3). In contrast, strains belonging to ST1722 exhibited very low MICs.

A finding of low MICs of temocillin in OXA-484 producers compared with OXA-48 producers aligned with previous reports regarding OXA-244 producers (*11*) that exhibited the same Arg214Gly mutation within the β5–β6 loop. Because increased susceptibility to temocillin was responsible for screening issues of OXA-244 (*11*), we evaluated the accuracy of several screening media to detect OXA-484 producers. We selected 46 OXA-484 producers with varying temocillin MICs alongside control strains producing OXA-48 or other carbapenemases. We streaked the strains with 10 µL of 0.5 McFarland bacterial suspension onto 2 commercially available CPE screening media (ChromID CARBA SMART [bioMérieux,

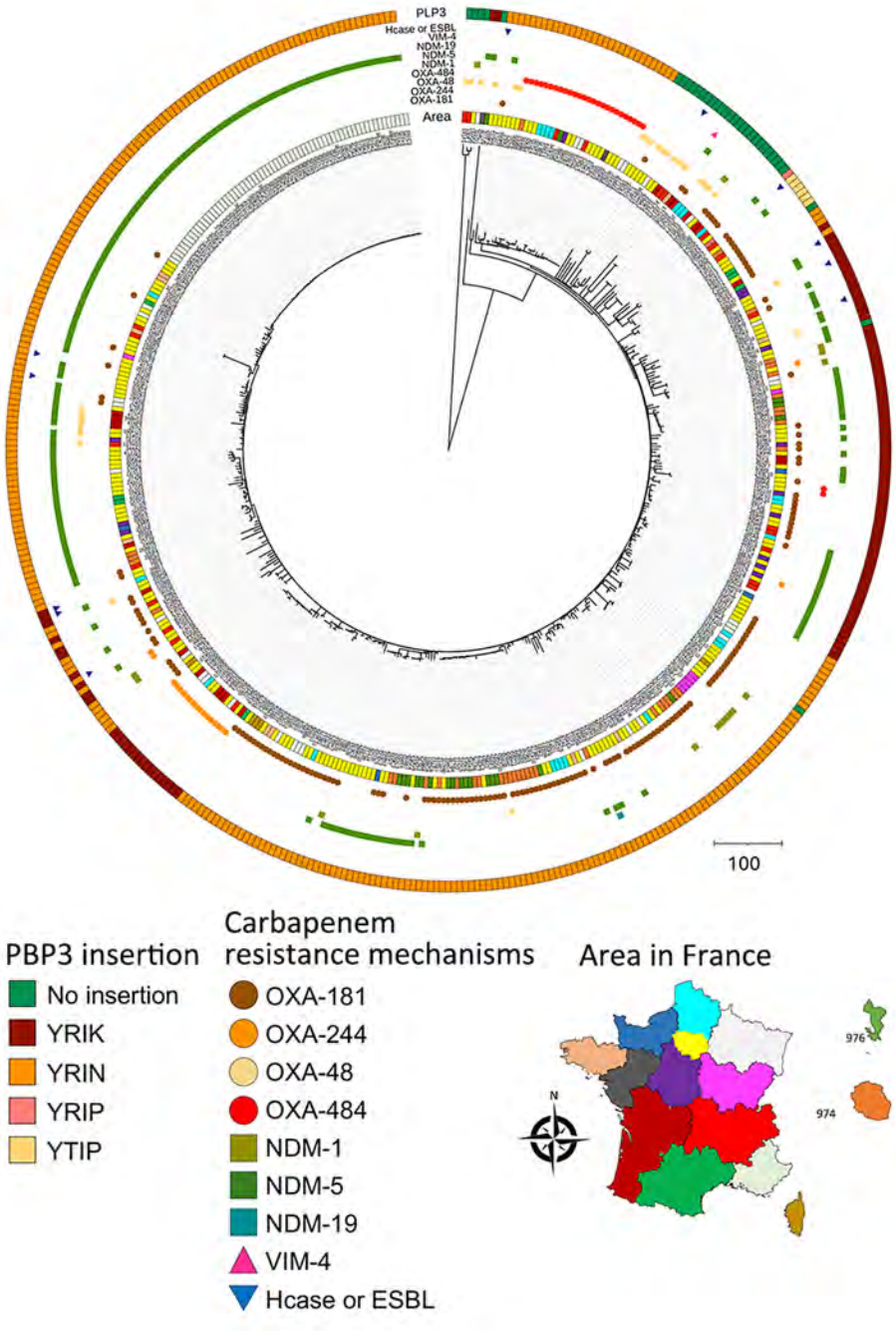

Figure 2. Phylogenetic tree and location map for carbapenem-resistant *Escherichia coli* sequence type (ST) 410 isolates received at the French National Reference Center for Carbapenem-Resistant Enterobacterales, France, 2012–2023. Carbapenemases are classified into 3 of the 4 Ambler classes: class A (mainly *Klebsiella pneumoniae* carbapenemase); class B or metallo-β-lactamases (predominantly NDM, VIM, or imipenemase types); and class D, primarily OXA-48–like types, including OXA-484 producers. Carbapenemase types are detailed and OXA-484 producers are indicated. ST410 strains are distinguished by whether there are amino acid insertions (YRIK, YRIN, YRIP, or YTIP motifs) in PBP3. We conducted the single-nucleotide polymorphism analysis on a common genome representing 89.05% of the entire genome of the reference strain 303D1. Map shows locations where specific mechanisms were found. ESBL, extended-spectrum β-lactamase; Hcase, helicase; NDM, New Delhi metallo-β-lactamase; OXA, oxacillinase; PBP3, penicillin-binding protein 3; VIM, Verona integron-encoded metallo-β-lactamase.

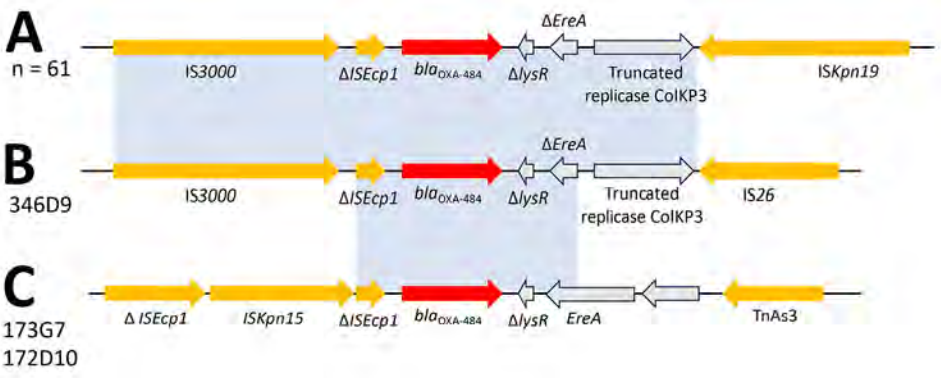

Figure 3. Genetic environments of $bla_{OXA-484}$ genes for 64 strains included in a study of oxacillinase-484–producing isolates received at the French National Reference Center for Carbapenem-Resistant Enterobacterales, France, 2012–2023. A) All strains; B) strain 346D9; C) strains 173G7 and 172D10. The $bla_{OXA-484}$ genes are shown in red, mobile elements are in yellow, and other genes in gray. The sequence homologies represented in light blue show an identity of >99.95%.

https://www.biomerieux.com] and mSuperCARBA [Mast Diagnostic, https://www.mast-group.com/fr]). As expected, after 16–24 hours' incubation, only 2 strains cultured on the CARB-side and only 11 on the OXA-side of the ChromID CARBA SMART medium. Those 11 isolates displayed temocillin MICs ≥128 mg/L. The mSuperCARBA agar yielded positive results for all OXA-484 producers.

Conclusions

As previously reported for OXA-244 producers (*11*), we found that the prevalence of OXA-484 producers is likely underestimated because of detection failure related to a lack of sensitivity of ChromID CARBA SMART, the most common screening medium in France. Whereas mSuperCARBA agar appears to be well suited, this medium possesses

Table. Antimicrobial susceptibility of OXA-484–producing isolates received at the French National Reference Center for Carbapenem-Resistant Enterobacterales, 2018–2023*

Species and carbapenemase type	MICs for antimicrobial drugs												
	ERT	IMI	IMI/REL	MEM	MEM/VAB	CPM	CTZ	CTZ/AVI	CFT/TAZ	AZT	AZT/AVI	TMC	COL
Escherichia coli OXA-484													
None, n = 26													
MIC	≤0.25–8	≤0.25–1	≤0.25–1	≤0.25–2	≤0.25–2	≤1–2	≤0.25–8	≤0.25–1	0.5–>8	≤0.25–2	≤0.25–2	32–>128	0.25–1
MIC_{50}	0.5	≤0.25	≤0.25	≤0.25	≤0.25	≤1	≤0.25	≤0.25	2	≤0.25	≤0.25	64	0.5
MIC_{90}	1	0.5	0.5	0.5	0.5	≤1	2	0.5	>8	1	1	>128	1
ESBL, n = 5													
MIC	≤0.25–1	≤0.25	≤0.25	≤0.25	≤0.25	2–>16	1–>16	≤0.25–0.5	1–>8	2–>16	≤0.25–1	32–128	0.25–0.5
MIC_{50}	0.5	≤0.25	≤0.25	≤0.25	≤0.25	16	4	0.5	8	>16	≤0.25	32	0.25
MIC_{90}	1	≤0.25	≤0.25	≤0.25	≤0.25	>16	>16	0.5	>8	>16	1	128	0.5
Acquired, n = 26													
MIC	0.5–4	≤0.25–2	≤0.25–1	≤0.25–2	≤0.25–1	≤1–16	4–>16	≤0.25–4	1–>8	1–>16	≤0.25–8	32–>128	0.5
MIC_{50}	1	≤0.25	≤0.25	≤0.25	≤0.25	8	>16	2	>8	>16	2	>128	0.5
MIC_{90}	4	0.5	0.5	0.5	0.5	4	>16	4	>8	>16	4	>128	0.5
E. coli OXA-484 + NDM													
ESBL, n = 2,	>16	8–>8	8–>8	>16	>16	>16	>16	>16	>8	>16	1–2	>128	0.5
Acquired, n = 2,	2–4	>8	>8	>16	>16	>16	>16	>16	>8	>16	4–2	>128	0.5
E. coli OXA-484 + OXA-48, acquired, n = 1	0.5	2	1	4	2	8	1	0.5	>8	4	2	32	0.5
Citrobacter youngae OXA-484, acquired, n = 1	2	0.5	0.5	0.5	0.5	1	4	≤0.25	>8	1	≤0.25	>128	0.5
Klebsiella pneumoniae OXA-484, n = 1	1	≤0.25	≤0.25	0.5	≤0.25	≤1	≤0.25	≤0.25	1	≤0.25	≤0.25	128	0.5
Total, n = 64													
MIC_{50}	2	≤0.25	≤0.25	≤0.25	≤0.25	4	8	0.5	>8	16	1	128	0.5
MIC_{90}	4	1	1	2	1	>16	>16	2	>8	>16	4	>128	0.5
% Susceptible†	31.3	95.3	93.8	92.2	93.8	42.2	39.1	93.8	34.4	35.9	54.7	0	100

*AVI, avibactam; AZT, aztreonam; CFT, ceftolozane; COL, colistin; CPM, cefepime; CTZ, ceftazidime; ESBL, extended-spectrum β-lactamase; IMI, imipenem; ERT, ertapenem; MEM, meropenemNDM, New Delhi metallo-β-lactamase; ; OXA, oxacillinase; REL, relebactam; TAZ, tazobactam; TMC, temocillin; VAB, vaborbactam.
†Interpreted according to EUCAST guidelines.

lower specificity, leading to a rise in additional confirmatory tests (*12*).

Most previously reported OXA-484 producers belong to *E. coli ST410*, a widely distributed, high-risk clone (*13*) that usually exhibits reduced susceptibility to multiple antimicrobial drugs, complicating treatment options. Given the number of SNPs between all OXA-484–producing *E. coli* ST410 isolates of our collection and their geographic distribution, those strains do not originate from a single outbreak. However, OXA-484–producing *E. coli* ST410 strains clustered together, suggesting the circulation of a single clone in France during 2018–2023. In addition, most OXA-484–producing *E. coli* belonged to ST1722. This clone has not been recognized for its prevalence nor for its role in the spread of carbapenem resistance but has been associated with the production of extended-spectrum β-lactamases in France (*14*).

We found $bla_{\text{OXA-484}}$ genes localized on different plasmids but with a common close genetic environment characterized by IS*3000* upstream and IS*Kpn19* downstream. The ST410 *E. coli* carried $bla_{\text{OXA-484}}$ on a 51-kb IncX3 plasmid similar to the one described by Moser et al. (*4*), whereas the ST1722 *E. coli* carried it on an IncF plasmid similar to the one described by Findlay et al (*6*). The genetic environment of $bla_{\text{OXA-484}}$ described on IncX3 or IncF-type plasmids is close to that of $bla_{\text{OXA-181}}$, likely the result of a mutation in $bla_{\text{OXA-181}}$ (*8*). However, the genetic environment observed around the $bla_{\text{OXA-484}}$ gene located on the IncP1-type plasmid does not match any known structures of other $bla_{\text{OXA-48}}$–like genes, questioning its potential origin. In summary, the growing prevalence of OXA-484 producers highlight the urgent need for improved surveillance of these pathogens.

About the Author

Dr. Emeraud is an assistant professor at the Institut National de la Santé et de la Recherche Médicale. Her primary research interests include epidemiology, genetics, and biochemistry of β-lactamases in gram-negative bacteria.

References

1. Naas T, Oueslati S, Bonnin RA, Dabos ML, Zavala A, Dortet L, et al. Beta-Lactamase DataBase (BLDB)—structure and function. J Enzyme Inhib Med Chem. 2017;32:917–9.
2. Findlay J, Hopkins KL, Loy R, Doumith M, Meunier D, Hill R, et al. OXA-48–like carbapenemases in the UK: an analysis of isolates and cases from 2007 to 2014. J Antimicrob Chemother. 2017;72:1340–9. https://doi.org/10.1093/jac/dkx012
3. Sommer J, Gerbracht KM, Krause FF, Wild F, Tietgen M, Riedel-Christ S, et al. OXA-484, an OXA-48-type carbapenem-hydrolyzing class D β-lactamase from *Escherichia coli*. Front Microbiol. 2021;12:660094. https://doi.org/10.3389/fmicb.2021.660094
4. Moser AI, Campos-Madueno EI, Sendi P, Perreten V, Keller PM, Ramette A, et al. Repatriation of a patient with COVID-19 contributed to the importation of an emerging carbapenemase producer. J Glob Antimicrob Resist. 2021;27:267–72. https://doi.org/10.1016/j.jgar.2021.10.012
5. Hooban B, Fitzhenry K, O'Connor L, Miliotis G, Joyce A, Chueiri A, et al. A longitudinal survey of antibiotic-resistant Enterobacterales in the Irish environment, 2019-2020. Sci Total Environ. 2022;828:154488. https://doi.org/10.1016/j.scitotenv.2022.154488
6. Findlay J, Duran JB, Poirel L, Nordmann P. Emergence of OXA-484, an OXA-48-type beta-lactamase, in Switzerland. J Glob Antimicrob Resist. 2023;32:131–3. https://doi.org/10.1016/j.jgar.2023.01.010
7. Ramsamy Y, Mlisana KP, Amoako DG, Abia ALK, Ismail A, Allam M, et al. Mobile genetic elements-mediated Enterobacterales-associated carbapenemase antibiotic resistance genes propagation between the environment and humans: A One Health South African study. Sci Total Environ. 2022;806:150641. https://doi.org/10.1016/j.scitotenv.2021.150641
8. Ge H, Qiao J, Xu H, Liu R, Zhao J, Chen R, et al. Emergence of OXA-484-Producing *Klebsiella variicola* in China. Infect Drug Resist. 2023;16:1767–75. https://doi.org/10.2147/IDR.S404551
9. Girlich D, Bonnin RA, Proust A, Naas T, Dortet L. Undetectable production of the VIM-1 carbapenemase in an *Atlantibacter hermannii* clinical isolate. Front Microbiol. 2021;12:741972. https://doi.org/10.3389/fmicb.2021.741972
10. Sato T, Ito A, Ishioka Y, Matsumoto S, Rokushima M, Kazmierczak KM, et al. *Escherichia coli* strains possessing a four amino acid YRIN insertion in PBP3 identified as part of the SIDERO-WT-2014 surveillance study. JAC Antimicrob Resist. 2020;2:dlaa081. https://doi.org/10.1093/jacamr/dlaa081
11. Emeraud C, Biez L, Girlich D, Jousset AB, Naas T, Bonnin RA, et al. Screening of OXA-244 producers, a difficult-to-detect and emerging OXA-48 variant? J Antimicrob Chemother. 2020;75:2120–3. https://doi.org/10.1093/jac/dkaa155
12. Girlich D, Anglade C, Zambardi G, Nordmann P. Comparative evaluation of a novel chromogenic medium (chromID OXA-48) for detection of OXA-48 producing Enterobacteriaceae. Diagn Microbiol Infect Dis. 2013;77:296–300. https://doi.org/10.1016/j.diagmicrobio.2013.08.015
13. Ba X, Guo Y, Moran RA, Doughty EL, Liu B, Yao L, et al. Global emergence of a hypervirulent carbapenem-resistant *Escherichia coli* ST410 clone. Nat Commun. 2024;15:494. https://doi.org/10.1038/s41467-023-43854-3
14. Muller A, Gbaguidi-Haore H, Cholley P, Hocquet D, Sauget M, Bertrand X. Hospital-diagnosed infections with *Escherichia coli* clonal group ST131 are mostly acquired in the community. Sci Rep. 2021;11:5702. https://doi.org/10.1038/s41598-021-85116-6

Address for correspondence: Laurent Dortet, Service de Bactériologie-Hygiène, Hôpital de Bicêtre, 78 rue du Général Leclerc, 94275 Le Kremlin-Bicêtre Cedex, France; email: laurent.dortet@aphp.fr

Clustering of Polymorphic Membrane Protein E Clade in *Chlamydia trachomatis* Lineages from Men Who Have Sex with Men

Morika Mitobe, Hiroaki Kubota, Kai Kobayashi, Hirofumi Miyake, Misao Takano, Daisuke Mizushima, Hiroyuki Gatanaga, Shinichi Oka, Jun Suzuki, Kenji Sadamasu

Several *Chlamydia trachomatis* lineages identified through outer membrane protein A genotyping or multilocus sequence typing have been circulating worldwide among men who have sex with men. In a study in Tokyo, Japan, we demonstrate that such lineages commonly belong to a specific polymorphic membrane protein E clade across genotypes.

Chlamydia trachomatis infection is the most common sexually transmitted infection (STI) worldwide. Because most infections are asymptomatic, sexual transmission generally occurs without notification. This aspect of transmission creates a risk for persistent undiagnosed *C. trachomatis* infection, which can lead to ascending infection in the female genital tract and result in serious conditions, such as pelvic inflammatory disease, ectopic pregnancy, and infertility.

The standard epidemiologic marker used for *C. trachomatis* genotyping is *ompA*, which encodes the major outer membrane protein. *C. trachomatis* is classified into 18 genotypes on the basis of *ompA* diversity, and the genotypes are further categorized into 3 groups on the basis of their predominant anatomic sites: ocular (A–C), urogenital and anorectal (D–K), and lymphogranuloma venereum (L1–L3). The molecular epidemiology of *C. trachomatis* is characterized by the predominance of *ompA* genotypes D, G, and J among men who have sex with men (MSM) in many countries (*1*–*8*). Multilocus sequence typing (MLST) has revealed that MSM-specific sequence types (STs) are present in these genotypes (*5*–*8*) and that those STs are distributed globally, suggesting the presence of specific international transmission networks among MSM. However, how the specific STs were selectively disseminated among MSM across several *ompA* genotypes or whether they have any shared underlying characteristics are unclear. The purpose of this study was to characterize the molecular epidemiology of *C. trachomatis* among MSM in Tokyo, Japan.

Author affiliations: Tokyo Metropolitan Institute of Public Health, Tokyo, Japan (M. Mitobe, H. Kubota, K. Kobayashi, H. Miyake, J. Suzuki, K. Sadamasu); National Center for Global Health and Medicine, Tokyo (M. Takano, D. Mizushima, H. Gatanaga, S. Oka)

DOI: https://doi.org/10.3201/eid3010.240852

The Study

We focused on *C. trachomatis* polymorphic membrane protein (Pmp) variation, which is considered to play a key role in the initial infection process (*9*,*10*). Among 9 Pmp groups (PmpA–PmpH), PmpE is the most diverse, and a specific clade has been identified in rectal samples from MSM (*11*), suggesting a potential target for molecular epidemiologic studies of *C. trachomatis*.

The clinical specimens were collected from MSM at an outpatient clinic at the National Center for Global Health and Medicine in Tokyo that specializes in providing care for MSM. We collected 7,200 pharyngeal and 1,904 urogenital specimens during October 2018–March 2021, and collected 703 rectal specimens during April 2019–March 2021. The men were participants in an HIV-negative cohort study on implementation of preexposure prophylaxis. The specimen collection methods have been described previously (*12*). In addition, 200 urogenital specimens and 42 cervical specimens were collected as non-MSM samples from outpatients attending general clinics (not specifically for MSM) with urinary or genital tract infections during the same period. The major departments of those clinics were obstetrics and gynecology (clinic A), gastroenterology (clinic B), and urology (clinic C). We selected patients who had clinically suspected

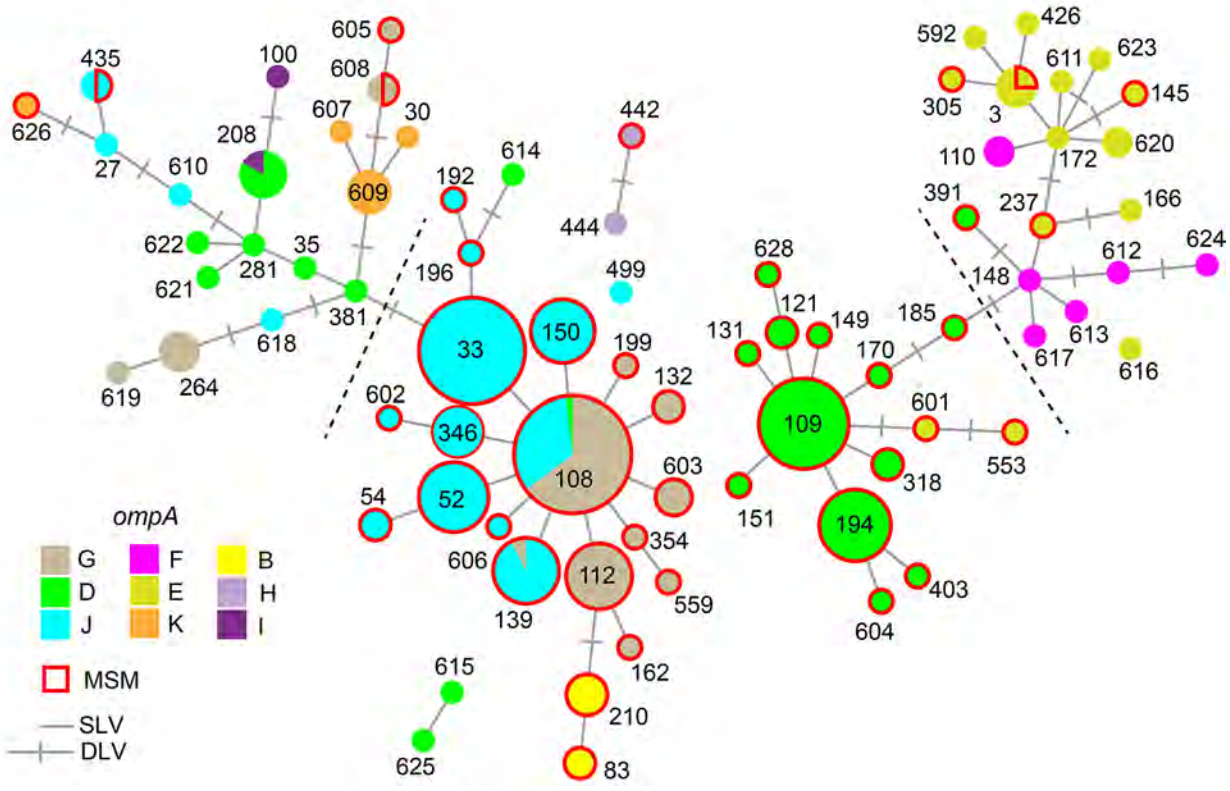

Figure 1. Minimum spanning tree based on sequence types (STs) and *ompA* of 298 *Chlamydia trachomatis* samples in study of clustering of specific polymorphic membrane protein E clade in *C. trachomatis* lineages from MSM, Japan. Each node indicates the ST number. SLVs and DLVs are linked. Samples from MSM are outlined in red, reflecting the proportion of samples in each node. The colors represent the *ompA* genotype. Nodes that contain several genotypes are shown as pie charts. Dashed lines are the assumed borders between the MSM and non-MSM lineages. DLV, double-locus variant; MSM, men who have sex with men; SLV, single-locus variant.

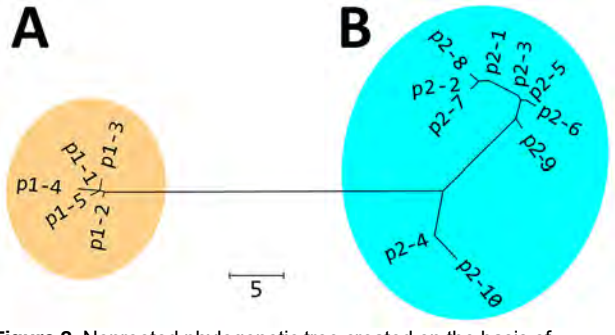

Figure 2. Nonrooted phylogenetic tree created on the basis of polymorphic membrane protein E of 298 *Chlamydia trachomatis* samples in study of clustering of specific polymorphic membrane protein E clade in *C. trachomatis* lineages from MSM, Japan. A) Cluster of 96.7% MSM (237 samples) and 0% non-MSM (0 samples); B) cluster of 3.3% MSM (8 samples) and 100% non-MSM (53 samples). p1 and p2 are 2 clades representing the MSM (p1) and non-MSM (p2) populations. The amino acid sequences of p1–1 to p2–10 are shown in Appendix 2 Figure (https://wwwnc.cdc.gov/EID/article/30/10/24-0852-App1.pdf). Numbers of samples included in each sequence: p1-1, n = 178; p1-2, n = 56; p1-3, n = 1; p1-4, n = 1; p1-5, n = 1; p2-1, n = 16; p2-2, n = 14; p2-3, n = 10; p2-4, n = 9; p2-5, n = 6; p2-6, n = 2; p2-7, n = 1; p2-8, n = 1; p2-9, n = 1; and p2-10, n = 1. Scale bar indicates the number of amino acid differences.

Neisseria gonorrhoeae or *C. trachomatis* infection. This study was approved by the ethics committee of the Tokyo Metropolitan Institute of Public Health (approval no. 3KENKENKENDAI465GOU).

We sequenced the *C. trachomatis*–positive specimens, confirmed using an Aptima Combo 2 transcription-mediated amplification test (Hologic, https://www.hologic.com), to determine the *ompA* genotypes, as described previously (*13*). We performed MLST targeting 5 regions (*hctB*, *CT058*, *CT144*, *CT172*, and *pbpB*) using the Uppsala scheme as described in the PubMLST website (https://pubmlst.org/organisms/chlamydiales-spp), assigning new STs when they were discovered. On the basis of the determined STs, we constructed a minimum-spanning tree using the GrapeTree tree visualization program (*14*) with the MSTreeV2 algorithm. We amplified the near–full length of PmpE-encoding regions (2740 bp), which includes 5 variable regions (*11*), by nested PCR using primer sets. We used pmpE_1st_F (5′-GAAAAAAGCGTTTTTCTTTTTCCTTATCG-3′) and pmpE_1st_R (5′-TCCCCATTGAGATAATTA-

Table. Detected polymorphic membrane protein E clades of *Chlamydia trachomatis* according to study population and anatomic source of sample in study of *C. trachomatis* lineages from MSM, Japan*

Sample type	No. (%) samples		
	p1	p2	Total
MSM samples			
Rectal	201 (97.6)	5 (2.4)	206 (100)
Pharyngeal	25 (93)	2 (7)	27 (100)
Urogenital	11 (92)	1 (8)	12 (100)
Total	237 (96.7)	8 (3.3)	245 (100)
Non-MSM samples			
Urogenital	0	35 (100)	35 (100)
Cervix	0	18 (100)	18 (100)
Total	0	53 (100)	53 (100)

*The proportions of p1 and p2 in the MSM population did not differ significantly among the rectal, pharyngeal, and urogenital specimens (p = 0.141 by Fisher exact test). MSM, men who have sex with men.

CAGAAGGTTGA-3′) for the first PCR and used pmpE_2nd_F (5′-AACTCAGTTCCAGATCCTAC-GAAAGAGTC-3′) and pmpE_2nd_R (5′-ACTG-GAAATGGAGAGTTAACCAACTCAAAG-3′) for the second PCR. We sequenced the PCR products through amplicon sequencing using MiSeq (Illumina, https://www.illumina.com). We constructed a non-rooted phylogenetic tree with the neighbor-joining method on the basis of the amino acid differences with MEGA7 software (https://www.megasoftware.net) using the amino acid sequences (907 aa) obtained by computational translation of DNA sequences corresponding to nucleotide numbers 1,025,723–1,028,443 of the *C. trachomatis* D/UW-3/CX genome (AE001273) (*15*).

We fully analyzed a total of 298 *C. trachomatis*–positive specimens (245 from MSM and 53 from non-MSM) with *ompA* genotyping, MLST, and

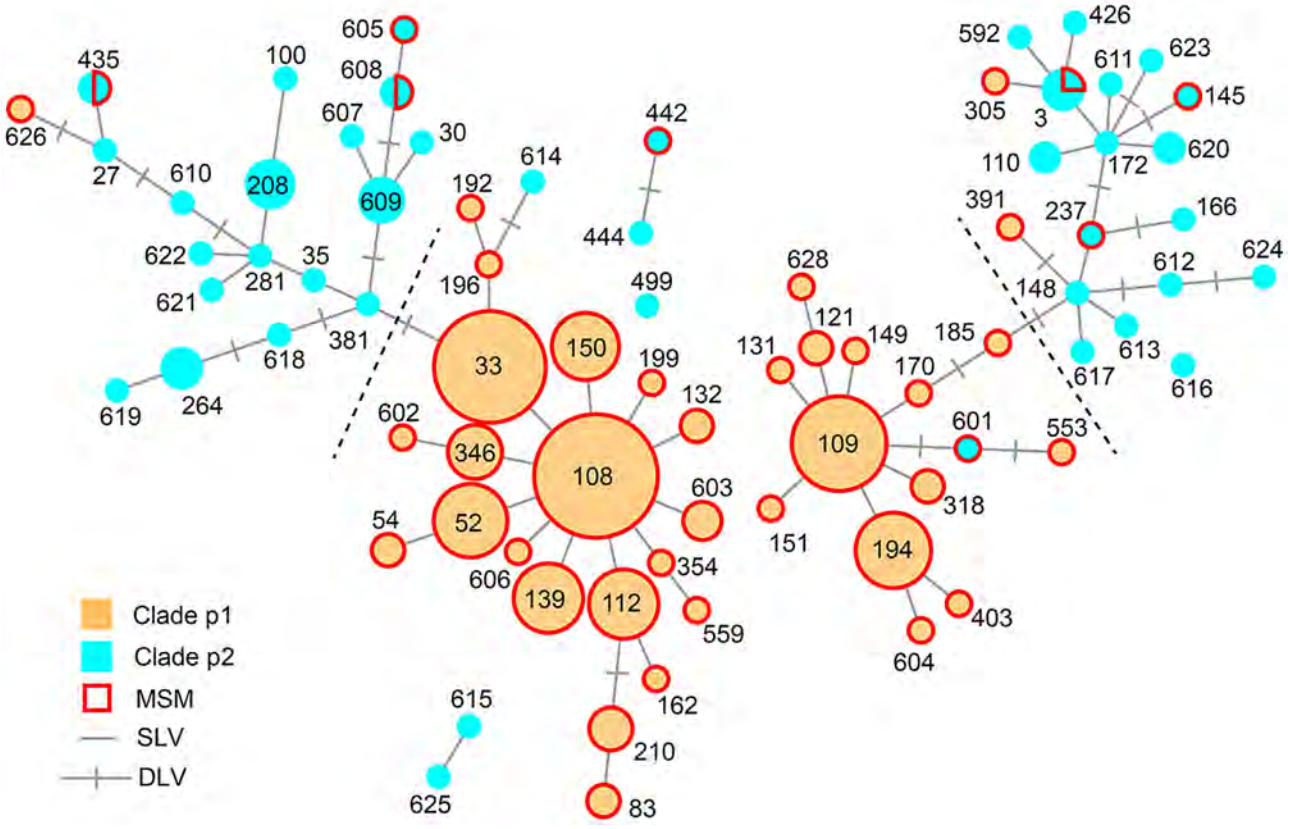

Figure 3. Minimum spanning tree based on sequence types (STs) and polymorphic membrane protein E (PmpE) of 298 *Chlamydia trachomatis* samples in study of clustering of specific PmpE clade in *C. trachomatis* lineages from MSM, Japan. Each node indicates the ST number. SLVs and DLVs are linked. Samples from MSM are outlined in red, reflecting the proportion of samples in each node. The PmpE clades p1 and p2 are colored using the same color codes as those used in Figure 2. Dashed lines are the assumed borders between the MSM and non-MSM lineages. DLV, double-locus variant; MSM, men who have sex with men; SLV, single-locus variant.

PmpE sequencing (Appendix 1, https://wwwnc.cdc.gov/EID/article/30/10/24-0852-App1.xlsx). Although specimens were repeatedly collected from several MSM participants on different dates, no duplicate data (identical ST detection from the same site on different collection dates) were collected. The predominant *ompA* genotypes in the MSM population were D, G, and J (Figure 1; Appendix 2 Table 1, https://wwwnc.cdc.gov/EID/article/30/10/24-0852-App2.pdf), as previously reported in several countries (*5*–*8*). The most frequently detected STs were ST108 and its single-locus variants (SLVs) (e.g., ST33, ST52) and ST109 and its SLV (e.g., ST194). The main *ompA* genotypes were G/J in the ST108 lineage and D in the ST109 lineage (Appendix 2 Table 2). ST108 and ST109 are quadruple-locus variants of each other.

We detected 15 PmpE sequences in the 298 samples (p1–1 to p1–5 and p2–1 to p2–10), and those were clearly separated into 2 clades (named as p1 and p2) reflecting the MSM and non-MSM populations (Figure 2; Appendix 2 Figure). A few MSM samples were classified as p2, whereas no non-MSM samples were classified as p1. In MSM, the prevalence of the p1 clade did not differ significantly in urogenital, pharyngeal, and rectal samples ($p = 0.141$ by Fisher exact test) (Table), suggesting that the difference in clade between MSM and non-MSM samples was not attributable to differences in the anatomic sample collection sites. To investigate the phylogenetic relationships between the PmpE clades, we created a minimum spanning tree from STs showing the relationship to p1 and p2 (Figure 3). We further divided both lineages into likely sublineages corresponding to the difference in the PmpE clades (Figures 1, 3).

Tokyo is a capital city with a population of >10 million and is connected to the 2 largest international airports in Japan; therefore, the similarity of the genotype distribution observed in this study to that observed in other countries is not surprising. The predominant *C. trachomatis* lineages among MSM in this study were centered around ST108 and ST109. Of the samples from MSM in this study, 89.4% (219/245) were major STs or their SLVs had been previously reported among MSM in other countries (*5*–*8*), demonstrating that the circulating lineages among MSM in Tokyo were typical of STs circulating internationally in MSM populations. In contrast, none of the STs of non-MSM samples were classified as major MSM STs, suggesting that the samples from non-MSM patients in this study were not linked to STs circulating in the global MSM population.

Conclusions

This study revealed that most MSM-associated *C. trachomatis* STs belonged to the specific PmpE clade p1. This finding indicates that nonsimplex *C. trachomatis* lineages with shared microbiological characteristics involved in the infection process (*9*,*10*) likely disseminated in parallel through international MSM networks and that those shared characteristics might be involved in the infection process and transmission. Taken together, this study demonstrates the importance of PmpE as a target for molecular epidemiologic investigation to clarify the dynamics of *C. trachomatis* transmission.

Acknowledgments

We thank Shigenobu Nishijima, Shinsuke Watanabe, and Toshihisa Iwabuchi for collecting the clinical specimens.

This work was supported by the National Center for Global Health and Medicine (grant nos. 19A1002 and 20A1020), JSPS KAKENHI (grant no. 24K10230), and the Takeda Science Foundation.

About the Author

Ms. Mitobe is a pharmacist who works as a senior scientist at the Tokyo Metropolitan Institute of Public Health, Tokyo, Japan. Her primary research interest is sexually transmitted diseases.

References

1. Klint M, Löfdahl M, Ek C, Airell A, Berglund T, Herrmann B. Lymphogranuloma venereum prevalence in Sweden among men who have sex with men and characterization of *Chlamydia trachomatis ompA* genotypes. J Clin Microbiol. 2006;44:4066–71. https://doi.org/10.1128/JCM.00574-06
2. Twin J, Moore EE, Garland SM, Stevens MP, Fairley CK, Donovan B, et al. *Chlamydia trachomatis* genotypes among men who have sex with men in Australia. Sex Transm Dis. 2011;38:279–85. https://doi.org/10.1097/OLQ.0b013e3181fc6944
3. Li JH, Cai YM, Yin YP, Hong FC, Shi MQ, Feng TJ, et al. Prevalence of anorectal *Chlamydia trachomatis* infection and its genotype distribution among men who have sex with men in Shenzhen, China. Jpn J Infect Dis. 2011;64:143–6. https://doi.org/10.7883/yoken.64.143
4. Qin X, Zheng H, Xue Y, Ren X, Yang B, Huang J, et al. Prevalence of *Chlamydia trachomatis* genotypes in men who have sex with men and men who have sex with women using multilocus VNTR analysis—*ompA* typing in Guangzhou, China. PLoS One. 2016;11:e0159658. https://doi.org/10.1371/journal.pone.0159658
5. Piñeiro L, Villa L, Salmerón P, Maciá MD, Otero L, Vall-Mayans M, et al. Genetic characterization of non-lymphogranuloma venereum *Chlamydia trachomatis* indicates distinct infection transmission networks in Spain. Int J Mol Sci. 2023;24:6941. https://doi.org/10.3390/ijms24086941

6. Bom RJ, van der Helm JJ, Schim van der Loeff MF, van Rooijen MS, Heijman T, Matser A, et al. Distinct transmission networks of *Chlamydia trachomatis* in men who have sex with men and heterosexual adults in Amsterdam, The Netherlands. PLoS One. 2013;8:e53869. https://doi.org/10.1371/journal.pone.0053869
7. Herrmann B, Isaksson J, Ryberg M, Tångrot J, Saleh I, Versteeg B, et al. Global multilocus sequence type analysis of *Chlamydia trachomatis* strains from 16 countries. J Clin Microbiol. 2015;53:2172–9. https://doi.org/10.1128/JCM.00249-15
8. Versteeg B, Bruisten SM, van der Ende A, Pannekoek Y. Does typing of *Chlamydia trachomatis* using housekeeping multilocus sequence typing reveal different sexual networks among heterosexuals and men who have sex with men? BMC Infect Dis. 2016;16:162. https://doi.org/10.1186/s12879-016-1486-2
9. Debrine AM, Karplus PA, Rockey DD. A structural foundation for studying chlamydial polymorphic membrane proteins. Microbiol Spectr. 2023;11:e0324223. https://doi.org/10.1128/spectrum.03242-23
10. Favaroni A, Hegemann JH. *Chlamydia trachomatis* polymorphic membrane proteins (Pmps) form functional homomeric and heteromeric oligomers. Front Microbiol. 2021;12:709724. https://doi.org/10.3389/fmicb.2021.709724
11. Suchland RJ, Carrell SJ, Ramsey SA, Hybiske K, Debrine AM, Sanchez J, et al. Genomic analysis of MSM rectal *Chlamydia trachomatis* isolates identifies predicted tissue-tropic lineages generated by intraspecies lateral gene transfer-mediated evolution. Infect Immun. 2022;90:e0026522. https://doi.org/10.1128/iai.00265-22
12. Mizushima D, Takano M, Uemura H, Yanagawa Y, Aoki T, Watanabe K, et al. High prevalence and incidence of rectal *Chlamydia* infection among men who have sex with men in Japan. PLoS One. 2019;14:e0220072. https://doi.org/10.1371/journal.pone.0220072
13. Yoshida H, Kishi Y, Shiga S, Inoue S, Hagiwara T. Serotyping of *Chlamydia trachomatis* by polymerase chain reaction [in Japanese]. Sex Transm Infect. 1995;6:40–5.
14. Zhou Z, Alikhan NF, Sergeant MJ, Luhmann N, Vaz C, Francisco AP, et al. GrapeTree: visualization of core genomic relationships among 100,000 bacterial pathogens. Genome Res. 2018;28:1395–404. https://doi.org/10.1101/gr.232397.117
15. Kumar S, Stecher G, Tamura K. MEGA7: Molecular Evolutionary Genetics Analysis version 7.0 for bigger datasets. Mol Biol Evol. 2016;33:1870–4. https://doi.org/10.1093/molbev/msw054

Address for correspondence: Hiroaki Kubota, 3-24-1 Hyakunincho, Shinjuku-ku, Tokyo 169-0073, Japan; email: hiroaki_kubota@member.metro.tokyo.jp

etymologia revisited

Influenza

[in''floo-en'zə]

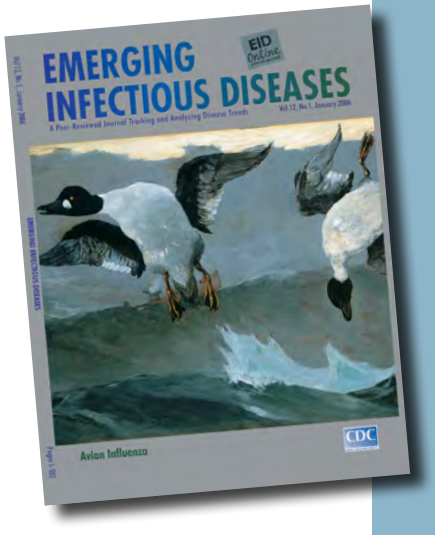

Originally published in January 2006

An acute viral infection of the respiratory tract. From Latin influentia,"to flow into"; in medieval times, intangible fluid given off by stars was believed to affect humans. The Italian influenza referred to any disease outbreak thought to be influenced by stars. In 1743, what Italians called an influenza di catarro ("epidemic of catarrh") spread across Europe, and the disease came to be known in English as simply "influenza."

Reference

Dorland's illustrated medical dictionary. 30th ed. Philadelphia: Saunders; 2003 and Quinion M. World wide words. 1998 Jan 3 [cited 2005 Dec 5]. http://www.worldwidewords.org/topicalwords/tw-inf1.htm

Investigation of a Human Case of *Francisella tularensis* Infection, United Kingdom, 2023

Ameeka Thompson, Tim Brooks, Catherine Houlihan, Tommy Rampling, Helen Umpleby, Kayleigh Hansford, Jolyon Medlock, Alexander Vaux, Julie Logan, Andrew Frost, Sue Neale, Stephen Wyllie, Kirsty Dodgson, Dominic Haigh, Isra Halim, Raqib Huq, Michael Riste, N. Claire Gordon

Tularemia, caused by *Francisella tularensis*, is not known to occur in the United Kingdom. We report a case of tularemia diagnosed in July 2023 in a UK patient with no travel in the 6 weeks before symptom onset. We describe the subsequent multiagency investigation into possible routes of acquisition.

Tularemia is a zoonotic disease caused by *Francisella tularensis*, currently considered absent from the United Kingdom. We report a human case of *F. tularensis* subspecies *holarctica* infection diagnosed in the United Kingdom and the resulting cross-agency investigations. We obtained written consent from the patient for publication of our findings.

The Study

In May 2023, a 47-year-old man sought treatment at a primary care facility 48 hours after he had fever and cervical lymphadenopathy develop. The working diagnosis was a dental infection, but there was no response to the oral antimicrobial drugs amoxicillin/clavulanic acid and metronidazole or to subsequent dental extraction. The patient was referred to the otorhinolaryngology department for further investigation. Over the next few weeks, the lymph nodes became suppurative, but there was no growth on routine bacterial culture. We aspirated his lymph nodes in June 2023 but found no growth on bacterial or mycobacterial cultures and sent the sample for 16S rRNA gene PCR (16S PCR) and sequencing. *F. tularensis* was identified on 16S PCR and confirmed by subsequent *Francisella*-specific PCR at the UK Health Security Agency (UKHSA) Rare and Imported Pathogens Laboratory.

We initially assumed that the infection had been acquired during a trip to Sweden. However, after the *F. tularensis* diagnosis was confirmed, we obtained a detailed travel and exposure history from the patient. The patient's symptoms had manifested 6 weeks before the trip to Sweden and remained unchanged after the trip. His only other relevant overseas travel was a 4-day trip to southern Portugal in March 2023, >6 weeks before symptom onset. Before that time, he had not left the United Kingdom since 2019.

The patient had 3 pet degus, chinchilla-like rodents originating in Chile, bought in the United Kingdom 6 years earlier. One degu had died suddenly in early July 2023, two months after the patient's symptom onset. The corpse of the animal was disposed of without examination. A second degu became unwell with jaw swelling a few days later. Cytological examination of the swelling was in keeping with inflammation and infection, but no samples were sent for bacteriology. The patient reported no other animal contact apart from occasional contact with dogs of a family member. Those dogs were fed commercial nonraw pet food and had had no recent illnesses.

The patient lived near a nature reserve in the northwest of England where he took regular walks; he had not seen any lagomorphs or rodents or noticed

Author affiliations: UK Health Security Agency Rare and Imported Pathogens Laboratory, Salisbury, UK (A. Thompson, T. Brooks, C. Houlihan, T. Rampling, H. Umpleby, N.C. Gordon); UK Health Security Agency Medical Entomology and Zoonoses Ecology, Salisbury (K. Hansford, J. Medlock, A. Vaux); UK Health Security Agency Bacterial Identification Section, London, UK (J. Logan); Animal and Plant Health Agency Veterinary Advice Services, London (A. Frost); Animal and Plant Health Agency Surveillance and Laboratory Service Department, Cumbria, UK (S. Neale); Animal and Plant Health Agency Veterinary Advice Services, Surrey, UK (S. Wyllie); Manchester University NHS Foundation Trust, Manchester, UK (K. Dodgson, D. Haigh, I. Halim, R. Huq, M. Riste)

DOI: https://doi.org/10.3201/eid3010.240479

any insect bites. He had no history of drinking contaminated water or consuming raw meat, lagomorphs, or rodents and had not handled any animal carcasses. The patient was examined again by the local infection team. Because of ongoing discharge from the neck lesions, antimicrobial drugs were changed from doxycycline to ciprofloxacin.

We collected additional swab and serum samples for *F. tularensis* antibody testing. *F. tularensis* subsp. *holarctica* subtype was confirmed by specific PCR by using an in-house multitarget real-time TaqMan PCR differentiation assay developed as described elsewhere (*1*). We submitted the PCR product for next-generation sequencing, which confirmed subspecies identification. Unfortunately, we could not culture the organism from either the original or later swab samples. A commercial assay (Seramun Diagnostica, https://www.seramun.com) was positive for combined *F. tularensis* IgG/IgM. We took samples from the surviving degus and their bedding and food. All tested negative for *F. tularensis* by specific PCR, and the bacterium was not isolated on culture.

The United Kingdom has many potential mammal reservoirs of *F. tularensis*, including the brown hare (*Lepus europaeus*), black rat (*Rattus rattus*), and several mice and vole species, but the organism has never been isolated from animals in the United Kingdom. The Animal and Plant Health Agency through its Diseases of Wildlife Scheme conducts passive surveillance for wildlife diseases; no local wildlife dieoffs had been reported. Rewilding programs reintroducing beavers (*Castor fiber*) into the United Kingdom present another possible source; however, no beavers had been released near the patient's locale, and imported beavers must test negative for *F. tularensis* as a condition of release.

Tickborne transmission of *F. tularensis* subsp. *holarctica* has been described for *Ixodes ricinus* and *Dermacentor reticulatus* ticks, both present in the United Kingdom. Although the likely date of the patient's tularemia acquisition was compatible with seasonal activity of *I. ricinus* ticks, there were no records of that tick in the local area, based on 15 years of passive surveillance data (*2*). Similarly, *D. reticulatus* ticks are not known to be present in that area. Mosquitoes represent another potential vector. Data from national mosquito surveillance indicate that potential mosquito vectors, such as *Aedes cinereus*, are present in the United Kingdom but would have been active 2 weeks after symptom onset. No nuisance biting was reported in the area at that time.

Site visits were conducted by the UKHSA Medical Entomology and Zoonoses Ecology team in August 2023 and May 2024. We found no evidence of active tick populations after sampling. Mosquito traps did not yield any human-biting species.

Although the patient's travel dates made acquisition in Portugal highly unlikely, we notified authorities in that country using its National International Health Regulations Focal Point in accordance with the World Health Organization International Health Regulations (2005) (*3*). The Portugal authorities have reported no recent imported or autochthonous cases of tularemia. European Centre for Disease Prevention and Control tick surveillance data show that both *I. ricinus* and *D. reticulatus* ticks are present in southern Portugal (*4*,*5*). A surveillance study project conducted in northern Portugal detected *F. tularensis* DNA in 1 human and 1 tick (*6*). Both imported (*7*) and autochthonous (*8*) cases of tularemia have been described in Portugal, although the autochthonous case was diagnosed by agglutination testing only. If the patient did acquire the infection in Portugal, the incubation period would have been substantially longer than usual because he returned from Portugal 47 days before symptom onset (*9*). The longest incubation period reported is 43 days in 1 case report (*10*).

Several hypotheses have been proposed and investigated to explain the transmission route for the case-patient. Whereas acquisition in Portugal was a possibility, the unusually long incubation period and reported local absence of *F. tularensis* in both humans and wildlife makes that scenario unlikely. Similarly, the patient was unlikely to have acquired the infection from his companion animals given the timelines and negative testing of the animals. We cannot rule out acquisition within the United Kingdom, potentially from an as-yet unidentified environmental reservoir, with the possibility that it was transmitted by a biting arthropod. Following antimicrobial treatment, the patient's systemic symptoms resolved. The lymph nodes ceased suppurating but remained enlarged, although without pain.

Conclusions

UKHSA issued a briefing note (*11*) to inform clinicians of the possible presence of *F. tularensis* in the United Kingdom. Passive surveillance for reports of wildlife dieoffs in the area will continue, and the nature reserve will be incorporated into a nationwide mosquito surveillance project. *F. tularensis* testing will be conducted on ticks collected as part of ongoing surveillance and research.

This multidisciplinary investigation demonstrates the difficulties of establishing the origin of a cryptic infection. Clinicians should be aware of tularemia and consider it in differential diagnoses of patients with compatible clinical syndromes, even in the absence of a recent relevant history of travel.

Acknowledgments

Many thanks to the other members of the investigating team: Jane Osborne, Richard Vipond, Clare Warrell, Daniel Bailey, Wendi Shepherd, Zoe Gibney, Eva Emanuel, Shivaj Bhardwaj, Elizabeth Stratford, Adrienne Mackintosh, Paul Holmes, Megan Rawlins, and Susannah Penney.

About the Author

Dr. Thompson is an infectious diseases and medical microbiology trainee in the United Kingdom, currently working at the UK Health Security Agency's Rare and Imported Pathogens Laboratory, Porton Down. Clinical interests include leptospirosis, imported infection, and tuberculosis.

References

1. Versage JL, Severin DD, Chu MC, Petersen JM. Development of a multitarget real-time TaqMan PCR assay for enhanced detection of *Francisella tularensis* in complex specimens. J Clin Microbiol. 2003;41:5492–9.
2. Hansford KM, Gandy SL, Gillingham EL, McGinley L, Cull B, Johnston C, et al. Mapping and monitoring tick (Acari, Ixodida) distribution, seasonality, and host associations in the United Kingdom between 2017 and 2020. Med Vet Entomol. 2023;37:152–63.
3. World Health Organization. International Health Regulations. 3rd edition. Geneva: The Organization; 2005.
4. European Centre for Disease Prevention and Control. *Ixodes ricinus*—current known distribution: October 2023 [cited 2023 Dec 8]. https://www.ecdc.europa.eu/en/publications-data/ixodes-ricinus-current-known-distribution-october-2023
5. European Centre for Disease Prevention and Control. *Dermacentor reticulatus*—current known distribution: October 2023 [cited 2023 Dec 8]. https://www.ecdc.europa.eu/en/publications-data/dermacentor-reticulatus-current-known-distribution-october-2023
6. de Carvalho IL, Escudero R, Garcia-Amil C, Falcão H, Anda P, Núncio MS. *Francisella tularensis*, Portugal. Emerg Infect Dis. 2007;13:666–7.
7. Lopes de Carvalho I, Nascimento P, Núncio MS, Toscano Rico M. First case of tularemia reported in Portugal: probably of imported origin. Front Public Health. 2018;6:325.
8. Cunha F, Lopes de Carvalho I, Torres C, Gonçalves R. A multidisciplinary approach to the first autochthonous case of tularemia reported in Portugal. Acta Med Port. 2022;35.
9. Maurin M, Gyuranecz M. Tularaemia: clinical aspects in Europe. Lancet Infect Dis. 2016;16:113–24.
10. Darmon-Curti A, Darmon F, Edouard S, Hennebique A, Guimard T, Martin-Blondel G, et al. Tularemia: a case series of patients diagnosed at the National Reference Center for Rickettsioses from 2008 to 2017. Open Forum Infect Dis. 2020;7:ofaa440.
11. UK Health Security Agency. UKHSA Briefing Note 2023/038. Changing epidemiology of zoonotic and vector borne infections. 2023.

Address for correspondence: Ameeka Thompson, Rare and Imported Pathogens Laboratory, UK Health Security Agency, Manor Farm Road, Porton Down, Salisbury SP40JG, UK; email: amy.thompson@ukhsa.gov.uk

Rift Valley Fever Epizootic, Rwanda, 2022

Eric Remera, Edson Rwagasore, Olivier Nsekuye, Muhammed Semakula, Misbah Gashegu, Robert Rutayisire, Leandre Ishema, Clarisse Musanabaganwa, Yvan Butera, Sabin Nsanzimana, Claude M. Muvunyi, Ayman Ahmed

A Rift Valley fever epizootic affected livestock in Rwanda during March–October 2022. We confirmed 3,112 infections with the virus, including 1,342 cases, 1,254 abortions, and 516 deaths among cattle, goats, and sheep. We recommend a One Health strategy for investigations and response to protect animal and human health.

Rift Valley fever (RVF) is a zoonotic arthropod-borne viral (arboviral) disease that affects a wide range of susceptible hosts, including livestock (cattle, sheep, goats), wildlife, and humans (*1*). It is caused by RVF virus (RVFV), which is mainly transmitted by *Aedes* and *Culex* mosquito vectors. Infection can also be acquired through close contact with infected animals or consumption of their infected products (e.g., raw milk, uncooked meat). In addition, vertical and sexual transmission of RVFV among humans, animals, and disease vectors has been documented (*2*). The disease affects health security and socioeconomics, leading to food insecurity and poverty, mainly among animal resource–dependent communities (*3*). RVFV transmission is influenced by climate, increased mobility, and contact between infected and susceptible hosts (e.g., humans, animals, and vectors) (*4*,*5*). Emergence of RFV epidemics, epizootics, and outbreaks is associated with extreme whether events, such as heavy rains and flooding (*2*,*6*).

Apart from Saudi Arabia and Yemen, RVF is confined to Africa; countries in East Africa (e.g., Sudan, Somalia, and Kenya) are affected the most (*2*,*7*). Little is known about the epidemiology and transmission of RVFV in Rwanda; however, high seroprevalence of RVFV was detected in the country during 2012–2013, and an outbreak occurred in 2018 (*8*,*9*). To help fill in knowledge gaps and evidence to guide strategic planning and interventions to prevent RVF outbreaks in Rwanda, we report an epizootic of RVF among livestock in Rwanda that occurred in 2022.

Author affiliations: Rwanda Biomedical Center, Kigali, Rwanda (E. Remera, E. Rwagasore, O. Nsekuye, M. Gashegu, R. Rutayisire, L. Ishema, C. Musanabaganwa, C.M. Muvunyi, A. Ahmed); Ministry of Health, Kigali (M. Semakula, Y. Butera, S. Nsanzimana); University of Khartoum, Khartoum, Sudan (A. Ahmed)

DOI: https://doi.org/10.3201/eid3010.240264

The Study

In response to a sudden increase in abortion rate among livestock that was reported by animals' owners in mid-March 2022, Rwanda Biomedical Centre (Kigali, Rwanda), the leading implementer of health systems in the country, initiated an epidemiologic investigation. Initial serologic analysis confirmed exposure of the dead and aborted animals to RVFV. Accordingly, a national health emergency alert was released to engage the community of the animals' owners, animal health authorities, and community health workers, as well as healthcare providers to enhance collaborative surveillance to strengthen national preparedness, response, and resilience to the health emergency (*10*). The collaborative surveillance included syndromic surveillance implemented through community engagement and supported by molecular epidemiology analysis.

We initially confirmed active RVFV infections by molecular analysis (PCR) on March 22, 2022, in the Nyagatare district in the northeastern region of Rwanda, near the borders with Tanzania and Uganda. However, the epizootic grew and spread rapidly among the populations of livestock throughout the country (Appendix Figure 1, https://wwwnc.cdc.gov/EID/article/30/10/24-0264-App1.pdf). The epizootic peaked at 77 cases reported on April 14, 2022, and disease fatalities peaked at 41 deaths reported on May 26 (Figure). The epizootic ended by October 14, 2022.

During the epizootic, March–October 2022, a total of 3,112 infections were confirmed among livestock, representing 0.2% of the total population of animal resources (livestock) in the country. Confirmed RVFV infections included 1,342 cases, 1,254 abortions, and 516 deaths (Table). Most cases were reported from

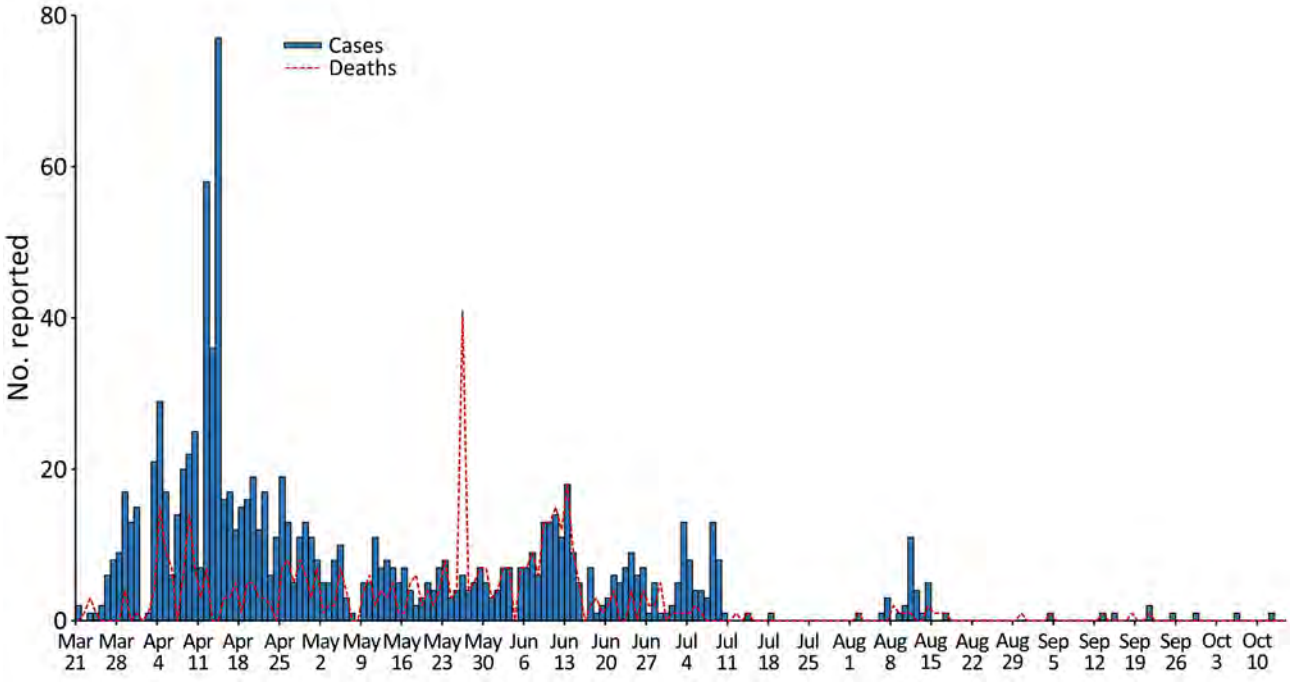

Figure. Cases and deaths among livestock, by date reported, during Rift Valley fever epizootic in Rwanda, March 21–October 14, 2022.

Eastern 535 (40%) and Southern 450 (33%) Provinces, as were abortions (41% were reported from Eastern and 41% from Southern Provinces). Most fatalities (225 [44%]) were reported from Southern Province, closely followed by Eastern Province (145 [28%]) (Table). Of note, the lowest proportion of RFV cases was in Western Province: 49 (4%) cases, 13 (1%) abortions, and 18 (3%) deaths. Cross-species analysis indicated that most RVF cases (1,285; 96%) affected the bovine population (Table); however, the reporting of abortions and deaths was not disaggregated by animal species.

Although cases of RVF in cattle were distributed throughout the country, the heavy burden was reported from the central and southern regions of Rwanda (Appendix Figure 2). Cases of RVF in goats were scattered throughout the northern and southwestern regions of the country. Cases of RVF in sheep were distributed from northern to southern Rwanda. However, it was not possible to investigate the drivers behind the sudden emergence and spread of the outbreak (*1*,*6*).

The capacity of entomologic surveillance and response in Rwanda is limited. Therefore, no entomologic investigations were performed to identify the vector species involved in the epizootic.

Conclusions

The emergence of the countrywide RVF epizootic in Rwanda suggests changes in disease transmission in the country, which could be attributed to increased density and mobility of livestock and to changes in vector composition resulting from emergence of invasive disease vectors (*11*). Because no entomologic investigations were undertaken during the epizootic, information about vector species involved in the outbreak, as well as the presence and distribution of RVF-competent vectors, is not available. The potential change in the composition of vectors might have been influenced by the recent expansion of rice farming in the country. Nevertheless, considering the growing risk for invasive-disease vectors and the growing burden of vector-borne diseases in the region, more investment

Table. Epidemiologic characteristics of the Rift Valley fever epizootic in Rwanda, 2022

Province	No. animals	Epidemiologic characteristics, no. (%)				Distribution of cases by species		
		Cases	Abortions	Fatalities	Affected animals	Bovine	Caprine	Ovine
Central	73,539	99 (7)	122 (10)	45 (9)	266 (9)	96	1	2
Eastern	1,171,793	535 (40)	511 (41)	145 (28)	1,191 (38)	532	0	3
Northern	635,259	209 (16)	87 (7)	83 (16)	379 (12)	178	18	13
Southern	911,211	450 (33)	521 (41)	225 (44)	1,196 (38)	435	11	4
Western	625,256	49 (4)	13 (1)	18 (3)	80 (3)	44	4	1
Total	1,880,591	1,342 (100)	1,254 (100)	516 (100)	3,112 (100)	1,285	34	23

should be made in building technical expertise and capacity to routinely implement comprehensive vector surveillance and control, with a focus on early detection of invasive vectors (*11*,*12*). Raising awareness and engaging the community in implementing syndromic surveillance will help with early detection and response (*10*). However, further investigations are needed to understand the driving factors behind the development and spread of RVF outbreaks (*13*).

To shed some light on the cross-border dynamics of RVFV in Rwanda, further genomic investigations are warranted (*14*) and should generate evidence that helps strengthen implementation of the International Health Regulations (2005) (https://www.who.int/publications/i/item/9789241580496) to prevent and control cross-country transmission of diseases including RVF (*6*,*15*). However, RVF is on lists of the World Health Organization, GAVI (https://www.gavi.org), and the Coalition for Epidemic Preparedness Innovations (https://cepi.net) for "disease X" pathogens and for pandemic-prone diseases. Therefore, stakeholders of human, animal, and environment health in Rwanda should prioritize strengthening the local pandemic preparedness, prevention, and response framework through a multisectoral transdisciplinary One Health strategy (*1*,*15*).

Widespread RVF infections among livestock in Rwanda suggest that the disease is endemic to the country and that factors such as increased density and mobility of livestock and changes in climate or vector composition might have enhanced transmission. Therefore, a strategy of strengthening the pandemic preparedness, prevention, and response framework in the country, including community-based syndromic surveillance, would be helpful. Because of the wide range of hosts susceptible to RVF, the framework should incorporate a multisectoral transdisciplinary One Health strategy to effectively protect humans, animals, and the environment from the devastating health, safety, food insecurity, and socioeconomic effects of RVF outbreaks.

About the Author

Dr. Remera is a senior data scientist and lead of the Research, Innovation, and Data Science Division at Rwanda Biomedical Centre. His research focuses on disease epidemiology and modeling and developing innovative prevention and control measures.

References

1. Ahmed A, Ali Y, Elduma A, Eldigail MH, Mhmoud RA, Mohamed NS, et al. Unique outbreak of Rift Valley fever in Sudan, 2019. Emerg Infect Dis. 2020;26:3030–3. https://doi.org/10.3201/eid2612.201599
2. Ahmed A, Dietrich I, LaBeaud AD, Lindsay SW, Musa A, Weaver SC. Risks and challenges of arboviral diseases in Sudan: the urgent need for actions. Viruses. 2020;12:81. https://doi.org/10.3390/v12010081
3. Davies FG. The historical and recent impact of Rift Valley fever in Africa. Am J Trop Med Hyg. 2010;83(Suppl):73–4. https://doi.org/10.4269/ajtmh.2010.83s2a02
4. Carlson CJ, Albery GF, Merow C, Trisos CH, Zipfel CM, Eskew EA, et al. Climate change increases cross-species viral transmission risk. Nature. 2022;607:555–62. https://doi.org/10.1038/s41586-022-04788-w
5. Ahmed A, Mohamed NS, Siddig EE, Algaily T, Sulaiman S, Ali Y. The impacts of climate change on displaced populations: a call for actions. The Journal of Climate Change and Health. 2021;3:100057. https://doi.org/10.1016/j.joclim.2021.100057
6. Ahmed A, Mahmoud I, Eldigail M, Elhassan RM, Weaver SC. The emergence of Rift Valley fever in Gedaref State urges the need for a cross-border One Health Strategy and enforcement of the International Health Regulations. Pathogens. 2021;10:885. https://doi.org/10.3390/pathogens10070885
7. Himeidan YE, Kweka EJ, Mahgoub MM, El Rayah A, Ouma JO. Recent outbreaks of Rift Valley fever in East Africa and the Middle East. Front Public Health. 2014;2:169. https://doi.org/10.3389/fpubh.2014.00169
8. Dutuze MF, Ingabire A, Gafarasi I, Uwituze S, Nzayirambaho M, Christofferson RC. Identification of Bunyamwera and possible other *Orthobunyavirus* infections and disease in cattle during a Rift Valley fever outbreak in Rwanda in 2018. Am J Trop Med Hyg. 2020;103:183–9. https://doi.org/10.4269/ajtmh.19-0596
9. Umuhoza T, Berkvens D, Gafarasi I, Rukelibuga J, Mushonga B, Biryomumaisho S. Seroprevalence of Rift Valley fever in cattle along the Akagera-Nyabarongo Rivers, Rwanda. J S Afr Vet Assoc. 2017;88:e1–5. https://doi.org/10.4102/jsava.v88i0.1379
10. World Health Organization. Defining collaborative surveillance: a core concept for strengthening the global architecture for health emergency preparedness, response, and resilience (HEPR) [cited 2024 Sep 3]. https://www.who.int/publications/i/item/9789240074064
11. Ahmed A, Abubakr M, Sami H, Mahdi I, Mohamed NS, Zinsstag J. The first molecular detection of *Aedes albopictus* in Sudan associates with increased outbreaks of chikungunya and dengue. Int J Mol Sci. 2022;23:11802. https://doi.org/10.3390/ijms231911802
12. Hemming-Schroeder E, Ahmed A. *Anopheles stephensi* in Africa: vector control opportunities for cobreeding *An. stephensi* and *Aedes* arbovirus vectors. Trends Parasitol. 2023;39:86–90. https://doi.org/10.1016/j.pt.2022.11.011
13. Métras R, Porphyre T, Pfeiffer DU, Kemp A, Thompson PN, Collins LM, et al. Exploratory space-time analyses of Rift Valley fever in South Africa in 2008-2011. PLoS Negl Trop Dis. 2012;6:e1808. https://doi.org/10.1371/journal.pntd.0001808
14. Freire CCM, Iamarino A, Soumaré POL, Faye O, Sall AA, Zanotto PMA. Reassortment and distinct evolutionary dynamics of Rift Valley fever virus genomic segments. Sci Rep. 2015;5:11353. https://doi.org/10.1038/srep11353
15. Ahmed A. Urgent call for a global enforcement of the public sharing of health emergencies data: lesson learned from serious arboviral disease epidemics in Sudan. Int Health. 2020;12:238–40. https://doi.org/10.1093/inthealth/ihz122

Address for correspondence: Eric Remera, Rwanda Biomedical Centre, Research Innovation and Data Science Division, PO Box 7162, KG 644 St, Kimihurura, Kigali, Rwanda; email: eric.remera@rbc.gov.rw

Correlation between Viral Wastewater Concentration and Respiratory Tests, Oregon, USA

Noah Lininger,[1] Rebecca Falender, Paul Cieslak, Arilene Novak, M. Andraya Hendrick, Devrim Kaya, Casey Kanalos, Oumaima Hachimi, David Mickle, Christine Kelly, Tyler Radniecki, Melissa Sutton

Author affiliations: Oregon Health Authority, Portland, Oregon (N. Lininger, R. Falender, P. Cieslak, A. Novak, M.A. Hendrick, M. Sutton); Oregon State University, Corvallis, Oregon, USA (D. Kaya, C. Kanalos, O. Hachimi, D. Mickle, C. Kelly, T. Radniecki).

DOI: https://doi.org/10.3201/eid3010.240637

We evaluated the association between wastewater concentration and weekly percent positivity of patient testing for SARS-CoV-2, influenza, and respiratory syncytial virus in Oregon, USA. We found strong, positive correlations for SARS-CoV-2 ($\rho = 0.84$, $p<0.001$), influenza ($\rho = 0.73$, $p<0.001$) and respiratory syncytial virus ($\rho = 0.69$, $p<0.001$).

Since the 1940s, wastewater surveillance has been used to track pathogens that are shed in feces (*1*). Testing wastewater for respiratory viral pathogens avoids potential biases found in case-based surveillance methods. Wastewater surveillance captures information from persons who are asymptomatic or not ill enough to seek care, who reside in rural areas or underserved communities with limited access to care, or who test at home and do not report their results (*2*).

Community transmission of SARS-CoV-2, influenza, and respiratory syncytial virus (RSV) are primarily monitored through test percent positivity. Previous studies have found positive regional correlations between wastewater viral concentration and percent positivity for COVID-19, influenza, and RSV (*3*–*5*). In this study, we compared weekly SARS-CoV-2, influenza, and RSV wastewater concentrations with patient test positivity during September 6, 2020–May 11, 2023, in Oregon, USA.

Our study included wastewater-treatment facilities that submitted ≥1 sample to Oregon's surveillance system during September 6, 2020–May 11, 2023. Sites located on sovereign tribal territories were excluded. Wastewater testing for SARS-CoV-2 was performed year-round. Influenza and RSV wastewater testing was conducted during the influenza and RSV respiratory seasons (September 15, 2021–June 24, 2022, and August 28, 2022–April 30, 2023, for influenza; August 22, 2022–April 30, 2023, for RSV). We collected 24-hour composite samples from wastewater treatment facility influents 1–2 times weekly. We quantified SARS-CoV-2, influenza, and RSV RNA concentrations by using reverse transcription droplet digital PCR, as described previously (*6*). We derived primers and probes for SARS-CoV-2 testing from the 2019-nCoV CDC droplet digital PCR triplex probe assay (BioRad Laboratories, https://www.bio-rad.com) and those for influenza testing from the Center for Disease Control and Prevision influenza SARS-CoV-2 multiplex assay (Integrated DNA Technology, https://idtdna.com); we adopted those for RSV testing from previous studies (*7*). We calculated statewide weekly wastewater viral concentrations by averaging log gene copies per person per day normalized for population and flow across all participating sites. For sites that submitted >1 sample per week, the average concentration of the 2 samples was used.

Human test positivity is the count of positive patient tests divided by the count of tests performed. The National Respiratory and Enteric Virus Surveillance System (NREVSS) is a sentinel laboratory surveillance system that collects aggregate patient test results for 7 viral pathogens including SARS-CoV-2, influenza, and RSV (*8*). A total of 24 sentinel laboratories in Oregon are registered in NREVSS.

We used pairwise correlation to assess the relationship between the statewide weekly wastewater concentration and human test positivity for each pathogen. We assessed the normality of continuous variables with a visual inspection of histograms and quantile-quantile plots and the Shapiro-Wilk test ($\alpha = 0.05$). The assumption of normality was not met, so we used the Spearman rank correlation (ρ) for all analyses. We used SAS 9.4 (SAS Institute Inc., https://www.sas.com) for the analyses.

A total of 48 wastewater treatment plants, serving 62.3% of the population of Oregon, submitted ≥1 sample during the study period. Of 7,185 wastewater samples tested for SARS-CoV-2, a total of 6,910 (96.2%) were positive; of 4,081 wastewater samples tested for influenza, 767 (18.8%) tested positive; and of 1,689 wastewater samples tested for RSV, 473 (28.0%) tested positive. We paired human test positivity with statewide viral concentrations, by week, over 140 weeks for SARS-CoV-2, over 76 weeks for influenza, and over 36 weeks for RSV. We found strong positive correlations between wastewater

[1]Current affiliation: Oregon State University, Corvallis, Oregon, USA.

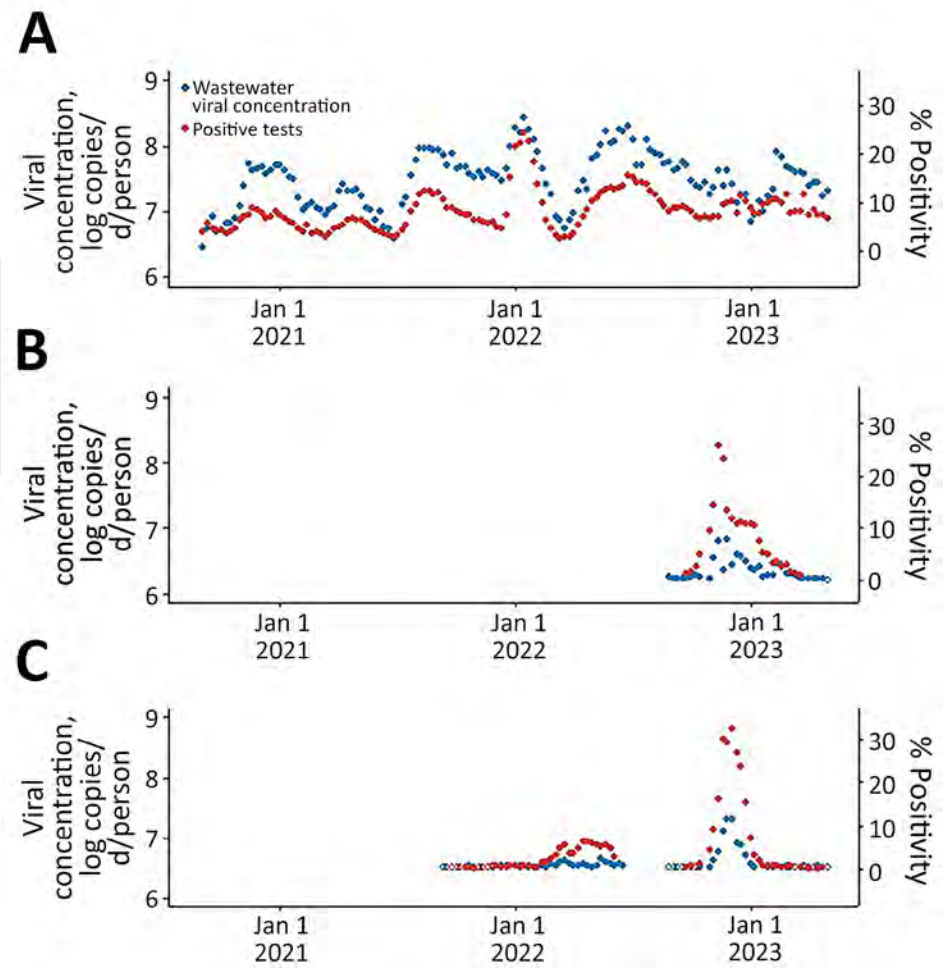

Figure. Statewide weekly wastewater viral concentration (log copies/d/person) and clinical human test positivity over time for respiratory pathogens, Oregon, USA, September 6, 2020–May 11, 2023. A) SARS-CoV-2; B) respiratory syncytial virus; C) influenza. Nondetect values were assigned the mean 1/2 limit of detection for each pathogen. Open circles indicate no detections for that week.

concentration and human test positivity for SARS-CoV-2 (ρ = 0.84, $p<0.0001$), influenza (0.73, $p<0.0001$), and RSV (ρ = 0.69, $p<0.0001$) (Figure).

A limitation of this study is that wastewater surveillance excludes people without access to municipal sewer service. Septic tanks are more prevalent in rural communities than in urban communities, which might have biased our results if people outside of sewersheds are infected at different rates than those within. In addition, whereas SARS-CoV-2 remained a reportable disease throughout the study period, influenza and RSV did not. Fewer influenza and RSV cases might have been reported (outside of NREVSS) during the study period, and statewide human test positivity metrics might not be fully representative of the 3 pathogens, weakening their associations with statewide wastewater data.

Our study found positive correlations between wastewater viral concentration and human test percent positivity for SARS-CoV-2, influenza, and RSV. The strength of association observed suggests wastewater surveillance acts as an indicator of community transmission for those pathogens. Wastewater data are not affected by healthcare-seeking behavior or testing biases, can be analyzed nearly in real-time from pooled community samples, and can be localized to the sewershed level, informing local public health decisions. Our results demonstrate how wastewater surveillance can strengthen our understanding of SARS-CoV-2, influenza, and RSV community transmission.

Acknowledgments

We thank the participating Oregon wastewater utilities and Oregon State University staff and students.

About the Author

At the time of this study, Mr. Lininger was an epidemiologist with the Acute and Communicable Disease Prevention Section at the Oregon Health Authority. His research interests include wastewater surveillance of respiratory viral pathogens and COVID-19 genomic surveillance.

References

1. Schmidt C. Watcher in the wastewater. Nat Biotechnol. 2020;38:917–20. https://doi.org/10.1038/s41587-020-0620-2
2. Larsen DA, Wigginton KR. Tracking COVID-19 with wastewater. Nat Biotechnol. 2020;38:1151–3. https://doi.org/10.1038/s41587-020-0690-1
3. Hopkins L, Persse D, Caton K, Ensor K, Schneider R, McCall C, et al. Citywide wastewater SARS-CoV-2 levels strongly correlated with multiple disease surveillance indicators and outcomes over three COVID-19 waves. Sci Total Environ. 2023;855:158967. https://doi.org/10.1016/j.scitotenv.2022.158967
4. Acosta N, Bautista MA, Waddell BJ, McCalder J, Beaudet AB, Man L, et al. Longitudinal SARS-CoV-2 RNA wastewater monitoring across a range of scales correlates with total and regional COVID-19 burden in a well-defined urban population. Water Res. 2022;220:118611. https://doi.org/10.1016/j.watres.2022.118611
5. Boehm AB, Hughes B, Duong D, Chan-Herur V, Buchman A, Wolfe MK, et al. Wastewater concentrations of human influenza, metapneumovirus, parainfluenza, respiratory syncytial virus, rhinovirus, and seasonal coronavirus nucleic-acids during the COVID-19 pandemic: a surveillance study. Lancet Microbe. 2023;4:e340–8. https://doi.org/10.1016/S2666-5247(22)00386-X
6. Sutton M, Radniecki TS, Kaya D, Alegre D, Geniza M, Girard A-M, et al. Detection of SARS-CoV-2 B.1.351 (Beta) variant through wastewater surveillance before case detection in a community, Oregon, USA. Emerg Infect Dis. 2022;28:1101–9. https://doi.org/10.3201/eid2806.211821
7. Sanghavi SK, Bullotta A, Husain S, Rinaldo CR. Clinical evaluation of multiplex real-time PCR panels for rapid detection of respiratory viral infections. J Med Virol. 2012;84:162–9. https://doi.org/10.1002/jmv.22186
8. Centers for Disease Control and Prevention. The national respiratory and enteric virus surveillance system (NREVSS) [cited 2024 Mar 12]. https://www.cdc.gov/surveillance/nrevss/index.html

Address for correspondence: Noah Lininger, Oregon State University, 116 Johnson Hall, 105 SW 26th St, Corvallis, OR 97331, USA; email: nlininger@gmail.com

Spatiotemporal Epidemiology of Oropouche Fever, Brazil, 2015–2024

Paulo Ricardo Martins-Filho, Thialla Andrade Carvalho, Cliomar Alves dos Santos

Author affiliations: Federal University of Sergipe, Aracaju, Brazil (P.R. Martins-Filho, T.A. Carvalho); Government of Sergipe State, Aracaju (C.A. dos Santos)

DOI: https://doi.org/10.3201/eid3010.241088

We assessed the spatiotemporal dynamics of Oropouche fever in Brazil during 2015–2024. We found the number of cases substantially increased during that period, particularly in the Amazon region. Our findings underscore the need for improved surveillance and public health measures in response to the disease's potential spread beyond endemic areas.

Oropouche fever is an emerging arboviral disease caused by Oropouche virus (OROV) and primarily transmitted by *Culicoides paraensis* biting midges. OROV is endemic to the Americas, predominantly the Amazon region of Brazil; estimates show ≈5 million persons live in areas at high risk for OROV transmission (*1*). Despite potential widespread transmission, Oropouche fever has been neglected, and limited data complicate implementation of effective disease control measures. In Brazil, OROV infection has caused numerous outbreaks, particularly in the Amazon region (*2*), where the climate and forest environment lead to vector proliferation. In 2024, the Pan American Health Organization and World Health Organization issued alerts of increased cases outside the Amazon (*3*) and possible vertical transmission events (*4*). Geographic spread affecting both rural areas and densely populated urban centers in non–Amazon region states underscores the virus' adaptability to varied environments and highlights the urgent need for intensified surveillance and proactive prevention strategies. We assessed the spatiotemporal dynamics of Oropouche fever in Brazil during January 2015–March 2024.

We used anonymized data from the General Coordination of Arbovirus Surveillance of the Ministry of Health (protocol no. 25072.020334/2024-62) and included cases confirmed by reverse transcription PCR or enzyme immunoassay. We extracted information on sex, age, symptom onset, sample collection date, diagnostic method, and location of case notification. We mapped case distributions and calculated cumulative incidence rates per 100,000 inhabitants by using 2022 population census data. We identified high-risk clusters through retrospective spatiotemporal scanning by using SaTScan version 10.1.3 (https://www.satscan.org), QGIS version 3.36.3 (https://qgis.org), and the discrete Poisson model adjusted for population size. For temporal analysis, we used sample collection dates as reference points, given their enhanced precision and reliability within our dataset. We ran Monte Carlo simulations for significance testing and applied the annual percentage change technique by using Joinpoint Regression Program version 5.0.2 (https://surveillance.cancer.gov/joinpoint) to analyze disease incidence trends. We considered $p \leq 0.05$ statistically significant in all analyses.

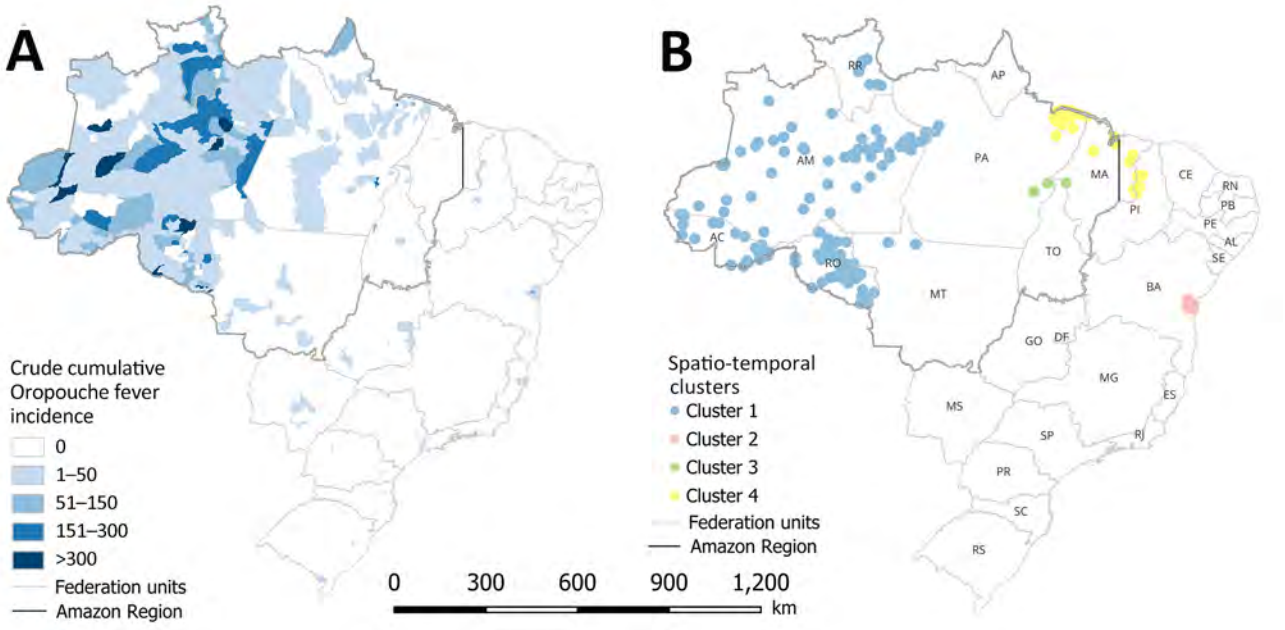

Figure 1. Spatiotemporal maps of epidemiology of Oropouche fever, Brazil, 2015–2024. A) Cumulative incidence (cases per 100,000 inhabitants); B) high-risk spatiotemporal clusters identified across municipalities. AC, Acre; AL, Alagoas; AM, Amazonas; AP, Amapá; BA, Bahia; CE, Ceará; DF, Federal District; ES, Espírito Santo; GO, Goiás; MA, Maranhão; MG, Minas Gerais; MS, Mato Grosso do Sul; MT, Mato Grosso; PA, Pará; PB, Paraíba; PE, Pernambuco; PI, Piauí; PR, Paraná; RJ, Rio de Janeiro; RN, Rio Grande do Norte; RO, Rondônia; RR, Roraima; RS, Rio Grande do Sui; SC, Santa Catarina; SE, Sergipe; SP, São Paulo; TO, Tocantins.

During January 2015–March 2024, Brazil recorded 5,407 Oropouche fever cases; 52% were among male and 48% among female persons. Most (71.4%) cases occurred among persons 20–59 years of age. In total, 18/27 (66.7%) states and 278/5,570 (5%) municipalities reported cases. Among notified cases, 97.1% (5,252 cases) occurred in the Amazon region; only 2.9% (155 cases) were reported outside that area (Appendix Table 1, https://wwwnc.cdc.gov/EID/article/30/10/24-1088-App1.pdf). Within the Amazon, Amazonas (82.4 cases/100,000 inhabitants), Rondônia (69 cases/100,000 inhabitants), and Acre (42.2 cases/100,000 inhabitants) states had the highest incidence rates. Among non–Amazon region states, Piauí (0.8 cases/100,000 inhabitants) and Bahia (0.7/100,000 inhabitants) had the highest rates (Figure 1, panel A).

Spatiotemporal analysis identified 4 major transmission clusters: one across Amazonas, Rondônia, Acre, Roraima, and Mato Grosso starting in 2023; another in Bahia in 2024; a third in Maranhão and Pará in 2021; and a fourth in Pará, Maranhão, and Piauí in 2018 (Figure 1, panel B; Appendix Table 2). Temporal analysis also revealed a statistically significant annual increase in incidence of 145.3% (95% CI 76.5%–240.7%) and a sudden rise in reported cases during December 2023–March 2024 (Figure 2).

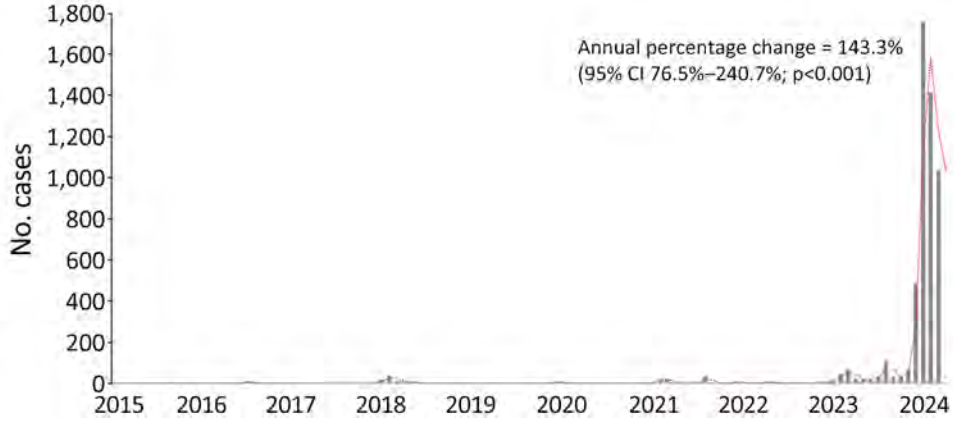

Figure 2. Annual cases in a study of spatiotemporal epidemiology of Oropouche fever, Brazil, 2015–2024. Bars depict distribution of cases per year and month of notification; red dotted line shows an analysis of temporal trends from January 2015 to March 2024 when case numbers rose sharply.

The first limitation of this study is incomplete travel history data, which might have missed imported cases. Another limitation is potential underdiagnosis, which might have underestimated case numbers. Finally, possible residual or cross-protection immunity could have resulted in uncertainty regarding the at-risk population.

Oropouche fever is predominantly endemic to the Amazon region, where several factors create a favorable scenario for its persistence. The humid and warm climate, complemented by dense vegetation and frequent rainfall, provide ideal conditions proliferation of *C. paraensis* midges, the primary OROV vector. Concurrently, expansion of human activities, including deforestation and urbanization, modify that vector's natural habitats, increasing transmission risks by reducing the spaces between humans and vectors (*1*,*5*,*6*). Moreover, increasing case numbers in non–Amazon region states might be linked to heightened human mobility and climate changes that extend the geographic distribution of vector habitats. That dynamic could be exacerbated by rapid urbanization without adequate infrastructure, enabling establishment of new urban transmission hotspots (*7*,*8*). In addition, potential novel OROV reassortment could enable adaptation to new vectors or enhance virulence, further contributing to expansion to previously unaffected areas (G.C. Scachetti et al., unpub. data, https://doi.org/10.1101/2024.07.27.24310296).

Oropouche fever has symptoms similar to other arboviruses, like dengue, which contributes to underreporting and complicates accurate diagnosis (*9*). Two Oropouche fever deaths were confirmed in state of Bahia, Brazil, on July 25, 2024 (https://www.gov.br/saude/pt-br/canais-de-atendimento/sala-de-imprensa/notas-a-imprensa/2024/ministerio-da-saude-confirma-dois-obitos-por-oropouche-no-pais). Furthermore, recent reports from Pernambuco and Acre documented cases of vertical transmission, mirroring the complex epidemiologic challenges observed during the 2015–16 Zika virus outbreak (*10*).

In conclusion, the spatiotemporal dynamics of Oropouche fever in Brazil highlight critical aspects of its epidemiology, particularly its concentration within the Amazon region and statistically significant annual incidence rate increases. Considering the geographic expansion and potential vertical OROV transmission events flagged by the Pan American Health Organization and World Health Organization, this study underscores the pressing need for an integrated surveillance and response system that includes epidemiologic surveillance and public health strategies to effectively manage the expansion of Oropouche fever in Brazil.

The datasets used and analyzed during the current study are available from the corresponding author on reasonable request.

P.R.M.F. is a research productivity fellow at the at National Council for Scientific and Technological Development (CNPq), Brazil.

About the Author

Dr. Martins-Filho is an epidemiologist and the head of the Investigative Pathology Laboratory at the University Hospital, Federal University of Sergipe, and holds a research productivity fellowship with the National Council for Scientific and Technological Development (CNPq) in Brazil. His primary research focuses include epidemiology, clinical research, and evidence synthesis.

References

1. Romero-Alvarez D, Escobar LE, Auguste AJ, Del Valle SY, Manore CA. Transmission risk of Oropouche fever across the Americas. Infect Dis Poverty. 2023;12:47. https://doi.org/10.1186/s40249-023-01091-2
2. Mourão MP, Bastos MS, Gimaque JBL, Mota BR, Souza GS, Grimmer GHN, et al. Oropouche fever outbreak, Manaus, Brazil, 2007–2008. Emerg Infect Dis. 2009;15:2063–4. https://doi.org/10.3201/eid1512.090917
3. Pan American Health Organization/World Health Organization. Epidemiological alert: Oropouche in the region of the Americas, 9 May 2024. Washington: The Organizations; 2024.
4. Pan American Health Organization/World Health Organization. Epidemiological alert: Oropouche in the region of the Americas: vertical transmission event under investigation in Brazil, 17 July 2024. Washington: The Organizations; 2024.
5. Moreira HM, Sgorlon G, Queiroz JAS, Roca TP, Ribeiro J, Teixeira KS, et al. Outbreak of Oropouche virus in frontier regions in western Amazon. Microbiol Spectr. 2024; 12:e0162923. https://doi.org/10.1128/spectrum.01629-23
6. Sciancalepore S, Schneider MC, Kim J, Galan DI, Riviere-Cinnamond A. Presence and multi-species spatial distribution of Oropouche virus in Brazil within the One Health framework. Trop Med Infect Dis. 2022;7:111. https://doi.org/10.3390/tropicalmed7060111
7. Fonseca LMDS, Carvalho RH, Bandeira AC, Sardi SI, Campos GS. Oropouche virus detection in febrile patients' saliva and urine samples in Salvador, Bahia, Brazil. Jpn J Infect Dis. 2020;73:164–5. https://doi.org/10.7883/yoken.JJID.2019.296
8. Sah R, Srivastava S, Kumar S, Golmei P, Rahaman SA, Mehta R, et al. Oropouche fever outbreak in Brazil: an emerging concern in Latin America. Lancet Microbe. 2024;1:100904. https://doi.org/10.1016/S2666-5247(24)00136-8
9. Martins-Filho PR, Soares-Neto RF, de Oliveira-Júnior JM, Alves dos Santos C. The underdiagnosed threat of Oropouche fever amidst dengue epidemics in Brazil. Lancet Reg Health Am. 2024;32:100718. https://doi.org/10.1016/j.lana.2024.100718
10. Martins-Filho PR, Carvalho TA, Dos Santos CA. Oropouche fever: reports of vertical transmission and deaths in Brazil. Lancet Infect Dis. 2024 Aug 22 [Epub ahead of print]. https://doi.org/10.1016/S1473-3099(24)00557-7

Address for correspondence: Paulo Ricardo Martins-Filho, Universidade Federal de Sergipe, Hospital Universitário, Laboratório de Patologia Investigativa, Rua Cláudio Batista, s/n. Sanatório, Aracaju, Sergipe 49060-100, Brazil; email: prmartinsfh@gmail.com

Respiratory Syncytial Virus Prevalence and Risk Factors among Healthy Term Infants, United States

Ferdinand Cacho, Tebeb Gebretsadik, Larry J. Anderson, James D. Chappell, Christian Rosas-Salazar, Justin R. Ortiz, Tina Hartert

Author affiliations: Vanderbilt University Medical Center, Nashville, Tennessee, USA (F. Cacho, T. Gebretsadik, J.D. Chappell, C. Rosas-Salazar, T. Hartert); Emory University School of Medicine and Children's Healthcare of Atlanta, Atlanta, Georgia, USA (L.J. Anderson); University of Maryland School of Medicine, Baltimore, Maryland, USA (J.R. Ortiz)

DOI: http://doi.org/10.3201/eid3010.240609

In a population-based birth cohort study of respiratory syncytial virus surveillance in the United States, 897/1,680 (53.4%) children were infected during infancy; 25/897 (2.8%) of those were hospitalized. Among symptomatic infants, 143/324 (44.1%) had lower respiratory tract infections. These data provide benchmarks to monitor effects of maternal vaccines and extended half-life monoclonal antibodies.

Respiratory syncytial virus (RSV) is a leading cause of illness in infants (*1*). Previous epidemiologic studies of RSV infection during infancy have focused on symptomatic illness, predominantly lower respiratory tract infections (LRTI) and hospitalizations (*2*). However, population-based surveillance studies to determine prevalence of and risk factors for RSV infection among healthy infants in the United States are lacking.

We determined prevalence of RSV infection by 1 year of age in a population-based birth cohort of healthy term infants in the United States. We excluded infants from the parent study, Infant Susceptibility to Pulmonary Infections and Asthma Following RSV Exposure (INSPIRE) (*3*,*4*), if they were not enrolled during well-child visits from 1 of 11 participating regional pediatric practices. We ascertained RSV infections by active surveillance using quantitative reverse transcription PCR (qRT-PCR) testing of nasal samples collected based on symptom surveys every 2 weeks and by passive surveillance by serum RSV antibody testing of all infants at 1 year of age during 2 RSV seasons, 2012–13 and 2013–14. If an infant met specified criteria for an acute respiratory infection, we conducted an in-person respiratory illness assessment and collected a nasal wash sample, which we used for the molecular detection of RSV by qRT-PCR. We also collected blood samples from all participating infants at 1 year of age and measured RSV serum antibody titers by ELISA using published protocols (*5*). We calculated 1-year prevalence of RSV infections, upper respiratory tract infections, LRTI, and healthcare utilization. We estimated the adjusted association and relative

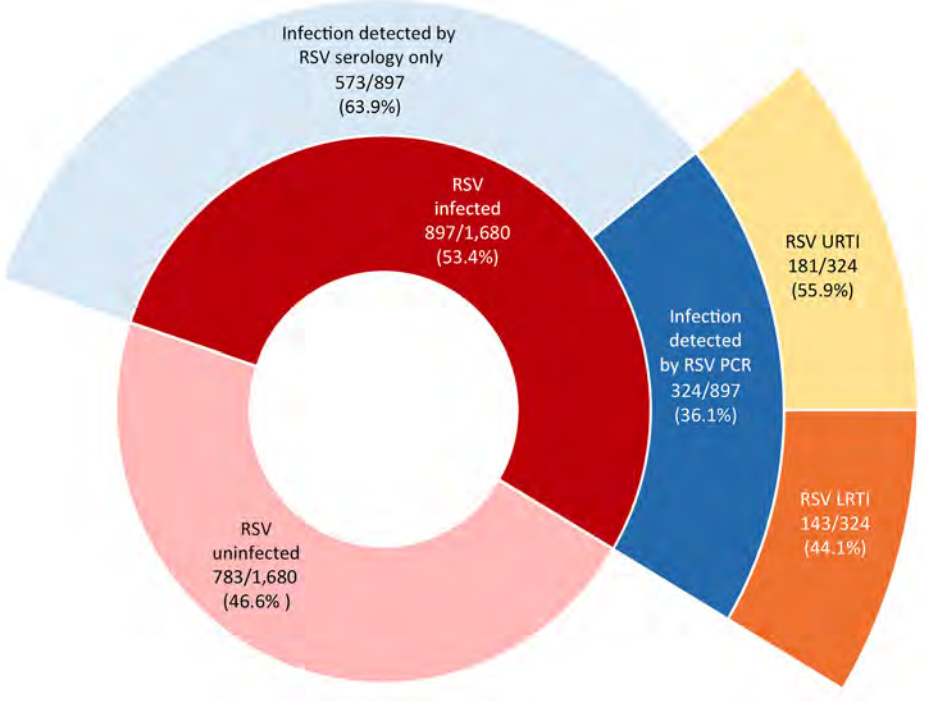

Figure 1. Percentages of RSV infection, symptomatic disease, LRTI, and URTI in the first year of life among healthy term infants, United States. Each ring represents the subset of the inner ring and adds to 100%. LRTI, lower respiratory tract infection; RSV, respiratory syncytial virus; URTI, upper respiratory tract infections.

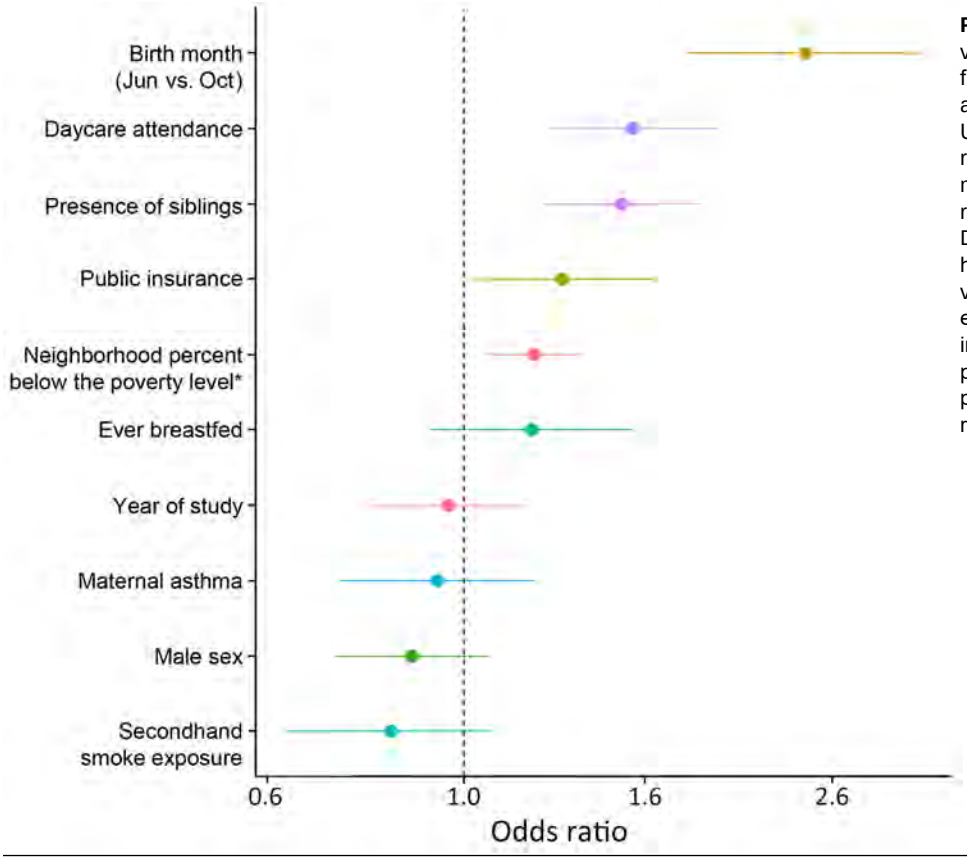

Figure 2. Respiratory syncytial virus infection risk factors in the first year of life in study of RSV among healthy term infants, United States. Adjusted odds ratios were estimated using multivariable logistic regression, referent is October birth month. Dots indicate odds ratio and horizontal line 95% CI. Dashed vertical line indicates the null effect. Asterisk indicates residence in a census tract with increasing percentage of people below the poverty level (interquartile range difference).

contribution of risk factors for RSV infection in the first year of life using multivariable logistic regression. The Institutional Review Board of Vanderbilt University approved INSPIRE, and 1 parent of each child provided written informed consent. INSPIRE methods have been published, and full study methods are available (*3*,*4*) (Appendix, https://wwwnc.cdc.gov/EID/article/30/10/24-0609-App1.pdf).

Among 1,680 infants who met inclusion criteria for our study, 897 (53.4%) were infected with RSV in the first year of life and 783 (46.6%) were not (Figure 1; Appendix Figure). Active surveillance detected 36.1% of RSV infections in symptomatic infants, whereas 63.9% were ascertained by serology alone. In all study infants, 1.5% (95% CI 0.96%–2.1%; n = 25) were hospitalized for RSV and 8.5% (95% CI 7.2%–9.9%; n = 143) had RSV LRTI. Among the subset with RSV infection, 2.8% (95% CI 1.9%–4.1%; n = 25) were hospitalized for RSV and 15.9% (95% CI 13.6%–18.4%; n = 143) had RSV LRTI. Restricted to the subset with symptomatic RSV infections meeting study criteria for a respiratory illness visit (n = 324), 55.9% had upper respiratory tract infections and 44.1% LRTIs. There were no infant deaths from RSV infection. We found that more than half of infants were RSV-infected in the first year of life. The rates of symptomatic disease, LRTI, and healthcare utilization demonstrate the considerable burden of respiratory illness in otherwise healthy infants; 1.5% of the cohort, or 2.8% of those infected, experienced RSV-associated hospitalizations.

Risk factors for RSV infection during infancy in order of contribution were infant birth month (June vs. referent October, OR 2.42 [95% CI 1.78–3.29]), presence of siblings (OR 1.50 [95% CI 1.22–1.84]), daycare attendance (OR 1.54 [95% CI 1.24–1.93]), increasing percentage below the poverty level in the residential neighborhood (21% vs. 8%; OR 1.19 [95% CI 1.05–1.36]), and public insurance (OR 1.28, 95% CI 1.02–1.62) (Figure 2). Secondhand smoke exposure, sex, ever being breastfed, maternal asthma, and study year were not significantly associated with likelihood of infant RSV infection.

The risk factors we identified increase viral exposure and underscore the potential for nonpharmacologic interventions to prevent infection (*6*). Earlier birth month was the strongest risk factor; we speculate that parental behaviors based on infant age affect exposure intensity (e.g., age at which infants are started in daycare). The risk factors of neighborhood percentage poverty and public insurance indicate the need to address socioeconomic determinants of RSV prevention.

The first limitation of our study is that eligibility criteria and sociodemographic characteristics might not be generalizable to other populations. In addition, our cohort represents a population that may be healthier, because they were term infants; however, this group represents half of RSV hospitalizations who are eligible for RSV prevention products. There is also potential for misclassification of infants categorized as uninfected with RSV in infancy (*4*). However, the proportions of both those with symptomatic respiratory illness and overall RSV serologic positivity are very similar to estimates from other studies (*7*–*9*). Although this cohort represents 2 RSV seasons during 2012–2014, we do not expect that time period to significantly affect the rates or risk factors for infection, which were similar across both RSV seasons.

In conclusion, our data are important estimates of the burden of RSV disease and risk factors for infection in healthy term infants. Our findings provide a benchmark to monitor the effects in the United States of recently available maternal vaccines and extended half-life monoclonal antibodies for severe RSV illness prevention in early life (*10*).

Acknowledgments

We thank the middle Tennessee pediatric practice sites and all the INSPIRE participants and their families for their involvement in and dedication to this study.

This work was supported with funds from the US National Institute of Allergy and Infectious Diseases (award nos. U19AI095227, UG3OD023282, and K24AI77930); the Vanderbilt Institute for Clinical and Translational Research (grant support from the National Center for Advancing Translational Sciences, award no. UL1TR000445); the US National Heart, Lung, and Blood Institute (award no. K23HL148638); the Department of Pediatrics at Vanderbilt University Medical Center (grant support from the Eunice Kennedy Shriver National Institute of Child Health and Human Development, award no. K12HD087023); and the Vanderbilt University Training Program in Environmental Toxicology (NIH T32 ES007028). The content is solely the responsibility of the authors and does not necessarily represent the official views of the funding agencies. The National Institutes of Health had no role in the design and conduct of the study.

Author contributions: F.C. conceptualized and designed the study, created the figures, drafted the initial manuscript, and critically reviewed and revised the manuscript. T.G. performed the statistical analysis, created the figures, and critically reviewed and revised the manuscript. L.J.A. and J.D.C. contributed to acquisition of data and biospecimen analysis and critically reviewed and revised the manuscript. C.R.-S. and J.R.O. contributed to analysis and interpretation of data and critically reviewed and revised the manuscript. T.H. designed the cohort and acquired study funding, coordinated and supervised study conduct, conceptualized and designed the current analysis, and critically reviewed and revised the manuscript. All authors approved the final manuscript as submitted and agreed to be accountable for all aspects of the work.

About the Author

Dr. Cacho is a pediatric pulmonology fellow at Vanderbilt University Medical Center and a graduate student in the MPH program at Vanderbilt University School of Medicine. His research interests are in the impact of early-life respiratory infections and the characterization of childhood asthma phenotypes.

References

1. Li Y, Wang X, Blau DM, Caballero MT, Feikin DR, Gill CJ, et al.; Respiratory Virus Global Epidemiology Network; RESCEU investigators. Global, regional, and national disease burden estimates of acute lower respiratory infections due to respiratory syncytial virus in children younger than 5 years in 2019: a systematic analysis. Lancet. 2022;399:2047–64. https://doi.org/10.1016/S0140-6736(22)00478-0
2. Rha B, Curns AT, Lively JY, Campbell AP, Englund JA, Boom JA, et al. Respiratory syncytial virus–associated hospitalizations among young children: 2015–2016. Pediatrics. 2020;146:e20193611. https://doi.org/10.1542/peds.2019-3611
3. Larkin EK, Gebretsadik T, Moore ML, Anderson LJ, Dupont WD, Chappell JD, et al.; INSPIRE Study. Objectives, design, and enrollment results from the Infant Susceptibility to Pulmonary Infections and Asthma Following RSV Exposure Study (INSPIRE). BMC Pulm Med. 2015;15:45. https://doi.org/10.1186/s12890-015-0040-0
4. Rosas-Salazar C, Chirkova T, Gebretsadik T, Chappell JD, Peebles RS Jr, Dupont WD, et al. Respiratory syncytial virus infection during infancy and asthma during childhood in the USA (INSPIRE): a population-based, prospective birth cohort study. Lancet. 2023;401:1669–80. https://doi.org/10.1016/S0140-6736(23)00811-5
5. Jadhao SJ, Ha B, McCracken C, Gebretsadik T, Rosas-Salazar C, Chappell J, et al. Performance evaluation of antibody tests for detecting infant respiratory syncytial virus infection. J Med Virol. 2021;93:3439–45. https://doi.org/10.1002/jmv.26736
6. Binns E, Koenraads M, Hristeva L, Flamant A, Baier-Grabner S, Loi M, et al. Influenza and respiratory syncytial virus during the COVID-19 pandemic: time for a new paradigm? Pediatr Pulmonol. 2022;57:38–42. https://doi.org/10.1002/ppul.25719
7. Wildenbeest JG, Billard MN, Zuurbier RP, Korsten K, Langedijk AC, van de Ven PM, et al.; RESCEU Investigators. The burden of respiratory syncytial virus in healthy term-born infants in Europe: a prospective birth cohort study. Lancet Respir Med. 2023;11:341–53. https://doi.org/10.1016/S2213-2600(22)00414-3

8. Munywoki PK, Koech DC, Agoti CN, Cane PA, Medley GF, Nokes DJ. Continuous invasion by respiratory viruses observed in rural households during a respiratory syncytial virus seasonal outbreak in coastal Kenya. Clin Infect Dis. 2018;67:1559–67. https://doi.org/10.1093/cid/ciy313
9. Zylbersztejn A, Pembrey L, Goldstein H, Berbers G, Schepp R, van der Klis F, et al. Respiratory syncytial virus in young children: community cohort study integrating serological surveys, questionnaire and electronic health records, Born in Bradford cohort, England, 2008 to 2013. Euro Surveill. 2021;26:2000023. https://doi.org/10.2807/1560-7917.ES.2021.26.6.2000023
10. Langedijk AC, Bont LJ. Respiratory syncytial virus infection and novel interventions. Nat Rev Microbiol. 2023;21:734–49. https://doi.org/10.1038/s41579-023-00919-w

Address for correspondence: Ferdinand Cacho, Department of Pediatrics, Vanderbilt University Medical Center,. 2200 Children's Way, DOT 11215, Nashville, TN 37232, USA; email: ferdinand.cacho@vumc.org

Prosthetic Valve Endocarditis Caused by *Pasteurella dagmatis*, Germany

Felix A. Rottmann, Peter Schorle, Roland Giesen, Christoph Jäger

Author affiliation: University of Freiburg Faculty of Medicine, Freiburg, Germany

DOI: https://doi.org/10.3201/eid3010.240727

An 81-year-old male patient in Germany had prosthetic valve endocarditis caused by *Pasteurella dagmatis* after a domestic cat bite. We surgically treated a paravalvular abscess and administered definitive antibiotic therapy consisting of penicillin G and levofloxacin. The patient was discharged from the intensive care unit in good condition 21 days after the surgery.

Pasteurella spp. are gram-negative, facultative anaerobic bacteria. They are part of the oral flora of domestic animals, including cats and dogs. In cases of animal bites, *Pasteurella* spp. bacteria can be detected culturally in 50%–75% of cases (*1*). Infections are typically caused by *Pasteurella multocida*, whereas *P. dagmatis* are rarely isolated from wounds, and severe *P. dagmatis* infections are exceedingly uncommon or unreported. Few cases of infective endocarditis (IE) attributable to *P. dagmatis* bacteria have been reported in the English-language literature (*2*–*5*). We report an additional case in a man in Germany. Given the rarity of gram-negative non-HACEK endocarditis (i.e., caused by species other than *Haemophilus* species, *Actinobacillus actinomycetemcomitans*, *Cardiobacterium hominis*, *Eikenella corrodens*, or *Kingella*) and the unfavorable prognosis associated with it, the contribution of case reports is essential to improve the management of affected patients (*6*).

An 81-year-old male patient was admitted to the hospital with a fever of up to 39.3°C. He reported weight loss of 10 kg during the preceding month. Vital signs and physical examination revealed no relevant pathologies. A domestic cat bite on the foot 2 months before admission was the only potential source of infection, but the wound had already healed weeks before. Underlying medical conditions included a mechanical aortic valve implanted 20 years previously because of a combined vitium.

After obtaining a set of blood cultures, we administered empiric antibiotic therapy with piperacillin/tazobactam. Results of chest radiograph, urine dipstick, and venous blood gas analyses were unremarkable. Results of point-of-care respiratory PCR testing for influenza and SARS-CoV-2 were negative. Blood testing showed mild anemia (hemoglobin 10.2 g/dL [reference range 11.6–15.5 g/dL]) but unremarkable leukocyte and platelet levels. C-reactive protein was moderately elevated at 47 mg/L (reference range <5 mg/L). Creatinine, urea, and liver function test results were unremarkable except for an international normalized ratio of 2.3 as a result of phenprocoumon therapy.

A set of blood cultures showed bacterial growth after 5 hours (anaerobic) and 10 hours (aerobic). We identified *P. dagmatis* bacteria by using matrix-assisted laser desorption/ionization time-of-flight mass spectrometry (MALDI Biotyper Sirius System; Bruker, https://www.bruker.com). The antibiogram demonstrated susceptibility to penicillin G, doxycycline, cotrimoxazole, and levofloxacin. Transthoracic echocardiography revealed a paravalvular abscess. We diagnosed prosthetic valve IE on the basis of modified Duke criteria (1 major clinical criterion, imaging; 3 minor clinical criteria, predisposition, fever, and microbiologic evidence falling short of a major criterion) (*7*).

The abscess measured at 24 ×14 × 31 mm on the subsequent computed tomography scan (Figure) and was communicating with the left ventricular outflow tract. The cardiac surgery department recommended

abscess removal and surgical replacement of the mechanical valve and ascending aorta. The patient underwent paravalvular abscess resection and replacement of the prosthetic valve and ascending aorta with a 25-mm biological valve (Carpentier-Perimount Magna Ease; Edwards Lifesciences, https://www.edwards.com) and bovine pericardial patch plasty. Intraoperative molecular diagnostic tests (16S rRNA PCR) were positive for *P. dagmatis* bacteria.

After surgery, the patient cardiogenic shock develop, requiring extracorporeal life support (ECLS). Because of bleeding attributable to ECLS, open chest management was necessary for 3 days. Acute kidney failure with anuria and hypervolemia (KDIGO acute kidney injury stage 3 [https://kdigo.org/guidelines/acute-kidney-injury]) resulted in dialysis for 5 days. ECLS could be explanted after 6 days. We treated sinus node dysfunction with a cardiac resynchronization therapy (pacemaker) device (Enitra 8 HF-T QP; Biotronik, https://www.biotronik.com) before intensive care unit discharge.

We continued to administer antibiogram-appropriate penicillin G therapy for a total of 6 weeks after the initial negative blood culture results. We administered levofloxacin, which we selected over an aminoglycoside antibiotic because of its superior abscess penetration, for the first 20 days as a combined therapy. The patient was discharged from the intensive care unit on the 21st day after surgery, exhibiting full consciousness and only mild focal neurologic deficits (dysphagia). He was discharged from the hospital shortly afterward and began rehabilitation treatment.

The choice of treatment in this case was complicated by the paucity of evidence regarding IE caused by *P. dagmatis* (*2*–*5*,*8*). Gump and Holden (*5*) reported IE caused by a new species of *Pasteurella* bacteria in 1972. In 1994, Sorbello et al. (*2*) reported another case, complicated by vertebral osteomyelitis. In 2001, Rosenbach et al. (*4*) reported prosthetic valve IE caused by *P. dagmatis*. A more recent case was reported in 2012 by Strahm et al. (*3*) (Appendix Table, https://wwwnc.cdc.gov/EID/article/30/10/24-0727-App1.pdf). Four of the 5 reported cases (including the case we describe) resulted from domestic cat bites, and all definitive therapies included either penicillin G or ceftriaxone. All patients survived infection. Antimicrobial therapy for *P. multocida* infection is similar to the course we describe, and penicillin has been recommended in all specimens that tested susceptible to it (*9*).

Empiric antibiotic therapy for animal wounds varies by severity (ranging from amoxicillin/clavulanate to piperacillin/tazobactam) and also needs to target other potential pathogens. Cat bites can be easily underestimated and justify careful therapy and follow-up. Animal contact could have been missed in this case because the wound had healed fully before the first symptoms of IE. Obtaining the patient's history greatly helped in the diagnosis.

Figure. Preoperative contrast-enhanced computed tomography (sagittal) of an 81-year-old male patient in Germany who had *Pasteurella dagmatis* infection after a domestic cat bite, indicating a paravalvular abscess of 24 × 14 × 31 mm. The large abscess near his mechanical valve, combined with *P. dagmatis* bacteria in blood cultures, confirmed a diagnosis of infective endocarditis based on Duke criteria (*7*).

About the Author

Dr. Rottmann studied medicine at the University of Freiburg in Germany. He is currently in training at the Department of Medicine IV, Nephrology and Primary Care, at the University of Freiburg Medical Center. His primary research interests include kidney function in critical care medicine, including care for patients on extracorporeal membrane oxygenation therapy.

References

1. Talan DA, Citron DM, Abrahamian FM, Moran GJ, Goldstein EJ; Emergency Medicine Animal Bite Infection Study Group. Bacteriologic analysis of infected dog and cat bites. N Engl J Med. 1999;340:85–92. https://doi.org/10.1056/NEJM199901143400202
2. Sorbello AF, O'Donnell J, Kaiser-Smith J, Fitzharris J, Shinkarow J, Doneson S. Infective endocarditis due to *Pasteurella dagmatis*: case report and review. Clin Infect Dis. 1994;18:336–8. https://doi.org/10.1093/clinids/18.3.336
3. Strahm C, Goldenberger D, Gutmann M, Kuhnert P, Graber P. Prosthetic valve endocarditis caused by a *Pasteurella dagmatis*-like isolate originating from a patient's cat. J Clin Microbiol. 2012;50:2818–9. https://doi.org/10.1128/JCM.00973-12
4. Rosenbach KA, Poblete J, Larkin I. Prosthetic valve endocarditis caused by *Pasteurella dagmatis*. South Med J. 2001;94:1033–5. https://doi.org/10.1097/00007611-200194100-00020

5. Gump DW, Holden RA. Endocarditis caused by a new species of *Pasteurella*. Ann Intern Med. 1972;76:275–8. https://doi.org/10.7326/0003-4819-76-2-275
6. Delgado V, Ajmone Marsan N, de Waha S, Bonaros N, Brida M, Burri H, et al.; ESC Scientific Document Group. 2023 ESC guidelines for the management of endocarditis. Eur Heart J. 2023;44:3948–4042. https://doi.org/10.1093/eurheartj/ehad193
7. Fowler VG Jr, Durack DT, Selton-Suty C, Athan E, Bayer AS, Chamis AL, et al. The 2023 Duke–International Society for Cardiovascular Infectious Diseases criteria for infective endocarditis: updating the modified Duke criteria. Clin Infect Dis. 2023;77:518–26. https://doi.org/10.1093/cid/ciad271
8. Porter RS, Hay CM. *Pasteurella* endocarditis: a case report and statistical analysis of the literature. Case Rep Infect Dis. 2020;2020:8890211. https://doi.org/10.1155/2020/8890211
9. Wei A, Dhaduk N, Taha B. Wrist abscess due to drug-resistant *Pasteurella multocida*. IDCases. 2021;26:e01277. https://doi.org/10.1016/j.idcr.2021.e01277

Address for correspondence: Felix A. Rottmann, Department of Medicine IV, Nephrology and Primary Care, University of Freiburg, Hugstetterstrasse 55, 79106 Freiburg, Germany; email: felix.rottmann@uniklinik-freiburg.de

etymologia

Pasteurellaceae [pas′′-tər-ə-lā′-sē-ī]

Clyde Partin

A novel member of the family Pasteurellaceae, *Emayella augustorita*, was introduced in the August 2024 issue of Emerging Infectious Diseases, by Meyer and colleagues of Limoges, France. Isolated from a patient in France, the bacterium is a new member of the family Pasteurellaceae, named in honor of Louis Pasteur. Pasteur was deemed by medical historian Robert P. Gaynes to be the "most notable nonphysician in the history of medicine." His name is most recognized for the eponymous pasteurization process, but he is also lauded in Linnaean taxonomy with the family name Pasteurellaceae, formally accepted in 1981. The designation was conceived to accommodate a collection of gram-negative organisms currently representing 34 genera and 105 species, described as "specialized commensals, primarily and potential pathogens of vertebrates—mainly mammals and birds."

Figure. This 1885 painting by Albert Edelfelt (1854–1905), currently in the collection of the Musée d'Orsay (Paris, France), shows Louis Pasteur in his laboratory. Pasteur was an accomplished artist, and examples of his artwork, done as early as age 15, are on display at the Pasteur Institute in Paris. Before pursuing his scientific career, Pasteur aspired to become an art teacher. Image source: Wikimedia Commons.

The constituent bacteria of this family have a propensity to inhabit the mucosal membrane of the mouth, respiratory, and genital tracts. The species *Haemophilus influenzae* and *Aggregatibacter actinomycetemcomitamitans* are well-known Pasteurellaceae that contribute to human illness. Of note, the *Pasteurellaceae* family is polyphyletic, and the taxonomy of some of the species is in need of further study.

Sources

1. Meyer S, Tilloy V, Durand-Fontanier S, Lafon T, Garnier F, Martin C, et al. *Emayella augustorita,* new member of Pasteurellaceae, isolated from blood cultures of septic patient. Emerg Infect Dis. 2024;30:1719–21. https://doi.org/10.3201/eid3008.231651
2. Gaynes RP. Louis Pasteur and the germ theory of disease. In: Germ theory: medical pioneers in infectious diseases. Washington: ASM Press; 2011. p. 143–71.
3. Leibniz Institute DSMZ—German Collection of Microorganisms and Cell Cultures GmbH. List of Prokaryotic names with Standing in Nomenclature. Family *Pasteurellaceae* [cited 2024 May 18]. https://lpsn.dsmz.de/family/pasteurellaceae
4. Bisgaard M. Taxonomy of the family Pasteurellaceae Pohl 1981. In: Donachie W, Lainson FA, Hodgson JC, editors. Haemophilus, Actinobacillus, and Pasteurella. Boston: Springer; 1995 [cited 2024 May 18]. https://doi.org/10.1007/978-1-4899-0978-7_1
5. Christensen H, Bossé J, Angen Ø, Nørskov-Lauritsen N, Bisgaard M. Immunological and molecular techniques used for determination of serotypes in *Pasteurellaceae*. In: Pavia CS, Gurtler V, editors. Methods in microbiology, vol. 47. Immunological methods in microbiology. Cambridge: Academic Press; 2020 [cited 2024 May 18]. https://www.sciencedirect.com/science/article/pii/S0580951720300027

Author affiliation: Emory University School of Medicine, Atlanta, Georgia, USA

Address for correspondence: Clyde Partin, Emory Clinic,1365 Clifton Rd NE, Bldg A, 1st Fl, Atlanta, GA 30322, USA; email: wpart01@emory.edu

DOI: https://doi.org/10.3201/eid3010.240735

SARS-CoV-2 and Other Coronaviruses in Rats, Berlin, Germany, 2023

Kerstin Wernike, Calvin Mehl, Andrea Aebischer, Lorenz Ulrich, Mario Heising, Rainer G. Ulrich, Martin Beer

Author affiliations: Friedrich-Loeffler-Institut, Greifswald-Insel Riems, Germany (K. Wernike, C. Mehl, A. Aebischer, L. Ulrich, R.G. Ulrich, M. Beer); Deutsches Zentrum für Infektionsforschung, Hamburg-Lübeck-Borstel-Riems, Germany (C. Mehl, R.G. Ulrich); SchaDe Umwelthygiene und Schädlingsbekämpfung GmbH, Berlin, Germany (M. Heising)

DOI: https://doi.org/10.3201/eid3010.241079

We tested 130 rats captured in Berlin for coronaviruses. SARS-CoV-2 antibodies were detected in 1 rat, but all animals were negative by reverse transcription PCR, suggesting SARS-CoV-2 was not circulating in the rat population. However, alphacoronaviruses were found. Monitoring rodent populations helps to determine coronavirus occurrence, transmission, and zoonotic potential.

SARS-CoV-2 was initially reported in 2019 in China and spread rapidly worldwide, causing the COVID-19 pandemic in humans. Since the pandemic unfolded, the role of animals as amplifying or reservoir hosts has been hypothesized. Because of the long-term association between rodents and coronaviruses (*1*), the wide range of coronaviruses occurring in wild rodents (*2*), and the ubiquitous distribution of commensal rodents, investigations of SARS-CoV-2 and other coronaviruses in rats is warranted. In experiments that used high infection doses, rats have been reported as receptive SARS-CoV-2 hosts, particularly for the Delta variant of concern (VOC); however, experimental infections with Alpha, Beta, and Omicron variants have also been described in rats (*3*,*4*), suggesting a theoretical risk for effective transmission chains in nature. Accordingly, field studies were initiated early during the pandemic to investigate SARS-CoV-2 infections in wild rats. Indeed, serologic and molecular evidence of SARS-CoV-2 infection was found in a few animals in some studies (*2*,*3*,*5*), whereas other studies consistently reported negative results (*6*,*7*). However, all of those studies were conducted before the emergence and worldwide large-scale spread of the Omicron VOC and its subvariants. In laboratory settings, lungs from Omicron virus–infected rats showed significantly lower infectious virus titers compared with rats infected with the Delta variant (*3*), but field studies on wild rats after Omicron VOC emergence and dominance within the human populations are missing. Therefore, we investigated SARS-CoV-2 infections in Norway rats (*Rattus norvegicus*) captured in Berlin, the very densely populated (>4,000 inhabitants/km^2) capital of Germany, during 2023, when Omicron was the dominant SARS-CoV-2 variant in

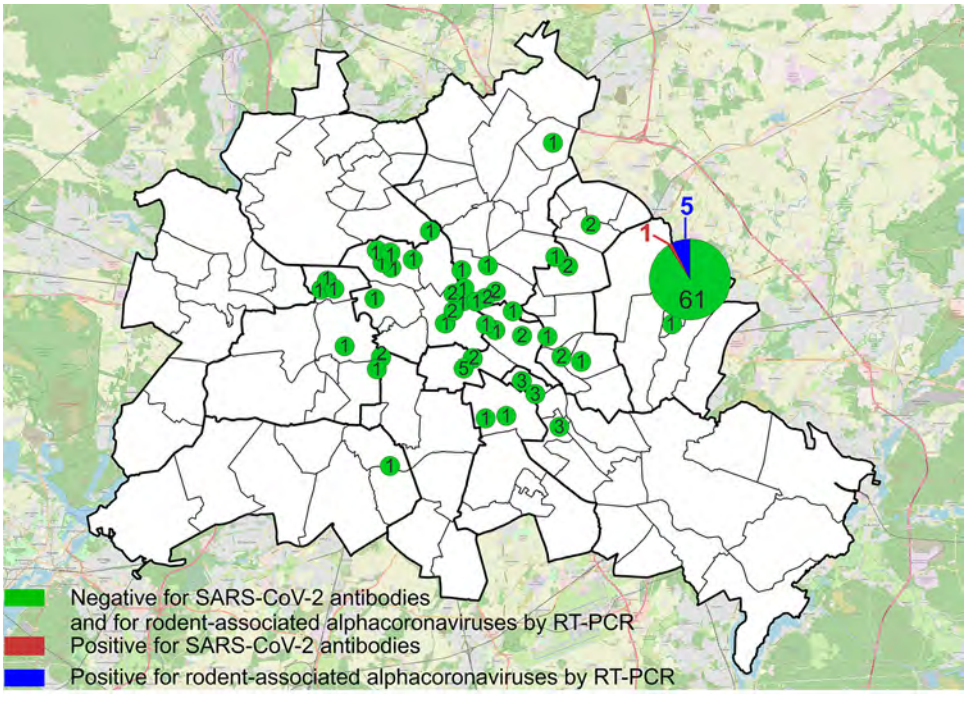

Figure 1. Locations of trapped rats tested in study of SARS-CoV-2 and other coronaviruses in rats, Berlin, Germany, 2023. Numbers indicate numbers of rats tested in each location. Overlay map of Berlin, in which the circles were printed, was retrieved from Geoportal Berlin, dataset Geoportal Berlin/ Ortsteile von Berlin (https://daten.odis-berlin.de/de/dataset/ortsteile), data license Germany–attribution–Version 2.0 (https://www.govdata.de/dl-de/by-2-0). Map of the area surrounding Berlin was created by using OpenStreetMap (https://www.openstreetmap.org). RT-PCR, reverse transcription PCR.

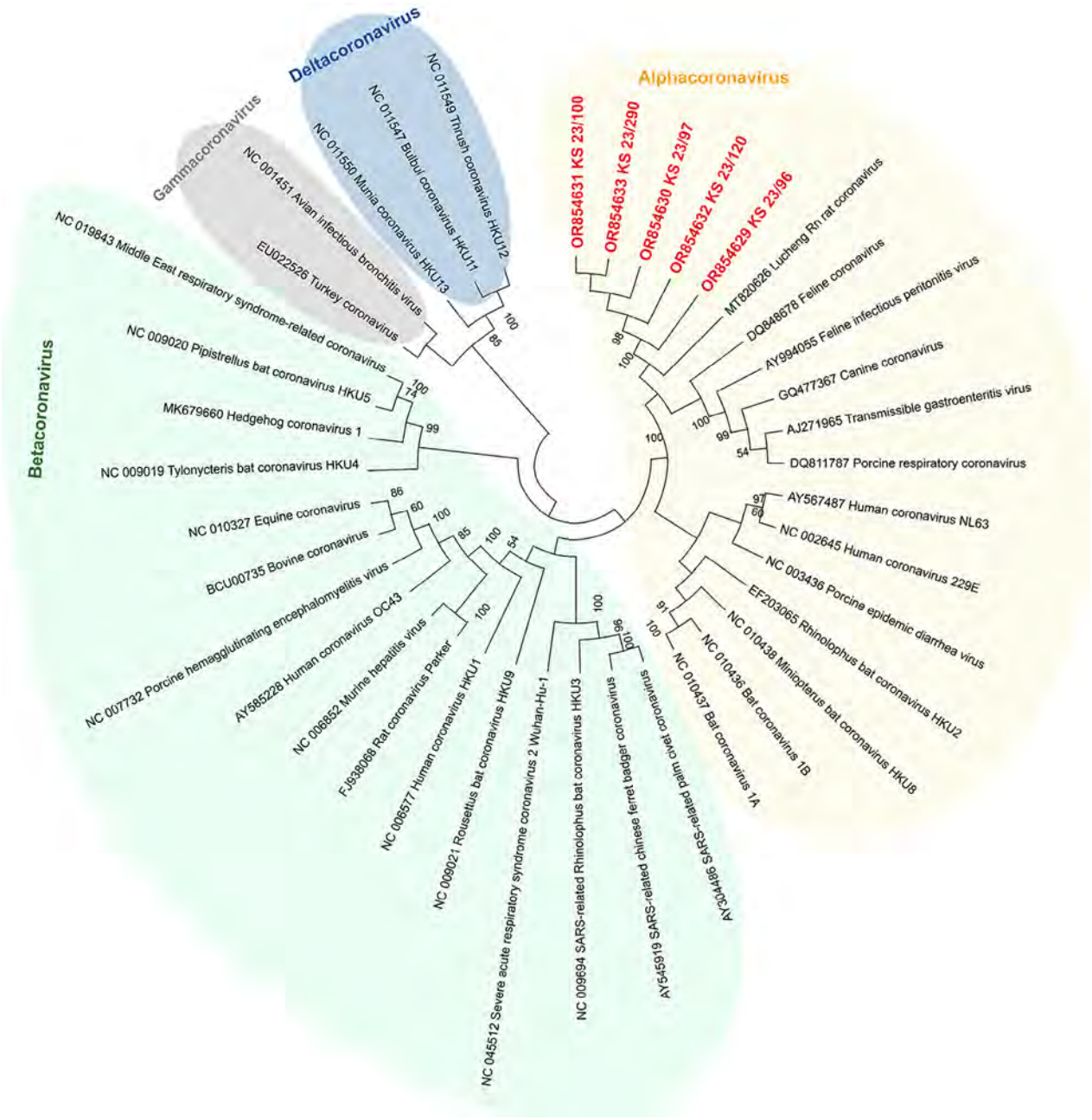

Figure 2. Phylogenetic analysis of SARS-CoV-2 and other coronaviruses in rats, Berlin, Germany, 2023. Partial sequences of the RNA-dependent RNA polymerase gene from coronaviruses isolated from rats in Berlin (red text) were compared with other coronavirus sequences obtained from GenBank. Background colors indicate viruses belonging to the same coronavirus genus. The maximum-likelihood tree was calculated by using MEGA X software (https://www.megasoftware.net). Statistical support for nodes was obtained by bootstrapping (1,000 replicates); only bootstrap values ≥50% are shown. GenBank accession numbers are provided. Tree not drawn to scale.

the human population. Rat samples were collected during rodent pest control activities; sample collection did not require a specific permit.

We collected samples of lung and chest cavity lavage fluid from 130 Norway rats caught at 44 trapping sites (Figure 1) by rinsing the chest cavity with 1 mL phosphate-buffered saline during necropsy. We tested lavage fluids for antibodies against SARS-CoV-2 by using a receptor-binding domain (RBD)–based multispecies ELISA and a cutoff value of ≥0.3 for positivity, as previously described (*8*). We used 2 RBD protein orthologs in parallel, the wild-type

virus RBD and that of the Omicron XBB1.5 variant. We prediluted the samples 1:10 as described for rodent lavage samples (*6*).

One of 130 rats tested positive; the optical density values were 1.16 (wild-type RBD) and 1.53 (Omicron RBD) (Appendix Figure, https://wwwnc.cdc.gov/EID/article/30/10/24-1079-App1.pdf). To confirm the positive result, we tested the sample by using a surrogate virus neutralization test (cPass SARS-CoV-2 Neutralization Antibody Detection Kit; GenScript, https://www.genscript.com) and 2 different RBD orthologs according to the manufacturer's instructions (cutoff for positivity was ≥30% inhibition). That test, in its original composition, enables the detection of antibodies against wild-type SARS-CoV-2 and all VOCs except Omicron. For Omicron and its subvariants, we used a specific RBD provided by the manufacturer (GeneScript). The ELISA-positive rat sample was positive against Omicron-specific RBD in the neutralization test (33.9% inhibition for Omicron, 23.4% for wild-type RBD), suggesting the rat had a previous infection with an Omicron subvariant. However, only 1 rat tested positive, indicating a single spillover event from humans into the rat population and lack of autonomous virus circulation in rats, especially considering 66 additional rats were caught in the same building as the seroreactive animal (Figure 1), and all of those tested negative. Potential cross-reactivity with other coronaviruses could account for the single positive result, although cross-reactivity of some animal coronaviruses was excluded during initial validation of the RBD-based ELISA (*8*).

To further confirm that no virus circulated in the sampled rat population, we tested lung samples by using SARS-CoV-2–specific real-time reverse transcription PCR (RT-PCR) targeting the RNA-dependent RNA polymerase (*RdRp*) gene (*9*) and by using an *RdRp*-based, generic pancoronavirus RT-PCR (*10*). Using the SARS-CoV-2–specific test, all samples were negative, verifying the absence of SARS-CoV-2. Nevertheless, 5 lung samples were positive in the pancoronavirus RT-PCR; all 5 animals were trapped at the same location (Figure 1). For further characterization, we sequenced the RT-PCR products in both directions by using the PCR amplification primers. We deposited the sequences in GenBank (accession nos. OR854629–33) and compared them with other representative coronavirus sequences obtained from GenBank. Virus typing according to the partial *RdRp* sequences revealed that the viruses found in Berlin rats belonged to the genus *Alphacoronavirus* and were closely related to each other (99.4%–100.0% nucleotide sequence identity) and to the Lucheng Rn rat coronavirus (Figure 2). Hence, in contrast to SARS-CoV-2, rodent-associated alphacoronaviruses were circulating within the Berlin rat population, which agrees with previous studies of coronaviruses in rats in other locations (*2*,*5*).

In conclusion, research into rodent coronaviruses contributes to a broader understanding of those viruses and aids in the development of strategies for managing both animal and public health. Coronavirus monitoring of rodent populations aids in determining virus occurrence, transmission characteristics, pathogenesis, and zoonotic potential.

Acknowledgments

We thank Bianka Hillmann, Dennis Karnatz, and Janina Beyer for excellent technical assistance, our institute colleagues for help during animal dissections, and the rodent pest controllers from Berlin for providing rats.

The study was supported by intramural funding from the German Federal Ministry of Food and Agriculture provided to the Friedrich-Loeffler-Institut, partial funding to M.B. from the European Union Horizon 2020 project (Versatile Emerging Infectious Disease Observatory, grant no. 874735), and funding to R.G.U. from the German Center for Infection Research, thematic translational unit Emerging Infections.

About the Author

PD Dr. Wernike is a veterinarian and senior scientist at the Friedrich-Loeffler-Institut, Greifswald-Insel Riems, Germany. Her research interests focus on emerging viruses, host-virus-interaction, and immunoprophylaxis.

References

1. Tsoleridis T, Chappell JG, Onianwa O, Marston DA, Fooks AR, Monchatre-Leroy E, et al. Shared common ancestry of rodent alphacoronaviruses sampled globally. Viruses. 2019;11:125. https://doi.org/10.3390/v11020125
2. Fisher AM, Airey G, Liu Y, Gemmell M, Thomas J, Bentley EG, et al. The ecology of viruses in urban rodents with a focus on SARS-CoV-2. Emerg Microbes Infect. 2023;12:2217940. https://doi.org/10.1080/22221751.2023.2217940
3. Wang Y, Lenoch J, Kohler D, DeLiberto TJ, Tang CY, Li T, et al. SARS-CoV-2 exposure in Norway rats (*Rattus norvegicus*) from New York City. mBio. 2023;14:e0362122. https://doi.org/10.1128/mbio.03621-22
4. Zhang C, Cui H, Li E, Guo Z, Wang T, Yan F, et al. The SARS-CoV-2 B.1.351 variant can transmit in rats but not in mice. Front Immunol. 2022;13:869809. https://doi.org/10.3389/fimmu.2022.869809
5. Miot EF, Worthington BM, Ng KH, de Lataillade LG, Pierce MP, Liao Y, et al. Surveillance of rodent pests for

SARS-CoV-2 and other coronaviruses, Hong Kong. Emerg Infect Dis. 2022;28:467–70. https://doi.org/10.3201/eid2802.211586
6. Wernike K, Drewes S, Mehl C, Hesse C, Imholt C, Jacob J, et al. No evidence for the presence of SARS-CoV-2 in bank voles and other rodents in Germany, 2020–2022. Pathogens. 2022;11:1112. https://doi.org/10.3390/pathogens11101112
7. Colombo VC, Sluydts V, Mariën J, Broecke BV, Van Houtte N, Leirs W, et al. SARS-CoV-2 surveillance in Norway rats (*Rattus norvegicus*) from Antwerp sewer system, Belgium. Transbound Emerg Dis. 2022;69:3016–21. https://doi.org/10.1111/tbed.14219
8. Wernike K, Aebischer A, Michelitsch A, Hoffmann D, Freuling C, Balkema-Buschmann A, et al. Multi-species ELISA for the detection of antibodies against SARS-CoV-2 in animals. Transbound Emerg Dis. 2021;68:1779–85. https://doi.org/10.1111/tbed.13926
9. World Health Organization. Real-time RT-PCR assays for the detection of SARS-CoV-2 [cited 2024 Sep 1]. https://www.who.int/docs/default-source/coronaviruse/real-time-rt-pcr-assays-for-the-detection-of-sars-cov-2-institut-pasteur-paris.pdf
10. Chidoti V, De Nys H, Pinarello V, Mashura G, Missé D, Guerrini L, et al. Longitudinal survey of coronavirus circulation and diversity in insectivorous bat colonies in Zimbabwe. Viruses. 2022;14:781. https://doi.org/10.3390/v14040781

Address for correspondence: Kerstin Wernike, Institute of Diagnostic Virology, Friedrich-Loeffler-Institut, Südufer 10, 17493 Greifswald-Insel Riems, Germany; email: kerstin.wernike@fli.de

Establishment of *Amblyomma maculatum* Ticks and *Rickettsia parkeri* in the Northeastern United States

Goudarz Molaei, Noelle Khalil, Carmen J. Ramos, Christopher D. Paddock

Author affiliations: Yale School of Public Health, New Haven, Connecticut, USA (G. Molaei); Connecticut Agricultural Experiment Station, New Haven (G. Molaei, N. Khalil); Centers for Disease Control and Prevention, Atlanta, Georgia, USA (C.J. Ramos, C.D. Paddock)

DOI: https://doi.org/10.3201/eid3010.240821

We document a case of *Rickettsia parkeri* rickettsiosis in a patient in Connecticut, USA, who became ill after a bite from a Gulf Coast tick (*Amblyomma maculatum*). We used PCR to amplify *R. parkeri* DNA from the detached tick. The patient showed a 4-fold rise in IgG reactive with *R. parkeri* antigens.

Native and invasive tick species pose serious public health concerns in the United States, particularly in northeastern states. Recent and rapid expansion of the lone star tick (*Amblyomma americanum*) into ranges with pervasive blacklegged tick (*Ixodes scapularis*) populations has increased the number of recognized tickborne pathogens that circulate in that densely populated region. In addition to *Borrelia burgdorferi*, the causative agent of Lyme disease, ≥7 additional tickborne pathogens are now endemic to the northeastern United States: *Ehrlichia chaffeensis*, *Ehrlichia ewingii*, Heartland virus, *Anaplasma phagocytophilum*, *Borrelia miyamotoi, Babesia microti*, and Powassan virus (*1*). Multiple factors, including climate change and anthropogenic modifications to the environment, have affected rapid expansion of the ranges of medically relevant tick species and associated pathogens. That expansion has been reflected by dramatic increases in the numbers of reported cases of tickborne diseases in the northeastern United States since the beginning of the 21st Century (*1*).

The Gulf Coast tick (*Amblyomma maculatum*) was first identified in the United States in 1844. As recently as the middle of the 20th Century, the tick's range was restricted predominantly to coastal regions of states bordering the Gulf of Mexico as far west as Texas and the southern Atlantic coast only as far north as southern North Carolina (Figure 1) (*2*,*3*). Established *A. maculatum* tick populations now exist in states hundreds of miles inland (Arkansas, Missouri, Kentucky, Illinois, Indiana) and along the Atlantic coast as far north as Connecticut (*4*–*9*). Migratory grassland birds serve a crucial role in the spread of Gulf Coast ticks to locations in central and northern states that possess favorable environmental conditions for the tick's survival (*2*,*8*).

The Gulf Coast tick was relatively unknown and infrequently studied until recognition of *Rickettsia parkeri* spotted fever rickettsiosis in 2004 (*2*). In contrast to its more widely recognized cousins, blacklegged and lone star ticks, which prefer predominantly woodland habitats, Gulf Coast ticks favor grassland habitats. During the past 250 years, huge swathes of native grasslands and savannahs in the eastern United States have been transformed into agricultural areas and rangeland, creating habitats no longer favorable for Gulf Coast ticks. Paradoxically, contemporary reclamation of native grasslands through conservation

efforts in the northeastern United States might have inadvertently led to establishment of Gulf Coast ticks in that region. The recent discovery of established populations of Gulf Coast ticks in reclaimed grasslands at the former Freshkills landfill on Staten Island, New York, is a salient example of this phenomenon (*7*,*8*). Of note, restored grassland habitats often occur near or within shorelines, parks, and wildlife areas proximate to and frequented by persons residing in densely populated metropolitan areas.

The Gulf Coast tick is the principal vector of *R. parkeri*, a pathogen that causes a rickettsiosis similar to but milder than Rocky Mountain spotted fever (*2*). Rates of *R. parkeri* infection are as high as 56% among questing adult Gulf Coast ticks in some regions, and 23%–53% of adult specimens obtained in Connecticut, New York, and New Jersey are infected (*6*–*9*). Gulf Coast ticks readily bite humans, posing another risk for tickborne disease in northeastern United States, particularly among persons who reside and recreate near or within New York, New York; New Haven, Connecticut; Newark, New Jersey; and Philadelphia, Pennsylvania, where recently established tick populations have been identified in areas where human infections with this pathogen had not been previously documented (Figure 1).

In August 2023, a 29-year-old woman discovered a tick attached to the nape of her neck after visiting a beach in Fairfield County, Connecticut. The tick (Figure 2, panels A, B) was attached for ≤4 hours before it was removed. Within 3 days, a small, erythematous, crusted lesion with a smaller satellite papule developed at the bite site (Figure 2, panel C), after which the patient experienced chills, fatigue, cervical lymphadenopathy, myalgia, severe headache, and mild confusion. Approximately 10 days later, several small erythematous macules developed on her arm and legs (Figure 2, panel D). The patient recovered rapidly after treatment with doxycycline. We performed PCR to amplify *R. parkeri* DNA from the detached tick; indirect immunofluorescence antibody assay results of patient serum samples revealed IgG reactive with antigens of *R. parkeri* at titers of <32 at 15 days and 256 at 24 days after illness onset (Appendix, https://wwwnc.cdc.gov/EID/article/30/10/24-0821-App1.pdf).

Because of morphologic similarities between Gulf Coast ticks and American dog ticks (*Dermacentor variabilis*, the principal vector of Rocky Mountain spotted fever in the northeastern United States), the 2 species can be misidentified. Because most tick species are associated with a unique suite of pathogens, it is critical to improve regional capacity for accurately detecting and identifying specific ticks and the pathogens they transmit in the northeastern United States, an area already endemic for Lyme disease, hard tick relapsing fever, Rocky Mountain spotted fever, ehrlichiosis, anaplasmosis, and Powassan virus infections (*10*). The rapidly changing dynamics and evolving risks of tickborne diseases across this region reinforce the need for awareness of and education on tick bite prevention strategies, including using repellents registered with the Environmental

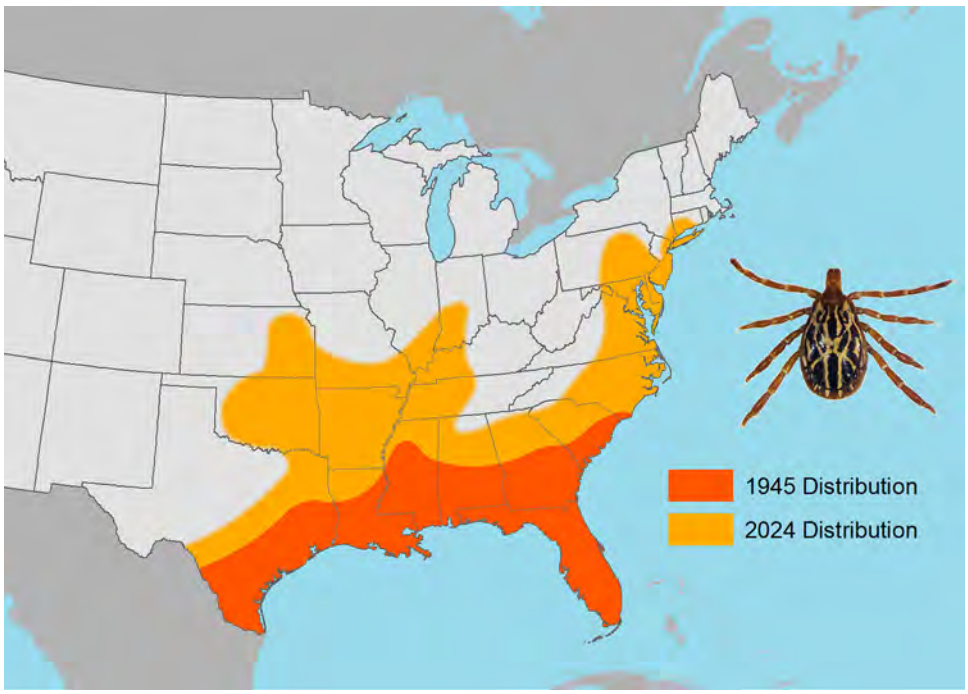

Figure 1. Generalized distributions of the Gulf Coast tick, *Amblyomma maculatum* (pictured), a human-biting tick species newly established in the northeastern United States, in 1945 compared with 2024. Establishment was defined as >6 ticks of the same life stage identified within a 12-month period or ticks of >1 life stage identified within a 12-month period. Data from references *2*–*9*, https://www.dep.pa.gov/Business/ProgramIntegration/Vector-Management/Ticks/Pages/default.aspx, and https://www.in.gov/health/idepd/zoonotic-and-vectorborne-epidemiology-entomology/vector-borne-diseases/tick-borne-diseases/amblyomma-maculatum-gulf-coast-tick/#Geographic_Distribution.

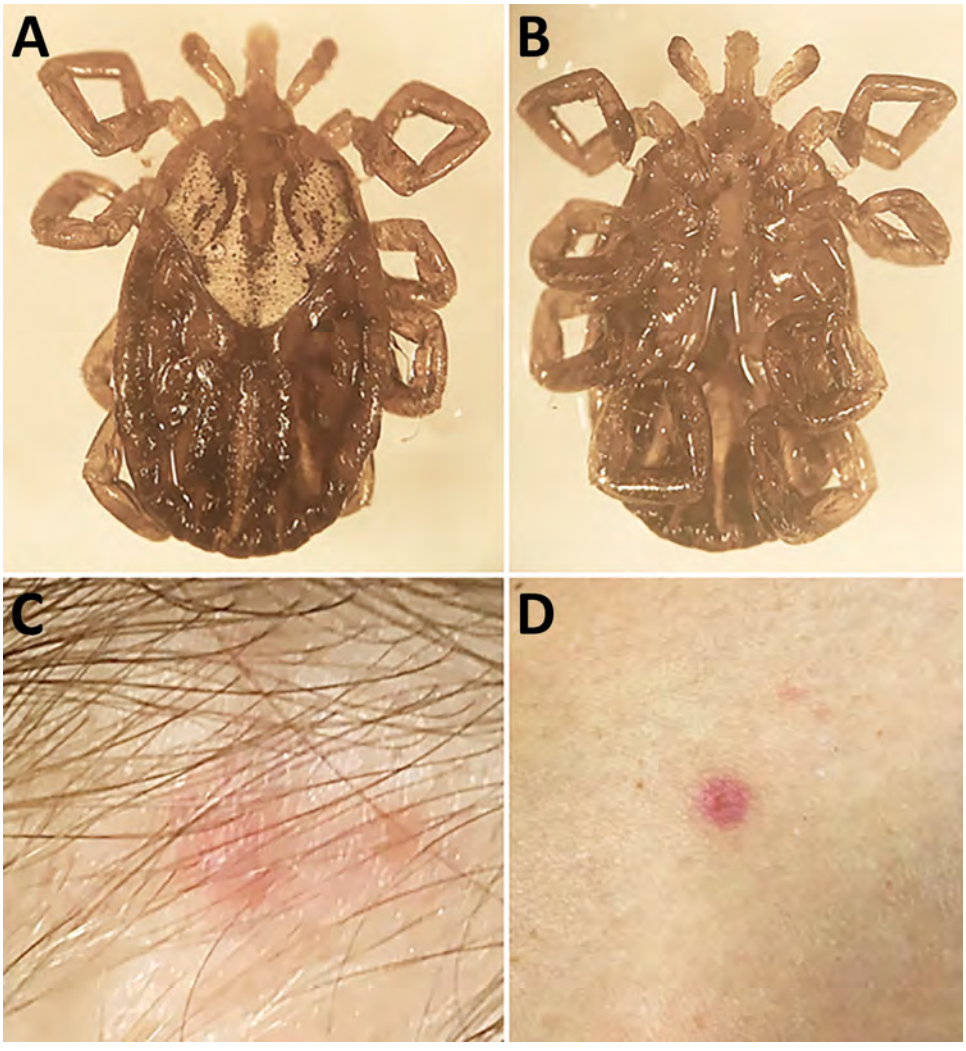

Figure 2. Biting *Amblyomma maculatum* tick removed from a woman in Connecticut, USA, and signs of *Rickettsia parkeri* rickettsiosis. A, B) Dorsal (A) and ventral (B) images of the tick. C, D) A small, erythematous, crusted lesion with a smaller satellite papule that developed at the bite site (C) and 1 of several small erythematous macules that developed on her arm and legs (D).

Protection Agency and performing regular, thorough tick checks after exposure to tick-infested areas.

Acknowledgments

The authors thank Jay Kiser for assistance in creating Figure 1, and Lorelei Sandland for assistance with creating Figure 2.

About the Author

Dr. Molaei is a research scientist and director of the Tick and Tick-borne Pathogen Surveillance Program at the Center for Vector Biology and Zoonotic Diseases and the Northeast Regional Center for Excellence in Vector-Borne Diseases of the Connecticut Agricultural Experiment Station, and also an associate clinical professor at the Yale School of Public Health. His current research interests include the ecology and epidemiology of tickborne and mosquitoborne pathogens of human health concern.

References

1. Molaei G, Eisen LM, Price KJ, Eisen RJ. Range expansion of native and invasive ticks: a looming public health threat. J Infect Dis. 2022;226:370–3. https://doi.org/10.1093/infdis/jiac249
2. Paddock CD, Goddard J. The evolving medical and veterinary importance of the Gulf Coast tick (Acari: Ixodidae). J Med Entomol. 2015;52:230–52. https://doi.org/10.1093/jme/tju022
3. Bishopp FC, Trembley HL. Distribution and hosts of certain North American ticks. J Parasitol. 1945;31:1–54. https://doi.org/10.2307/3273061
4. Phillips VC, Zieman EA, Kim CH, Stone CM, Tuten HC, Jiménez FA. Documentation of the expansion of the Gulf Coast tick (*Amblyomma maculatum*) and *Rickettsia parkeri*: first report in Illinois. J Parasitol. 2020;106:9–13. https://doi.org/10.1645/19-118
5. Maestas LP, Reeser SR, McGay PJ, Buoni MH. Surveillance for *Amblyomma maculatum* (Acari: Ixodidae) and *Rickettsia parkeri* (Rickettsiales: Rickettsiaceae) in the state of Delaware, and their public health implications. J Med Entomol. 2020;57:979–83. https://doi.org/10.1093/jme/tjz255
6. Molaei G, Little EAH, Khalil N, Ayres BN, Nicholson WL, Paddock CD. Established population of the Gulf Coast tick,

Amblyomma maculatum (Acari: Ixodidae), infected with *Rickettsia parkeri* (Rickettsiales: Rickettsiaceae), in Connecticut. J Med Entomol. 2021;58:1459–62. https://doi.org/10.1093/jme/tjaa299
7. Bajwa WI, Tsynman L, Egizi AM, Tokarz R, Maestas LP, Fonseca DM. The Gulf Coast tick, *Amblyomma maculatum* (Ixodida: Ixodidae), and spotted fever group *Rickettsia* in the highly urbanized northeastern United States. J Med Entomol. 2022;59:1434–42. https://doi.org/10.1093/jme/tjac053
8. Ramírez-Garofalo JR, Curley SR, Field CE, Hart CE, Thangamani S. Established populations of *Rickettsia parkeri*-infected *Amblyomma maculatum* ticks in New York City, New York, USA. Vector Borne Zoonotic Dis. 2022;22:184–7. https://doi.org/10.1089/vbz.2021.0085
9. Musnoff BL, Cuadera MKQ, Birney MR, Zipper L, Nicholson W, Ayres B, et al. The first record of an established population of *Amblyomma maculatum* (Acari: Ixodidae) in New Jersey, USA. J Med Entomol. 2024;61:1081–5. https://doi.org/10.1093/jme/tjae056
10. Eisen RJ, Paddock CD. Tick and tickborne pathogen surveillance as a public health tool in the United States. J Med Entomol. 2021;58:1490–502. https://doi.org/10.1093/jme/tjaa087

Address for correspondence: Goudarz Molaei, Department of Entomology, Connecticut Agricultural Experiment Station, 123 Huntington St, New Haven, CT 06511, USA; email: goudarz.molaei@ct.gov

Fort Sherman Virus Infection in Human, Peru, 2020

Edmilson F. de Oliveira-Filho, César Augusto Cabezas Sánchez, Dora Esther Valencia Manosalva, Maribel Dana Figueroa Romero, Nancy Susy Merino Sarmiento, Adolfo Ismael Marcelo Ñique, Edward Málaga-Trillo, Andres Moreira-Soto, Maria Paquita García Mendoza, Jan Felix Drexler

Author affiliations: Charité-Universitätsmedizin Berlin, Freie Universität Berlin and Humboldt-Universität zu Berlin, Institute of Virology, Berlin, Germany (E.F. de Oliveira-Filho, A. Moreira-Soto, J.F. Drexler); Instituto Nacional de Salud, Lima, Peru (C.A. Cabezas Sánchez, M.D. Figueroa Romero, N.S. Merino Sarmiento, A.I.M. Ñique, M.P. Garcia Mendoza); Laboratorio de Referencia Regional de Salud Pública de Lambayeque, Lambayeque, Perú (D.E. Valencia Manosalva); Universidad Peruana Cayetano Heredia, Lima (E. Málaga-Trillo); German Centre for Infection Research, Berlin (J.F. Drexler)

DOI: https://doi.org/10.3201/eid3010.240124

Fort Sherman virus (FSV) was isolated in Panama in 1985 from a US soldier. We report a case of human FSV infection in a febrile patient from northern coastal Peru in 2020. FSV infections spanning ≈35 years and a distance of 2,000 km warrant diagnostics, genomic surveillance, and investigation of transmission cycles.

In 1985, the orthobunyavirus Fort Sherman virus (FSV) was discovered in a US soldier with acute febrile disease who was based in a jungle warfare training center in Panama (*1*). Two FSV strains were isolated from mosquitoes in Argentina in 1965 and 1982 (*2*). FSV was found in healthy horses in Brazil in 2018, (*2*) and in horses in Argentina showing neurologic and abortive disease in 2013 (*3*). Serologic analyses of horse-associated FSV strains have suggested a broad vertebrate host range in peridomestic animals; seroprevalence has ranged from 2.9% in goats to 22.0% in horses in Brazil (*2*) and 5.7% in humans in Argentina (*4*).

We describe a case of human FSV infection in a patient with febrile illness sampled in March 2020 in the city of Chiclayo in Lambayeque department on the northern coast of Peru (Figure 1). The patient was a 61-year-old man with no recent travel history and fever of 38°C. Results of diagnostic tests were negative, including dengue virus (DENV)–specific real-time reverse transcription PCR (RT-PCR) and broadly reactive nested RT-PCRs targeting flaviviruses and alphaviruses. Expanded diagnostic investigation yielded a positive result for orthobunyaviruses using a broadly reactive RT-PCR (Appendix, https://wwwnc.cdc.gov/EID/article/30/10/24-0124-App1.pdf). We identified the virus as FSV by sequencing of the screening PCR amplicon (Appendix). We obtained complete coding sequences of all 3 genome segments by amplifying overlapping genome fragments using nested RT-PCR, followed by Sanger sequencing (Appendix). Virus isolation failed despite repeated attempts, potentially because of sample degradation and a relatively low viral load of 3.7×10^2 viral RNA copies/mL of blood quantified using published FSV-specific real-time RT-PCR (*2*).

To investigate the extent of FSV infection in Lambayeque, we examined all 582 available serum samples from febrile persons sent for diagnostics to the local reference laboratory from Peru's Ministry of Health during 2020 using RT-PCR for orthobunyaviruses. Of the samples, 70.4% (410/582 [95% CI 66.6–74.0]) tested positive for DENV, but no samples tested positive for FSV, other orthobunyaviruses, alphaviruses, or other flaviviruses (Appendix Table 3, Appendix Figure).

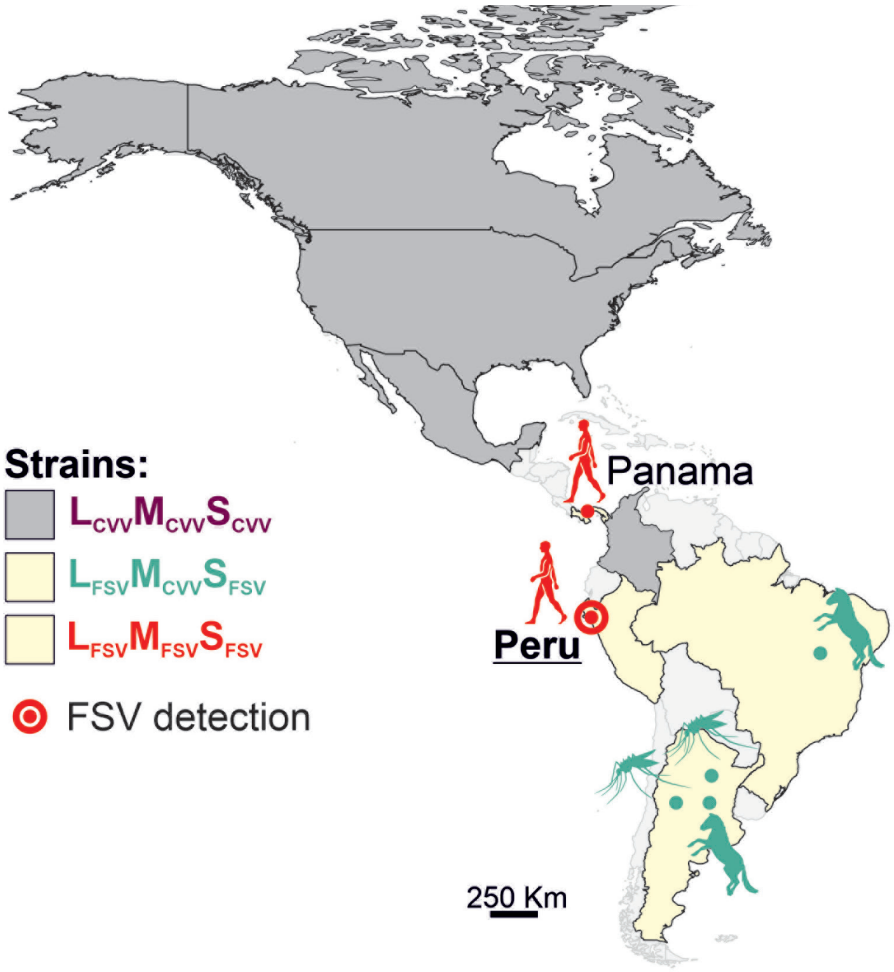

Figure 1. Geographic distribution of CVV and both FSV strains along the North and South American continents in study of FSV infection, Peru, 2020. Additional information on the sequences used to build the figure is provided (Appendix Table 1, https://wwwnc.cdc.gov/EID/article/30/10/24-0124-App1.pdf). CVV, Cache Valley virus; FSV, Fort Sherman virus; L, large segment; M, medium segment; S, small segment.

The genetic identity of the human-derived FSV strains from Panama and Peru was notable because those 2 strains were sampled over a distance of 2,000 km and nearly 4 decades apart. Nucleotide distances of the complete coding sequences compared with the prototypic FSV were 2.0% for large, 2.3% for medium (M), and 1.0% for small gene sequences. Translated amino acid sequence distances were low at all coding sequences, ranging from 0 to 1.5% (Appendix Table 4), which is compatible with strong purifying selection acting on arthropod-borne viruses, such as FSV (*5*).

In phylogenetic reconstructions, the Peru FSV clustered with the Panama FSV prototype strain in all 3 viral genes. In the M gene–based phylogeny, the Panama and Peru FSV strains were monophyletic and nested in the Cache Valley virus (CVV) clade with robust bootstrap support (Figure 2). In contrast, mosquito- and horse-derived FSV strains from Argentina and Brazil differed from the FSV prototype in the phylogeny of their glycoprotein-encoding M gene (Figure 2). Phylogenetic inference of human-derived strains suggested an evolutionary origin of M genes involving a nonrecent reassortment event involving CVV (*2*). CVV frequently infect ruminants in North America, causing severe disease and congenital defects (*6*). Febrile disease in CVV-infected humans has been reported sporadically (*6*). The range of potential vertebrate or invertebrate hosts in which FSV and CVV reassortment might have occurred is thus wide.

Orthobunyavirus reassortment predominantly involves the M segment that encodes proteins responsible for viral receptor binding, thus potentially altering viral host range (*7*). Because CVV has been detected in several mosquito species (*6*), the human-derived FSV containing a CVV-like M

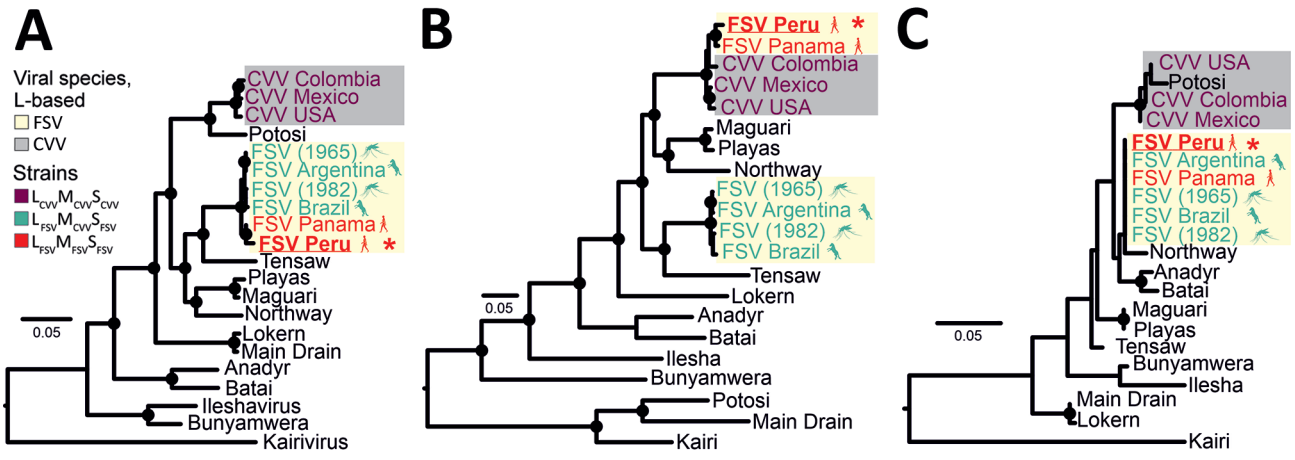

Figure 2. Maximum-likelihood phylogenetic trees based on deduced amino acid sequences of the L (A), M (B), and S (C) gene segments in study of Fort Sherman virus infection, Peru, 2020. Red asterisks indicate the FSV strain sequenced in this study. Black circles at nodes represent support values of ≥0.70 from 1,000 bootstrap replicates. Additional information on the reference sequences used to build the tree is provided (Appendix Table 1, https://wwwnc.cdc.gov/EID/article/30/10/24-0124-App1.pdf). Scale bars indicate genetic distance. CVV, Cache Valley virus; FSV, Fort Sherman virus; L, large segment; M, medium segment; S, small segment.

protein might have a relatively broad host range, potentially including mosquito species that enable urban transmission cycles. This possibility is worrying because the Lambayeque region is a hot spot for the *Aedes* spp. mosquito–borne DENV, and during the COVID-19 pandemic, vector control activities were stopped (*8*). Although lack of another FSV-positive patient with febrile disease during 2020 in Lambayeque refuted an FSV outbreak, future outbreaks in humans cannot be excluded. Genetic monitoring of FSV will be required given that even single amino acid exchanges might affect the arboviral host range, as was demonstrated by the E1-A226V exchange in the Chikungunya virus envelope coding sequence that dramatically enhanced infection of *Aedes albopictus* (*9*).

The lack of studies describing FSV in humans is intriguing. One explanation could be the insufficient diagnostic capacity in areas where FSV potentially circulates. Another reason could be that human FSV infections are rare, potentially because of strong purifying selection that hinders the virus's adaptation to human hosts (*10*). Our data highlight infection of humans with FSV in 2 ecologically distinct settings (coastal desert in Peru and coastal forest in Panama; https://www.oneearth.org) ≈2,000 km and 35 years apart in Latin America. The transmission cycle of both the human- and horse-derived FSV strains needs to be elucidated to identify risk groups and design intervention strategies. FSV should be considered in the differential diagnosis of febrile disease in Latin America, ideally including the development of robust serologic tests.

Acknowledgments

We thank José Encinas Marroquin, Victor Carvalho Urbieta, and Sebastian Brünink for their technical support.

The procedures in this study were carried out with the approval of the institutional bioethics committee under the ethic protocol number 6528 from VIA LIBRE and EA2/031/22 from Charité-Universitaetsmedizin Berlin.

This work was supported by the German Federal Ministry of Economic Cooperation and Development (BMZ) via the Deutsche Gesellschaft für Internationale Zusammenarbeit (GIZ) GmbH (project no. 81262528).

About the Author

Dr. Oliveira-Filho is a virologist at the Institute of Virology, Charité Universitätsmedizin Berlin. His research interests include the epidemiology and evolution of emerging viruses.

References

1. Mangiafico JA, Sanchez JL, Figueiredo LT, LeDuc JW, Peters CJ. Isolation of a newly recognized Bunyamwera serogroup virus from a febrile human in Panama. Am J Trop Med Hyg. 1988;39:593–6. https://doi.org/10.4269/ajtmh.1988.39.593
2. de Oliveira Filho EF, Carneiro IO, Ribas JRL, Fischer C, Marklewitz M, Junglen S, et al. Identification of animal hosts of Fort Sherman virus, a New World zoonotic orthobunyavirus. Transbound Emerg Dis. 2020;67:1433–41. https://doi.org/10.1111/tbed.13499
3. Tauro LB, Rivarola ME, Lucca E, Mariño B, Mazzini R, Cardoso JF, et al. First isolation of Bunyamwera virus (*Bunyaviridae* family) from horses with neurological disease and an abortion in Argentina. Vet J. 2015;206:111–4. https://doi.org/10.1016/j.tvjl.2015.06.013

4. Tauro LB, Venezuela RF, Spinsanti LI, Konigheim BS, Contigiani MS. First case of human infection with a Bunyamwera serogroup virus in Argentina. J Clin Virol. 2012;54:98–9. https://doi.org/10.1016/j.jcv.2012.01.023
5. Woelk CH, Holmes EC. Reduced positive selection in vector-borne RNA viruses. Mol Biol Evol. 2002;19:2333–6. https://doi.org/10.1093/oxfordjournals.molbev.a004059
6. Waddell L, Pachal N, Mascarenhas M, Greig J, Harding S, Young I, et al. Cache Valley virus: a scoping review of the global evidence. Zoonoses Public Health. 2019;66:739–58. https://doi.org/10.1111/zph.12621
7. Briese T, Calisher CH, Higgs S. Viruses of the family Bunyaviridae: are all available isolates reassortants? Virology. 2013;446:207–16. https://doi.org/10.1016/j.virol.2013.07.030
8. Plasencia-Dueñas R, Failoc-Rojas VE, Rodriguez-Morales AJ. Impact of the COVID-19 pandemic on the incidence of dengue fever in Peru. J Med Virol. 2022;94:393–8. https://doi.org/10.1002/jmv.27298
9. Tsetsarkin KA, Vanlandingham DL, McGee CE, Higgs S. A single mutation in chikungunya virus affects vector specificity and epidemic potential. PLoS Pathog. 2007;3:e201. https://doi.org/10.1371/journal.ppat.0030201
10. Orf GS, Perez LJ, Meyer TV, Luk KC, Forberg K, Rodgers MA, et al. Purifying selection decreases the potential for Bangui orthobunyavirus outbreaks in humans. Virus Evol. 2023;9:vead018. https://doi.org/10.1093/ve/vead018

Address for correspondence: Jan Felix Drexler, Institute of Virology, Charitéplatz 1, 10117 Berlin, Germany; email: felix.drexler@charite.de

Fatal Renal Abscess Caused by *Porphyromonas gingivalis* and Subcapsular Hemorrhage, Japan

Yuichiro Atagi, Yoshito Homma, Sadamu Yamashi, Ken Kikuchi, Yoji Nagashima

Author affiliations: Ehime Prefectural Central Hospital, Matsuyama, Japan (Y. Atagi, Y. Homma, S. Yamashi); Tokyo Women's Medical University School of Medicine, Tokyo, Japan (K. Kikuchi, Y. Nagashima)

DOI: https://doi.org/10.3201/eid3010.240078

A 61-year-old man in Japan with abdominal pain was suspected of having a renal tumor. Despite initial treatment, his condition rapidly deteriorated, leading to death. Postmortem examination revealed a renal abscess and sepsis caused by *Porphyromonas gingivalis*. This case underscores the need to consider atypical pathogens in renal masses.

Renal abscesses are rare and often difficult to distinguish from malignant renal tumors. Renal abscesses typically are caused by gram-negative bacteria, such as *Escherichia coli* and *Proteus* species, as well as gram-positive *Staphylococcus aureus* (*1*). *Porphyromonas gingivalis*, an anaerobic, gram-negative bacterium primarily associated with periodontal disease, is an uncommon cause of systemic infections (*2*). We report a fatal case of renal abscess and sepsis caused by *P. gingivalis* in a man in Japan.

The patient was a 61-year-old man with a body mass index of 22.3 kg/m^2 who had a history of hypertension, hyperuricemia, dyslipidemia, and cerebral hemorrhage. However, he had no residual effects from the cerebral hemorrhage and worked without any problems. He was undergoing follow-up for an intraductal papillary mucinous tumor of the pancreatic duct in the internal medicine department at Ehime Prefectural Central Hospital in Matsuyama, Japan. One week before admission, he experienced a brief fever and gum pain. Three days before admission, routine imaging revealed a mass in his right kidney (Figure 1, panel A), leading to a referral to the urology department.

At admission, the patient was in severe pain. A contrast-enhanced computed tomography (CT) scan of the abdomen revealed a subrenal capsular hematoma caused by tumor rupture (Figure 1, panel B). Spontaneous rupture of a renal tumor was diagnosed and considered a grade 1 renal injury. After examination, we admitted the patient for conservative therapy. We performed a follow-up contrast-enhanced CT scan of the abdomen a day after admission, which showed no changes in hematoma size or effusion progression (Figure 1, panel C). We continued conservative treatment, but 2 days after admission, the patient showed signs of poor oxygenation, tachycardia, and hypotension. On day 3 of admission, the patient's respiratory function deteriorated, and he required intubation.

During the patient's hospitalization, no fever was observed. However, blood tests indicated an elevated inflammatory response. We suspected a hematoma infection, drew blood for cultures, and started the patient on meropenem. However, the patient's general condition did not improve, and he died on the fourth day after admission.

Two sets of blood cultures obtained before initiating antimicrobial drug therapy were both negative. A urine culture detected only the presence of streptococci. The family requested an autopsy to determine the cause of death.

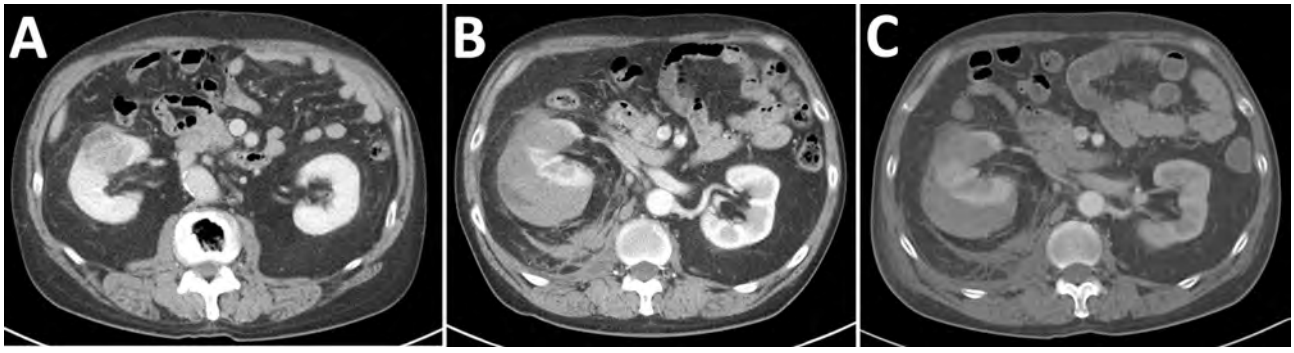

Figure 1. CT scans in a case of fatal renal abscess caused by *Porphyromonas gingivalis* and subcapsular hemorrhage, Japan. A) Contrast enhanced CT 3 days before patient admission shows a 3.5-cm large right renal mass, which was suspected to be renal carcinoma based on imaging findings. B) Contrast enhanced CT at admission. The patient was hospitalized for bleeding from the renal mass. C) Contrast enhanced CT 1 day after admission, showing a shrinking hematoma. CT, computed tomography.

The autopsy was approved and revealed that the right renal mass was not a tumor but a renal abscess. We found turbid ascites and pleural effusions in the abdominal and thoracic cavities. The pathology report revealed that the cause of death was renal abscess, associated sepsis, and respiratory failure due to acute respiratory distress syndrome. The renal subcapsular hematoma caused disruption of cortical vessels around the abscess. Because blood culture results were negative, we performed immunostaining of the pathology specimen from the renal abscess (Figure 2). We also performed 16srRNA gene sequencing of isolates from renal abscess specimens, which identified the causative organism as *P. gingivalis*.

P. gingivalis is a known etiologic agent of periodontitis and has been observed to cause abscesses in various body parts, including the brain and liver (*3*–*5*). However, reports of renal abscesses caused by this pathogen are lacking. Although primarily associated with periodontitis, *P. gingivalis* has also been implicated in various systemic diseases and systemic infections, highlighting its potential as a versatile pathogen (*6*). The pathogenesis of *P. gingivalis* involves several virulence factors, including fimbriae, hemagglutinins, and gingipains, which enable the bacterium to invade tissues and evade the host immune response (*7*,*8*). *P. gingivalis* also is reported to have biofilm formation, intravenous dipeptidyl peptidase activity, strong induction of inflammatory cytokine secretion, and the ability to infiltrate epithelial cells to evade the immune response activation (*9*). The route of infection in this case remains unclear, but hematogenous spread from a subclinical oral infection is plausible.

Renal abscesses are typically associated with underlying conditions, such as diabetes mellitus, urinary tract obstructions, or immunosuppression (*10*). However, our patient had no notable immunodeficiency or recent urologic interventions that could predispose him to such an infection. The atypical clinical manifestations, without classic signs of sepsis-like fever or leukocytosis, likely delayed the diagnosis and appropriate treatment.

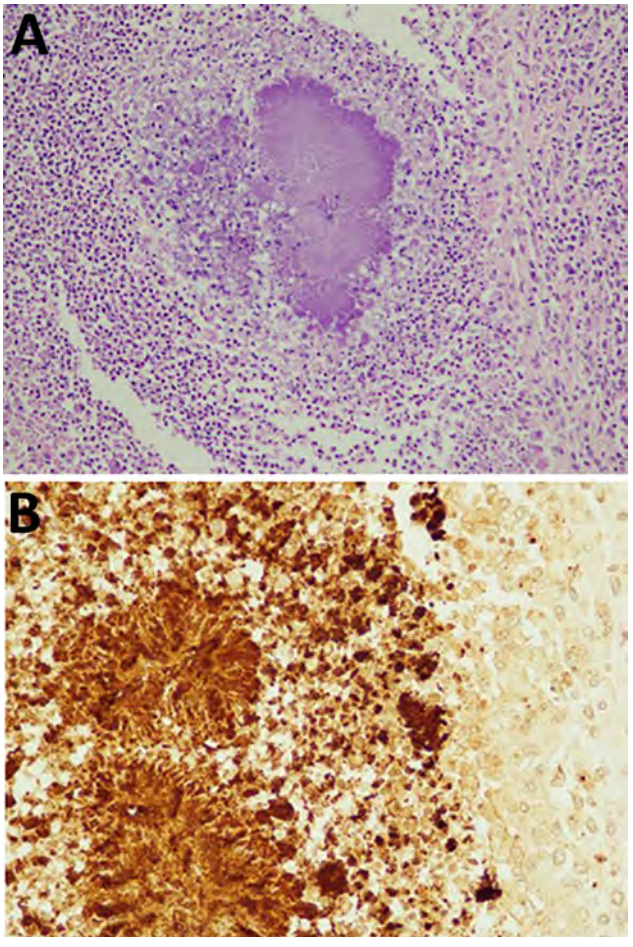

Figure 2. Immunology of mass in a case of fatal renal abscess caused by *Porphyromonas gingivalis* and subcapsular hemorrhage, Japan. A) Hematoxylin and eosin stain. Original magnification ×100. B) Immunohistochemistry with antibody diluted 100 times. Original magnification × 200.

Early recognition and aggressive treatment are critical in managing renal abscesses. Appropriate imaging studies, prompt abscess drainage, and targeted antimicrobial therapy are key to successful renal abscess outcomes. Identification of *P. gingivalis* in this case highlights the importance of comprehensive diagnostic workups, including advanced molecular techniques, to detect uncommon pathogens.

In summary, we identified a rare case of fatal renal abscess and sepsis caused by *P. gingivalis*. Early diagnosis and aggressive management are crucial to improving patient outcomes in such complex infections. This case underscores the need for clinicians to maintain a high index of suspicion for atypical pathogens in patients with renal masses and systemic symptoms, even when classic risk factors are absent.

During the preparation of this work, we used Grammarly (https://www.grammarly.com) and ChatGPT4o (OpenAI, https/openai.com) to correct English grammar. After using this service, we reviewed and edited the content as needed and take full responsibility for the publication's content.

About the Author

Dr. Atagi is a urologist at Ehime Prefectural Central Hospital. His work focuses on urological oncology.

References

1. Rafiei M, Kiani F, Sayehmiri F, Sayehmiri K, Sheikhi A, Zamanian Azodi M. Study of *Porphyromonas gingivalis* in periodontal diseases: a systematic review and meta-analysis. Med J Islam Repub Iran. 2017;31:62. https://doi.org/10.18869/mjiri.31.62
2. Bostanci N, Belibasakis GN. *Porphyromonas gingivalis*: an invasive and evasive opportunistic oral pathogen. FEMS Microbiol Lett. 2012;333:1–9. https://doi.org/10.1111/"j.1574-6968.2012.02579.x
3. Zhang Y, Zhu Y, Wan H. Case report: multiple abscesses caused by *Porphyromonas gingivalis* diagnosed by metagenomic next-generation sequencing. Front Med (Lausanne). 2023;9:1089863. https://doi.org/10.3389/fmed.2022.1089863
4. Ohyama H, Nakasho K, Yamanegi K, Noiri Y, Kuhara A, Kato-Kogoe N, et al. An unusual autopsy case of pyogenic liver abscess caused by periodontal bacteria. Jpn J Infect Dis. 2009;62:381–3. https://doi.org/10.7883/yoken.JJID.2009.381
5. Van der Cruyssen F, Grisar K, Maes H, Politis C. Case of a cerebral abscess caused by *Porphyromonas gingivalis* in a subject with periodontitis. BMJ Case Rep. 2017; 2017:bcr2016218845. https://doi.org/10.1136/bcr-2016-218845
6. Arimatsu K, Yamada H, Miyazawa H, Minagawa T, Nakajima M, Ryder MI, et al. Oral pathobiont induces systemic inflammation and metabolic changes associated with alteration of gut microbiota. Sci Rep. 2014;4:4828. https://doi.org/10.1038/srep04828
7. Fiorillo L, Cervino G, Laino L, D'Amico C, Mauceri R, Tozum TF, et al. *Porphyromonas gingivalis*, periodontal and systemic implications: a systematic review. Dent J. 2019;7:114. https://doi.org/10.3390/dj7040114
8. Mei F, Xie M, Huang X, Long Y, Lu X, Wang X, et al. *Porphyromonas gingivalis* and its systemic impact: current status. Pathogens. 2020;9:944. https://doi.org/10.3390/pathogens9110944
9. Mysak J, Podzimek S, Sommerova P, Lyuya-Mi Y, Bartova J, Janatova T, et al. *Porphyromonas gingivalis*: major periodopathic pathogen overview. J Immunol Res. 2014;2014:476068. https://doi.org/10.1155/2014/476068
10. Zhang JQ, Fielding JR, Zou KH. Etiology of spontaneous perirenal hemorrhage: a meta-analysis. J Urol. 2002;167:1593–6. https://doi.org/10.1016/S0022-5347(05)65160-9

Address for correspondence: Yuichiro Atagi, Ehime Prefectural Central Hospital Department of Urology, Kasuga-machi 83, Matsuyama 790-0024, Japan; email: yatagi.170326@gmail.com

Correction: Vol. 30, Supplement 1

The vertical axis of Figure 2 was mislabeled in HIV Risk and Interest in Preexposure Prophylaxis in Justice-Involved Persons (A.E. Nijhawan et al.). The article has been corrected online (https://wwwnc.cdc.gov/eid/article/30/13/23-0739_article).

Correction: Vol. 30, No. 1

Figures were mislabeled and the author list was incorrect in Clade I–Associated Mpox Cases Associated with Sexual Contact, the Democratic Republic of the Congo (E.M. Kibunguet al.). The article has been corrected online (https://wwwnc.cdc.gov/eid/article/30/1/23-1164_article).

Infectious Disease Physicians' Knowledge and Practices Regarding Wastewater Surveillance, United States, 2024

Carly Adams, Libby Horter, Susan E. Beekmann, Philip M. Polgreen, Jessica N. Ricaldi, Souci Louis, Scott Santibañez

Author affiliations: Centers for Disease Control and Prevention, Atlanta, Georgia, USA (C. Adams, L. Horter, J.N. Ricaldi, S. Louis, S. Santibañez); Goldbelt Professional Services, Chesapeake, Virginia, USA (L. Horter); University of Iowa, Iowa City, Iowa, USA (S.E. Beekmann, P.M. Polgreen)

DOI: https://doi.org/10.3201/eid3010.240719

A survey of US infectious disease physicians indicated that few regularly reviewed wastewater surveillance (WWS) data but many reported examples of the effect or potential effect of WWS on clinical practice. WWS data can be useful for physicians, but increased communication between public health professionals and physicians regarding WWS could improve its utility.

Although clinical reporting is critical to infectious disease surveillance, it is limited to the interaction of individual patients with the healthcare system. Wastewater surveillance (WWS) has a history of detecting disease early, independent of healthcare-seeking behavior or access to healthcare and testing (*1*). WWS data often correlate with transmission levels found in case-based surveillance and can strengthen efforts to prevent disease transmission (*1*). To enhance the capacity to detect SARS-CoV-2 and additional microbial and chemical targets in wastewater, the US Centers for Disease Control and Prevention (CDC; Atlanta, GA, USA) established the National Wastewater Surveillance System (https://www.cdc.gov/nwss/wastewater-surveillance.html) during the COVID-19 pandemic (*2*). As of April 2024, a total of 1,690 NWSS sites in all 50 states and several cities and tribal communities have been monitoring wastewater for infectious diseases. Data on SARS-CoV-2 and monkeypox virus are publicly available (*3*–*6*).

Often, the first to diagnose and report infectious diseases are physicians (*7*). However, before physicians' initial interactions with case-patients, public health and clinical awareness of infections can be enhanced by WWS. To describe the knowledge and practices of US infectious disease physicians regarding WWS, we surveyed the Emerging Infections Network (EIN), a provider-based network supported by CDC and the Infectious Diseases Society of America (*8*). The activity was reviewed by CDC and conducted consistent with applicable federal law and CDC policy (e.g., 45 C.F.R. part 46, 21 C.F.R. part 56; 42 U.S.C. §241(d); 5 U.S.C. §552a; 44 U.S.C. §3501 et seq.).

Table 1. Characteristics of 448 infectious disease specialists responding to Emerging Infections Network survey regarding wastewater surveillance, February–March 2024*

Respondent practice characteristics	No. (%) respondents
Experience since infectious disease fellowship, y	
<5	63 (14)
5–14	132 (30)
15–24	92 (21)
≥25	161 (36)
Practice type	
Adult	356 (80)
Pediatric	92 (21)
Type of hospital in which respondent primarily practices	
City/county	25 (6)
Community	94 (21)
Nonuniversity teaching	106 (24)
University	195 (44)
Outpatient only	3 (1)
US Department of Veterans Affairs or Department of Defense	25 (6)
US Census Bureau region in which respondent resides	
Northeast	108 (24)
Midwest	107 (24)
South	126 (28)
West	107 (24)

*The Infections Disease Society of America Emerging Infections Network is a provider-based emerging infections sentinel network established in 1995 to assist the Centers for Disease Control and Prevention and other public health authorities with surveillance for emerging infectious diseases and related phenomena. The electronic survey was distributed via 3 email messages in February and March 2024 to all US Emerging Infections Network infectious disease physician members.

Table 2. Perspectives of 448 infectious disease specialists regarding wastewater surveillance, Emerging Infections Network survey responses, February–March 2024*

Survey responses	No. (%) respondents
Wastewater surveillance conducted in county or state of work	
Yes	286 (64)
No	18 (4)
Unsure	144 (32)
Awareness and frequency of review of wastewater surveillance data, n = 446	
Not aware of those data	97 (22)
Aware but do not review regularly	251 (56)
Aware and review regularly	98 (22)
Use CDC wastewater websites, n = 446	
Yes	194 (43)
No	252 (57)
Type of CDC wastewater websites used, n = 44†	
COVID WVAL map	150 (34)
COVID data tracker	142 (32)
COVID variants	74 (17)
Mpox	37 (8)
Use non-CDC wastewater websites, n = 440	
Yes	125 (28)
No	315 (72)
Targets respondents chose as potentially useful for wastewater surveillance‡	
Influenza A	302 (67)
Influenza B	254 (57)
Respiratory syncytial virus	247 (55)
Norovirus	245 (55)
Measles	245 (55)
Antimicrobial resistance	198 (44)
West Nile virus	172 (38)
Fungal	138 (31)
Bacterial	117 (26)
Adenovirus	110 (25)
Parasitic diseases	103 (23)
Dengue virus	100 (22)
Reported geographic reporting level as very useful‡§	
City, n = 424	281 (66)
County, n = 431	277 (64)
State, n = 426	103 (24)
Nation, n = 418	64 (15)
Reported facility reporting level as very useful‡§	
Hospital, n = 426	254 (60)
Long-term care facility, n = 423	230 (54)
K-12 school, n = 414	151 (37)
University, n = 408	121 (30)
Jail/detention center, n = 414	129 (31)
Homeless shelter, n = 410	138 (34)

*The Infections Disease Society of America Emerging Infections Network is a provider-based emerging infections sentinel network established in 1995 to assist the Centers for Disease Control and Prevention and other public health authorities with surveillance for emerging infectious diseases and related phenomena. The electronic survey was distributed via 3 email messages in February and March 2024 to all US EIN infectious disease physician members. n values indicate no. respondents when <448. K–12, kindergarten through 12th grade; WVAL, Wastewater viral activity levels.
†CDC COVID WVAL Map (https://www.cdc.gov/nwss/rv/COVID19-currentlevels.html); CDC COVID Data Tracker (https://covid.cdc.gov/covid-data-tracker/#wastewater-surveillance); CDC COVID variants (https://www.cdc.gov/nwss/rv/COVID19-variants.html); CDC Mpox (https://www.cdc.gov/nwss/wastewater-surveillance/mpox-data.html); non-CDC wastewater websites (e.g., from state/local health departments or private/academic organizations).
‡At the time of the survey, the National Wastewater Surveillance System was reporting wastewater surveillance data publicly for SARS-CoV-2 and monkeypox virus at the sampling site, state, and national levels.
§Respondents were asked "In your practice, please indicate the usefulness of the following potential levels of reporting..." and to rate geographic location and facility reporting levels for wastewater surveillance data as slightly, somewhat, or very useful.

During February–March 2024, we distributed a 9-question cross-sectional survey to EIN members (Appendix, https://wwwnc.cdc.gov/EID/article/30/10/24-0719-App1.pdf). We described the survey responses received from 448 (25%) of 1,809 US-based infectious disease physician members and summarized them by respondent characteristics. We identified example quotations that summarized themes identified most frequently from the open-ended question.

Although 64% of respondents knew of WWS in their county or state of work, 36% reported uncertainty or no WWS occurrence (Tables 1, 2). Respondents in the midwestern and western United States were more aware of WWS than those in the

northeastern and southern United States (Appendix Table 1). A total of 22% respondents reviewed WWS data regularly, 56% did not review regularly, and 22% were not aware of those data (Table 3). For data sources, 43% of respondents used CDC websites (*3*–*6*) and 28% used non-CDC websites. Among the 108 respondents who listed non-CDC websites, most reported state health department websites (58%), followed by local health department and private/academic institution websites (25% each). Targets considered most useful for WWS included influenza A (67%), influenza B (57%), respiratory syncytial virus (55%), norovirus (55%), and measles (55%). Providers with <15 years of experience were more likely to consider measles a useful target than were providers with ≥15 years of experience (Appendix Table 2). Facility-level reporting was most often considered very useful for hospitals (60%) and long-term care facilities (54%). Compared with providers of adult healthcare, providers of pediatric healthcare were less likely to consider reporting for long-term care facilities very useful and were more likely to

Table 3. Thematic summary of specific examples provided by infectious disease physicians to open-ended question of how wastewater surveillance has affected or could affect their clinical practice, Emerging Infections Network, February–March 2024*

Themes identified and subset of example responses, respondents providing free-text responses, n = 192	No. (%) respondents
Situational awareness	91 (47)
"In the absence of reliable Covid test reporting, we integrate wastewater with emergency department and admission data to assess risk."	
"Identify potential outbreaks early."	
"I look to tell immunocompromised patients' risk for COVID."	
"It has helped with discussions with my patients and their families."	
"Raises or lowers my clinical suspicion based on prevalence."	
"Potential early indicator of disease activity in the community."	
"Include the information in communicable diseases reports for my organization and county."	
IPC decisions	47 (24)
"Wastewater surveillance has helped us direct IPC and public health resources and can be very helpful."	
"We have used this information to support decisions to determine need for staff masking during respiratory virus season."	
"We are using it to inform masking policy and to a lesser extent visitation policy at our hospital."	
"Providing hospital personal protective equipment guidance."	
"For many COVID protocols particularly when de-implementing, such as when we were planning to discontinue pre procedure and inpatient admissions screening, this was one of the metrics we used."	
Diagnostic testing and differential diagnoses	29 (15)
"Increases/decreases suspicion for certain infections prior to results of testing."	
"Determining which respiratory virus panel is worth offering."	
"Knowing something is increasing before clinically evident has helped inform testing in our emergency department."	
"Affects decision to retest for COVID in patients with consistent symptoms with a negative initial test, who might be eligible for remdesivir or Paxlovid."	
Vaccinations	24 (13)
"Serves as educational and clinical tools to emphasize need for vaccination."	
"To encourage flu, mpox, and COVID vaccinations when the uptick is seen in the community."	
"Influenza activity and initiation of vaccination schedules."	
Healthcare preparedness	19 (10)
"Predicting COVID needs".	
"Hospital surge planning and resource allocation."	
"Used for staffing."	
"During the past few years, I used it as a leading indicator to help with hospital planning as part of my role as Medical Director for Infection Control in my Hospital System."	
Clinical management	18 (9)
"Increasing resistance genes in our area may lower my threshold to use broader empiric antibiotics."	
"Incidence of resistant organisms can guide therapy."	
"Management of vulnerable patient populations such as transplant recipients and other immunocompromised."	
"Lower thresholds towards treatment."	
Variant/emerging infections detection	8 (4)
"Watching for SARS-CoV-2 variant emergence."	
, "Perhaps detection of new strains of influenza."	
"Best use would be for novel pathogens of interest or antibiotic resistance in specific facilities."	
No effect	14 (7)
"No impact."	
"Unless there is practical and evidenced based guidance that is tied to wastewater surveillance results, I do not believe this will be useful for my clinical practice."	

*The Infections Disease Society of America Emerging Infections Network is a provider-based emerging infections sentinel network established in 1995 to assist the Centers for Disease Control and Prevention and other public health authorities with surveillance for emerging infectious diseases and related phenomena. The electronic survey was distributed via 3 email messages in February and March 2024 to all US EIN infectious disease physician members. IPC, infection prevention and control.

consider reporting for kindergarten–12th grade schools very useful (Appendix Table 3).

In 192 free-text responses, 178 (40%) of the 448 respondents reported how WWS has affected or could affect their clinical practice and 14 respondents reported that WWS does not affect their clinical practice (Table 3). The most common (47%) response was improving situational awareness, including advanced warning of surges and outbreaks to guide patient counseling. For example, a respondent noted, "If we see measles suddenly popping up in a community, we know we have to act." Respondents reported using WWS to guide healthcare infection prevention and control decisions (24%) and diagnostic testing and differential diagnoses (15%). When prompted for additional comments regarding WWS, 47 respondents replied. Providers described the utility of WWS (n = 10), how WWS is not useful (n = 5), and the need to better understand correlations with clinical disease (n = 4).

Results from our survey may not be generalizable to all US infectious disease physicians; respondents may have a greater interest in public health surveillance than nonparticipating physicians. However, respondents' practice characteristics were comparable to those of all EIN members (Appendix Figure). It is unknown how nonrespondents would have answered. If nonresponse resulted from lack of awareness or review of wastewater data, our findings underestimate the need for increased communication with physicians regarding WWS.

Among our findings, many respondents reported examples of how wastewater data affected or could affect their clinical practice, but few reviewed wastewater data regularly. Many respondents were not aware of WWS in their county or state; however, WWS is currently conducted in all 50 states. Increased messaging about the public availability of WWS data is needed. In addition, endemic respiratory viruses, including influenza A, were most commonly reported as useful pathogens for WWS. That finding is consistent with another national survey of infectious disease subject matter experts (*9*). Last, local WWS data were reported as most useful. Currently, CDC reports wastewater data publicly at the sampling site, state, and national levels. Our survey revealed that increased communication between public health professionals and physicians regarding WWS, along with more local reporting, could increase WWS utility.

Acknowledgments

We thank the Houston Health Department for providing information on their survey methods and results, EIN for their assistance drafting and distributing the survey and analyzing results, and Matthew Kuehnert for providing input on the manuscript.

This work was funded by CDC (cooperative agreement no. 5, grant no NU50CK000574).

About the Author

Dr. Adams is an epidemiologist at CDC in Atlanta. Her research interests include infectious disease transmission dynamics in healthcare facilities and wastewater surveillance for SARS-CoV-2 and other infectious diseases.

References

1. Kilaru P, Hill D, Anderson K, Collins MB, Green H, Kmush BL, et al. Wastewater surveillance for infectious disease: a systematic review. Am J Epidemiol. 2023;192:305–22. https://doi.org/10.1093/aje/kwac175
2. Adams C, Bias M, Welsh RM, Webb J, Reese H, Delgado S, et al. The National Wastewater Surveillance System (NWSS): from inception to widespread coverage, 2020-2022, United States. Sci Total Environ. 2024;924:171566. https://doi.org/10.1016/j.scitotenv.2024.171566
3. Centers for Disease Control and Prevention. COVID data tracker: wastewater surveillance. 2024 Apr 8 [cited 2024 Apr 8]. https://covid.cdc.gov/covid-data-tracker/#wastewater-surveillance
4. Centers for Disease Control and Prevention, National Wastewater Surveillance System. COVID-19 current wastewater viral activity levels map. 2024 Apr 4 [cited 2024 Apr 8]. https://www.cdc.gov/nwss/rv/COVID19-currentlevels.html
5. Centers for Disease Control and Prevention, National Wastewater Surveillance System. COVID-19 variants in wastewater. 2024 Apr 4 [cited 2024 Apr 8]. https://www.cdc.gov/nwss/rv/COVID19-variants.html
6. Centers for Disease Control and Prevention, National Wastewater Surveillance System. U.S. mpox wastewater data. 2024 Apr 3 [cited 2024 Apr 8]. https://www.cdc.gov/nwss/wastewater-surveillance/mpox-data.html
7. Thacker SB, Choi K, Brachman PS. The surveillance of infectious diseases. JAMA. 1983;249:1181–5. https://doi.org/10.1001/jama.1983.03330330059036
8. Pillai SK, Beekmann SE, Santibanez S, Polgreen PM. The Infectious Diseases Society of America Emerging Infections Network: bridging the gap between clinical infectious diseases and public health. Clin Infect Dis. 2014;58:991–6. https://doi.org/10.1093/cid/cit932
9. Sheth K, Hopkins L, Domakonda K, Stadler L, Ensor KB, Johnson CD, et al. Wastewater target pathogens of public health importance for expanded sampling, Houston, Texas, USA. Emerg Infect Dis. 2024;30:14–7.

Address for correspondence: Libby Horter, Centers for Disease Control and Prevention, 4770 Buford Hwy, Mailstop S106-3, Atlanta, GA 30341, USA; email: qsw2@cdc.gov

Alfred Sisley (1839–1899), Flood at Port-Marly, 1872. Oil on canvas, 18 1/4 in × 24 in/46.4 cm × 61 cm. Collection of Mr. and Mrs. Paul Mellon. National Gallery of Art, Washington, DC, USA. Open access image.

Following the Flood

Byron Breedlove

"Great floods have flown from simple sources."
—William Shakespeare, *All's Well that Ends Well*, Act 2, Scene 1, line 142

Flooding is the most frequently occurring natural disaster worldwide. According to the data portal Statista, 164 floods were reported in 2023, and no doubt others occurred. Hydrologists categorize the most common types of flooding as coastal floods, river floods, storm surges, and flash floods. Regardless of whether it's a roiling torrent or a seemingly languid flow, floods can damage and destroy cities, towns, building, bridges, and roads; decimate natural landscapes, farms, and crops; displace human and animal populations; disrupt commerce, travel, and healthcare; and cause loss of life during the flooding and afterwards.

This month's cover features *Flood at Port-Marly*, an event French impressionistic artist Alfred Sisley witnesses and recorded. Biographies of Sisley note that he was born in Paris, France, and his parents were British expatriates. He lived in France and occasionally visited England. In 1862, Sisley received training at the Paris studio of Swiss artist Marc Gabriel Charles Gleyre, where he met Claude Monet, Pierre Renoir, and Frederic Bazille. The four became

Author affiliation: Centers for Disease Control and Prevention, Atlanta, Georgia, USA

DOI: https://doi.org/10.3201/eid3010.AC3010

friends, sharing studio space and exchanging ideas, and are credited as being among the originators of Impressionism. Despite his associations with other Impressionistic artists and a portfolio of around 900 oil paintings, 100 pastels, and numerous drawings, Sisley received little recognition and lived much of his life in poverty.

The Getty Museum says of Sisley: "A pure landscape painter unconcerned with the challenge of history painting, he celebrated the intimate qualities of the places he lived in, exploring the effects of changing light and weather and mapping scenes from a variety of viewpoints in different seasons." The U.S. National Gallery of Art, home to this work, notes that "Flooding early in the spring of 1872 drew Sisley to Port-Marly, a village on the Seine near Louveciennes, the artist's home. The water here is calm and human activity is minimal. Rather than dramatic or picturesque incident, the artist's attention was engaged by purely visual effects of rain-laden clouds and water-covered streets."

In this traditionally composed painting, eddying, pink-tinted clouds float over gently rippling water. The river Seine has spilled over its banks, covered the street, and stranded people. There is no sense of eminent danger from surging floodwaters nor havoc and horror following a ruinous deluge. The water has either just stopped short from or receded from the entrances of the two-toned building. The National Gallery of Art offers relates, "Two women in long skirts stand at a darkened, open doorway near the front corner of the structure. A sign on the side of the building hangs from a horizontal arm over three men in and near a shallow boat, which is being propelled by a man who stands in the stern with a long stick. The street is so wet that it first appears to be a canal or river. It is only when we notice dashes of mauve, pale pink, and gray to our left that we realize the cobblestone road is flooded."

This village has apparently escaped direct devastation from flooding, but indirect effects might still occur. Accumulations of standing water that linger could increase the risk for transmission of various vectorborne diseases, such as malaria, dengue fever, West Nile virus disease, and yellow fever. However, although floodwaters could create ideal breeding grounds for mosquitoes and other arthropod vectors in some circumstances, heavy flooding might also wash away larval breeding habitats, decreasing the population of adult mosquitos.

The relationship between vectorborne infections and flooding is not cut and dried. The dynamics of transmission for such diseases are complex and depend on interactions of multiple biologic and environmental factors, adding to the challenges hampering public health efforts to predict, prevent, and respond to outbreaks of vectorborne diseases that may follow flooding.

Bibliography

1. Getty Museum Collection. Alfred Sisley [cited 2024 Aug 23]. https://www.getty.edu/art/collection/person/103KXZ
2. National Gallery of Art. Alfred Sisley. Flood at Port-Marly, 1872 [cited 2024 Aug 23]. https://www.nga.gov/collection/art-object-page.66436.html
3. Statista. Number of natural disasters worldwide in 2023, by type [cited 2024 August 25]. https://www.statista.com/statistics/269653/natural-disasters-on-the-continents-by-nature-of-the-disaster
4. Tate. Alfred Sisley: 1839–1899 [cited 2024 Aug 23]. https://www.tate.org.uk/art/artists/alfred-sisley-1948
5. Wen LS. Mosquito-borne illnesses pose a serious threat. We're not ready for them [cited 2024 Sep 4]. https://www.washingtonpost.com/opinions/2024/09/04/mosquito-illness-eee-west-nile

Address for correspondence: Byron Breedlove, EID Journal, Centers for Disease Control and Prevention, 1600 Clifton Rd NE, Mailstop H16-2, Atlanta, GA 30329-4018, USA; email: wbb1@cdc.gov

EMERGING INFECTIOUS DISEASES®

Upcoming Issue
Respiratory Infections • November 2024

- Flexible Development Programs for Antibacterial Drugs to Address Unmet Medical Needs
- Clinical and Genomic Epidemiology of Coxsackievirus A21 and Enterovirus D68 in Homeless Shelters, King County, Washington, 2019–2021
- Wastewater Surveillance for Poliovirus in Selected Jurisdictions, United States, 2022–2023
- Spatial-Temporal Ecologic Analysis of COVID-19 Vaccination Coverage and Outcomes, Oklahoma, USA, February 2020–December 2021
- Detection of Predominant Azole-Resistant Candida tropicalis Genotype in Orchards Causing Human Candidemia, Taiwan
- Clinical and Molecular Characterization of Human Burkholderia mallei Infection, Brazil
- Emerging Monkeypox Virus Sublineage C.1 Causing Community Transmission, Vietnam, 2023
- Fatal Oropouche Virus Infections in Nonendemic Region, Brazil, 2024
- Epidemiology of Streptococcus pyogenes Disease Before, During, and After COVID-19 Pandemic, Germany, 2005–2023
- Outbreak of Listeriosis Associated with Baker's Yeast Products, Switzerland, 2022–2024
- Mpox Hepatic and Pulmonary Lesions in HIV/Hepatitis B Virus Co-Infected Patient, France
- Foodborne Outbreak Size Is Dependent on How the Outbreak Is Detected
- Risk for Facial Palsy after COVID-19 Vaccination, South Korea, 2021–2022
- Tuberculosis Posttreatment Mortality Rates, Georgia, USA, 2008–2019

Complete list of articles in the November issue at https://wwwnc.cdc.gov/eid/#issue-315

Earning CME Credit

To obtain credit, you should first read the journal article. After reading the article, you should be able to answer the following, related, multiple-choice questions. To complete the questions (with a minimum 75% passing score) and earn continuing medical education (CME) credit, please go to http://www.medscape.org/journal/eid. Credit cannot be obtained for tests completed on paper, although you may use the worksheet below to keep a record of your answers.

You must be a registered user on http://www.medscape.org. If you are not registered on http://www.medscape.org, please click on the "Register" link on the right hand side of the website.

Only one answer is correct for each question. Once you successfully answer all post-test questions, you will be able to view and/or print your certificate. For questions regarding this activity, contact the accredited provider, CME@medscape.net. For technical assistance, contact CME@medscape.net. American Medical Association's Physician's Recognition Award (AMA PRA) credits are accepted in the US as evidence of participation in CME activities. For further information on this award, please go to https://www.ama-assn.org. The AMA has determined that physicians not licensed in the US who participate in this CME activity are eligible for AMA PRA Category 1 Credits™. Through agreements that the AMA has made with agencies in some countries, AMA PRA credit may be acceptable as evidence of participation in CME activities. If you are not licensed in the US, please complete the questions online, print the AMA PRA CME credit certificate, and present it to your national medical association for review.

Article Title

Pasteurella Infections in South Korea and Systematic Review and Meta-analysis of *Pasteurella* Bacteremia

CME Questions

1. Which was the predominant *Pasteurella* species isolated among patients in South Korea in the current study?

A. *P. canis*
B. *P. multocida*
C. *P. dagmatis*
D. *P. stomatis*

2. Which of the following epidemiologic trends was noted in the infection results from South Korea in the current study?

A. Patient sex had no effect on the risk for *Pasteurella* infection
B. Over 85% of patients had a history of companion animal exposure
C. More cases of *Pasteurella* infection were related to exposure to cats vs dogs
D. Less than 4% of patients had a polymicrobial infection

3. Which of the following statements regarding management and outcomes of *Pasteurella* infection in the current study is most accurate?

A. The most common antibiotics prescribed were macrolides
B. The overall prevalence of bacteremia was around 3%
C. Being a man was the main risk factor for bacteremia
D. There were no fatalities related to *Pasteurella* infection

4. Which of the following statements regarding the results of the meta-analysis analyzing the global burden of *Pasteurella* infections is most accurate?

A. Women had higher rates of *Pasteurella* infection than men in all included studies
B. Over 70% of patients had animal exposure
C. The mortality rate of infection was less than 5%
D. Bacteremia was present in 3% to 6% of patients

Earning CME Credit

To obtain credit, you should first read the journal article. After reading the article, you should be able to answer the following, related, multiple-choice questions. To complete the questions (with a minimum 75% passing score) and earn continuing medical education (CME) credit, please go to http://www.medscape.org/journal/eid. Credit cannot be obtained for tests completed on paper, although you may use the worksheet below to keep a record of your answers.

You must be a registered user on http://www.medscape.org. If you are not registered on http://www.medscape.org, please click on the "Register" link on the right hand side of the website.

Only one answer is correct for each question. Once you successfully answer all post-test questions, you will be able to view and/or print your certificate. For questions regarding this activity, contact the accredited provider, CME@medscape.net. For technical assistance, contact CME@medscape.net. American Medical Association's Physician's Recognition Award (AMA PRA) credits are accepted in the US as evidence of participation in CME activities. For further information on this award, please go to https://www.ama-assn.org. The AMA has determined that physicians not licensed in the US who participate in this CME activity are eligible for AMA PRA Category 1 Credits™. Through agreements that the AMA has made with agencies in some countries, AMA PRA credit may be acceptable as evidence of participation in CME activities. If you are not licensed in the US, please complete the questions online, print the AMA PRA CME credit certificate, and present it to your national medical association for review.

Article Title

Age- and Sex-Specific Differences in Lyme Disease Health-Related Behaviors, Ontario, Canada, 2015–2022

CME Questions

1. Which of the following statements regarding temporal trends in cases of Lyme disease in Ontario, Canada, between 2015 and 2022 in the current study is most accurate?

A. Incidence rates increased 3-fold during the study period
B. The peak incidence of Lyme disease was between April and June
C. Incidence rates increased annually between 2015 and 2022
D. Incidence rates were flat between 2015 and 2018, and then accelerated sharply

2. What were the peak ages of incident Lyme disease in the current study?

A. 14 to 19 and 20 to 29 years
B. 30 to 39 and 50 to 59 years
C. 40 to 49 and 70 to 79 years of age
D. 5 to 9 and 60 to 79 years of age

3. Which of the following statements regarding gender and the epidemiology of Lyme disease in the current study is most accurate?

A. Most cases of Lyme disease occurred among female persons
B. There was no difference in the incidence of Lyme disease based on gender
C. Male persons with Lyme disease had a lower median age compared with female cases
D. Female persons between the ages of 5 and 9 years had higher incidence rates of Lyme disease than male patients

4. Which of the following statements regarding risk factors for Lyme disease among patients in the current study is most accurate?

A. A history of camping was the most common exposure risk factor
B. A history of visiting a hiking or cycling trail was the most common exposure risk factor
C. Most patients recalled an exposure to ticks or a tick bite
D. Most patients had employed using adequate clothing to prevent tick bite or the use of insect repellent

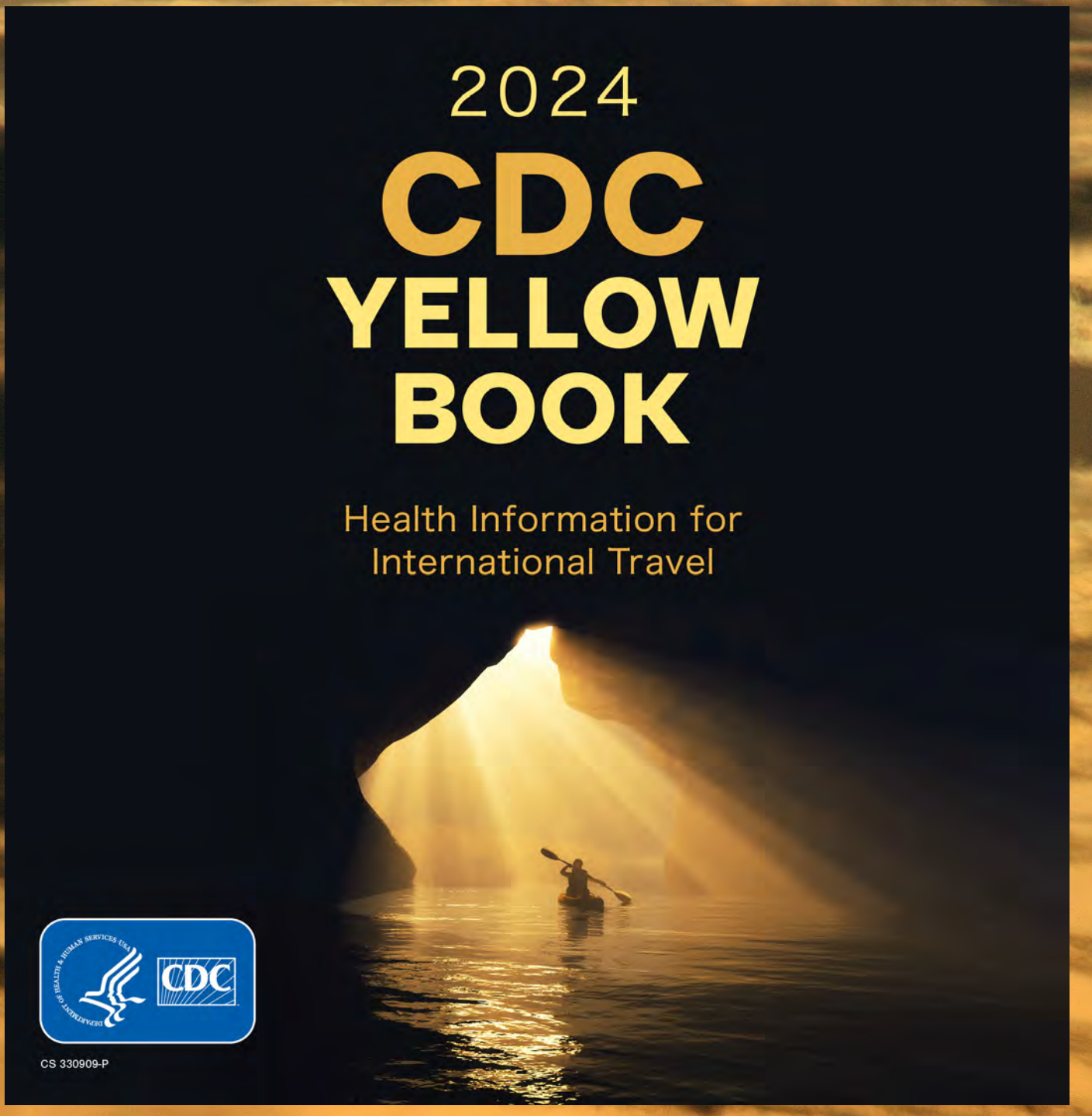

Launch of CDC Yellow Book 2024 – A Trusted Travel Medicine Resource

CDC is pleased to announce the launch of the CDC Yellow Book 2024. The CDC Yellow Book is a source of the U.S. Government's recommendations on travel medicine and has been a trusted resource among the travel medicine community for over 50 years. Healthcare professionals can use the print and digital versions to find the most up-to-date travel medicine information to better serve their patients' healthcare needs.

The CDC Yellow Book is available in print through Oxford University Press and online at www.cdc.gov/yellowbook.